

Department of Chemistry

University of Glasgow

ALLOY FORMATION IN BIMETALLIC REFORMING

CATALYSTS

BY

NORMAN MACLEOD

THESIS

SUBMITTED FOR THE DEGREE

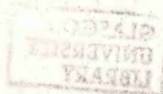
OF

DOCTOR OF PHILOSOPHY

DEPARTMENT OF CHEMISTRY

OCTOBER 1997

© NORMAN MACLEOD, 1997



ProQuest Number: 13815381

All rights reserved

INFORMATION TO ALL USERS

The quality of this reproduction is dependent upon the quality of the copy submitted.

In the unlikely event that the author did not send a complete manuscript and there are missing pages, these will be noted. Also, if material had to be removed, a note will indicate the deletion.



ProQuest 13815381

Published by ProQuest LLC (2018). Copyright of the Dissertation is held by the Author.

All rights reserved.

This work is protected against unauthorized copying under Title 17, United States Code
Microform Edition © ProQuest LLC.

ProQuest LLC.
789 East Eisenhower Parkway
P.O. Box 1346
Ann Arbor, MI 48106 – 1346

Summary

The aim of this study was to obtain a clearer understanding of the role played by promoters such as Re, Ir, Sn and Ge in modifying the properties of Pt/Al₂O₃ reforming catalysts. Particular emphasis was placed on alloy formation in these systems.

A variety of bi and multimetallic catalysts were prepared and characterised by transmission electron microscopy and energy dispersive X-Ray analysis. The results of these studies were correlated with catalytic performance measurements obtained using a microreactor system operated under realistic reforming conditions (110 psig, 510 °C)

For 0.3 wt% Pt - 0.3 wt% Re/Al₂O₃ and 0.3 wt% Pt - 0.3 wt% Ir/Al₂O₃ catalysts, which showed the highest stability, it was concluded that hydrogenolysis/hydrogenation of coke precursors by Re⁰ and Ir⁰ species resulted in the observed improvement in catalytic properties. TEM observations revealed that the metallic component of the 0.3 wt% Pt - 0.3 wt% Ir/Al₂O₃ catalyst consisted of PtIr alloy particles. TEM studies of the 0.3 wt% Pt - 0.3 wt% Re/Al₂O₃ catalyst found no evidence for Re⁰ or PtRe alloys. However, the similarities between the reforming properties of these catalysts strongly suggests that rhenium metal was present.

Addition of germanium to iridium containing catalysts (0.3 wt% Ir - 0.3 wt% Ge/Al₂O₃, 0.3 wt% Pt - 0.3 wt% Ir - 0.3 wt% Ge/Al₂O₃ and 0.3 wt% Pt - 0.3 wt% Ir - 0.03 wt% Ge/Al₂O₃) was found to strongly suppress structure sensitive hydrogenolysis reactions. This was due to a geometric/ensemble effect, i.e. dilution of the active metal surface into smaller clusters or ensembles of adjacent surface metal atoms. These smaller ensembles were unable to catalyse the undesirable hydrogenolysis reaction but were active for aromatisation and isomerisation (essentially dehydrogenation reactions). These ensembles were also less susceptible to coke deposition, which is also known to be structure sensitive. However, in the

case of the 0.3 wt% Pt - 0.3 wt% Ir - 0.3 wt% Ge/Al₂O₃ catalyst, the formation of germanium alloy particles contributed to the overall rate of deactivation of this system.

In the case of 0.3 wt% Pt - 0.3 wt% Sn/Al₂O₃ and 0.3 wt% Pt - 0.3 wt% Ge/Al₂O₃ catalysts, an initial improvement in catalytic properties relative to 0.3 wt% Pt/Al₂O₃ was observed due to geometric/ensemble effects. Again, however, the formation of germanium and tin containing alloy particles contributed to the overall rate of deactivation in these systems. A number of alloy phases were identified in each case.

Addition of V₂O₅ (which is known to exhibit strong metal support interactions) to iridium containing catalysts produced similar alterations in the reforming properties to the addition of germanium. However, the suppression of hydrogenolysis was not as great in this case.

Catalysts containing the rare-earth oxides CeO₂ and Pr₂O₃ were also prepared and tested. It was found that these oxides significantly altered the acidic nature of the support and thus improved the properties of Pt/Al₂O₃ catalysts. No evidence for a significant interaction between the rare-earth oxide and the metal component was obtained although the presence of such an interaction could not be ruled out.

Acknowledgments

I would like to express my thanks to my supervisors Dr J.R. Fryer, Dr D. Stirling and Prof. G. Webb for all their help and advice throughout the course of this study.

Thanks also to everyone in the Electron Microscopy group, particularly Victoria Thompson and David Thom for technical assistance.

I am also indebted to the Engineering and Physical Science Research Council for the award of a studentship at the University of Glasgow.

Finally, I would like to thank my parents, family and friends for all their support and encouragement during the course of my studies.

CONTENTS

Page No.

Summary

Acknowledgments

1. Introduction

1.1	Catalytic Reforming	
1.1.1	Industrial Significance	1
1.1.1	Reforming Reactions and Thermodynamic Considerations	4
1.2	Mechanistic and Kinetic Considerations	
1.2.1	Bifunctional Catalysis	7
1.2.2	Isomerisation Reactions	9
1.2.3	Dehydrocyclisation Reactions	12
1.2.4	Hydrogenolysis Reactions	14
1.2.5	Hydrocracking Reactions	16
1.3	Reforming Catalysts	
1.3.1	Early Reforming Catalysts	17
1.3.2	The Alumina Support	18
1.3.3	Bimetallic Catalysts:	20
1.3.3A	Platinum - Rhenium Catalysts	21
1.3.3B	Platinum - Tin Catalysts	31
1.3.3C	Platinum - Germanium Catalysts	39
1.3.3D	Platinum - Iridium Catalysts	42
1.3.4	Rare-earth Oxides as Promoters in Reforming Catalysts	48
1.4	Catalysts Deactivation by Carbonaceous Residues	50
1.4.1	Characterisation of Coke Deposits	51
1.4.2	Mechanism of Coke Formation	52
1.4.3	Effect of Operating Conditions on Coking	54
1.4.4	Influence of Bimetallic Catalysts on Coking	55
1.4.5	Influence of Carbonaceous Residues on Reforming Reactions	56
1.5	Sintering	58
1.5.1	Sintering Mechanisms	59

2. Objectives

2.1	Objectives of the Present Study	63
-----	---------------------------------	----

3. Transmission Electron Microscopy and Energy Dispersive X-ray Analysis

3.1	Transmission Electron Microscopy	64
3.2	Contrast Mechanisms in the TEM	66
3.2.1	Elastic Scattering	66
3.2.2	Inelastic Scattering	67
3.3	Contrast Transfer and Retrieval of High Resolution Information	69
3.4	Limitations of Information Recovery	
3.4.1	Spherical Aberration	71
3.4.2	Astigmatism	71
3.4.3	Chromatic Aberration	72
3.4.4	Radiation Damage	72
3.4.5	Mechanical Stability	72
3.5	Electron Diffraction	73
3.6	Energy Dispersive X-ray Analysis	
3.6.1	Production and Analysis of X-rays	76
3.6.2	Spectrum Acquisition and Processing	78

4. Experimental 80

4.1	Catalyst Preparation	80
4.1.1	EuroPt-4	81
4.1.2	Coimpergnated Catalysts	81
4.2	Catalysts Characterisation: Chemisorption	82
4.3	Catalysts Characterisation: n-Octane Reforming	83
4.3.1	The Feed System	84
4.3.2	The Reactor System	84
4.3.3	Reactor Pressure Control	85
4.3.4	Gas Sampling	86
4.3.5	The Analytical System	86
4.3.6	PNA Operation	87
4.3.7	Summary of PNA Columns	89
4.3.8	Hydrocarbon Detection and Calibration	90
4.3.9	Materials	90
4.3.10	Activation of Catalysts	91
4.3.11	Catalyst Testing	91

4.3.12	Treatment of Results	92
4.4	Surface Carbon Analysis	94
4.5	Electron Microscopy	
4.5.1	Microscope Operation	94
4.5.2	Quantitative EDX Analysis	95

5. Results 99

5.1	0.3 wt% Pt/Al ₂ O ₃	99
5.2	0.3 wt% Pt - 0.3 wt% Sn/Al ₂ O ₃	105
5.3	0.3 wt% Pt - 0.3 wt% Ge/Al ₂ O ₃	111
5.4	0.3 wt% Pt - 0.3 wt% Re/Al ₂ O ₃	118
5.5	0.3 wt% Pt - 0.3 wt% Ir/Al ₂ O ₃	122
5.6	0.3 wt% Ir/Al ₂ O ₃	126
5.7	0.3 wt% Ir - 0.3 wt% Ge/Al ₂ O ₃	128
5.8	0.03 wt% Ir - 0.3 wt% Ge/Al ₂ O ₃	132
5.9	0.3 wt% Ir - 0.3 wt% V/Al ₂ O ₃	135
5.10	0.3 wt% Pt - 0.3 wt% Ir - 0.03 wt% Ge/Al ₂ O ₃	138
5.11	0.3 wt% Pt - 0.3 wt% Ir - 0.3 wt% Ge/Al ₂ O ₃	143
5.12	0.3 wt% Pt - 0.3 wt% Ir - 0.3 wt% V/Al ₂ O ₃	149
5.13	0.3 wt% Pt/Al ₂ O ₃ [Pt(acac) ₂]	153
5.14	0.3 wt% Pt - 0.3 wt% Ce/Al ₂ O ₃	156
5.15	0.3 wt% Pt - 0.3 wt% Pr/Al ₂ O ₃	159
5.16	0.3 wt% Ni/Al ₂ O ₃	162
5.17	0.3 wt% Ni - 0.3 wt% Ge/Al ₂ O ₃	164
5.18	0.3 wt% Ru - 0.3 wt% Ge/Al ₂ O ₃	166
5.19	Coke Deposition	169
5.20	Chemisorption of CO and O ₂ over Ir/Al ₂ O ₃ , Pt - Ir/Al ₂ O ₃ and Pt - Ir - Ge/Al ₂ O ₃	170

6. Discussion 172

6.1	Pt/Al ₂ O ₃	172
6.2	Pt - Sn/Al ₂ O ₃ and Pt - Ge/Al ₂ O ₃	176
6.3	Pt - Re/Al ₂ O ₃ and Pt - Ir/Al ₂ O ₃	184
6.4	Ir/Al ₂ O ₃ , Ir - Ge/Al ₂ O ₃ , 0.03Ir - Ge/Al ₂ O ₃ and Ir - V/Al ₂ O ₃	192

6.5	Pt - Ir - 0.03Ge/Al ₂ O ₃ , Pt - Ir - Ge/Al ₂ O ₃ and Pt - Ir - V/Al ₂ O ₃	200
6.6	Pt/Al ₂ O ₃ [Pt(acac) ₂] and Rare-earth Containing Catalysts	204
6.7	Ni/Al ₂ O ₃ , Ni - Ge/Al ₂ O ₃ and Ru - Ge/Al ₂ O ₃	208
6.8	General Conclusions	209

References

Chapter One: Introduction

1.1 Catalytic Reforming

1.1.1 Industrial Significance

Catalytic reforming is one of the principal petroleum refining processes and has developed over the last four decades to the point where it is now one of the most important industrial applications of catalysis^{1,2,3}.

The main aim of the process is to produce the high octane fuels that are required for the modern internal combustion engine. Reforming is also the major source of aromatic compounds used in the petrochemical industry for the production of plastics, paints, dyes and detergents.² The process also generates large quantities of hydrogen which are subsequently used in additional refining processes such as hydrotreating and hydrocracking.

The hydrocarbon feedstocks used in the reforming process is referred to by the generic term "naphtha". Naphtha fractions, which are obtained from fractional distillation (and to a lesser extent catalytic cracking) of crude oil, are composed of hydrocarbons with boiling points in the approximate temperature range 40-200°C. These fractions are composed of a mixture of alkanes, cycloalkanes and aromatics, the exact composition of which varies widely between different geographical sources of crude oil. Table 1.1 presents a detailed analysis of two reforming feedstock naphthas; feedstock (a) is a paraffinic Middle East crude and feedstock (b) is a naphthenic Nigerian crude.³

Although the aromatic concentration rarely exceeds 20% by volume in these feedstocks the alkane and cycloalkane contents can vary considerably. Naphtha feedstocks are further characterised by their sulphur, nitrogen and trace metal concentrations.

Table 1.1 also gives the research octane number (RON) of these feedstocks.

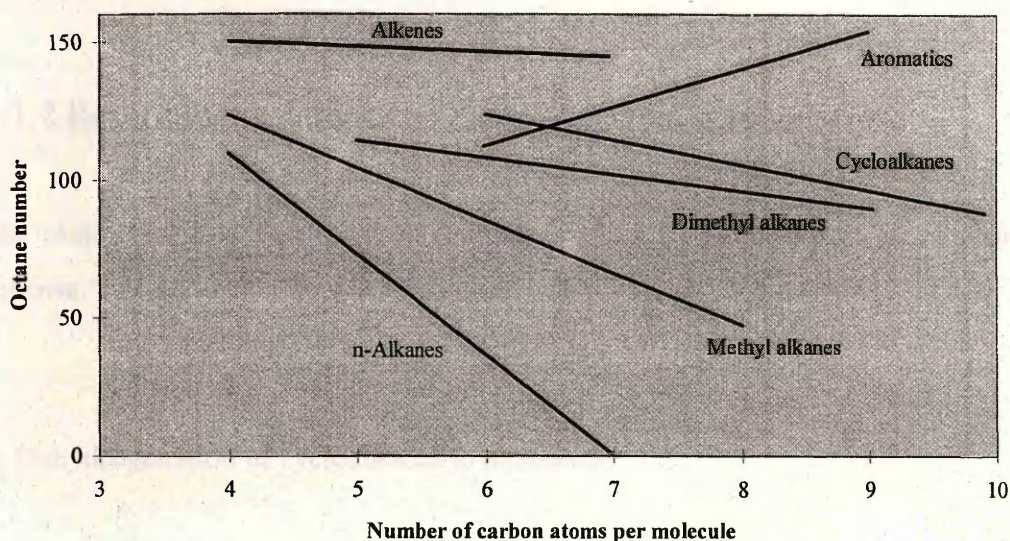
Table 1.1 - Detailed analysis of two reforming feedstocks by weight %.³

	Alkanes	Cycloalkanes	Aromatics
<u>Feedstock (a)</u>			
C ₅	0.00	0.00	0.00
C ₆	5.49	2.30	0.41
C ₇	16.83	5.80	3.18
C ₈	21.38	8.27	6.80
C ₉	17.26	5.59	3.08
C ₁₀	<u>2.59</u>	<u>0.63</u>	<u>0.00</u>
Total	63.55	22.95	13.47
RON = 50			
<u>Feedstock (b)</u>			
C ₅	1.16	0.27	0.00
C ₆	3.31	5.78	0.20
C ₇	6.13	14.24	1.20
C ₈	9.79	14.47	3.54
C ₉	3.89	17.14	4.29
C ₁₀	<u>3.59</u>	<u>11.17</u>	<u>0.88</u>
Total	26.81	63.07	10.10
RON = 66			

The octane rating of a fuel is a measure of its anti-knock properties, i.e. its ability to resist detonation under a rise in temperature due to compression.^{2,4-5} The octane number of a fuel is obtained by comparing its knocking characteristics with blends of iso-octane (2,2,4-trimethylpentane), arbitrarily assigned a value of 100, and n-heptane, assigned a value of zero. A fuel which matches the knocking characteristics of a mixture of 90 parts iso-octane and 10 parts n-heptane by volume is assigned an octane number of 90 (if a sample fuel's octane number exceeds 100, tetraethyl lead is added to iso-octane to improve the reference). Typically modern internal combustion engines require a high octane fuel value of between 92 and 98 RON.⁴

Figure 1.1 shows the relationship between research octane number and molecular structure for various low molecular weight hydrocarbons.² It is apparent from this figure that the octane number of hydrocarbons increase with (1) the degree of branching and (2) the degree of unsaturation. With the exception of aromatic hydrocarbons the octane number decreases with increasing carbon number or molecular weight. High concentrations of alkenes in fuel are known to cause engine fouling problems. Consequently, despite their high anti-knock ratios, their production is undesired.

Figure 1.1. Variation in octane number with respect to chemical structure



In catalytic reforming therefore, the aim is to produce aromatic hydrocarbons as selectively as possible, since their RON always exceeds 100. This is achieved by the dehydrocyclisation of alkanes and the dehydrogenation of cycloalkanes. An increase in the concentration of iso-alkanes and a corresponding decrease in their overall molecular weight also contributes, although to a lesser extent.

Although the production of aromatic compounds provides the largest increase in octane number, there is growing concern regarding the presence of large quantities of

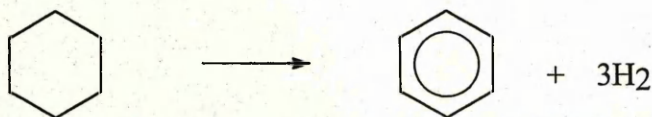
carcinogenic compounds such as benzene in motor fuels. These environmental considerations, which in the past ended the addition of tetraethyl lead to improve octane ratings, may result in a reduction in the amounts of aromatics which can be added to motor fuels. This would result in a shift in emphasis in reforming towards the production of iso-alkanes.

Industrial reforming is typically carried out in the temperature range 480 to 530°C. Reaction pressures may vary between 10 and 35 atmospheres.⁶ The exact conditions used depend on several factors, including the feedstock composition and product requirements.

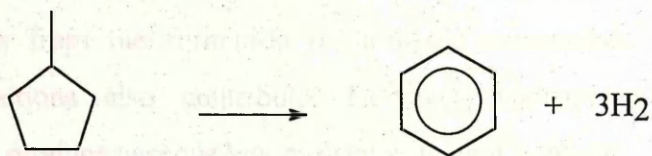
1.1.2 Reforming reactions and thermodynamic considerations

The major reactions that occur in reforming, using C₆ molecules as an example, are as follows:

1. Dehydrogenation of cycloalkanes to aromatics.



2. Dehydroisomerisation of alkyl cyclopentanes to aromatics.



The dehydrogenation of cyclohexanes is the most readily occurring of these reactions. Isomerisation reactions also occur readily, but at a slower rate than that of cyclohexane dehydrogenation. The limiting reactions in most catalytic reforming operations are hydrocracking and dehydrocyclisation, which generally occur at much slower rates.⁶

Thermodynamic data for various reactions of C₆ hydrocarbons are listed in Table 1.2.⁷⁸ The equilibrium constant *K* is defined in terms of the partial pressures of the reactants and products expressed in atmospheres at 500°C. For higher molecular weight hydrocarbons the thermodynamic considerations are qualitatively similar.

Table 1.2 Thermodynamic data on reactions of C₆ hydrocarbons.

Reaction	<i>K</i>	Δ <i>H_R</i> kJ/mol
Cyclohexane → Benzene + 3H ₂	6 × 10 ⁵	221
Methylcyclopentane → Cyclohexane	0.086	-160
n-Hexane → Benzene + 4H ₂	0.78 × 10 ⁵	226
n-Hexane → 2-Methylpentane	1.1	-5.9
n-Hexane → 3-Methylpentane	0.76	-4.6
n-Hexane → 1-Hexene + H ₂	0.037	130

The dehydrogenation of cyclohexane and the dehydrocyclisation of n-hexane are endothermic and, from the viewpoint of equilibrium, are favoured by high temperatures and low partial pressures. The formation of alkenes is favoured by similar conditions and, although their overall concentration remains very low under typical reforming conditions, their production is nevertheless of considerable importance as alkenes are intermediates in a number of the reactions that occur. This will be discussed in more detail in the following section.

Isomerisation reactions are pressure independent and the equilibria are much less temperature sensitive since the heats of reaction are relatively small. The equilibrium

The dehydrogenation of cyclohexanes is the most readily occurring of these reactions. Isomerisation reactions also occur readily, but at a slower rate than that of cyclohexane dehydrogenation. The limiting reactions in most catalytic reforming operations are hydrocracking and dehydrocyclisation, which generally occur at much slower rates.⁶

Thermodynamic data for various reactions of C₆ hydrocarbons are listed in Table 1.2.⁷⁸ The equilibrium constant *K* is defined in terms of the partial pressures of the reactants and products expressed in atmospheres at 500°C. For higher molecular weight hydrocarbons the thermodynamic considerations are qualitatively similar.

Table 1.2 Thermodynamic data on reactions of C₆ hydrocarbons.

Reaction	<i>K</i>	Δ <i>H_R</i> kJ/mol
Cyclohexane → Benzene + 3H ₂	6 x 10 ⁵	221
Methylcyclopentane → Cyclohexane	0.086	-160
n-Hexane → Benzene + 4H ₂	0.78 x 10 ⁵	226
n-Hexane → 2-Methylpentane	1.1	-5.9
n-Hexane → 3-Methylpentane	0.76	-4.6
n-Hexane → 1-Hexene + H ₂	0.037	130

The dehydrogenation of cyclohexane and the dehydrocyclisation of n-hexane are endothermic and, from the viewpoint of equilibrium, are favoured by high temperatures and low partial pressures. The formation of alkenes is favoured by similar conditions and, although their overall concentration remains very low under typical reforming conditions, their production is nevertheless of considerable importance as alkenes are intermediates in a number of the reactions that occur. This will be discussed in more detail in the following section.

Isomerisation reactions are pressure independent and the equilibria are much less temperature sensitive since the heats of reaction are relatively small. The equilibrium

between methylcyclopentane and cyclohexane favours the former, indicating that the five membered ring is more stable. In the equilibrium between n-hexane and methylpentanes, 2-methylpentane is the favoured isomer as would be predicted by statistical considerations. Also, thermodynamic calculations predict that 30-35% of the total hexane isomers at 500°C should be dimethylbutanes. This is not observed in practice and suggests that a strong kinetic barrier opposes formation of doubly branched isomers.⁹

Hydrogenolysis and hydrocracking reactions, involving rupture of carbon-carbon bonds and subsequent hydrogenation, are exothermic and very favourable from a thermodynamic point of view. In practice these reactions are limited only by kinetic factors.

It is therefore desirable to operate the reforming reaction at high temperatures and low hydrogen partial pressures, to maximise the preferred dehydrogenation and dehydrocyclisation reactions. However, these conditions also favour coke deposition which results in catalyst deactivation. In industrial reforming the conditions actually employed are chosen to balance product requirements with the rate of catalysts deactivation.

1.2 Mechanistic and kinetic considerations

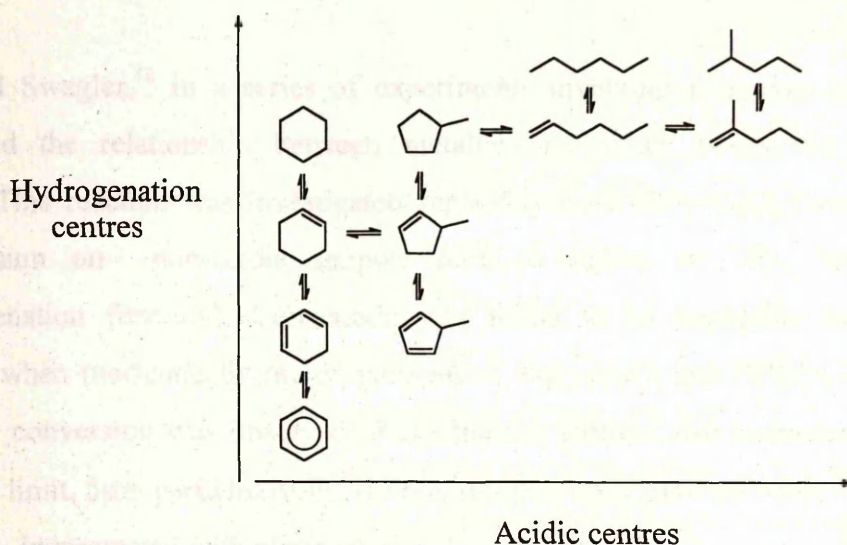
1.2.1 Bifunctional catalysis

Reforming catalysts are bifunctional in nature, i.e. they possess two different types of catalytic activity. The hydrogenation/dehydrogenation activity is associated with a metallic component (e.g. platinum), while the activity for isomerisation and cracking reactions is associated with acid sites on the alumina support.

The original reaction scheme proposed by Mills et. al.¹⁰ to describe the reforming of C₆ hydrocarbons is shown in Figure 1.2. Although incomplete, this scheme gives a good

qualitative description of the overall process. Reactions drawn parallel to the y-axis occur at the hydrogenation/dehydrogenation centres and reactions drawn parallel to the x-axis occur at the acidic centres of the catalyst.

Figure 1.2. Reaction paths in the reforming of C₆ hydrocarbons¹⁰



The reactant n-hexane is first dehydrogenated on the metal to give hexene. The hexene migrates to a neighboring acid centre where it is converted into a secondary carbonium ion by the addition of a proton. The carbonium ion then undergoes skeletal rearrangement and returns a proton to the support. This skeletal rearrangement may produce either isohexene or methylcyclopentane. Isohexene is subsequently hydrogenated by the metal function to produce the product isohexane. Methylcyclopentane may then undergo a similar series of steps resulting in the production of cyclohexene, which is dehydrogenated by the metal yielding benzene.

The above reaction scheme, as for example in the conversion of n-hexane to iso-hexane, involves three separate adsorption/desorption steps with gas phase transfer of the relative intermediates between metallic and acidic components.

Roessner and Roland¹¹ recently put forward a modified view of the classical model to take account of some experimental results which could not be explained by this scheme. These authors considered that a reaction mechanism involving three separate adsorption-desorption steps was unlikely. Their proposal contains a single adsorption step on the acidic component of the catalyst and involves spillover of adsorbed H^+ ions and H^\bullet radicals from the metal to the support, where they react with the adsorbed hydrocarbon.

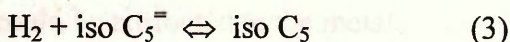
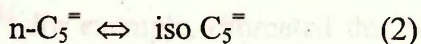
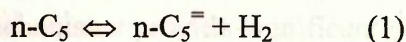
Weisz and Swegler,¹² in a series of experiments involving n-heptane isomerisation, investigated the relationship between metallic and acidic centres in bifunctional catalysts. This reaction was investigated separately over $SiO_2-Al_2O_3$ (acidic-function) and platinum on non-acidic support such as carbon or SiO_2 (hydrogenation /dehydrogenation function). Conversion was found to be negligible in each case. However, when mechanically mixed particles of $SiO_2-Al_2O_3$ and Pt/SiO_2 were studied significant conversion was observed. Reducing the particle size increased conversion and, in the limit, 5 μm particles of Pt/Al_2O_3 and $SiO_2-Al_2O_3$ gave the same conversion as $SiO_2-Al_2O_3$ impregnated with platinum.

These results were explained in terms of gas phase diffusion limitations between the metallic and acidic components. However, under the scheme proposed by Roessner and Roland, these results could also be explained in terms of limitations in the surface migration of adsorbed hydrogen species from metal to acid sites.

1.2.2 Isomerisation reactions

To further substantiate the bifunctional nature of reforming catalysts and to illustrate the reaction kinetics for isomerisation reactions it is useful to refer to a specific example. Sinfelt and coworkers¹³ investigated the isomerisation of n-pentane over platinum on alumina at low conversions. Rate measurements were determined in a flow system at 372°C in the presence of hydrogen at total pressures of between 7.7 and 27.7

atmospheres. The kinetic data was interpreted in terms of a reaction proceeding on the metal and support via the following mechanism.



For a typical reforming catalyst reaction (2) is assumed to be slow and reactions (1) and (3) are assumed to be close to equilibrium. Based on the assumption that the rate of reaction is proportional to the concentration of adsorbed olefin on the acid sites and that equilibrium is established between n-pentene in the gas phase and n-pentene adsorbed on the acid sites then kinetic analysis leads to the following rate equation:

$$r = k [(n-C_5)/(H_2)]^n \quad (1)$$

Where: r = reaction rate

k = rate constant

n = a constant

The rate of reaction is therefore obtained in terms of the n-pentane and hydrogen partial pressures. This expression states that the isomerisation rate is independent of total pressure and dependent only on the ratio of the n-pentane partial pressure to hydrogen partial pressure. The observed reaction kinetics are indeed consistent with this proposal and provide good supporting evidence for the bifunctional mechanism illustrated.

Further support for the above kinetic analysis was presented by Sinfelt and co-workers when they reported that the rate of isomerisation of pent-1-ene on Pt-free alumina (no hydrogenation-dehydrogenation function) was in close agreement with that for n-pentane isomerisation on a bifunctional reforming catalyst.¹³

Although the bifunctional mechanism is the major pathway for the formation of iso-alkanes and aromatics, it is now accepted that these reactions may also occur on the metal function alone. The available data on commercial reforming operations indicates that these mono-functional mechanisms provide significant contributions to the overall process. Weisz and Swegler,¹¹ for example, estimated that between 10 and 15% of n-heptane isomerisation could be attributed to the metal.

Two mechanisms have been proposed to account for skeletal isomerisation of hydrocarbons on platinum. Anderson and Avery¹⁴ proposed a bond-shift mechanism involving an $\alpha\alpha$ -triadsorbed intermediate bonded to two adjoining platinum atoms. For example, in the isomerisation of neopentane:

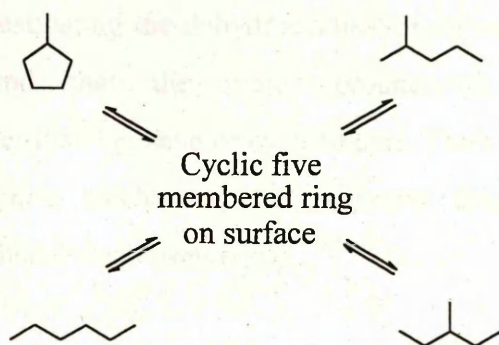


Gault proposed a mechanism which proceeds via formation of a cyclic five-membered ring.^{3,15} This reaction sequence may be represented as three consecutive steps:

- (1) 1,5 dehydrocyclisation to form an adsorbed cyclopentane intermediate.
- (2) Desorption of the ring species can occur allowing for readsorption through different carbon atoms, or alternatively, the intermediate cyclic hydrocarbon may displace the points of attachment to the metal without desorption.
- (3) Ring cleavage followed by desorption of the isomeric product.

Step (2) allows the ring to be opened at a different position from where it was closed and accounts for skeletal isomerisation. Figure 3. illustrates the reaction scheme for C₆ alkane isomerisation on a metal surface.

Figure 1.3. Reaction scheme for the isomerisation of C₆ alkanes on a metal surface³.



The relative importance of bond-shift and cyclic isomerisation reactions has been determined using ¹³C-radiotracer techniques.¹⁶ Supported metal particle size was shown to be critical in determining which mechanism prevailed. For 2-methylpentane-2 ¹³C, isomerisation to give 3-methylpentane proceeded almost exclusively by the cyclic mechanism on well dispersed Pt crystallites (12 Å). On larger Pt crystallites (180 Å) the bond shift mechanism was predominant.

1.2.3 Dehydrocyclisation reactions

In a similar manner to isomerisation, the dehydrocyclisation of alkanes can occur via two mechanisms. A bifunctionally catalysed reaction pathway and a mechanism involving the metal function alone.

In the bifunctionally catalysed reaction scheme (Figure 1.2) the dehydrocyclisation of, for example, n-hexane proceeds via formation of n-hexene on the platinum sites followed by cyclisation of the intermediate alkene to methylcyclopentane on the acidic support. Similarly, conversion to methylcyclopentene followed by isomerisation yields cyclohexene. Cyclohexene may then return to hydrogenation-dehydrogenation sites on the catalyst were, depending on the reaction conditions, it can either be hydrogenated to form cyclohexane or further dehydrogenated to form benzene.

Sinfelt and Roher,¹⁷ investigating the dehydrocyclisation of n-hexane on a 0.3 wt% Pt-alumina catalyst, found that the major product at low conversion was methylcyclopentane rather than benzene or cyclohexane. Their results strongly indicated that the preferred reaction mechanism for n-hexane dehydrocyclisation involved formation of a five membered ring intermediate.

The effect of hydrogen partial pressure on the kinetics of n-heptane dehydrocyclisation on a Pt/Al₂O₃ catalyst was also investigated by Sinfelt et. al.¹⁸ No dehydrocyclisation was found in the absence of hydrogen. In the presence of hydrogen the rate of dehydrocyclisation was found to increase with increasing hydrogen pressure until a given point. Thereafter the rate decreased as the hydrogen pressure further increased. The change in the nature of the hydrogen pressure dependence was interpreted as follows. At low pressures, the metal sites became covered with carbonaceous residues resulting in the reaction rate being limited by the dehydrogenation activity of the catalyst. Increasing the hydrogen pressure resulted in beneficial removal of such surface residues, freeing platinum sites and increasing the overall rate of dehydrocyclisation. Above a certain point however, the rate did not continue to increase. The formation of alkenes was no longer the rate controlling step and the overall reaction became limited by the cyclisation of alkenes on the acidic centres of the catalyst. Any further increase in hydrogen pressure only served to attenuate the concentration of alkene intermediate at equilibrium and hence decreased the rate of dehydrocyclisation.

In addition to the bifunctionally catalysed dehydrocyclisation mechanism there is evidence for a monofunctional pathway involving dehydrogenation and cyclisation on the metal. Sinfelt and co-workers¹⁹ observed that the rate of n-heptane dehydrocyclisation increased significantly when the metal content of a Pt/Al₂O₃ catalyst was increased from 0.1 to 0.6% by weight. The increased rate was not directly proportional to platinum content but the results did indicate that the rate of dehydrocyclisation was not solely determined by an acid site controlled bifunctional mechanism.

Dehydrocyclisation activity on monofunctional catalysts has been reported by Dautzenberg and Patteeuw²⁰ and Davis.²¹ Since bifunctional catalysis on the non-acidic catalysts was assumed to be eliminated, the dehydrocyclisation activity was attributed to platinum metal alone. Davis reported evidence for direct (1,6)-ring closure of straight chain alkanes. Similarly, the aromatic products from dehydrocyclisation of C₈ and C₉ alkanes, catalysed at atmospheric pressure and 482°C, were those predicted for C₆ cyclisation.²² In contrast, Gault and co-workers have postulated a 5-membered ring enlargement over non-acidic platinum catalysts.¹⁵

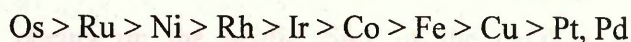
1.2.4 Hydrogenolysis reactions

Hydrogenolysis involves only the metal component of the catalyst and leads to the formation of methane along with smaller amounts of ethane. Hydrocarbon hydrogenolysis reactions on metal catalysts have been extensively studied and particular attention is drawn to a review by Sinfelt.²³

The mechanism of hydrogenolysis is reasonably well established and involves chemisorption of adjacent carbon atoms on adjacent metal sites. Hydrocarbon adsorption on the metal surface involves rupture of carbon-hydrogen bonds. The hydrogen-deficient surface species, multiply bonded to the metal, then undergoes carbon-carbon bond

scission followed by rehydrogenation of the intermediates, producing methane or ethane and an alkane from the second fragment.

It has been demonstrated that the order of activities of metals for ethane hydrogenolysis decreases in the order:²³



Similar trends have also been observed using different hydrocarbons.²⁴ Despite attempts to relate hydrogenolysis activity to percentage d-character, it is clear that this criterion alone does not adequately describe the catalytic activity of transition metals for this reaction. The low hydrogenolysis activity of platinum combined with its established dehydrogenation activity makes it the preferred choice of metallic species in reforming catalysts.

With regards to platinum, it is generally accepted that hydrogenolysis is a demanding structure-sensitive reaction, e.g. experimental evidence shows that large ensembles of atoms are required.^{25,26} Information about the size of metal-atom ensembles required to catalyse the hydrogenolysis reaction has been inferred from alloying platinum with inactive atoms such as gold, tin and lead. Very dilute Pt-Au alloys have been prepared in which the metal surface is almost pure gold.^{27,28} It was observed that under such conditions the isomerisation reaction alone was catalysed, suggesting a single atom site for this reaction. Hydrogenolysis reactions were found to require significantly larger ensembles. As will be seen in the following sections this dilution of the active platinum surface into smaller ensembles by alloying with an inactive species is one of the most often quoted explanations to account for the improved properties of bimetallic catalysts.

In addition Blakley and Somorjai²⁹ have proposed that the hydrogenolytic sites on platinum are high index, low coordination sites such as those found at corners, edges, kinks etc. and furthermore that these sites are preferred by the atoms of a second metal

(or sulphur). The hydrogenolysis activity is therefore selectively poisoned by the addition of these species, provided the second metal is not active in its own right.

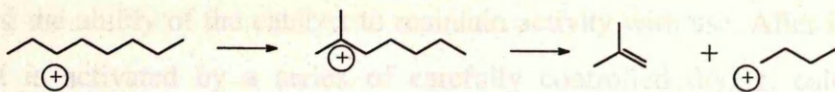
1.2.5 Hydrocracking reactions

The second type of reaction that involves carbon-carbon bond scission is termed hydrocracking and occurs on the acidic sites of the catalyst support. Bifunctional catalysis is involved in the mechanism and alkenes are regarded as key intermediates. In this sense hydrocracking is similar to isomerisation except that the alkene undergoes a fragmentation reaction rather than a skeletal rearrangement. The hydrocracking mechanism is understood to require the formation of a carbonium ion as the first step in the reaction.³⁰ This is facilitated by the formation of alkenes on the metal surface of the catalyst. Such alkenes readily react with a proton from the acidic support to produce a carbonium ion. The next step in the process is the decomposition of the carbonium ion by beta-scission:



This cracking produces an α -alkene and a new hydrogen-deficient species. The new carbonium ion is converted to a more stable secondary configuration by a simple proton shift. The secondary carbonium ion undergoes further cleavage at the beta position and cracking may then proceed until a carbonium ion which cannot yield fragments of three or more atoms is produced.

A characteristic feature of catalytic cracking is the formation of large amounts of iso-alkanes. This is readily explained by a rearrangement of a secondary ion prior to cracking:



Saturated alkanes predominate among the cracked products because the alkenes formed are hydrogenated on the metal component of the catalyst.

1.3 Reforming catalysts

1.3.1 Early reforming catalysts

As already stated reforming catalysts are bifunctional in nature. They possess both acidic and metallic functions, each contributing to the overall reforming process.

The first commercial catalytic naphtha reforming process, introduced in the 1940's, employed molybdenum or chromium oxide-alumina catalysts. The supported oxides in these systems provided both the hydrogenation-dehydrogenation and isomerisation functions.³¹ However, due to their rapid deactivation and costly regeneration, these catalysts were eventually replaced, in the early 1950's, by an alumina supported platinum catalyst. This new catalyst, as well as having improved activity maintenance, also showed improved selectivity to the desired reaction products compared to that of the supported oxide based catalysts.

Monometallic platinum-alumina catalysts are usually prepared by impregnation of alumina with aqueous solutions of hydrochloric and chloroplatinic (H_2PtCl_6) acids. The quantities involved are chosen to give a catalyst with the desired metal loading, typically between 0.2 and 1 % platinum by weight. The loading of platinum used is a fine balance between the cost of the metal, the intrinsic hydrogenation-dehydrogenation activity

required and the ability of the catalyst to maintain activity with use. After impregnation the catalyst is activated by a series of carefully controlled drying, calcination and reduction steps. Very highly dispersed catalysts are obtained using these impregnation and activation procedures, usually with $Pt_{\text{surface}}/Pt_{\text{bulk}}$ ratios close to unity as determined by chemisorption of H_2 , O_2 or CO .

1.3.2 The alumina support

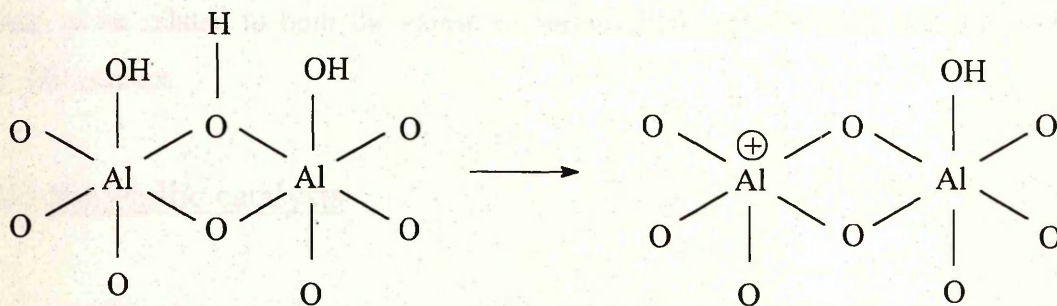
Acid catalysed reforming reactions are associated with sites on the surface of the alumina support. The use of aluminas as supports is widespread and their preparation and properties have been extensively investigated.^{32,33,34} Aluminas of high surface area ($100\text{-}600\text{ m}^2/\text{g}$) are usually prepared by the thermal decomposition of crystallised aluminium hydroxides or by the precipitation of colloidal gels. The latter process is often favoured since it yields more control over the surface area and porosity of the aluminas produced. The properties of aluminas are dependent upon choice of gelation conditions.³⁵

Aluminas exist in several allotropic forms and again their exact structure is related to the method of preparation.³ The favoured materials for reforming catalysts are η - and γ -alumina. The crystallographic structure of both materials is a defect lattice of the spinel type. The η and γ -alumina allotropes are distinguished by the distribution of the cations in tetrahedral and octahedral sites created by the cubic close packed oxygen.³⁶ Due to the economic simplicity of its manufacture and high thermal stability the most widely used form is γ -alumina.⁴

Uncalcined alumina surfaces are terminated by a near monolayer coverage of hydroxyl groups, the presence of which is well established and has been demonstrated by deuterium exchange and infra-red spectroscopy studies.^{37,38} These hydroxyl groups do not contribute significantly as a source of Brønsted acidity. Parry³⁹ used infra-red

spectroscopy of adsorbed ammonia and pyridine to study the acidity of uncalcined γ - Al_2O_3 . No adsorption bands due to ammonium or pyridium ions, anticipated if protonic acid sites were present, were observed.

On calcination however, a variety of surface groups are formed. The most significant change which occurs is the removal of most hydroxyl groups. Pevi reported that about 67% of the surface hydroxyl content was removed by heating γ -alumina at 500°C ; this value increased to 90% at 670°C .³⁸ The removal of hydroxyl groups from the surface involves a condensation reaction between two neighbouring groups and leads to the elimination of water:



The process leaves an oxide ion in the outermost surface layer and an exposed, incompletely coordinated aluminium ion in the layer below. This exposed cation is electron deficient and behaves as a Lewis acid site.

Activated aluminas are therefore weakly acidic and are capable of catalysing skeletal isomerisation reactions typical of carbonium ion chemistry. Pines and Haag,⁴⁰ using various indicator tests, confirmed that the source of acidity in γ - Al_2O_3 consisted of Lewis rather than Brønsted acid sites.

The acidity of hydroxyl groups on the surface of γ - Al_2O_3 can be markedly enhanced by deliberately incorporating halogens such as chlorine^{41,42,43} or fluorine^{44,45} onto the

alumina surface. The incorporation of chlorine, for example, will partially convert a fully hydrated surface to one consisting of Cl^- and OH^- groups (by treating with HCl). The close proximity of highly electronegative chloride species draws electron density away from the O-H bond, thereby increasing the Brønsted acidity of these groups.⁴⁶ It would also appear that the acidity of a group on the alumina surface can be progressively increased as more of the OH^- groups surrounding it are replaced by Cl^- ions.⁴⁷ Halides can also be introduced if a metal halide compound such as H_2PtCl_6 is used in the preparation of the catalyst.

In the case of chlorinated alumina surfaces therefore, both Brønsted and Lewis acid sites may be active in promoting hydrocarbon conversion reactions. The importance of each source of acidity is difficult to quantify. However the relative contribution of each would appear to be related to both the extent of surface hydroxyl coverage and the level of chloride content.

1.3.3 Bimetallic catalysts

Monometallic platinum-alumina catalysts dominated naphtha reforming for many years until Chevron introduced the first bimetallic platinum-rhenium catalyst in 1967.⁴⁸ The new Pt-Re catalyst offered improved activity and stability as compared to its monometallic predecessor. A number of bimetallic systems have since been introduced including Pt-Ir, Pt-Sn and Pt-Ge, all of which have improved properties. Although these bimetallic systems have been in use for many years there is still considerable debate about how the second metal brings about the improvement in catalytic properties.

The literature regarding each of these four systems will now be reviewed, with particular emphasis on the often conflicting results that have been reported.

1.3.3A Platinum-Rhenium catalysts

The main focus of attention in Pt-Re/Al₂O₃ catalysts has been on the oxidation state of rhenium and whether or not rhenium is alloyed with platinum.

Johnson and LeRoy⁴⁹ and Johnson⁵⁰ used infra-red spectroscopy (IR) and X-ray diffraction (XRD) to study a series of Pt-Re catalysts prepared by the impregnation of η - and γ -alumina with aqueous solutions of chloroplatinic acid and ammonium perrhenate. They also measured hydrogen consumption during reduction of the catalysts at 482°C. The platinum and rhenium contents ranged from 0.31 to 0.66 wt% and 0.2 to 1.18 wt% respectively and the catalysts were calcined at 482°C. The H₂ consumption studies indicated complete reduction of Pt^{IV} to Pt⁰ and partial reduction of Re^{VII} to Re^{IV} during the reduction process.

The X-Ray diffraction studies, performed after the alumina support had been removed by treatment with HBF₄, revealed no evidence for rhenium metal or platinum-rhenium alloy formation. This lead the authors to conclude that the rhenium was present as a highly dispersed oxide such as ReO₂ supported on the surface of the alumina.

In contrast a study by Webb⁵¹ on rhenium-alumina catalysts calcined in air at 482°C, in which the degree of reduction was monitored by the amount of H₂ consumed, indicated that rhenium was completely reduced to the metal by hydrogen at temperatures of 400-450°C.

Two possible explanations were proposed to account for these different results. The higher concentration of rhenium used by Webb (3.5 wt%) may have resulted in easier reduction of rhenium, since interaction of rhenium oxide with the support is greater at lower concentrations. The second explanation involved the amount of water present on the catalysts during these experiments. The experiments of Johnson and LeRoy were conducted in a static system, with the water produced by the reduction process remaining

in contact with the catalyst, whilst Webb used a system employing recirculation of hydrogen from which water had been removed by means of a nitrogen trap. Subsequent experiments, using chemisorption, electron spin resonance and temperature-programmed reduction, confirmed the results of Webb and showed a change in oxidation state of rhenium from +7 to 0.^{52,53,54}

However, in the study by Yao and Shelef,⁵² who used chemisorption, ESR and TPR to study a series of Re/Al₂O₃ catalysts (1.2-2.6 wt% loading), it was found that a high temperature N₂ or O₂ treatment prior to reduction resulted in the formation of a dispersed two dimensional rhenium oxide phase which was difficult to reduce. The peak maximum in the TPR profile occurred at 550°C. This contrasts with the Re/Al₂O₃ catalysts which were not subjected to the high temperature treatment, in which complete reduction of Re^{VII} to Re⁰ was found to occur at \approx 360°C.

These results suggested that the oxidation state of rhenium in these systems is highly dependent on the methods of preparation and activation. In subsequent studies TPR was used extensively to determine the oxidation state of rhenium and its interaction with platinum.

McNicol⁵⁴ used TPR to study a series of mono and bimetallic catalysts with total metal loadings less than 1 wt%. The catalysts were dried at 120°C and calcined at 525°C. For the monometallic catalysts, Pt/Al₂O₃ reduced in a single peak at 280°C and Re/Al₂O₃ in a single peak at 550°C. The platinum catalyst consumed the equivalent of four and the rhenium the equivalent of seven hydrogen atoms per metal atom thus indicating that complete reduction of both metal oxides to the metallic state had occurred. For the bimetallic catalysts, McNicol concluded that the TPR profile was simply the addition of the corresponding monometallic catalysts, suggesting that no interaction between platinum and rhenium occurred.

However, in the study by Bolivar et. al.,⁵³ who also observed complete reduction of Pt and Re when studying the reduction of Pt-Re/Al₂O₃ catalysts, it was found that the reduction profile of the bimetallic catalyst was not simply the sum of the corresponding monometallic catalysts. It was observed that the presence of platinum on the catalyst strongly catalysed the reduction of rhenium. The authors postulated that hydrogen spillover was responsible for the reduction of rhenium by platinum. The differences in the results of Bolivar et. al. and McNicol were explained in terms of the degree of hydration of the metal oxide.⁵⁴ McNicol calcined the catalyst at 525°C and then dried in nitrogen at 400°C prior to reduction whereas Bolivar et. al. dried their catalyst at 110°C.

Further TPR studies by Isaacs and Petersen⁵⁵ on the effect of drying temperature noted that the maximum reduction temperatures of monometallic Pt/Al₂O₃ and Re/Al₂O₃ were strongly dependent upon the calcination temperature, and only weakly dependent on the drying temperature. In general Pt/Al₂O₃ and Re/Al₂O₃ calcined at 500-550°C reduced with TPR peaks at approximately 275 and 600°C respectively. However, after calcination at 300°C or less the TPR peaks for Pt/Al₂O₃ and Re/Al₂O₃ fell to about 150 and 350°C respectively. This drop suggested that a higher calcination temperature enhanced the interaction between the metal oxide and the support, as found by Yao and Shelef.⁵² For a precalcined bimetallic Pt-Re/Al₂O₃ catalysts these authors found that, in contrast to the monometallic catalysts, the drying temperature had a marked effect on the TPR profile (however the effect of varying the calcination temperature was not investigated). Both the number and position of peaks were highly dependent on the drying temperature. For Pt-Re catalysts dried at 100 or 200°C the TPR profile consisted of a single peak with a maximum temperature similar to that of a monometallic Pt/Al₂O₃ catalyst. The size of the peak corresponded to simultaneous reduction of both Pt and Re. Similar observation were made by Bolivar⁵³ and Wagstaff and Prins.⁵⁶ At higher drying temperatures (500°C) two TPR peaks were found, one at a temperature characteristic of monometallic Pt/Al₂O₃ and one at a temperature characteristic of monometallic Re/Al₂O₃, similar to the observations made by McNicol and Wagstaff and Prins.

Three different proposals were made to explain the contrasting TPR profiles obtained for Pt-Re/Al₂O₃ catalysts dried at different temperatures:

- (1) The degree of hydration influenced the ease of reduction of the metal oxide.⁵⁴
- (2) The degree of hydration influenced the rate of hydrogen spillover.^{55,59}
- (3) The degree of hydration influenced the mobility of Re₂O₇.^{55,56,60}

Isaacs and Petersen⁵⁵ dismissed the first proposal after observing that the degree of hydration did not significantly affect the reduction of either Pt/Al₂O₃ or Re/Al₂O₃. The oxidation temperature in the calcination step and not the drying temperature was the important factor in determining the temperature of reduction of monometallic catalysts.

The second explanation for the two forms of TPR profile observed was based upon activated hydrogen spillover. Atomic hydrogen, produced by dissociation of molecular hydrogen on reduced platinum sites, migrates by way of the alumina support to the rhenium precursor. As water is known to be a necessary co-catalyst for hydrogen spillover,⁵⁷ the difference in the reducibility of rhenium with drying temperature was due to variations in the water content of the support. However, calculations based on kinetic data, obtained by Kramer and Andre,⁵⁸ implied that insufficient active hydrogen could be generated under these conditions.

More recently, Mievile⁵⁹ proposed a mechanism which required only sufficient active hydrogen to reduce a small portion of the rhenium oxide. It was suggested by the author that the rhenium nucleus thus created subsequently catalysed the reduction of the remaining oxide. This mechanism assumes that reduction of rhenium and platinum oxide precursors occur at separate sites on the alumina surface.

The catalytic reduction of rhenium was rationalised by Isaacs and Petersen,⁵⁵ Wagsaff and Prins,⁵⁶ and Bolivar et. al.⁶⁰ by assuming a high mobility of hydrated Re_2O_7 species. Following migration to hydrogen covered platinum centres, reduction of rhenium and subsequent alloying with platinum took place. For catalysts predried at higher temperatures, dehydroxylation hindered surface migration of Re_2O_7 . It was concluded that the platinum exhibited much less interaction with rhenium under these conditions resulting in at least two peaks in the TPR profile and by implication no formation of bimetallic alloy.

A summary of the TPR results therefore suggests that the degree of reduction of rhenium in these catalysts is dependent on the calcination temperature and the water content of the catalysts. Higher calcination temperatures induce strong interaction between the supported oxides and alumina, which makes reduction of rhenium more difficult. Decreasing the water content hinders the interaction between platinum and rhenium, either by reducing H_2 spillover or decreasing the mobility of Re_2O_x , which again results in higher temperatures being required to reduce the rhenium species present completely to Re^0 .

X-ray photoelectron spectroscopy (XPS) has also been used to study the valence state of rhenium and its interaction with platinum. Biloen et.al.⁶¹ studied a series of Pt-Re/SiO_2 and $\text{Pt-Re/Al}_2\text{O}_3$ catalysts and concluded that rhenium was in the reduced form and alloyed with platinum. However, no preparation or activation details were given. Shpiro et. al.⁶² studied a series of silica and alumina supported monometallic Re catalysts prepared using a variety of precursors (3.4-4.8 wt% Re, dried at 120°C prior to reduction). Alumina supported Re was found to be much more difficult to reduce. This was ascribed to a stronger interaction between ReO_2 and the alumina support than with silica. For an alumina catalyst reduced at 500°C in flowing hydrogen, it was concluded that all the rhenium was reduced to Re^0 . However, the XPS spectrum differed from that of bulk Re^0 . This observation was explained in terms of an interaction between Re^0 and the support resulting in electron density transfer from Re^0 to $\gamma\text{-Al}_2\text{O}_3$, i.e. $\text{Re}^{\delta+}$.

EXAFS (Extended X-ray Absorption Fine Structure) has also been used to study these systems. Short et. al.⁶³ studied Pt-Re/Al₂O₃ catalysts, with metal loadings typical of commercial catalysts, after reduction (no calcination step) at 485°C. They found that rhenium was present in the +4 oxidation state and highly dispersed on the surface of alumina.

However, Meitzner et. al.⁶⁴ also used EXAFS to study Pt-Re/Al₂O₃ and Pd-Re/Al₂O₃ catalysts with similar metal loadings to those used by Short et. al. and concluded that in the Pt-Re/Al₂O₃ catalyst rhenium was completely reduced to Re⁰ and alloyed with platinum after calcination in air at 500°C and reduction in H₂ also at 500°C. This platinum containing catalyst was studied in a hydrogen atmosphere (as were those studied by Short. et. al.). In the case of the palladium containing catalysts it was necessary to perform the EXAFS measurements in a helium atmosphere to preclude the formation of a palladium hydride phase. In this case it was found that a substantial fraction of the rhenium present was coordinated to oxygen, possibly as ReO₂. It was suggested by the authors that this interaction of rhenium with oxygen had occurred after switching from hydrogen to helium, to facilitate a high temperature helium purge prior to the EXAFS experiments. It was concluded that, in the absence of hydrogen, some rhenium reacted with oxygen from the alumina lattice. There was still significant coordination of rhenium with palladium in bimetallic clusters however.

Kelley et. al.⁶⁵ performed studies incorporating scanning transmission electron microscopy (STEM), energy dispersive X-ray analysis (EDX) and ion scattering spectroscopy (ISS). Under the conditions used by these authors, rhenium was found to be widely dispersed over the surface of alumina and not significantly alloyed with platinum.

Infra-red spectroscopy experiments on adsorbed probe molecules performed by Peri⁶⁶ could also find no evidence for the formation of an alloy phase or bimetallic cluster. It was concluded that the catalysts studied (prepared and activated under typical reforming

conditions) contained both Re^0 and Re^{4+} species. However these Pt-Re catalysts exhibited spectra similar to the combined spectra of monometallic Pt/ Al_2O_3 and Re/ Al_2O_3 catalysts, suggesting that no alloy formation had occurred.

H_2/O_2 titrations have also been used extensively to provide information about Pt-Re interactions in these systems.^{60,67,68} The bimetallic Pt-Re supported catalysts studied showed a decrease in hydrogen chemisorption and an increase in titratable oxygen compared with the monometallic platinum catalyst. This led the authors to conclude that alloy formation had occurred. In a further H_2/O_2 titration study⁶⁹ it was concluded that the pretreatment conditions, which affect the ease of reduction of rhenium, also had a major influence on the degree of alloy formation between reduced platinum and reduced rhenium, i.e. whether Pt^0 and Re^0 were in intimate contact or separated on the support.

It is clear that the extent to which rhenium is reduced, and also the degree of alloy formation between any reduced rhenium and platinum, is highly sensitive to the preparation and activation procedures involved. To investigate these systems further, a number of studies have been performed using catalytic probes (including structure sensitive and insensitive reactions) to determine the role played by rhenium in these systems.

Jossens and Petersen,⁷⁰ investigating the effect of Re addition to platinum catalysts on a number of reactions related to reforming, found that the rates for structure sensitive reactions decreased whilst those of the insensitive reactions were unaffected. This was interpreted in terms of an interaction between platinum and rhenium, possibly involving bimetallic cluster or alloy formation.

Betizeau et. al.⁷¹ found that the catalytic properties of a bimetallic Pt-Re/ Al_2O_3 catalyst, the characterisation of which had found evidence for complete reduction of both Pt and Re,⁵³ differed from the predicted additive behaviour of pure platinum and pure rhenium.

The authors explained this observation by suggesting an electronic modification of platinum and rhenium brought about by alloy formation.

Augustine and Sachtler,²⁶ investigating hydrogenolysis of cyclopentane on supported Pt-Re catalysts, found that the rate of reaction was much higher over the bimetallic catalysts than either monometallic Pt or Re. This led the authors to conclude that alloy formation had occurred.

Biloen et. al.⁶¹ and Parera and Beltramini⁷² also found that addition of rhenium to a Pt/Al₂O₃ catalyst increased the rate of hydrogenolysis in the reaction on n-hexane. This was explained by alloying of Pt with metallic rhenium. Parera and Beltramini also found that addition of Re improved the resistance to deactivation of the catalyst.

Bond and Cunningham⁷³, studying the hydrogenolysis of various alkanes over Pt and Pt-Re catalysts also found that the hydrogenolysis activity was increased by the addition of rhenium and this was explained in terms of alloy formation. Similar conclusions were made by Biloen et. al.⁶¹ and Parera and Beltramini⁷² studying the reactions of n-heptane over mono and bimetallic Pt-Re catalysts

In contrast to the above evidence for the formation of Pt-Re alloys, Bertolacini and Pellet⁷⁴ provided evidence against alloy formation in working catalysts. A mixed bed of monometallic platinum and rhenium on separate pellets was observed to perform similarly to co-supported platinum and rhenium. Moreover, post-analysis of the mechanical mixture established that no metal transfer had taken place. On the basis of these results the authors concluded that alloy formation, if it occurred, was not necessary for the reforming catalyst to benefit from rhenium addition.

Due to the high hydrogenolysis activity of rhenium and iridium, catalysts containing these metals are presulphided before use. This selectively diminishes the initial high hydrogenolysis activity associated with Pt-Re/Al₂O₃ catalysts. In addition, it is known

that coke formation on the metal is reduced by adding sulphur, thereby improving yield stability.^{75,76} Sulphur is therefore a selective poison which, when used in a controlled manner, improves the catalytic properties of the metal. Several different sulphur compounds may be used to treat the catalysts, e.g. thiophene, H_2S etc. In all cases the catalysts undergo a final high temperature reduction step in a hydrogen atmosphere. Under these conditions some of the deposited sulphur is removed as hydrogen sulphide while some is retained by the catalysts. It is this strongly bound or "irreversible" sulphur which modifies the catalytic properties.

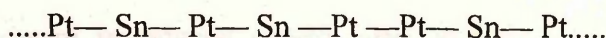
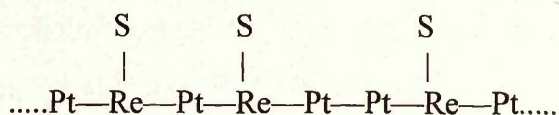
In the case of monometallic $\text{Pt}/\text{Al}_2\text{O}_3$ several possible mechanisms have been proposed to account for the beneficial effects of controlled sulphur addition. One generally accepted consequence is the dilution of the active surface into smaller ensembles.⁷⁷ This geometric effect reduces hydrogenolysis and formation of carbonaceous residues. Both are demanding reactions and require an ensemble of several atoms in each active site.^{78,79}

Parera and co-workers⁸⁰ suggested that modification of the platinum selectivity may be due to the influence of an electronic transfer from platinum to sulphur. The strong chemical bond formed with sulphur changes the chemical bonding of platinum with other adsorbates and hence alters the catalyst selectivity. In a later paper the same authors considered that both electronic and geometric effects acted together in influencing the selectivity changes.⁸¹

When considering geometric effects it should be noted that alloying platinum with catalytically inactive atoms such as gold, tin, or germanium can have similar effects to that of sulphur.⁸²

In the bimetallic platinum-rhenium catalysts the effect of sulphur addition is similar but more pronounced. Indeed, a number of studies have concluded that the addition of rhenium is only beneficial to the overall reforming properties of the catalyst if it is also treated with sulphur.⁶¹ Rhenium is known to adsorb sulphur more strongly than platinum

and therefore the majority of rhenium and only a portion of the platinum is in the sulphided state in modified Pt-Re/Al₂O₃ catalysts.^{83,84} The undesirable hydrogenolysis activity of rhenium is therefore selectively poisoned by the addition of sulphur. If a Pt-Re alloy is formed during reduction the sulphided rhenium atom may also be considered as an inert diluent, similar to tin for example:



In both cases the size of surface metal ensembles is reduced and certain undesirable reactions are selectively poisoned.⁶¹

A recent study performed in this department by Huang et. al.,⁸⁵ in which TEM/EDX and chemisorption were used to study a series of mono and bimetallic Pt-Re catalysts, found no evidence for alloy formation and concluded that the rhenium was present mainly as highly dispersed ReO₂ which interacted strongly with the alumina support.

It is clear from the above discussion that there is considerable debate about the role played by rhenium in these systems. The uncertainty over the oxidation state(s) of rhenium has been caused, at least in part, by the different preparation and activation procedures employed. With regards to the modification of the catalytic properties of Pt/Al₂O₃ by the addition of rhenium, four main proposals have been suggested:

(1) Electronic modification of Pt by interaction with Re^{IV}

(2) Electronic modification of Pt by alloying with Re⁰

(3) Dilution of Pt surface by Re-S

(4) Reduction in coke formation on the metal due to presence of Re^0

It is possible that under typical reforming conditions a number of these effects are in operation.

1.3.3B Platinum-Tin catalysts

Pt-Sn/ Al_2O_3 catalysts were introduced shortly after Pt-Re/ Al_2O_3 but were not used extensively until recently. The renewed interest in these catalysts has come about due to improvements in the catalyst regeneration processes used in reforming operations.

The main advantage of Pt-Sn catalysts are that they allow use at lower pressures and higher temperatures (i.e. more severe operating conditions) to maximise yields of aromatics without inducing corresponding increases in hydrogenolysis or deactivation by coke formation.^{86,87} Also, their preparation and activation is simpler than for Pt-Re and Pt-Ir as no sulphur treatment is required prior to use.

Extensive investigations have been performed by many workers in an attempt to determine the nature of the beneficial effects of tin⁸⁸⁻⁹⁷ Despite these numerous studies, as with Pt-Re, several points of contention still exist. These include the oxidation state of tin, the interaction of tin with platinum and the support and the role played by alloy formation.

TPR has been used in a number of studies to determine the oxidation state of tin in these systems under typical reforming conditions. Burch⁸⁸ found that the average valence state of tin in bimetallic catalysts was Sn^{II} , present as an oxide species stabilised by the γ -

alumina support. Using reduction and reoxidation cycles in a static system and measuring the consumption of H_2 or O_2 , Burch concluded that all the tin was reduced to Sn^{II} and that no Sn^0 was formed. Similar results were obtained by Sexton et. al.⁹⁸ and Muller et. al.⁹⁴

Duatzenberg et al.,⁸⁹ again using TPR and static H_2/O_2 consumption experiments, concluded that 0.6 ± 0.2 wt% Sn was chemically complexed with the alumina support in such a way that it could not be reduced to the metallic state. Any additional tin present above these loadings was found to be completely reduced to Sn^0 .

Studies by Lieske and Völter⁹⁰ concluded that only a minor fraction of tin was reduced to Sn^0 and alloyed with platinum. The majority of tin was again found to be present as Sn^{II} which was strongly stabilised by the alumina support. These authors also found that the degree of alloy formation increased with platinum and tin loading. Similar results were obtained by Bariås et.al.⁹⁹

Chemisorption studies have also been performed in an attempt to determine the interaction between platinum and tin in these systems. Völter et. al.,⁹⁰ Palazov et. al.⁹² and Lieske and Völter⁹⁶ all found that addition of tin to platinum decreased the amount of hydrogen chemisorbed by the catalyst. This was taken as evidence for alloy formation between platinum and tin. Palazov et. al. concluded that this was consistent with alloy formation causing a reduction in the number of surface Pt atoms available for chemisorption (metallic tin does not chemisorb H_2) whilst Völter et. al. concluded that the effect was more likely to be due to electronic modification of platinum when alloyed with tin.

In contrast to these studies Burch,⁸⁸ Muller⁹⁴ and Bariås et. al.⁹⁹ observed an increase in hydrogen uptake with increasing tin content. Balakrishnan and Schwank¹⁰⁰ found an initial increase in hydrogen uptake upon addition of small quantities of tin ($Sn/Pt < 0.5$), but the amount of hydrogen chemisorbed tended to decrease with further additions of tin. These increased hydrogen uptakes were attributed to an increase in platinum dispersion

by Burch, Balakrishnan and Schwank, and Bariás et. al. Muller proposed that with tin addition hydrogen is able to migrate by a spillover mechanism onto Sn^{II} sites.

XPS has also been used in a number of studies to determine the chemical state of tin. Sexton et. al.⁹⁸ concluded from their XPS experiments that tin was not reduced further than Sn^{II} . Similar results were obtained by Balakrishnan and Schwank¹⁰⁰ for alumina supported Pt-Sn catalysts.

Adkins and Davis,¹⁰¹ in an early paper employing XPS, again concluded that no metallic tin was present. However, the validity of these early studies is questionable since Davis et. al.¹⁰² later reported that the early work from their laboratories had been biased by use of oxygen-containing pump oils in the XPS system. A subsequent paper by Li et. al.¹⁰³ found evidence for metallic tin. The proportion of tin reduced to Sn^0 was found to be dependent on the method of preparation and the loading of tin used.

Similar results were obtained in a recent study by Merlen et. al.¹⁰⁴ who proposed two models to account for the effect of tin in these systems. The models are based on the degree of dispersion in these catalysts. For a highly dispersed catalyst it was concluded that a $\text{Pt}/\text{SnO}_x/\text{Al}_2\text{O}_3$ system (with Sn^{II} and Sn^{IV}) was obtained in which platinum had a strong interaction with tin oxide which subsequently induced a modification of the platinum particle structure. For a catalyst with lower dispersion, (larger particles) it was concluded that PtSn alloys were formed, which induced electronic modification of platinum.

X-ray and electron diffraction studies^{105,106} have been carried out in an attempt to characterise the alloy phases formed in these systems. Detection of alloy phases using XRD has been severely hampered by the highly dispersed nature of these systems.

Srinivasan et. al.¹⁰⁴ used XRD to study a series of mono and bimetallic alumina catalysts prepared using PtCl_2 and a Pt-Sn complex $[(\text{C}_2\text{H}_5)_4\text{N}]_2\text{Pt}_3\text{Sn}_8\text{Cl}_{20}$ respectively. For high

metal loadings (5 wt%), both Pt and PtSn phases were found (but no Pt_3Sn , PtSn_2 or PtSn_4) in the bimetallic system. For lower loadings (0.6 wt% Pt), only the PtSn phase was observed. The tin present in excess of that required to form the 1:1 alloy was present in an X-ray “amorphous” form and therefore could not be characterised.

A later study by the same group¹⁰⁶ employed XRD, TEM, electron microdiffraction and EDX to study two Pt-Sn catalysts prepared by more conventional means. One catalyst was prepared by coprecipitating tin and alumina and then impregnating the calcined material with chloroplatinic acid to give a Pt:Sn atomic ratio of 1:3. The second catalyst was prepared by coimpregnating γ -alumina with the relevant quantities of $\text{SnCl}_4 \cdot 5\text{H}_2\text{O}$ and H_2PtCl_6 to also give a Pt:Sn ratio of 1:3. It was found that for the coimpregnated catalyst the major phase was PtSn (1:1, hcp) alloy. For the coprecipitated catalysts, although alloy particles were detected, the major phase was pure platinum, with the majority of tin being in a state which could not be detected by the EDX system.

Mössbauer spectroscopy has also been used extensively to characterise these systems. Bacaud and Bussière¹⁰⁷ found evidence for the presence of significant quantities of Sn^{IV} and Sn^{II} species and Sn^0 alloyed with platinum. They also found that a significant quantity of the platinum was probably not alloyed, although its adsorption/desorption characteristics were modified by the presence of tin.

Li et. al.¹⁰⁸ used Mössbauer spectroscopy to study a series of alumina and silica supported Pt-Sn catalysts. For the alumina system they reached similar conclusions to those of Bacaud and Bussière. For the silica catalysts it was found that more of the tin had been reduced to Sn^0 , again suggesting a strong interaction between ionic tin and the alumina support. They also found that the fraction of platinum alloyed with tin increased with tin loading. Similar results were obtained by Hobson et. al.¹⁰⁹ who, when studying a catalyst with 0.34 wt% Sn loading, found that 70-80% of the tin interacted strongly with the alumina and did not alloy with platinum.

EXAFS and EXANES have also been used to study the state of tin in these catalysts. Meitzer et. al.¹¹⁰ concluded that, for an alumina supported catalyst, the tin was present mainly as Sn^{II} on the alumina surface. They also found that the presence of tin increased the platinum dispersion, although no evidence for PtSn alloys were found. In the case of a silica supported catalysts however, treatment under the same conditions resulted in most of the tin being reduced to Sn^0 and alloyed with platinum

Caballero et. al.¹¹¹ used EXAFS to study Pt-Sn/ Al_2O_3 catalysts prepared using organometallic precursors. These authors found evidence for both Sn^{II} and Sn^0 and concluded that their results could be rationalised by assuming formation of highly dispersed bimetallic particles which were stabilised on the alumina surface through Pt-O- Sn^{2+} bonds. These authors suggested that the differences between their results and those of Meitzner et. al.¹¹⁰ were due to the different starting materials and the preparation procedures (impregnation versus precipitation) employed in these studies.

It is evident therefore that the degree to which tin is reduced and alloyed with platinum is (as with Pt-Re) sensitive to a number of factors such as: support, starting materials, activation procedures, metal loading etc. The general consensus appears to be that for an alumina supported Pt-Sn catalysts, used under typical reforming conditions, both tin oxide and tin metal species will be present, although the proportion of each may vary widely depending on the factors mentioned above. To investigate what influence these tin species have on the corresponding catalytic properties a number of studies have been performed employing specific test reactions as probes.

Dautzenberg et. al.⁸⁹ studied n-hexane reforming over a series of Pt and Pt-Sn catalysts supported on non-acidic supports (metal function only). These author concluded that the differences in selectivity observed between Pt and Pt-Sn were due to alloy formation and subsequent dilution of the platinum surface (ensemble effect).

Coq and Figueras¹¹² studied the conversion of methylcyclopentane over acidic Pt/Al₂O₃ catalysts to which varying amounts of tin had been added (0.06 - 4.00 wt% Sn). The effect of tin addition on the hydrogenolysis reaction was interpreted by the authors as being due to an ensemble effect, with the activity decreasing as more tin was added. It was also found that sulphur and coke had similar effects on the hydrogenolysis activity. The activity for aromatisation to benzene however, which passed through a maximum and then decreased as more tin was added, could not be reproduced by the addition of sulphur or gradual coking and was interpreted in terms of an electronic modification of platinum by alloying with tin. This modification was said to involve electron donation from tin to platinum which subsequently weakened the Pt-C bond. These authors also found that the bimetallic catalyst was less susceptible to poisoning than monometallic platinum.

Burch and Garla⁹³ studied a number of reaction over a Pt-Sn catalysts which they had characterised previously⁸⁸ and in which it had been found that the majority of tin had been present as Sn^{II}. These authors concluded that tin had a number of effects on the catalytic properties. As well as improving the resistance of the catalysts to deactivation and modifying the selectivity of the metal, they also found that Sn^{II} species poisoned the highly acidic sites of the support, resulting in a decrease in hydrocracking reactions and a corresponding increase in isomerisation.

The modification of platinum in these systems was interpreted in terms of an electronic effect due to interaction of platinum with Sn^{II} ions. However, the authors could not rule out that the small amounts of Sn⁰ present were not at least partially responsible for the observed changes in catalytic properties.

The small quantities of Sn⁰ present in their catalysts led the authors to propose a possible geometric effect that is electronic in origin. Their argument was as follows: It is known that the formation of a strong metal-carbon bond is essential for C-C bond breaking to occur. The strength of this metal-carbon bond will depend on the electronic properties of

the surface atom involved, and in an alloy the properties of a surface atom must be affected to some extent by its ligand environment. If you assume that a metal, such as platinum, can only form a sufficiently strong bond to carbon when the Pt atom is surrounded exclusively by other Pt atoms, and that at least three adjacent platinum atoms are required for hydrogenolysis^{27,28} (certainly it is known that this reaction cannot occur on isolated atoms) then it becomes apparent that a single tin atom next to any one of the three platinum atoms is enough to poison the entire site. Therefore a very small concentration of Sn^0 could have a dramatic effect on the overall catalytic properties.

Schwank and co-workers, in a number of studies,^{95,100,113-115} concluded that the electronic interaction between ionic tin and platinum is the main contributor to the beneficial effects of the bimetallic catalyst, since tin was always located in close proximity to platinum particles and the few Pt-Sn alloy particles observed were not thought to play a significant role in controlling the catalytic behaviour.

Bari s et. al.⁹⁹ studied propane dehydrogenation over a series of alumina and silica supported Pt-Sn catalysts. For the alumina supported catalyst they concluded that the main effect of tin was to modify the support properties, particularly the ability to transport chemisorbed species from the Pt surface. Tin also poisoned the acidic sites on the Al_2O_3 (as reported by Burch and Garla⁹³), resulting in a reduction in cracking.

Srinivasan and Davis and coworkers studied n-octane dehydrocyclisation at atmospheric¹¹⁶ and elevated¹¹⁷ pressures. They found that the properties of Pt-Sn catalysts were highly dependent on the Pt:Sn ratio and the method of preparation (coimpregnation or coprecipitation). They concluded that tin had a number of effects such as:

- (1) Enhancing Pt dispersion at low loadings.

- (2) Forming a Pt-Sn = 1:1 alloy with a higher dehydrocyclisation activity than Pt.

(3) Modifying the distribution of aromatic products, and

(4) Poisoning acid sites on the support.

Beltamini and Trimm¹¹⁸ studied reforming of n-heptane over a series of bimetallic catalysts including Pt-Sn. They found that although less coke was formed on bimetallic catalysts, the main benefit of the bimetallic system originated from control of where the coke was deposited on the catalyst. This change in properties was interpreted as being due to either electronic modification of platinum by tin or dilution of the platinum surface into smaller ensembles by tin.

Coq et. al.¹¹⁹ studied the reactions of n-hexane, methylcyclopentane and 2,2,3,3-tetramethylbutane on Pt-Sn/Al₂O₃ catalysts prepared using organometallic precursors. These authors found that when small concentrations of tin were added to a Pt/Al₂O₃ catalyst, the reduced tin preferentially occupied sites of low coordination in the Pt crystallites (corners, edges etc.) thus selectively poisoning the reactions that occur more readily on these sites (hydrogenolysis etc.). These findings are similar to those of Blakley and Somorjai.²⁹ Further addition of tin resulted in dilution of the platinum surface by tin.

In a previous study performed in this department,¹²⁰ utilizing TEM, EDX, electron microdiffraction and chemisorption studies, it was found that the majority of tin was present as Sn^{II} after reduction, while a minor part was reduced to Sn⁰ and alloyed with platinum. With further oxidation/reduction cycles or use in reforming it was found that a greater proportion of tin was reduced and the degree of alloying subsequently increased. A number of alloy phases were identified including PtSn, Pt₃Sn, Pt₂Sn and Pt rich solid solutions.

It is clear therefore that there is no consensus in the literature about the state of tin and its role in modifying the catalytic properties of these catalysts. It is likely however that both

Sn^{II} and Sn^0 will be present in these systems under the conditions typically employed in industrial reforming.

In those studies that have found evidence for Sn^0 it was always observed that tin alloyed with platinum. This alloying was said to modify the properties of platinum either by an electronic effect^{112,118} or by dilution of the platinum surface^{89,118,119} (ensemble/geometric effect).

In the case of Sn^{II} , which is always found to interact strongly with the support, perhaps as tin-aluminate as proposed by Adkins and Davis,¹⁰¹ a number of effects have been proposed including:

- (1) Modification of support acidity.^{93,99}
- (2) Anchoring of metal particles.¹¹¹
- (3) Modification of electronic properties of Pt by interaction with Sn^{II} .^{93, 95, 100, 113-115, 120}

Many of the debates currently running concerning Pt-Sn catalysts are mirrored in the related Pt-Ge system, as will be seen in the next section.

1.3.3C Platinum-germanium catalysts

Although extensive studies have been performed on Pt-Re, Pt-Sn and Pt-Ir/ Al_2O_3 catalysts, much less attention has been directed towards Pt-Ge catalysts. As will become apparent, this system is similar to Pt-Sn in many respects.

Again TPR has been used to study the oxidation state of Ge in these systems. McNicol,¹²¹ studying a Pt-Ge/ Al_2O_3 catalyst, found that the hydrogen consumption in the

Ge region of his TPR profile ($\approx 600^\circ\text{C}$) was 40% less than that required for total reduction of Ge^{4+} to Ge^0 . Therefore he concluded that some of the germanium remained in an oxidised form in combination with the support (as Ge^{IV}) and that the remainder was reduced to Ge^0 and alloyed with platinum. Support for these conclusions came from hydrogen chemisorption measurements¹²² that showed that the H/Pt ratio for a Pt-Ge catalyst had a value of one if the reduction temperature of the calcined catalyst was 450°C but progressively fell as the reduction temperature was raised into the region where the germanium component was reduced. This suggested that, as Ge^{IV} was reduced to Ge^0 , Ge^0 built up in the platinum surface, diluting it and causing hydrogen chemisorption to fall.

Goldwasser et. al.¹²³ also used TPR to characterise these systems. For a series of Pt-Ge/ Al_2O_3 catalysts precalcined at 400°C , their TPR results were in agreement with those of McNicol. However, XPS experiments could find no evidence for Ge^0 and therefore they interpreted their results in terms of partial reduction of Ge^{IV} to Ge^{II} . For a series of catalysts precalcined at 600°C it was found that no Ge was reduced even at temperatures of 973°C . These authors also performed H_2 chemisorption experiments but did not find a reduction in H_2 uptake with germanium addition. Benzene hydrogenation and n-butane hydrogenolysis experiments were also performed and these led the authors to conclude that the special properties of Pt-Ge catalysts were due to electronic modification of small platinum particles by interaction with Ge^{II} .

Bouwman and Biloen¹²⁴ used XPS to study Pt-Ge/ Al_2O_3 catalysts reduced at a range of temperatures. These authors found that for reduction at 550°C the Ge was present as a mixture Ge^{IV} and Ge^{II} species, while after reduction at 650°C it contained Ge^{II} and Ge^0 . It was also observed that platinum catalysed the reduction of germanium, an conclusion not shared by McNicol.¹²¹

Miguel et. al.^{125,126} in a series of studies, used TPR, chemisorption and test reactions (cyclohexane dehydrogenation and cyclopentane hydrogenolysis) to study these systems.

They concluded that the oxidation state(s) of germanium and subsequent interactions with platinum were dependent on the reduction temperature. At reduction temperatures below 350°C, only Ge^{II} and Ge^{IV} species were present. When used for hydrogenolysis of cyclopentane these catalysts showed a large drop in activity which was interpreted as a geometric effect, i.e. dilution of the platinum surface by Ge^{IV} and Ge^{II} species.

At higher reduction temperatures, e.g. 500°C, it was found that 50% of the germanium was in the zero valent state. In this case both hydrogenation (structure-insensitive) and hydrogenolysis (structure-sensitive) reactions were found to be strongly suppressed. It was concluded that this was due to an electronic effect on alloying platinum with germanium. In agreement with Jenkins,¹²² these authors also found that the H_2 chemisorption capacity of these systems decreased with increasing reduction of Ge. This was interpreted in terms of a decrease in dispersion.

Beltramini and Trimm^{118,127} used TPR and n-heptane reforming to study these systems. They concluded that for a catalyst calcined and reduced at 500°C, 50% of the Ge had been reduced to Ge^0 , the remainder remaining as a germanium oxide species on the support. It was found by these authors that the presence of Ge reduced coke formation on the metal and also improved the selectivity of the catalyst. This was interpreted as being due to a geometric effect induced by alloy formation. It was also found that the presence of Ge oxide increased the hydrocracking activity of these catalysts, due to the acidity of this species. However, Miguel et. al. could find no evidence for this effect.

A recent study in this department by Huang et. al.,^{128,129} employing TEM, EDX, electron microdiffraction and chemisorption experiments, concluded that the majority of germanium was present in an ionic state after reduction at 400°C, whilst a minor part was reduced to Ge^0 and alloyed with platinum. Use in reforming and oxidation/reduction cycles increased the degree of alloying. A number of alloy phases were identified including PtGe, Pt_3Ge_2 , Pt_3Ge and Pt rich solid solutions.

1.3.3D Platinum-Iridium catalysts

The bimetallic Pt-Ir/Al₂O₃ catalyst was first introduced by Exxon¹³⁰ in the late 70's and like Pt-Re offered improved activity and resistance to deactivation as compared to the monometallic catalyst. As with Pt-Re, this catalyst must be treated with sulphur before use to reduce its intrinsically high hydrogenolysis activity.

TPR has been used extensively to study the oxidation state of Ir and the degree of alloy formation in these systems.^{131,135} In contrast to Pt-Re, Pt-Sn and Pt-Ge, where there is considerable debate in the literature about the oxidation state of the second metal under typical reforming conditions, in this case there is general agreement that Ir is completely reduced and alloyed with platinum.

It should be stated that although these studies are in agreement about the final state of the catalyst, there has been debate between Wagstaff and Prins^{131,133} and Fogar and Jaeger¹³² about the interpretation of their TPR profiles and the species that are present after calcination and/or reoxidation following reduction. However, these considerations are of secondary importance. The crucial point being the state of the reduced form of the catalyst and on this point both groups agreed that Ir was completely reduced and alloyed with platinum.

In an early paper on this system Sinfelt and Via¹³⁶ used XRD and H₂ chemisorption to study a series of Pt-Ir silica or alumina supported catalysts. It was found that H/M chemisorption ratios were higher on alumina than silica, indicating a higher dispersion on this support. Unfortunately, XRD studies on alumina were unsuccessful due to interference from the alumina diffraction pattern. However, on the silica supported catalyst the presence of bimetallic particles was confirmed. These alloy particles exhibited diffraction line positions midway between the positions of the corresponding lines for platinum and iridium metals.

This study also illustrated the sensitivity of Pt-Ir catalysts to high temperature oxygen treatments. This is important when considering calcination and coke burn-off/regeneration treatments. It was found that a calcination temperature of 375°C was satisfactory to produce a highly dispersed alloy catalyst. However, a calcination temperature of 500°C resulted in the formation of large IrO₂ crystallites, which on subsequent reduction were converted into large particles of iridium. Catalysts prepared under these conditions would therefore consist of highly dispersed platinum or platinum rich clusters and large iridium particles. It is therefore apparent that any high temperature oxygen treatments performed on these catalysts must be closely controlled to prevent Ir agglomeration.

It should be noted that the catalysts studied by Sinfelt and Via¹³⁶ contained relatively high metal loadings, 5-20 wt% (resulting in relatively large particle sizes), which is not the case for industrial catalysts. To overcome this problem, and also the problems associated with using XRD to study alumina supported catalysts, Garten and Sinfelt¹³⁷ turned to Mössbauer spectroscopy studies employing ⁵⁷Fe as a probe. The catalysts studied consisted of 1.75 wt% each of platinum and iridium to which 0.1 wt% ⁵⁷Fe had been added. The results obtained were interpreted by the authors as being consistent with alloy formation between platinum and iridium. The effect of oxygen treatment was also studied and similar results were obtained regarding Ir agglomeration as those reported in their earlier study.¹³⁶ It was found that a calcination temperature of 375°C was adequate while calcination at temperatures ≥ 450°C resulted in Ir agglomeration.

In an attempt to study even more highly dispersed systems Sinfelt and co-workers¹³⁸ used EXAFS to study a series of catalysts containing 1 wt% each of platinum and iridium supported on silica or alumina. The results of these EXAFS studies provided evidence for bimetallic clusters. Interestingly however, it was found that the data suggested that the bimetallic clusters were not homogeneous, i.e. the catalyst contained platinum rich and iridium rich regions. Two proposals were suggested to account for these findings.

Either the catalyst contained a distribution of metal clusters of varying composition (some platinum rich, some iridium rich), or alternatively the platinum rich and iridium rich regions were contained within individual particles. On the basis of surface energy considerations also presented in this paper the authors favoured the later proposal. For highly dispersed systems the authors went on to propose a two-dimensional "raft like" shape for the metal clusters (rather than spherical) composed of a central iridium rich raft surrounded by a perimeter of platinum atoms.

Rasser et. al.¹³⁹ used Auger electron spectroscopy (AES) to study the surface composition of a series of Ir, Pt and PtIr alloy powders both before and after contact with propane. They also used n-heptane and n-hexane reforming to study the properties of a series of supported catalysts.

The AES studies revealed that even at high bulk iridium concentrations the iridium surface concentration was very low. It was stated that this result may explain why their Pt-Ir catalysts were more platinum like in character. When these powders were contacted with propane, even at low Ir surface concentrations, it was found that the formation of carbonaceous deposits was suppressed, as compared with pure platinum. This agreed with their finding that PtIr supported catalysts were resistant to deactivation by coking. It was concluded that carbon atoms, deposited on platinum, can migrate over a number of platinum sites to the iridium centres in the surface where they are hydrogenated to methane.

It is likely therefore that Pt-Ir/Al₂O₃ is a true "bimetallic" system, with both supported metals completely reduced and in intimate contact with each other, i.e. in the form of bimetallic clusters or alloys particles. To investigate what influence iridium has on the catalytic properties a number of workers have used test reactions using a variety of alkanes. At this point it must be emphasized that Ir has a very high hydrogenolysis activity and therefore a Pt-Ir catalyst, in the "as prepared" form, cannot be used for reforming due to its high selectivity to methane. To overcome this problem Pt-Ir (as with

Pt-Re) are presulphided before use.¹⁴⁰ The sulphur dilutes the metal surface into smaller ensembles which cannot catalyse the hydrogenolysis reaction. This selective poisoning of structure-sensitive reactions is also thought to lower coke deposition on the metal. Although in the case of PtRe sulphur is thought to bind preferentially to Re^{83,84} (due to the strength of the Re-S bond) it is unlikely that a similar effect occurs in PtIr catalysts.

Sinfelt and co-workers¹⁴⁰ used n-heptane and methylcyclopentane reforming (at elevated pressures) to study the properties of these systems along with extended naphtha reforming experiments. The catalysts studied contained 0.3 wt% each of platinum and iridium and was pretreated with H₂S before testing. Platinum and Pt-Re catalysts were prepared and tested in a similar manner for comparison.

It was found that both Pt-Ir and Pt-Re exhibited increased resistance to deactivation as compared with Pt. In the case of platinum-iridium this improved activity maintenance was attributed, at least in part, to a lower rate of formation of carbonaceous residues on the catalyst. The decreased formation of such residues, as compared with Pt alone, was attributed to the increased hydrogenolysis activity resulting from the presence of iridium and was taken as an indication of an interaction between platinum and iridium. It was concluded that hydrogenolysis provides a mechanism for removal of coke residues (or the precursors of coke residues) from the surface.

In the case of platinum-rhenium catalysts, the improved stability relative to platinum could not be rationalised in this manner since the rate of formation of carbonaceous residues was not significantly affected by the presence of rhenium. This point is interesting because metallic rhenium also has a high hydrogenolysis activity. It was suggested that the difference between platinum-rhenium and platinum-iridium was due to the strong retention of sulphur by rhenium (as already mentioned the inhibiting effect of sulphur on hydrogenolysis is well known). The improved activity maintenance of a platinum-rhenium catalyst relative to platinum was achieved despite the fact that the quantity of coke formed was essentially unaffected.

When considering the beneficial effect of the high hydrogenolysis activity of iridium in suppressing formation of carbonaceous residues, it must be remembered the such activity may simultaneously have an adverse effect on product distribution. The authors maintained that by controlling the level of hydrogenolysis it is possible to obtain a satisfactory product distribution while at the same time realise large improvements in activity maintenance over catalysts containing platinum alone.

In comparing the activity of Pt-Ir and Pt-Re catalysts in naphtha reforming it was found that the activity of the Pt-Ir catalyst was generally twice as high as that of Pt-Re, although the yields of methane and ethane were higher. The yields of benzene and toluene were also higher over the Pt-Ir catalyst. Data on the reactions of n-heptane and methylcyclopentane indicated that Pt-Re was more selective for conversion of cycloalkanes to aromatics, while Pt-Ir was more selective for the dehydrocyclisation of alkanes.

Rice and Lu¹⁴¹ studied the reforming of n-heptane over a number of presulphided platinum and platinum-iridium catalysts at different pressures (135kPa and 790kPa). In agreement with Sinfelt's work,¹⁴⁰ these authors found that the Pt-Ir catalyst had a higher activity and was more resistant to deactivation. Again this was explained in terms of the ability of Ir or Pt-Ir to hydrogenate coke precursors more effectively than Pt. It was also found that the behavior of the Pt-Ir catalyst was distinctly different from that of a mechanical mixture of separate Pt and Ir catalysts, which was taken as indirect evidence for alloy formation. It was also found in this study that reforming tests at atmospheric pressure were not good indicators of the relative behaviour under commercial conditions. These authors concluded that there were two possible means by which iridium "promoted" the activity of these catalysts, both of which involved bimetallic clusters.

The first was that the incorporation of Ir into platinum to form bimetallic clusters altered the electronic properties of these clusters, improving their selectivity for favourable

reactions and suppressing coke formation. It was also stated that these alloy clusters would have special geometrical features such as metal-metal bond lengths, although this effect was not considered as important as the electronic effect.

The second possibility put forward was the dilution of the Pt surface into smaller ensembles by Ir in a similar manner to the explanation put forward by Biloen et. al.⁶¹ for the promoting effect of Re (actually Re-S). However, due to the fact that rhenium and iridium differ significantly in chemical behavior, it was considered debatable whether a close similarity in their promotional mechanisms with respect to Pt should be expected.

Huang et. al.¹³⁵ investigated n-hexane reforming over a series of non sulphided Pt, Ir and Pt-Ir catalysts. However, the catalysts were contacted with the reactant mixture at 400°C for 12 hours prior to the actual reforming experiments, which were performed at 500°C. This was done to poison the high hydrogenolysis activity by coking the catalyst (this has a similar effect to addition of sulphur). These authors also found that the bimetallic catalyst was more resistant to coking and again this was attributed to the high hydrogenolysis activity of iridium destroying coke precursors. It was also found that the addition of Pt to an Ir/Al₂O₃ catalyst altered significantly the cracking activity of iridium.

Ponec and Dees¹⁴² investigated the influence of sulphur addition on the reforming of n-hexane over a series of alumina and silica supported catalysts. The total metal content on each catalyst was kept at 5 wt% although the % Ir (or Pt) was varied between 0 and 100% of the total content. The reforming experiments were carried out under various temperatures at atmospheric pressure. In general, their results were in agreement with those already reported. It was stated that addition of sulphur resulted in Ir and PtIr catalysts showing a "Pt like" selectivity (i.e. low hydrogenolysis, high dehydrogenation) and again this was explained in terms of an ensemble effect. However, in this case it was reported that sulphided Ir and Pt-Ir catalysts showed increased yields when compared to sulphided Pt catalysts. It was concluded that this may be due to the higher dehydrogenating activity of Ir.

Pt and Pt-Y catalysts at 500°C it was found that the addition of Y decreased the Bonivardi et. al.¹⁴³ studied the reactions of n-hexane over bimetallic PtIr polycrystalline foils with various surface compositions (as determined by AES) at 720K, $H_2/n\text{-hexane} = 67$ and total pressure of 0.9 MPa. The effects of sulphur addition on these foils was also studied. The findings made by this study are in close agreement with those of Carter et. al.¹⁴⁰ It was also found that a Pt-Ir bimetallic surface with a composition Pt_2Ir showed higher activities for n-hexane isomerisation and cyclisation than pure platinum or iridium. This rate enhancement remained on addition of sulphur. It was suggested that this was caused by iridium speeding up the rate determining adsorption step, i.e. iridium sites can adsorb and dissociate hydrocarbons easily which then diffuse to platinum where they can isomerise. Thus Pt-rich catalysts cannot adsorb and dissociate fast enough and Ir-rich catalysts adsorb molecules too strongly which causes higher hydrogenolysis. At this composition it was considered that the number of Pt-Ir nearest neighbours would be high and the Ir-Ir neighbours low.

In conclusion therefore it is likely that Pt-Ir is a true bimetallic system with alloy/bimetallic clusters of PtIr formed on the support surface. In this case the high hydrogenolysis activity of Ir is generally believed to account for the improved resistance to deactivation, although this activity must be controlled to some degree to maintain adequate product distributions.

1.3.4 Rare earth oxides as promoters in reforming catalysts

A number of studies have been made by Fengyi and co-workers^{144,145,146,147} on the effects of addition of various rare-earth oxides to Pt/Al_2O_3 catalysts.

In a study on the influence of addition of yttrium and ytterbium to Pt-alumina catalysts¹⁴⁴ (0.3 wt% Pt - 0.3 wt% Y or Yb), it was concluded that the addition of the rare-earth increased the dispersion of the active Pt phase. In conversion of methylcyclopentane over

Pt and Pt-Y catalyst at 500°C it was found that the addition of Y decreased the hydrogenolysis selectivity and increased the isomerisation and aromatisation selectivity due to an ensemble effect. In the case of n-hexane reforming at 480°C over Pt and Pt-Yb it was also found that the hydrogenolysis selectivity decreased and the aromatisation selectivity increased (the isomerisation activity remained unchanged). The overall conversions were relatively unaffected in both cases. It was also found that the addition of the rare-earth decreased the influence of sulphur poisoning on these systems.

In a related study on the influence of dysprosium on Pt/Al₂O₃^{145,146} (0.5 wt% Pt and Dy loading varied from 0.05-1.00 wt%) in the hydrogenation of benzene and reforming of n-hexane and cyclopentane it was concluded that an electronic modification of platinum was responsible for the improved catalytic properties observed.¹⁴⁵ In the reforming of n-hexane¹⁴⁶ the addition of dysprosium was found to increase the overall conversion and yield of benzene, whilst decreasing yields of iso-hexanes. The hydrogenolysis and cracking activities were essentially unchanged from those of Pt/Al₂O₃.

In a further study performed by this group¹⁴⁷ a series of Pt-R.E./Al₂O₃ catalysts were prepared (R.E = La, Nd, Tb, Ho, Tm or Y). These catalysts contained 0.3 wt% Pt and 0.3 wt% of the rare-earth element. In general, for the reforming of n-hexanes, it was reported that the presence of a rare-earth decreased hydrogenolysis (although the figure quoted for hydrogenolysis was actually the sum of all species less than C₆) and increased the selectivity to isomerisation and aromatisation.

In an unrelated study Fan et. al.¹⁴⁸ examined the influence of samarium oxide on the properties of a Pt-Sn/Al₂O₃ catalyst. The catalyst studied contained 0.38 wt% Pt, a Sn/Pt atomic ratio of 3 and varying quantities of Sm from Sm/Pt = 3 to Sm/Pt = 6. The catalysts were studied using Mössbauer spectroscopy (¹¹⁹Sn enriched catalysts), H₂ chemisorption and HREM and the corresponding catalytic properties were monitored using n-butane as a test reactant.

It was concluded by these authors that the beneficial effect of tin in Pt-Sn catalysts was due to the presence of Sn^{II} species. During oxidation and reduction cycles it was found that the fraction of tin present as Sn^{II} fell significantly and the quantities of Sn^{IV} and Sn^0 consequently increased. The Sn^0 produced was found to be alloyed with platinum and this caused a significant decrease in catalyst activity. The incorporation of samarium oxide into these catalysts was found to stabilise Sn^{II} and prevent alloy formation, significantly improving the activity maintenance of the catalysts. In direct contrast to the results of Fengyi et. al.,¹⁴⁴⁻¹⁴⁷ it was found that the rare-earth oxide had no effect on the initial reforming properties of these systems. The only influence of samarium was to stabilise tin in the Sn^{II} state.

i.e. no sulphur treatment step is required.

1.4.1 Characterisation of coke deposits

1.4 Catalyst deactivation by carbonaceous residues

A number of techniques have been employed to characterise the coke deposits.

The formation of carbonaceous residues on the surface of reforming catalysts is one of the major causes of deactivation in these catalysts.

XRD, IR and TGA.

The deposition of coke onto these systems not only reduces the catalyst's activity but also modifies the catalyst's selectivity which is manifest in a lowering of reformat octane number and a decrease in hydrogen yield. In order to maintain the same anti-knock qualities in the reformat product, the operating temperature is gradually increased as the catalyst deactivates. The maximum temperature that can be achieved is determined by plant design and product requirements, as high reaction temperatures also favour side reactions such as hydrocracking and hydrogenolysis⁴ (high activation energies).

Plaza et al. demonstrated the influence of temperature on the rate of coke formation.

Commercial catalysts may be operated for periods of 1-2 years and accumulate high levels of carbonaceous deposits, which may be as high as 20% by weight.¹⁴⁹ These carbonaceous deposits are gradually converted into graphitic structures which blocks metal sites and plugs the porous support, rendering the catalyst inactive. At this stage

plant shutdown is required and the catalyst is regenerated using a lengthy and expensive procedure involving carbon burn-off, metal redispersion, chlorine level adjustment and, in the case of Pt-Re and Pt-Ir catalysts, sulphur treatment.

A recent development in reforming technology is the introduction of continuous regeneration reactors. These allow the continuous circulation of catalyst material between the reformer and the regeneration equipment.^{4,150} This process allows the reforming of naphtha under more severe conditions (lower pressures) thereby improving reformat quality. These continuous regeneration procedures have also been partially responsible for the interest in Pt-Sn and Pt-Ge catalysts due to their ease of regeneration, i.e. no sulphur treatment step is required.

1.4.1 Characterisation of coke deposits

A number of techniques have been employed to characterise the location, composition and structure of coke deposits on reforming catalysts. These include temperature programmed oxidation (TPO),^{151,152} Raman^{153,157} and infra-red spectroscopy,¹⁵⁸⁻¹⁶³ XRD^{155,164} and TEM.¹⁶⁴⁻¹⁶⁷

In general the findings are as follows. Initially there is rapid deposition of coke on the metal which, after reaching a certain level, remains relatively constant. Coke formation on the support is slower initially but continues throughout the whole length of the run, gradually increasing the quantity of carbon deposited.¹⁶⁸ Coke deposited on the support tends to be more dehydrogenated and polymeric.

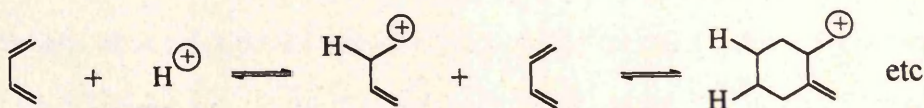
Biswas et. al.¹⁷² demonstrated the existence of two types of coke on the metal surface of reforming catalysts. The first type of coke was easily removed by hydrogen and termed reversible. The second type was more resistant to hydrogen removal and was termed irreversible coke. The presence of reversible and irreversible coke on hydrocarbon conversion catalysts has been proposed by a number of authors.^{173,174} Single crystal

studies by surface scientists have characterised these coke types, the reversible coke being hydrogenated surface species (H/C ratios 1.5-2.0) and the irreversible being graphitic in nature (H/C ratio ≈ 0.2).¹⁷⁵ Biswas noted that the graphitic coke was favoured by high temperatures and low partial pressures and increased with time on stream, corresponding with the drop in catalyst activity.

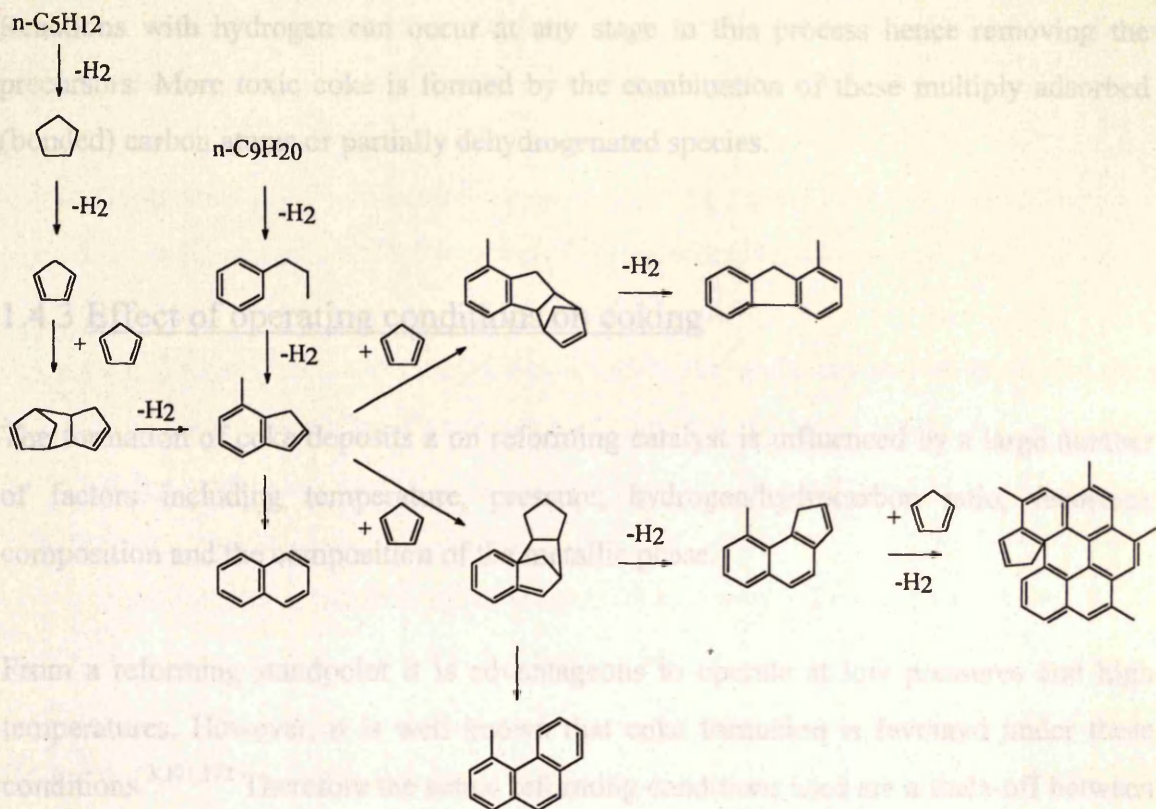
1.4.2 Mechanism of coke formation

A number of mechanisms have been proposed to account for coke formation on reforming catalysts.¹⁶⁹⁻¹⁷¹ They all involve an initial dehydrogenation step resulting in formation of unsaturated species on the catalyst surface which can subsequently undergo polymerisation reactions to produce extensive deposits of hydrogen-deficient carbonaceous material.

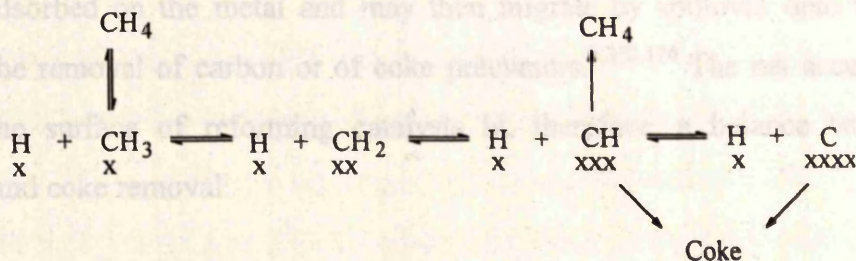
As already stated, the coke deposits formed on the acid support are known to be different from those formed on the metal. It is generally believed that coke formation on acidic sites of the catalyst proceed via polymerisation of unsaturated material. The following mechanism involving carbonium ions produced from alkenes has been reported by Trimm:¹⁶⁹



Parera and co-workers¹⁷⁰ proposed a Diels-Alder type condensation mechanism, catalysed by Lewis acid sites, to account for the high coking activity of five membered ring compounds (this will also be discussed in the next section):



These reactions are catalysed by the support and continue until there are no terminal C_5 rings present in the species, e.g. as with naphthalene and fluorene. Coking of the metal function of the catalyst is generally thought to involve dehydrogenated species. For example, Trimm¹⁷¹ proposed that the production of coke on platinum surfaces takes place via a series of fragmentation and successive dehydrogenation reactions:



Reactions with hydrogen can occur at any stage in this process hence removing the precursors. More toxic coke is formed by the combination of these multiply adsorbed (bonded) carbon atoms or partially dehydrogenated species.

1.4.3 Effect of operating conditions on coking

The formation of coke deposits on a reforming catalyst is influenced by a large number of factors including temperature, pressure, hydrogen/hydrocarbon ratio, feedstock composition and the composition of the metallic phase.

From a reforming standpoint it is advantageous to operate at low pressures and high temperatures. However, it is well known that coke formation is favoured under these conditions.^{3,171,172} Therefore the actual reforming conditions used are a trade-off between product requirements and rate of catalyst deactivation. The major advantage of bimetallic over monometallic platinum catalysts are that their improved resistance to deactivation allows operation under more severe conditions.

The H_2 /hydrocarbon ratio also has a marked effect on coke formation. Low hydrogen pressures encourage the formation of highly unsaturated precursors on the catalyst surface and also encourage the conversion of pregraphitic carbonaceous residues into toxic graphitic species.¹⁷² By increasing the hydrogen pressure the catalyst surface is able to cleanse itself of carbonaceous deposits. The availability of activated atomic hydrogen, which is adsorbed on the metal and may then migrate by spillover onto the support, results in the removal of carbon or of coke precursors.^{3,172,176} The net accumulation of coke on the surface of reforming catalysts is, therefore, a balance between coke formation and coke removal.

It has been shown by a number of studies¹⁷⁷⁻¹⁸⁰ that the feedstock composition can have a major influence on the rate of deactivation. Zhoroz et. al.¹⁷⁴ classed the coking ability

of various hydrocarbons and compared them with that of cyclohexane, which was given a reference coefficient of one. The order of coking efficiency was found to be as follows:

Cyclopentane(670) > indene(250) > methylcyclopentane(130) > n-nonane(41) > n-hexane(35) > ethylbenzene(23) > benzene(3) > cyclohexane(1)

Cooper and Trimm¹⁷⁸ obtained similar results when investigating the coking of Pt/Al₂O₃ with various C₆ hydrocarbons. These authors found that the coking potential decreased in the following order:

methylcyclopentane > 3-methylpentane > n-hexane > 2-methylpentane > benzene > cyclohexane

Beltramini et. al.¹⁷⁹ found that coke formation was not directly related to molecular weight (although there was higher coke deposition for C₇ and higher alkanes) but was more strongly influenced by hydrocarbon structure.

An important feature that is apparent from the above discussion is the potency of C₅ ring structures towards formation of coke as discussed earlier in the mechanism given by Parera and co-workers.¹⁷⁰

1.4.4 Influence of bimetallic catalysts on coking.

Addition of Re, Ir, Sn or Ge and/or sulphur are all known to increase the resistance to deactivation of reforming catalysts. These additives also influence the rate of coking of these systems. However, there is no simple relationship between the rate of deactivation of these catalysts and the quantity of carbon deposited. These additives also modify the type of coke produced and where these carbonaceous residues are deposited on the catalyst.

Carter et. al.¹⁴⁰ observed a decrease in coke deposition on addition of iridium to a Pt/Al₂O₃ catalyst. Since iridium is known to have high hydrogenolysis activity, these authors proposed that the observed decrease in coking was due to removal of coke, or coke precursors, by hydrogenolysis. Similar conclusions about the influence of both Re and Ir on coking have been reached by a number of studies.^{75a,181}

A number of studies have concluded that reduction in the ensemble size of Pt by alloying with inactive species such as tin or germanium makes the metal surface less susceptible to deactivation by coke formation^{89,118,127} (coke deposition is considered to be structure sensitive in a similar manner to hydrogenolysis). A similar dilution mechanism has been proposed to account for the influence of S and Re-S, where sulphur binds preferentially to Re.^{61,75b,82,179}

Modification of the electronic properties of platinum by alloy formation^{112,71} or interaction with an oxide species of the promoter (i.e. GeO_x, SnO_x, ReO_x)^{93,95,113-115,123} has been considered by some authors to influence the coking characteristics of these systems. The electronic effect is stated to reduce the strength of the Pt-C bond and therefore reduce the susceptibility of the metal surface to deactivation by coke formation.

1.4.5 Influence of carbonaceous residues on reforming reactions

The deposition of carbonaceous residues onto reforming catalysts not only reduces the overall activity but also results in changes in selectivity. This effect has been demonstrated by Christoffel and Paál.¹⁸³ According to these workers both fresh and partly deactivated Pt/Al₂O₃ catalysts lose isomerisation and hydrogenolysis activity during reaction with methylcyclopentane. Dehydrogenation activity, however, remains unchanged. These authors also observed that the formation of carbonaceous deposits favoured metal-catalysed bond-shift skeletal rearrangements in preference to the cyclic

mechanism of isomerisation. The authors attributed these effects to dilution of the larger metal ensembles, required in the later mechanism, by surface carbon.

In agreement with these results Barbier¹⁸⁴ found that, for the reaction of various hydrocarbons over Pt/Al₂O₃, the hydrogenolysis reaction was the most sensitive to coke deposition, whereas hydrogenation and dehydrogenation reactions were essentially unaffected.

Beltamini and Trimm¹⁸⁵ also provided evidence for the selective loss of hydrogenolysis selectivity over a Pt/Al₂O₃ catalyst. However, in contrast to Christoffel and Paál,¹⁸² these workers reported that the isomerisation selectivity of their catalyst increased with time. In addition, Figoli and co-workers¹⁸⁶ established from naphtha reforming studies that the increasing coke content induces a selective loss of dehydrocyclisation activity.

A more recent study by Beltramini and Trimm¹¹⁸ indicated that the main benefit in using bimetallic reforming catalysts originates in their ability to control the position on which coke is deposited on the catalysts. The Pt/Al₂O₃ catalyst studied showed a very rapid initial decline in overall activity (i.e. conversion of n-heptane) due to coke formation on the metal. This was accompanied by a decrease in selectivity for hydrogenolysis, hydrocracking and aromatisation and an increase in selectivity for isomerisation. For the bimetallic catalysts studied (Pt-Ge, Pt-Sn and Pt-Ir) it was found that the initial high conversion levels were virtually unchanged throughout the length of the run. The selectivities did change with use however, although these changes were not the same for each catalyst.

It is clear therefore that coke deposition on reforming catalysts can have a significant effect on both the activity and selectivity of reforming catalysts. However, there is no simple relationship between the degree of coking and the corresponding changes in catalytic activity, particularly for bimetallic systems.

1.5 Sintering

Sintering of the metal function in reforming catalysts is, like the formation of coke, a major cause of deactivation in these systems. The resulting loss of metal surface area free to interact with the gaseous hydrocarbons results in a decrease in the overall activity. The selectivity of these catalysts is also affected due to the different structure sensitivities of the reactions involved, as discussed in section 1.2. A review of particle size effects in catalysis is given by Bond.¹⁸⁷

Several factors affect the rate of sintering of supported metal particles: the nature of the support, the nature of the metal, temperature, chemical atmosphere, loading etc.

(1) The crystalline migration model

White et. al.^{188,189,190} studied model systems and supported Pt/ γ -Al₂O₃ by electron microscopy. It was found that the average particle sizes increased with increasing temperature, treatment time and metal loading. It was also observed that treatment in an oxygen environment led to larger platinum particles than in a reducing environment. Similar results have been reported in other studies.¹⁸⁸⁻¹⁹⁴

Chu and Ruckenstein^{191,192} studied the effect of chemical atmosphere on the sintering of platinum-alumina model catalysts. Electron microscopy was used to characterise these systems both before and after treatment in H₂, N₂, O₂, wet N₂ and wet H₂ atmospheres. Significant increases in sintering were reported in a wet hydrogen atmosphere. It was also found that the rate of sintering increased with increasing treatment temperature.

Yao et. al.¹⁹⁴ studied the effect of atmosphere, temperature and metal loading on the sintering of platinum supported on alumina. TEM, TPR and selective gas adsorption were used to study the catalyst after various treatments. The authors reported that heating the catalyst at 500°C in H₂ caused an increase in particle size, and hence decrease in surface area. Subsequent heating in O₂ at 500°C (and subsequent reduction) increased the surface area. However, O₂ treatment at temperatures >600°C caused further sintering

of metal particles. Higher rates of sintering were reported with high metal loadings. These results were explained by assuming the formation of a platinum oxide phase after treatment in oxygen at 500°C, which resulted in redispersion of the metal. Above 600°C however, this oxide decomposed to platinum which agglomerated, resulting in a decrease in metal surface area.

1.5.1 Sintering Mechanisms

Two models have been proposed to explain the sintering of supported metal catalysts:

(1) The crystallite migration model

This model was proposed by Ruckenstein and Pulvermacher.¹⁹⁵ They suggested that sintering occurs by migration of metal crystallites over the surface of the support, followed by collision and subsequent coalescence of the metal particles.

(2) The atomic migration model

This model was proposed by Flynn and Wanke^{196,197} and is based on migration of individual atoms (or molecules) leaving crystallites and migrating over the support until they collide and are captured by larger metal crystallites.

Ruckenstein and Pulvermacher's crystallite migration model is based on a two step process: (a) migration of the metal crystallites on the support and (b) sintering of the migrating particles by collision and subsequent coalescence.

The crystallite migration model was used to explain the results obtained by Chu and Ruckenstein^{191,192} from electron microscopy studies of model catalyst systems. In these studies the size, shape and position of individual crystallites were monitored following treatment in various chemical atmospheres. In the first study,¹⁹¹ examining platinum on a carbon substrate, migration of particles larger than 20 nm was reported. In the second study of Pt on alumina,¹⁹² direct evidence for migration of particles larger than 10 nm was reported.

In a later related paper from this laboratory,¹⁹³ employing the same technique to study a Pt/Al₂O₃ catalyst, it was concluded that sintering of supported metal crystallites occurred by two mechanisms:

(1) Short-distance, direction-selective (non random) migration of particles followed by (a) collision and coalescence or (b) direct transfer of atoms between two approaching particles.

(2) Localised ripening (direct ripening) between stationary adjacent particles.

There are a number of observations which cannot be adequately explained by the crystallite migration model, such as the increased rate of sintering in an oxidising environment as compared to a reducing environment. Wynblatt and Gjostein,¹⁹⁸ in a theoretical discussion of supported metal crystallites, concluded that particle migration was too slow a process to explain sintering of particles greater than 5 nm.

The atomic (or molecular) diffusion model can be used to explain differences in sintering with changes in chemical atmosphere, the migrating species being platinum atoms in a reducing atmosphere and molecules of platinum oxide in an oxidising atmosphere.

Flynn and Wanke¹⁹⁶ used the atomic migration model to explain results obtained on the sintering of alumina supported platinum. McVicker et. al.¹⁹⁹ studied Ir/Al₂O₃ catalysts by electron microscopy and concluded that sintering occurred in an oxygen environment via a molecular migration mechanism. This is important due to the known tendency of Ir to agglomerate into large crystallites of IrO₂ when heated in O₂ at high temperatures.^{136,137}

The basis of the atomic migration model is the growth of larger particles at the expense of smaller ones (Ostwald ripening). Small particles have larger surface energy than large particles and, therefore, the driving force for sintering is an overall decrease in surface energy.

Wynblatt and Ahn²⁰⁰ considered mathematical models for sintering and concluded that particle growth of supported metals was due to ripening.

Harris et. al.²⁰¹ studied the sintering of alumina supported catalysts by TEM. The samples were sintered in air at 600°C for various lengths of time ranging from 30 minutes to 24 hours. Examination of the sintering data suggested that a change in sintering mechanism occurred after 2 hours. The authors proposed that in the initial stages platinum particles grew by the migration and subsequent coalescence of small Pt particles. In the latter stages the presence of fast growing large platinum crystallites suggested that sintering occurred via an Ostwald ripening process.

These results were supported by a later study²⁰² in which the catalysts were treated in O₂ at 700°C for time periods of 10 minutes to 8 hours. The particle structures and size distribution were noted after each treatment. It was concluded that the initial sintering mechanism was dominated by the migration and coalescence of small particles. Many twinned platinum particles were observed. In the later stages the presence of abnormally large particles (> 1500 Å) suggested growth via an Ostwald ripening process with PtO₂ as the migrating molecular species. It was suggested that the twin boundaries formed in the initial stages of particle sintering (with reentrant surface features) could provide

preferential nucleation sites for growth via molecular migration. Sintering at 700°C ²⁰² caused an increase in the rate of particle growth compared to sintering at 600°C .²⁰¹

Chapter two: Objectives

2.1 Objectives of the present study

The principal aim of this study was to gain a clearer understanding of the role played by the various parameters noted in Table 1.1 in determining the rate of polymerization and to establish the relative importance of each of these factors in the overall process.

Chapter two: Objectives

This work is a continuation of the work of the author's previous studies.

The main objectives of this study are:

1. To determine the effect of the concentration of the reactants on the rate of polymerization.

2. To determine the effect of the temperature on the rate of polymerization.

3. To determine the effect of the catalyst on the rate of polymerization.

4. To determine the effect of the solvent on the rate of polymerization.

5. To determine the effect of the initiator on the rate of polymerization.

6. To determine the effect of the monomer on the rate of polymerization.

To this end, a series of experiments were carried out under the following conditions:

1. The concentration of the reactants was varied by a factor of 10.

2. The temperature was varied by a factor of 10.

3. The catalyst was varied by a factor of 10.

4. The solvent was varied by a factor of 10.

5. The initiator was varied by a factor of 10.

6. The monomer was varied by a factor of 10.

2.1 Objectives of the present study

The principal aim of this study was to gain a clearer understanding of the role played by the various promoters added to Pt/Al₂O₃ reforming catalysts to improve their selectivity and stability. Particular emphasis was placed on alloy formation in these systems.

This work is a continuation of a number of studies performed in this department by Huang et. al.^{85,120,128,129} In these studies it was found that Pt-Sn and Pt-Ge alloys were formed on Pt-Sn/Al₂O₃ and Pt-Ge/Al₂O₃ catalysts during use in reforming. It was the aim of this study to examine these system in more detail to determine the influence exerted by alloy formation on the corresponding catalytic properties. A further aim was to extend these studies to include a variety of iridium containing catalysts. It was hoped that the high hydrogenolysis activity of iridium would provide a useful means of studying geometric/ensemble effects in these systems.

To this end a number of bi and multimetallic reforming catalysts were prepared and characterised by transmission electron microscopy and energy dispersive X-Ray analysis. This characterisation was performed both before and after reaction. The results obtained were correlated with reforming data obtained using a pressurised continuous flow microreactor system. n-Octane was used as a model feed in these experiments and the reactions were carried out under conditions typical of industrial reforming (110 psig, 510 °C).

Chapter Three: Transmission Electron Microscopy and Energy Dispersive X-ray Analysis

3.1 Transmission Electron Microscopy

The wave-nature of electrons was first proposed by De Broglie²⁰³ in 1925. Electron diffraction was demonstrated by Davisson and Germer in 1926.²⁰⁴ At that time it was known that the resolving power of any microscope was related to the wavelength of the radiation employed. Therefore de Broglie's proposal led to the realisation that the use of high energy electrons, which can be focused (unlike X-rays) and whose wavelengths are considerably shorter than visible light, offered the potential for a large improvement in resolution as compared with conventional optical microscopes.

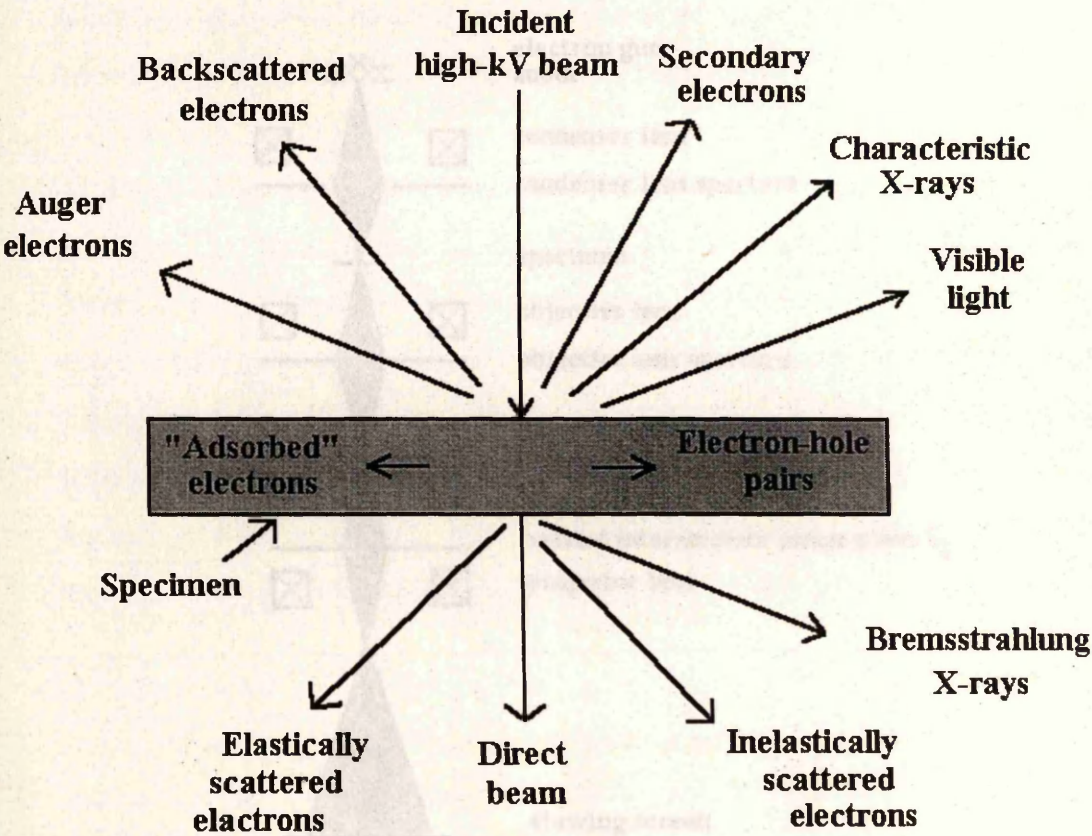
Knoll and Ruska²⁰⁵ built the first electron microscope in 1931 and within one year of its construction the resolution limit of the light microscope (≈ 300 nm) was surpassed. Since that time improvements in microscope design and technology have led to gradual improvement in resolving power, with some modern instruments being capable of atomic resolution.

Although the initial impetus for the use of electrons was the potential of improved resolution, it has since become apparent that there are many other advantages in using electrons. This is due to the variety of interactions that occur between the incident electron beam and the specimen, as detailed in figure 3.1. Modern analytical electron microscopes are designed to take advantage of these interactions to obtain as much information about the specimen under examination as possible.

The basic layout of a modern high resolution transmission electron microscopes is shown in figure 3.2. The microscope consists of three main sections; the electron gun and accelerator, the illuminating system, and the imaging system.

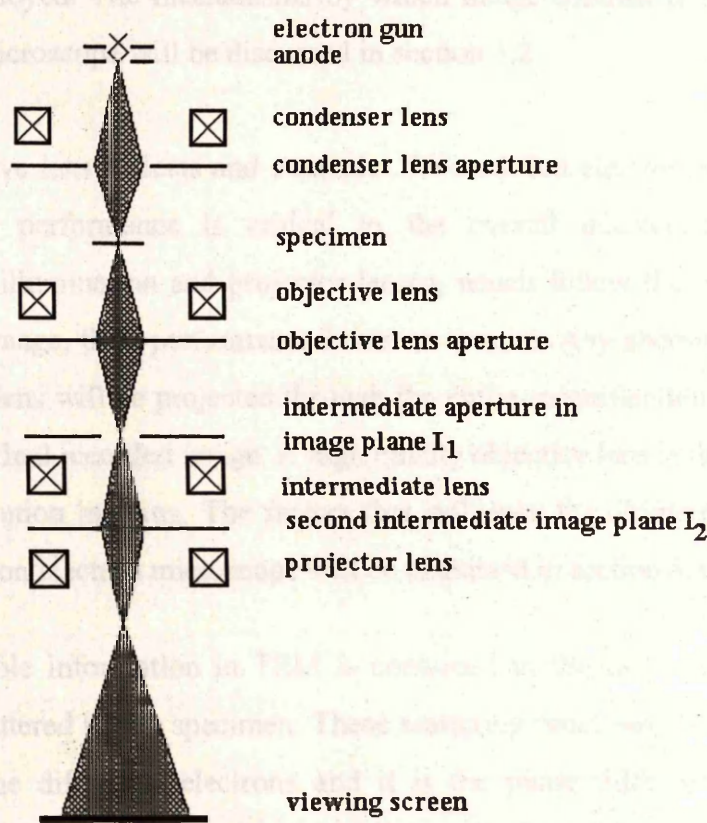
In modern high resolution electron microscopes the electron source is usually a heated LaB₆ cathode or a field emission gun. These are used in preference to conventional tungsten filaments due to their improved brightness and coherence. The fine beam of electrons produced is then accelerated through a potential difference, typically between 200 kV and 400 kV for HREM, and focused into a spot by a series

Figure 3.1 Signals generated when a high-energy beam of electrons interacts with a thin specimen



of electromagnetic condenser lenses. A variable aperture is inserted below the final condenser lens, the function of which is to improve the coherence of the illuminating radiation.

Figure 3.2 Basic layout of a transmission electron microscope



The recoverable information in TEM is contained in the elastically scattered electrons. These carry information about changes in the atomic structure. Most of the primary electrons are absorbed in the specimen and the unscattered transmitted beam which carries the high resolution lattice imaging in the TEM. However, the imaging lenses do not pass the phases of transmitted electrons and therefore complete image formation is not possible. This will be discussed in more detail in section 3.3.

As well as high resolution imaging, the electron microscope may also be used to obtain electron diffraction patterns and to perform analytical spectroscopy such as energy dispersive X-ray analysis (EDX) and electron energy loss spectroscopy (EELS). Electron diffraction and EDX, two techniques that have been employed in this study, will be discussed in more detail in sections 3.5 and 3.6 respectively.

of electromagnetic condenser lenses. A variable aperture is inserted below the final condenser lens, the function of which is to improve the coherence of the illuminating radiation.

After passing through the specimen the electron image produced is magnified by a series of imaging electromagnetic lenses and projected onto the fluorescent viewing screen. The range of magnifications typically available extend from about 1000 times to over 1 million. To record image detail photographic film or TV/CCD cameras are generally employed. The mechanisms by which image contrast is brought about in the electron microscope will be discussed in section 3.2.

As the objective lens collects and transmits the modified electron beam leaving the specimen, its performance is critical to the overall microscope performance. Although the illumination and projector lenses, which follow the objective, further magnify the image, their performance is not so crucial. Any aberrations induced by the objective lens will be projected through the entire magnification system and will appear in the final recorded image. A high quality objective lens is therefore essential for high resolution imaging. The factors that influence the ultimate performance of the transmission electron microscope will be discussed in section 3.4.

The recoverable information in TEM is contained in the electrons that have been elastically scattered by the specimen. These scattering processes also introduce phase changes in the diffracted electrons and it is the phase difference between these electrons and the unscattered transmitted beam which forms the basis of high resolution lattice imaging in the TEM. However, the imaging lenses can also perturb the phases of transmitted electrons and therefore complicate image interpretation. This will be discussed in more detail in section 3.3.

As well as high resolution imaging, the electron microscope may also be used to obtain electron diffraction patterns and to perform analytical spectroscopies such as energy dispersive X-ray analysis (EDX) and electron energy loss spectroscopy (EELS). Electron diffraction and EDX, two techniques that have been employed in this study, will be discussed in more detail in sections 3.5 and 3.6 respectively.

3.2 Contrast mechanisms in the TEM

Contrast in transmission electron microscope images is brought about either by the physical exclusion of electrons that have been scattered by the specimen, or by recombination of scattered and undeviated electrons to produce interference effects. The scattering of electrons by atoms can involve both elastic and inelastic processes.

3.2.1 Elastic scattering

Elastic scattering results mainly from coulombic interactions between incident electrons and the electric charge of the atomic nucleus. This type of scattering increases with increased atomic number of the specimen nuclei. It decreases with increased incident beam energy.

If elastic scattering occurs to high angles such that some electrons are physically stopped by the microscope column, then contrast will result in the image. This is termed “mass” or “amplitude” contrast, the magnitude of which can be increased by inserting an objective aperture in the beam path. This aperture cuts out electrons scattered at angles greater than the angle subtended by the aperture on the specimen.

Mass contrast due to scattering by thick regions, or regions of high Z , is incoherent in nature, i.e. there is no phase relationship between the scattered electrons. However, in a crystal where there is an ordered arrangement of atomic planes, and if the planes are aligned parallel to the electron beam direction then a series of coherent diffracted beams will result. These beams will appear at angles satisfying the Bragg condition. If an aperture is inserted to intercept some or all of these diffracted beams then contrast will result in the image. This is termed diffraction contrast.

However, if a number of these diffracted beams are permitted to enter the objective lens, then recombination of these beams with the undeviated electrons will result in

interference effects producing areas of increased and diminished intensity in the image. This is termed phase contrast and is the basis of high resolution lattice imaging in the TEM. A detailed review of high resolution lattice imaging can be found in the texts by Spence²⁰⁶ and Busek et. al.²⁰⁷ Such lattice images can only be obtained from periodicities parallel to the electron beam direction and under the correct objective defocus conditions (section 3.3).

As the angle of scattering for a diffracted beam is inversely proportional to the lattice spacing from which it was produced, small periodicities will produce widely elastically scattered electrons. These electrons will be focused by off-axis regions of the objective lens and consequently lens aberrations such as spherical aberration severely effect the retrieval and interpretation of information obtained by phase contrast.

3.2.2 Inelastic Scattering

Inelastic scattering processes involve mainly interaction of the incident electrons with orbital electrons in the specimen, generally resulting in relatively small deflections in electron trajectory. However, these processes are of considerable importance as the energy transfer that occurs from the electron beam to the specimen generates a range of signals which can be used to obtain additional information about the specimen. The main consequences of the inelastic processes which occur are as follows:

- a) Plasmon excitation
- b) Excitation of conduction electrons leading to secondary electron emission
- c) Ionisation of inner shells resulting in the production
of X-rays and Auger electrons
- d) Bremsstrahlung X-rays
- e) Phonon excitations

Plasmon excitations are brought about by interaction on the incident electrons with loosely held or free electrons. A coulombic interaction between the incident beam electron and the electron "gas" in the specimen can cause the electron gas to oscillate and these oscillations are known as plasmons. The incident electrons thus lose discrete amounts of energy by excitation of plasmon oscillations.

The removal of inner shell electrons resulting in the emission of X-rays (or Auger electrons) and is the basis of EDX analysis which will be discussed in more detail in section 3.6.

Phonon scattering occurs when a high energy electron "strikes" an atom and causes the lattice to vibrate. This vibration of the lattice is equivalent to heating of the specimen. Although phonon excitations usually involve very small energy losses (0.1 eV) the electrons can be scattered to relatively high angles and these interactions account for the diffuse background intensity present between the Bragg spots in diffraction patterns.

Although inelastic processes are useful in terms of the information we can obtain from spectroscopies such as EELS and EDX, they can be detrimental from the viewpoint that energy transfer from the electron beam to the specimen can result in specimen damage and degradation (section 3.4.2).

Just as elastically scattered electrons can be recombined to produce interference effects, inelastically scattered electrons (whose energies and hence wavelengths have been altered) can be recombined to produce areas of increased or diminished intensity in the image. This is termed inelastic phase contrast. The effects of this type of contrast only become apparent at very high resolution.

Where $\Delta\theta$ = Scattering angle of diffracted beam

C_s = Spherical aberration coefficient of the objective lens

Δf = Lens defocus value

3.3 Contrast Transfer and Retrieval of High Resolution Information

Elastic and inelastic phase contrast can only be simply interpreted for thin specimens (< 10 nm), for which single electron scattering events occur and the specimen behaves as a weak phase object.²⁰⁷ In reality, in most specimens, multiple scattering of electrons by the specimen occurs and a more rigorous dynamical treatment has been developed to calculate scattering amplitudes and phases in this case.²⁰⁷⁻²⁰⁹

Furthermore, to interpret high resolution transmission electron microscopy images it is also necessary to take account of the effect of the electron optics, as well as the specimen, in modifying the transmitted electron wave. Scherzer²¹⁰ considered the theoretical resolution limit of the TEM and derived a wave-mechanical formulation of image formation. This work formed the basis for the transfer theory of electron microscopy.

Phase contrast effects in high resolution electron microscopy are modified by a phase distortion function, $\sin\chi$, due to aberrations associated with the objective lens. For a perfect lens $\sin\chi = 1$. The presence of wave aberrations can be accounted for by an instrumental modulation factor $\chi_{(s)}$ where:

$$\chi_{(s)} = \frac{2\pi}{\lambda} \left[\Delta f \frac{\alpha_{(s)}^2}{2} - C_s \frac{\alpha_{(s)}^4}{4} \right]$$

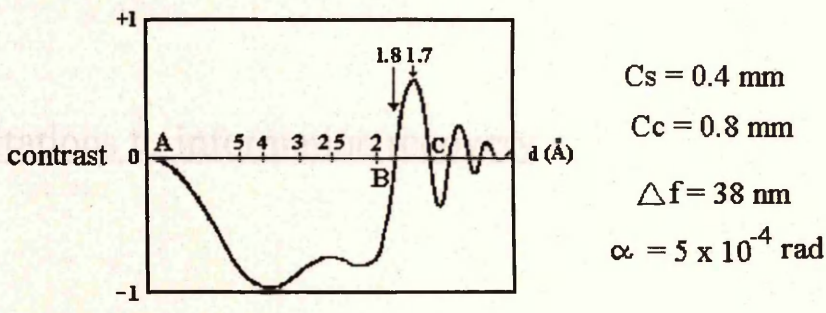
Where $\alpha_{(s)}$ = Scattering angle for diffracted beam

C_s = Spherical aberration coefficient of the objective lens

Δf = Lens defocus value

The function $\sin\chi(s)$ can be plotted against spatial frequency, giving the Phase Contrast Transfer Function (PCTF). This is a function of defocus, Δf , and spherical aberration, C_s . Figure 3.3 shows the PCTF for the TOPCON 002B microscope used in this study, with $C_s = 0.4$ mm and $\Delta f = 38$ nm. Spatial frequencies between A and B will appear in reverse contrast to those in region BC. Frequencies corresponding to values of $\sin\chi(s) = 0$ will not be visible in the image.

Figure 3.3. Phase contrast transfer function for the TOPCON 002B



For most applications it is desirable to operate the microscope at a defocus value where the appropriate transfer function value is identical and near unity for the maximum range of spatial frequencies without contrast reversal. This “optimum defocus” value $\Delta f'$, first found by Scherzer is given by:

$$\Delta f' = 1.2\sqrt{C_s} \lambda$$

For the TOPCON 002B, $\Delta f' = 38$ nm, as in figure 3.3. The Scherzer cut-off, d_{\min} was calculated as:²¹¹

$$d_{\min} = 0.65C_s^{1/4} \lambda^{3/4}$$

and for the 002B $d_{\min} = 1.8\text{\AA}$.

The optimum defocus defines the limit of most faithful reproduction over the maximum range of spatial frequencies. However, smaller lattices can be resolved, in good contrast, if the appropriate defocus value is chosen, but great care is required in image interpretation as the absence of image detail from other periodicities can lead to spurious effects and erroneous observations.

3.4 Limitations to information recovery

3.4.1 Spherical Aberration

The focal length of a magnetic lens is not constant across its diameter. Electrons off the optical axis experience a magnetic field stronger than those near the axis and are therefore brought to a focus at a point closer to the lens. As a result, a point object is imaged as a disk of finite size. This is the most important lens defect and ultimately the spherical aberration coefficient of the objective lens determines the limit of resolution obtainable in a TEM.

3.4.2 Astigmatism

The effect of astigmatism, which is again most crucial in the objective lens, can, if not corrected, also limit the information available from TEM. Astigmatism arises from rotational variation in the field strength (focal length) of the lens. Some astigmatism is inherent in all electromagnetic lenses due to the manufacturing process but can also be induced by contamination within the microscope column, the

charging of which can produce distorting electric fields. A correcting field produced by a series of stigmators is used to balance the inhomogeneities caused by astigmatism.

3.4.3 Chromatic Aberration

Chromatic aberration arises due to variations in both the electrical stability (lens currents) and the energy of the electrons. To minimise this effect, the lens currents must be stabilised to avoid a lens with continually altering focal length. The high voltage power supply must also be stabilised to allow sufficiently monoenergetic electrons to be obtained. Inelastic scattering events which occur in the specimen increase the energy spread of the electron beam and therefore induce an increase chromatic aberration. This effect becomes more pronounced as the specimen thickness increases.

3.4.4 Radiation Damage

Specimen damage under electron beam irradiation is significant in most cases and is prohibitive to the study of many organics and polymers. Loss of spot intensity has been used as a measure of radiation damage. Fryer²¹¹ has tabulated critical doses for various organic and polymer species and the topic has been reviewed by Jones²¹² and Glaeser et. al. (in Siegel and Beaman).²¹³ The catalysts samples that provided the focus of this study were relatively beam stable and thus did not require any special procedures to minimise radiation damage. However, heavy metal compounds such as platinum oxide or chloroplatinic acid are rapidly decomposed by the electron beam.

3.4.5 Mechanical Stability

Mechanical instabilities, mainly residual drift in the specimen stage, can adversely affect the quality of high resolution images, resulting in an incoherent blurring of the

image. To minimise drift it is important that thermal equilibrium is established in the specimen and stage.

Figure 3.4 Ray paths in the electron microscope for

3.5 Electron Diffraction

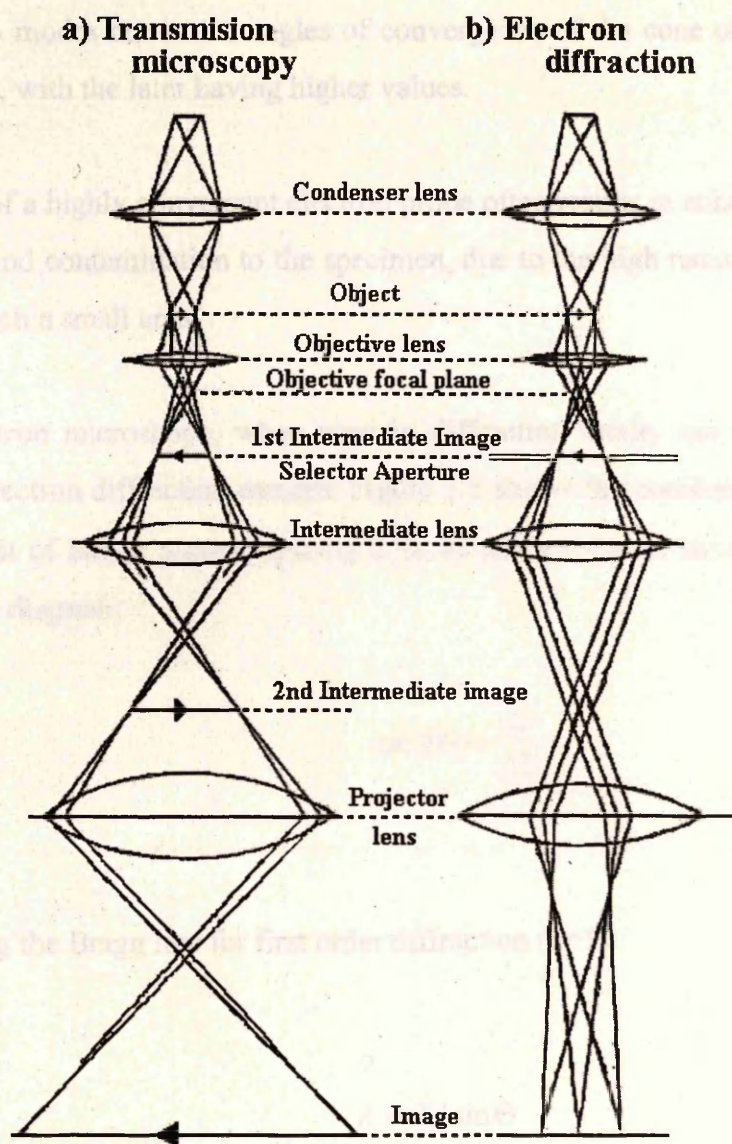
Areas of the specimen with crystal planes parallel to the electron beam diffract electrons in accordance with the Bragg law. The undeviated incident beam and diffracted beams are focused at the back focal plane of the objective lens, and there form a diffraction pattern.

Figure 3.4 presents a schematic diagram of ray paths for both imaging and diffraction modes in the TEM. The diffraction pattern and the intermediate image are always present in the microscope, and the intermediate lens setting determines which is projected onto the image plane. In transmission mode, the intermediate lens is focused on the intermediate image (Figure 3.4.a), whilst for electron diffraction, the intermediate lens is focused on the back focal plane of the objective lens, which contains the diffraction pattern and corresponding adjustment of the following projector lenses system magnifies this onto the final screen (Figure 3.4.b).

In order to single out an area of the specimen from which to obtain a diffraction pattern selected area or micro-beam electron diffraction techniques are employed. For selected area diffraction an aperture is inserted in the first intermediate image plane, as shown in figure 3.4.b. This is equivalent to insertion of an aperture in the specimen plane, but smaller by the magnification factor of the objective lens. Using this technique it is possible to select areas down to a few hundred nanometres in diameter.

Micro-beam electron diffraction²¹⁴ employs a highly condensed electron probe to illuminate only the area of interest in the specimen. Using this technique on the 002B microscope a minimum probe diameter of 2 nm is obtainable. The highly convergent

Figure 3.4 Ray paths in the electron microscope for



nature of the electron probe causes the diffraction spots to spread out into disks, the diameter of which is controlled ultimately by the size of the condenser aperture employed. The 002B instrument allows two different probe forming conditions to be employed, one termed micro-beam electron diffraction and one termed convergent beam electron diffraction. As these names suggest the main differences between these two modes are in the angles of convergence of the cone of electrons forming the probe, with the later having higher values.

The use of a highly convergent electron probe often results in enhanced rates of beam damage and contamination to the specimen, due to the high radiation dose contained within such a small area.

The electron microscope, when used in diffraction mode, can be considered as a simple electron diffraction camera. Figure 3.5 shows the construction for diffraction from a set of lattice planes, spacing d , at an angle θ to the incident electron beam. From the diagram:

$$\tan 2\Theta = \frac{D}{2L} \quad (\text{equation 3.5.1})$$

and using the Bragg law for first order diffraction ($n=1$):

$$\lambda = 2d \sin \Theta \quad (\text{equation 3.5.2})$$

Since θ is very small the approximation

$$\tan 2\Theta = 2 \sin \Theta = 2\Theta \quad (\text{equation 3.5.3})$$

can be used and combined with equations 3.5.1 and 3.5.2 above gives:

$$Ld = 2\lambda L \quad \text{or} \quad Dd = K \quad (\text{equation 3.5.4})$$

where L = effective camera length
 K = camera constant

Figure 3.5 The electron microscope as a simple diffraction camera

The effective camera length is the physical distance between the diffraction plane and the final image screen given by:

$$L = f_o M_1 M_2 M_3 \quad (\text{equation 3.5.5})$$

where L = focal length of the objective lens

$M_{1,2,3}$ = magnification of intermediate and final lenses

L = the distance between the specimen and the screen

A standard electron microscope setup is shown in Figure 3.5. The incident beam is parallel to the specimen surface. The diffracted beam is at an angle 2θ to the incident beam. The distance between the specimen and the screen is L . The distance between the specimen and the screen is L . The distance between the specimen and the screen is L .

The restriction that only lattice planes are parallel to the incident beam allows determination of the specimen orientation. The geometry of the diffraction pattern allows determination of the specimen orientation, lattice spacing and unit cell parameters. Formulae for the calculation of interplanar spacings, angles between planes, and the direction normal to the diffracting planes and angles between zone axes for the common crystal systems are given in Table 3.5.1.

The geometry of the diffraction pattern allows determination of the specimen orientation, lattice spacing and unit cell parameters. Formulae for the calculation of interplanar spacings, angles between planes, and the direction normal to the diffracting planes and angles between zone axes for the common crystal systems are given in Table 3.5.1.

Diffraction spots also contain intensity information which can be used to determine the position of atoms within the unit cell. This forms the basis of electron crystallography.

$$Dd = 2\lambda L \quad \text{or} \quad Dd = K \quad (\text{equation 3.5.4})$$

where L = effective camera length
 K = camera constant

The effective camera length, L , is the equivalent physical distance between the diffraction plane and the final image screen given by:

$$L = f_0 M_1 M_2 M_3 \quad (\text{equation 3.5.5})$$

where f_0 = focal length of the objective lens

$M_{1,2,3}$ = magnification of intermediate and projector lenses

λ = the electron wavelength, fixed by the accelerating voltage.

A standard is used to determine the camera constant and then unknown diffraction patterns are identified by comparing the spacing with tabulated X-ray data in the JCPDS-ICDD powder diffraction file (formerly the ASTM index).²¹⁵

The restriction that only lattice planes near parallel to the electron beam will contribute to the diffraction pattern allows determination of specimen orientation, since the specimen lies normal to the planes giving rise to the recorded reflections. The geometry of the diffraction pattern allows determination of the specimen orientation, lattice spacings and unit cell parameters. Formulae are available which allow calculation of interplanar spacings, angles between planes, zone axes (the direction normal to the diffracting planes) and angles between zone axes for the common crystal systems.²¹⁶⁻²¹⁸

Diffraction spots also contain intensity information which can be used to locate and position atoms within the unit cell. This forms the basis of electron crystallography.²¹⁹

3.6 Energy dispersive X-ray analysis

3.6.1 Production and analysis of X-rays

As discussed in section 3.2.2 , inelastic scattering of incident electrons leads to the generation of X-rays by two different processes:

A) Deceleration of the electrons in the Coulombic field of the atom core (i.e. the nucleus and tightly bound electrons) which leads to the formation of a continuous spectrum of X-ray energies from zero energy up to the value of the incident electron energy - Bremsstrahlung X-rays.

B) Interaction of a beam electron with an inner-shell electron in the specimen can result in the ejection of the bound electron. This leaves the atom in an excited state with a vacancy in the electron shell. During subsequent deexcitation, an electron transition occurs from an outer shell to fill this vacancy. This transition involves a change in energy and this energy is released in the form of an X-ray (or alternatively as an Auger electron).

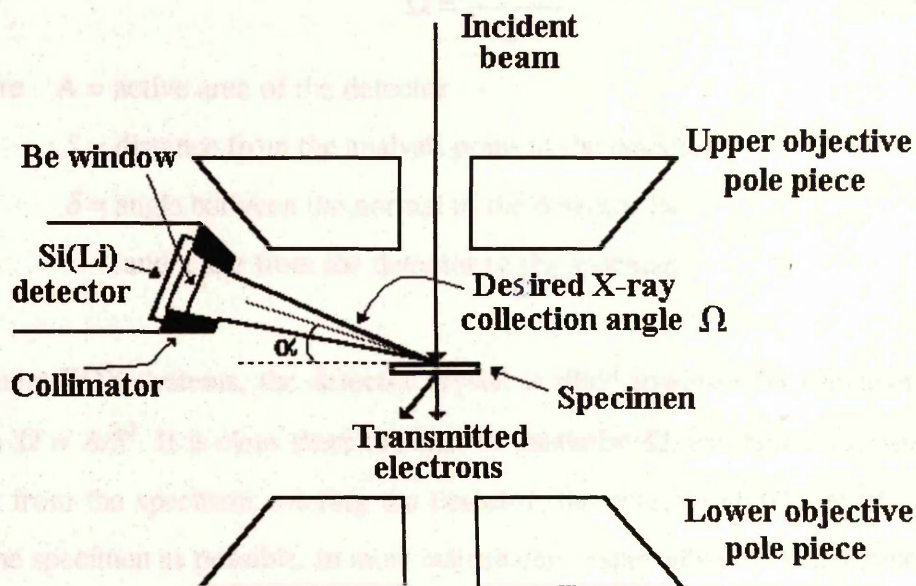
In the later process, as the energy of the emitted X-rays are related to the difference in energy between the sharply defined levels in the atom, the X-rays are characteristic of the element from which they were produced. Therefore by analysing the X-rays produced when a specimen is irradiated by high energy electrons it is possible to determine the chemical composition of the specimen.

In order to obtain a EDX spectrum a solid state Si(Li) or Ge detector is placed in close proximity to the specimen during electron beam bombardment and the X-rays produced are analysed. Figure 3.6 shows a schematic diagram of the X-ray analysis geometry.

The EDX detector has a collimator in front of the detector crystal to reduce entry of undesired radiation from the stage region of the microscope i.e. to select only X-rays produced from the area of specimen under examination.

The detector collection angle Ω is the solid angle subtended at the analysis point on the specimen by the active area of the front face of the detector, which is usually

Figure 3.6 Schematic diagram of the X-ray analysis geometry



The rate of entry of X-rays depends on the area of the active area of the detector, as shown in figure 3.7. The area of the active area of the detector of bulk specimens is the value of d is kept at the minimum. The thickness of the specimen they travel through bulk specimen is also kept at the minimum.

The EDX detector has a collimator in front of the detector crystal to reduce entry of undesired radiation from the stage region of the microscope i.e. to selected only X-rays produced from the area of specimen under examination.

The detector collection angle Ω is the solid angle subtended at the analysis point on the specimen by the active area of the front face of the detector, which is usually about 30 mm². The collection angle is defined as:

$$\Omega = \frac{A \cos \delta}{S} \quad \text{(equation 3.6.1)}$$

where A = active area of the detector

S = distance from the analysis point to the detector

δ = angle between the normal to the detector face

and a line from the detector to the specimen

In most EDX systems, the detector crystal is tilted towards the specimen so $\delta = 0$; then $\Omega = A/S^2$. It is clear therefore that to maximise Ω , and hence the number of X-rays from the specimen entering the detector, the detector should be placed as close to the specimen as possible. In most instruments, especially with thermionic sources, it is the low X-ray count rate that limits the accuracy of the experiment. The magnitude of Ω is limited as the upper polepiece of the objective lens gets in the way of the collimator thus limiting S . To overcome this limitation it is possible to increase the polepiece gap, however this results in an increase in spherical aberration and degradation of image resolution. Therefore in the design of an analytical electron microscope a compromise has to be made between the beam current (and resolution) and collection angle.

The take off angle α is the angle between the specimen surface and a line to the centre of the detector, as shown in figure 3.6. Traditionally in electron probe microanalysis of bulk specimens the value of α is kept high to minimise the adsorption of x-rays as they travel through bulk specimens. In AEMs the value of α

is again restricted by the upper polepiece. Fortunately this is not generally a problem since the thin specimens employed in TEM mean that the effects of adsorption are much reduced. This effect can also be reduced by tilting the specimen towards the detector and thereby increasing α .

2.6.2 Spectrum acquisition and processing

Once an X-ray photon has entered the semiconducting Si(Li) detector it produces a large number of electron hole pairs (the energy required to transfer an electron from the valence to the conduction band in Si ≈ 3.8 eV whilst the energy of a characteristic X-ray is usually > 1 keV) which are swept away by an applied bias. The resulting charge pulse is converted to a voltage which is amplified and identified electronically as resulting from a specific X-ray energy. Although the incident X-ray photon does not give up all its energy to the production of electron hole pairs, the number produced are directly proportional to the energy of the incident photon and sufficient signal is generated to distinguish most elements in the periodic table with good statistical precision.

In order to reduce the thermal production of electron-hole pairs, giving a noise level which would swamp the X-ray signal, it is necessary to cool the detector with liquid nitrogen. However, this has some undesirable consequences. Hydrocarbons and water vapour from the microscope environment can condense on the cold detector surface, causing adsorption of lower energy X-rays. To overcome this problem a thin window, often beryllium, is placed in front of the detector (figure 3.6). These windows are too thick to admit X-rays with energies less than 1 keV, limiting analysis to element above sodium in the periodic table. Ultra-thin composite Al/polymer or diamond windows can also be used which allow detection of lighter elements. In a microscope which can sustain an efficient clean vacuum, it is sometimes possible to operate with a windowless detector, which allows detection of elements down to Be.

The amplified voltage pulse originating from the detector is further amplified several thousand times by a pulse processor, and shaped so that an analog-to-digital

converter can recognise the pulse coming from an X-ray of specific energy. A computer then assigns the pulse to the appropriate channel in a multi-channel analyser (MCA) display.

The accumulation of pulses or counts entering each energy channel at various rates produces a histogram of counts (intensity) versus energy that is a digital representation of the X-ray spectrum. The MCA display offers multiples of 1024 channels in which to display the spectrum, and various energy ranges can be assigned to these channels e.g. for 1024 channels a display resolution of 20 eV per channel gives a full horizontal scale of 0 - 20 keV.

The X-ray spectrum obtained contains the Bremsstrahlung background and characteristic specimen peaks. To perform quantitative analysis the background intensity must first be removed. This can be done using one of several available software routines. The procedure used to obtain elemental ratios from peak intensities in the EDX spectrum is detailed in section 4.5.2. A detailed discussion of the theory and practice of energy dispersive X-ray analysis can be found in a number of texts.²²⁰⁻²²²

Chapter Four: Experimental

A list of the catalysts studied in this work is given in figure 4.1. In the following chapter the preparation, characterisation and testing of these catalysts will be detailed.

4.1.1 EUROPT-4

Figure 4.1 Catalysts Studied

1. 0.3 wt % Pt/Al₂O₃
2. 0.3 wt % Pt - 0.3 wt% Sn/Al₂O₃
3. 0.3 wt % Pt - 0.3 wt % Ge/Al₂O₃
4. 0.3 wt % Pt - 0.3 wt % Re/Al₂O₃ (EUROPT 4)
5. 0.3 wt % Pt - 0.3 wt % Ir/Al₂O₃
6. 0.3 wt % Ir/ Al₂O₃
7. 0.3 wt % Ir - 0.3 wt % Ge/Al₂O₃
8. 0.03 wt % Ir - 0.3 wt % Ge/Al₂O₃
9. 0.3 wt % Ir - 0.3 wt % V/Al₂O₃
10. 0.3 wt % Pt - 0.3 wt % Ir - 0.3 wt % Ge/Al₂O₃
11. 0.3 wt % Pt - 0.3 wt % Ir - 0.03 wt % Ge/Al₂O₃
12. 0.3 wt % Pt - 0.3 wt % Ir - 0.3 wt % V/Al₂O₃
13. 0.3 wt % Pt /Al₂O₃ (prepared using Pt(acac)₂)
14. 0.3 wt % Pt - 0.3 wt % Ce/Al₂O₃
15. 0.3 wt % Pt - 0.3 wt % Pr/Al₂O₃
16. 0.3 wt % Ni/Al₂O₃
17. 0.3 wt % Ni - 0.3 wt % Ge/Al₂O₃
18. 0.3 wt % Ru - 0.3 wt % Ge/Al₂O₃

4.1 Catalyst Preparation

All of the catalysts studied were prepared using a standard wet impregnation procedure with the exception of EUROPT-4 which was purchased. The same commercial pelletised

γ -alumina support (CK-300, Akzo Chemie Ketjen) was used in each case. This support was chosen as EUROPT-4 is manufactured by Akzo using this high purity γ -alumina.

4.1.1 EUROPT-4

The chemical composition and some physical characteristics, as supplied by the manufacturer, for EUROPT-4 are listed in table 4.1.

Table 4.1 Chemical and physical characteristics of EUROPT-4

	EUROPT-4
Surface area (m^2g^{-1})	187
N_2 pore volume	0.53
Pt (wt %)	0.296
Re (wt %)	0.311
Cl (wt %)	0.95
Fe (wt %)	0.02
S (ppm)	50

This catalyst contains an optimum level of chlorine to enhance the acidic sites of the support. The γ -alumina support is supplied as pellets about 4.0 mm in length and 1.7-1.8 mm in diameter.

4.1.2 Coimpregnated Catalysts

The remaining catalysts, as listed in figure 4.1, were prepared in the laboratory in Glasgow by a standard wet impregnation technique. This involved coimpregnation of the alumina pellets with aqueous and hydrochloric acid solutions of the appropriate metal salts. The only exception to this was catalysts number 13 which was prepared using $\text{Pt}(\text{acac})_2$ and toluene as solvent. The metal salt concentration was varied to give the

required loading and in each case 1 ml of impregnating solution per gram of support was used. The support was left in contact with the impregnating solution for 24 hours prior to drying. Drying was performed at 110°C in air for 4 hours.

The chlorine content of the impregnating solution was varied by changing the concentration of HCl used, in an attempt to keep the Cl content of the resulting catalysts fixed at approximately 1 wt%.

The metal salts (solution in the case of germanium) used in the impregnation procedures were as follows:

Pt:- H_2PtCl_6 , Aldrich chemical company, and $\text{Pt}(\text{acac})_2$ also from Aldrich.*

Ir:- $\text{IrCl}_3 \cdot 3\text{H}_2\text{O}$, Aldrich chemical company.

Sn:- $\text{SnCl}_2 \cdot 2\text{H}_2\text{O}$, Aldrich chemical company.

Ge:- Germanium ICP/DCP standard solution, Aldrich chemical company (10200 $\mu\text{g}/\text{ml}$).

Ni:- $\text{NiCl}_2 \cdot 6\text{H}_2\text{O}$, B.D.H. Laboratory chemicals division.

Ru:- RuCl_3 , Aldrich chemical company.

Ce:- $\text{CeCl}_3 \cdot 7\text{H}_2\text{O}$, B.D.H. Laboratory chemicals division.

Pr:- $\text{PrCl}_3 \cdot 6\text{H}_2\text{O}$, Aldrich chemical company.

V:- V_2O_5 , Aldrich chemical company.

* $\text{Pt}(\text{acac})_2$ — Platinum acetylacetonate

4.2 Catalyst Characterisation: Chemisorption

Carbon monoxide and oxygen chemisorption studies on $\text{Pt}/\text{Al}_2\text{O}_3$, $\text{Pt-Re}/\text{Al}_2\text{O}_3$, $\text{Pt-Sn}/\text{Al}_2\text{O}_3$ and $\text{Pt-Ge}/\text{Al}_2\text{O}_3$ catalysts have been performed in previous studies undertaken in this department.^{85,120,128} To extend these chemisorption studies a number of iridium containing catalysts were examined in this work, namely 0.3 wt% $\text{Ir}/\text{Al}_2\text{O}_3$, 0.3 wt% $\text{Ir-0.3 wt% Ge}/\text{Al}_2\text{O}_3$ and 0.3 wt% $\text{Pt-0.3 wt% Ir-0.3 wt% Ge}/\text{Al}_2\text{O}_3$.

The chemisorption system used was similar to one described by Jackson et. al.²²³ The catalyst precursors were reduced in situ in this system. Approximately 0.5 g of catalyst was used in each experiment. The sample was ramped from ambient temperature to 400°C (5°/min) in flowing hydrogen (60 ml/min) and held at this temperature for 2 hours. Following reduction the catalyst was flushed with helium (1 hour) and then cooled to room temperature. The adsorbate gas (CO or O₂) was admitted to the reduced catalyst by injecting fixed pulses (4.70 cm³, 10 mmHg) into the carrier gas stream. The quantity of adsorbate retained by the catalysts was monitored using a TCD detector in conjunction with a chart recorder. The volume of gas used was chosen so that a number of pulses would be completely consumed by the catalyst. Several pulses of adsorbate were passed over the catalyst until the adsorbate peak stabilised, indicating that adsorption had ended. The amount of gas adsorbed onto the catalyst was calculated from the difference in the peak areas. CO/M and O/M ratios were then determined.

4.3 Catalyst Characterisation: n-Octane Reforming

In order to determine the activity, selectivity and resistance to deactivation of the catalysts studied in this work a high pressure continuous flow microreactor system was employed.²²⁴ This system was capable of operating at temperatures of 600°C and pressures up to 200 psig. The system consisted of three main sections:

(1) The feed system

(2) The reactor system

(3) The analytical system

4.3.1 The Feed System

The feed system allowed a constant regulated flow of n-octane and hydrogen, at the required ratio, to be delivered to the reactor. A schematic diagram of this section is shown in figure 4.2

The n-octane was delivered at a constant rate by means of a Labatron (LDP-20) precision metering pump, which is capable of operating at back-pressures of up to 50 atmospheres. The liquid n-octane feed was driven through a vapourisation unit maintained at approximately 250°C, well above the boiling point of n-octane (125-127°C), ensuring instant vapourisation of the feed. All metal tubing beyond this point was held at elevated temperatures (>150°C) to ensure that no n-octane, or reaction products, condensed out in the line. The hydrogen flow to the reactor was regulated by means of a calibrated mass flow control unit (position 1).

In addition to hydrogen, the feed system was also capable of delivering other gases such as air, helium and nitrogen. These gases were used at different stages of the catalyst activation as will be discussed. Nitrogen was also used to flush out the reactor after each reforming run.

4.3.2 The Reactor System

A diagram of the reactor system is shown in figure 4.3.

The reactor and bypass tubes, consisting of 20 cm lengths of 1/8" stainless steel tubing, were contained within a rectangular brass reactor block. This reactor block was contained within an insulated box along with the vapourisation unit. When the reactor was at reaction temperature, the temperature within the box remained constant at approximately 250 °C, thus ensuring that the vapourisation unit and all metal tubing needed no additional heating to avoid condensation of products.

Figure 4.3 The Reactor System

Figure 4.2 The Feed system

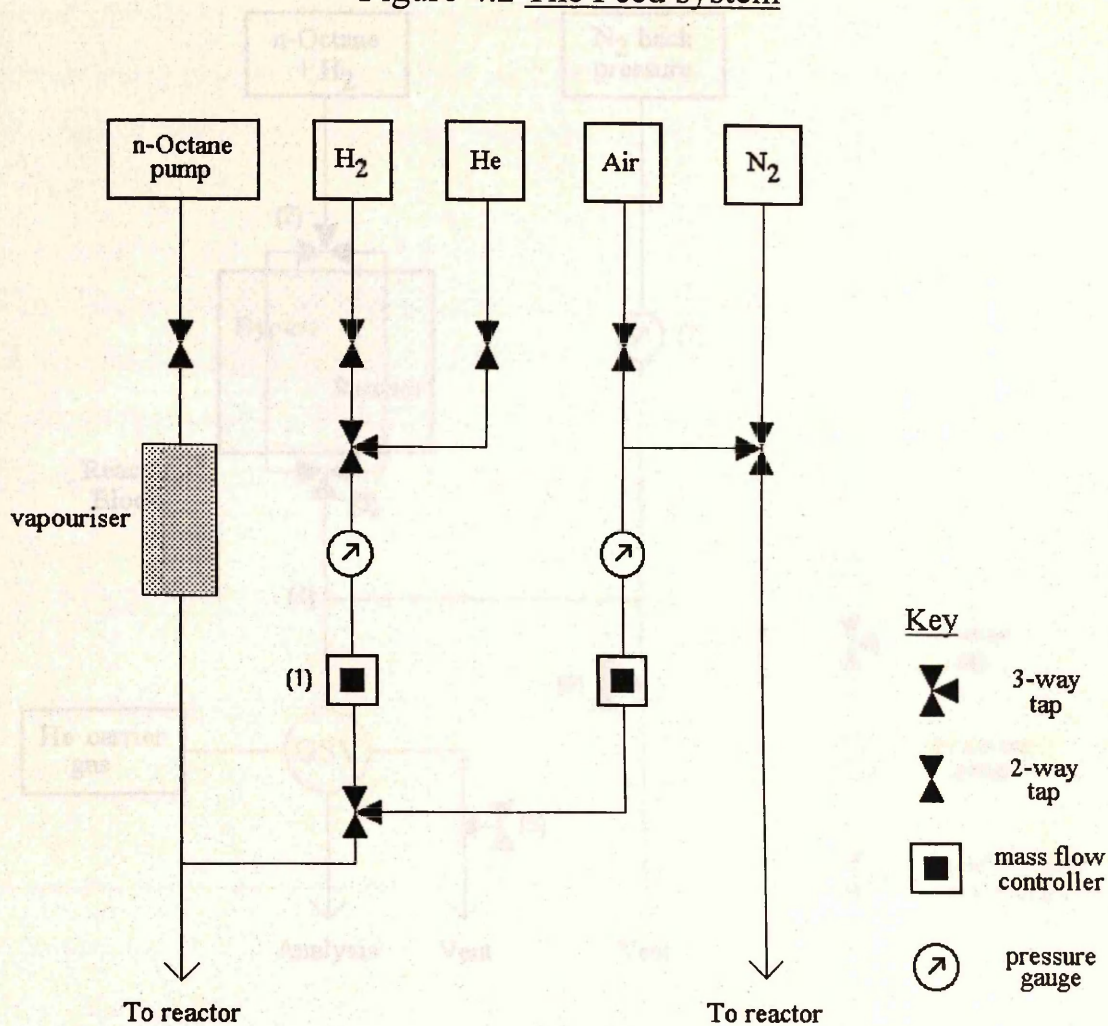
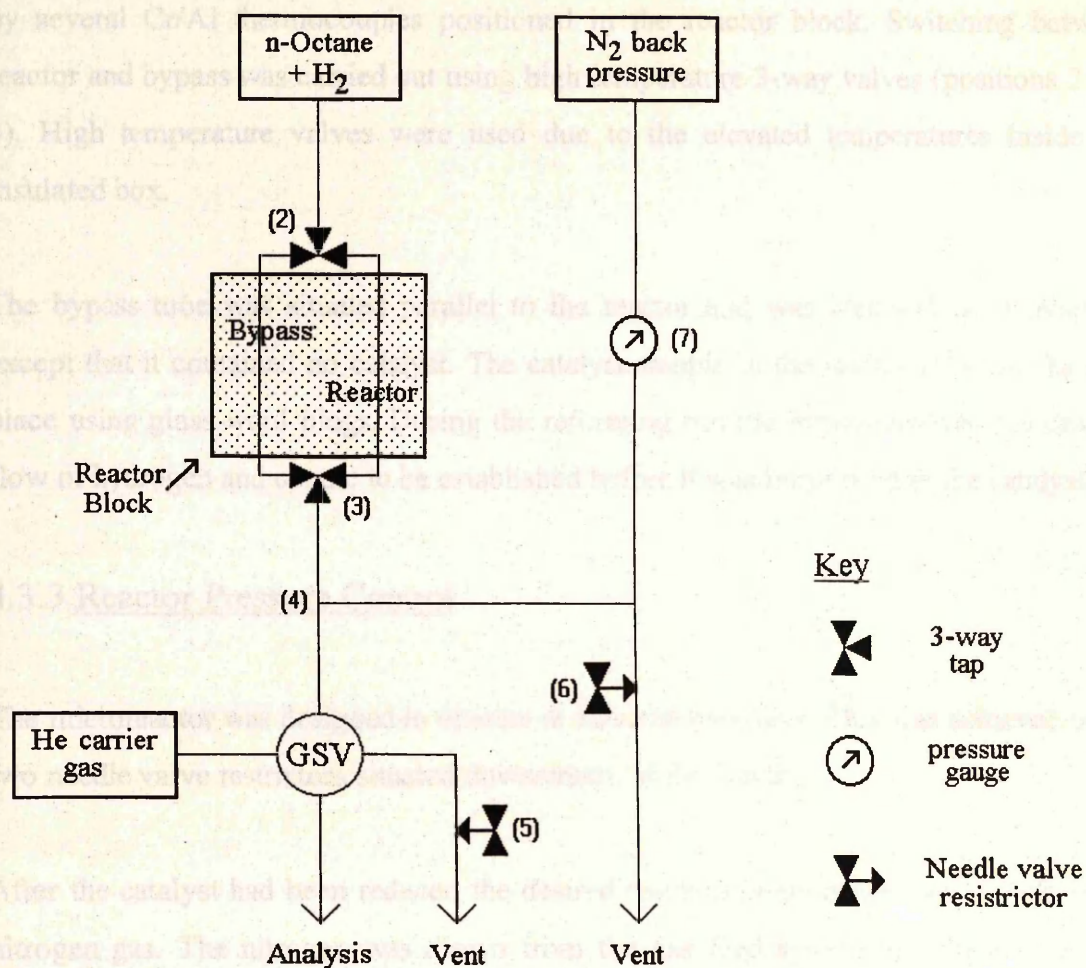


Figure 4.3 The Reactor System



The temperature of the reactor block was accurately controlled by means of an F.G.H. temperature programmer in conjunction with a 10A solid state relay and four 240W cartridge heaters. The temperature during a reforming run was monitored continuously by several Cr/Al thermocouples positioned in the reactor block. Switching between reactor and bypass was carried out using high temperature 3-way valves (positions 2 and 3). High temperature valves were used due to the elevated temperatures inside the insulated box.

The bypass tube was situated parallel to the reactor and was identical in all respects except that it contained no catalyst. The catalyst sample in the reactor tube was held in place using glass wool plugs. During the reforming run the bypass enabled the desired flow of hydrogen and octane to be established before it was introduced to the catalyst.

4.3.3 Reactor Pressure Control

The microreactor was designed to operate at elevated pressures. This was achieved using two needle valve restrictors situated downstream of the reactor.

After the catalyst had been reduced the desired reaction pressure was set initially using nitrogen gas. The nitrogen was drawn from the gas feed system described in section 4.3.1. and shown in figure 4.2. Having set the pressure at the desired level, hydrogen and gaseous n-octane were allowed to flow through the reactor. The gas stream eluting from the reactor was split into two fractions by a T junction (position 4). The nitrogen line was connected to the reactor system after this T junction and before one of the restrictors.

The restrictor at position (5) was set such that the total outflow through this needle valve was slightly less than total inflow of n-octane and hydrogen into the reactor. If this condition was met, and the restrictor at position (6) was opened sufficiently to prevent pressure buildup, then the reactor pressure remained constant when the feed gases were

introduced (inducing a corresponding decrease in the contribution of nitrogen to the absolute pressure) and nitrogen vented only via the restrictor at (6), i.e. no N₂ was present in the G.S.V.

Reactor pressure was monitored using a Budenberg gauge (0-300 psig, position (7)).

4.3.4 Gas Sampling

The gas stream from the reactor was sampled at regular intervals using an eight port high temperature gas sampling valve (G.S.V.). This GSV was situated inside an oven (Perkin Elmer F11) held at a constant temperature of 150°C, thus ensuring no hydrocarbon condensed out in the metal tubing. The two sample loops (2.00 ml) in use were also maintained at this temperature. The effluent gas was vented to the atmosphere. A schematic diagram of the gas sampling valve is shown in figure 4.4.

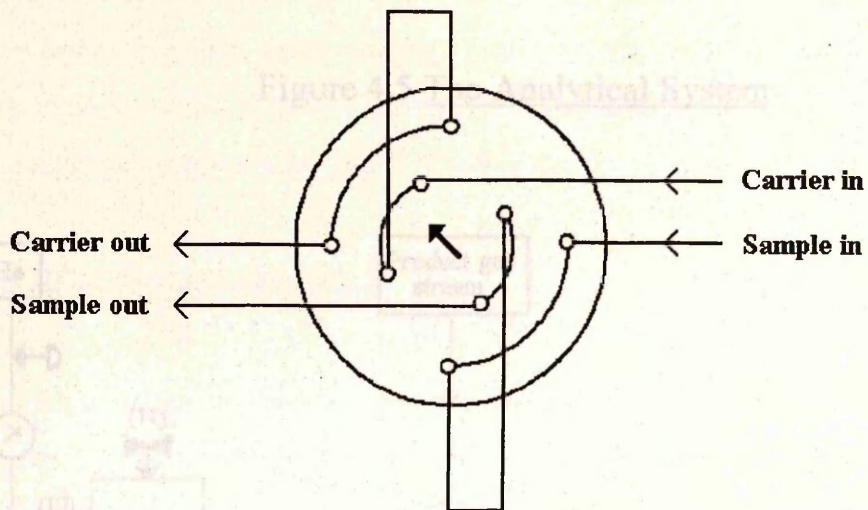
4.3.5 The Analytical System

A schematic diagram of the analytical system is shown in figure 4.5.

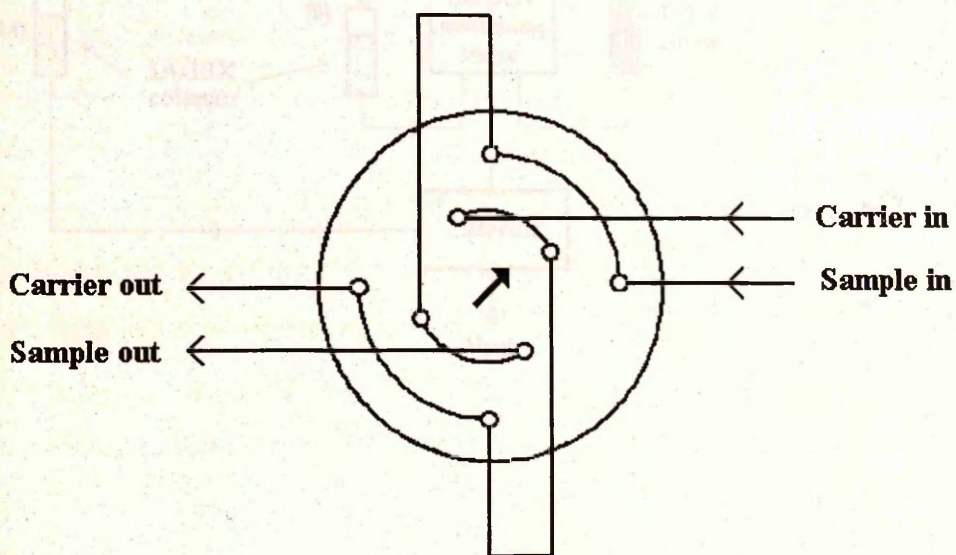
The reforming of n-octane produces a wide range of products from light aliphatic gases through medium alkanes (both normal and branched isomers) and cycloalkanes to aromatic species such as benzene. A quantitative separation of these products was required and the analytical system used was based upon a method established by I.C.I for the resolution of mixtures of alkanes (paraffins), cycloalkanes (naphthenes) and aromatics. The acronym PNA is used to refer to this system.

The PNA system involves first the separation of aromatic hydrocarbons from alkanes and cycloalkanes. These non-aromatic hydrocarbons are then resolved by a combination of 5A and 13X activated molecular sieves.

Figure 4.4 The Gas Sampling Valve

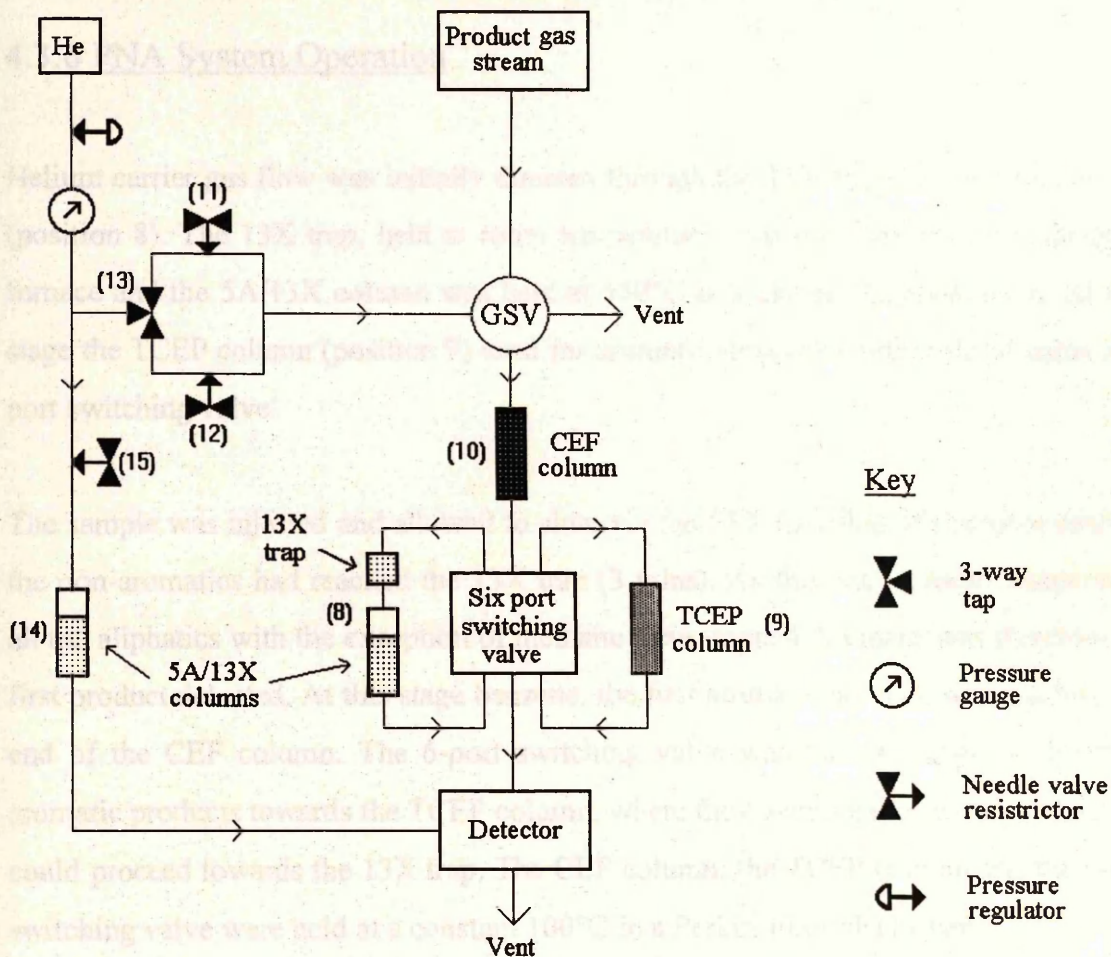


Position A



Position B

Figure 4.5 The Analytical System



Molecular sieves 5A and 13X are alumina silicate frameworks characterised by a uniform pore size distribution. Activated molecular sieves differ from other adsorbent types in that they only accept molecules or parts of molecules which fit within their micropores; that is they exhibit shape selectivity. Adsorbed molecules can subsequently be removed from the pores by heating. The most significant difference between 5A and 13X molecular sieves is pore size (5Å versus 13Å)

4.3.6 PNA System Operation

Helium carrier gas flow was initially directed through the 13X trap and 5A/13X column (position 8). The 13X trap, held at room temperature, was enclosed by a tubular glass furnace and the 5A/13X column was held at 150°C in a chromatographic oven. At this stage the TCEP column (position 9) used for aromatic separation was isolated using a 6-port switching valve.

The sample was injected and allowed to elute via the CEF (position 10) column until all the non-aromatics had reached the 13X trap (3 mins). As this was at room temperature all the aliphatics with the exception of methane were trapped. Methane was therefore the first product detected. At this stage benzene, the first aromatic product, was reaching the end of the CEF column. The 6-port switching valve was then switched to direct all aromatic products towards the TCEP column, where they were separated, before benzene could proceed towards the 13X trap. The CEF column, the TCEP column and the 6-port switching valve were held at a constant 100°C in a Perkin Elmer F11 oven.

Detection of the aromatics was complete within 35 minutes, during which time the non-aromatics were held in the 13X trap. Unfortunately separation of meta- and para-xylenes could not be achieved on the TCEP column. Figure 4.6 shows a typical chromatogram of aromatic reforming products.

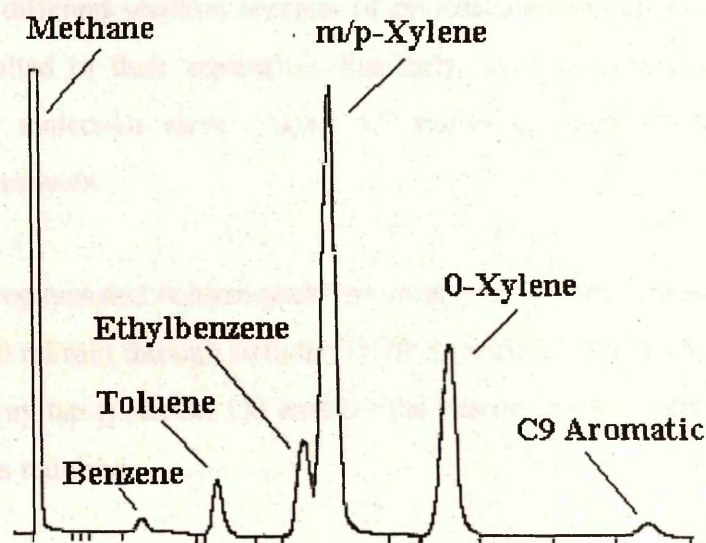
After the detection and measurement of aromatics was complete the 6-port valve was switched to allow the carrier gas to flow through the 5A/13X column. Both the 13X trap and 5A/13X column were held at their initial temperatures for a further 10 minutes allowing ethane to elute. Then the 13X trap was heated rapidly to 450°C (about 2 minutes) whilst the 5A/13X column was maintained at 150°C. After 15 minutes, when all the non-aromatics had been displaced onto the 5A/13X column, the 13X trap was cooled.

Figure 4.6 Typical chromatogram of methane and aromatic reformat products.

The 5A/13X column was then ramped at 1°/min to 400°C and held at this temperature until all the aliphatics had eluted. Raising the temperature at the end of the run allowed the adsorbed hydrocarbons to be removed irrespective of their boiling point or carbon number. The column was then cooled to 150°C and the 6-port valve was switched to allow the carrier gas to flow through the 5A/13X column. The flow rate was then set at 30 ml/min and the 6-port valve was switched to position 12. A 3-way tap was used to divert the carrier gas either to the detector or to a waste line.

Due to the different retention times of the various components, the flow rate was set at 30 ml/min for the first 10 minutes of the run. After 10 minutes the flow rate was increased to 40 ml/min for the remainder of the run. The reference flow was split into two streams, one to the detector (position 4) and the other to the waste line (position 12). The flow rate was then set at 30 ml/min and the 6-port valve was switched to position 11. The flow rate was then set at 30 ml/min and the 6-port valve was switched to position 11.

In order to avoid condensation of the sample in the transfer lines, the transfer lines and analytical sections of the system was maintained at a constant temperature. This was achieved by building the system into a water jacket. The water jacket was maintained at elevated temperatures to avoid cold spots within the line. All the components were



After the detection and measurement of aromatics was complete the 6-port valve was switched to allow the carrier gas to flow through the 5A/13X column. Both the 13X trap and 5A/13X column were held at their initial temperatures for a further 10 minutes allowing ethane to elute. Then the 13X trap was heated rapidly to 450°C (about 2 minutes) whilst the 5A/13X column was maintained at 150°C. After 15 minutes, when all the non-aromatics had been displaced onto the 5A/13X column, the 13X trap was cooled to room temperature.

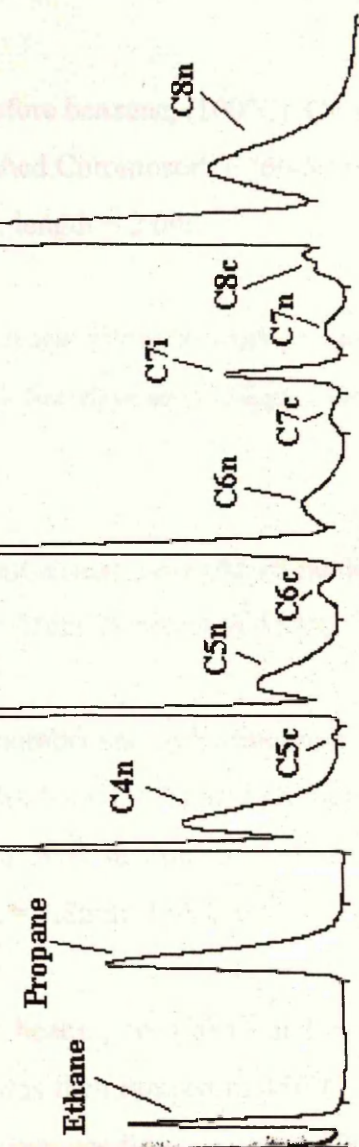
The 5A/13X column was then ramped at 3°/min to 400°C and held at this temperature until all the aliphatics had eluted. Raising the temperature at the optimum rate of 3°/min allowed the adsorbed hydrocarbons to be removed sequentially in order of increasing carbon number. The different sorption energies of cycloalkanes and alkanes on the 13X molecular sieve resulted in their separation. Similarly, iso and normal alkanes were resolved on the 5A molecular sieve. Figure 4.7 shows a typical chromatogram of aliphatic reforming products.

Due to the different regimes and column packings employed, needle valves were used to set the flow rate at 30 ml/min through both the TCEP (position 11) and 5A/13X columns (position 12). A 3-way tap (position 13) enabled the carrier gas to be directed through either needle valve as required.

The carrier gas flow rate through the 5A/13X column decreased with increasing temperature. This results in a rising baseline in the non-aromatic chromatogram. To attenuate this, the reference flow was diverted through a second identical 5A/13X column (position 14). Initial flow through this second 5A/13X column was set using a further needle valve (position 15).

In order to avoid condensation of gaseous hydrocarbons, all metal tubing in the reactor and analytical sections of the system was maintained at elevated temperatures. This was achieved by building the system inside a series of ovens. These were maintained at elevated temperatures to avoid cold spots within the line. All tubing situated outside

Figure 4.7 Typical chromatogram of aliphatic reforming products



these ovens was maintained at approximately 160°C by means of electrothermal heating tape, lagged with high temperature insulating tape, again to avoid cold spots and any condensation within the line. The temperature of the heating tape was maintained using Variac transformers.

4.3.7 Summary of PNA Columns

1. CEF Allows elution of aliphatics $<C_{10}$ before benzene, (100°C). Cyano ethyl formamide, 22.5 %w/w on acid washed Chromosorb P (60-80 mesh).
Stainless steel column i.d. = 1.8mm, length = 2.0m
2. TCEP Aromatics separation (100°C). Tris cyano ethoxy propane, 5 %w/w on acid washed Chromosorb P (60-80 mesh). Stainless steel column, i.d. = 2.4mm, length = 3.0m
3. 13X trap Entrapment of non-aromatics, 13X molecular sieve (60-80 mesh). Stainless steel column, i.d. = 1.8mm, length = 15cm. Ambient to 450°C
4. 5A/13X Separation of aliphatics by carbon number and by hydrocarbon type. 5A molecular sieve section (60-80 mesh), length = 30cm. 13X molecular sieve section (60-80 mesh), length = 90cm. Both sections contained within one length of stainless steel column, i.d. = 1.8mm. 150-450°C @ 3°/minute.

Columns 3 and 4 were initially activated by heating to 100°C and holding at this temperature for half an hour. The temperature was then ramped to 450°C at 3°/min and held at this temperature for a further 4 hours. Carrier gas flow was set at 30ml/min.

4.3.8 Hydrocarbon Detection and Calibration

Table 4.2 Chromatographic Retention Times

A thermal conductivity detector and a Shimadzu Chromatopac integrator were used in the detection, measurement and display of the chromatographic data.

The retention times and response factors of all potential reaction products were determined by injecting a known volume of each potential product into the PNA system. By varying the volume a corresponding range of peak areas was obtained. Therefore all retention times and response factors represent averaged values. Table 4.2 shows the retention times and response factors for all the relevant compounds.

4.3.9 Materials

(1) n-Octane

The n-octane used throughout the course of this study was supplied by the Aldrich chemical company. The purity, as measured by gas chromatography was > 99%. It was used without further purification.

(2) Hydrogen

Cylinder hydrogen (B.O.C. Ltd.) was used without further purification.

(3) Air

Cylinder air (B.O.C. Ltd.) was used without further purification.

(4) Nitrogen

Cylinder nitrogen (B.O.C. Ltd.) was used without further purification.

(5) Helium

Cylinder helium (B.O.C. Ltd.) was used without further purification.

**Table 4.2 Chromatographic Retention Times
and Response Factors**

<u>Product</u>	<u>Retention Time</u> (Minutes)	<u>Response Factor</u> (Area units x 10 ⁻¹² mol ⁻¹)
Methane	1.8	6.97
Ethane	3.4	4.81
Propane	26.7	3.59
i-Butane	43.4	2.83
n-Butane	46.9	2.62
c-Pentane	59.0	2.47
i-Pentane	62.6	2.35
n-Pentane	66.6	2.33
C ₆ Cycloalkane	76.8	2.29
i-Hexane	80.6	2.20
n-Hexane	86.4	2.05
C ₇ Cycloalkane	92.9	1.85
i-Heptane	97.4	1.97
n-Heptane	101.1	1.70
C ₈ Cycloalkane	108.5	1.60
i-Octane	113.3	1.62
n-Octane	123.6	1.49
Benzene	8.2	2.40
Toluene	11.8	2.20
Ethylbenzene	15.9	1.88
o/m-Xylene	17.7	1.81
p-Xylene	22.9	1.89
C9 Aromatics	32.5	1.65

4.3.10 Activation of Catalysts

All the catalysts tested in these studies were activated *in situ* in the microreactor using a standard procedure. This consisted of 3 steps:

(1) Calcination

Heating to 400°C at 5°/min in flowing air (60ml/min). Held at 400°C for 4 hours then cooled to room temperature.

(2) Flushing

Switch to He flow (60ml/min). Held for 1 hour at room temperature.

(3) Reduction

Switch to hydrogen flow (60ml/min) and heated to 400°C at 5°/min. Held at 400°C for 2 hours.

Prior to removal from the reactor all catalyst samples were passified in a 1% air/helium mix..

4.3.11 Catalyst testing

All the reforming experiments carried out in this work were performed under a standard set of conditions. These were as follows:

H_2 / n-octane molar ratio = 6/1

Temperature = 510 °C

Pressure = 110 psig

Weight hourly space velocity = 2 h⁻¹

4.3.12 Treatment of Results

The yield, conversion and selectivity values quoted throughout this work are defined as follows:-

Yield:- the amount of a given reaction product related to the amount of starting component, expressed as a percentage. Thus, for a product i , the yield is expressed by the relationship:

$$\%yield = \frac{n_i(M_i)}{N(x)} \times \frac{100}{1}$$

where: n_i = the number of carbon atoms in product species i .

M_i = the number of moles of product species i .

N = the number of carbon atoms in the reactant molecule.

x = the number of moles of hydrocarbon reactant.

Conversion: the amount of a given reaction component transformed into products related to the initial quantity of that same component, expressed as a percentage. This was obtained by summing all the individual product yields. Thus for j product species:

$$\%conversion = \frac{\sum_{i=1}^{j} n_i(M_i)}{N(x)} \times \frac{100}{1}$$

Selectivity: the amount of a given product related to the amount of starting material converted, expressed as a percentage. Selectivity values for individual product species are calculated by dividing the appropriate yield values by conversion. Selectivity is therefore expressed by the relationship:

$$\%selectivity = \frac{n_i(M_i)}{\sum_{i=1}^{i=j} n_i(M_i)} \times \frac{100}{1}$$

The molar quantity of each individual hydrocarbon species present in a fixed volume of the product gas stream was determined by gas chromatography as described in section 3.3.8. The post reactor gas stream was sampled at regular intervals by a gas sampling valve maintained at 150°C; the precision gas sampling loops each had a volume of 2.00 ml. The number of moles of hydrocarbon reactant x is defined as the quantity of n-octane that would have been present in the fixed volume sample loops had no reaction occurred. Knowing the molar ratios of hydrogen to hydrocarbon and the values of pressure, temperature and volume the value of x could be readily calculated.

The selectivities to the four major reforming reactions were also calculated. For this purpose the selectivities were defined as follows:

- (a) Aromatisation- defined as the sum of the selectivities for all aromatic species.
- (b) Isomerisation- defined as the sum of the selectivities of iso-heptane and iso-octane.
- (c) Hydrocracking- defined as the sum of selectivities of iso-butane, iso-pentane, and iso-hexane.
- (d) Hydrogenolysis- defined as the selectivity for methane.

In this way any changes in the selectivities to the major reforming reactions were followed throughout a reforming run.

4.4 Surface Carbon Analysis

Samples of the spent catalyst were analysed for carbonaceous residue content after use in reforming using a combustion technique. The carbonaceous residues on each catalyst were converted to carbon dioxide and water by pyrolysis in an oxygen rich atmosphere. A quantitative measure of carbon dioxide production was provided by on-line analysis in a calibrated gas chromatogram. The volume of carbon dioxide produced was used to determine the % weight of carbon present on each catalyst.

4.5 Electron microscopy

4.5.1 Microscope operation

The microscope employed in this study was a TOPCON 002B instrument in which the EDX system LINK 2000QX was installed. The microscope was operated at 200kV with an improved LaB₆ filament. The energy resolution of the EDX system was 138eV at 5.9 keV.

TEM specimens were prepared by placing a drop of ethanol solution, containing the ground catalyst powder in suspension, onto a carbon film coated copper grid. HREM studies were performed prior to diffraction or EDX to minimise the specimen damage and/or contamination. MBED patterns and EDX spectra were obtained from individual particles by focusing the electron probe onto the particle under examination. The minimum probe diameter obtainable was 2 nm. The collection time for EDX spectra was typically 100 seconds. During collection the beam was sometimes momentarily spread (under or overfocused) to obtain an image of the particle and relocated to compensate for

any specimen drift. The sensitivity of the EDX system was about 500-800 platinum atoms, or between 2-3 nm particle size.

A double tilt ($\pm 10^\circ$) specimen stage was used to obtain zone-axis microbeam diffraction patterns for particles. Beam tilt was sometimes used for final precise alignment. The MBED pattern for platinum, the elemental identity of which was verified by EDX analysis, was used as an in-situ standard for calibration of the camera length. All the MBED patterns were recorded at the same camera length (11 cm) and are printed in the text at the same optical enlargement.

The combination of MBED and quantitative EDX analysis was used to identify the phases present in the bi and multimetallic catalysts studied. Tables 4.5.1 to 4.5.5 list all the relevant crystalline phases and some of their crystallographic properties.

4.5.2 Quantitative EDX analysis.

For quantitative EDX analysis, generally:

$$\frac{C_\alpha}{C_\beta} = \frac{k_\alpha}{k_\beta} \times \frac{I_\alpha}{I_\beta}$$

where $C_\alpha (C_\beta)$ = weight percent of element $\alpha (\beta)$

$k_\alpha (k_\beta)$ = elemental sensitivity factor of $\alpha (\beta)$

$I_\alpha (I_\beta)$ = EDX intensity of $\alpha (\beta)$

Or alternatively:

$$\frac{C_\alpha}{C_\beta} = \frac{k_\alpha}{k_\beta} \times \frac{\text{at. wt. } \beta}{\text{at. wt. } \alpha} \times \frac{I_\alpha}{I_\beta}$$

where $C_\alpha (C_\beta)$ = atomic percent of element $\alpha (\beta)$

The elemental sensitivity factors (k factors) used were those supplied with the LINK Pentafet system for total intensities of K, L and M lines:

$$K_{total} = (K_{\alpha_1} + K_{\alpha_2} + K_{\beta_1})$$

$$L_{total} = (L_{\alpha_1} + L_{\beta_1})$$

$$M_{total} = (M_{\alpha_1} + M_{\beta_2})$$

The k factors relevant to this study are as follows:

$$k_{Pt_{L_{total}}} = 2.398$$

$$k_{Pt_{M_{total}}} = 1.563$$

$$k_{Ir_{L_{total}}} = 2.355$$

$$k_{Ir_{M_{total}}} = 1.563$$

$$k_{Ge_{K_{total}}} = 1.543$$

$$k_{Ge_{L_{total}}} = 2.398$$

$$k_{Sn_{L_{total}}} = 1.682$$

$$k_{Ni_{K_{total}}} = 1.146$$

$$k_{Ni_{L_{total}}} = 5.760$$

$$k_{Ru_{L_{total}}} = 1.604$$

The following calculations were used to obtain atomic percent ratios based on the particular choice of X-ray lines employed in the quantitative analysis.

1). Platinum-Germanium Due to the overlap of the platinum L_{β_1} (11.068 keV) and the germanium K_{β_1} (10.982 keV) lines the atomic percentage ratio in this system was based on the intensities of Pt L_α and Ge K_α lines. The relative intensities of the K lines of germanium are as follows: K_{α_1} (9.885 keV) 100, K_{α_2} (9.854 keV) 50, K_{β_1} (10.981 keV) 14. The relative intensities of the L lines for platinum are as follows: L_{α_1} (9.441 keV) 100, L_{β_1} (11.068 keV) 54. Therefore the k factor for the Ge K_α line is:

$$(100 + 50 + 14)/(100 + 50) \times 1.543 = 1.687,$$

and for the Pt L_{α_1} is:

$$(100 + 54)/100 \times 2.398 = 3.693.$$

The atomic percent ratios based on the ratio of Pt L_{α_1} and Ge K_{α} are therefore given by:

$$\frac{Pt}{Ge} = \frac{3.693}{1.687} \times \frac{72.59}{195.08} \times \frac{I_{Pt_{L_{\alpha_1}}}}{I_{Ge_{K_{\alpha}}}} = 0.81 \frac{I_{Pt_{L_{\alpha_1}}}}{I_{Ge_{K_{\alpha}}}}$$

Alternatively the Pt_M line can be used which, again using $Ge_{K_{\alpha}}$, results in the following relationship:

$$\frac{Pt}{Ge} = 0.344 \frac{I_{Pt_M}}{I_{Ge_{K_{\alpha}}}}$$

2) Platinum - Tin In this case there is no overlap of X-ray intensity. Using Pt_L ($Pt_{L_{\alpha_1} + L_{\beta_1}}$) and Sn_L ($Sn_{L_{\alpha_1}} - 3.444\text{keV}$) and following the same procedure as outlined above we obtain:

$$\frac{Pt}{Sn} = 0.87 \frac{I_{Pt_L}}{I_{Sn_L}}$$

3) Platinum - Iridium Due to the close proximity of these metals in the periodic table there is considerable overlap of X-ray lines. The M lines (Pt_M 2.05 keV, Ir_M 1.98 keV) are completely unresolved and there is also considerable overlap of the L_{α_1} lines ($Pt_{L_{\alpha_1}}$ 9.441 keV, $Ir_{L_{\alpha_1}}$ 9.137 keV). The $Ir_{L_{\alpha_1}}$ is also somewhat obscured by its proximity to the large $Cu_{K_{\beta}}$ systems peak (8.907 keV). Approximate quantitative analysis can be

performed on the L_{β_1} peaks ($Pt_{L_{\beta_1}}$ 11.069 keV, $Ir_{L_{\beta_1}}$ 10.706 keV) although the low intensities of these lines and a certain degree of overlap lowers the accuracy of the results obtained. The k factors are sufficiently close ($k_{Pt_L} = 2,398$, $k_{Ir_L} = 2.355$) to allow atomic ratios to be estimated directly from the intensity data.

4) Platinum - Iridium - Germanium In this trimetallic system the $Pt_{L_{\beta_1}}$ and $Ir_{L_{\beta_1}}$ lines were first used to obtain a value for Pt/Ir, although in this case the accuracy of this method is further decreased by overlap with the $Ge_{K_{\beta_1}}$ line at 10.981 keV. The concentration of Ge was then related to Pt/Ir using the sum of the $Pt_M + Ir_M$ lines and the $Ge_{K_{\alpha}}$ line. Therefore:

$$\frac{Pt + Ir}{Ge} = 0.35 \frac{I_{Pt_M + Ir_M}}{I_{Ge_{K_{\alpha}}}}$$

5) Nickel - Germanium In this case the nickel K ($Ni_{K_{\alpha}}$ - 7.472 keV, K_{β} - 8.265 keV) and germanium K lines were used. Therefore:

$$\frac{Ni}{Ge} = 0.919 \frac{I_{Ni_K}}{I_{Ge_K}}$$

6) Ruthenium - Germanium Here the Ru_L ($Ru_{L_{\alpha_1}}$ - 2.558 keV) lines and the Ge_K lines were used. Therefore:

$$\frac{Ru}{Ge} = 0.747 \frac{I_{Ru_L}}{I_{Ge_K}}$$

Table 4.5.1 Crystallographic information for the Pt - Ge system

Formula	Crystal structure	Lattice constant (Å)			Space group
		a	b	c	
Pt	Fcc	3.9231			<i>Fm3m</i>
Pt ₃ Ge	Monoclinic *	7.93	7.67	5.520	<i>C2/m</i>
Pt ₂ Ge	Hexagonal	6.68		3.53	<i>P321</i>
Pt ₃ Ge ₂	Orthorhombic	7.544	3.432	12.326	<i>Amma</i>
PtGe	Orthorhombic	6.088	5.733	3.701	<i>Pbnm</i>
Pt ₂ Ge ₃	Orthorhombic	16.430	3.378	6.22	<i>Pnma</i>
PtGe ₂	Orthorhombic	6.185	5.765	2.908	<i>Pnnm</i>
Ge	Cubic	5.6576			<i>Fd3m</i>

$$* \beta = 44.72^\circ$$

Table 4.5.2 Crystallographic information for the Pt-Sn system

Formula	Crystal structure	Lattice constant (Å)			Space group
		a	b	c	
Pt	Fcc	3.9231			<i>Fm3m</i>
Pt ₃ Sn	Fcc (Cu ₃ Au type)	4.0005			
PtSn	Hcp (NiAs type)	4.100		5.432	<i>P6₃/mmc</i>
Pt ₂ Sn ₃	Hcp	4.337		12.960	<i>P6₃/mmc</i>
PtSn ₂	Fcc (CaF ₂ type)	6.425			<i>Fm3m</i>
PtSn ₄	Orthorhombic	6.362	6.393	11.311	<i>C_{2v}</i>
Sn	Cubic	6.489			<i>Fd3M</i>

Table 4.5.3 Crystallographic information for the Ir-Ge system

Formula	Crystal structure	Lattice constant (Å)			Space group
		a	b	c	
Ir	Fcc	3.8394			<i>Fm3m</i>
IrGe	Orthorhombic	6.2811	5.611	3.4895	<i>Pbnm</i>
Ir ₄ Ge ₅	Tetragonal	5.615		18.308	<i>P4c2</i>
Ir ₃ Ge ₇	Cubic	8.735			<i>Im3m</i>
Ge	Cubic	5.6576			<i>Pd3m</i>

Table 4.5.4 Crystallographic information for the Ni-Ge system

Formula	Crystal structure	Lattice constant (Å)			Space group
		a	b	c	
Ni	Fcc	3.5238			<i>Fm3m</i>
Ni ₅ Ge ₂	Hexagonal	6.82		12.39	[P]
Ni ₂ Ge	Orthorhombic	5.11	3.83	7.26	
Ni ₅ Ge ₃	Monoclinic *	11.68	6.73	6.36	
Ni ₁₉ Ge ₁₂	Hexagonal	6.72		10.05	
NiGe	Orthorhombic	5.811	5.381	3.428	<i>Pbnm</i>
Ge	Cubic	5.65769			<i>Pd3m</i>

$$* \beta = 52.10^\circ$$

Chapter Five: Results

Table 4.5.5 Crystallographic information for the Ru-Ge system

Formula	Crystal structure	Lattice constant (Å)			Space group
		a	b	c	
Ru	Hcp	2.7058		4.2819	<i>P63/mmc</i>
RuGe	Cubic	4.846			<i>P213</i>
Ru ₂ Ge ₃	Orthorhombic	11.436	9.238	5.716	
Ge	Cubic	5.6576			<i>Pd3m</i>

Chapter Five: Results

In the following chapter each of the catalysts will be treated in turn. The results of TEM studies on each system will be followed by the reforming data obtained from that catalyst. Due to the large volume of data contained in the reforming results, the results obtained for each catalysts will be compared and contrasted with the results obtained for the basic Pt/Al₂O₃ (H₂PtCl₆ prepared) catalysts. This is done in order to highlight the influence exerted by the various promoters on the corresponding catalytic properties.

For simplicity each of the catalysts will be referred to by simply stating the supported metals that it contained, e.g., 0.3 wt% Pt - 0.3 wt% Sn/Al₂O₃ will be referred to as Pt-Sn or Pt-Sn/Al₂O₃ (Please note that this nomenclature does not define the oxidation state in which these species were found in the working catalysts). In the case of catalysts that contained the same components but at different loadings, the catalyst with a loading not equal to 0.3 wt% will be specified by noting the loading used, e.g., 0.3 wt% Pt - 0.3 wt% Ir - 0.3 wt% Ge/Al₂O₃ and 0.3 wt% Pt - 0.3 wt% Ir - 0.03 wt% Ge will be distinguished as Pt-Ir-Ge and Pt-Ir-0.03 Ge respectively.

One of the major sources of error in the reforming data presented was in the calculation of peak areas from chromatographic traces. This is especially true in the case of n-alkanes. For these products the uncertainty may be as great as $\pm 0.5\%$.

5.1 0.3 wt% Pt/Al₂O₃

5.1.A. TEM observations

A typical image of this catalyst obtained after calcination and reduction is shown in plate 1. No metal particles were observed in most regions of this catalysts that were analysed. This suggests that the average particle size of the metal particles was too low to allow them to be distinguished from the background support, i.e., $\leq 1\text{nm}$ in diameter. This

image is also typical of the $\gamma\text{-Al}_2\text{O}_3$ support used in all the catalysts tested in this work. The alumina crystallites were randomly oriented and showed a range of contrast between the different orientations.

It was sometimes difficult to determine whether an area of high contrast was caused by a metal particle or an alumina crystallite orientated to give strong diffraction. Provided the area in question was large enough, EDX analysis provided an effective method of distinguishing between the two. It was also observed that whilst both highly diffracting alumina crystallites and metal particles > 2 nm in diameter were usually imaged with well defined borders, the former tended to be highly faceted while the metal particles appeared more rounded in nature (see plate 58 for an example).

A small number of metallic particles in the size range 2-7 nm were observed at this stage however. An example is given in plate 2. This particle was approximately 6 nm in diameter. The lattice fringes visible in the image correspond to the 0.227 nm $\{111\}$ fringes of crystalline platinum. The EDX spectrum obtained from this particle (inset) contained platinum peaks along with aluminum and oxygen peaks from the alumina support. The large Cu peaks originate from the copper grids used to support the specimen. These larger particles were very infrequently observed at this stage and must only have represented a small percentage of the total metal content.

After use in the reforming of n-octane for 144 hours, however, considerable sintering of the platinum component was seen to have occurred. This was manifest in an increase in both the number density of particles observed and also in an increase in their average particle size, with the largest particles being in the 20-30 nm size range. An example of a particle formed at this stage is given in plate 3. This particle was approximately 15 nm in diameter and again the EDX spectrum obtained confirmed that it was platinum. The corresponding MBED pattern obtained (inset) was indexed as the (110) pattern of the fcc metal. Again, the lattice fringes visible in this image correspond to the $\{111\}$ 0.227 nm plane of platinum.

Another example of a particle observed at this stage is given in plate 4. This particle was approximately 20 nm in diameter and again the EDX spectrum obtained confirmed its identity as platinum. In this case the MBED pattern obtained was indexed as the (121) pattern of crystalline platinum. These two diffraction patterns represent the most frequently observed particle orientations observed in the catalysts containing fcc metals. The only other orientation found in significant numbers was the (100) orientation.

It must be stated that these relatively large 10-30 nm sized particles were relatively infrequently observed. The majority of the particles observed were below 5 nm in diameter and it is likely that a significant proportion of the total metal content of this catalysts remained in the form of nanometer sized particles even after this length of time on line.

5.1.B. n-Octane reforming.

The reforming experiments on all the catalysts studied in this work were carried out under a specific set of reaction conditions as detailed in section 4.3.11. The yield and selectivity values quoted were calculated as defined in section 4.3.12.

The % yield of each individual product species, as defined in section 4.3.12, is presented in table 5.1.1 as a function of time on line and plotted in figures 5.1.1 to 5.1.6.

The yields of methane, ethane, propane, i-butane and n-butane over this catalysts are plotted in figure 5.1.1. The yield of methane over this catalyst was observed to undergo an initial period of rapid decline before reaching a relatively stable value of slightly over 4%. The yields of ethane, propane, i-butane and n-butane in comparison were found to decrease slowly but continuously throughout the entire length of the run. The relative

yields of these products decreased in the order (the values quoted are the initial yields obtained after 1 hour on line):

propane (7.0%) > n-butane (5.9%) > i-butane (3.9%) > ethane (3.4%)

The trend in the order of yields of these products was also observed for a large number of the catalysts studied. However, as will be shown, the yield of methane was more variable.

The yields of cycloalkanes over the Pt/Al₂O₃ are plotted in figure 5.1.2. It was observed that yields of these products were relatively low. In this case the yields of cyclopentane and C₆ species remained relatively constant, at 0.1-0.2% and 0.5-0.6% respectively, whilst the yields of cyclic C₇ and C₈ species were observed to increase with time on line. The rate of increase was greatest in the initial stages of the run with the yields of each product increasing from approximately 0.2% and 0.3% respectively to 0.95 and 2.1%. Again these trends and the relative amounts of each product produced will be found to be quite similar on a number of the catalysts studied.

The yields of i-alkane products over this catalyst are plotted in figure 5.1.3. As with the yield of cyclic C₈ products, the yield of i-octane was observed to increase very significantly with time on line, from 5.3% to 23%. In contrast, the yields of i-pentane (between 5 and 7%), i-hexane (between 5 and 6%) and i-heptane (between 1-2%) were observed to remain relatively constant throughout the run. The yields of i-pentane and i-hexane did, however, decrease slightly with time on line.

The yields of n-alkanes over this catalysts are plotted in figure 5.1.4. The yields of n-pentane (~ 4%) and n-hexane (~2-3%) remained relative stable throughout the run whilst the yield of n-heptane increased slightly in the initial stages, from approximately 0.35 to 1.3%. Again these are trends which were also observed for a number of the catalysts studied.

Figure 5.1.4 is useful in highlighting the nature of the trendlines used to fit the reforming data in all the graphs presented in this work. These trendlines were produced by polynomial expressions used to obtain a curve that best fitted the data series. However, small fluctuations in the slope or gradient of these lines, especially for low yield products, should not be taken as indicative of a corresponding variation in the product yield. These lines are intended to highlight only the major trends and to make the graphs easier to interpret. It will also be noted that the plotted data for n-alkanes show rather large fluctuations. This is an experimental artifact due to the low, broad nature of n-alkane peaks in the chromatographic trace (see figure 4.7). This makes the measurement of peak areas rather inaccurate.

The yields of aromatic products over the $\text{Pt}/\text{Al}_2\text{O}_3$ catalysts are plotted in figure 5.1.5. It is clear that the major aromatic species produced were xylenes. Unfortunately, however, the TCEP column (section 4.3.6) used to separate these species could not resolve meta and para xylenes. Therefore the data presented for this and all subsequent catalysts represents the sum of the yields for these two species. The aromatic species produced, in order of decreasing yield, were as follows (again the yields quoted are the initial yields):

m/p-xylene (19.4%) > o-xylene (10.2%) > ethylbenzene (8.8%)
> toluene (3.7%) > benzene (1.3%), C_9 aromatics (1.0%)

The yields of the main aromatic species were observed to decrease most rapidly during the initial stages of the run. This was followed by a period of more gradual yield loss.

The total conversion of n-octane, as defined in section 4.3.12, is also presented in table 5.1.1 and is plotted versus time on line in figure 5.1.6. The conversion was initially very high under the conditions employed in this study (98.4%). However, the level of conversion was found to decrease continuously during the length of the run. As with the

Plate 1
yields of aromatics and methane, the rate of deactivation was found to be more severe initially and gradually tailed off as the run progressed.

The selectivities to the four main reforming reactions, as defined in section 4.3.12, are presented versus time on line in table 5.1.2 and plotted in figure 5.1.7. The selectivities to hydrocracking and hydrogenolysis (after the initial decrease) were found to remain relatively constant throughout the run (15-17% and 4-5% respectively) whilst the selectivity to aromatisation was found to decrease. This decrease was mirrored by a corresponding increase in the yield of isomerisation. Indeed, after 144 hours on line the isomerisation reaction was found to be the main reforming process occurring using this catalyst. Again, the rate of increase or decrease of these reactions was observed to be greatest in the initial stages of the run followed by a period of more gradual change.

Plate 1

10 nm

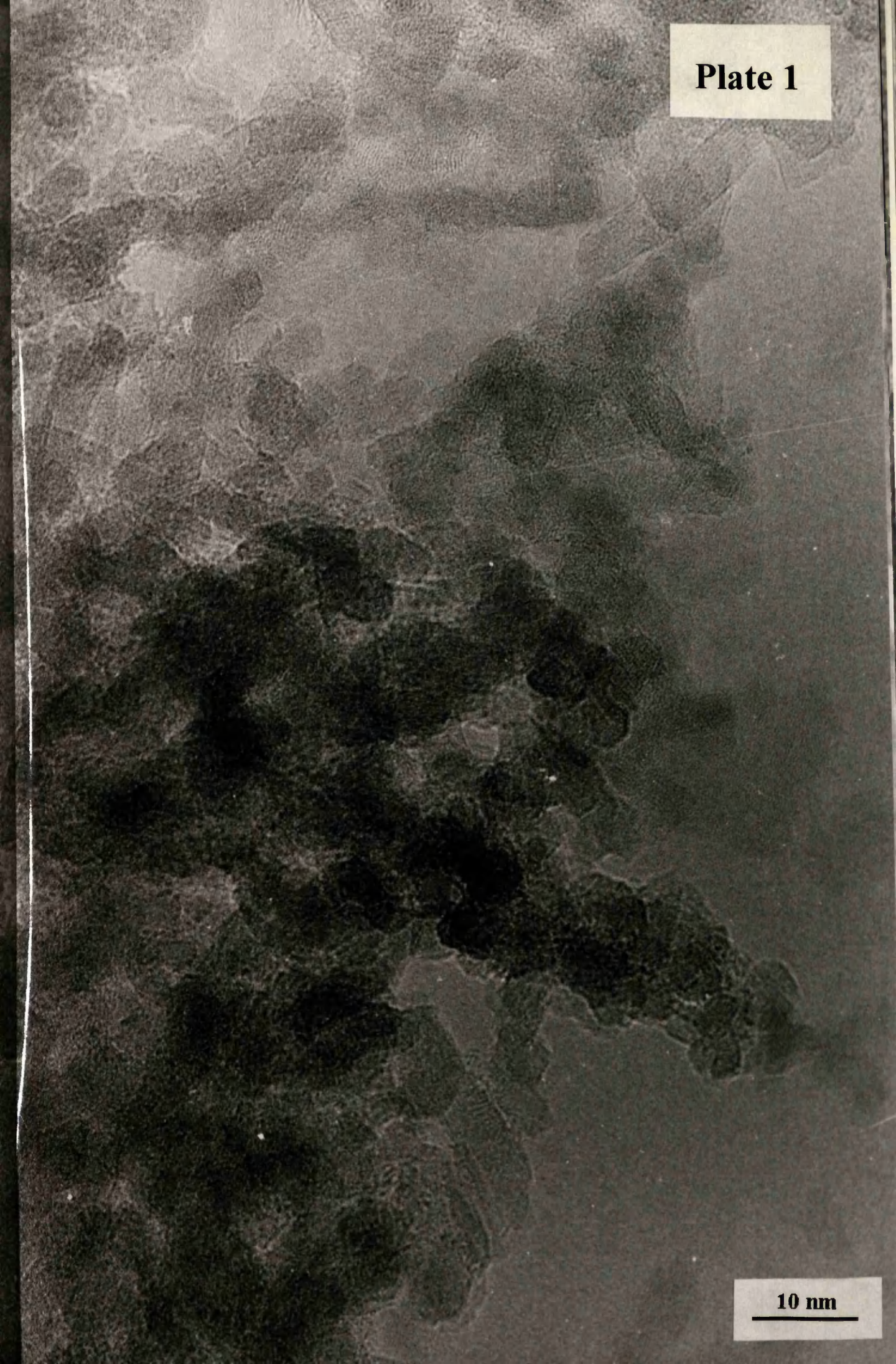
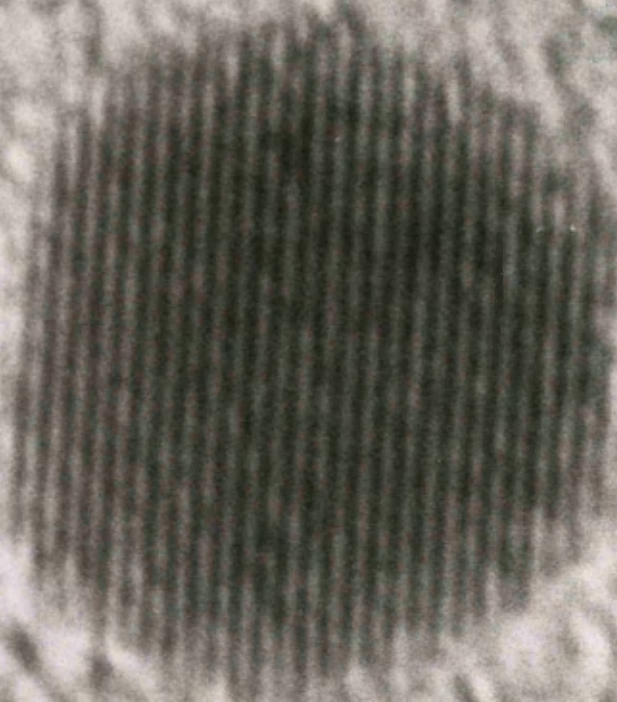
This is a high-magnification electron micrograph showing a complex, dark, and irregularly shaped biological structure, possibly a cell or a large protein complex, against a lighter, textured background. The structure has a mottled appearance with varying shades of gray and black, suggesting different internal components or densities. A scale bar in the bottom right corner indicates a length of 10 nm.

Plate 2



2 nm

Horizontal Scale - 0-20 keV

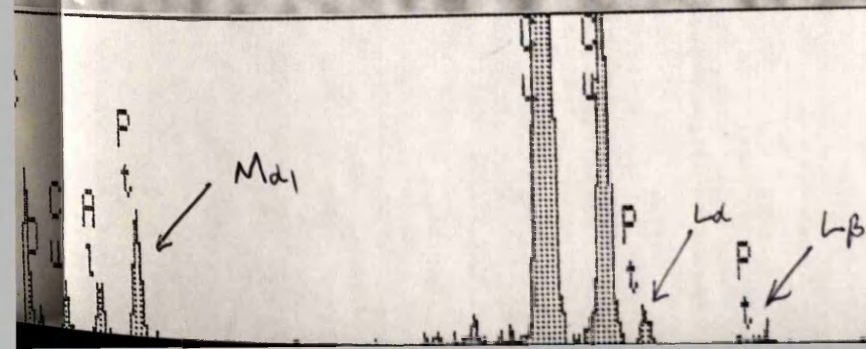
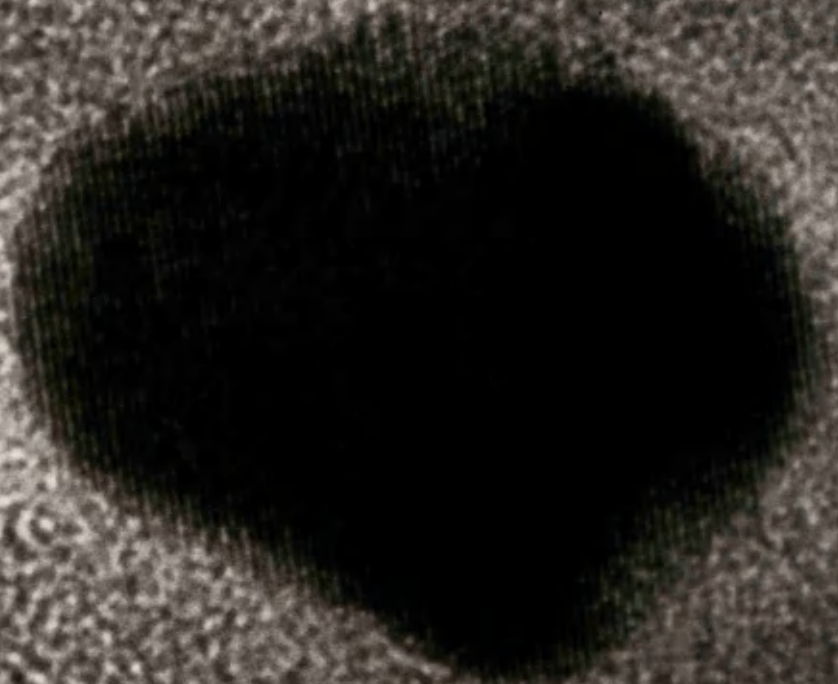


Plate 3



3 nm

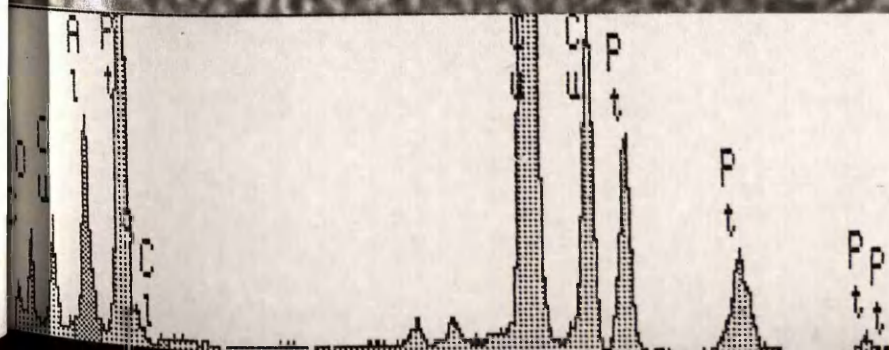


Plate 4

5 nm

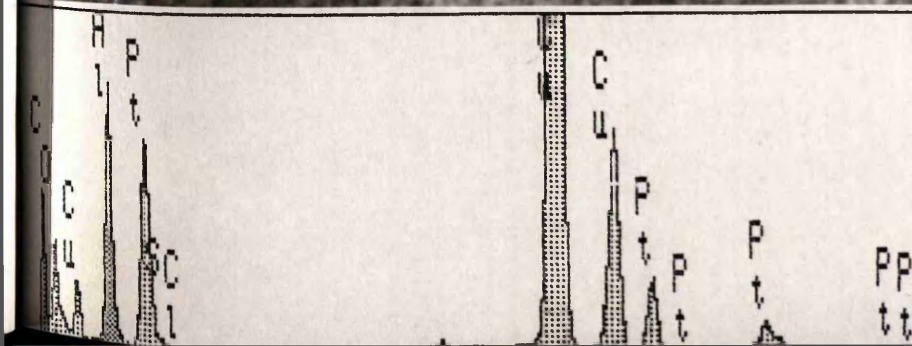


Table 5.1.1 Yields of individual products for catalyst 0.3 wt% Pt/Al₂O₃

Time (hours)	Methane	Ethane	Propane	i-Butane	n-Butane	c-Pentane	i-Pentane	n-Pentane
1.0	5.8	3.4	7.0	3.9	5.9	0.2	6.9	4.9
8.3	6.6	3.4	7.1	4.0	5.8	0.1	6.6	3.9
20.8	5.4	3.2	6.6	3.9	5.9	0.1	6.4	4.1
24.3	4.6	3.4	6.9	3.9	6.0	0.1	6.4	4.3
27.5	4.8	3.3	6.6	3.9	5.9	0.1	6.4	3.8
32.0	4.3	3.2	6.6	3.8	5.6	0.1	6.0	4.0
45.0	4.6	3.0	6.3	3.7	5.7	0.1	6.0	4.2
48.5	4.3	3.2	6.5	3.6	5.8	0.1	5.9	4.3
51.5	3.7	3.1	6.4	3.7	5.6	0.1	5.7	3.9
68.0	4.1	3.0	6.2	3.6	5.7	0.1	6.0	4.3
72.5	4.4	2.9	6.5	3.8	6.0	0.1	6.0	3.8
75.0	4.5	2.9	6.1	3.4	5.4	0.1	5.4	4.0
92.0	4.1	2.7	5.9	3.5	5.5	0.1	5.7	4.4
96.5	4.0	2.9	6.1	3.5	5.6	0.1	5.6	3.7
121.5	4.3	3.1	6.0	3.4	5.4	0.1	5.4	4.5
125.0	4.0	2.8	5.8	3.3	5.4	0.1	5.1	3.7
144.0	4.2	2.8	5.9	3.3	5.4	0.1	5.3	4.4

Table 5.1.1 (cont) Yields of individual products for catalyst 0.3 wt% Pt/Al₂O₃

Time (hours)	C6 c-Alkane	i-Hexane	n-Hexane	C7 c-Alkane	i-Heptane	n-Heptane	C8 c-Alkane	i-Octane
1.0	0.6	6.0	2.3	0.2	1.1	0.3	0.3	5.3
8.3	0.5	6.2	2.2	0.1	1.4	0.4	0.5	9.6
20.8	0.5	6.2	2.7	0.4	1.7	1.1	1.2	12.7
24.3	0.4	6.2	2.8	0.4	1.6	0.6	0.8	13.6
27.5	0.3	6.2	2.2	0.4	1.6	0.7	1.1	15.4
32.0	0.5	6.0	3.2	0.6	1.8	1.3	1.4	14.7
45.0	0.6	6.1	2.8	0.5	1.8	1.0	1.5	17.0
48.5	0.5	6.0	2.9	0.6	1.7	1.0	1.4	17.0
51.5	0.5	5.7	2.9	0.8	1.9	1.3	1.6	16.7
68.0	0.5	6.1	2.2	0.8	1.6	1.3	1.7	19.7
72.5	0.4	5.9	2.6	0.8	1.6	1.3	1.8	19.5
75.0	0.6	5.5	3.0	0.9	1.7	1.4	1.7	18.9
92.0	0.5	5.8	2.1	0.8	1.5	1.3	1.7	21.4
96.5	0.4	5.7	2.6	0.9	1.5	1.2	1.8	21.3
121.5	0.7	5.7	2.2	0.9	1.4	1.4	1.8	21.7
125.0	0.5	5.3	3.0	0.9	1.8	1.6	1.8	22.8
144.0	0.5	5.1	1.9	0.9	1.3	1.4	2.1	23.0

Table 5.1.1.1 (cont) Yields of individual products for catalyst 0.3 wt% Pt/Al₂O₃

Time (hours)	Benzene	Toluene	Ethyl- Benzene	m/p- Xylene	o-Xylene	C9 Aromatic	Total Conversion
1.0	1.3	3.7	8.8	19.4	10.2	1.0	98.4
8.3	1.0	3.1	6.6	19.3	8.6	0.8	97.8
20.8	0.7	2.7	5.3	17.1	7.3	0.9	96.0
24.3	0.8	2.7	5.3	17.3	7.3	0.9	96.3
27.5	0.7	2.7	5.0	16.6	6.9	0.9	95.5
32.0	0.7	2.6	4.8	16.2	6.8	0.8	95.0
45.0	0.6	2.4	4.5	14.9	6.3	0.9	94.4
48.5	0.6	2.4	4.7	15.0	6.2	0.9	94.8
51.5	0.7	2.6	4.5	15.8	6.4	0.9	94.3
68.0	0.6	2.2	3.9	13.7	5.5	0.8	93.5
72.5	0.6	2.3	4.0	13.0	5.6	0.9	93.5
75.0	0.6	2.3	3.9	13.9	5.6	0.9	92.8
92.0	0.5	2.1	3.5	12.8	5.2	0.8	92.3
96.5	0.5	2.2	3.7	12.8	5.2	0.8	92.1
121.5	0.5	2.1	3.3	12.2	4.9	0.8	91.7
125.0	0.5	2.1	3.3	12.1	4.8	0.8	91.4
144.0	0.5	2.0	3.1	11.7	4.6	0.8	90.2

Table 5.1.2 Selectivity to the major reforming reactions for 0.3 wt% Pt/Al₂O₃

Time (hours)	Selectivity to Aromatics	Selectivity to Isomerisation	Selectivity to Hydrocracking	Selectivity to Hydrogenolysis
1.0	45.2	6.5	17.1	5.9
8.3	40.3	11.2	17.1	6.8
20.8	35.4	15.0	17.1	5.6
24.3	35.6	15.8	17.1	4.8
27.5	34.4	17.7	17.3	5.0
32.0	33.7	17.4	16.5	4.5
45.0	31.3	19.9	16.7	4.8
48.5	31.5	19.8	16.3	4.6
51.5	32.6	19.6	16.1	3.9
68.0	28.6	22.8	16.7	4.4
72.5	28.1	22.5	16.7	4.7
75.0	29.4	22.2	15.4	4.9
92.0	27.0	24.9	16.3	4.5
96.5	27.3	24.8	16.1	4.4
121.5	25.9	25.1	15.7	4.7
125.0	25.9	26.9	14.9	4.3
144.0	25.1	26.9	15.2	4.6

Figure 5.1.1 Yields of individual products over 0.3 wt% Pt/Al₂O₃

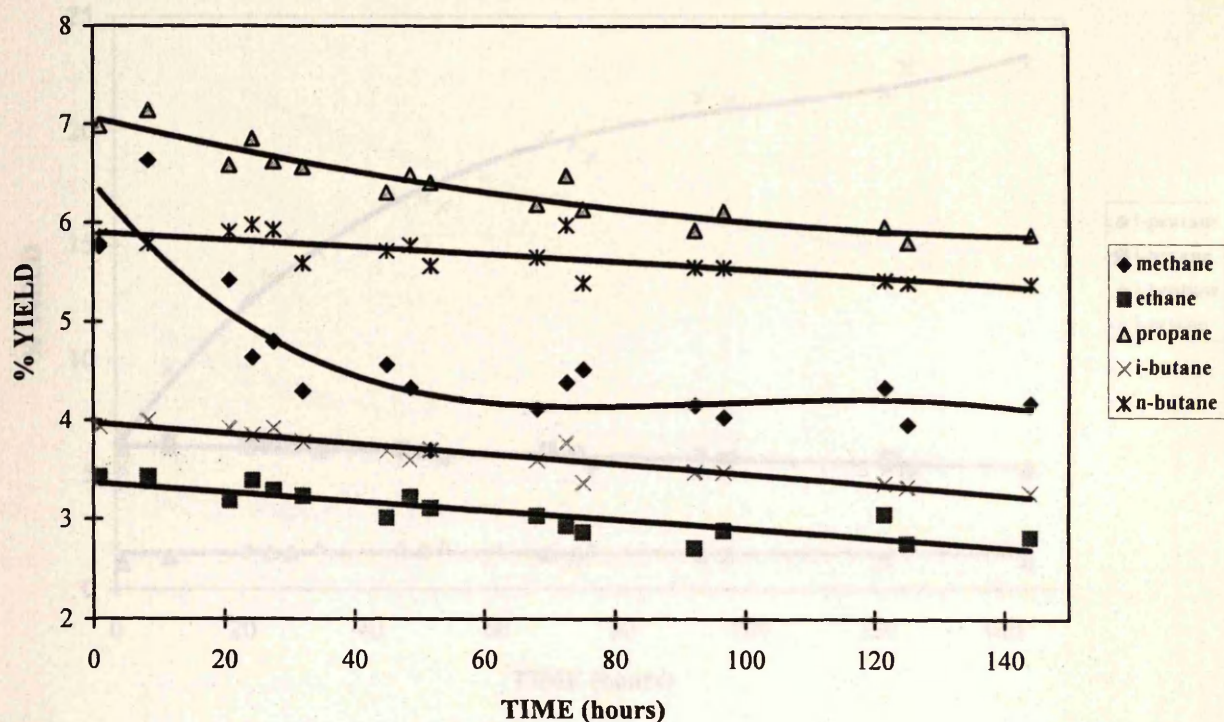


Figure 5.1.2 Yields of cycloalkanes over 0.3 wt% Pt/Al₂O₃

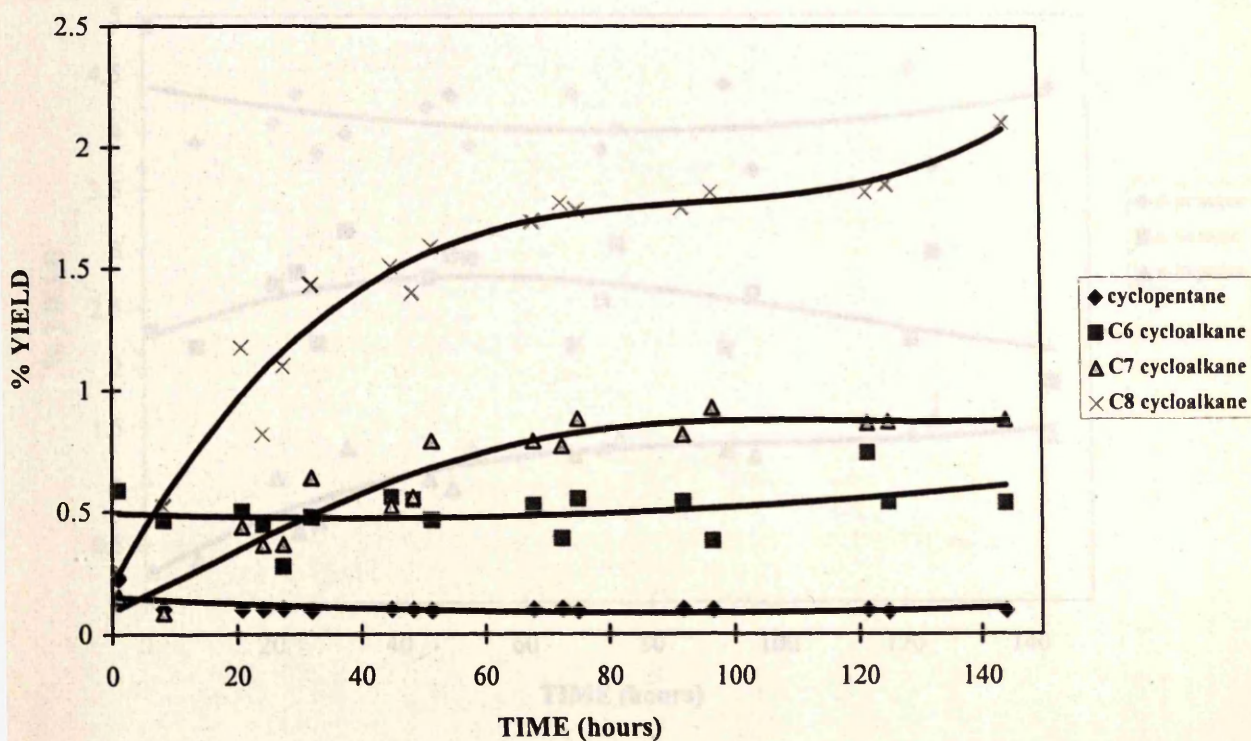


Figure 5.1.3 Yields of i-alkanes over 0.3 wt% Pt/Al₂O₃

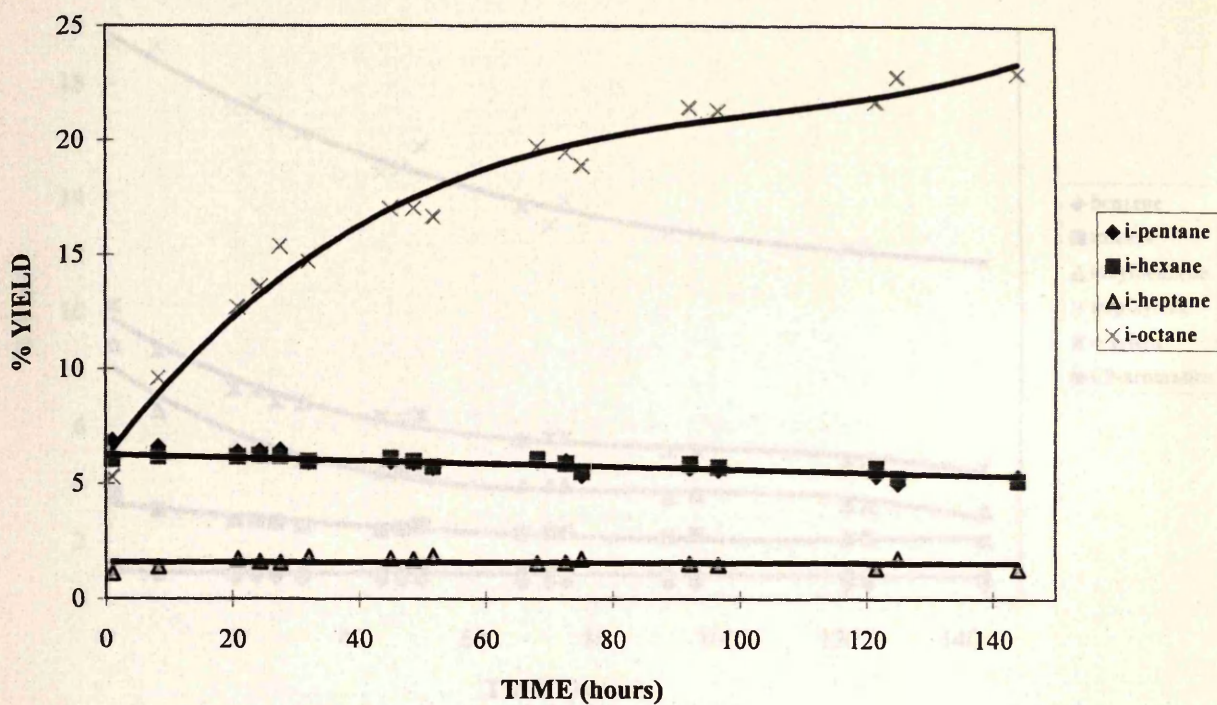


Figure 5.1.4 Yields of n-alkanes over 0.3 wt% Pt/Al₂O₃

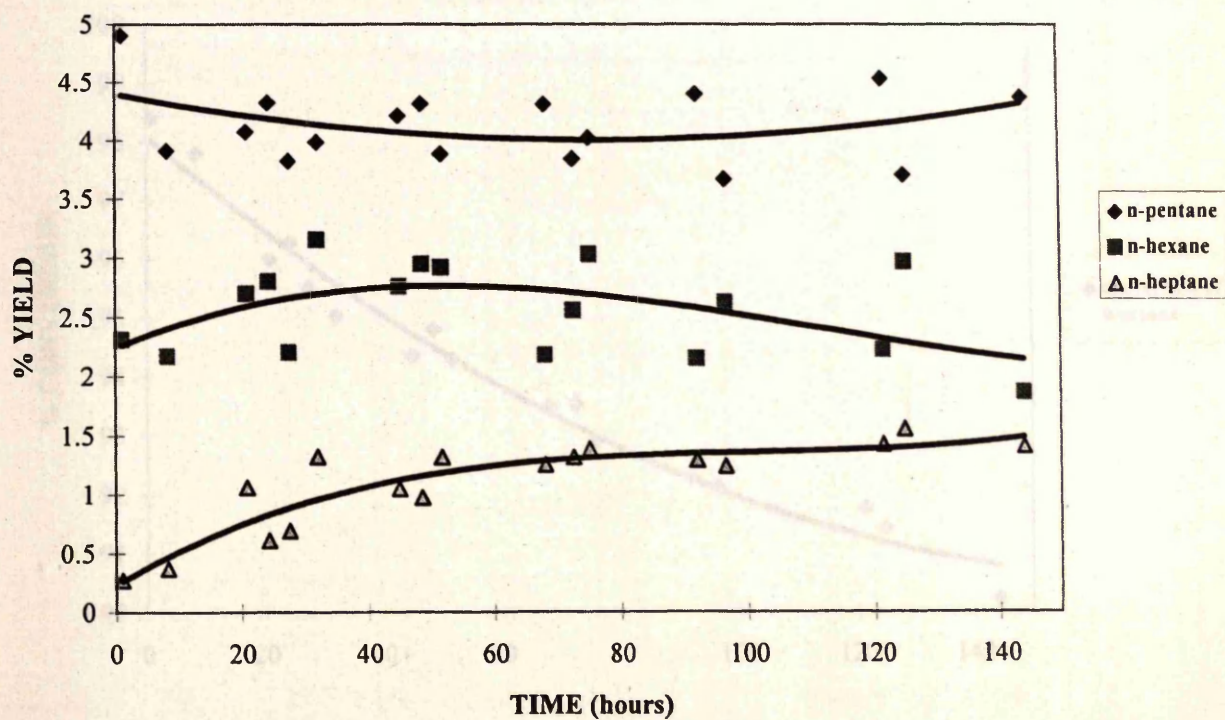


Figure 5.1.5 Yields of aromatics over 0.3 wt% Pt/Al₂O₃

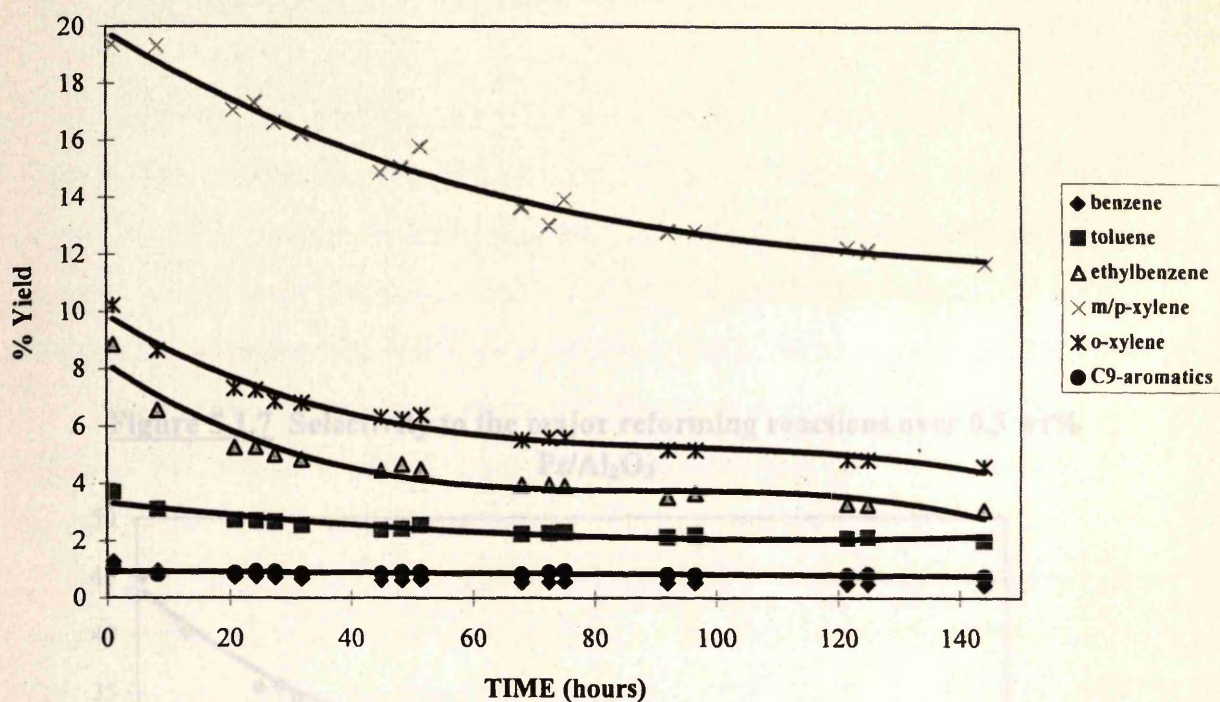
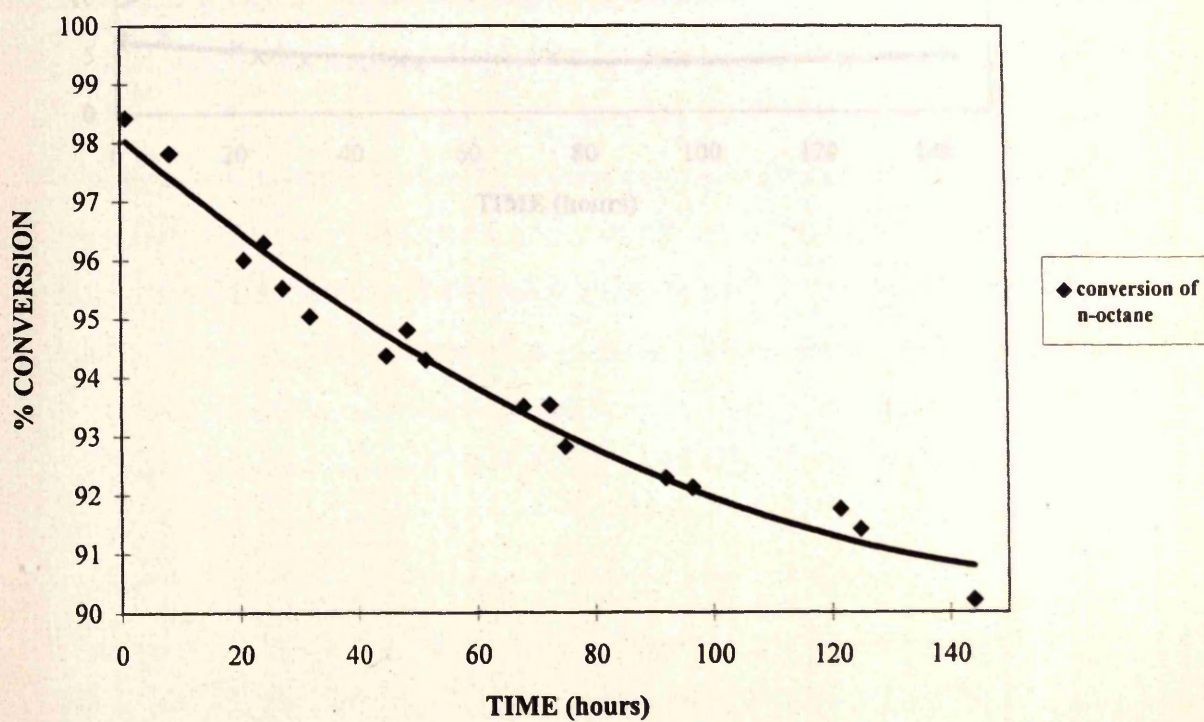


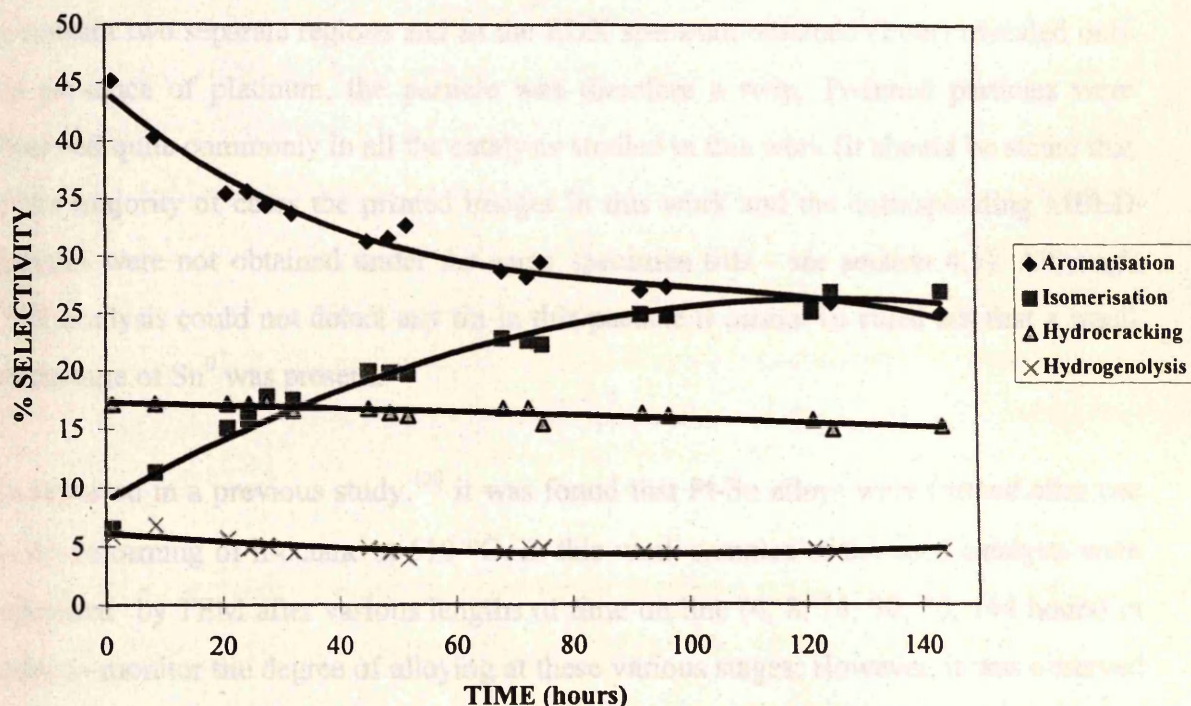
Figure 5.1.6 Conversion of n-octane over 0.3 wt% Pt/Al₂O₃



5.1.7 TEM observations

After preparation and reduction, this catalyst was found to closely resemble the Pt/Al₂O₃ catalyst. The metallic component was highly dispersed with only a small number of particles > 1 nm in diameter being observed. EDX analysis of these particles revealed that they were all pure platinum, at least to within the sensitivity of the EDX system. No Pt-Sn alloys were detected at this stage. An example is shown in plate 3. This particle

Figure 5.1.7 Selectivity to the major reforming reactions over 0.3 wt% Pt/Al₂O₃



5.2. 0.3 wt% Pt - 0.3 wt% Sn/Al₂O₃

5.2.A. TEM observations

After calcination and reduction, this catalyst was found to closely resemble the Pt/Al₂O₃ catalyst. The metallic component was highly dispersed with only a small number of particles > 1 nm in diameter being observed. EDX analysis of these particles revealed that they were all pure platinum, at least to within the sensitivity of the EDX system. No Pt-Sn alloys were detected at this stage. An example is shown in plate 5. This particle was approximately 6 nm in diameter and the corresponding MBED pattern (inset) obtained was indexed as the (121) pattern of crystalline platinum. The particle appeared to contain two separate regions and as the EDX spectrum obtained (inset) revealed only the presence of platinum, the particle was therefore a twin. Twinned particles were observed quite commonly in all the catalysts studied in this work (it should be stated that in the majority of cases the printed images in this work and the corresponding MBED patterns were not obtained under the same specimen tilts - see section 4.5). Although EDX analysis could not detect any tin in this particle it cannot be ruled out that a small percentage of Sn⁰ was present.

As reported in a previous study,¹²⁰ it was found that Pt-Sn alloys were formed after use in the reforming of n-octane at 510 °C. In this work samples of the used catalysts were examined by TEM after various lengths of time on line (4, 8, 16, 30, 70, 144 hours) in order to monitor the degree of alloying at these various stages. However, it was observed that after only 4 hours on line the majority of the larger particles (> 4 nm) had been converted into Pt-Sn alloys. The number of such particles were still relatively low, although there was a marked increase in particle number density and average particle size compared to the calcined/reduced catalyst, indicating that some sintering of the metallic component had occurred during these four hours.

An example of a Pt-Sn alloy formed at this stage is given in plate 6. This particle was approximately 10 nm in diameter and the corresponding EDX spectrum obtained revealed it to be an alloy particle with the approximate atomic ratio Pt/Sn of 1.0 (calculated as described in section 4.5.2). The lattice visible in the image, although not very clear, has a spacing of 0.35 nm, corresponding to the {100} plane of crystalline hcp PtSn ($d = 0.355$ nm). This particle was therefore assigned to the hcp PtSn structure. A number of platinum rich solid solutions were also observed at this stage. An example is shown in plate 7. This particle was approximately 10 nm in diameter and the EDX spectrum obtained revealed a Pt/Sn atomic ratio of 7.0.

With increasing time on line, further sintering of the metallic component was observed to occur. After 144 hours on line a small number of very large 20-30 nm sized alloy particles were observed. However, the majority of detectable metal particles remained in the size range 1-5 nm after this time. It is possible that a substantial proportion of the metal remained in the form of sub-nanometer particles which could not be imaged by TEM.

A number of alloy phases were found to coexist in this system, as was reported previously.¹²⁰ Examples of relatively large alloys formed after 144 hours on line are shown in plates 8-11.

The majority of the alloy particles found in this system at all stages of the reforming run were hcp PtSn. Plate 8 contains an image of a 20-30 nm particle formed after 144 hours. The corresponding EDX spectrum, obtained using an electron beam probe which covered the entire particle, revealed a Pt/Sn atomic ratio of 0.9. The particle was observed to contain three separate regions, marked (A), (B) and (C) in the image. A MBED pattern obtained from region (A) (inset (a)) was indexed as the (100) pattern of the hcp PtSn structure. The MBED pattern obtained from region (B) (inset (b)) was also indexed as PtSn, although in this case to the (011) orientation. No MBED pattern was obtained from region (C) as a zone axis orientation could not be obtained. The lattice

fringes visible in regions (A) (running vertically in the image) and (B) (running horizontally) both have spacings of approximately 0.35 nm corresponding to the {100} spacing of the hcp PtSn phase.

A further example of a particle of this phase is shown in plate 9. Again, this was a large 20 nm sized particle, although smaller particles of this phase, similar to that shown in plate 6, were also observed after 144 hours on line. The EDX spectrum obtained from this particle revealed a Pt/Sn atomic ratio of 1.0. In this case, the corresponding MBED pattern was indexed as the (121) pattern of PtSn and the lattice fringes visible in this image were found to have a spacing of 0.297 nm corresponding to the (101) spacing of PtSn.

Particles which consisted of platinum rich solid solutions were also observed after 144 hours on line in reforming. However, these particles were not as common as the PtSn structure. An example is given in plate 10. This was a relatively large particle about 15-20 nm in diameter. In this case the EDX spectrum obtained revealed a Pt/Sn atomic ratio of 4.5. The MBED pattern obtained (inset) was indexed as the (310) pattern of crystalline platinum. The lattice fringes visible in this image correspond to the (200) 0.196 nm lattice of platinum.

In addition to the alloy phases identified in the previous investigation,¹²⁰ a superlattice or superstructure phase was also observed. A similar structure was found in previous studies of the related Pt-Ge system.¹²⁹ An example of this structure is shown in plate 11. This particle was found to contain two separate phases. An EDX spectrum from the smaller region, marked (A) in the image, revealed a Pt/Sn atomic ratio of 0.7 (spectrum A). The lattice fringes visible in this region of the particle had a spacing of approximately 0.35 nm corresponding to the {100} spacing of hcp PtSn. This region of the particle was therefore assigned to the PtSn phase. The EDX spectrum obtained from region (B) (spectrum B) revealed a Pt/Sn atomic ratio of 3.1. A MBED pattern obtained from this region (inset) contained a series of bright spots which correspond exactly with

the (110) pattern of platinum. Also present in this pattern are a series of less intense spots midway between each bright spot (corresponding to the 100 and 110 forbidden reflections of fcc platinum). This is characteristic of a modified or superlattice type structure and is similar to a Pt-Ge alloy which has been described in a previous study.¹²⁹ However, although this phase was found to very common in the Pt-Ge/Al₂O₃ catalysts, as will be seen in the following sections, in the Pt-Sn/Al₂O₃ catalysts this type of particle was relatively infrequently observed. The edge of the particle imaged in plate 11 was surrounded by a layer with lower contrast which appeared to be poorly crystalline or amorphous. Similar features were observed in a number of the particles imaged in this catalyst. This may have been a layer of tin oxide which formed due to gradual oxidation of tin on exposure to atmospheric oxygen. A related study on Pt-Sn catalysts found that a fraction of the Sn⁰ originally present in these systems was slowly oxidised when exposed to oxygen over a period of days.¹⁰³ In order to ensure that the TEM observations made in this study were truly representative of the catalyst structures, a number of TEM grids were prepared for each sample and these were subsequently analysed over a period of days or weeks. It is possible therefore that some oxidation of tin occurred during this period.

5.2.B n-Octane reforming

The yields of individual products species over this catalyst are presented versus time on line in table 5.2.1. These results are plotted in figures 5.2.1 to 5.2.6.

The yields of methane, ethane, propane, i-butane and n-butane are plotted in figure 5.2.1. The yields of ethane, propane and butanes over this catalyst were found to be similar to those obtained over platinum (compare with figure 5.1.1). Therefore the addition of tin had very little effect on the production of these products. In the case of methane however, which gives a measure of the hydrogenolysis activity, the yields over these two catalysts were found to be quite different. Whilst over platinum the hydrogenolysis

activity declined rapidly initially, followed by a period of more gradual decline, over Pt-Sn this trend was reversed. Initially the decline in methane yield was slow but appeared to increase during the length of the reforming run. The factors believed to be responsible for this observation, and all the other differences between the various catalysts studied, will be discussed in chapter 6.

The yield of cyclic products over Pt-Sn/ Al_2O_3 are plotted in figure 5.2.2. Again these yields were very similar to those obtained over the Pt/ Al_2O_3 catalyst. The yields of C_5 and C_6 cycloalkanes remained relatively constant throughout the run whilst the C_7 and particularly C_8 yields increased significantly.

The yields of iso-alkanes over this catalysts are plotted in figure 5.2.3. The trends for these four products were similar to those observed over Pt/ Al_2O_3 (figure 5.1.3); the yield of i-pentane, i-hexane and i-heptane remained relatively constant whilst the yield of i-octane increased sharply throughout the run. In this case the rate of increase of i-octane yield was more constant than that observed over platinum. An interesting point however is that although the trends were similar, the initial yields of i-hexane, i-heptane and i-octane were markedly lower over the Pt-Sn (4.2%, 0.5% and 1.9% respectively) catalysts than over Pt (6.0%, 1.1% and 5.3% respectively). Again the factors believed to be involved in this observation will be discussed in the following chapter.

The yields of n-alkanes are plotted in figure 5.2.4. Again the yields are roughly equivalent to those obtained over Pt/ Al_2O_3 with no major changes having occurred on addition of tin.

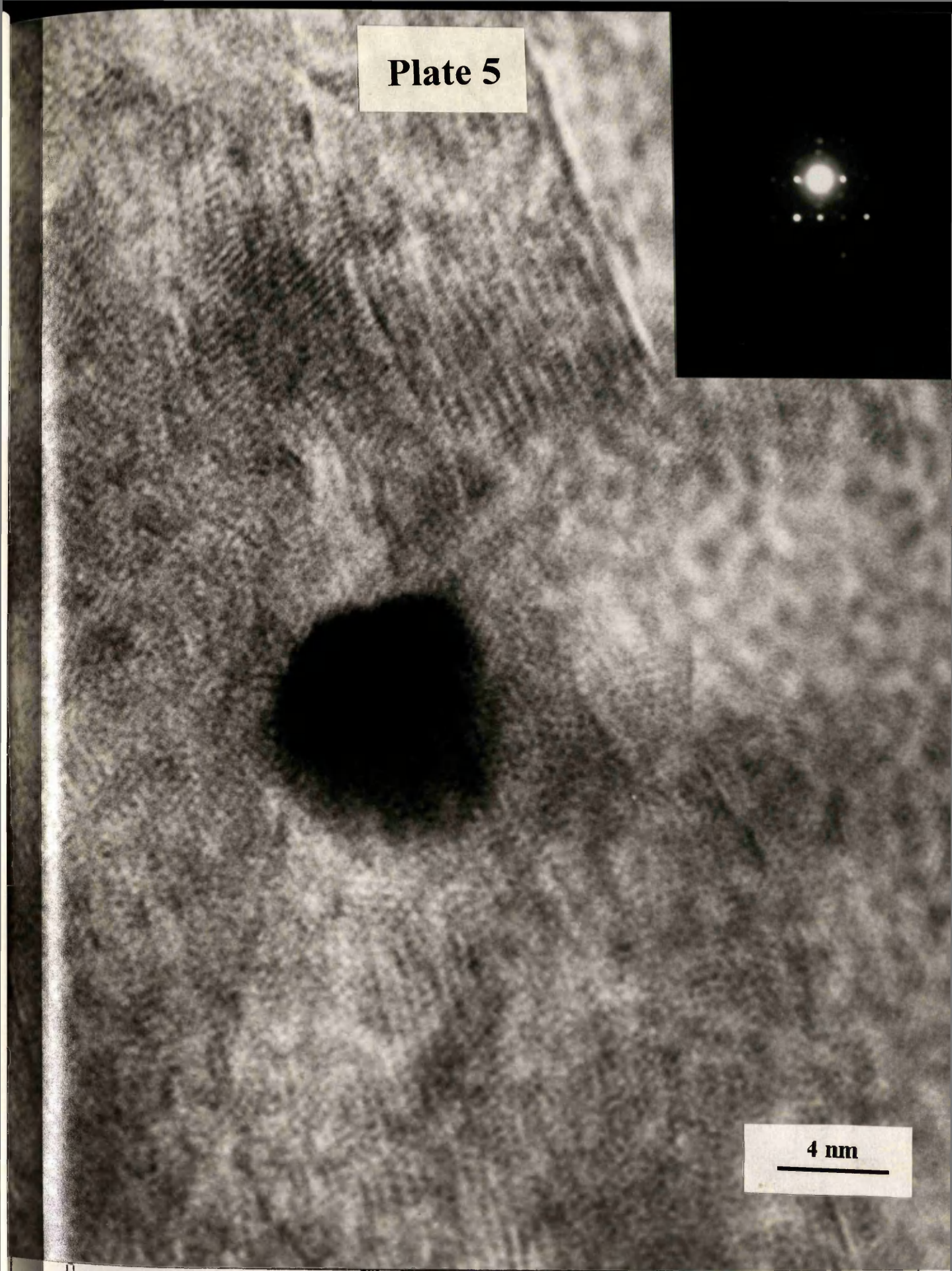
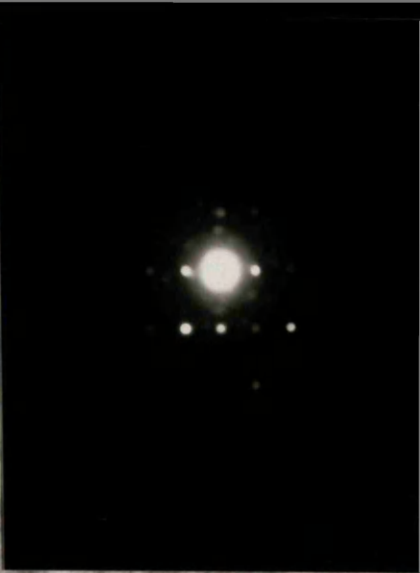
One of the major changes that did occur on the addition of tin however was in the yields of aromatic products produced. The yields of these products over Pt-Sn/ Al_2O_3 are plotted in figure 5.2.5. Although the same order of production of aromatics (in order of decreasing yield: m/p-xylene > o-xylene > ethylbenzene > toluene > benzene, C_9 aromatics) was the same for both catalysts, the yield m/p-xylene showed a marked

increase on addition of tin, as to a lesser extent did that of o-xylene. Another major difference was in the way the yields of these products changed with time on line (compare figures 5.1.5 and 5.2.5) Over platinum the yields of xylenes and ethylbenzene showed an initial rapid decline whilst over Pt-Sn the yields decreased at a more constant rate throughout the run. This difference becomes more obvious when the selectivities of the catalysts are examined, as will be shown shortly.

The conversion of n-octane versus time on line over Pt-Sn/Al₂O₃ is plotted in figure 5.2.6. Comparing this with the conversion over Pt/Al₂O₃ (figure 5.1.6), it is clear that the initial conversion was slightly higher over the Pt-Sn catalysts. However, the main difference between these two was found to be in the slopes of these deactivation curves. Whilst the rate of deactivation of platinum was more rapid during the initial stages of the run and then occurred at a more gradual pace, the opposite occurred with Pt-Sn. The rate of deactivation actually increased during the run. In fact by 144 hours on line the level of conversion over Pt-Sn/Al₂O₃ had actually fallen below that of platinum (89.0% versus 90.2 %).

The selectivities to the four major reforming reactions are presented versus time on line in table 5.2.2. and plotted in figure 5.2.7. When comparing these results with those obtained over Pt/Al₂O₃ (figure 5.1.7), it is clear that in the initial stages the influence of tin was to decrease isomerisation and correspondingly increase aromatisation. Also, whilst over Pt/Al₂O₃ the decrease in aromatisation and corresponding increase in isomerisation was rapid in the initial stages and then leveled off, over Pt-Sn/Al₂O₃ this change in selectivity occurred at a more constant rate throughout the run.

Plate 5



4 nm

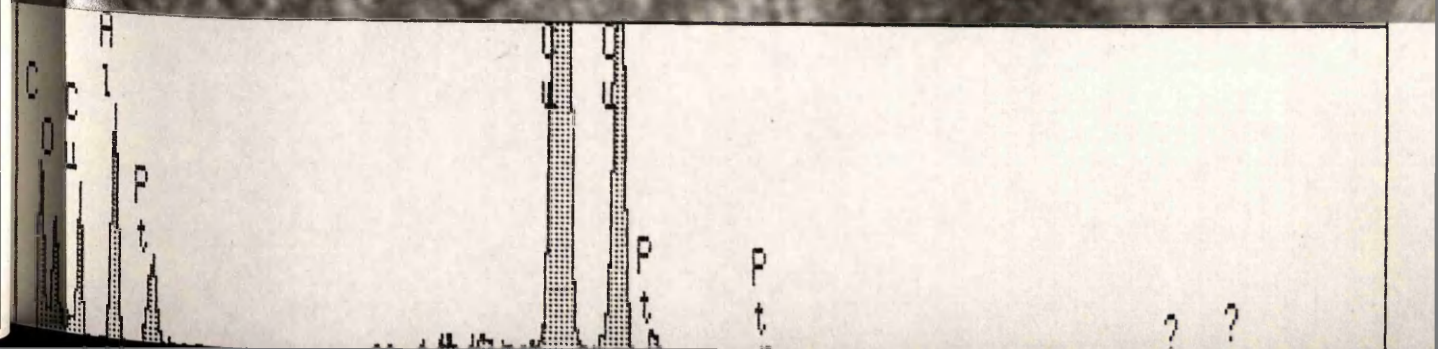
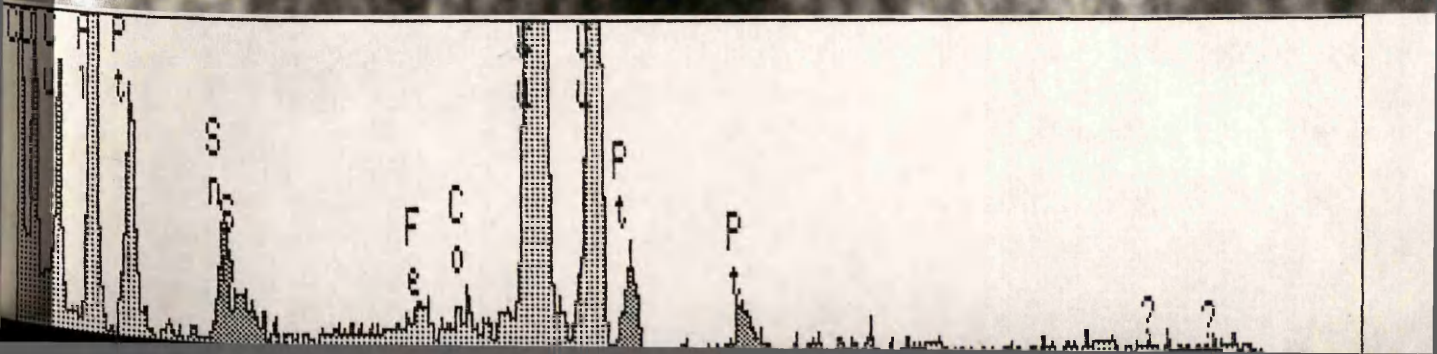
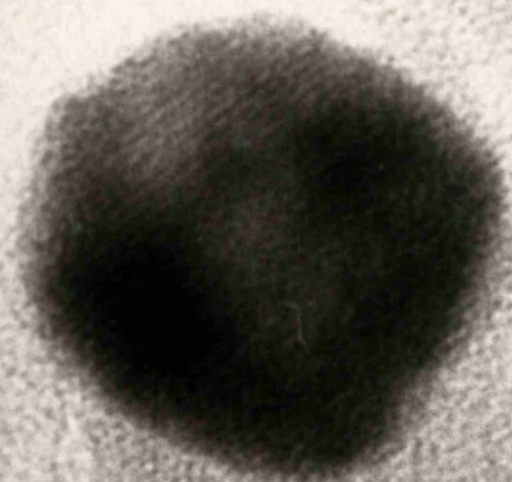


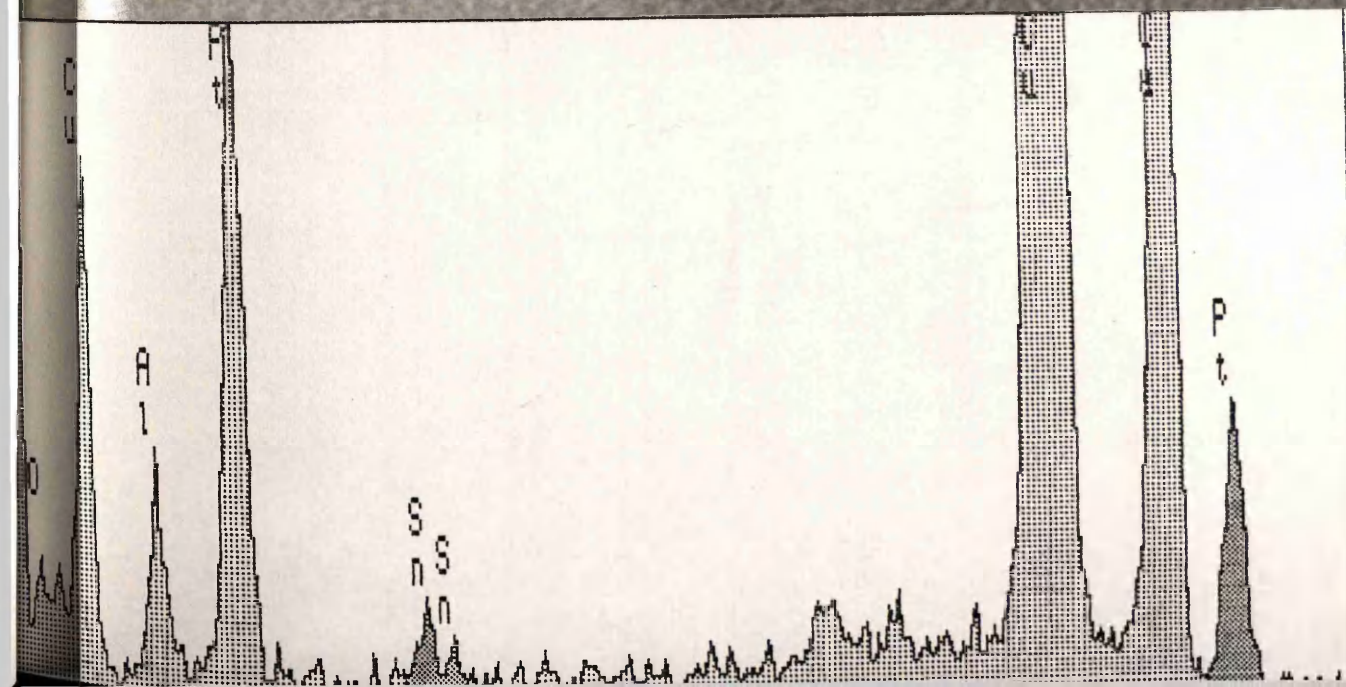
Plate 6

4 nm





4 nm



(b)



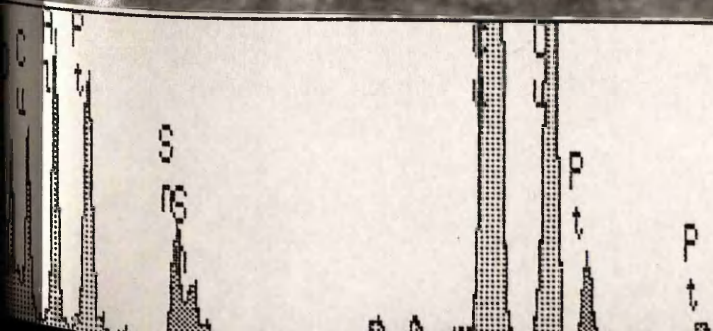
(B)

(A)

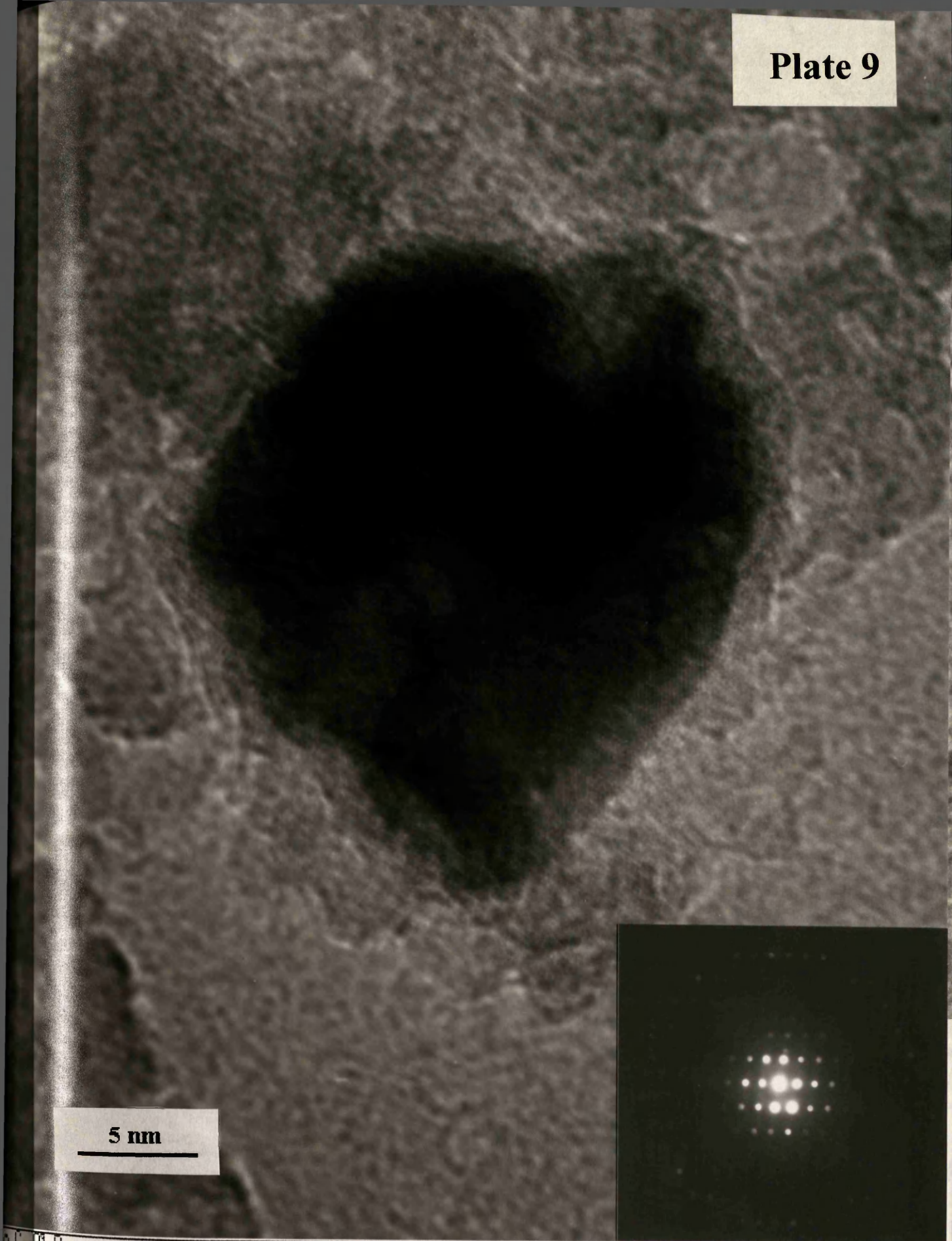
(C)

5 nm

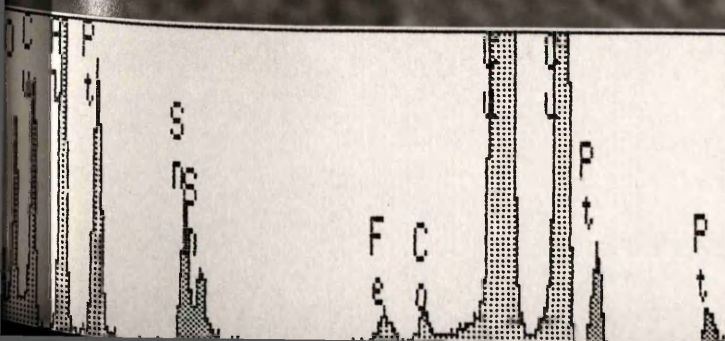
(a)



2 2



5 nm

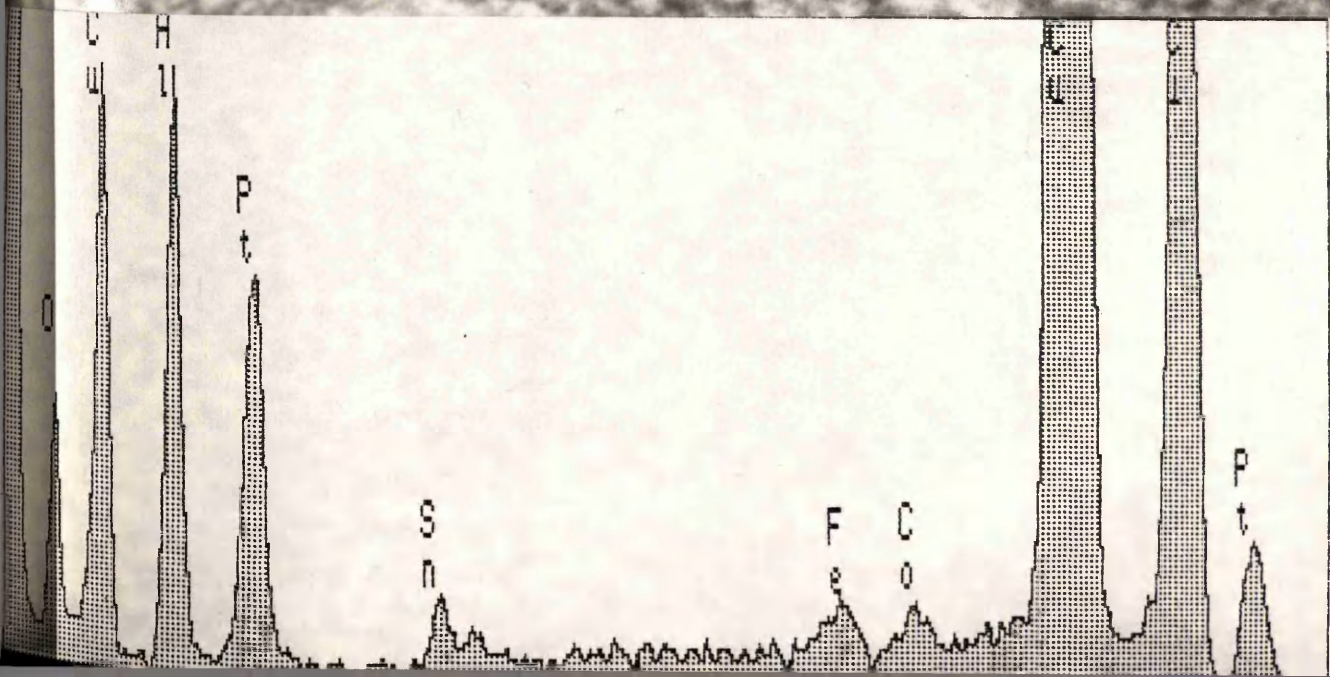


? ?

Plate 10



3 nm



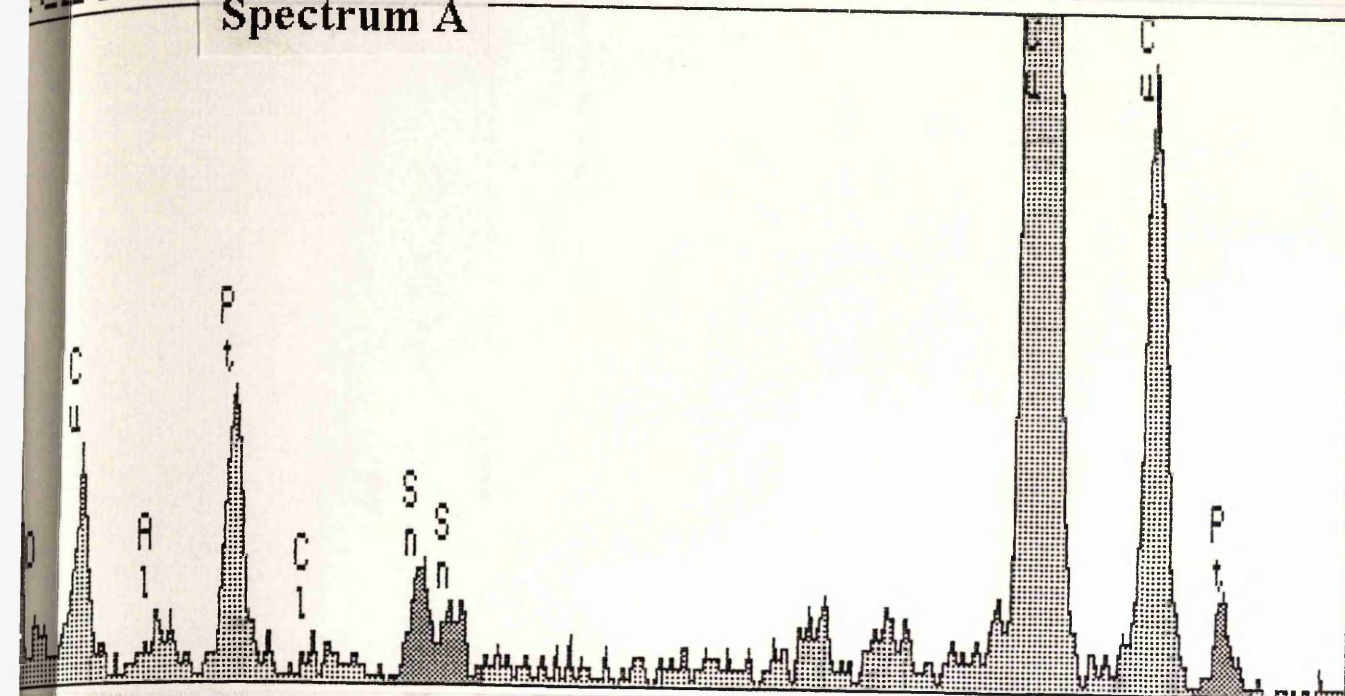
(A)

(B)

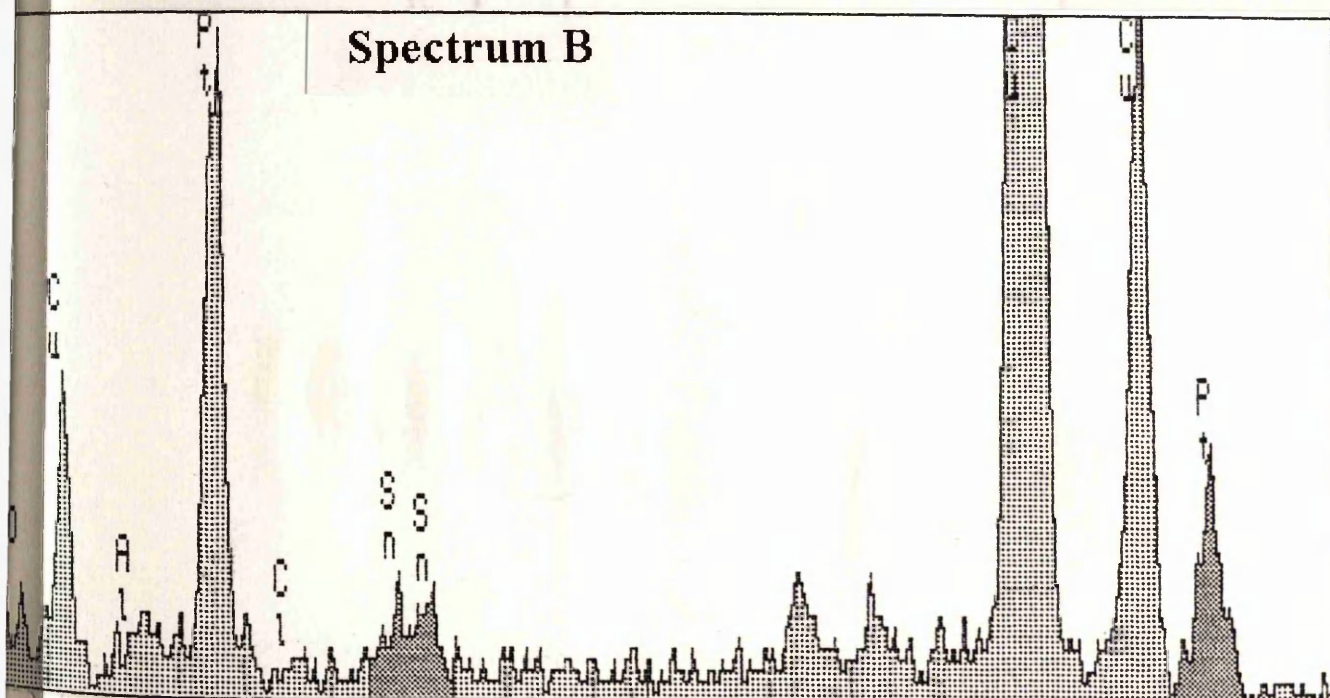
5 nm



Spectrum A



Spectrum B



Time (hours)	1.0	7.6	21.0	25.0	48.0	75.0	96.5	117.0	122.0	140.0	144.0
--------------	-----	-----	------	------	------	------	------	-------	-------	-------	-------

Table 5.2.1 Yields of individual products for catalyst 0.3 wt% Pt - 0.3 wt% Sn/Al₂O₃

Time (hours)	Methane	Ethane	Propane	i-Butane	n-Butane	c-Pentane	i-Pentane	n-Pentane
1.0	7.1	2.9	7.4	4.9	6.2	0.1	6.7	4.9
7.0	6.3	3.3	7.1	4.7	6.0	0.1	6.1	3.8
21.0	6.7	3.2	7.0	4.5	5.9	0.1	5.5	4.2
25.0	6.4	3.3	7.1	4.6	5.9	0.1	6.2	4.3
48.0	6.5	3.3	7.0	4.5	5.9	0.1	6.1	3.8
75.0	6.3	3.0	6.8	4.2	5.8	0.3	5.7	5.0
96.5	5.9	3.2	6.9	4.4	6.1	0.1	6.7	5.4
117.0	4.9	3.4	7.1	4.2	6.2	0.1	6.3	5.0
122.0	5.4	3.3	6.6	4.0	5.7	0.1	5.6	4.3
140.0	4.1	3.4	6.9	4.1	5.8	0.1	5.8	5.1
144.0	4.6	3.2	6.5	3.9	5.6	0.1	5.4	4.2

Table 5.2.1 (cont) Yields of individual products for catalyst 0.3 wt% Pt - 0.3 wt% Sn/Al₂O₃

Time (hours)	C6 c-Alkane	i-Hexane	n-Hexane	C7 c-Alkane	i-Heptane	n-Heptane	C8 c-Alkane	i-Octane
1.0	0.3	4.2	1.5	0.0	0.5	0.1	0.1	1.9
7.0	0.1	4.3	3.9	0.0	0.6	0.1	0.2	2.3
21.0	0.5	4.3	1.9	0.2	0.7	0.2	0.3	3.7
25.0	0.4	4.8	2.4	0.3	0.9	0.4	0.4	4.7
48.0	0.3	4.8	1.6	0.2	1.0	0.3	0.8	7.1
75.0	0.8	5.2	2.8	0.8	1.4	1.2	1.9	10.5
96.5	0.7	6.2	2.7	0.5	1.3	0.4	1.8	14.2
117.0	0.7	5.7	2.6	0.5	1.3	0.6	2.1	15.8
122.0	0.7	5.3	3.3	0.9	1.6	1.4	2.5	15.4
140.0	0.9	5.7	3.1	0.8	1.5	1.0	2.7	16.6
144.0	0.6	5.2	3.1	0.9	1.5	1.3	2.8	17.2

Table 5.2.1 (cont) Yields of individual products for catalyst 0.3 wt% Pt - 0.3 wt% Sn/Al₂O₃

Time (hours)	Benzene	Toluene	Ethyl- Benzene	m/p- Xylene	o-Xylene	C9 Aromatic	Total Conversion
1.0	1.4	2.8	6.3	27.4	11.3	1.5	99.4
7.0	1.2	4.0	6.1	26.7	10.7	1.2	99.0
21.0	1.1	4.5	5.8	26.3	11.2	1.3	99.1
25.0	1.0	4.4	4.9	24.8	10.2	1.2	98.7
48.0	0.9	4.4	4.6	23.3	9.5	1.2	97.2
75.0	0.7	3.3	3.6	17.7	7.1	1.0	94.9
96.5	0.5	2.6	2.7	14.1	5.8	0.8	93.1
117.0	0.4	2.4	2.6	13.2	5.4	0.8	91.4
122.0	0.4	2.4	2.6	13.0	5.2	0.9	90.6
140.0	0.4	2.3	2.4	12.0	4.8	0.7	90.1
144.0	0.4	2.2	2.4	12.2	4.9	0.9	89.0

Table 5.2.2 Selectivity to the major reforming reactions for 0.3 wt% Pt - 0.3 wt% Sn/Al₂O₃

Time (hours)	Selectivity to Aromatics	Selectivity to Isomerisation	Selectivity to Hydrocracking	Selectivity to Hydrogenolysis
1.0	51.0	2.4	15.9	7.1
7.0	50.5	2.9	15.3	6.4
21.0	50.7	4.4	14.4	6.8
25.0	47.1	5.8	15.8	6.5
48.0	45.2	8.3	15.8	6.7
75.0	35.1	12.6	15.9	6.7
96.5	28.6	16.7	18.5	6.3
117.0	27.3	18.7	17.8	5.3
122.0	27.1	18.8	16.4	6.0
140.0	25.1	20.1	17.3	4.5
144.0	25.8	21.0	16.3	5.1

Figure 5.2.1 Yields of individual products over 0.3 wt% Pt - 0.3 wt% Sn/Al₂O₃

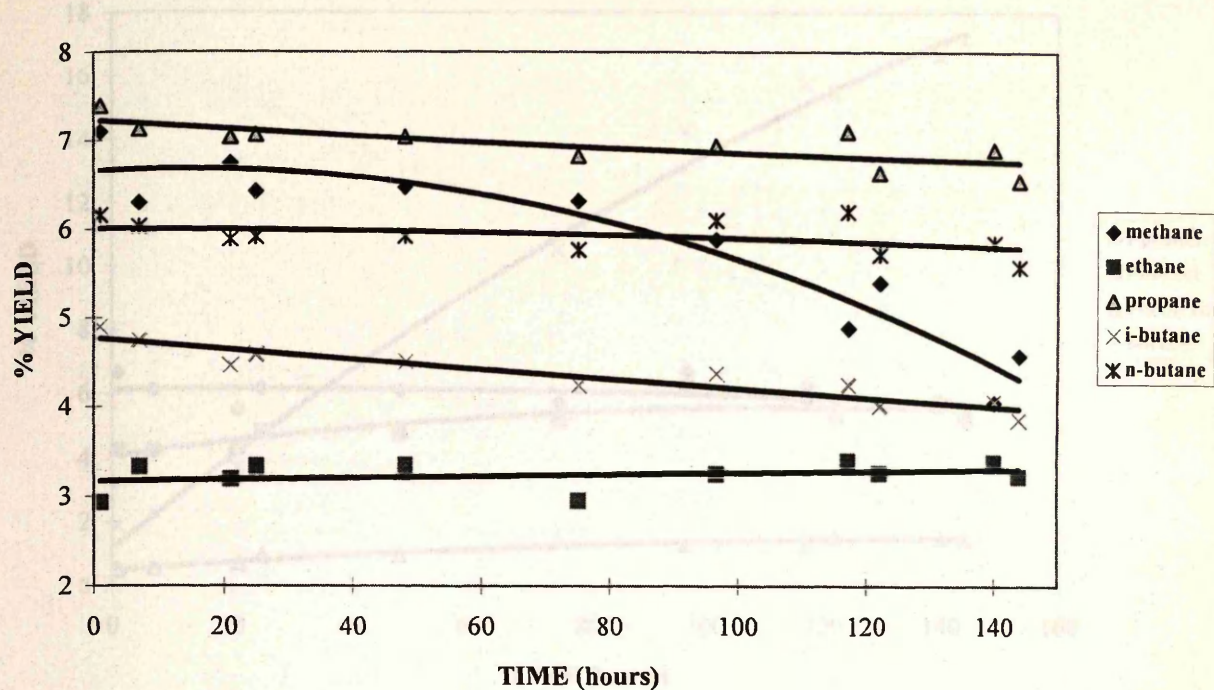


Figure 5.2.2 Yields of cycloalkanes over 0.3 wt% Pt - 0.3 wt% Sn/Al₂O₃

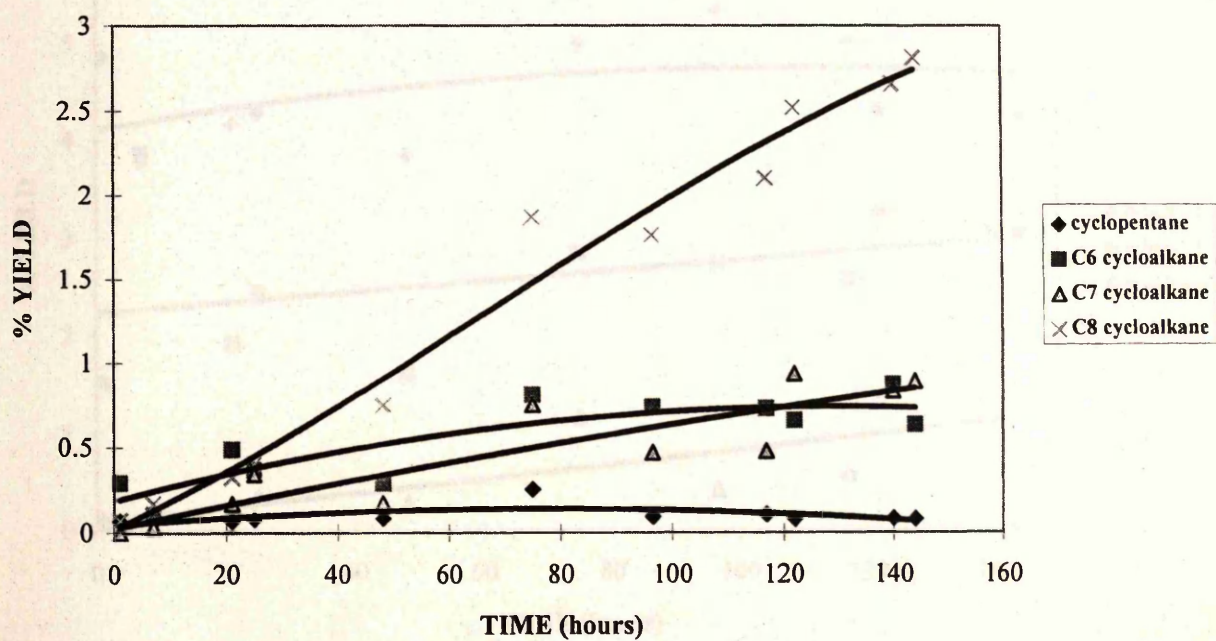


Figure 5.2.3 Yields of i-alkanes over 0.3 wt% Pt - 0.3 wt% Sn/Al₂O₃

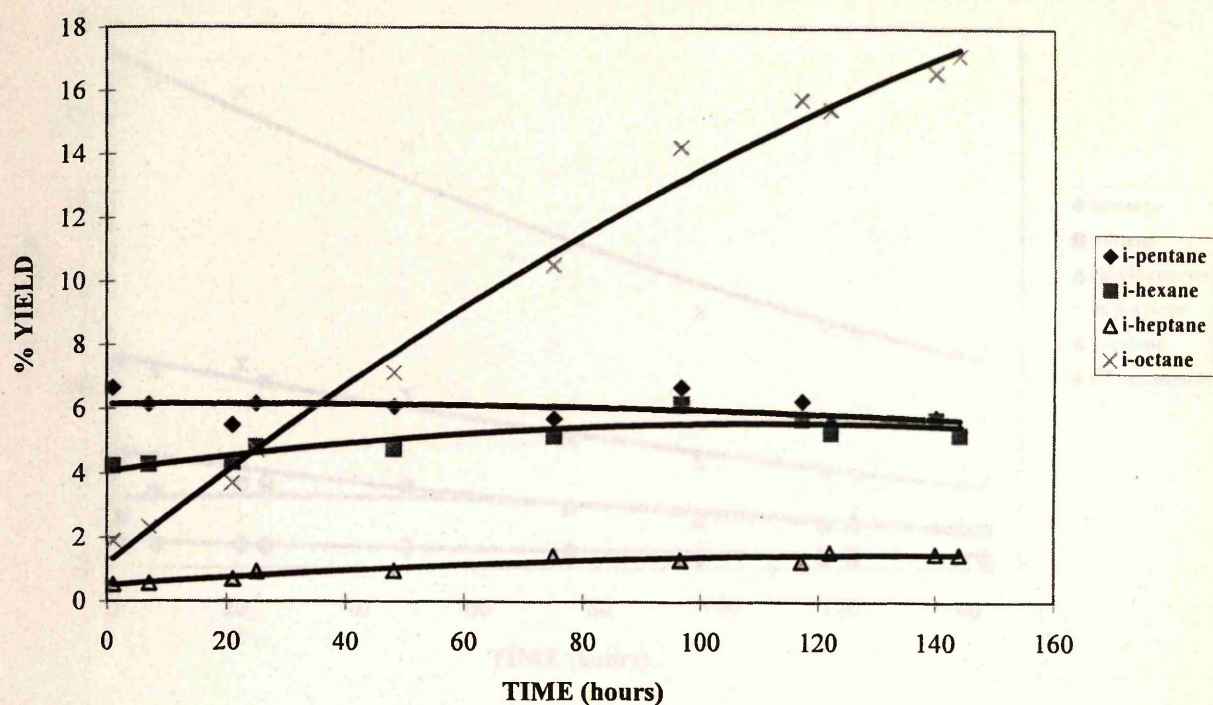


Figure 5.2.4 Yields of n-alkanes over 0.3 wt% Pt - 0.3 wt% Sn/Al₂O₃

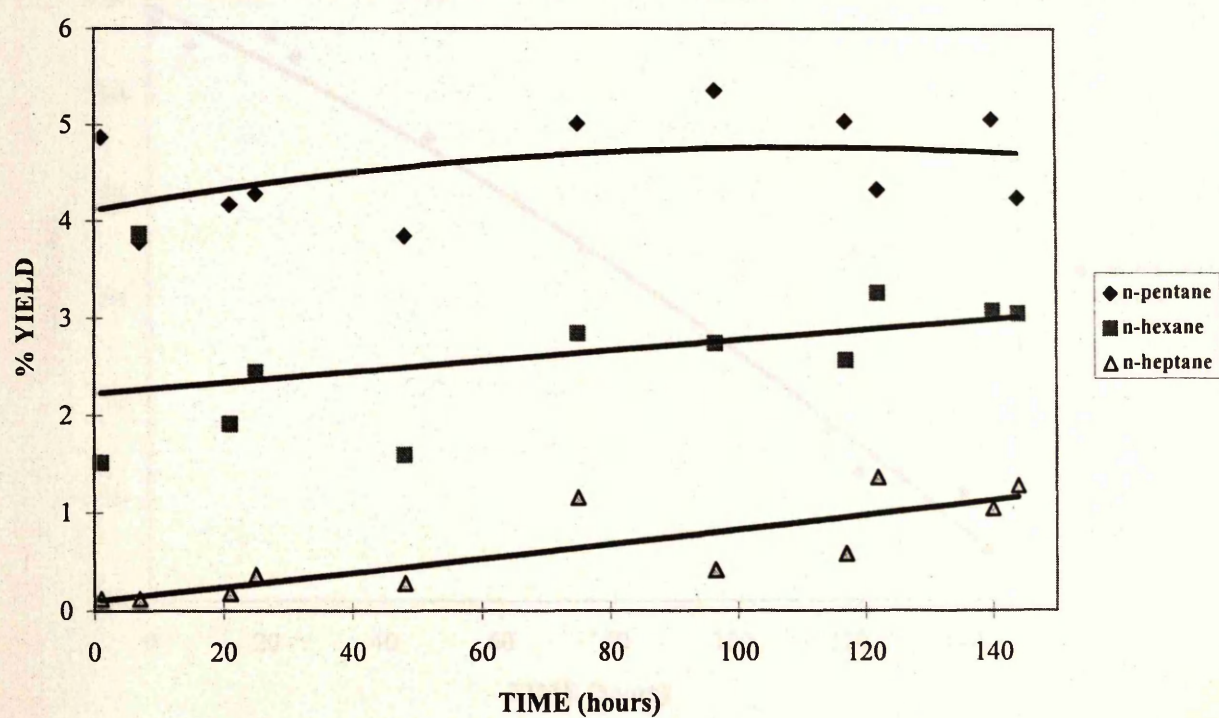


Figure 5.2.5 Yields of aromatics over 0.3 wt% Pt - 0.3 wt% Sn/Al₂O₃

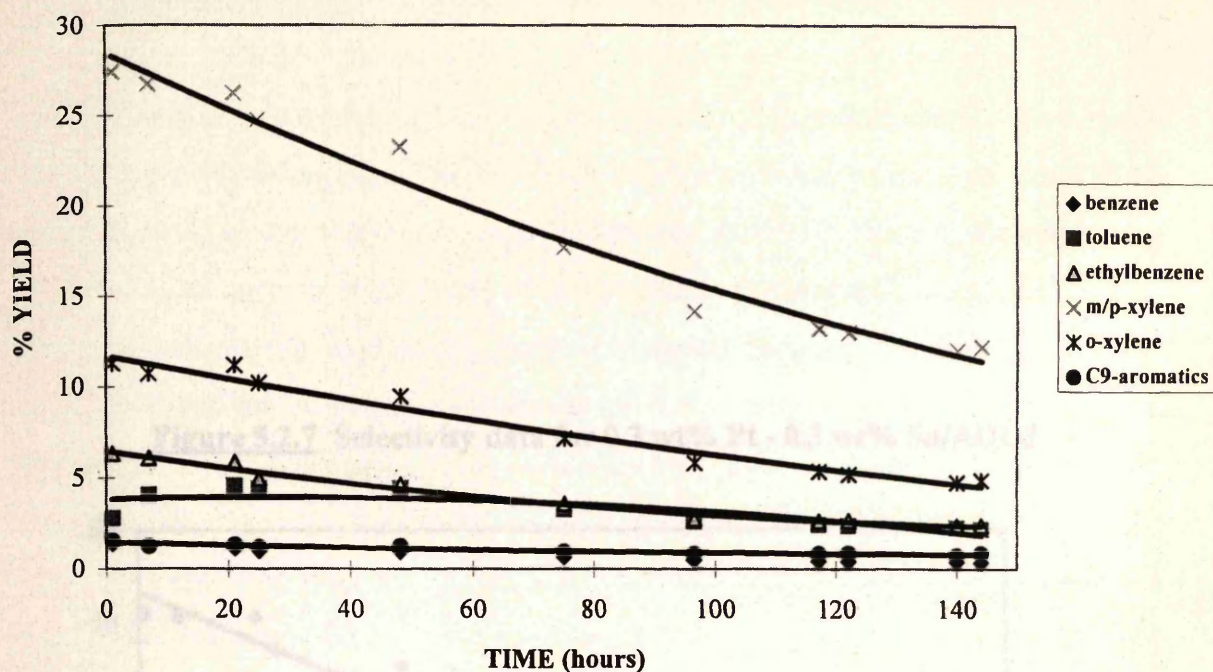
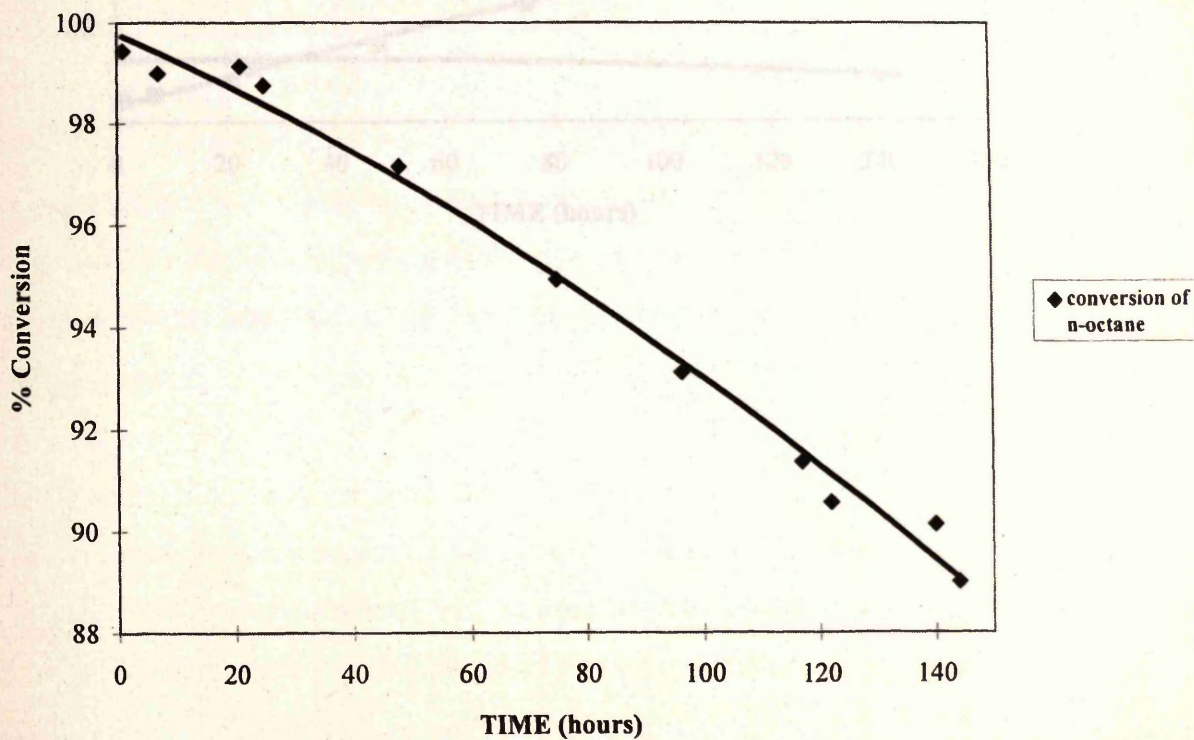


Figure 5.2.6 Conversion of n-octane over 0.3 wt% Pt - 0.3 wt% Sn/Al₂O₃

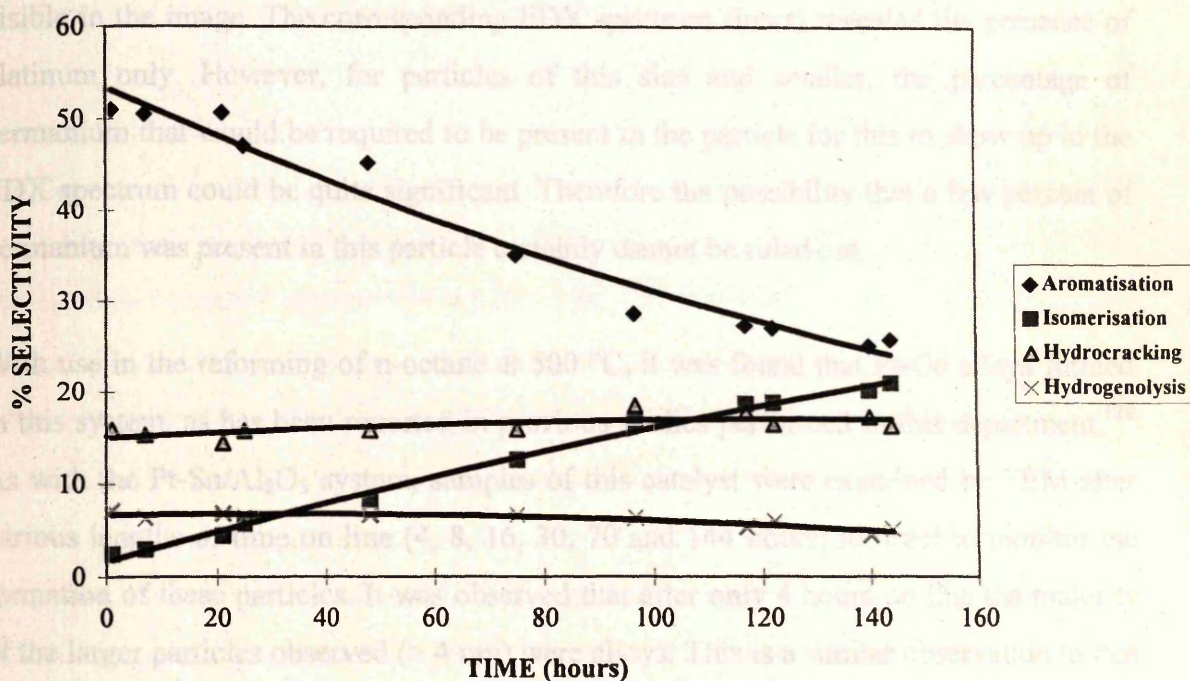


5.3. 0.3 wt% Pt - 0.3 wt% Ge/Al₂O₃

5.3.A TEM observations

After calcination and reduction this catalyst again showed similar features to the 0.3 wt% Pt/Al₂O₃ catalyst when examined by TEM. The metallic component was found to be very highly dispersed with only a small number of particles > 1 nm in diameter being observed. EDX analysis of the larger of these particles revealed the presence of platinum only. An example of a platinum particles is shown in plate 12. This particle was approximately 5 nm in diameter and was in the (110) orientation relative to the electron beam direction. The platinum (110) 0.227 nm and (200) 0.193 nm lattice fringes are visible in the image. The energy-dispersive EDX spectrum for this particle is presented in plate 13. It was found that the particles of this size and smaller, the percentage of platinum only. However, for particles of this size and smaller, the percentage of platinum only. However, for particles of this size and smaller, the percentage of platinum only.

Figure 5.2.7 Selectivity data for 0.3 wt% Pt - 0.3 wt% Sn/Al₂O₃



5.3. 0.3 wt% Pt - 0.3 wt% Ge/Al₂O₃

5.3.A TEM observations

After calcination and reduction this catalyst again showed similar features to the 0.3 wt% Pt/Al₂O₃ catalyst when examined by TEM. The metallic component was found to be very highly dispersed with only a small number of particles > 1 nm in diameter being observed. EDX analysis of the larger of these particles revealed the presence of platinum only. An example of a platinum particle is shown in plate 12. This particle was approximately 5 nm in diameter and was in the (110) orientation relative to the electron beam direction. The platinum {111} 0.227 nm and {200} 0.196 nm lattice fringes are visible in the image. The corresponding EDX spectrum (inset) revealed the presence of platinum only. However, for particles of this size and smaller, the percentage of germanium that would be required to be present in the particle for this to show up in the EDX spectrum could be quite significant. Therefore the possibility that a few percent of germanium was present in this particle certainly cannot be ruled out.

With use in the reforming of n-octane at 500 °C, it was found that Pt-Ge alloys formed in this system, as has been reported in previous studies performed in this department.¹²⁰ As with the Pt-Sn/Al₂O₃ system, samples of this catalyst were examined by TEM after various lengths of time on line (4, 8, 16, 30, 70 and 144 hours) in order to monitor the formation of these particles. It was observed that after only 4 hours on line the majority of the larger particles observed (> 4 nm) were alloys. This is a similar observation to that made with Pt-Sn. Some sintering of the metallic component was also observed to have occurred during these four hours, although the overall number of metal particles > 2 nm was still low.

An example of an alloy formed in this system after four hours on line is given in plate 13. This particle was approximately 10 nm in diameter. The EDX spectrum obtained revealed a Pt/Ge atomic ratio of 3.2. The particle was observed to contain two separate

regions, which are marked (A) and (B) in the image. The lattice spacings in both regions could be indexed as platinum, although to different lattice planes. The fringes in region (A) corresponded with the {111} 0.227 nm platinum lattice whilst those in region (B) corresponded with the {002} 0.196 nm lattice. Also visible in region (B) is a set of lattice fringes running perpendicular to the {002} planes. These were indexed as the {210} lattice of platinum with a spacing of 0.175 nm (reflections from this lattice are forbidden in a true fcc system). It was also observed that in region (B) every second dark band in the {002} lattice was much more intense than the band between. This is again characteristic of a modified superlattice or superstructure and occurs due to alloy formation between platinum and germanium. Region (A) was therefore assigned to platinum and region (B) to a Pt-Ge superlattice structure which has been described previously.¹²⁹ It was also observed that this particle contained a number of dislocations.

Another example of an alloy particle formed after four hours on line is shown in plate 14. This particle was approximately 12 nm in diameter. The corresponding EDX spectrum from this particle revealed a Pt/Ge atomic ratio of 2.3. The particle was observed to contain a number of regions with differently spaced and orientated lattice fringes. The main central region contained a set of bold lattice fringes (vertical in image) whose spacings were approximately 0.23 nm. Also present in this area was a second set of fringes (fainter) running at approximately 80° to the first set. The spacing of these fringes was approximately 0.32 nm. These spacings and the interplanar angle are consistent with the (101) and (021) planes of the orthorhombic PtGe structure. If this assignment is correct then the Pt/Ge ratio obtained from the EDX spectrum would suggest that the remaining regions of the particle were platinum.

Another example is shown in plate 15. This micrograph contained two particles. The EDX spectrum obtained from the larger 5 nm diameter particle (spectrum A) revealed that it was an alloy with an approximate Pt/Ge atomic ratio = 2.5. The EDX spectrum obtained from the smaller 3 nm diameter particle (spectrum B) contained peaks due to platinum only. This particle was observed to be in the (100) orientation (perpendicular

{200} lattice fringes visible). However, although the EDX spectrum from the smaller particle gave no evidence for the presence of germanium, the very low peak intensities in the spectrum, due to the small particle size, means that a significant concentration of germanium may have been present in this particle.

With further use in reforming, continued sintering of the metal component was observed to occur. As with Pt-Sn, very large 20-30 nm sized alloy particles were observed after 144 hours on line. However, the majority of metal particles detected even after this length of time on line were in the 2-10 nm size range. It is also possible that a significant proportion of the total metal content remained in the form of sub-nanometer sized particles.

As reported in a previous studies,^{128,129} a number of alloy phases were found to coexist in this catalyst. Unlike Pt-Sn, where the major alloy phase was hcp PtSn, in this catalyst there was a much greater variety in both the types of alloy formed and the relative distribution of the observed particles amongst the structures. Plates 16 to 21 give examples of all the alloy phases observed after 144 hours on line.

Plate 16 contains a particle that was approximately 20 nm in diameter. The EDX spectrum obtained from this particle revealed a Pt/Ge atomic ratio of 2.7. However, the lattice fringes visible had a spacing of 0.227 nm corresponding to the platinum {111} lattice. It is observed that some regions of the particle contained the characteristic features of a modified structure, i.e. alternating bright and weaker lattice fringes. This particle was therefore assigned to the Pt₃Ge superlattice phase.

Another example of this superlattice phase is shown in plate 17. Again this particle contained characteristic superlattice features with alternating strong and weak lattice fringes. The MBED pattern obtained (inset) was indexed as the (110) pattern of platinum with extra weaker spots between the main reflections. In this case the EDX spectrum contained a Pt/Ge atomic ratio equal to 5.4. It was observed that Pt-Ge alloy particles

with areas exhibiting superlattice features were found for compositions within the approximate range $\text{Pt/Ge} = 2$ to $\text{Pt/Ge} = 6$.

Another example of this phase is shown in plate 18. This particle was seen to contain two different regions, both of which exhibited superlattice features. The overall Pt/Ge atomic ratio was found to be 3.8. The MBED patterns obtained from the regions marked (A) and (B) in the image (taken with a 5 nm probe, marked as insets (a) and (b) respectively) can be indexed as platinum (110) with extra superlattice spots. However, pattern (b) is further away from the exact zone axis orientation.

It is interesting to compare the MBED patterns in plates 17 and 18 with the MBED pattern obtained from a Pt-Sn superlattice which is given in plate 11. The MBED patterns from the Pt-Ge alloys are observed to contain an extra set of superlattice reflections. As well as the superlattice spots corresponding to platinum {100} and {110}, an extra set of more closely spaced spots is observed (corresponding to $d = 0.454$ nm). The previous study performed in this department¹²⁹ found that these superlattice phases were similar to the well known Cu_3Au phase^{225,226} which has lattice parameters twice the size of platinum. The second set of superlattice reflections observed in plates 17 and 18 correspond to the {111} reflections of such a structure. These spots occur due to double diffraction.

Alloy phases such as orthorhombic Pt_3Ge_2 and PtGe were also observed. Plate 19 contains a very large particle which was formed after 144 hours on line. This particle was between 30-40 nm in diameter. The EDX spectrum obtained revealed a Pt/Ge atomic ratio of 1.7. The inserted MBED pattern was indexed as the (110) pattern of orthorhombic Pt_3Ge_2 . An example of the PtGe phase is given in plate 20. This particle was 35 nm in diameter. The EDX spectrum obtained revealed a Pt/Ge atomic ratio of 1.2. The MBED pattern obtained was indexed as the (110) pattern of the PtGe phase. Smaller examples of both of these phase were also observed after this length of time on line.

As with Pt-Sn, particles containing more than one phase were also often observed even after 140 hours on line. Plate 21 contains a particle 10-15 nm in diameter. It is clear from this image that the particle contained two different regions. The EDX spectrum obtained from the entire particle using a 20 nm probe revealed a Pt/Ge atomic ratio of 2.7. The larger bold lattice (region A) fringes visible had a spacing of approximately 0.32 nm which was assigned to the {101} spacing (0.316 nm) of the orthorhombic PtGe structure. The second, less visible, lattice (region B) had a spacing of approximately 0.22 nm which was assigned to the {111} spacing of platinum. These assignments correlate well with the observed EDX Pt/Ge atomic ratio of 2.7.

5.3.B n-Octane reforming

The yields of individual products species over the Pt-Ge catalysts are presented versus time on line in table 5.3.1 and plotted in figures 5.3.1 to 5.3.6.

The yields of methane, ethane, propane, i-butane and n-butane are plotted in figure 5.3.1. Relative to the Pt/Al₂O₃ catalysts (figure 5.1.1) it was observed that there was a marked increase in the yields of propane, i-butane and n-butane (all hydrocracked products) on the addition of germanium (after 1 hour: propane- 7.0% versus 7.5%, i-butane- 3.9% versus 5.5%, n-butane- 5.9% versus 7.6%). The yield of methane, although initially similar to that obtained over platinum (5-6%), did not undergo the initial rapid decline observed over the platinum catalysts. In this respect Pt-Ge/Al₂O₃ was similar to Pt-Sn/Al₂O₃. However, the rate of decline of the yield of methane was observed to increase with increasing time on line over this catalyst, again similar to Pt-Sn.

The yields of cyclic products over this catalyst are plotted in figure 5.3.2. In this case the initial yields of C₇ and C₈ cycloalkanes were observed to be slightly higher than those observed over Pt/Al₂O₃. The yield of cyclopentane was low throughout the run, as over

the previous catalysts. The yield of C₈ cycloalkanes was observed to increase sharply throughout the run, again in a similar manner to the two previous catalysts.

The yields of i-alkanes over Pt-Ge/Al₂O₃ are plotted in figure 5.3.3. The yields of these products over this catalyst were found to be roughly similar in most respects to those observed over Pt/Al₂O₃. The only slight differences being a small decrease in the yield of i-hexane and a small increase in the yield of i-pentane due to the addition of germanium. The yield of i-octane was observed to increase sharply throughout the run (from 3.3 to 21.5%) in a similar manner to Pt-Sn/Al₂O₃.

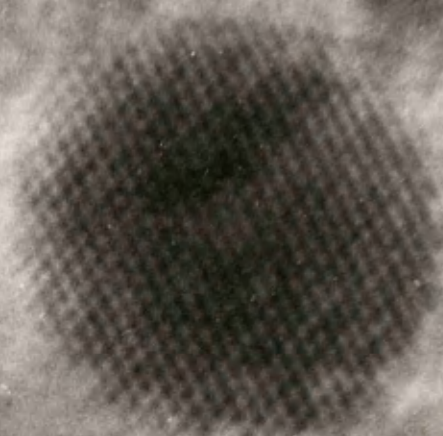
The yields of n-alkanes are plotted in figure 5.3.4. Again, no major changes in the yields of these products were observed due to the presence of germanium. Again, a similar finding was made with Pt-Sn/Al₂O₃.

However, the yields of aromatics, shown in figure 5.3.5, were significantly altered by the presence of germanium in the catalyst. The yields of xylenes were found to increase significantly on the addition of germanium. However, this increase was not as pronounced as that observed on addition of tin (m/p xylenes after 1 hour: Pt 19.4%, Pt-Sn 27.4%, Pt-Ge 23.6%). This improvement was completely nullified by a corresponding decrease in the yield of ethylbenzene (8.8% over Pt, 4.4% over Pt-Ge, 6.3 % over Pt-Sn). The presence of germanium also influenced the slopes of the trendlines for aromatic products. Again, as with Pt-Sn, the rapid initial decrease in the yields of aromatics observed over the Pt/Al₂O₃ catalyst did not occur on this catalyst. However, the yields of these products did decline continuously throughout the run.

Similar effects were observed with the overall conversion, figure 5.3.6. Comparing this figure with the conversion over Pt/Al₂O₃ (figure 5.1.6) we see that the initial conversion was slightly higher over the Pt-Ge catalysts (99.1% versus 98.4%). As with Pt-Sn, however, the major difference was in the change in the level of conversion with time on line. As was shown in section 5.1, the Pt/Al₂O₃ catalysts undergoes a period of rapid

deactivation in the initial stages, which was not observed over Pt-Ge or Pt-Sn/ Al_2O_3 . However, whilst the rate of deactivation over Pt/ Al_2O_3 decreased with time on line, the rate of deactivation over Pt-Ge actually increased. The overall result would be that, given a sufficiently long period of time, the level of conversion over the Pt-Ge catalyst would be likely to drop below that of monometallic platinum. (This was actually seen to occur after ~ 120 hours over Pt-Sn).

The selectivities to the major reforming reactions are listed in table 5.3.2 versus time in line and are plotted in figure 5.3.7. The first point to note is that the addition of germanium increased slightly the selectivity to hydrocracking (compare with table 5.1.2 and figure 5.1.7). This effect is more pronounced if the yields of propane and n-butane are also taken into consideration. The other major influence of germanium was to prevent the initial rapid decline in aromatisation and subsequent increase in isomerisation that occurred over Pt/ Al_2O_3 . Although both of these did occur over Pt-Ge/ Al_2O_3 , they occurred at a more gradual pace throughout the entire length of the run (again compare with figure 5.1.7).



2 nm

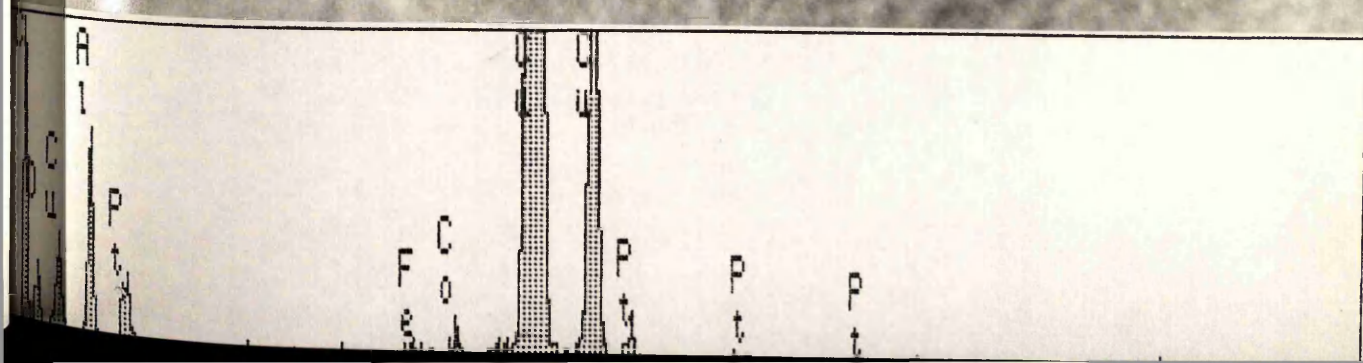
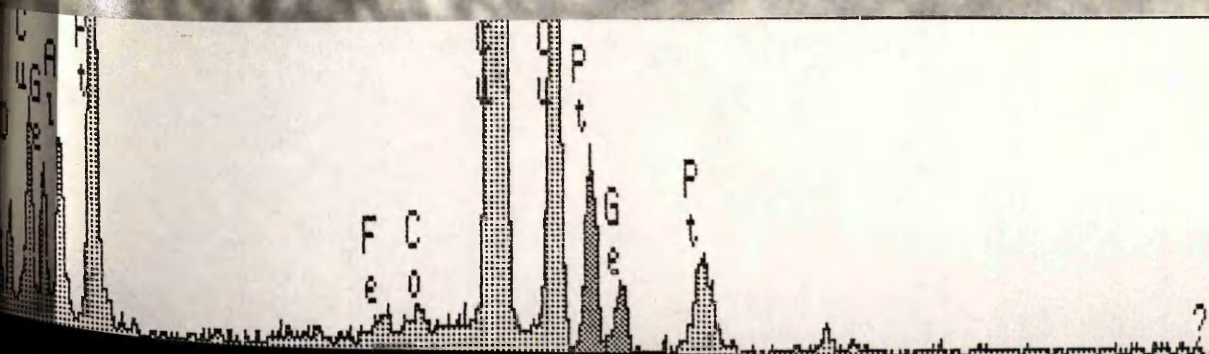


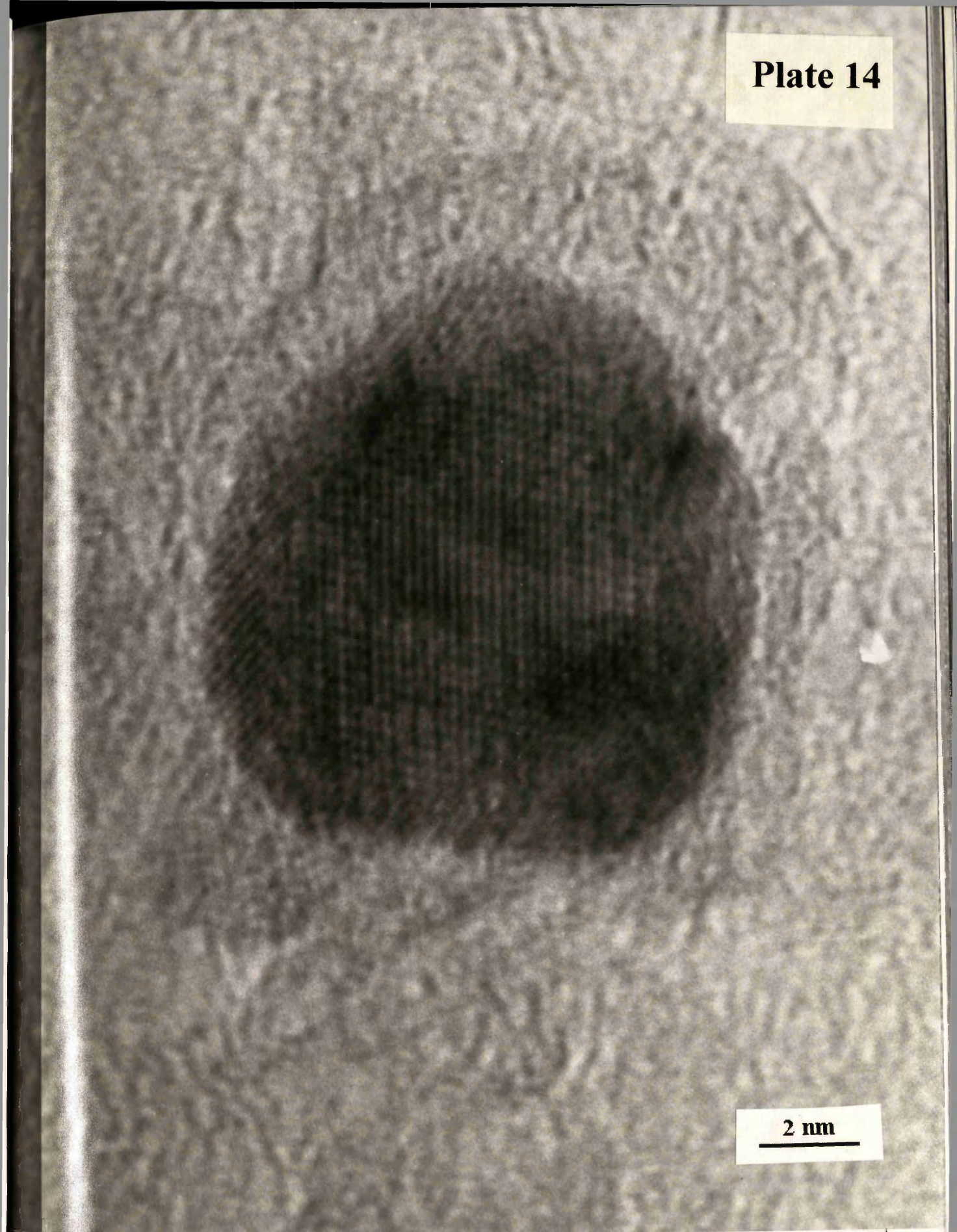
Plate 13

(A)

(B)

2 nm





2 nm

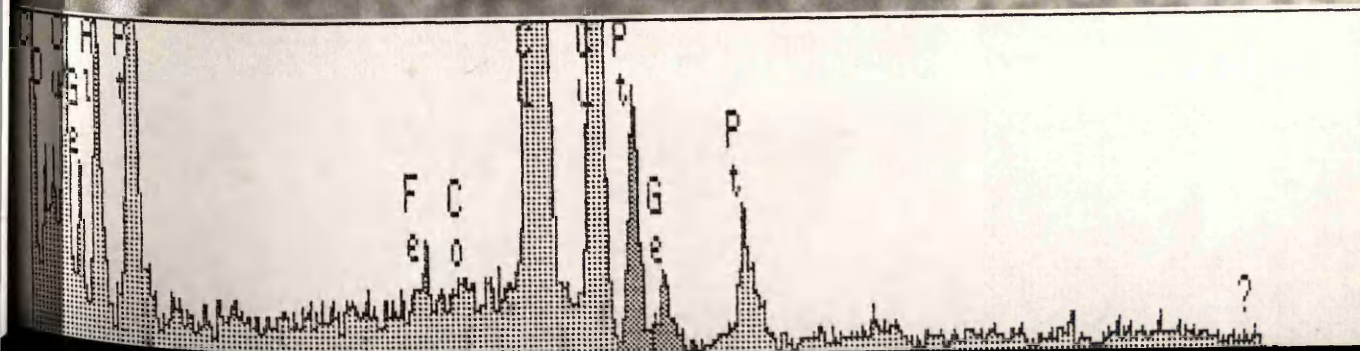
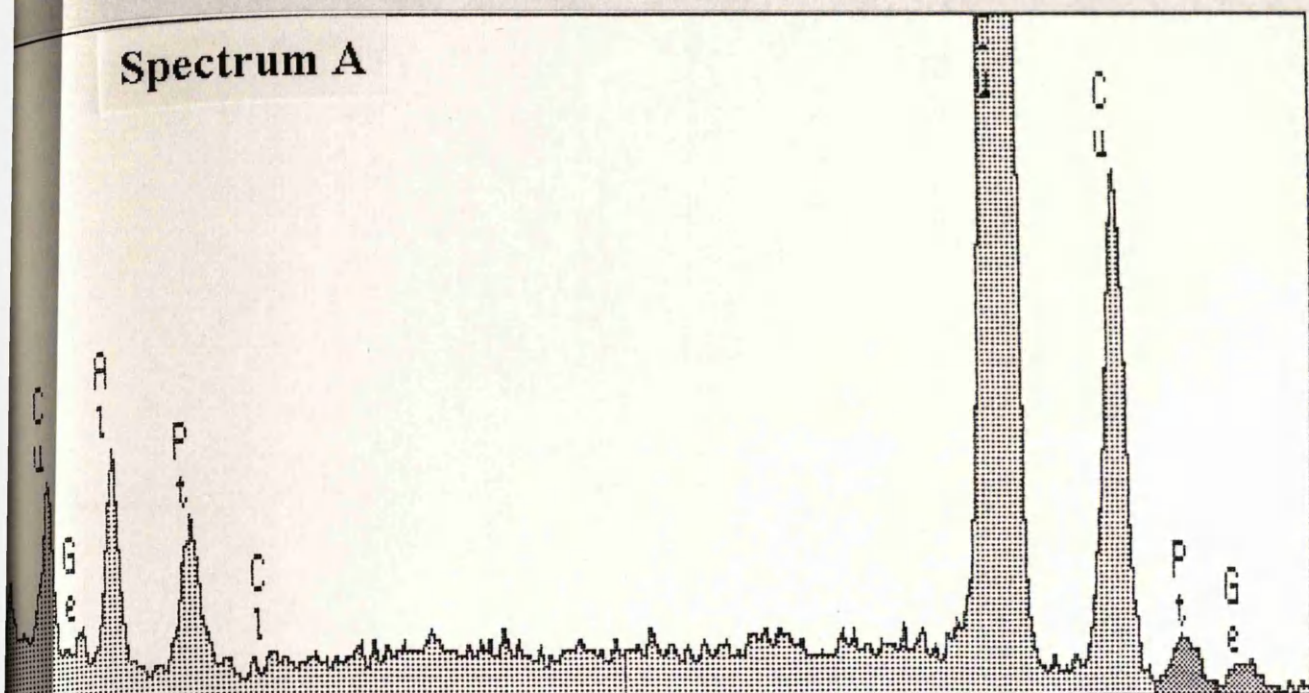


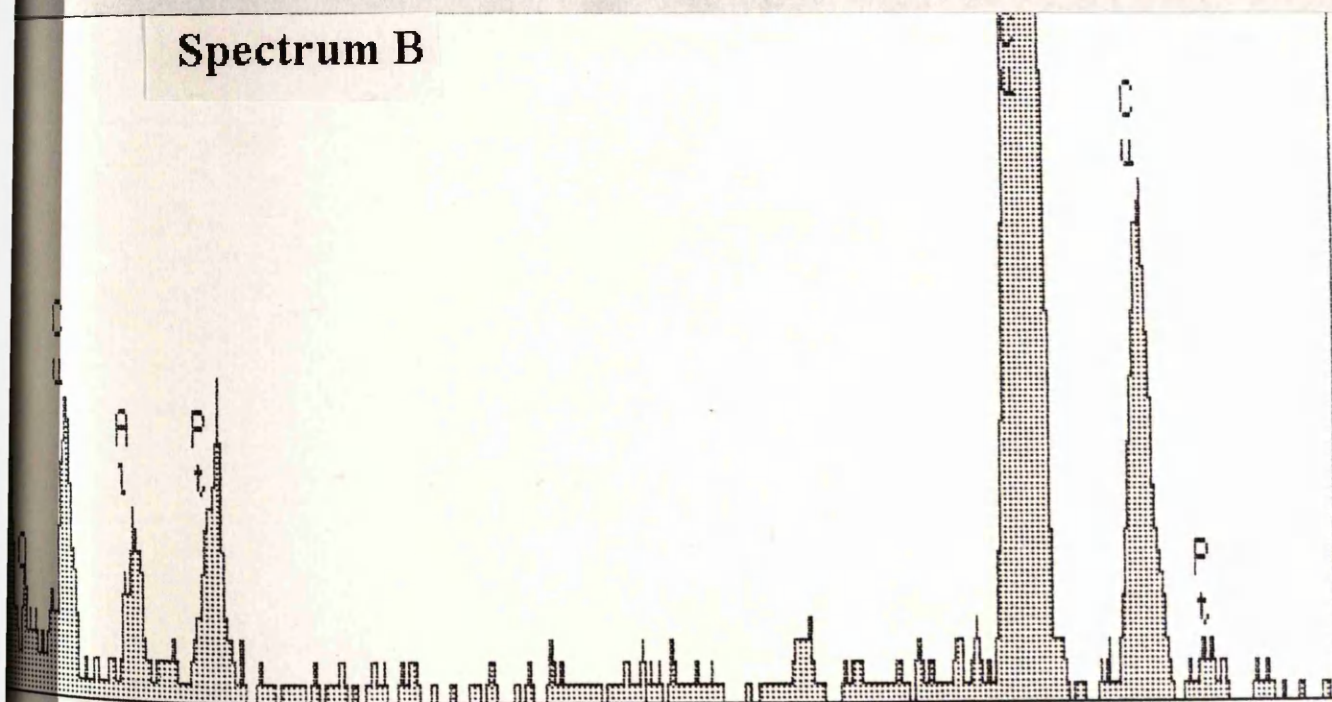
Plate 15

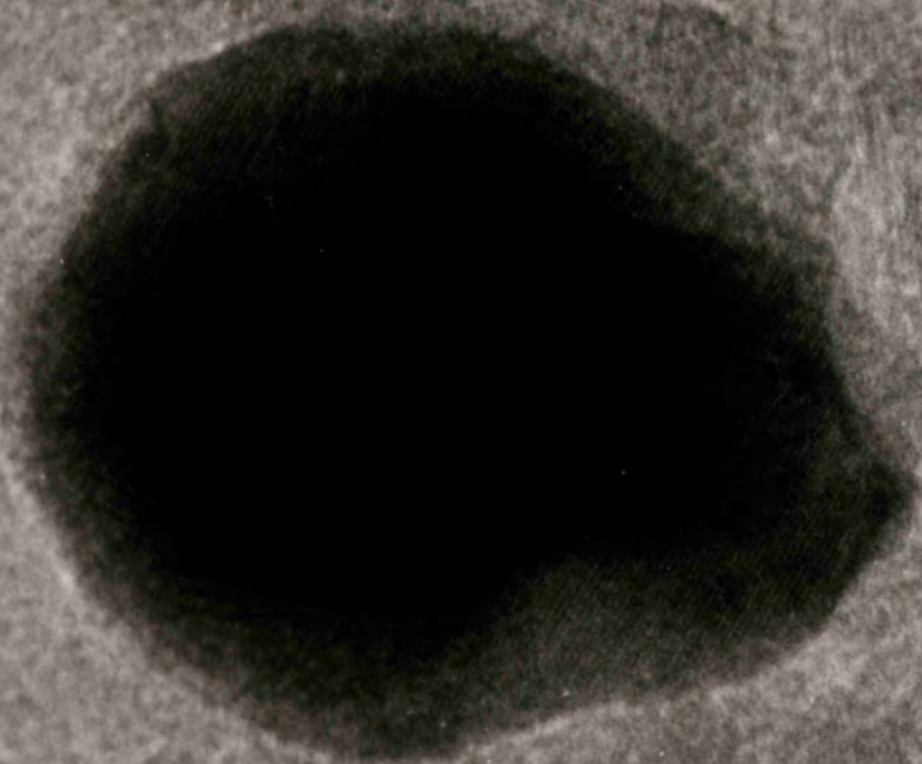
5 nm

Spectrum A

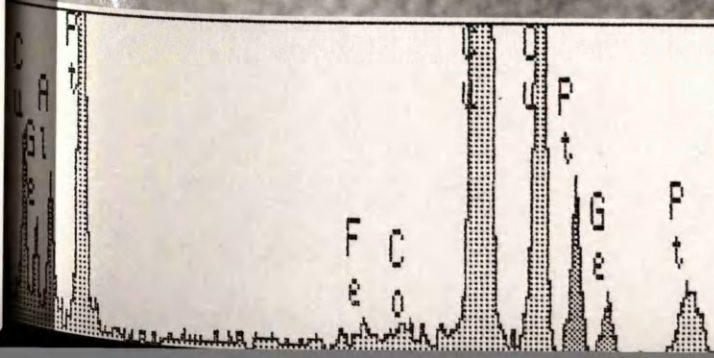


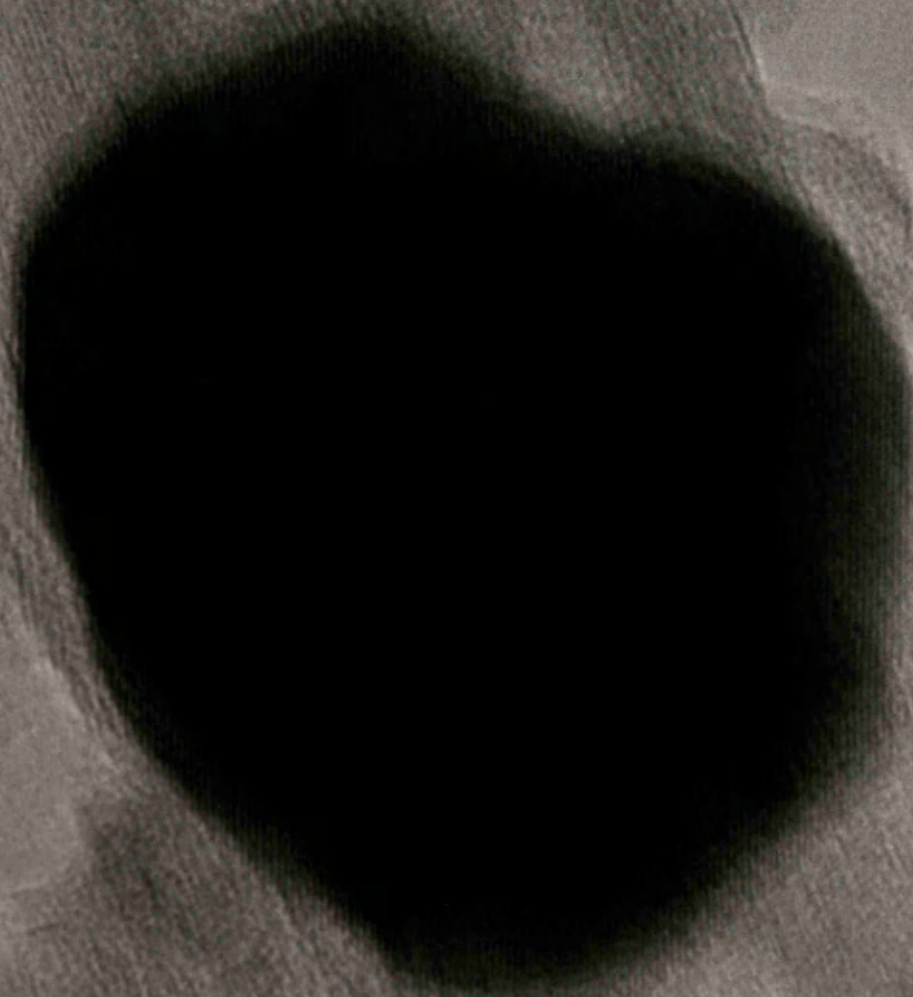
Spectrum B



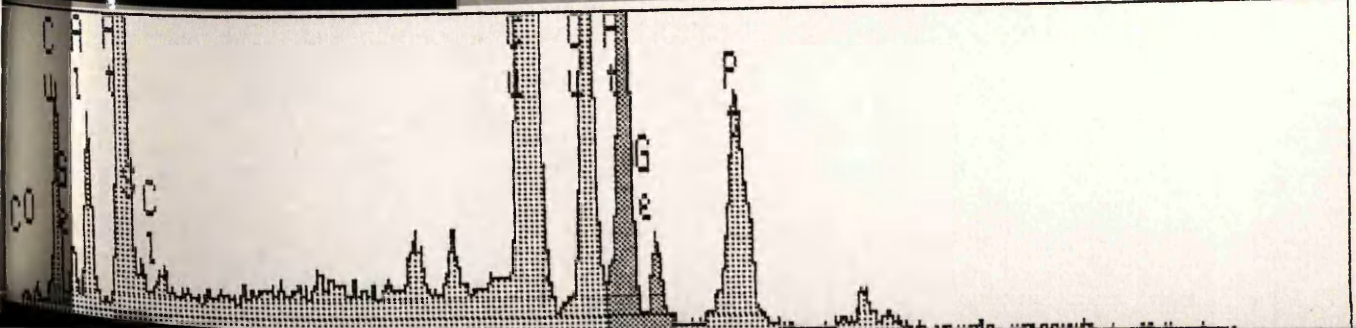


5 nm





5 nm



(b)

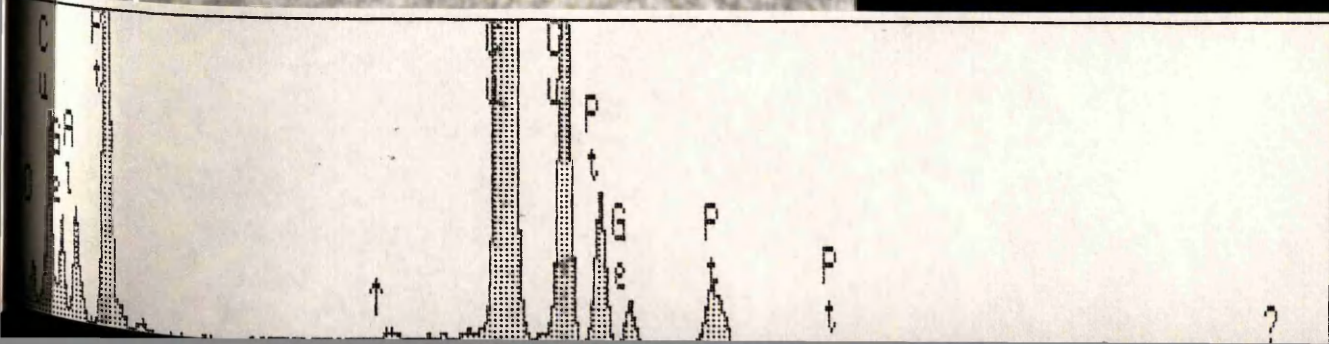
Plate 18

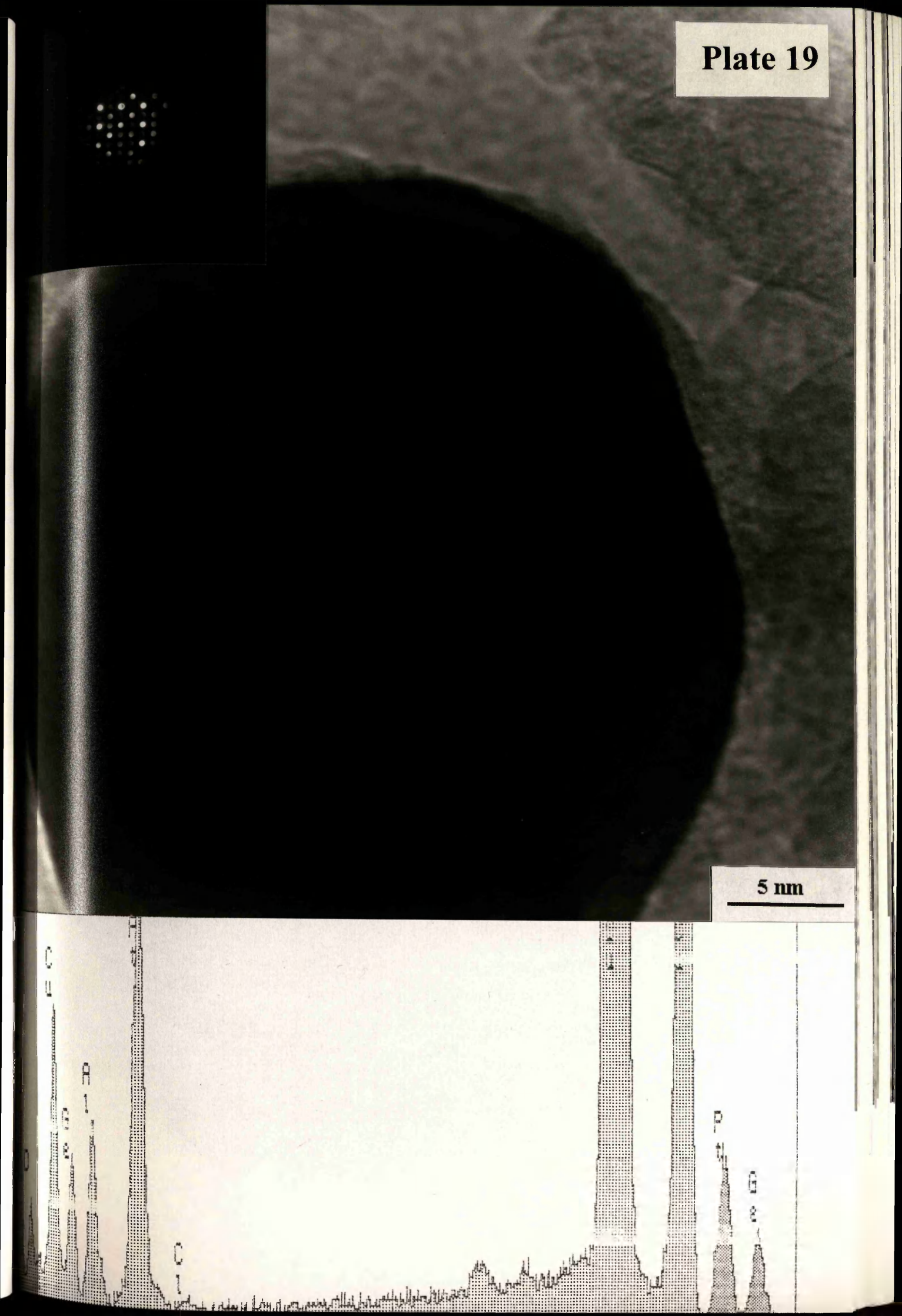
(A)

(B)

5 nm

(a)





5 nm

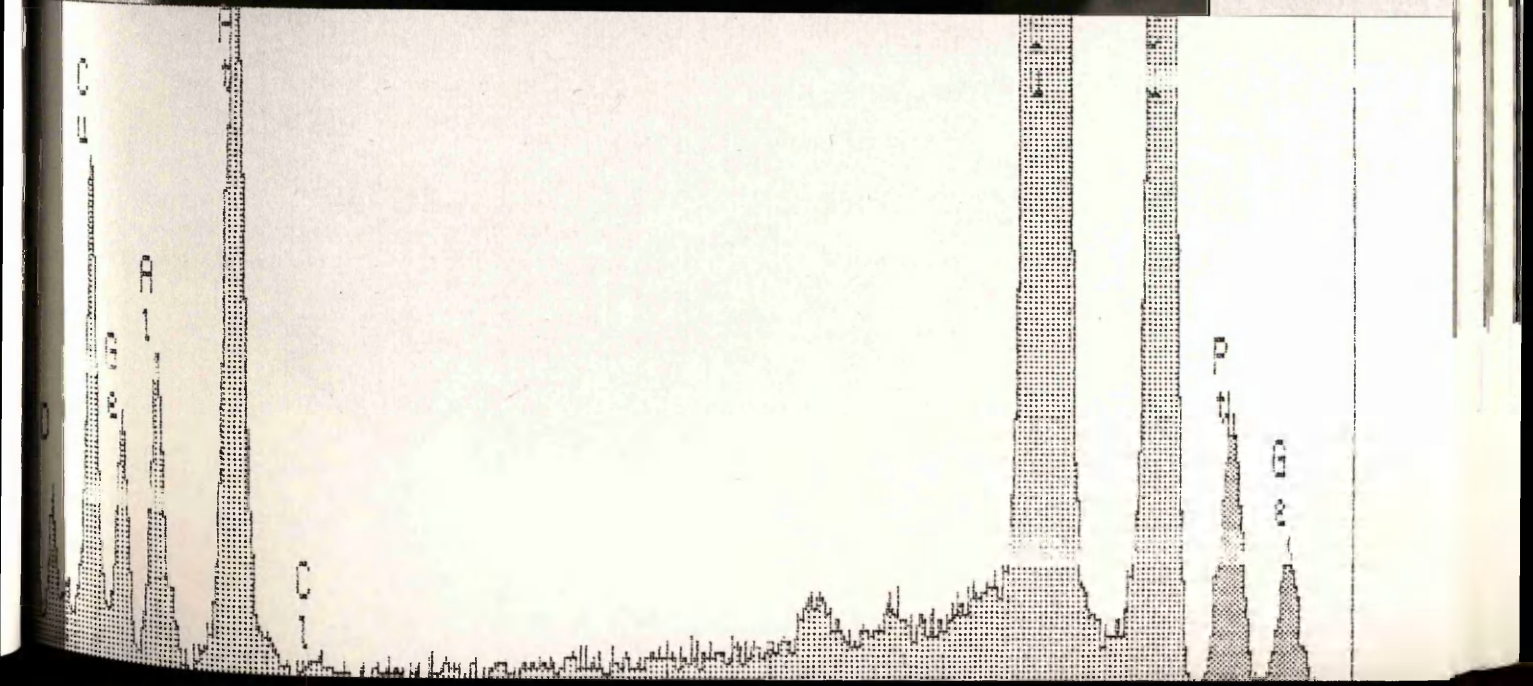
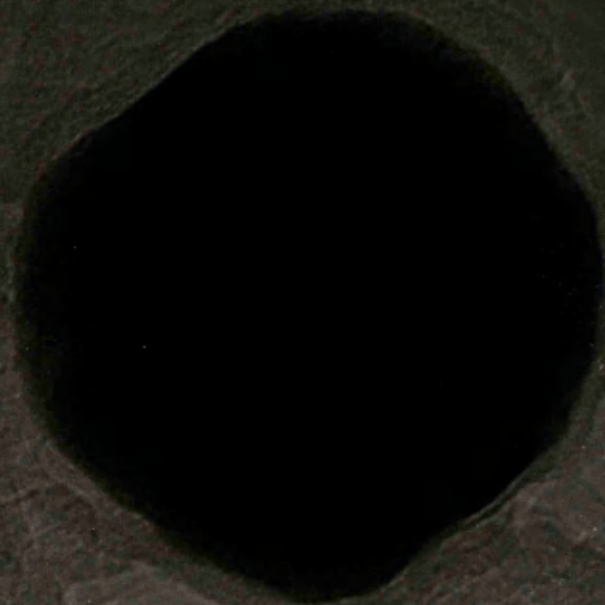
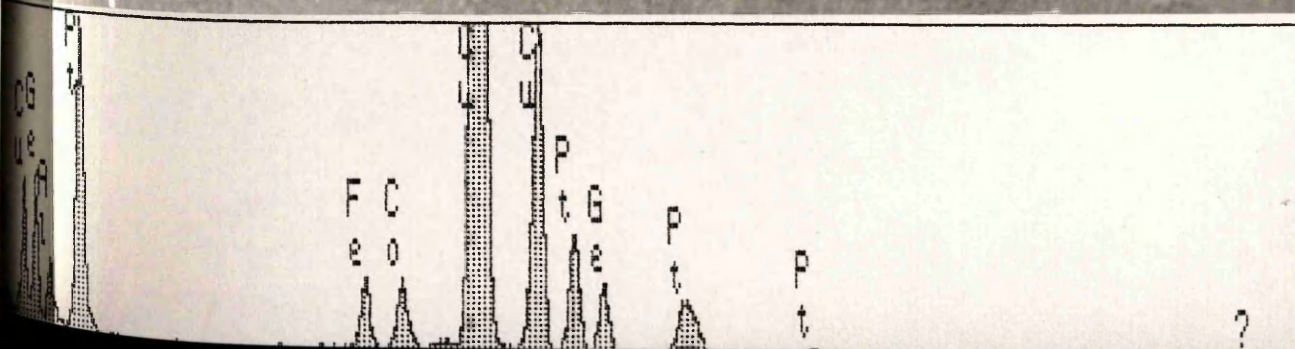


Plate 20



10 nm



(B)

(A)

2 nm

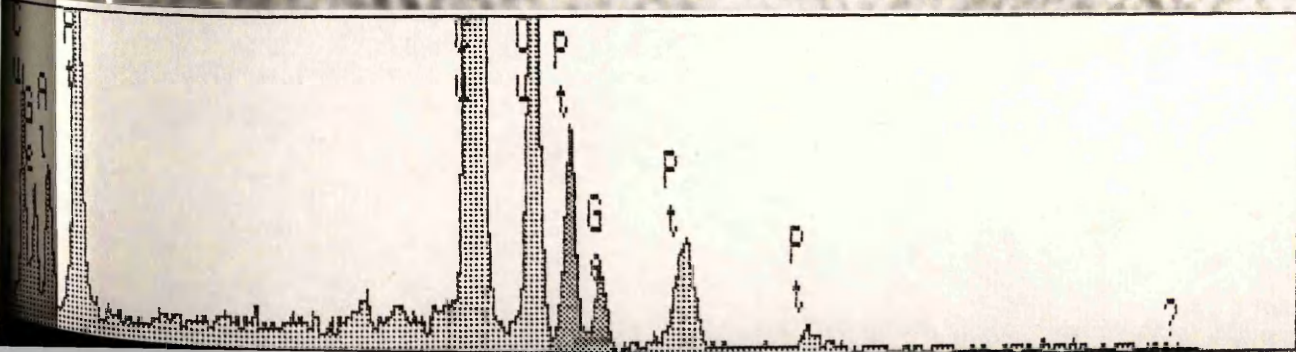


Table 5.3.1 Yields of individual products for catalyst 0.3 wt% Pt - 0.3 wt% Ge/Al₂O₃

Time (hours)	Methane	Ethane	Propane	i-Butane	n-Butane	c-Pentane	i-Pentane	n-Pentane
1.0	5.2	2.2	7.5	5.5	7.6	0.1	7.6	5.7
4.5	5.9	2.2	6.8	5.3	7.3	0.0	7.3	5.6
18.5	5.8	2.1	7.4	5.6	6.6	0.0	7.6	4.3
22.0	5.5	2.2	7.3	5.8	7.0	0.0	7.5	4.2
30.0	5.6	2.0	6.8	5.6	6.9	0.0	7.8	4.3
66.5	5.3	1.9	6.6	5.1	6.2	0.0	7.1	3.9
70.0	4.8	1.7	6.2	4.9	6.5	0.0	7.0	4.6
97.5	4.8	1.9	6.8	5.3	6.4	0.0	7.2	4.0
120.5	4.7	1.8	6.6	5.1	6.7	0.0	7.0	4.3
125.0	3.9	1.8	6.5	5.0	6.6	0.0	6.9	4.5
139.0	4.2	1.7	6.3	4.9	6.0	0.0	6.7	4.0
144.0	3.7	1.8	6.4	5.0	6.2	0.0	6.7	4.1

Table 5.3.1 (cont) Yields of individual products for catalyst 0.3 wt% Pt - 0.3 wt% Ge/Al₂O₃

Time (hours)	C6 c-Alkane	i-Hexane	n-Hexane	C7 c-Alkane	i-Heptane	n-Heptane	C8 c-Alkane	i-Octane
1.0	0.6	4.4	2.5	0.5	1.1	1.0	0.8	3.3
4.5	0.6	4.6	2.6	0.6	1.3	1.1	0.9	4.6
18.5	0.5	4.7	2.5	0.6	1.1	1.0	0.9	7.1
22.0	0.4	5.0	2.3	0.5	1.4	0.9	0.8	7.3
30.0	0.4	5.1	2.4	0.5	1.3	0.8	0.8	10.4
66.5	0.3	4.8	2.1	0.5	1.3	0.8	0.9	14.7
70.0	0.5	5.0	2.7	0.6	1.6	1.0	1.2	13.3
97.5	0.4	4.9	2.6	0.7	1.3	1.1	1.3	15.8
120.5	0.3	5.0	2.5	0.6	1.3	0.9	1.2	18.3
125.0	0.4	5.1	2.6	0.6	1.7	1.0	1.4	19.3
139.0	0.3	5.0	2.3	0.6	1.4	0.9	1.2	20.9
144.0	0.4	5.0	2.4	0.6	1.7	0.9	1.3	21.5

Table 5.3.1 (cont) Yields of individual products for catalyst 0.3 wt% Pt - 0.3 wt% Ge/Al₂O₃

Time (hours)	Benzene	Toluene	Ethyl- Benzene	m/p- Xylene	o-Xylene	C9 Aromatic	Total Conversion
1.0	0.7	2.5	4.4	23.6	11.5	0.9	99.1
4.5	0.7	2.5	4.0	23.3	10.6	0.9	98.9
18.5	0.6	2.4	4.0	22.7	10.9	0.9	99.2
22.0	0.5	2.0	3.8	22.2	10.8	0.9	98.5
30.0	0.4	1.8	3.7	21.1	9.9	0.8	98.4
66.5	0.4	1.7	3.4	18.9	9.3	0.8	96.2
70.0	0.2	1.6	3.5	18.3	9.2	0.8	95.3
97.5	0.3	1.5	3.5	16.4	7.6	0.8	94.6
120.5	0.3	1.6	3.2	15.1	7.0	0.9	94.4
125.0	0.3	1.5	2.9	13.9	6.4	0.8	93.2
139.0	0.2	1.4	2.8	13.6	6.2	0.8	91.5
144.0	0.2	1.4	2.6	13.1	5.9	0.8	91.6

Table 5.3.2 Selectivity to the major reforming reactions for 0.3 wt% Pt - 0.3 wt% Ge/Al₂O₃

Time (hours)	Selectivity to Aromatics	Selectivity to Isomerisation	Selectivity to Hydrocracking	Selectivity to Hydrogenolysis
1.0	43.9	4.5	17.7	5.3
4.5	42.5	6.0	17.4	6.0
18.5	41.7	8.3	18.1	5.8
22.0	40.9	8.9	18.6	5.6
30.0	38.3	11.9	18.7	5.7
66.5	36.0	16.6	17.7	5.5
70.0	35.4	15.7	17.7	5.1
97.5	31.9	18.1	18.3	5.1
120.5	29.8	20.8	18.0	5.0
125.0	27.7	22.6	18.2	4.2
139.0	27.4	24.3	18.2	4.6
144.0	26.2	25.3	18.3	4.1

Figure 5.3.1 Yields of individual products over 0.3 wt% Pt - 0.3 wt% Ge/Al₂O₃

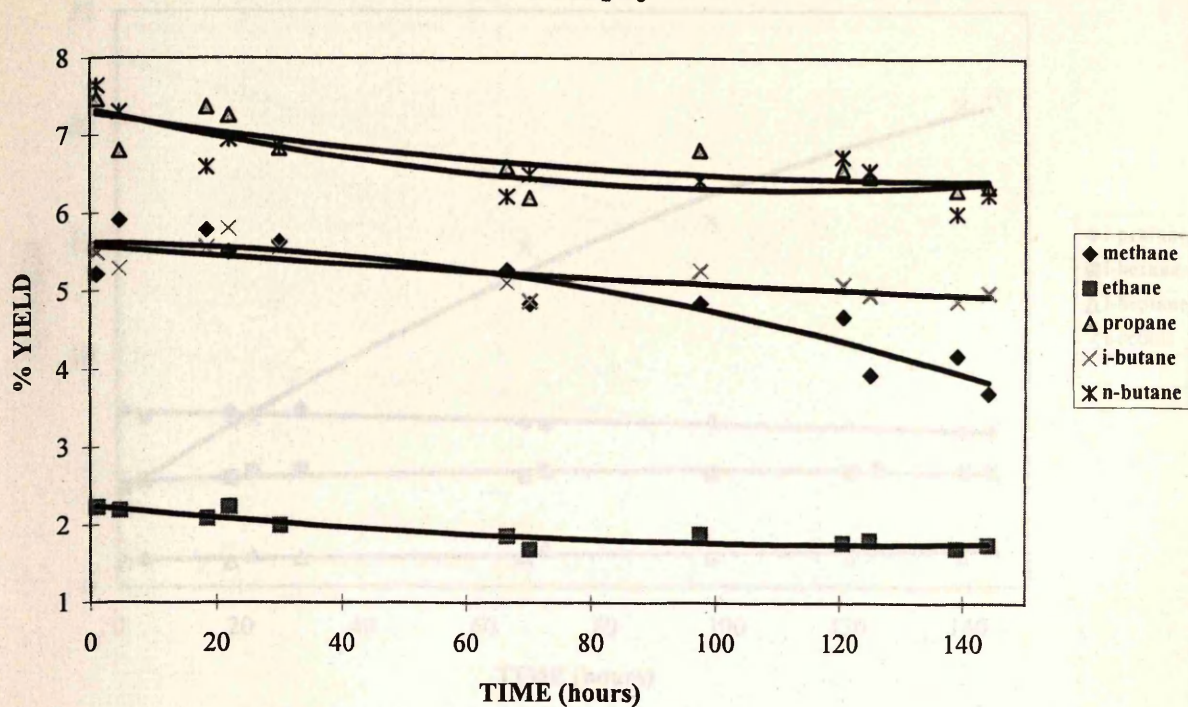


Figure 5.3.2 Yields of cycloalkanes over 0.3 wt% Pt - 0.3 wt% Ge/Al₂O₃

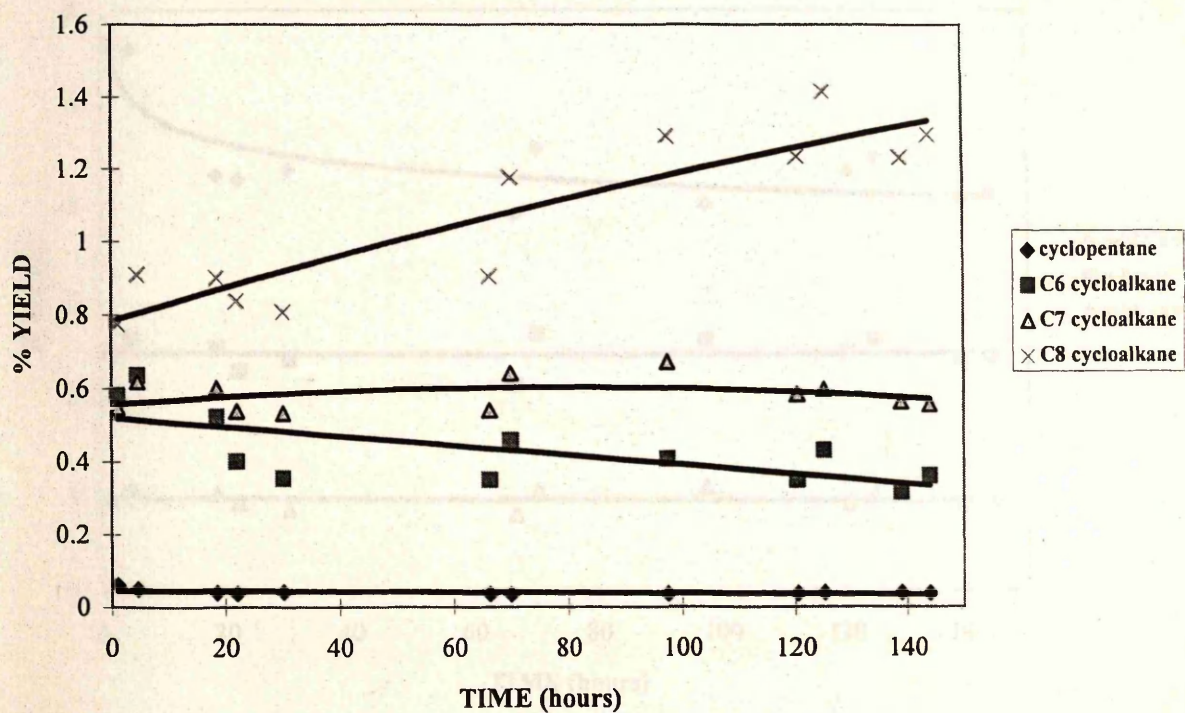


Figure 5.3.3 Yields of i-alkanes over 0.3 wt% Pt - 0.3 wt% Ge/Al₂O₃

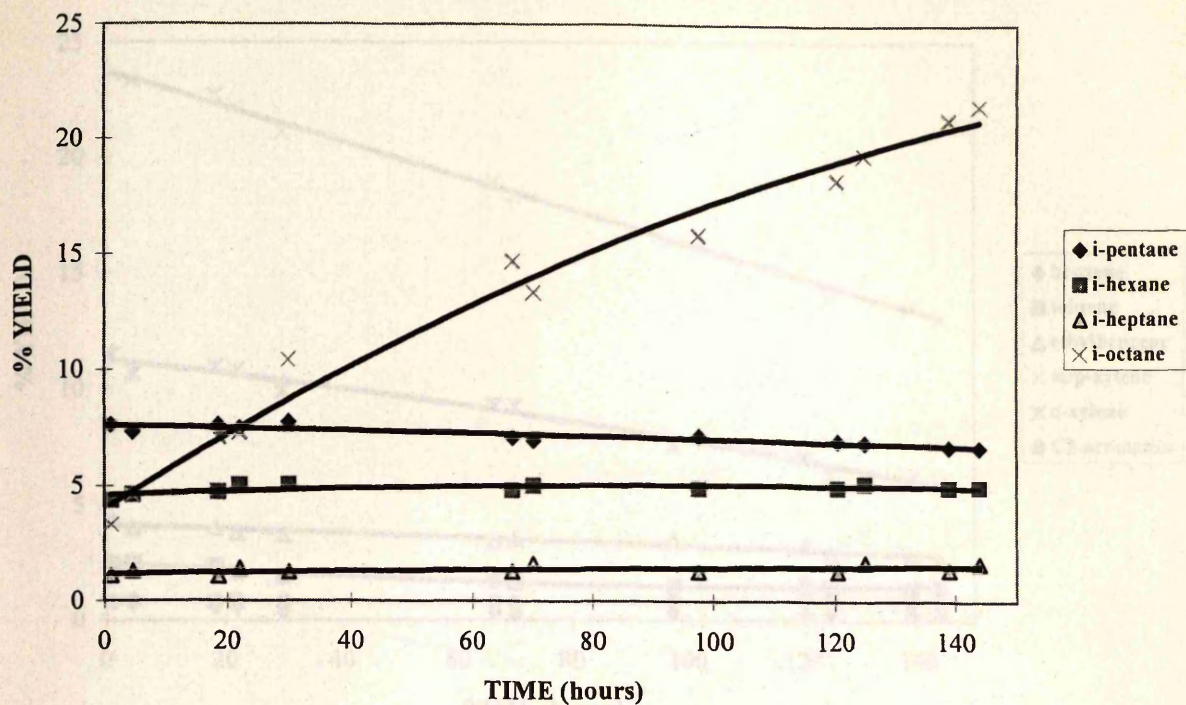


Figure 5.3.4 Yields of n-alkanes over 0.3 wt% Pt - 0.3 wt% Ge/Al₂O₃

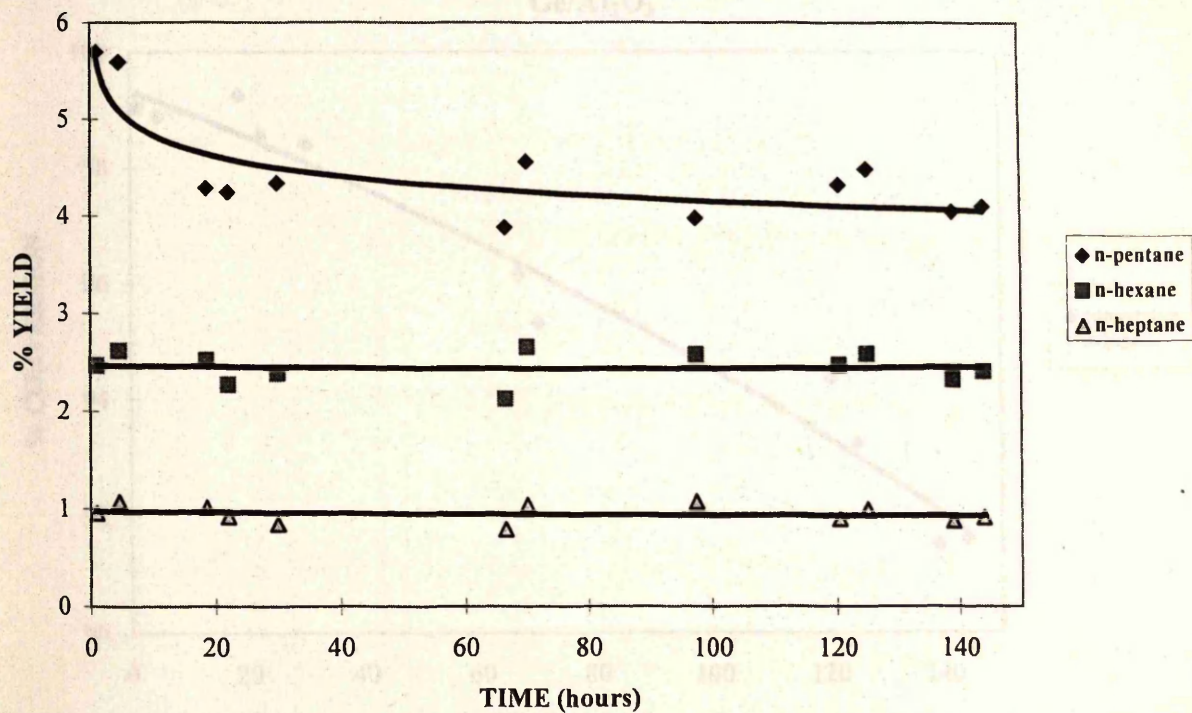


Figure 5.3.5 Yields of aromatics over 0.3 wt% Pt - 0.3 wt% Ge/Al₂O₃

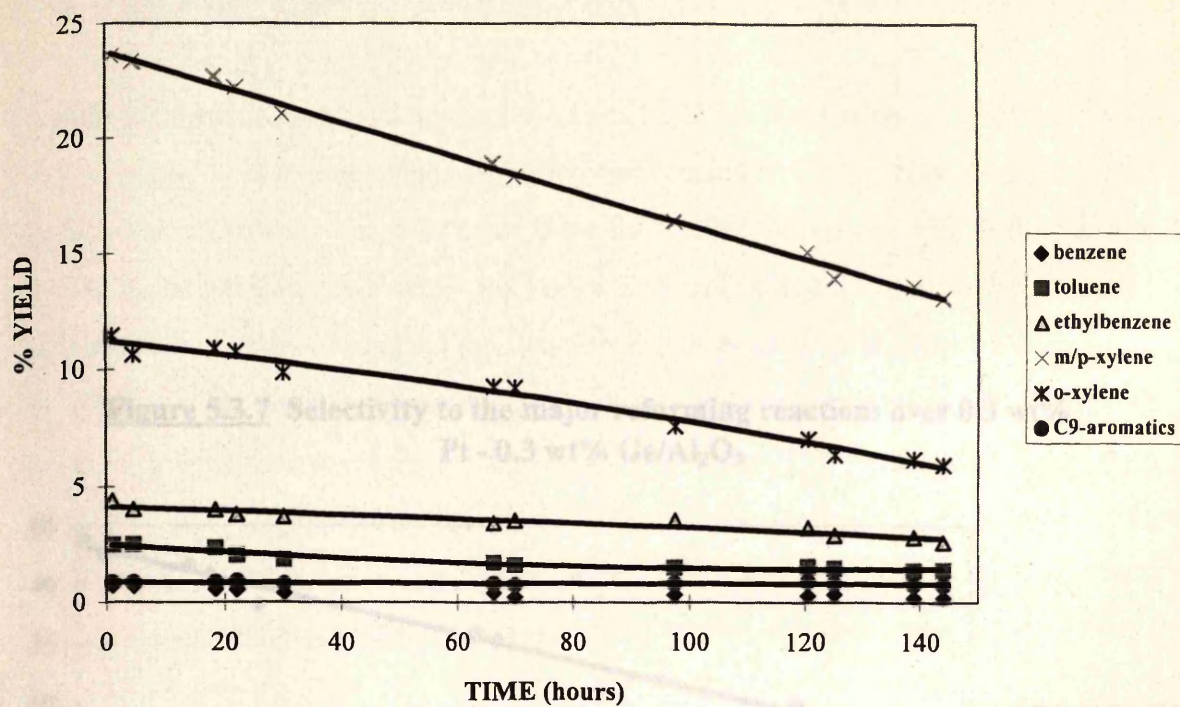
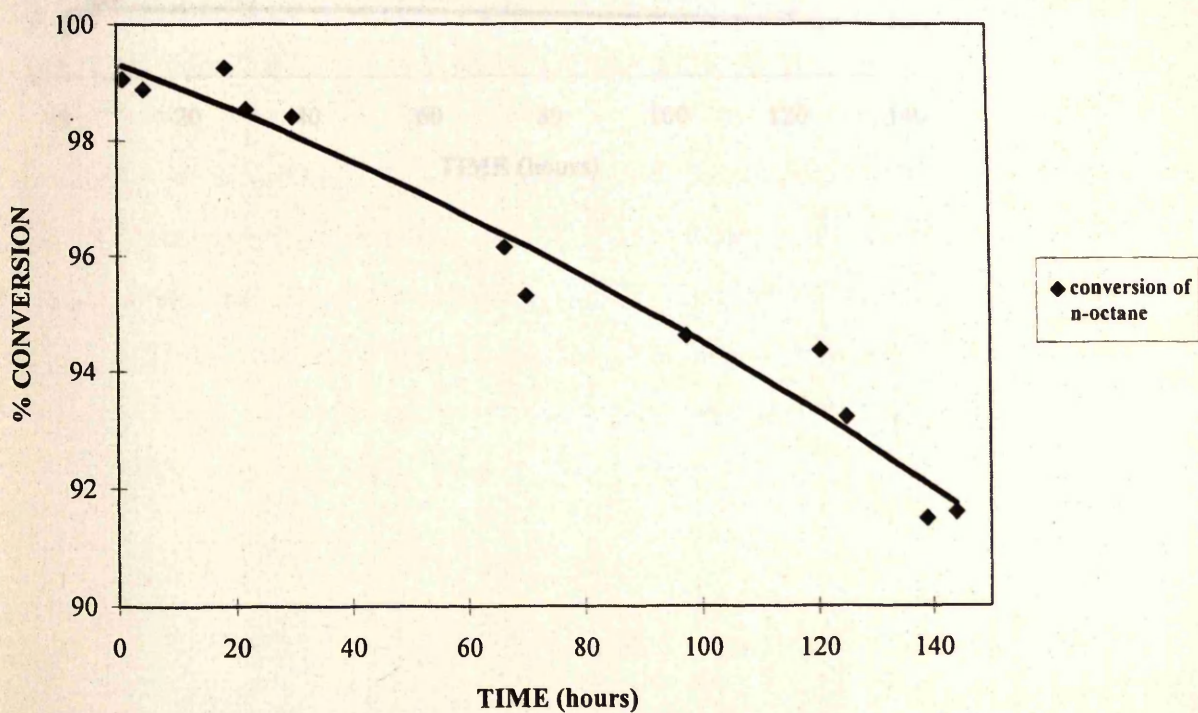


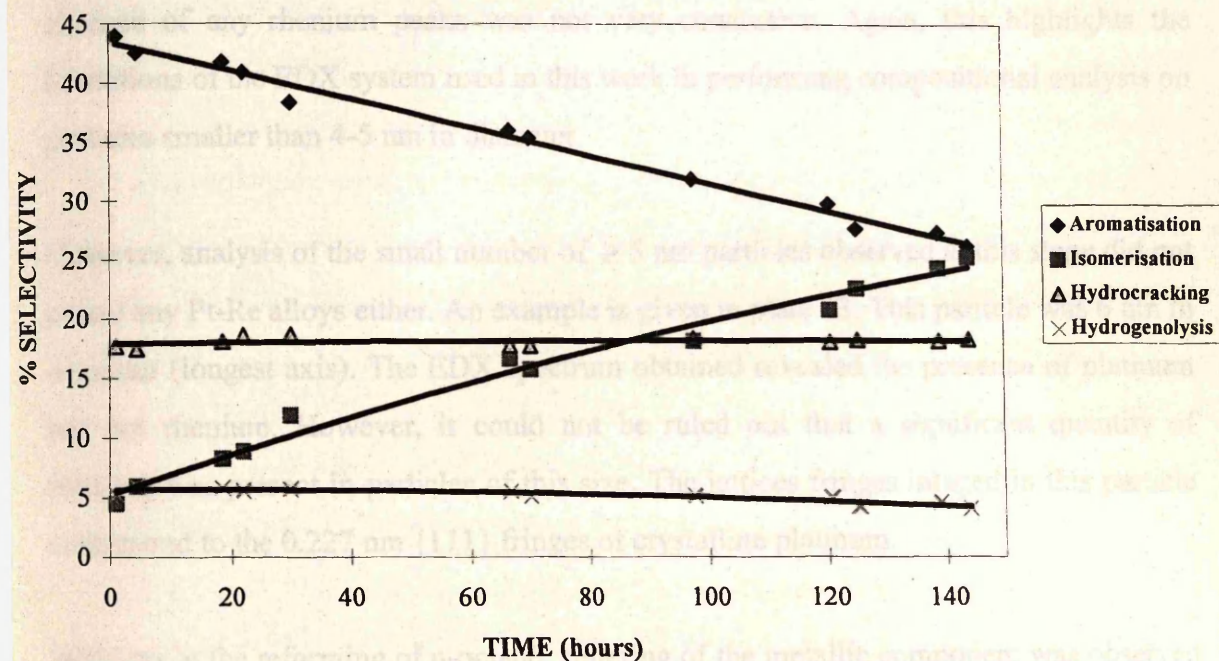
Figure 5.3.6 Conversion of n-octane over 0.3 wt% Pt - 0.3 wt% Ge/Al₂O₃



2.4.4. TEM observations

As with the previous catalysts studied, the metallic component of this system was found to be very highly dispersed after calcination and reduction. Only a small number of 2-5 nm sized particles were observed after these treatments. An example is shown in plate 22. The metal particle observed in this image was approximately 5 nm in diameter. The EDX spectrum obtained using a 5 nm diameter probe revealed peaks due to platinum but

Figure 5.3.7 Selectivity to the major reforming reactions over 0.3 wt% Pt - 0.3 wt% Ge/Al₂O₃



5.4 0.3 wt% Pt - 0.3 wt% Re/Al₂O₃

5.4.A. TEM observations

As with the previous catalysts studied, the metallic component of this system was found to be very highly dispersed after calcination and reduction. Only a small number of 2-5 nm sized particles were observed after these treatments. An example is shown in plate 22. The metal particle observed in this image was approximately 3 nm in diameter. The EDX spectrum obtained using a 5 nm diameter probe revealed peaks due to platinum but not rhenium (the position of the Re M_{α} and $L_{\alpha 1}$ lines are marked in the spectrum). However, this particle was near the detection limit of the EDX system and therefore the absence of any rhenium peaks was not very conclusive. Again, this highlights the limitations of the EDX system used in this work in performing compositional analysis on particles smaller than 4-5 nm in diameter.

However, analysis of the small number of ≥ 5 nm particles observed at this stage did not reveal any Pt-Re alloys either. An example is given in plate 23. This particle was 6 nm in diameter (longest axis). The EDX spectrum obtained revealed the presence of platinum but not rhenium. However, it could not be ruled out that a significant quantity of rhenium was present in particles of this size. The lattices fringes imaged in this particle correspond to the 0.227 nm {111} fringes of crystalline platinum.

With use in the reforming of n-octane, sintering of the metallic component was observed to occur. After 144 hours on line a number of large sintered particles were observed (10-30 nm) along with the more common 1-5 nm sized particles. The relative rates of sintering of these catalysts will be compared and discussed in chapter 6. However, unlike Pt-Sn and Pt-Ge, no alloy particles were detected in this system even after 144 hours on line. The only metallic particles observed being platinum.

An example is shown in plate 24. This particle was observed after 144 hours on line and was approximately 10 nm in diameter. The MBED pattern obtained was indexed as the (110) pattern of platinum. The corresponding EDX spectrum revealed the presence of platinum only.

Another example is shown in plate 25. This was a relatively large 20-25 nm sized particle. The MBED pattern obtained from this particle was again indexed as the (110) pattern of platinum. The lattice fringes visible in the image correspond to the {111} 0.227 nm lattice. Again the EDX spectrum obtained gave no evidence for the presence of rhenium. The accuracy of compositional analysis by EDX improves with the size of the metal particle analysed. Therefore, for relatively large particles such as the one in plate 25, an upper limit of a few percent rhenium is placed on the proportion of this metal that may have been present.

Although substantial sintering of the metallic component had occurred during 144 hours on line, large particles such as those in plates 24 and 25 were still relatively infrequently observed and it is likely that a substantial fraction of the metal remained in the form of nanometer sized particles. The same may be said of the Pt-Sn and Pt-Ge catalysts.

5.4.B n-Octane reforming

The yields of individual product species over Pt-Re/ Al_2O_3 are presented versus time on line in table 5.4.1 and plotted in figures 5.4.1 to 5.4.6.

The yields of methane, ethane, propane, i-butane and n-butane were all higher over this catalyst (figure 5.4.1) than over the Pt/ Al_2O_3 catalyst, particularly in the case of methane and ethane (initial methane: Pt 5.8%, Pt-Re 10.0%; initial ethane: Pt 3.45, Pt-Re 5.3%). However the change in the yields of these products with time on line was similar to that which occurred over Pt/ Al_2O_3 , i.e. the yields of all these products remained relatively

constant throughout the run with the exception of methane which underwent a period of rapid initial decline before reaching a more stable value. It will be remembered that Pt-Sn and Pt-Ge/Al₂O₃ did not show this behaviour in methane yield.

The yields of cycloalkanes over this catalysts are plotted in figure 5.4.2. The yields of these products over Pt-Re were roughly similar to those over platinum with one important exception. The production of C₈ cycloalkanes did not undergo the rapid increase which was observed over platinum (and also Pt-Ge and Pt-Sn) e.g. final yields:- Pt 2.1%, Pt-Re 0.2%.

The yields of i-alkanes over this catalyst are plotted in figure 5.4.3. The initial yields of i-hexane, i-heptane and i-octane were all observed to be considerably lower than over Pt/Al₂O₃ (See figure 5.1.3:- 3.9% versus 6.0%, 0.5% versus 1.1% and 0.6 versus 5.3% respectively). The yields of i-pentane were similar. However the main difference between these catalysts when considering i-alkane products was in the change in the yield of i-octane with time on line. Although the yield of i-octane did increase over this catalyst, the level of this increase was considerably lower over Pt-Re (final yield 5.7%) than over monometallic Pt (final yield 23%).

The yields of n-alkanes over this catalyst are plotted in figure 5.4.4. The yields of n-pentane and n-hexane were observed to be similar to those obtained over Pt/Al₂O₃ (figure 5.1.4). The yields of n-heptane however, were, in general, lower over this catalyst.

The yields of aromatic hydrocarbons over this catalyst, figure 5.4.5, were however found to be very different to those observed over platinum. The addition of rhenium had pronounced effects on both the initial yields of these species and also in the manner in which these values changed with time on line. The first point to note was the large increase in the yield of toluene, and to a lesser extent benzene, on this catalyst compared with Pt/Al₂O₃ (figure 5.1.5.) Initial yields of benzene: Pt 1.3%, Pt-Re 2.9%. Initial yields

of toluene: Pt 3.7%, Pt-Re 11%). Conversely, the initial yield of ethylbenzene was considerably lower.

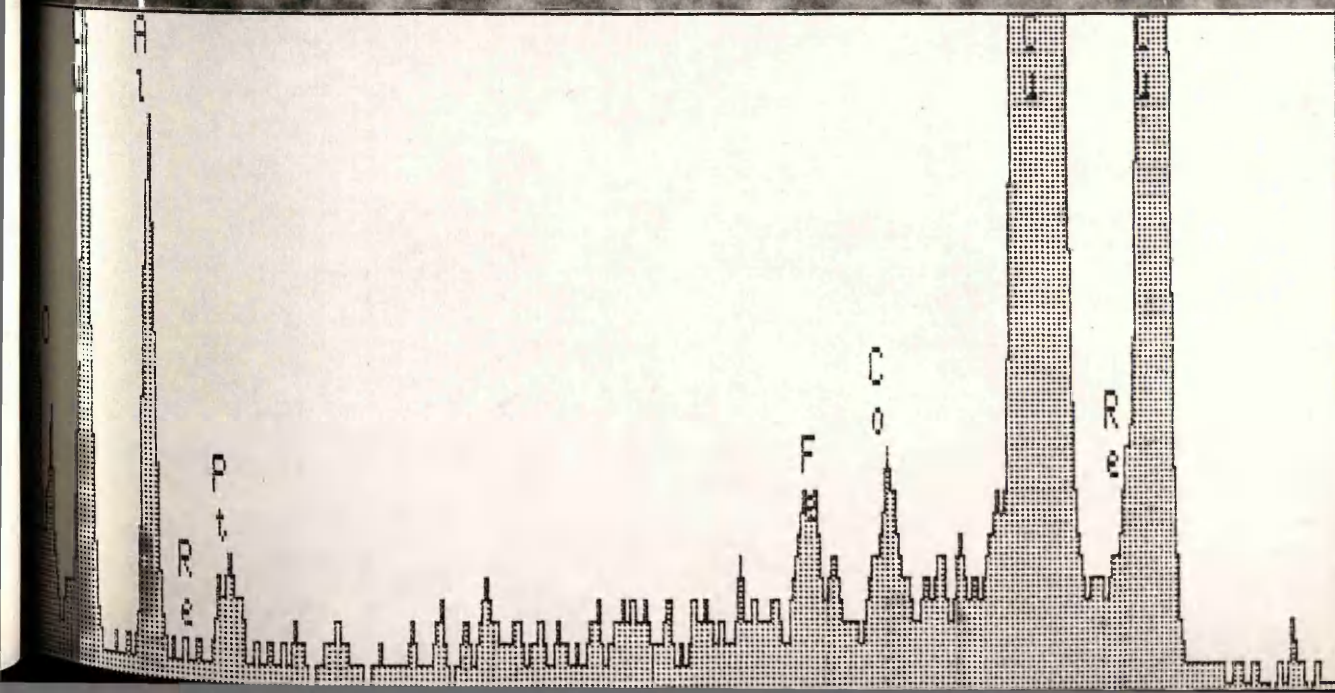
Whilst for the platinum catalyst the yields of ethylbenzene and xylenes were observed to decrease, particularly during the early stages, the yields of these products were almost constant with time on line over Pt-Re/ Al_2O_3 (with the exception of m/p xylene which appeared to increase by $\sim 3\%$ very rapidly in the initial few hours). Conversely, the yield of toluene over Pt-Re declined rapidly during the initial period before leveling off.

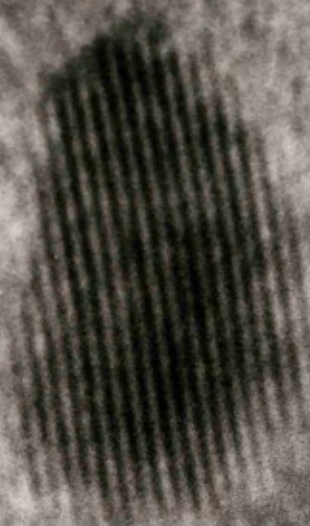
Perhaps the most significant difference between Pt/ Al_2O_3 and Pt-Re/ Al_2O_3 was observed in the level of conversion over these two catalysts. (compare figure 5.4.6 with figure 5.1.6). Although the initial conversion was slightly higher over Pt-Re, the main difference was that this bimetallic catalyst did not undergo the rapid decrease observed over platinum (or indeed the more gradual deactivation that occurred over Pt-Sn and Pt-Ge). After 144 hours on line the level of conversion over this catalyst was found to have dropped by only 1% (final conversions (144 h): Pt 90.2%, Pt-Re 98.7%).

The selectivities to the major reforming reactions are listed versus time on line in table 5.4.2 and plotted in figure 5.4.7. When comparing these values with those obtained over Pt/ Al_2O_3 (table 5.1.2 and figure 5.1.7) the most significant effect of rhenium addition was to prevent the loss of selectivity to aromatisation and subsequent increase in isomerisation that occurred on the monometallic catalyst. The selectivity toward hydrocracked products were similar over both catalysts and the selectivity towards hydrogenolysis, although significantly higher initially over Pt-Re, also reached comparable values by the end of the run.

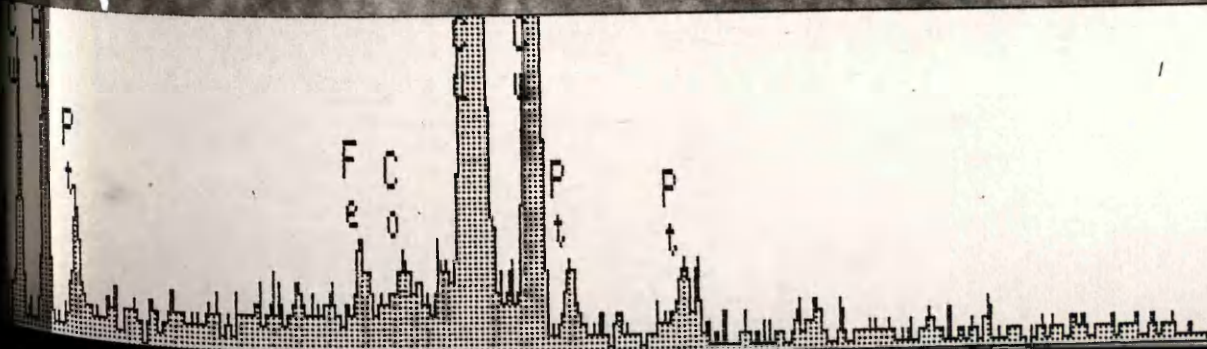
Plate 22

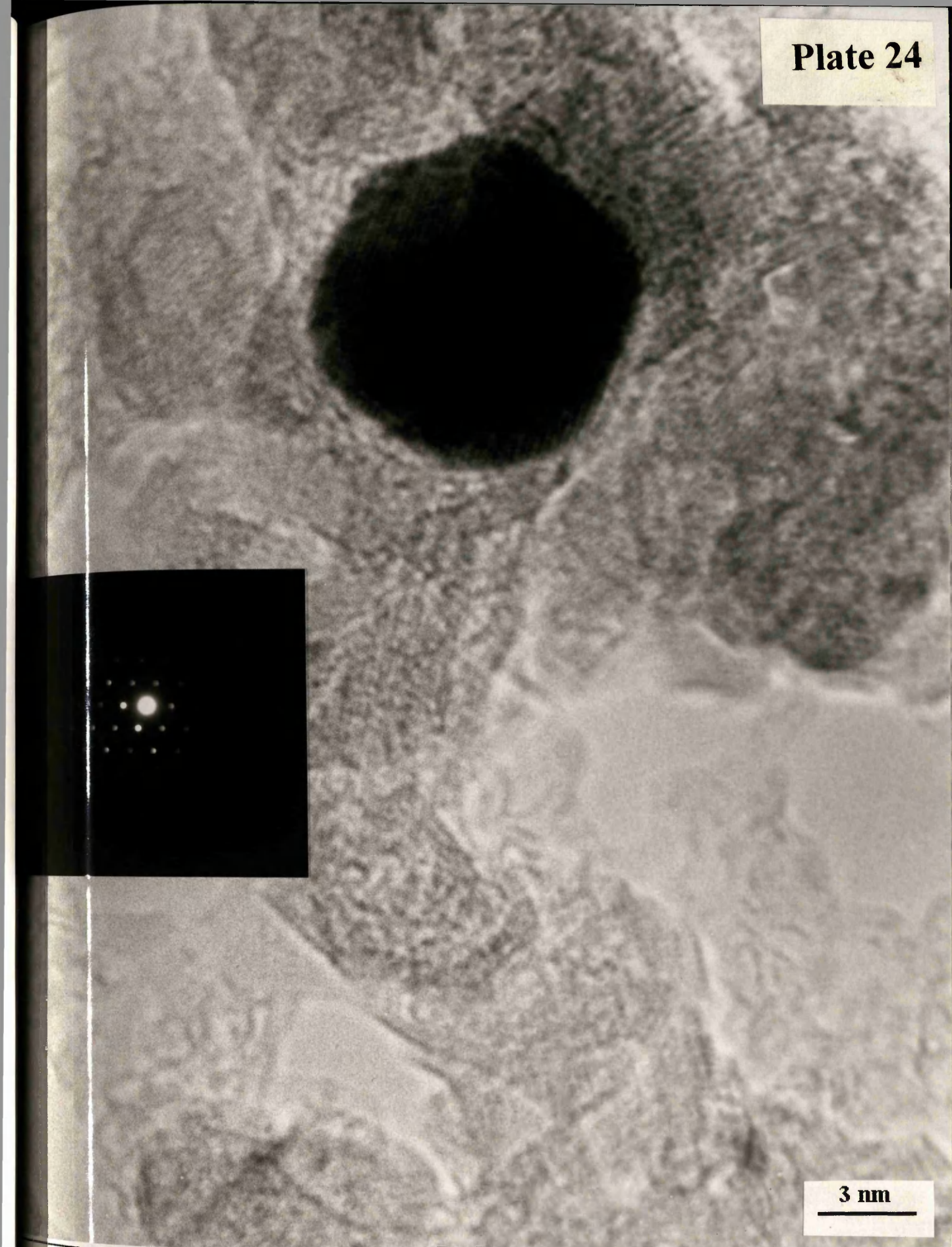
2 nm





2 nm





3 nm

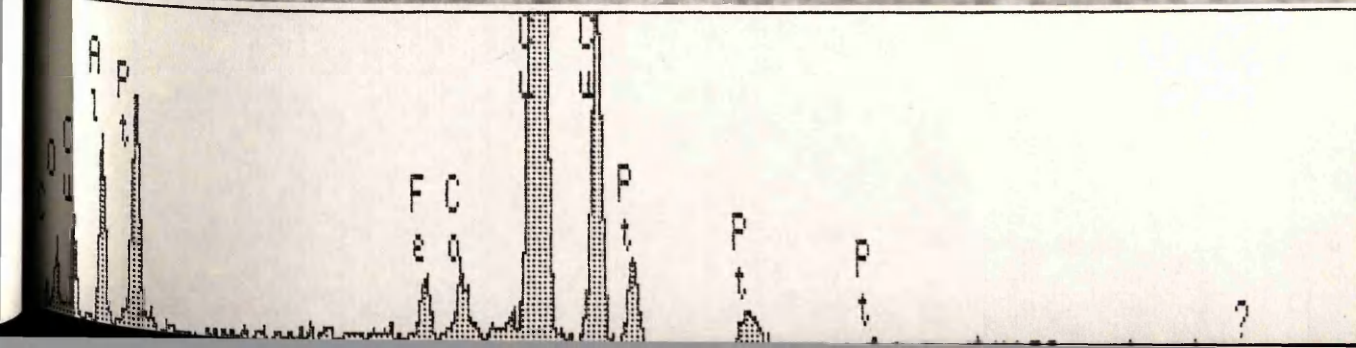
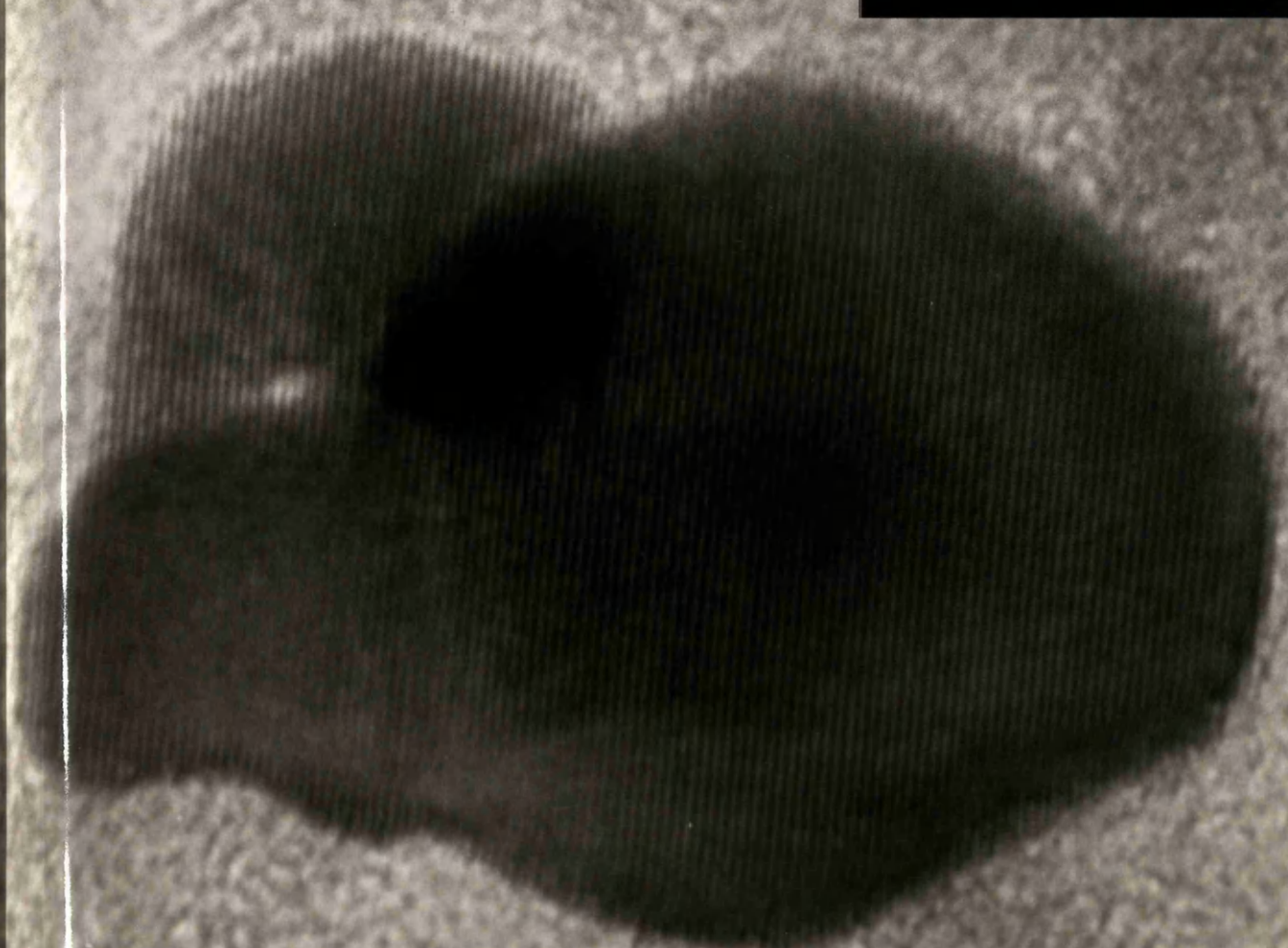


Plate 25



3 nm

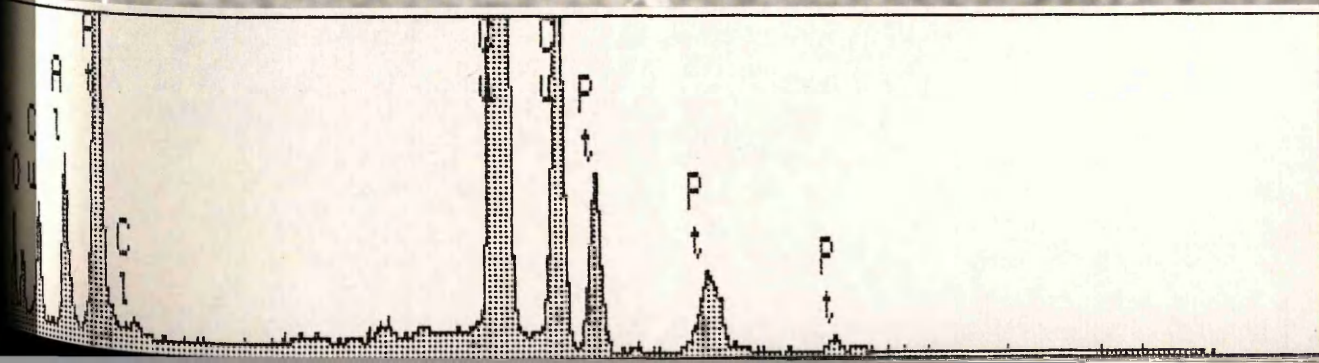


Table 5.4.1 Yields of individual products for catalyst 0.3 wt% Pt - 0.3 wt% Re/Al₂O₃

Time (hours)	Methane	Ethane	Propane	i-Butane	n-Butane	c-Pentane	i-Pentane	n-Pentane
0.8	10.0	5.3	8.8	4.4	6.7	0.1	6.6	4.6
3.8	7.3	4.5	8.3	4.5	6.4	0.1	6.6	4.3
16.0	8.4	4.5	8.2	4.6	6.3	0.1	6.6	4.7
20.0	7.3	4.5	8.2	4.6	6.5	0.1	6.9	4.4
23.0	7.0	4.3	7.9	4.5	6.1	0.1	6.6	4.3
43.8	6.3	4.3	8.4	4.7	6.7	0.1	7.2	5.1
47.5	6.0	4.2	7.8	4.4	6.4	0.1	6.7	4.9
70.5	6.7	4.3	8.1	4.6	6.5	0.1	6.9	4.5
75.5	6.5	4.2	8.1	4.6	6.3	0.1	6.9	4.3
90.0	6.5	4.0	7.8	4.5	6.3	0.1	6.9	4.9
93.0	5.5	3.8	7.5	4.4	6.3	0.1	6.8	4.7
112.5	6.1	3.9	7.6	4.5	6.1	0.1	6.8	5.2
116.0	5.1	3.8	7.4	4.5	6.3	0.1	6.7	4.9
118.8	5.6	3.9	7.4	4.2	6.2	0.1	6.6	4.6
136.0	5.7	3.9	7.7	4.5	6.2	0.1	7.1	5.0
139.0	5.2	3.6	7.2	4.3	6.4	0.1	6.9	4.8
144.0	5.1	4.0	7.6	4.4	6.1	0.1	6.7	4.2

Table 5.4.1 (cont) Yields of individual products for catalyst 0.3 wt% Pt - 0.3 wt% Re/Al₂O₃

Time (hours)	C6 c-Alkane	i-Hexane	n-Hexane	C7 c-Alkane	i-Heptane	n-Heptane	C8 c-Alkane	i-Octane
0.8	0.4	3.9	1.6	0.2	0.5	0.1	0.0	0.6
3.8	0.4	4.3	2.0	0.2	0.9	0.4	0.0	1.0
16.0	0.4	4.6	1.9	0.2	1.0	0.4	0.2	1.9
20.0	0.4	4.8	2.1	0.2	1.0	0.4	0.1	2.5
23.0	0.5	4.8	2.4	0.2	1.2	0.7	0.2	2.9
43.8	0.4	5.2	2.0	0.2	1.1	0.3	0.1	2.6
47.5	0.5	5.2	2.1	0.2	1.5	0.3	0.2	3.4
70.5	0.5	5.2	1.7	0.2	1.2	0.3	0.1	3.6
75.5	0.5	5.3	2.2	0.2	1.2	0.3	0.2	3.7
90.0	0.4	5.6	2.2	0.2	1.3	0.3	0.2	4.7
93.0	0.5	5.5	3.1	0.3	1.7	1.3	0.2	5.3
112.5	0.4	5.8	2.7	0.2	1.5	0.7	0.3	5.3
116.0	0.4	5.3	2.4	0.2	1.7	1.2	0.3	6.7
118.8	0.4	5.4	3.0	0.2	1.6	1.2	0.3	5.5
136.0	0.4	5.8	2.3	0.4	1.4	0.4	0.3	5.9
139.0	0.4	5.8	2.9	0.4	1.7	0.9	0.3	6.4
144.0	0.5	5.6	2.2	0.3	1.4	0.4	0.2	5.7

Table 5.4.1 (cont) Yields of individual products for catalyst 0.3 wt% Pt - 0.3 wt% Re/Al₂O₃

Time (hours)	Benzene	Toluene	Ethyl- Benzene	m/p- Xylene	o-Xylene	C9 Aromatic	Total Conversion
0.8	2.9	11.0	4.6	17.1	9.8	0.6	99.8
3.8	2.4	9.5	5.1	20.3	10.8	0.6	99.9
16.0	1.9	7.2	5.0	20.8	10.3	0.6	99.7
20.0	1.8	6.9	5.1	20.8	10.1	0.6	99.1
23.0	1.7	6.5	5.2	20.8	10.2	0.7	98.8
43.8	1.6	6.1	5.2	20.9	10.0	0.7	99.2
47.5	1.6	5.9	5.2	21.2	10.1	0.6	98.7
70.5	1.5	5.5	5.4	21.3	10.2	0.7	99.1
75.5	1.5	5.5	5.3	21.2	10.4	0.7	99.2
90.0	1.3	4.9	5.3	20.5	9.9	0.7	98.9
93.0	1.3	4.7	5.1	20.0	9.3	0.7	98.1
112.5	1.2	4.6	5.0	20.0	9.4	0.7	98.3
116.0	1.2	4.5	5.1	19.9	9.6	0.7	98.1
118.8	1.3	4.6	5.2	20.6	9.7	0.7	98.2
136.0	1.2	4.4	5.2	20.2	9.5	0.7	98.5
139.0	1.1	4.4	5.2	20.5	9.5	0.7	98.6
144.0	1.4	4.7	5.4	21.6	10.4	0.7	98.7

Table 5.4.2 Selectivity to the major reforming reactions for 0.3 wt% Pt - 0.3 wt% Re/Al₂O₃

Time (hours)	Selectivity to Aromatics	Selectivity to Isomerisation	Selectivity to Hydrocracking	Selectivity to Hydrogenolysis
0.8	46.1	1.1	14.9	10.0
3.8	48.8	1.9	15.4	7.3
16.0	45.9	2.9	15.9	8.4
20.0	45.7	3.6	16.4	7.4
23.0	45.6	4.1	16.2	7.1
43.8	44.9	3.7	17.2	6.3
47.5	45.4	5.0	16.6	6.1
70.5	45.0	4.8	16.8	6.8
75.5	45.0	4.9	16.9	6.5
90.0	43.1	6.1	17.2	6.6
93.0	42.0	7.2	17.0	5.6
112.5	41.8	7.0	17.4	6.2
116.0	41.8	8.6	16.7	5.2
118.8	42.8	7.2	16.5	5.7
136.0	41.9	7.5	17.7	5.8
139.0	42.0	8.2	17.2	5.3
144.0	44.7	7.1	16.9	5.2

Figure 5.4.1 Yields of individual products over 0.3 wt% Pt - 0.3 wt% Re/Al₂O₃

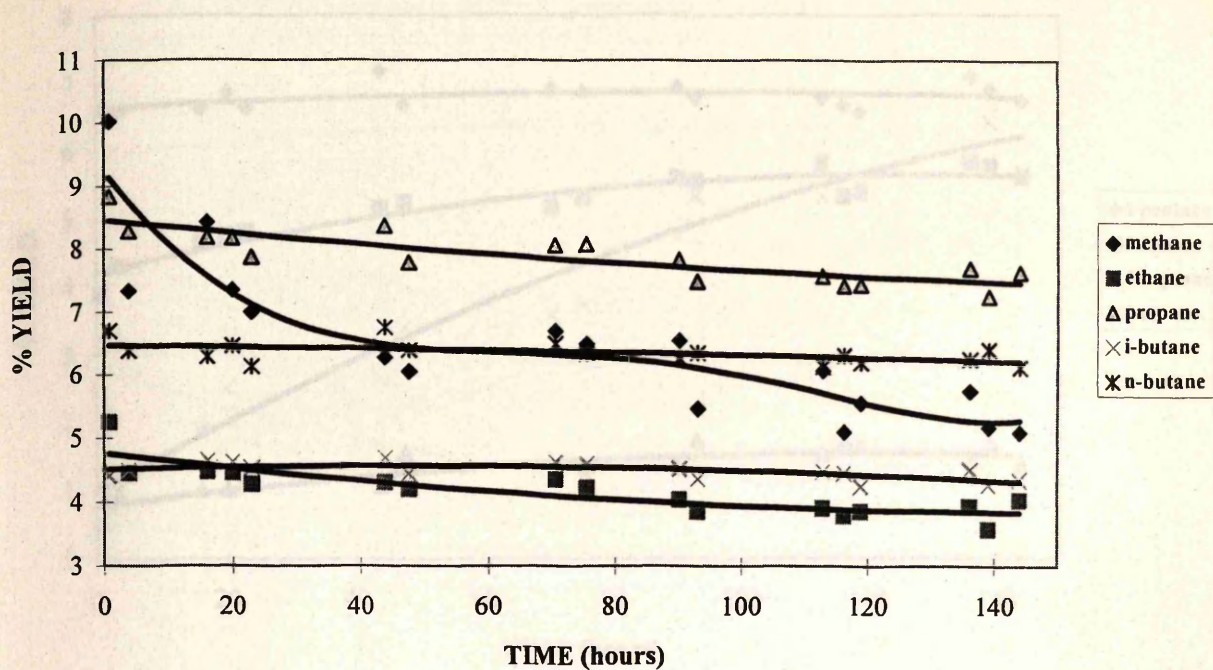


Figure 5.4.2 Yields of cycloalkanes over 0.3 wt% Pt - 0.3 wt% Re/Al₂O₃

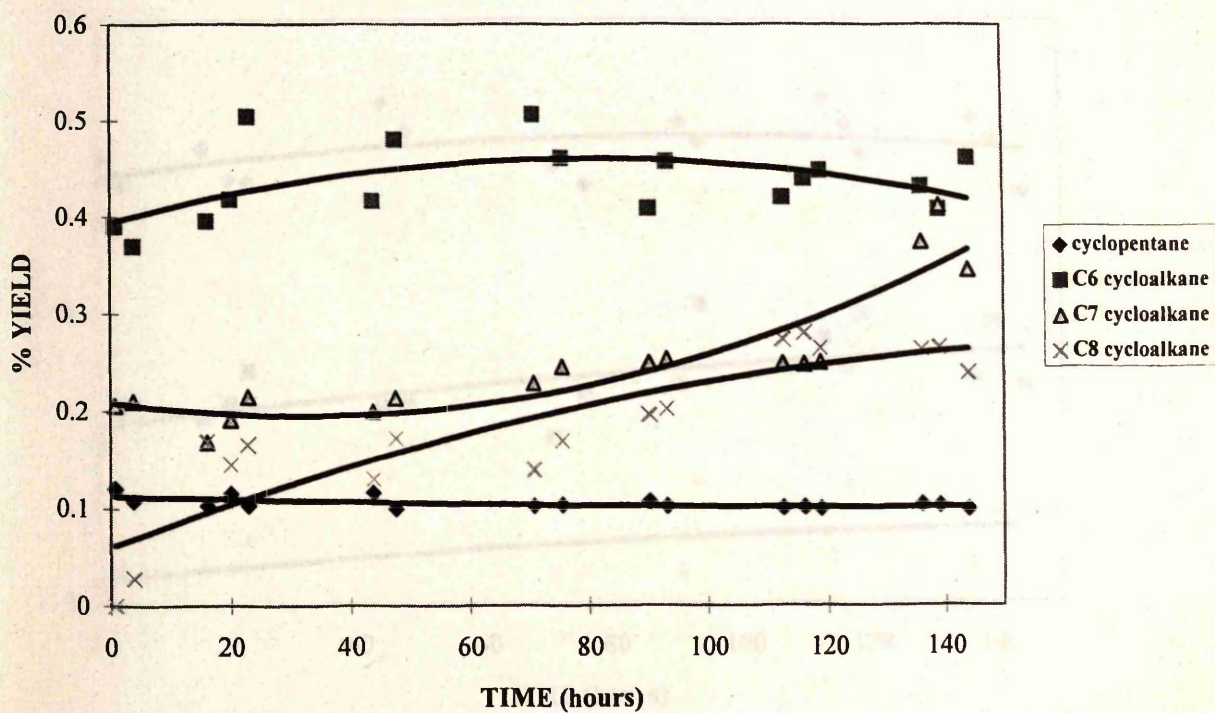


Figure 5.4.3 Yields of i-alkanes over 0.3 wt% Pt - 0.3 wt% Re/Al₂O₃

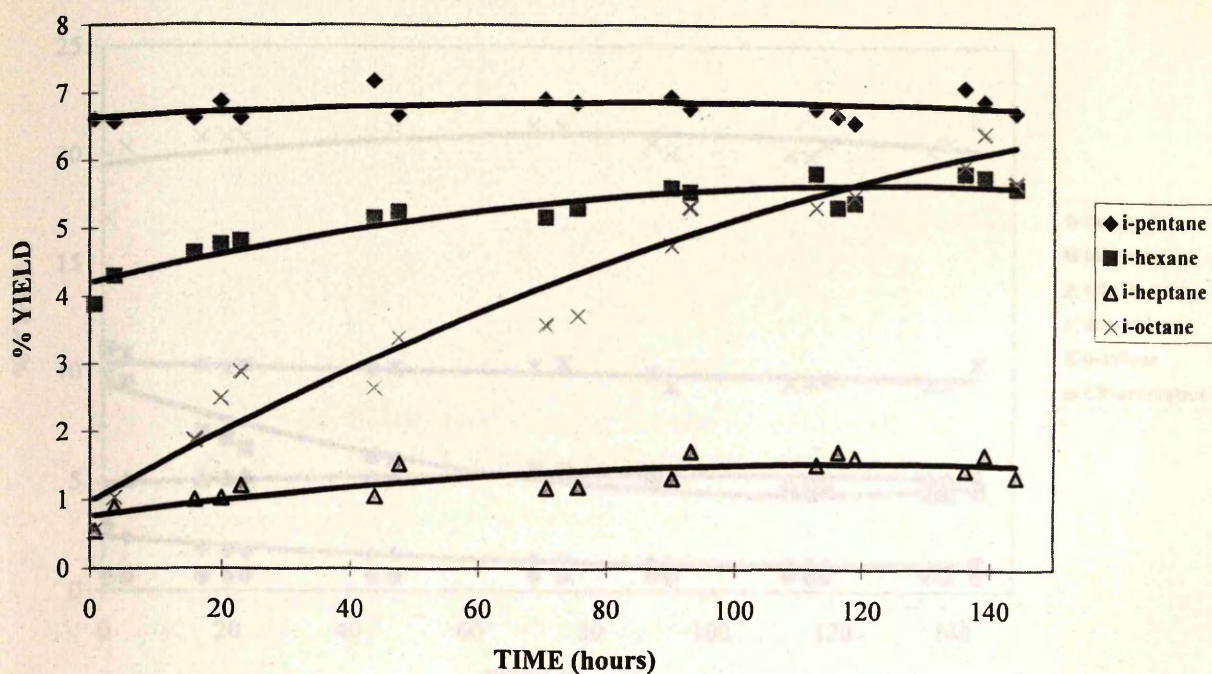


Figure 5.4.4 Yields of n-alkanes over 0.3 wt% Pt - 0.3 wt% Re/Al₂O₃

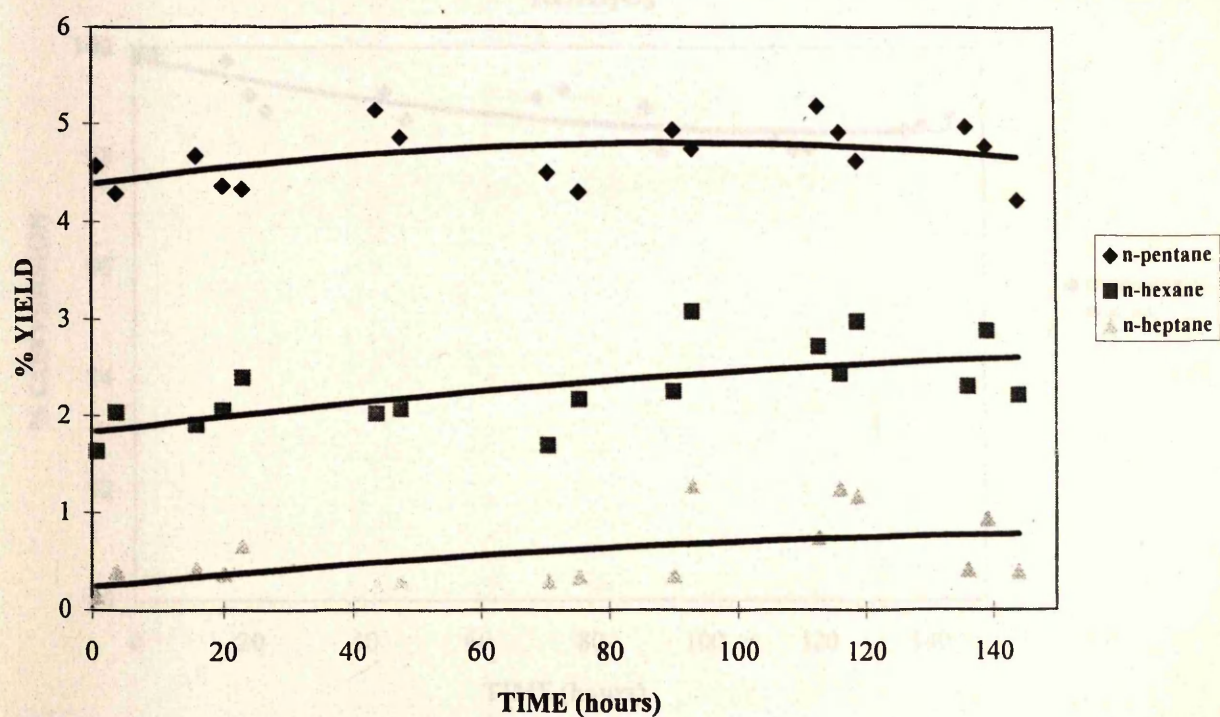


Figure 5.4.5 Yields of aromatics over 0.3 wt% Pt - 0.3 wt% Re/Al₂O₃

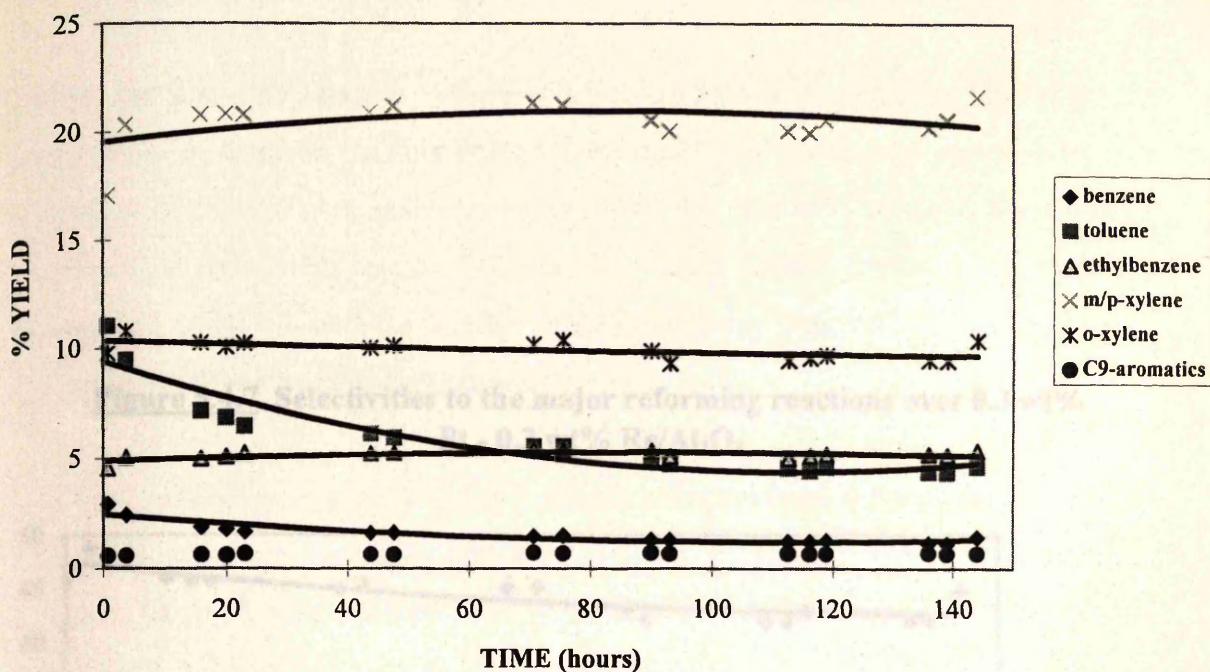
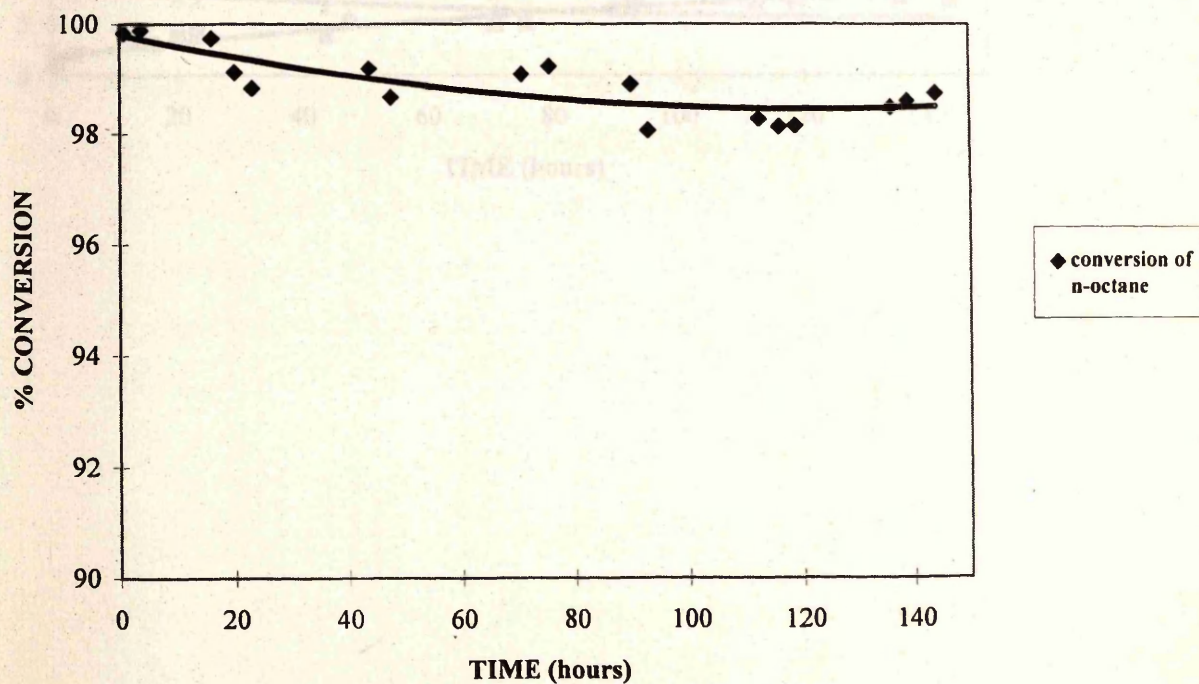


Figure 5.4.6 Conversion of n-octane over 0.3 wt% Pt - 0.3 wt% Re/Al₂O₃

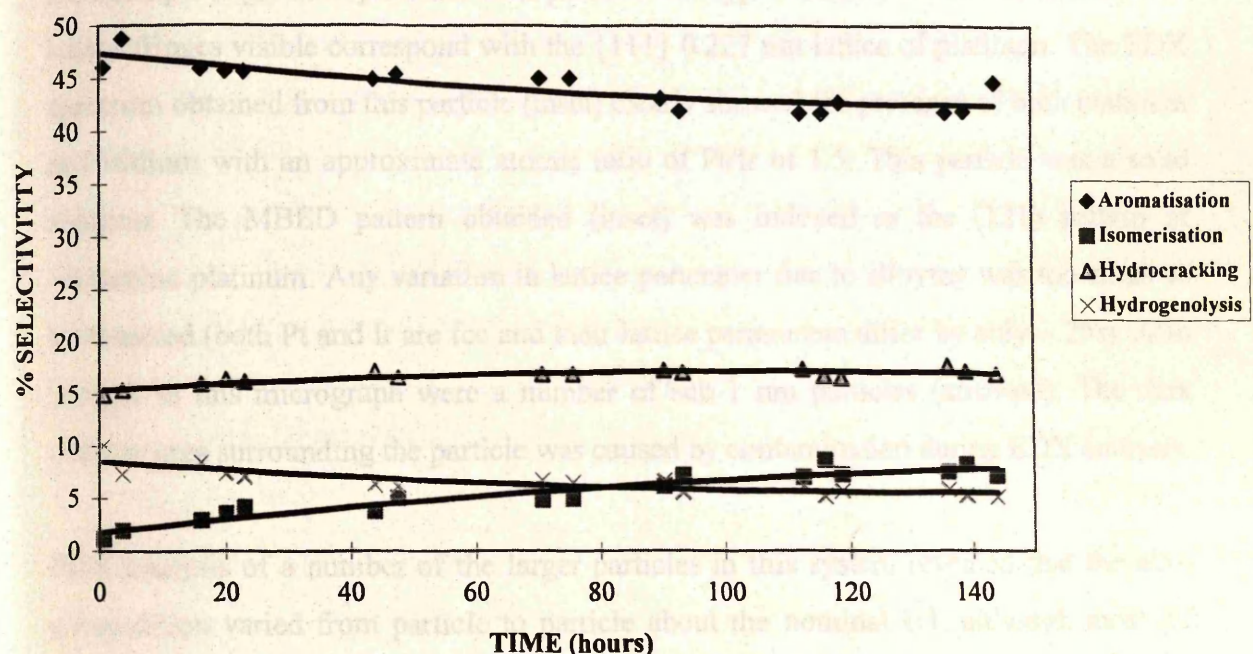


5.5. 0.3 wt% Pt - 0.3 wt% Ir/Al₂O₃

5.5.1. TEM observations

Unlike the previous catalysts, where after calcination and reduction only platinum particles were observed, in this system the majority of particles observed after the reduction procedures were platinum-iridium alloys. It must also be stated that although the metallic component in this system was again highly dispersed, there was a appreciable increase in both the number density of directly observable particles (per area).

Figure 5.4.7 Selectivities to the major reforming reactions over 0.3 wt% Pt - 0.3 wt% Re/Al₂O₃



5.5. 0.3 wt% Pt - 0.3 wt% Ir/Al₂O₃

5.5.A. TEM observations

Unlike the previous catalysts, where after calcination and reduction only platinum particles were observed, in this system the majority of particles observed after this activation procedures were platinum-iridium alloys. It must also be stated that although the metallic component in this system was again highly dispersed, there was a discernible increase in both the number density of directly observable particles (particles > 2 nm) and in their average particle size.

An example is given in plate 26. This particle was approximately 6 nm in diameter. The lattice fringes visible correspond with the {111} 0.227 nm lattice of platinum. The EDX spectrum obtained from this particle (inset) clearly showed the presence of both platinum and iridium with an approximate atomic ratio of Pt/Ir of 1.5. This particle was a solid solution. The MBED pattern obtained (inset) was indexed as the (121) pattern of crystalline platinum. Any variation in lattice parameter due to alloying was too small to be detected (both Pt and Ir are fcc and their lattice parameters differ by only ~2%). Also imaged in this micrograph were a number of sub 1 nm particles (arrowed). The dark circular area surrounding the particle was caused by contamination during EDX analysis.

EDX analysis of a number of the larger particles in this system revealed that the alloy composition varied from particle to particle about the nominal 1:1, although most did have a Pt/Ir ratio close to unity (the accuracy of quantitative EDX analysis must also be considered however). An example of an iridium rich particle is shown in plate 27. This particle was approximately 8-10 nm in diameter. The EDX spectrum obtained revealed a Pt/Ir atomic ratio of 0.7. The {111} 0.227 nm and {002} 0.197 nm lattice fringes are visible in the image.

As with the previous catalysts studied, use of this catalyst in the reforming of n-octane over a prolonged period of time resulted in gradual sintering of the metallic component. This was manifest in both an increase in both particle number density and average particle size. An example of a particle observed in this system after 144 hours on line is given in plate 28. This particle was approximately 12 nm in diameter. The EDX spectrum obtained revealed a Pt/Ir atomic ratio of 1.0. The MBED pattern was indexed as the (110) pattern of platinum(or iridium). The {111} 0.227 and {002} 0.196 nm lattice fringes are visible in the image. Although the particle compositions varied about the nominal 1:1, there was a slight bias towards platinum rich compositions in the particles analysed.

Iridium rich particles were also observed at this stage. An example is given in plate 29. This particle was approximately 20 nm in diameter. The corresponding MBED pattern was indexed as the (100) pattern of the fcc metals. The perpendicular {002} lattice fringes are visible in the image, although they were somewhat obscured due to a significant degree of specimen drift during exposure of the negative. The EDX spectrum obtained from this particle revealed a Pt/Ir atomic ratio of 0.8. Also imaged in this micrograph were a number of nanometer sized metal particles. Although considerable sintering of the Pt-Ir component had occurred during the 144 hours on line, large particles greater than > 10 nm were still rarely observed and it is likely therefore that a significant proportion of the metal component of this catalyst remained in the form of these nanometer sized particles.

5.5.B n-Octane reforming

The yields of individual products over this catalyst are listed versus time on line in table 5.5.1 and plotted in figures 5.5.1 to 5.5.6.

The yields of methane, ethane, propane, i-butane and n-butane are plotted in figure 5.5.1. It is clear that a major difference between this catalyst and the Pt/Al₂O₃ (figure 5.1.1)

was in the yields of methane and ethane produced. The presence of iridium induced a very large increase in the production of methane (initial values; Pt: 5.8% versus Pt-Ir: 42.8%) and ethane (Pt: 3.4% versus Pt-Ir: 26.6%). This resulted in a corresponding large decrease in the yields of the remaining reforming products. With time on line, the yields of these two products gradually decreased resulting in an increase in the yields of the remaining products. It is interesting to note that the rate of reduction in methane yield appears to be greater than that of ethane. The yield of propane was also very different over Pt and Pt-Ir. Although the initial values were similar, with increasing time on line the yield of propane actually increased over the Pt-Ir catalyst and after 144 hours on line was more than double (12.4% versus 5.9%) the corresponding value for the monometallic catalyst. The yields of i-butane and n-butane were also significantly lower initially over the Pt-Ir catalyst (1.2% and 0.7% respectively) than over Pt (3.9% and 5.9% respectively).

The yields of cycloalkanes over this catalyst, shown in figure 5.5.2 remained very low throughout the run, with just traces of these species being observed at various stages.

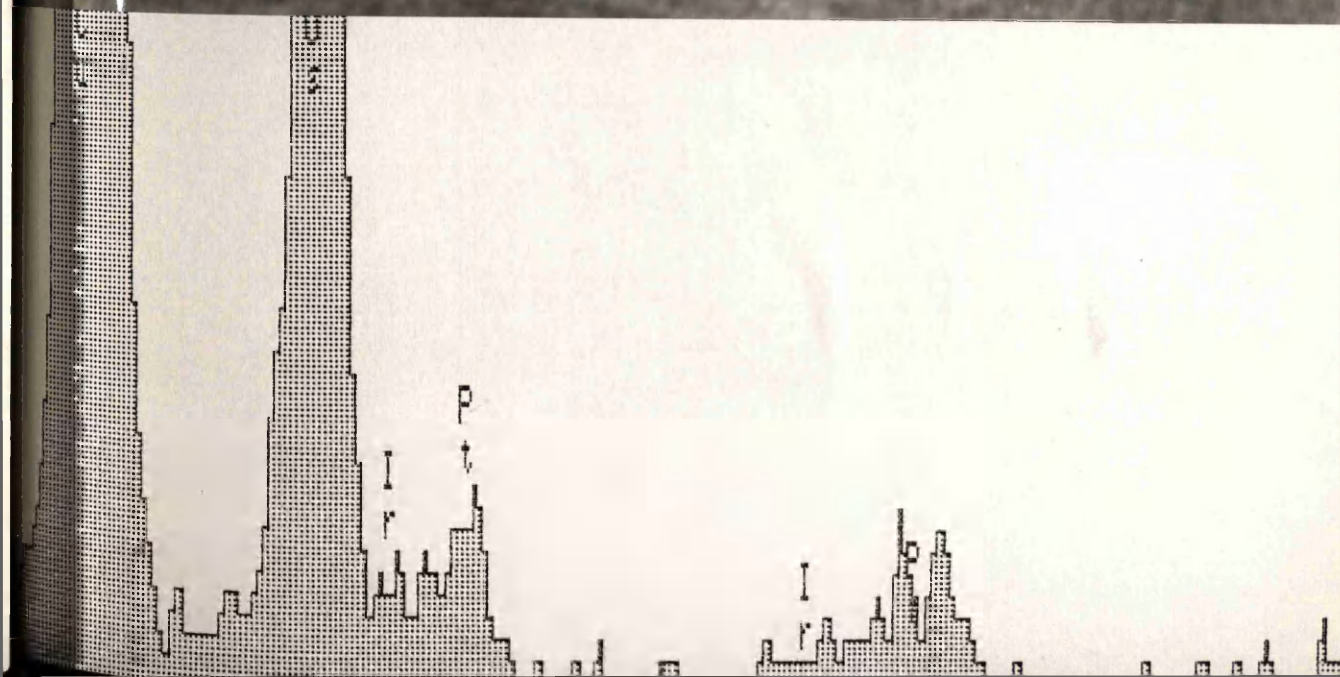
The yields of i-alkanes were also very low over the Pt-Ir/ Al_2O_3 , figure 5.5.2. With time on line the yields of i-pentane and i-hexane gradually increased. Those of i-heptane and i-octane remained essentially near zero.

A similar situation was observed for the yield of n-alkanes over this catalyst, figure 5.5.3. Initially no n-alkanes were detected. With increasing time on line small quantities of n-pentane and n-hexane began to be detected and these then continued to increase throughout the remainder of the run.

In addition to the large increase in the yields of methane and ethane, another major influence exerted by iridium in this catalyst was on the distribution of aromatic species produced. Whilst over platinum the main aromatics were xylenes and ethylbenzene, figure 5.1.5, over Pt-Ir the main products were benzene and toluene, figure 5.5.4. In the



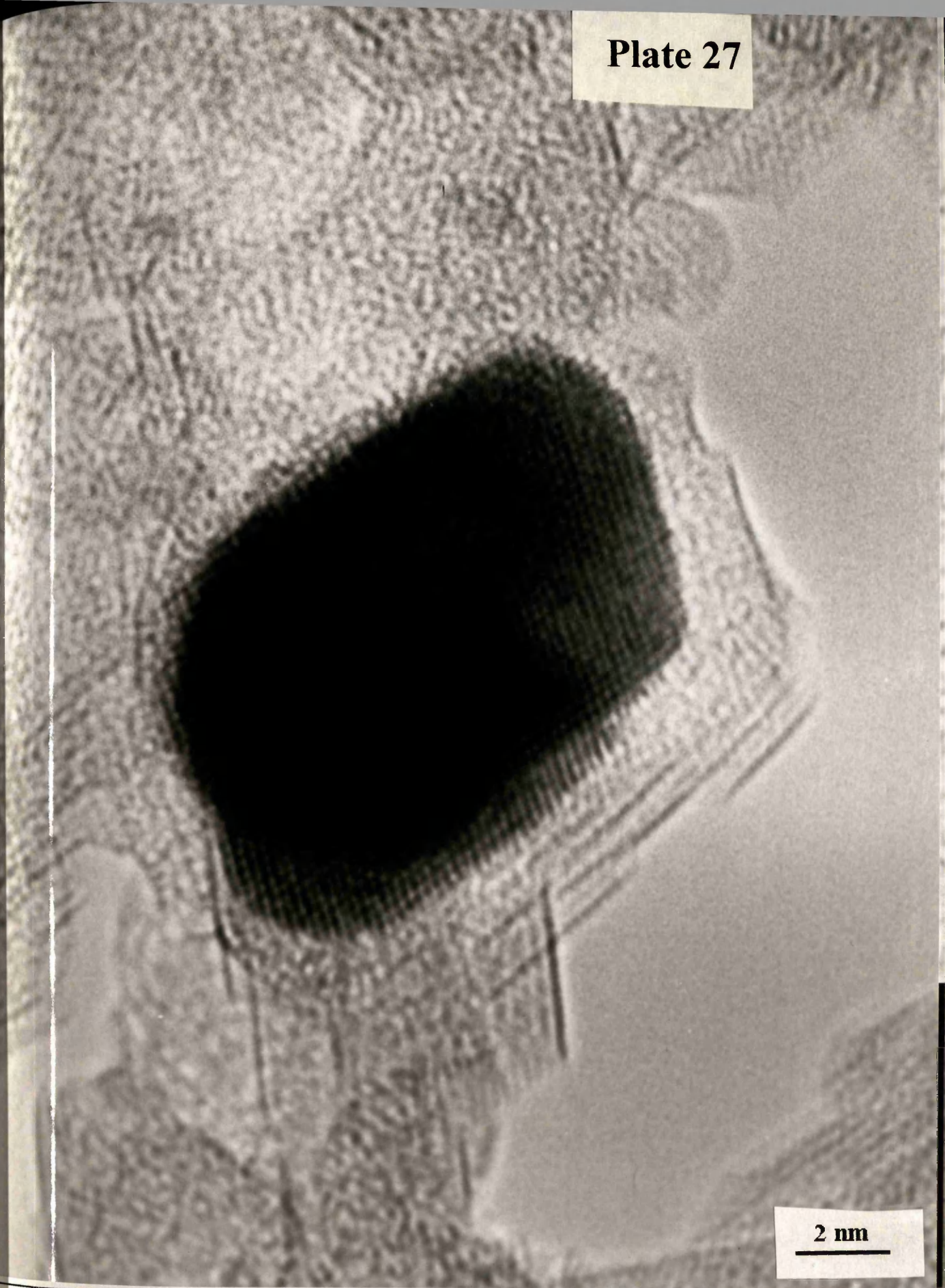
2 nm



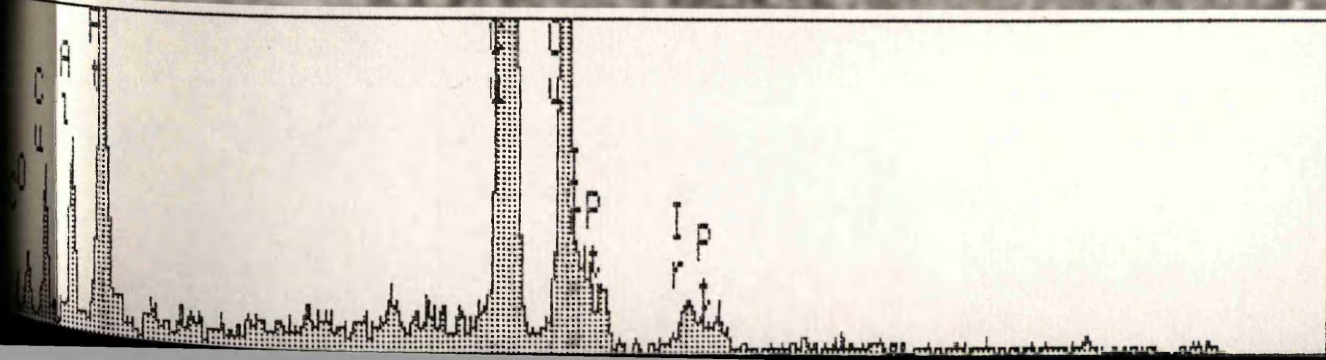
initial stages benzene was the major product formed followed by toluene and small quantities of xylenes. The benzene yield remained relatively stable for approximately 80 hours and then begun to decline. The toluene yield increased steadily throughout the entire length of the run, as did the yields of m/p and o-xylene. The overall result was that by 144 hours on line toluene had become the major aromatic product.

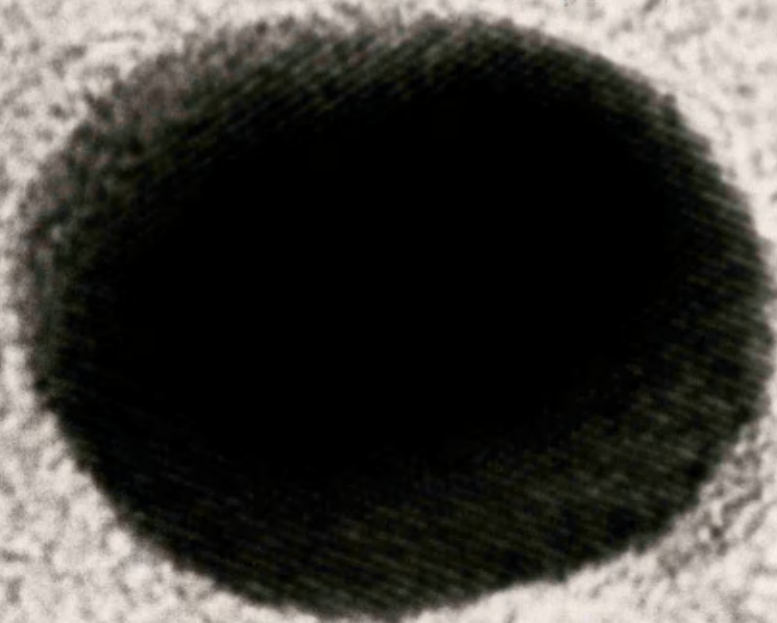
The conversion of n-octane versus time on line for this catalyst is plotted in figure 5.5.5. The level of conversion was initially 100% and decreased slowly but steadily throughout the run. When comparing the conversion over this catalyst with that of Pt/ Al₂O₃, figure 5.1.6, it is clear that the presence of iridium significantly improved the resistance to deactivation of the catalyst and in this respect was quite similar to Pt-Re. (Conversion after 144 hours: Pt 90.2%, Pt-Ir 98.6%.)

The selectivities to the four major reforming reactions are listed versus time on line in table 5.5.2. and plotted in figure 5.5.6. Although the presence of iridium was beneficial to the overall stability of the catalyst, it is clear from figure 5.5.6 that the very high selectivity of this catalyst towards methane production (and the subsequent low selectivity towards the remaining reactions) precludes the use of this unsulphided version of the catalyst in industrial reforming. However, as the selectivity towards hydrogenolysis decreased throughout the run the selectivity to the more desirable reactions increased. Indeed the selectivity of this catalysts for the production of aromatics after 144 hours on line was higher than the corresponding value over Pt/Al₂O₃ (35.8% versus 25.1% respectively) and was still on the increase.



2 nm





2 nm



FC
eo

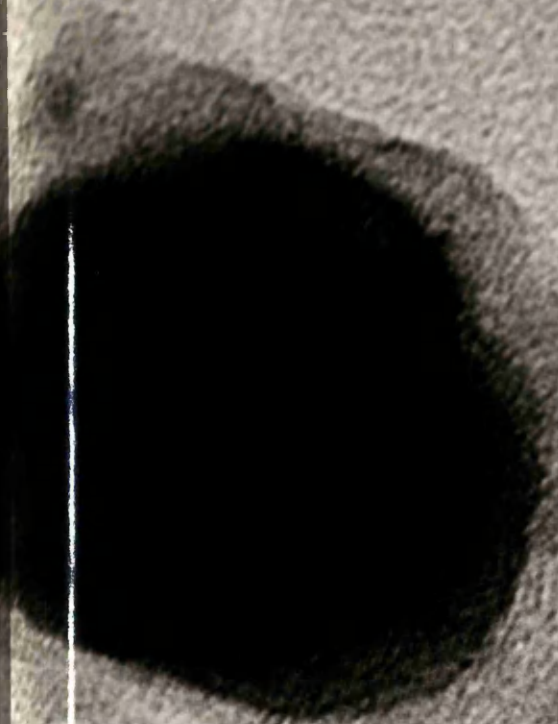
IP
rt

IP
rt

IP
rt

?

Plate 29



5 nm

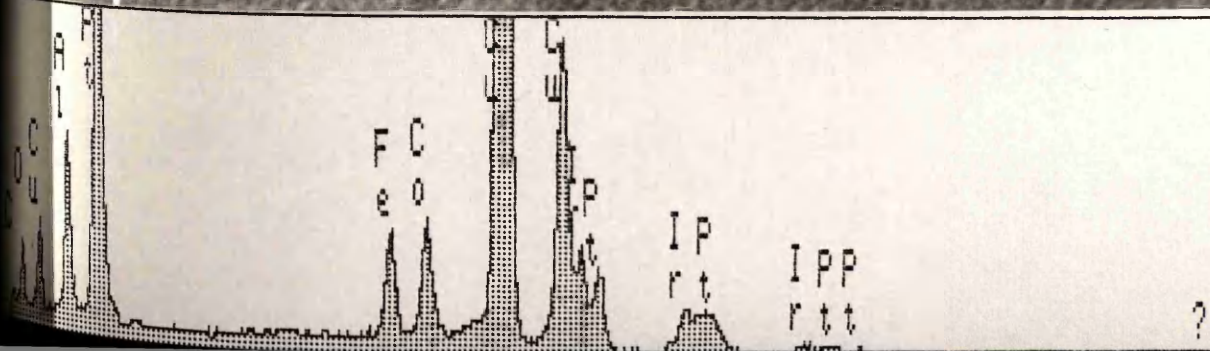


Table 5.5.1 Yields of individual products for catalyst 0.3 wt% Pt - 0.3 wt% Ir/Al₂O₃

Time (hours)	Methane	Ethane	Propane	i-Butane	n-Butane	c-Pentane	i-Pentane	n-Pentane
1.0	42.8	26.6	6.7	1.2	0.7	0.0	0.1	0.0
4.5	45.5	26.3	5.6	1.1	0.6	0.0	0.1	0.0
18.0	42.0	24.5	6.7	1.5	0.8	0.0	0.2	0.0
21.5	38.7	22.8	8.1	1.9	1.2	0.0	0.3	0.0
24.5	34.8	21.3	9.6	2.9	2.6	0.0	0.3	0.1
44.5	34.8	22.7	9.2	2.4	1.7	0.0	0.5	0.2
49.5	32.4	20.8	9.7	2.7	2.0	0.0	0.7	0.3
76.0	32.4	21.4	10.2	3.0	2.1	0.0	0.8	0.4
79.0	33.8	22.0	9.4	2.6	1.5	0.0	0.9	0.5
94.5	33.4	19.9	10.7	2.9	1.9	0.0	1.0	0.5
101.0	28.3	17.7	11.7	3.7	3.3	0.0	1.3	0.4
114.0	25.9	17.8	12.0	4.0	3.9	0.0	1.7	0.8
117.0	23.3	16.0	12.2	4.2	4.5	0.0	1.7	1.0
120.0	23.9	16.5	12.1	4.0	4.1	0.0	2.0	1.0
140.0	23.3	16.0	12.5	4.1	4.4	0.0	2.4	1.2
144.0	22.0	15.4	12.4	4.4	4.7	0.0	2.4	1.2

Table 5.5.1 (cont) Yields of individual products for catalyst 0.3 wt% Pt - 0.3 wt% Ir/Al₂O₃

Time (hours)	C6 c-Alkane	i-Hexane	n-Hexane	C7 c-Alkane	i-Heptane	n-Heptane	C8 c-Alkane	i-Octane
1.0	0.1	0.1	0.0	0.0	0.0	0.0	0.0	0.0
4.5	0.0	0.0	0.0	0.0	0.0	0.0	0.0	0.0
18.0	0.0	0.0	0.0	0.0	0.0	0.0	0.0	0.1
21.5	0.1	0.2	0.0	0.0	0.0	0.0	0.0	0.0
24.5	0.1	0.2	0.0	0.0	0.0	0.0	0.0	0.0
44.5	0.0	0.1	0.0	0.0	0.0	0.0	0.0	0.0
49.5	0.1	0.1	0.0	0.0	0.0	0.0	0.0	0.0
76.0	0.0	0.1	0.0	0.0	0.0	0.0	0.0	0.0
79.0	0.0	0.1	0.0	0.0	0.0	0.0	0.0	0.1
94.5	0.0	0.1	0.0	0.0	0.0	0.0	0.0	0.0
101.0	0.2	0.2	0.0	0.0	0.0	0.0	0.0	0.0
114.0	0.1	0.3	0.0	0.0	0.0	0.0	0.0	0.0
117.0	0.0	0.5	0.2	0.0	0.0	0.0	0.0	0.0
120.0	0.1	0.4	0.3	0.0	0.0	0.0	0.0	0.1
140.0	0.1	0.5	0.2	0.0	0.0	0.0	0.0	0.0
144.0	0.1	0.5	0.3	0.0	0.0	0.0	0.0	0.0

Table 5.5.1 (cont) Yields of individual products for catalyst 0.3 wt% Pt - 0.3 wt% Ir/Al₂O₃

Time (hours)	Benzene	Toluene	Ethyl- Benzene	m/p- Xylene	o-Xylene	C9 Aromatic	Total Conversion
1.0	13.9	7.1	0.0	0.5	0.2	0.0	100.0
4.5	13.8	6.0	0.0	0.5	0.2	0.0	99.8
18.0	15.8	7.4	0.0	0.5	0.2	0.0	99.8
21.5	16.0	9.2	0.0	0.9	0.4	0.0	99.8
24.5	14.8	9.4	0.0	2.4	1.1	0.1	99.8
44.5	16.0	10.3	0.0	1.0	0.5	0.0	99.6
49.5	15.8	12.5	0.0	1.6	0.7	0.0	99.6
76.0	15.6	11.4	0.0	1.3	0.6	0.0	99.4
79.0	14.5	12.7	0.0	1.0	0.5	0.0	99.4
94.5	13.9	13.7	0.0	0.9	0.4	0.0	99.3
101.0	14.2	14.5	0.0	2.4	1.2	0.1	99.3
114.0	13.2	14.9	0.0	2.8	1.4	0.1	98.8
117.0	11.7	16.8	0.0	4.2	2.2	0.2	98.8
120.0	12.4	16.2	0.0	3.6	1.9	0.1	98.7
140.0	11.8	16.3	0.0	3.7	1.9	0.1	98.6
144.0	11.5	17.2	0.1	4.2	2.2	0.1	98.6

Table 5.5.2 Selectivity to the major reforming reactions for 0.3 wt% Pt - 0.3 wt% Ir/Al₂O₃

Time (hours)	Selectivity to Aromatics	Selectivity to Isomerisation	Selectivity to Hydrocracking	Selectivity to Hydrogenolysis
1.0	21.7	0.0	1.4	42.8
4.5	20.6	0.0	1.2	45.6
18.0	24.0	0.1	1.7	42.1
21.5	26.6	0.0	2.3	38.8
24.5	27.9	0.0	3.4	34.8
44.5	28.0	0.0	3.0	35.0
49.5	30.8	0.0	3.5	32.6
76.0	29.2	0.0	3.9	32.6
79.0	28.8	0.1	3.6	34.0
94.5	29.1	0.0	4.0	33.7
101.0	32.6	0.0	5.3	28.5
114.0	32.7	0.0	6.0	26.2
117.0	35.5	0.0	6.5	23.6
120.0	34.7	0.1	6.4	24.2
140.0	34.3	0.0	7.1	23.6
144.0	35.8	0.0	7.5	22.3

Figure 5.5.1 Yields of individual products over 0.3 wt% Pt - 0.3 wt% Ir/Al₂O₃

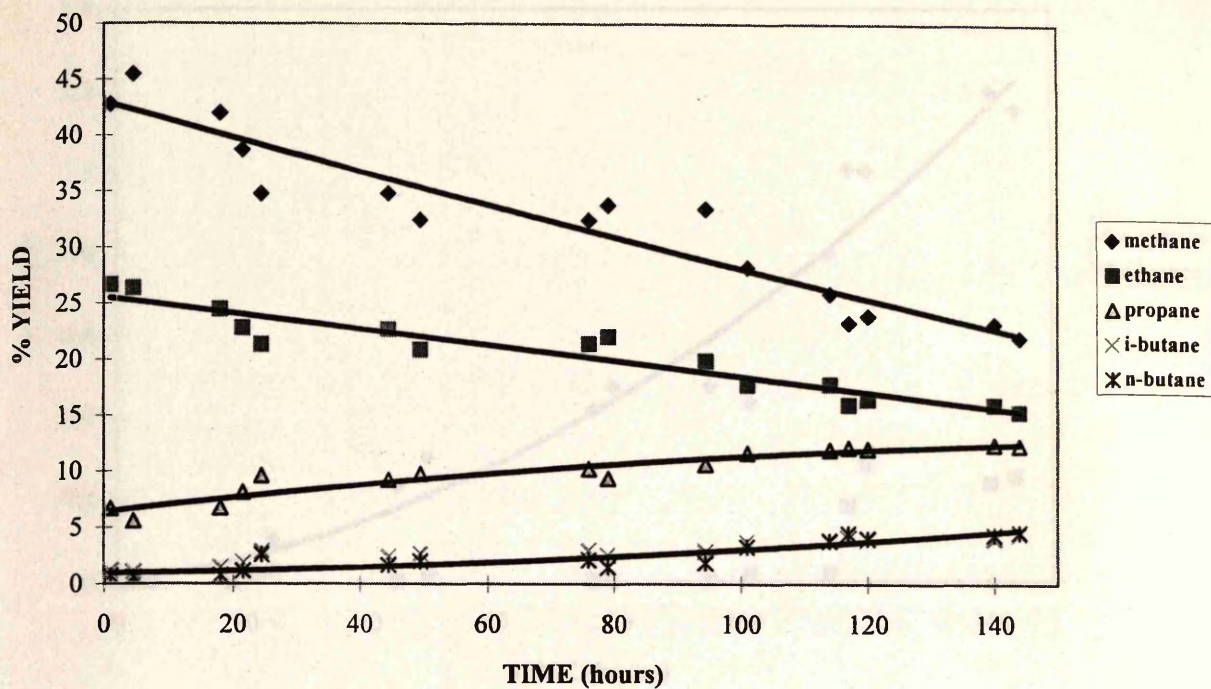


Figure 5.5.2 Yields of i-alkanes over 0.3 wt% Pt - 0.3 wt% Ir/Al₂O₃

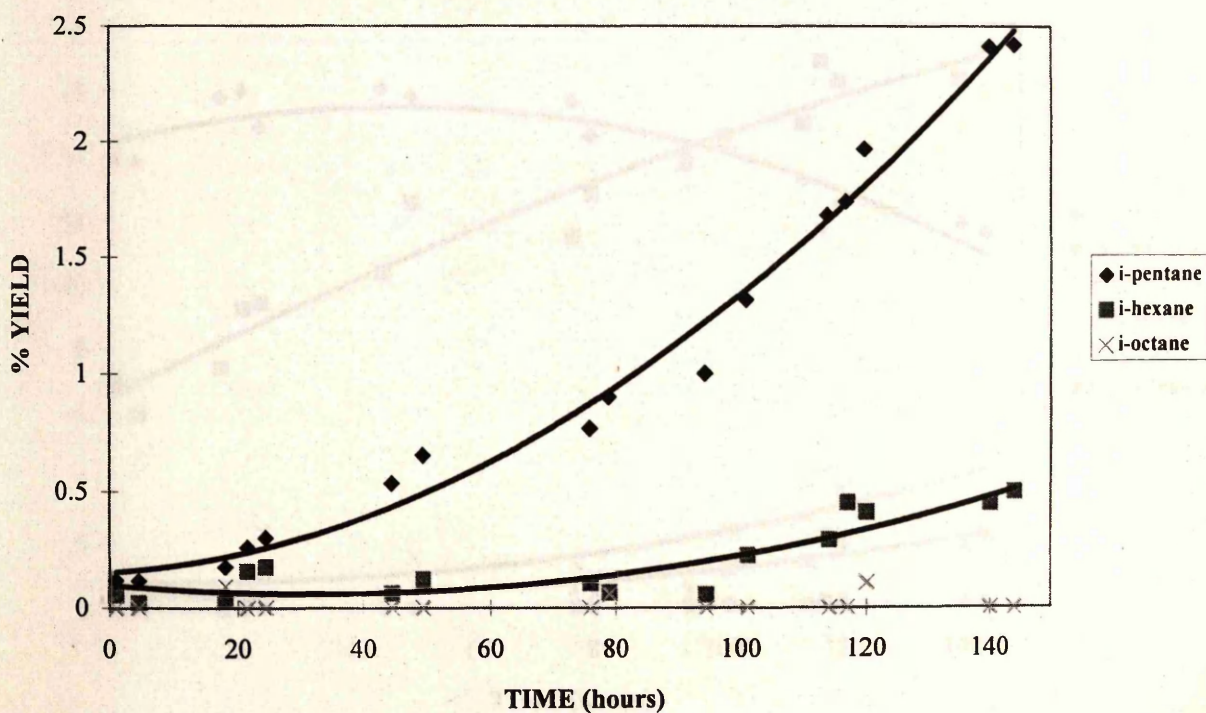


Figure 5.5.3 Yields of n-alkanes over 0.3 wt% Pt - 0.3 wt% Ir/Al₂O₃

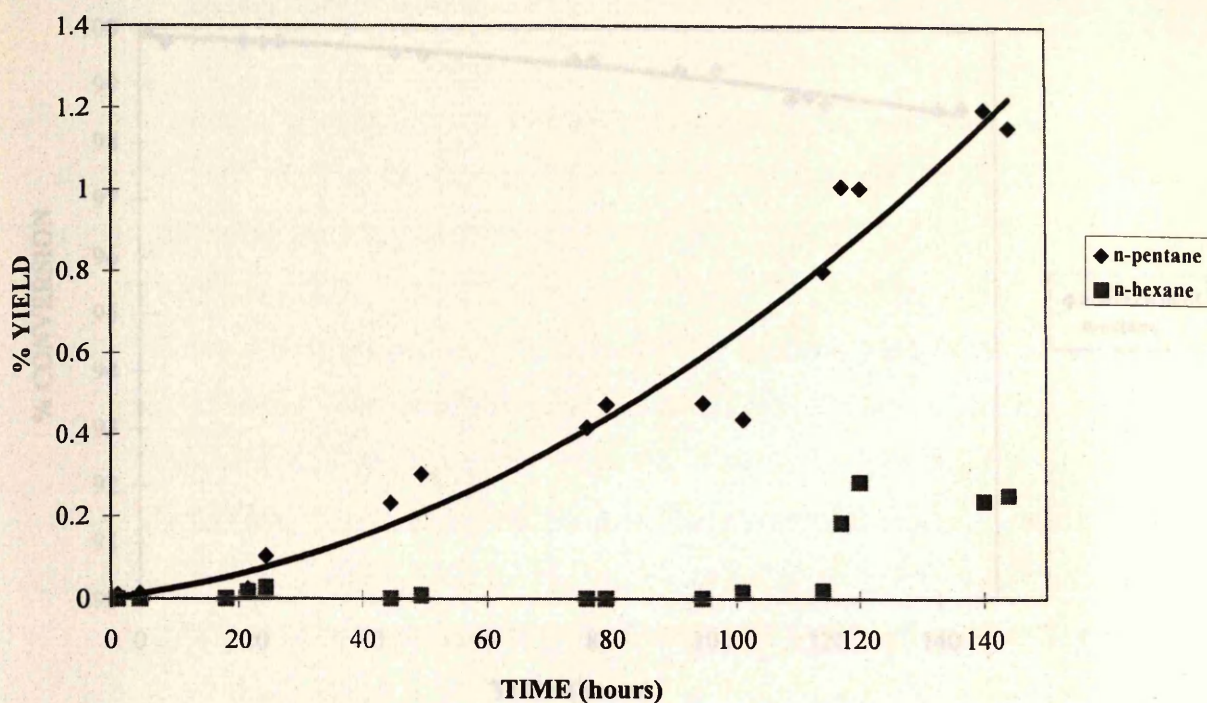


Figure 5.5.4 Yields of aromatics over 0.3 wt% Pt - 0.3 wt% Ir/Al₂O₃

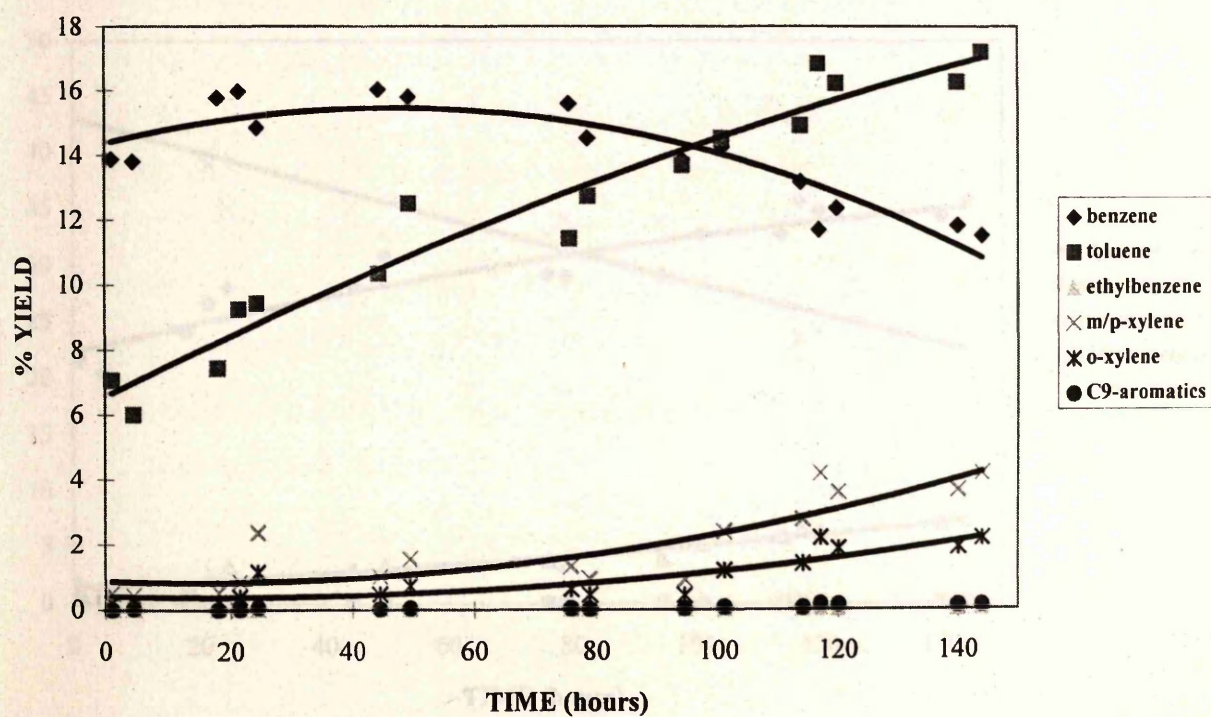


Figure 5.5.5 Conversion of n-octane over 0.3 wt% Pt - 0.3 wt% Ir/Al₂O₃

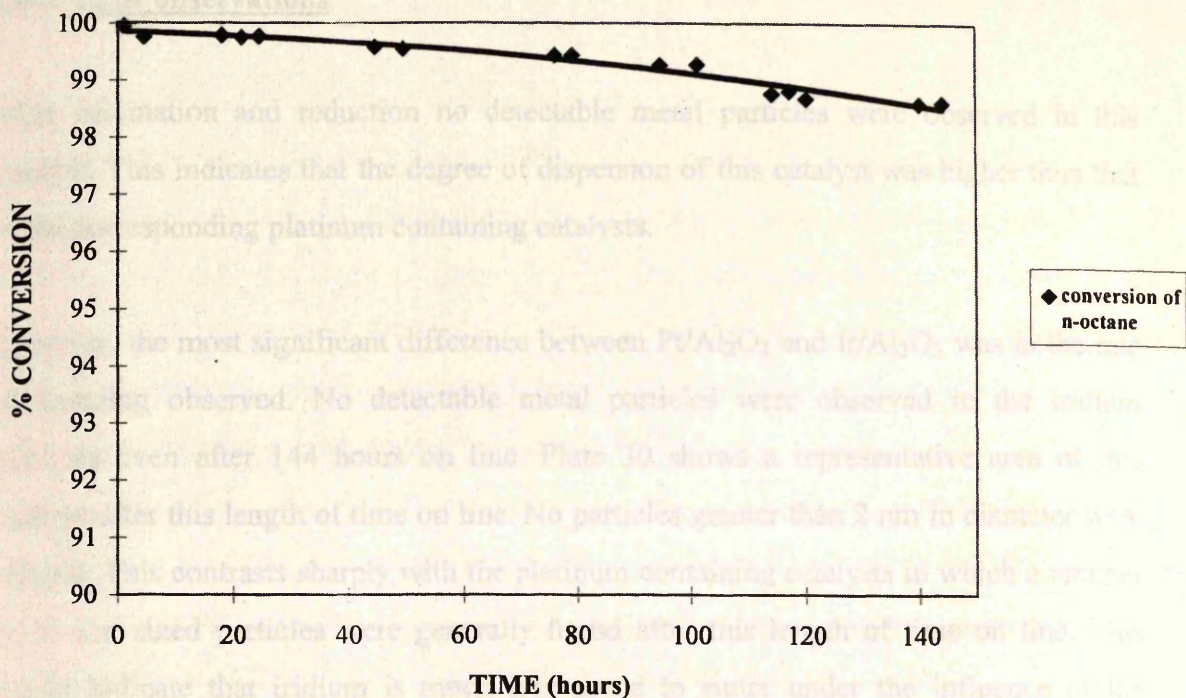
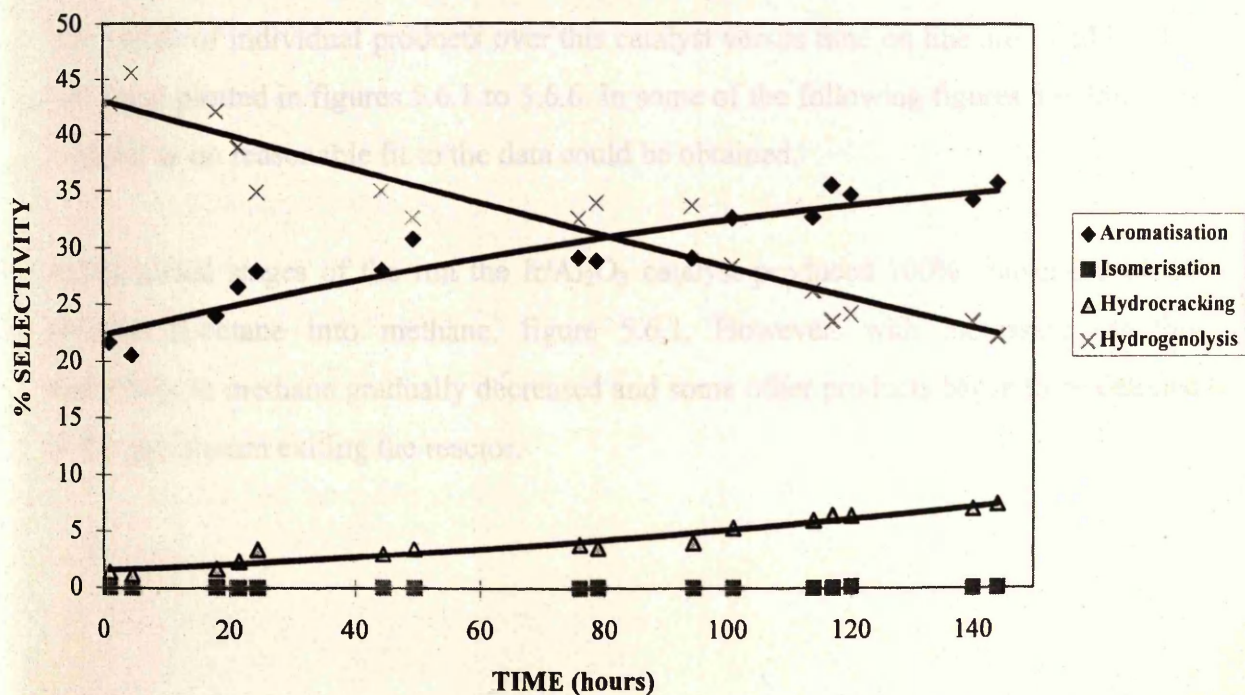


Figure 5.5.6 Selectivities to the major reforming reactions over 0.3 wt% Pt - 0.3 wt% Ir/Al₂O₃



5.6 . 0.3 wt% Ir/Al₂O₃

5.6.A TEM observations

After calcination and reduction no detectable metal particles were observed in this catalyst. This indicates that the degree of dispersion of this catalyst was higher than that of the corresponding platinum containing catalysts.

However, the most significant difference between Pt/Al₂O₃ and Ir/Al₂O₃ was in the rate of sintering observed. No detectable metal particles were observed in the iridium catalysts even after 144 hours on line. Plate 30 shows a representative area of this catalyst after this length of time on line. No particles greater than 2 nm in diameter were imaged. This contrasts sharply with the platinum containing catalysts in which a number of 20 nm sized particles were generally found after this length of time on line. This would indicate that iridium is much less prone to sinter under the influence of the hydrogen-rich atmospheres used in this study.

5.6.B n-Octane reforming

The yields of individual products over this catalyst versus time on line are listed in table 5.6.1 and plotted in figures 5.6.1 to 5.6.6. In some of the following figures trendlines are omitted as no reasonable fit to the data could be obtained.

In the initial stages of the run the Ir/Al₂O₃ catalyst produced 100% conversion of the reactant n-octane into methane, figure 5.6.1. However, with increasing use this selectivity to methane gradually decreased and some other products began to be detected in the gas stream exiting the reactor.

The yields of ethane, propane, i-butane and n-butane all increased steadily throughout the length of the run, figure 5.6.2. The yield of ethane after 144 hours on line was greater than the highest value obtained over the platinum catalysts and was still increasing.

The only cycloalkanes detected at any stage of the run were C_8 species, although the quantities involved remained low (0.2-0.3%). The yields of iso and normal alkanes were also very low. Figure 5.6.3 shows the yields of i-alkanes. In the initial stages the yields of these products were zero. As the run progressed the yields gradually increased. A similar finding was made with the yields of n-alkanes, figure 5.6.4, with the exception of n-heptane which was not detected at any stage. The yields of all these products remained much lower than the corresponding yields over Pt/Al_2O_3 .

The yields of aromatic species over this catalysts are plotted in figure 5.6.5. Initially the yield of aromatics was zero. However the yields of benzene and toluene increased quite sharply during the first 18 hours and then continued to increase at a more gradual pace throughout the remainder of the run. The yields of xylenes were found to increase slowly throughout the run. The overall yield of aromatics over this catalyst was much lower at all stages of the run than the corresponding yield over Pt/Al_2O_3 .

Although the product distributions were found to vary with time on line, the overall conversion, figure 5.6.6, remained at 100% throughout the length of the run.

The selectivities to the four major reforming reactions are presented versus time on line in table 5.6.2 and plotted in figure 5.6.7. As was stated the catalysts showed 100% selectivity to methane in the initial stages. However this selectivity decreased with time on line, particularly during the initial stages of the run, and there was a corresponding increase in the selectivities to the more desirable reforming reactions, i.e. aromatisation, isomerisation and hydrocracking. However, the selectivities to these reactions did remain comparatively low over this catalyst e.g. final selectivities to aromatisation: Pt - 25.1%, Ir - 6.0%.

10 nm

Table 5.6.1 Yields of individual products for catalyst 0.3 wt% Ir/Al₂O₃

Time (hours)	Methane	Ethane	Propane	i-Butane	n-Butane	c-Pentane	i-Pentane	n-Pentane
1.5	100.0	0.0	0.0	0.0	0.0	0.0	0.0	0.0
18.0	91.7	2.2	0.9	0.4	0.4	0.0	0.2	0.0
21.0	93.9	1.5	1.0	0.2	0.1	0.0	0.1	0.0
47.5	88.7	2.8	1.0	0.6	0.6	0.0	0.4	0.2
70.0	87.5	3.0	1.2	0.7	0.6	0.0	0.4	0.1
89.0	85.3	3.7	1.5	0.8	0.7	0.0	0.5	0.2
94.0	86.0	3.7	1.3	0.6	0.5	0.0	0.5	0.1
112.0	83.0	4.4	1.7	0.9	0.9	0.0	0.7	0.2
117.0	83.7	4.3	1.6	0.7	0.6	0.0	0.6	0.2
136.5	81.5	4.3	2.2	1.0	0.9	0.0	0.7	0.3
144.0	80.7	5.1	2.1	0.9	0.8	0.0	0.7	0.3

Table 5.6.1 (cont) Yields of individual products for catalyst 0.3 wt% Ir/Al₂O₃

Time (hours)	C6 c-Alkane	i-Hexane	n-Hexane	C7 c-Alkane	i-Heptane	n-Heptane	C8 c-Alkane	i-Octane
1.5	0.0	0.0	0.0	0.0	0.0	0.0	0.0	0.0
18.0	0.0	0.1	0.0	0.0	0.0	0.0	0.0	0.4
21.0	0.0	0.0	0.0	0.0	0.0	0.0	0.0	0.3
47.5	0.0	0.2	0.0	0.0	0.0	0.0	0.2	1.2
70.0	0.0	0.3	0.0	0.0	0.0	0.0	0.3	1.6
89.0	0.0	0.4	0.1	0.0	0.1	0.0	0.2	1.6
94.0	0.0	0.4	0.1	0.0	0.0	0.0	0.2	1.8
112.0	0.0	0.5	0.1	0.0	0.1	0.0	0.2	2.1
117.0	0.0	0.5	0.2	0.0	0.1	0.0	0.2	2.0
136.5	0.0	0.5	0.3	0.0	0.1	0.0	0.2	2.1
144.0	0.0	0.5	0.3	0.0	0.1	0.0	0.3	2.2

Table 5.6.1 (cont) Yields of individual products for catalyst 0.3 wt% Ir/Al₂O₃

Time (hours)	Benzene	Toluene	Ethyl- Benzene	m/p- Xylene	o-Xylene	C9 Aromatic	Total Conversion
1.5	0.0	0.0	0.0	0.0	0.0	0.0	100.0
18.0	2.1	1.0	0.0	0.3	0.1	0.0	100.0
21.0	1.9	1.1	0.0	0.1	0.0	0.0	100.0
47.5	2.6	1.2	0.0	0.2	0.1	0.0	100.0
70.0	2.7	1.2	0.0	0.2	0.1	0.0	100.0
89.0	2.9	1.4	0.0	0.3	0.1	0.0	100.0
94.0	3.0	1.5	0.0	0.3	0.1	0.0	100.0
112.0	2.9	1.7	0.0	0.4	0.2	0.0	100.0
117.0	3.0	1.6	0.0	0.4	0.3	0.0	100.0
136.5	3.1	2.1	0.0	0.6	0.2	0.0	100.0
144.0	3.0	2.1	0.0	0.6	0.3	0.0	100.0

Table 5.6.2 Selectivity to the major reforming reactions for 0.3 wt% Ir/Al₂O₃

Time (hours)	Selectivity to Aromatics	Selectivity to Isomerisation	Selectivity to Hydrocracking	Selectivity to Hydrogenolysis
1.5	0.0	0.0	0.0	100.0
18.0	3.6	0.4	0.8	91.7
21.0	3.0	0.3	0.3	93.9
47.5	4.2	1.2	1.1	88.7
70.0	4.2	1.7	1.4	87.5
89.0	4.8	1.7	1.8	85.3
94.0	4.9	1.8	1.4	86.0
112.0	5.2	2.2	2.0	83.0
117.0	5.5	2.1	1.7	83.7
136.5	6.0	2.2	2.1	81.5
144.0	6.0	2.2	2.2	80.7

Figure 5.6.1 Yield of methane over 0.3 wt% Ir/Al₂O₃

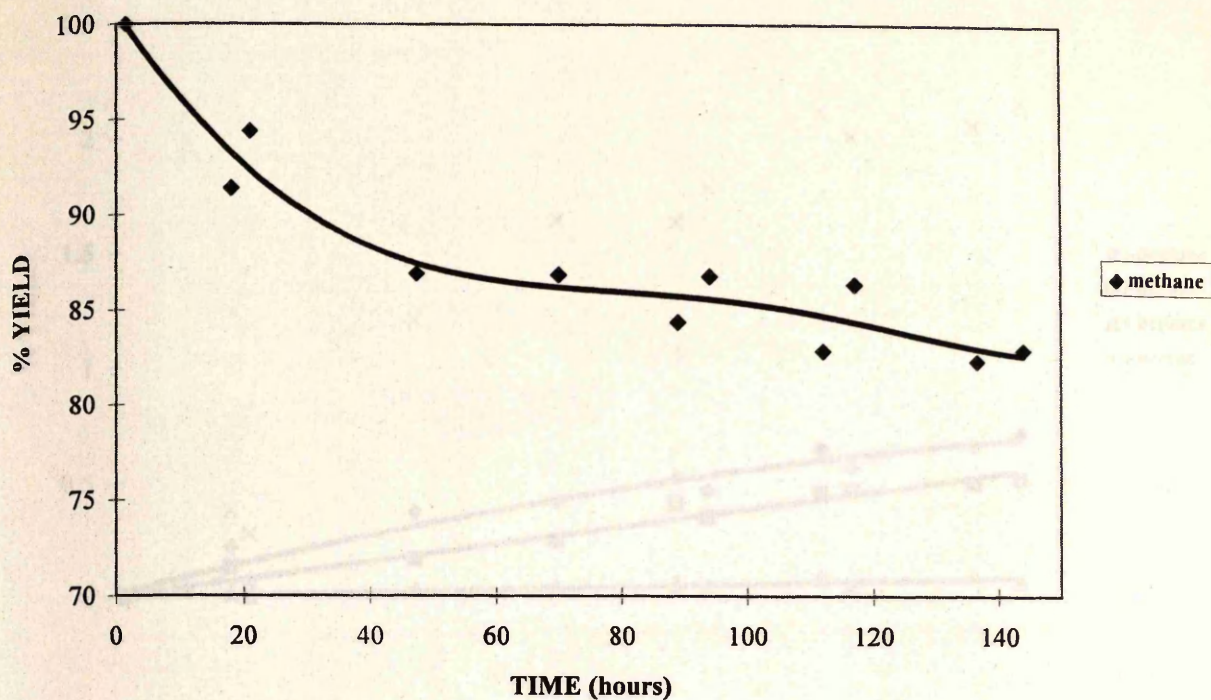


Figure 5.6.2 Yields of individual products over 0.3 wt% Ir/Al₂O₃

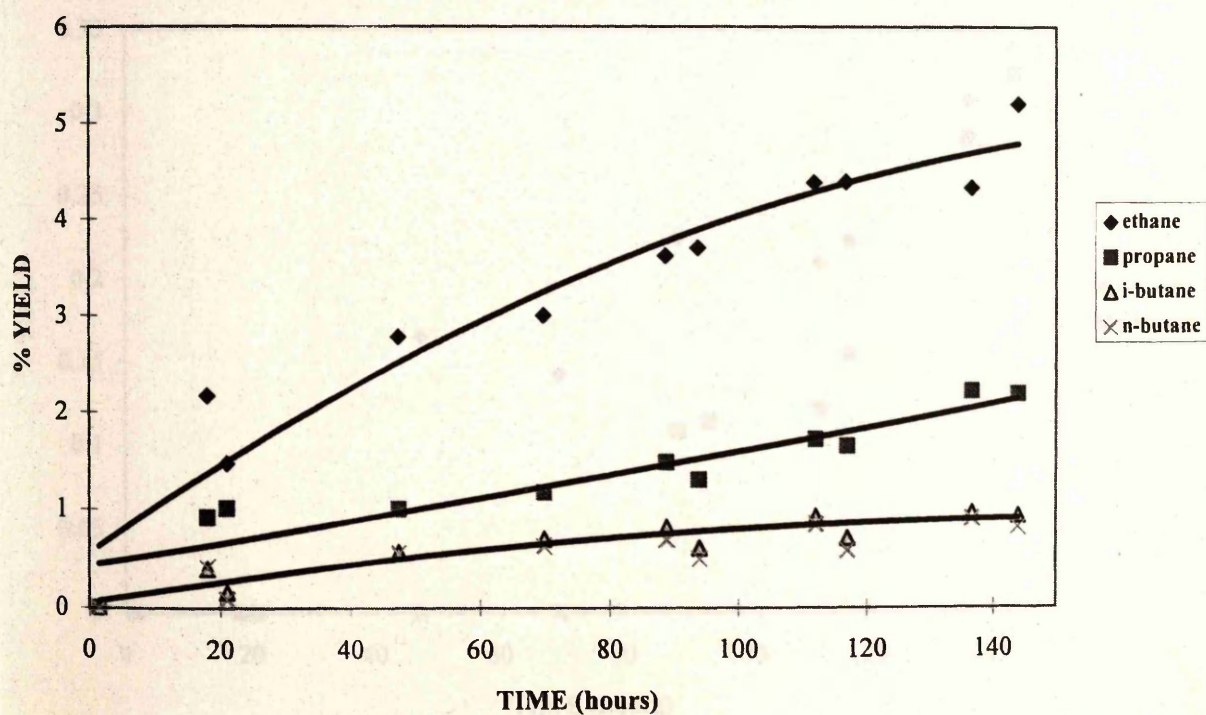


Figure 5.6.3 Yields of i-alkanes over 0.3 wt% Ir/Al₂O₃

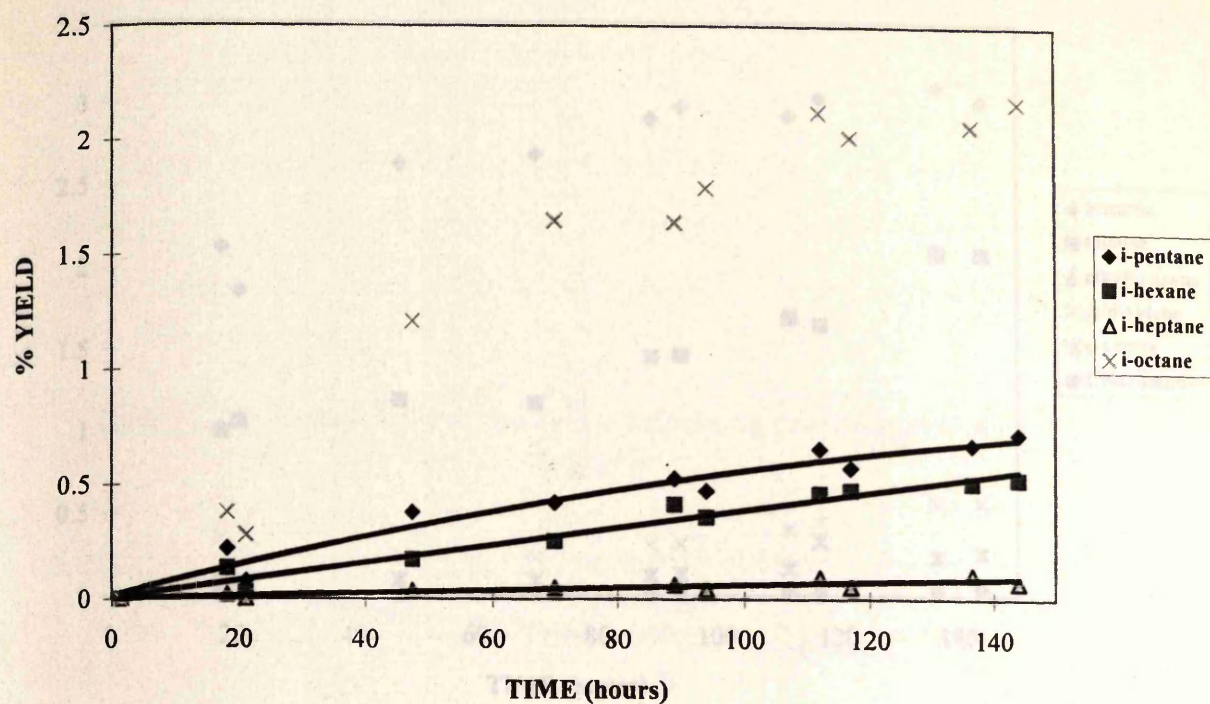


Figure 5.6.4 Yields of n-alkanes over 0.3 wt% Ir/Al₂O₃

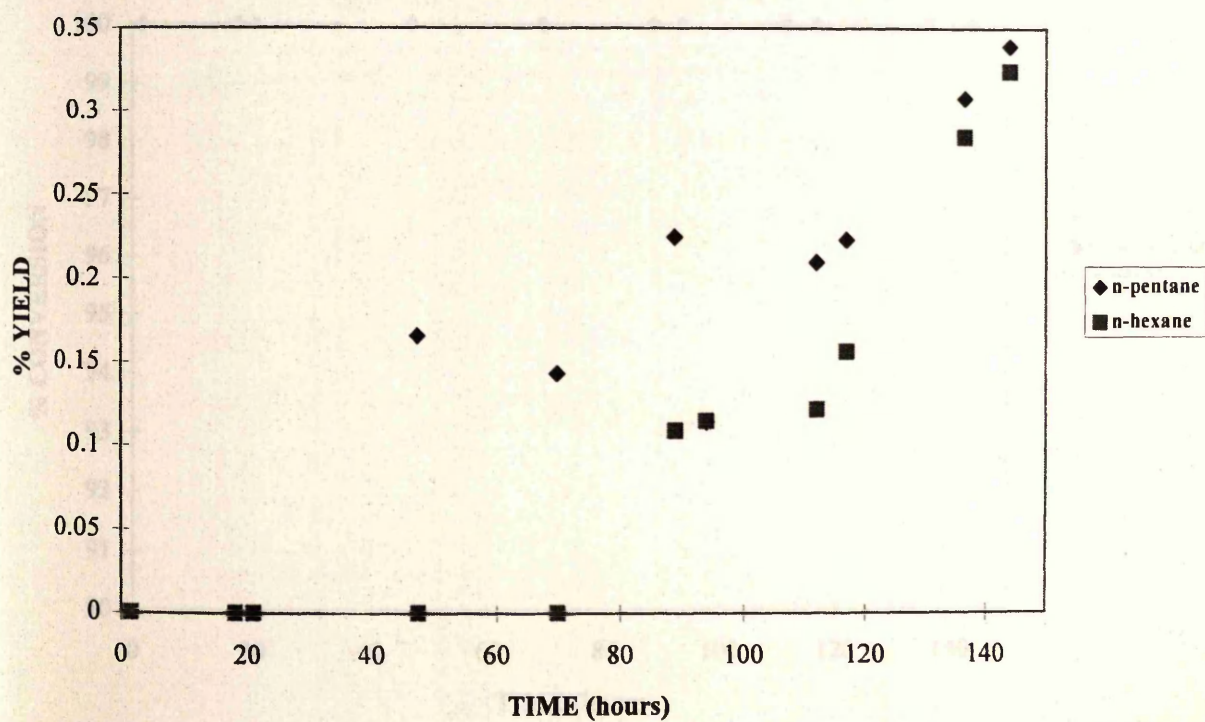


Figure 5.6.5 Yields of aromatics over 0.3 wt% Ir/Al₂O₃

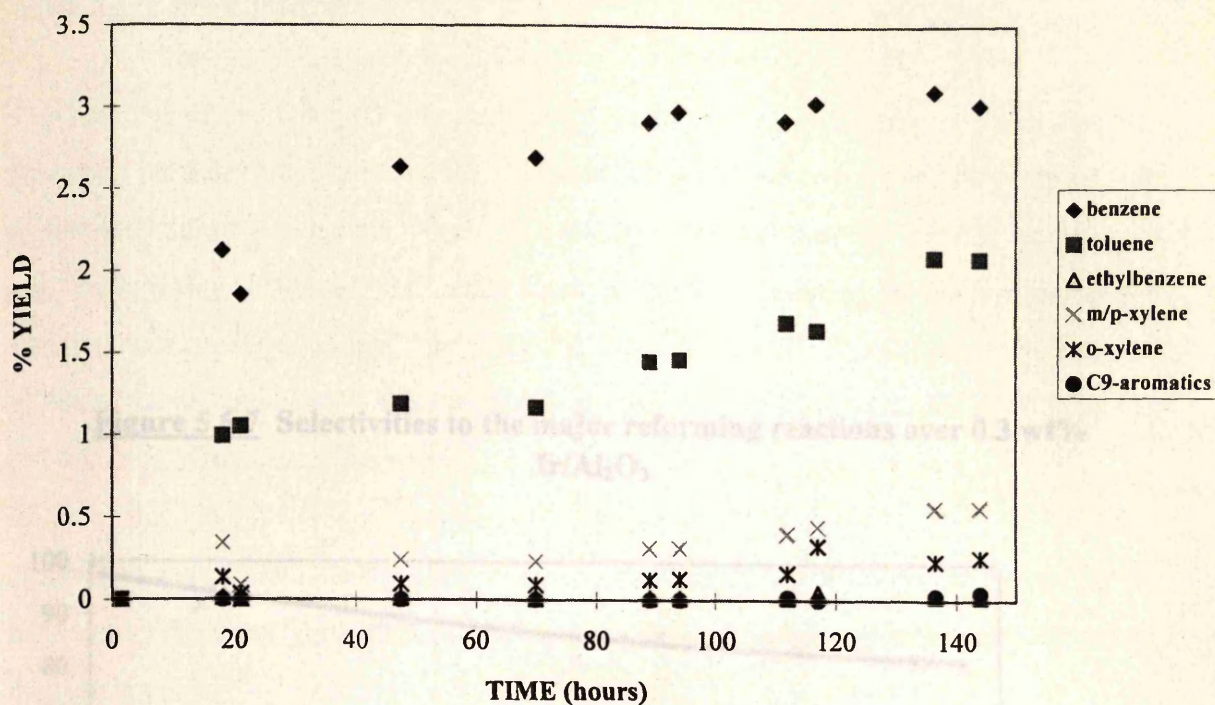
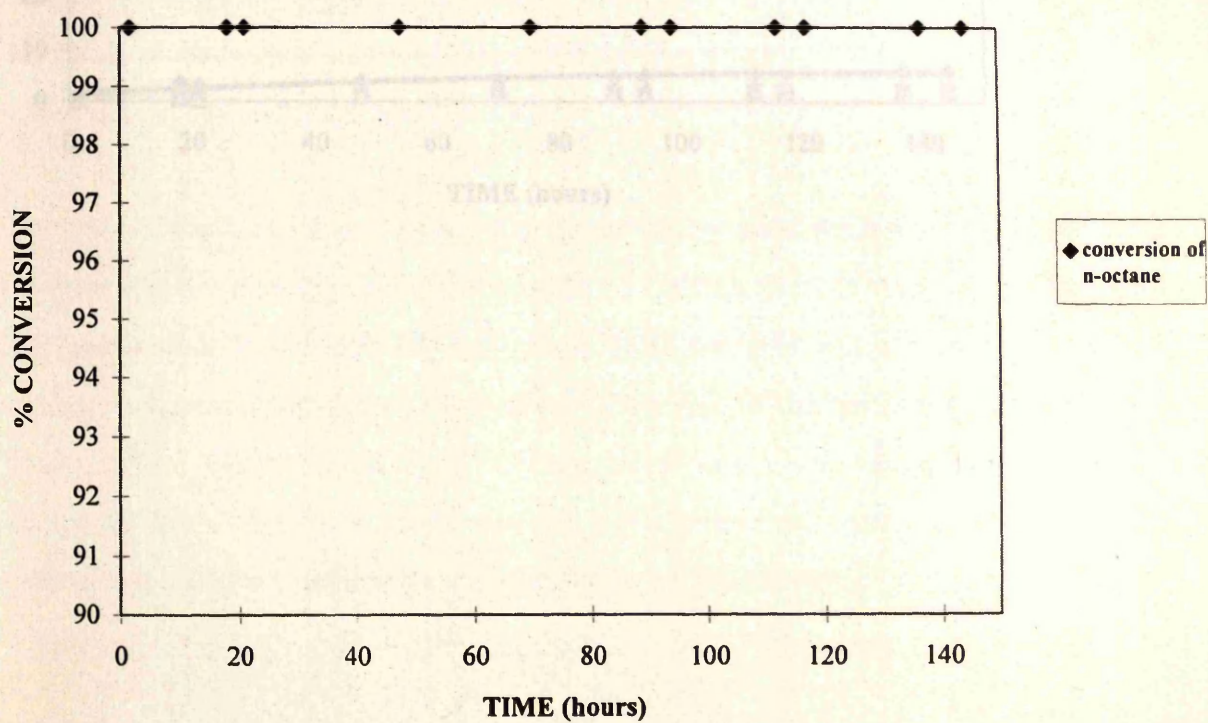


Figure 5.6.6 Conversion of n-octane over 0.3 wt% Ir/Al₂O₃

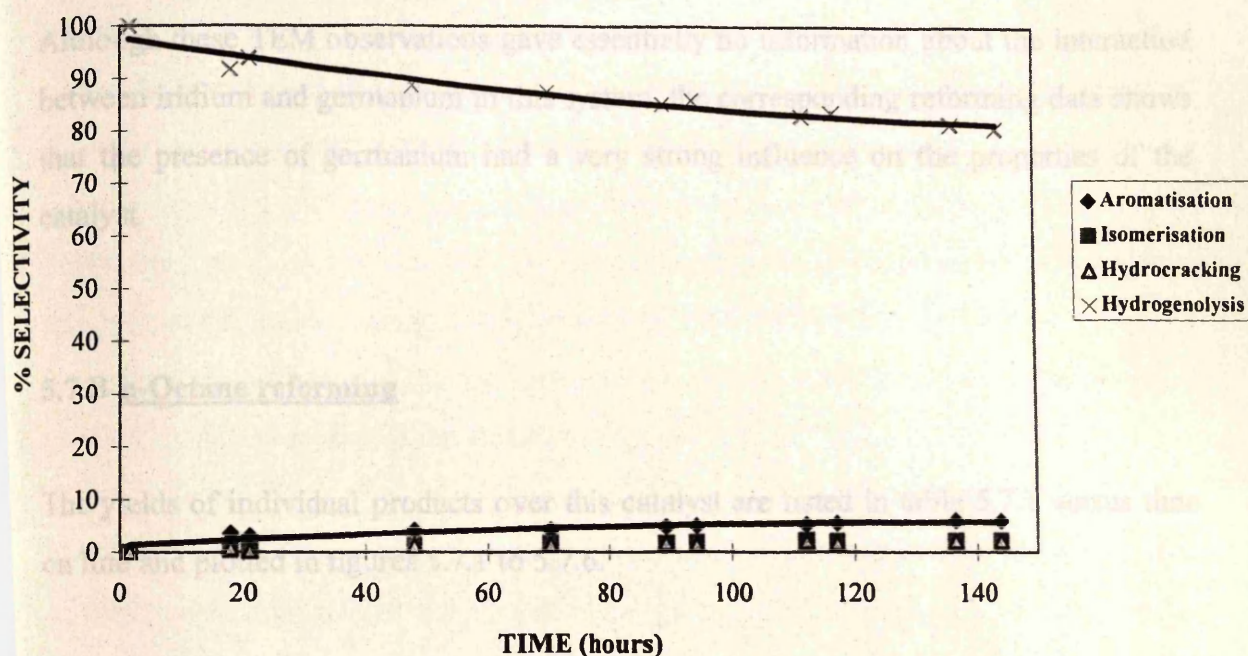


5.7. 0.3 wt% Ir - 0.3 wt% Ge/Al₂O₃

5.7.A TEM observations

TEM studies of this catalysts revealed identical results to the preceding Ir/Al₂O₃ catalyst. No metal particles were detected after calcination or reduction or after 144 hours on line in the reforming of n-octane. Again this strongly suggests that the metallic component was very highly dispersed and much more resistant to sintering in the hydrogen-rich atmospheres employed in this study than the corresponding Ir-Ge catalyst. Indeed, a TEM observation after 144 hours on line is shown in Figure 5.6.7, in which no particles greater than 2 nm were observed.

Figure 5.6.7 Selectivities to the major reforming reactions over 0.3 wt% Ir/Al₂O₃



5.7. 0.3 wt% Ir - 0.3 wt% Ge/Al₂O₃

5.7.A TEM observations

TEM studies of this catalysts revealed identical results to the preceding Ir/Al₂O₃ catalyst. No metal particles were detected after calcination or reduction or after 144 hours on line in the reforming of n-octane. Again this strongly suggest that the metallic component was very highly dispersed and much more resistant to sintering in the hydrogen rich atmospheres employed in this study than the corresponding Pt-Ge catalyst. A typical area of this catalyst after 144 hours on line is shown in plate 31. Again no metal particles greater than 2 nm were observed.

Although these TEM observations gave essentially no information about the interaction between iridium and germanium in this system, the corresponding reforming data shows that the presence of germanium had a very strong influence on the properties of the catalyst.

5.7.B n-Octane reforming

The yields of individual products over this catalyst are listed in table 5.7.1 versus time on line and plotted in figures 5.7.1 to 5.7.6.

The yields of methane, ethane, propane, i-butane and n-butane are plotted in figure 5.7.1. It is clear that the most significant consequence of adding germanium to this system was that it dramatically reduced the very high hydrogenolysis activity of iridium. This resulted in a corresponding large increase in the yields of the remaining products. The initial yield of methane over the Ir/Al₂O₃ catalyst was 100%, whilst over this Ir-Ge catalyst the initial yield of methane was just 3.8%. Indeed this value is below even that of the initial yield of methane over Pt-Ge/Al₂O₃ (5.2%). Another interesting feature of

this catalyst was that, relative to Pt/Al₂O₃ (figure 5.1.1) or Pt-Ge/Al₂O₃ (figure 5.3.1), the yields of propane, i-butane and n-butane were considerably higher (e.g. initial yields of n-butane Pt 5.9%, Pt-Ge 7.6%, Ir-Ge 14.4%).

The yields of cycloalkanes over this catalysts are plotted in figure 5.7.2. The first point to note is that the yields of these products were lower than the corresponding yields over platinum (figure 5.1.2). However, it was observed that the yields of C₇ and C₈ cycloalkanes, although zero initially, began to increase sharply after approximately 80 hours on line. This contrasts with the situation for these two products over Pt/Al₂O₃ where the largest increase in yield was observed in the initial stages of the run.

The yields of i-alkanes over this catalyst are plotted in figure 5.7.3. Relative to platinum (figure 5.1.3) it was observed that on this catalyst the yield of i-pentane was greater (9%) whilst the initial yield of i-hexane (2.2%) was lower (this compares with initial values of 6.9% for i-pentane and 6.0% for i-hexane over Pt/Al₂O₃). The yield of i-heptane was initially zero but increased continuously throughout the run reaching a final value of 1.5%. The yield of i-octane was also zero initially but this increased quite sharply throughout the run reaching a final value of 9.0%. Although the i-octane yield did increase noticeably throughout the run, this increase was not as great as that observed over the Pt/Al₂O₃ catalyst (final value 23.0%).

The yields of n-alkanes over this catalyst are plotted in figure 5.7.4. The yield of n-pentane over this catalyst was found to be greater at all stages of the run than the corresponding yield over Pt/Al₂O₃ (initial values: 7.15% and 4.9% respectively). The yields of n-hexane and n-heptane were similar to those over the platinum catalyst. It was observed that the yield of n-pentane decreased slightly with time on line whilst the yields of n-hexane and n-heptane increased.

The yields of aromatic products versus time on line over the Ir-Ge/Al₂O₃ are plotted in figure 5.7.5. In order of decreasing yield the major aromatic products were as follows:

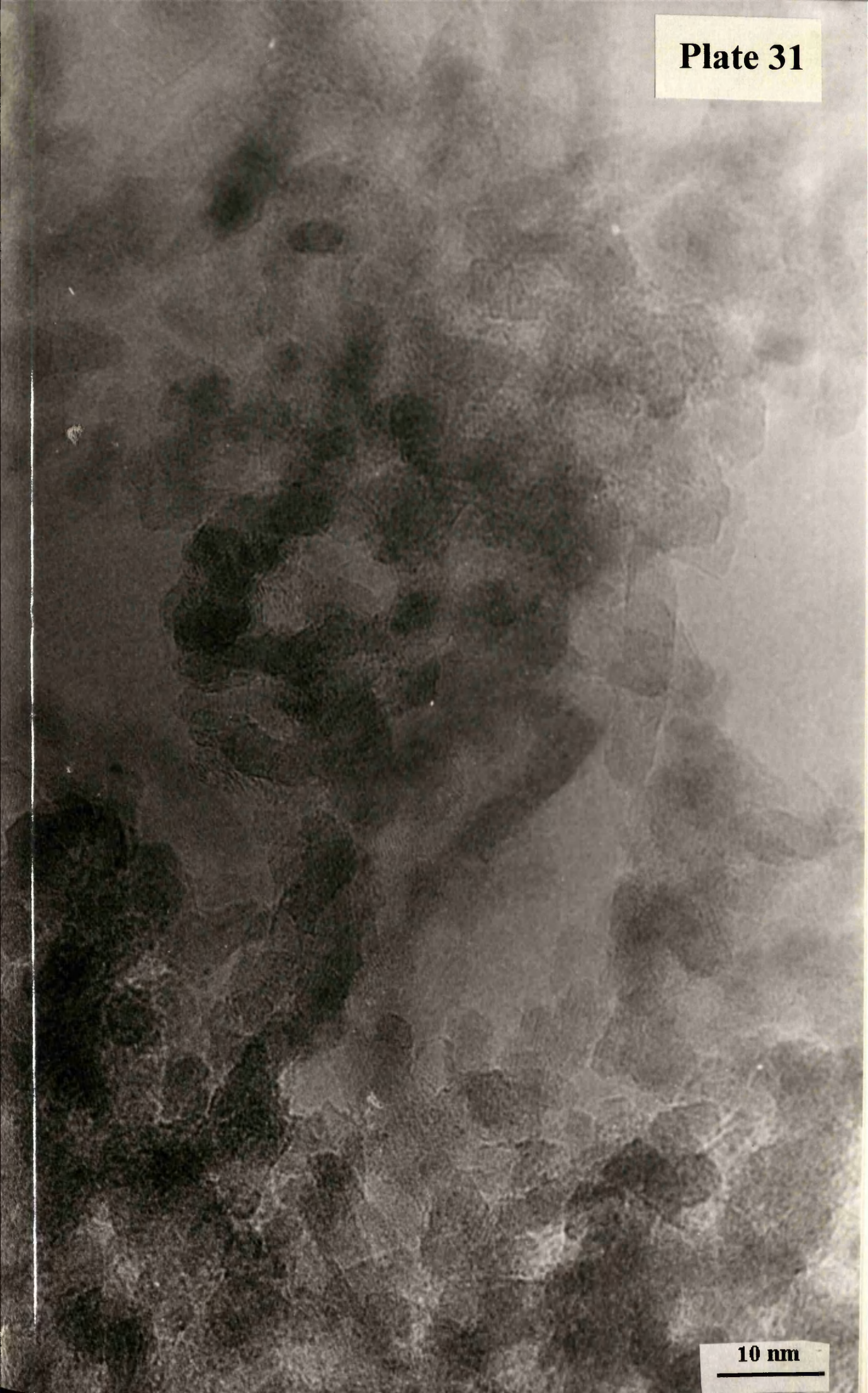
m/p-xylene > o-xylene > toluene ~ ethylbenzene > benzene ~ C₉ aromatics

This is not the same order as observed over platinum (see section 5.1). Whilst the yields of m/p-xylenes, toluene, benzene and C₉ aromatics were similar over these two catalysts, the initial yields of o-xylene and especially ethylbenzene were considerably lower over Ir-Ge/Al₂O₃ than over Pt/Al₂O₃ (o-xylene: Pt 10.2%, Ir-Ge 6.4%; ethylbenzene: 8.8%, Ir-Ge 2.5%). However, whilst over Pt/Al₂O₃ (figure 5.1.5) the yields of most aromatic products decreased significantly with time on line, the corresponding values over Ir-Ge were found to be considerably more stable. The overall result was that although Pt/Al₂O₃ produced more aromatics initially, the rapid deactivation of this catalyst meant that the Ir-Ge/Al₂O₃ catalysts was superior for the production of aromatics during the latter stages of the reforming run.

The conversion of n-octane over this catalyst is plotted in figure 5.7.6. Initially 100% conversion of n-octane was achieved although this did decline slightly throughout the run. This compares with the Ir/Al₂O₃ catalyst (figure 5.6.6) where 100% conversion was maintained throughout the entire run. However when this slight decrease is compared with the corresponding values over platinum (figure 5.1.6), Pt-Sn (figure 5.2.6) or Pt-Ge (figure 5.3.6) it is clear that it was much less than in these platinum containing catalysts (e.g. final conversions: Pt-Ge 91.6%, Ir-Ge 97.6%). Another interesting feature is that this catalyst was found to exhibit an "accelerating" deactivation curve similar to those found for Pt-Sn and Pt-Ge rather than the "decelerating" deactivation curve observed over Pt.

The selectivities to the four major reforming reactions are presented versus time on line in table 5.7.2 and plotted versus time on line in figure 5.7.7. When comparing these values to those obtained over the Ir/Al₂O₃ catalyst (figure 5.6.6), the major difference observed was the dramatic decrease in the selectivity to hydrogenolysis and the corresponding large increase in the selectivity to the remaining reactions. When

comparing these values with those obtained over $\text{Pt}/\text{Al}_2\text{O}_3$ (figure 5.1.7) a number of interesting differences were also observed. The selectivity to hydrocracking was much greater over the Ir-Ge catalyst and remained relatively constant throughout the run (21-22% over Ir-Ge, 15-17% over Pt). The selectivity to aromatics, although initially lower, was much more stable over Ir-Ge than Pt and by 144 hours on line the Ir-Ge catalysts was found to be more selective (final values: Ir-Ge 32.2; Pt 25.1%) . The selectivity to isomerisation was much lower initially over Ir-Ge than platinum but did increase throughout the run. This increase in isomerisation selectivity was not as pronounced as that observed over platinum however (final values Ir-Ge 10.8%, Pt 26.9%).



10 nm

Table 5.7.1 Yields of individual products for catalyst 0.3 wt% Ir - 0.3 wt% Ge/Al₂O₃

Time (hours)	Methane	Ethane	Propane	i-Butane	n-Butane	c-Pentane	i-Pentane	n-Pentane
1.5	3.8	4.0	14.8	9.7	14.4	0.2	9.1	7.1
4.5	4.4	3.7	13.6	9.1	13.4	0.2	9.2	6.8
17.0	4.7	3.3	11.1	10.1	13.9	0.2	9.7	6.8
20.5	4.9	3.0	12.1	9.0	12.3	0.2	9.4	6.1
41.0	4.6	3.2	11.2	8.8	12.6	0.2	9.9	6.0
44.5	5.2	2.9	10.9	8.2	10.9	0.1	8.9	5.9
70.5	3.9	3.1	11.8	8.5	11.1	0.1	8.8	6.0
74.0	3.3	3.1	10.0	7.3	9.6	0.1	8.5	6.0
91.5	3.2	3.0	10.0	7.7	9.9	0.1	8.9	5.8
100.0	3.5	3.2	10.0	7.3	9.3	0.1	8.6	5.6
114.0	4.4	2.9	9.3	7.2	9.4	0.1	8.6	5.7
118.5	3.4	3.1	9.5	6.9	8.9	0.1	8.3	5.4
136.5	2.9	2.7	9.3	7.1	9.3	0.1	8.8	6.0
144.0	2.8	2.3	9.2	7.0	8.9	0.1	8.3	5.6

Table 5.7.1 (cont) Yields of individual products for catalyst 0.3 wt% Ir - 0.3 wt% Ge/Al₂O₃

Time (hours)	C6 c-Alkane	i-Hexane	n-Hexane	C7 c-Alkane	i-Heptane	n-Heptane	C8 c-Alkane	i-Octane
1.5	0.0	2.2	1.1	0.0	0.0	0.0	0.0	0.0
4.5	0.0	2.6	1.6	0.0	0.1	0.1	0.0	0.0
17.0	0.0	3.8	1.7	0.0	0.2	0.1	0.0	0.2
20.5	0.1	3.6	1.9	0.0	0.3	0.2	0.0	0.3
41.0	0.1	5.0	2.1	0.0	0.5	0.2	0.0	1.2
44.5	0.1	4.4	2.2	0.0	0.6	0.5	0.0	2.4
70.5	0.2	4.6	3.0	0.0	1.2	0.8	0.0	3.6
74.0	0.2	5.0	2.6	0.0	1.0	0.5	0.0	3.3
91.5	0.2	5.5	2.6	0.0	1.1	0.4	0.1	4.6
100.0	0.2	5.4	2.3	0.1	1.0	0.3	0.2	4.3
114.0	0.3	5.5	2.5	0.1	1.0	0.3	0.2	5.3
118.5	0.3	5.4	2.5	0.2	1.1	0.4	0.2	5.2
136.5	0.4	5.9	3.0	0.4	1.4	0.9	0.7	7.7
144.0	0.4	5.6	2.9	0.5	1.5	0.9	0.8	9.0

Table 5.7.1 (cont) Yields of individual products for catalyst 0.3 wt% Ir - 0.3 wt% Ge/Al₂O₃

Time (hours)	Benzene	Toluene	Ethyl- Benzene	m/p- Xylene	o-Xylene	C9 Aromatic	Total Conversion
1.5	1.5	3.8	2.5	18.7	6.4	0.7	100.0
4.5	1.4	3.7	2.7	19.7	6.8	0.7	99.9
17.0	1.1	3.3	2.9	18.8	6.9	0.6	99.6
20.5	1.1	3.6	3.1	20.2	7.6	0.9	99.7
41.0	0.9	3.2	3.2	19.0	7.3	0.7	99.7
44.5	0.9	3.2	3.3	20.3	7.9	0.9	99.7
70.5	0.5	2.3	1.7	19.5	7.6	1.0	99.3
74.0	1.2	3.1	3.6	20.8	8.4	1.2	99.0
91.5	0.6	2.8	3.3	19.8	8.0	0.9	98.6
100.0	0.7	3.0	3.6	21.1	8.4	0.8	99.0
114.0	0.6	2.7	3.2	20.1	8.1	1.0	98.7
118.5	0.6	2.9	3.6	21.1	8.5	1.0	98.8
136.5	0.5	2.3	2.8	17.2	7.0	1.0	97.5
144.0	0.4	2.4	3.1	17.5	7.0	1.0	97.1

Table 5.7.2 Selectivity to the major reforming reactions for 0.3 wt% Ir - 0.3 wt% Ge/Al₂O₃

Time (hours)	Selectivity to Aromatics	Selectivity to Isomerisation	Selectivity to Hydrocracking	Selectivity to Hydrogenolysis
1.5	33.6	0.0	21.0	3.8
4.5	35.1	0.1	20.9	4.4
17.0	33.8	0.4	23.8	4.7
20.5	36.6	0.5	22.1	4.9
41.0	34.3	1.6	23.7	4.6
44.5	36.6	2.9	21.5	5.2
70.5	32.8	4.9	22.0	3.9
74.0	38.7	4.3	21.1	3.3
91.5	35.9	5.8	22.4	3.3
100.0	38.0	5.3	21.5	3.5
114.0	36.3	6.4	21.6	4.5
118.5	38.2	6.4	21.0	3.5
136.5	31.7	9.4	22.4	3.0
144.0	32.2	10.8	21.5	2.9

Figure 5.7.1 Yields of individual products over 0.3 wt% Ir - 0.3 wt% Ge/Al₂O₃

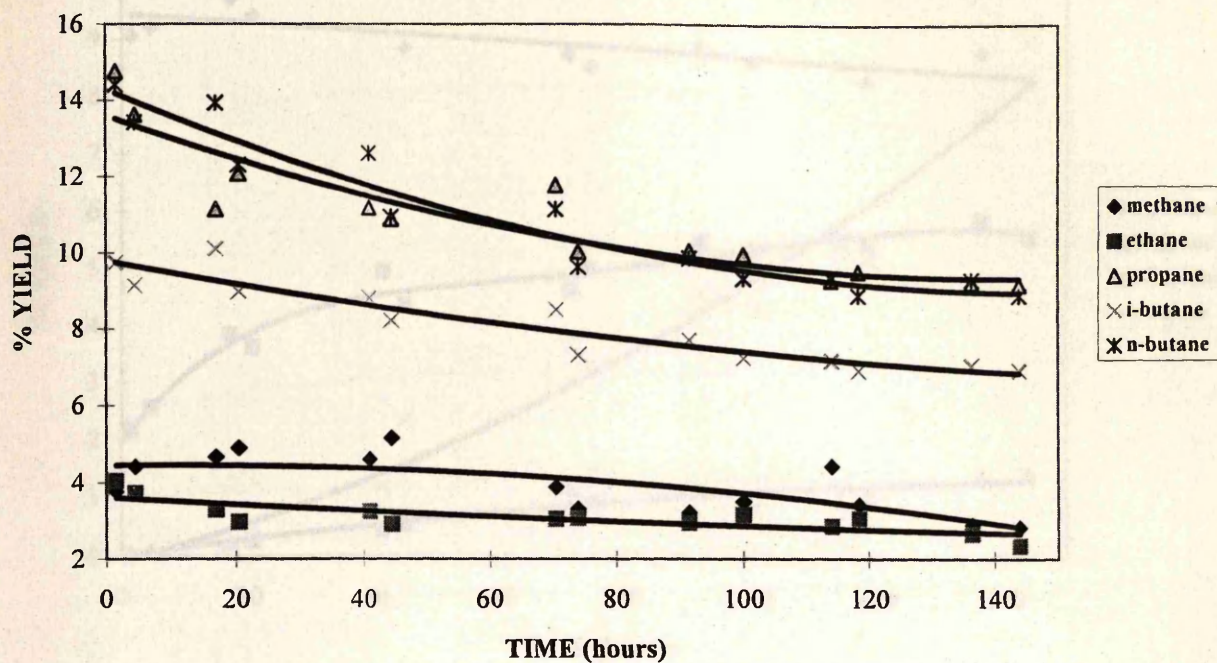


Figure 5.7.2 Yields of cycloalkanes over 0.3 wt% Ir - 0.3 wt% Ge/Al₂O₃

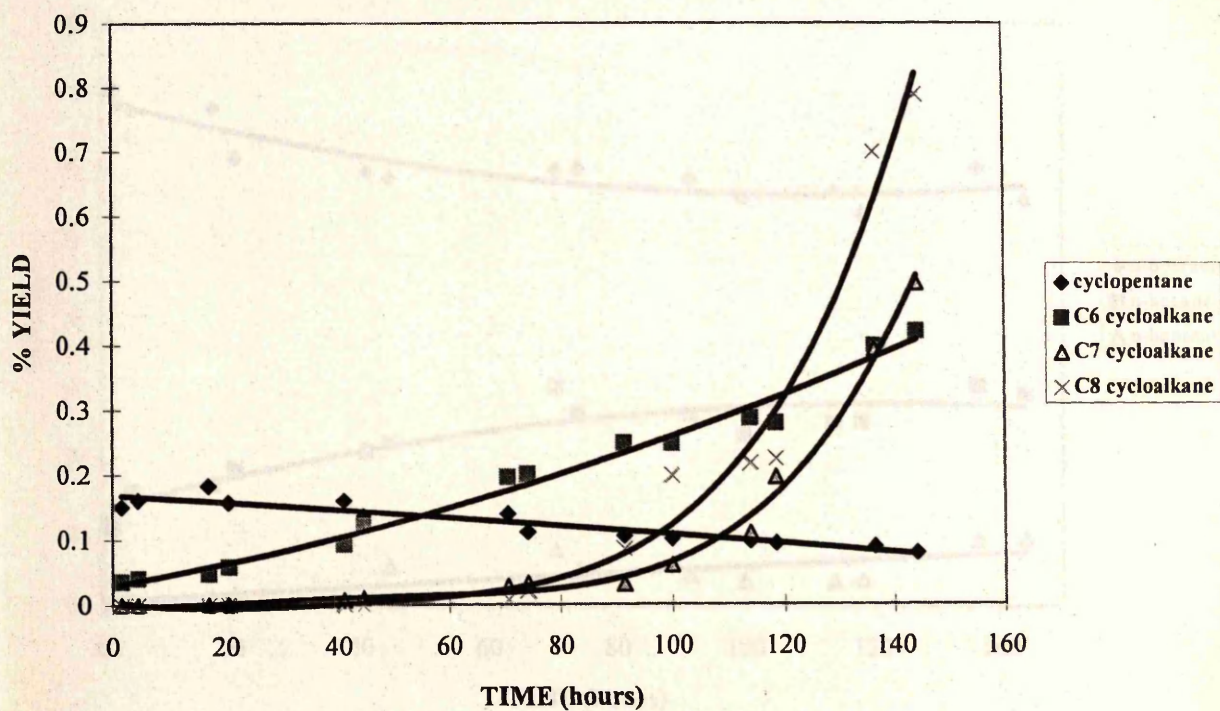


Figure 5.7.3 Yields of i-alkanes over 0.3 wt% Ir - 0.3 wt% Ge/Al₂O₃

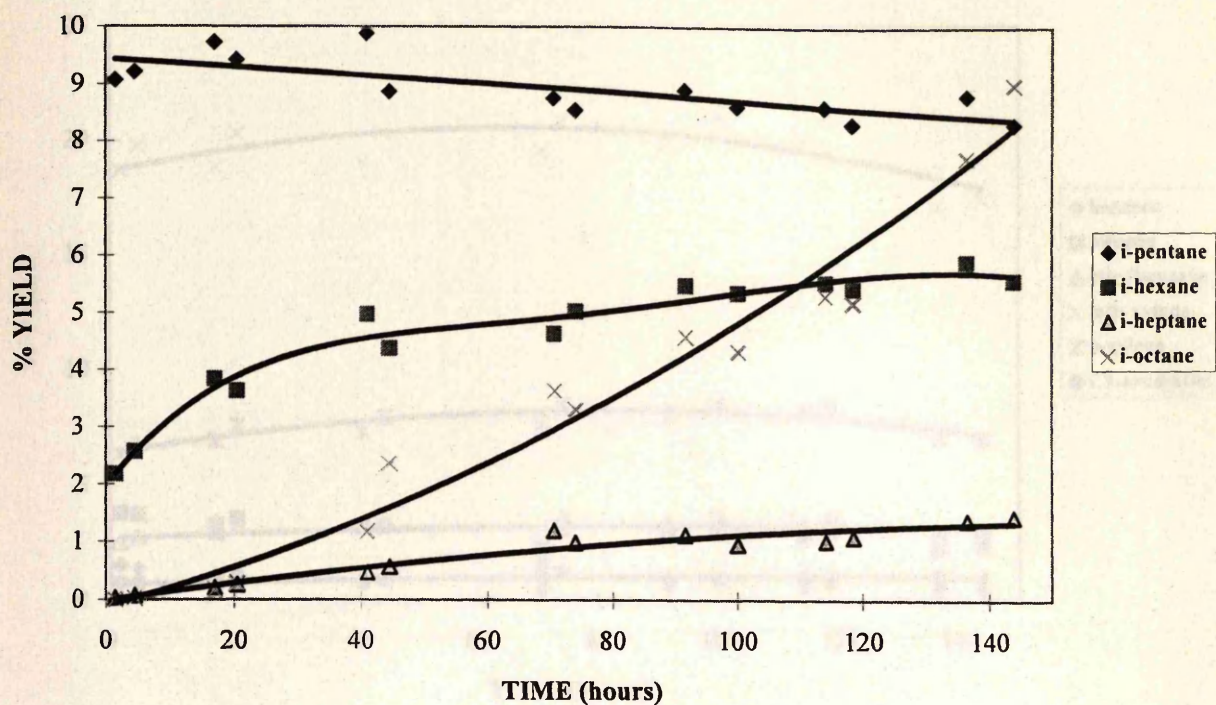


Figure 5.7.4 Yields of n-alkanes over 0.3 wt% Ir - 0.3 wt% Ge/Al₂O₃

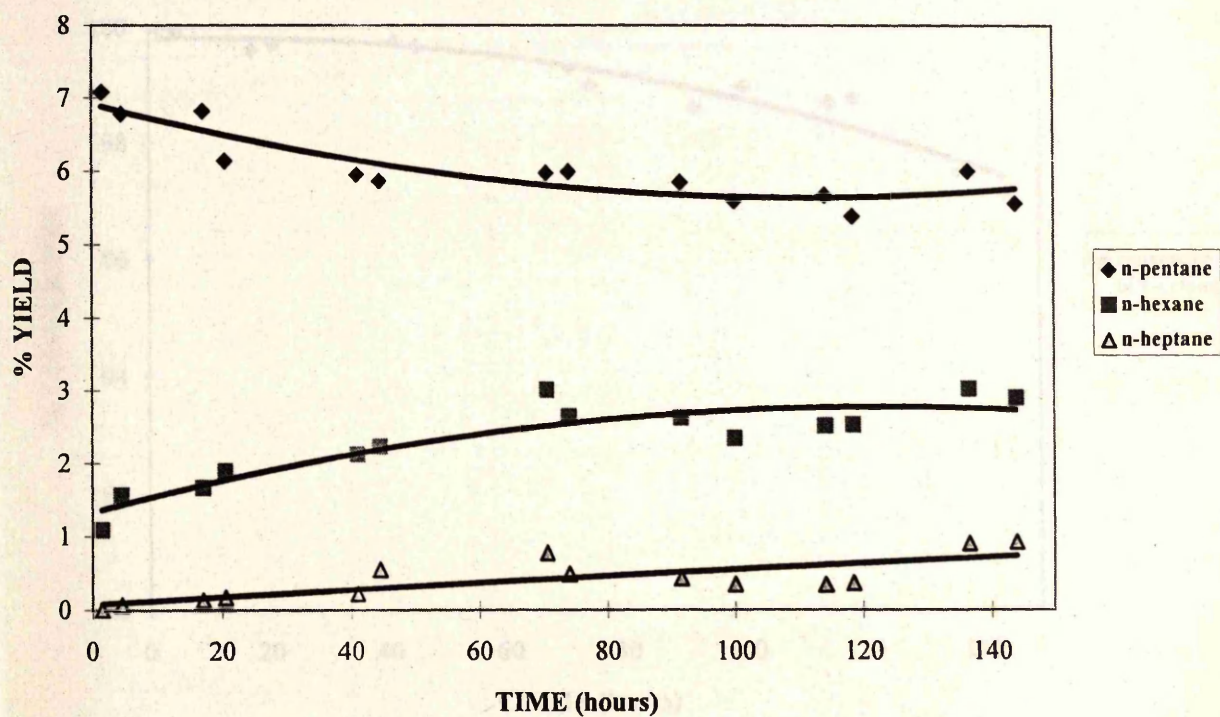


Figure 5.7.5 Yields of aromatics over 0.3 wt% Ir - 0.3 wt% Ge/Al₂O₃

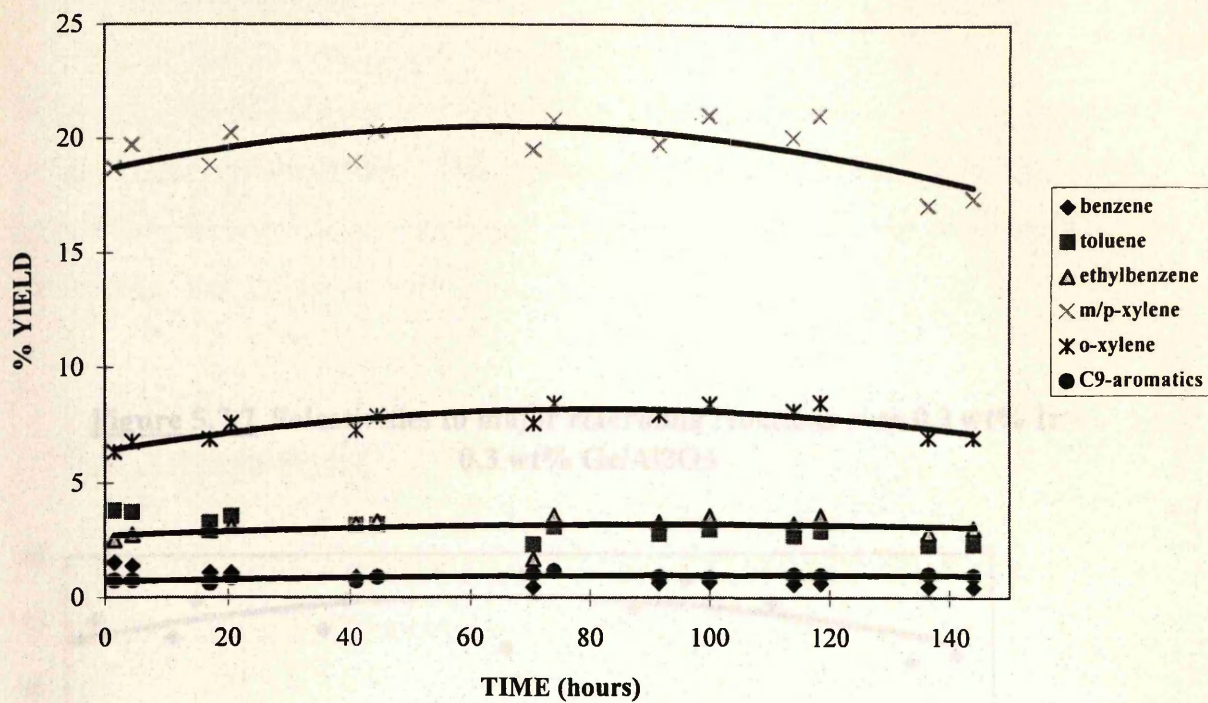
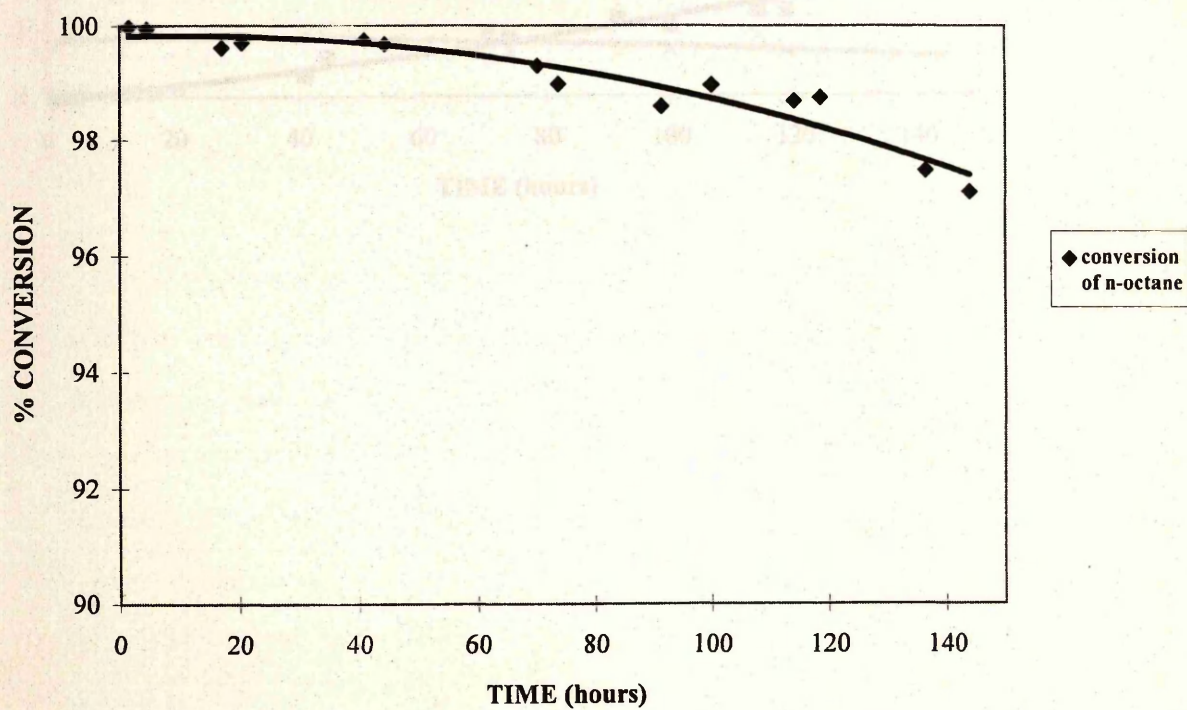


Figure 5.7.6 Conversion of n-octane over 0.3 wt% Ir - 0.3 wt% Ge/Al₂O₃

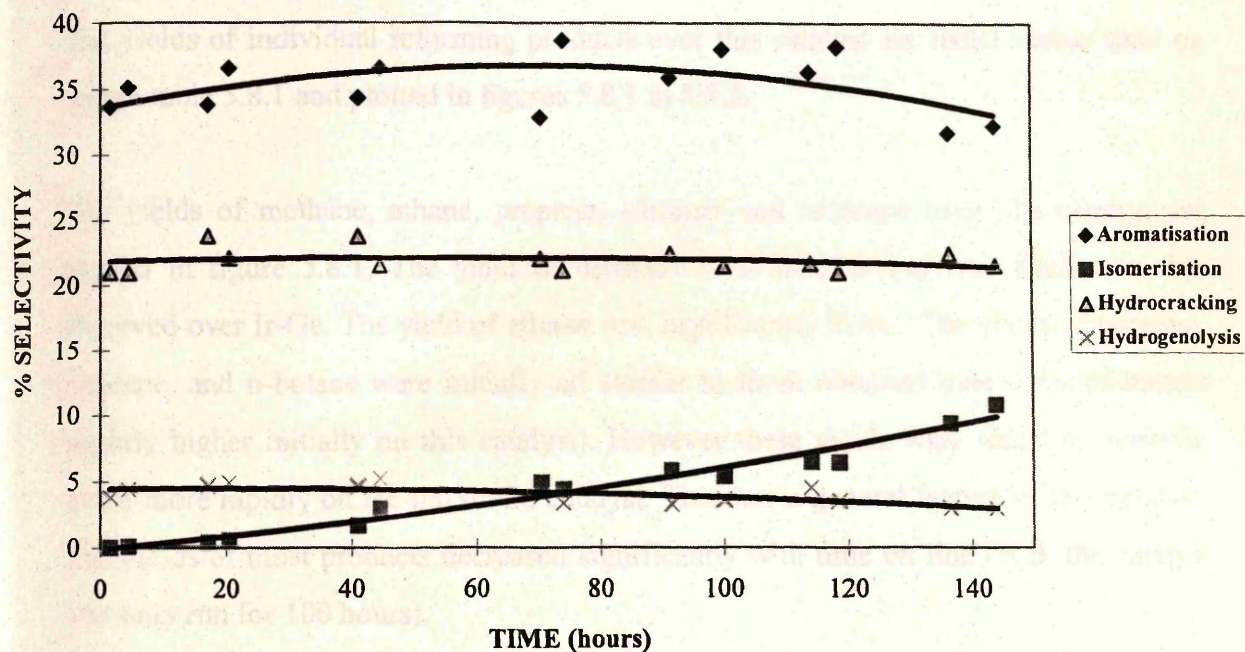


5.6. 0.03 wt% Ir - 0.3 wt% Ge/Al₂O₃

5.6.4 TEM observations

TEM studies of this catalyst after both calcination-reduction and use in reforming found no detectable metal particles. This finding was not very surprising in light of the observation made on the two previous catalysts studied and the fact that the catalysts contained a very low metal loading.

Figure 5.7.7 Selectivities to major reforming reactions over 0.3 wt% Ir - 0.3 wt% Ge/Al₂O₃



5.8. 0.03 wt% Ir - 0.3 wt% Ge/Al₂O₃

5.8.A TEM observations

TEM studies of this catalyst after both calcination/reduction and use in reforming found no detectable metal particles. This finding was not very surprising in light of the observation made on the two previous catalysts studied and the fact that this catalysts contained a very low metal loading.

5.8.B n-Octane reforming

The yields of individual reforming products over this catalyst are listed versus time on line in table 5.8.1 and plotted in figures 5.8.1 to 5.8.6.

The yields of methane, ethane, propane, i-butane and n-butane over this catalyst are plotted in figure 5.8.1. The yield of methane over this catalyst was similar to that observed over Ir-Ge. The yield of ethane was significantly lower. The yields of propane, i-butane, and n-butane were initially all similar to those obtained over Ir-Ge (n-butane slightly higher initially on this catalyst). However these yields were found to decrease much more rapidly on the 0.03Ir-Ge catalyst. This was a general feature of this catalyst. The yields of most products decreased significantly with time on line (N.B. the catalyst was only run for 100 hours).

The yields of cycloalkanes over this catalyst are plotted in figure 5.8.2. It is interesting to note that the yields of cycloalkanes over this catalyst were significantly greater than the corresponding yields over Ir-Ge (figure 5.7.2). The yields of cyclopentane and C₆, C₇ cycloalkanes remained relatively constant throughout the run whilst the yields of C₈ cycloalkanes were observed to increase steadily throughout the run.

The yields of i-alkanes over this catalyst are plotted in figure 5.8.3. The initial yield of i-pentane over 0.03Ir-Ge was found to be similar to the initial value over Ir-Ge (9.6). However, the yield of this product decreased much more rapidly over the 0.03Ir-Ge catalyst. The initial yields of i-hexane were also similar over these two catalysts. However the yield over the Ir-Ge catalyst increased with time on line whilst over the 0.03 Ir-Ge catalyst the yield remained relatively constant. The yields of i-heptanes were similar over these catalysts, although the increase in yield of i-heptane was greater and more pronounced over Ir-Ge. The initial yield of i-octane was higher over 0.03Ir-Ge (3.5%) than over Ir-Ge (0%). The yield over 0.03Ir-Ge increased steadily during the first ~ 70 hours on line and then remained relatively constant (perhaps began to decrease slightly). This compares with Ir-Ge where the yield of i-octane was observed to increase continuously throughout the run (100 hour values: 0.03Ir-Ge 7.9%, Ir-Ge 9%).

The yields of n-alkanes over the 0.03Ir-Ge catalyst are plotted in figure 5.8.4. The yields of n-alkanes over this catalyst and Ir-Ge were found to be relatively similar during the first 100 hours on line.

The yields of aromatic products over 0.03Ir-Ge are plotted in figure 5.8.5. It was observed that one of the major consequences of decreasing the active metal loading from 0.3 to 0.03 wt% was to significantly decrease the yields of aromatic products (compare with figure 5.7.5 e.g. initial m/p-xylene yields: 0.03Ir-Ge 9.7%, Ir-Ge 18.7%). Also, whilst the yields of aromatics over Ir-Ge were relatively stable during the run, the yields of the major aromatic products, xylenes, were found to decrease significantly with time on line over 0.03Ir-Ge.

The initial conversion of n-octane over 0.03Ir-Ge, figure 5.8.6, was considerably lower than the conversion observed in all the previous catalysts discussed. (90% versus 98-100% for the other systems) and was also found to decrease much more rapidly with time on line, reaching a value of 60.4 % after 100 hours.

The selectivities to the four major reforming reactions over this catalyst are presented versus time on line in table 5.8.2 and plotted in figure 5.8.7. It is interesting to note that the major reforming reaction over this catalyst was hydrocracking whilst on most of the catalysts studied the major reaction was aromatisation. The selectivity to hydrocracking on this catalysts (24.3%) was slightly higher than the initial selectivity over Ir-Ge (21%, figure 5.7.7). However, this selectivity decreased slowly through the run whilst over the Ir-Ge the selectivity to hydrocracking remained relatively stable. The selectivity to aromatisation was much lower over 0.03Ir-Ge but did not decrease significantly with time on line (initial values: 0.03Ir-Ge 18.9; Ir-Ge 33.6). The selectivity to isomerisation was initially higher over 0.03Ir-Ge than Ir-Ge (4.1% versus zero). This selectivity increased at a similar rate with time on line over both catalysts. The selectivity to hydrogenolysis was greater over the 0.03Ir-Ge catalyst than over the Ir-Ge.

Table 5.8.1 Yields of individual products for catalyst 0.03 wt% Ir - 0.3 wt% Ge/Al₂O₃

Time (hours)	Methane	Ethane	Propane	i-Butane	n-Butane	c-Pentane	i-Pentane	n-Pentane
1.0	4.3	2.4	14.9	10.0	16.3	0.5	9.6	6.2
6.0	4.2	1.9	13.3	8.5	14.3	0.6	8.2	7.8
19.0	5.0	2.3	11.5	7.7	12.4	0.4	7.5	6.8
23.5	4.7	2.0	11.0	7.3	11.7	0.5	7.2	6.7
45.5	4.5	2.0	9.3	6.6	10.4	0.4	6.6	6.0
71.5	4.9	2.0	7.6	6.2	9.9	0.4	6.4	4.7
76.5	4.7	1.6	8.3	5.7	8.1	0.4	5.6	4.0
95.0	4.1	1.4	6.9	5.1	7.6	0.3	4.8	3.8
100.0	3.6	1.3	6.7	4.4	6.7	0.3	4.5	4.6

Table 5.8.1 (cont) Yields of individual products for catalyst 0.03 wt% Ir - 0.3 wt% Ge/Al₂O₃

Time (hours)	C6 c-Alkane	i-Hexane	n-Hexane	C7 c-Alkane	i-Heptane	n-Heptane	C8 c-Alkane	i-Octane
1.0	0.6	2.4	0.9	0.6	0.3	0.1	0.7	3.5
6.0	0.6	2.7	2.5	0.8	0.7	0.4	1.3	4.2
19.0	0.4	2.8	2.1	0.5	0.4	0.3	1.3	5.4
23.5	0.8	2.9	2.6	0.8	0.7	0.4	1.7	6.1
45.5	0.7	2.8	2.4	0.6	0.5	0.2	1.8	7.7
71.5	0.5	2.8	2.1	0.4	0.5	0.2	2.1	9.2
76.5	0.5	2.5	1.6	0.5	0.5	0.4	2.5	9.2
95.0	0.4	2.1	2.1	0.5	0.5	0.4	2.6	8.8
100.0	0.4	2.4	2.7	0.6	0.8	0.6	2.6	7.9

Table 5.8.1 (cont) Yields of individual products for catalyst 0.03 wt% Ir - 0.3 wt% Ge/Al₂O₃

Time (hours)	Benzene	Toluene	Ethyl- Benzene	m/p- Xylene	o-Xylene	C9 Aromatic	Total Conversion
1.0	0.3	1.7	0.9	9.7	3.5	0.9	90.4
6.0	0.3	1.6	0.8	8.4	3.0	0.8	86.9
19.0	0.2	1.8	0.9	9.0	3.3	0.9	83.0
23.5	0.2	1.6	0.9	8.0	2.9	0.8	81.7
45.5	0.2	1.4	0.9	8.1	3.1	1.1	77.3
71.5	0.1	1.2	0.7	6.5	2.3	0.7	71.4
76.5	0.1	1.3	0.8	7.1	2.6	0.9	68.8
95.0	0.1	1.1	0.6	6.5	2.5	0.8	63.0
100.0	0.2	1.1	0.6	5.4	2.0	0.7	60.4

Table 5.8.2 Selectivity to the major reforming reactions for 0.03 wt% Ir - 0.3 wt% Ge/Al₂O₃

Time (hours)	Selectivity to Aromatics	Selectivity to Isomerisation	Selectivity to Hydrocracking	Selectivity to Hydrogenolysis
1.0	18.9	4.1	24.3	4.8
6.0	17.2	5.6	22.3	4.8
19.0	19.4	7.1	21.6	6.0
23.5	17.6	8.4	21.3	5.8
45.5	19.1	10.6	20.8	5.8
71.5	16.3	13.6	21.6	6.8
76.5	18.7	14.1	20.1	6.8
95.0	18.6	14.8	18.9	6.5
100.0	16.7	14.5	18.7	6.0

Figure 5.8.1 Yields of individual products over 0.03 wt% Ir - 0.3 wt% Ge/Al₂O₃

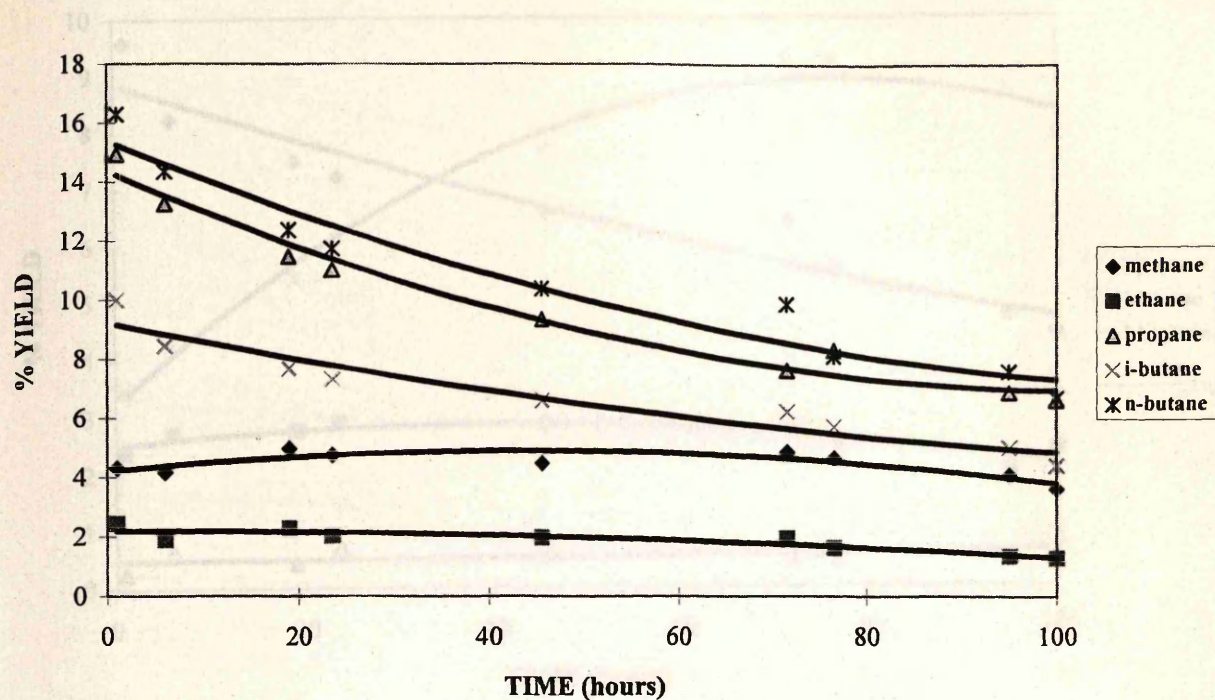


Figure 5.8.2 Yields of cycloalkanes over 0.03 wt% Ir - 0.3 wt% Ge/Al₂O₃

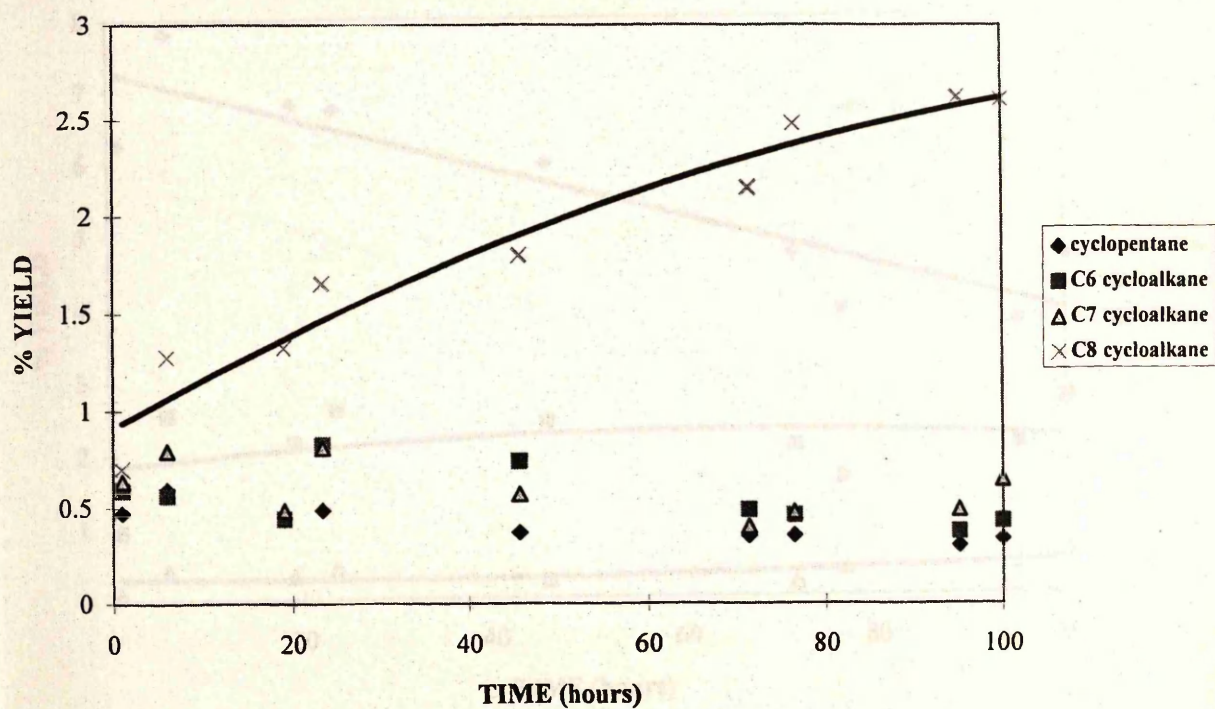


Figure 5.8.1 Yields of individual products over 0.03 wt% Ir - 0.3 wt% Ge/Al₂O₃

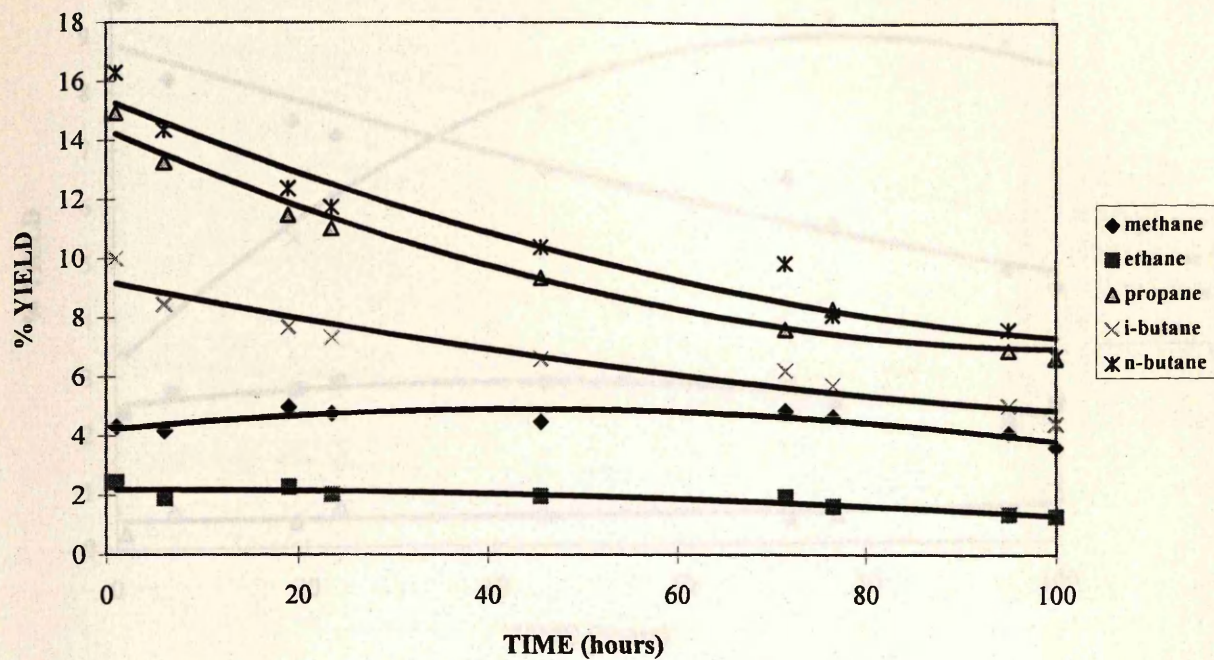


Figure 5.8.2 Yields of cycloalkanes over 0.03 wt% Ir - 0.3 wt% Ge/Al₂O₃

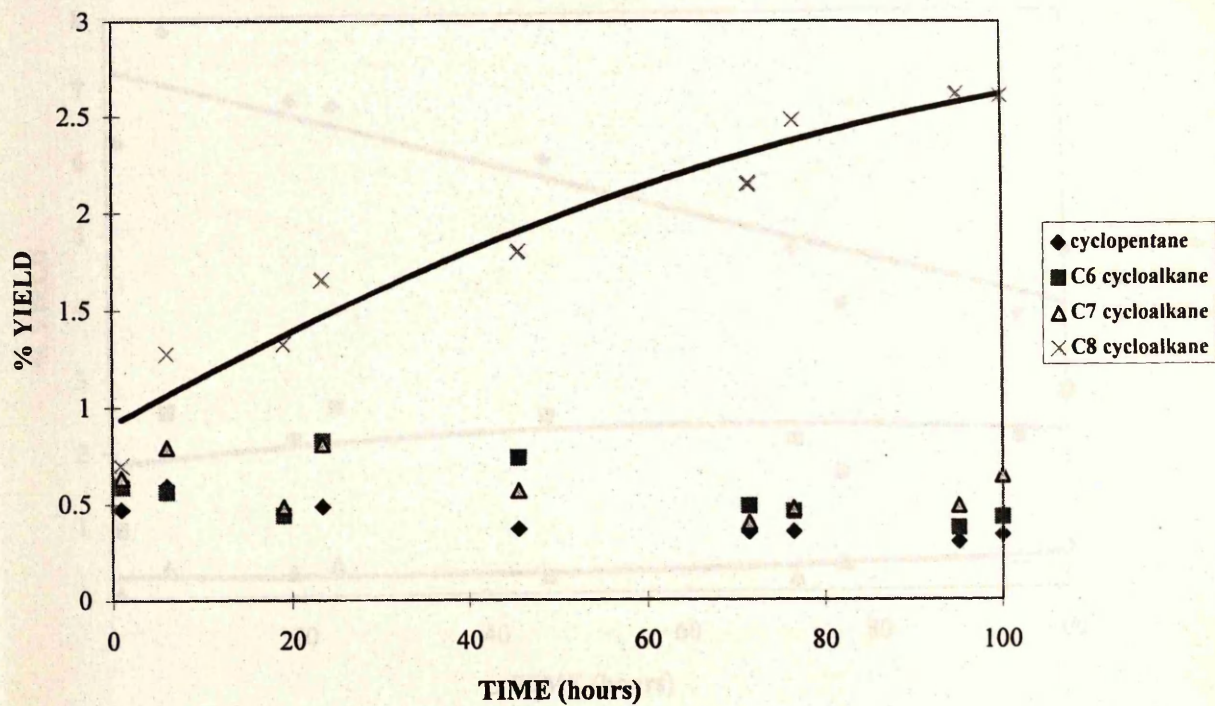


Figure 5.8.3 Yields of i-alkanes over 0.03 wt% Ir - 0.3 wt% Ge/Al₂O₃

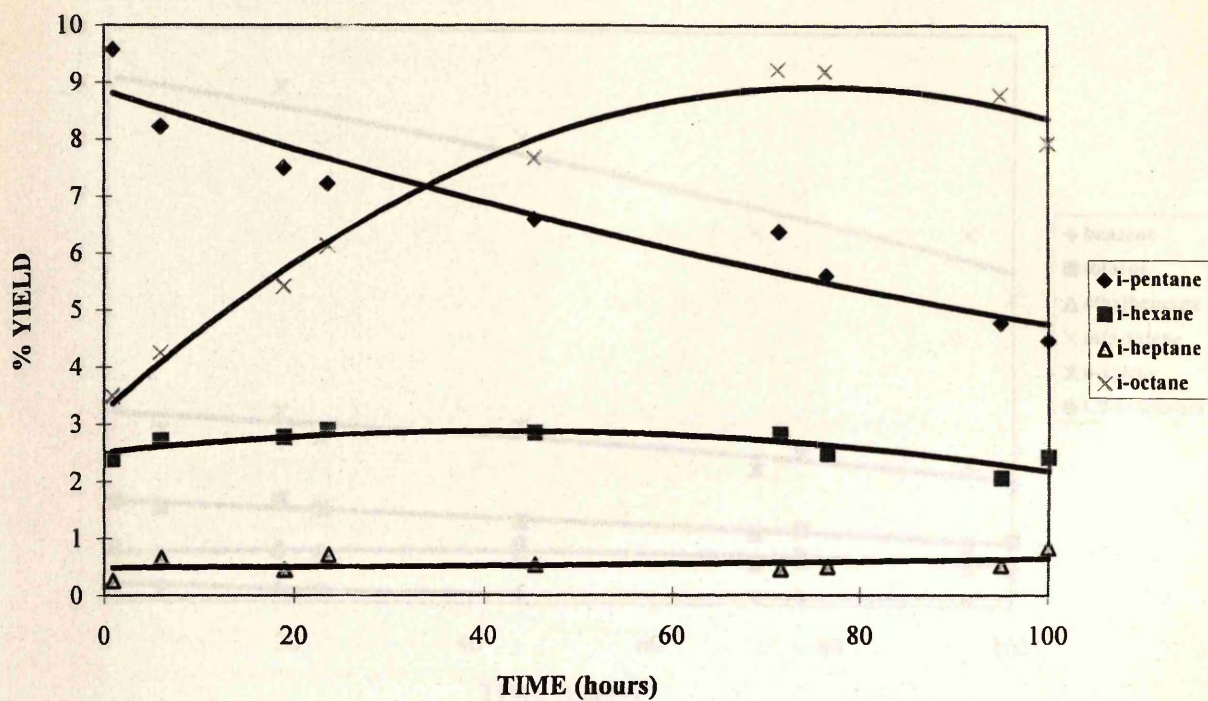


Figure 5.8.4 Yields of n-alkanes over 0.03 wt% Ir - 0.3 wt% Ge/Al₂O₃

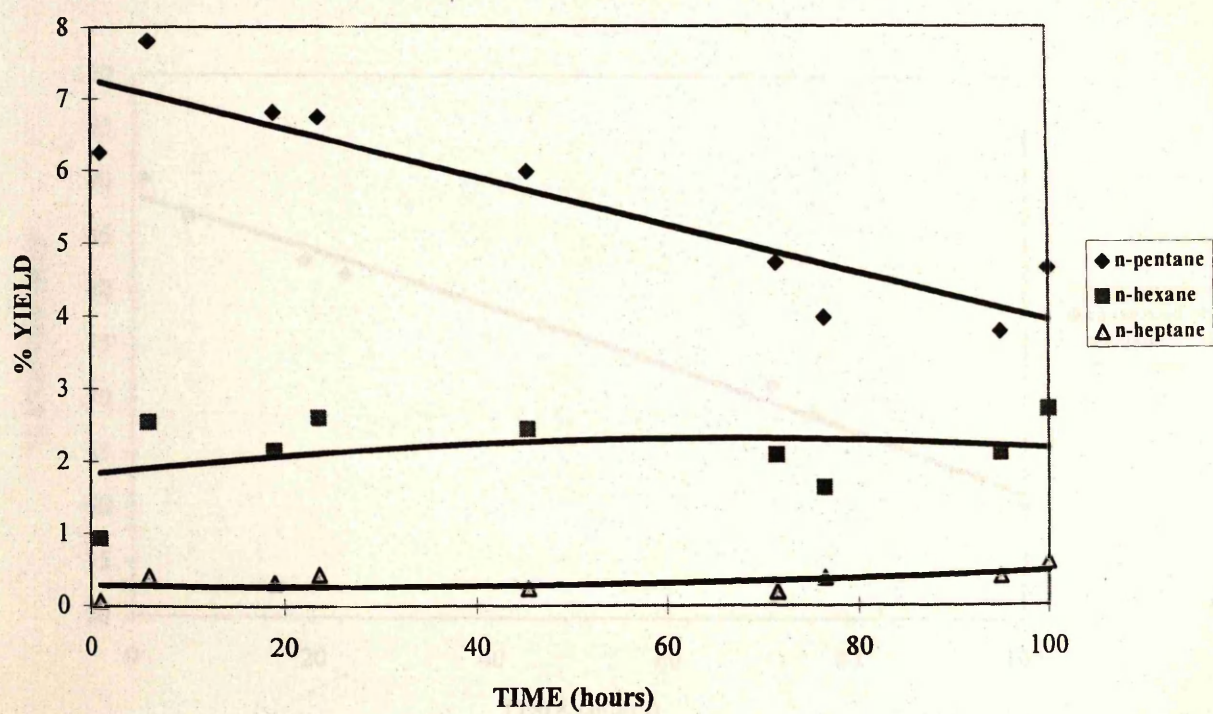


Figure 5.8.5 Yields of aromatics over 0.03 wt% Ir - 0.3 wt% Ge/Al₂O₃

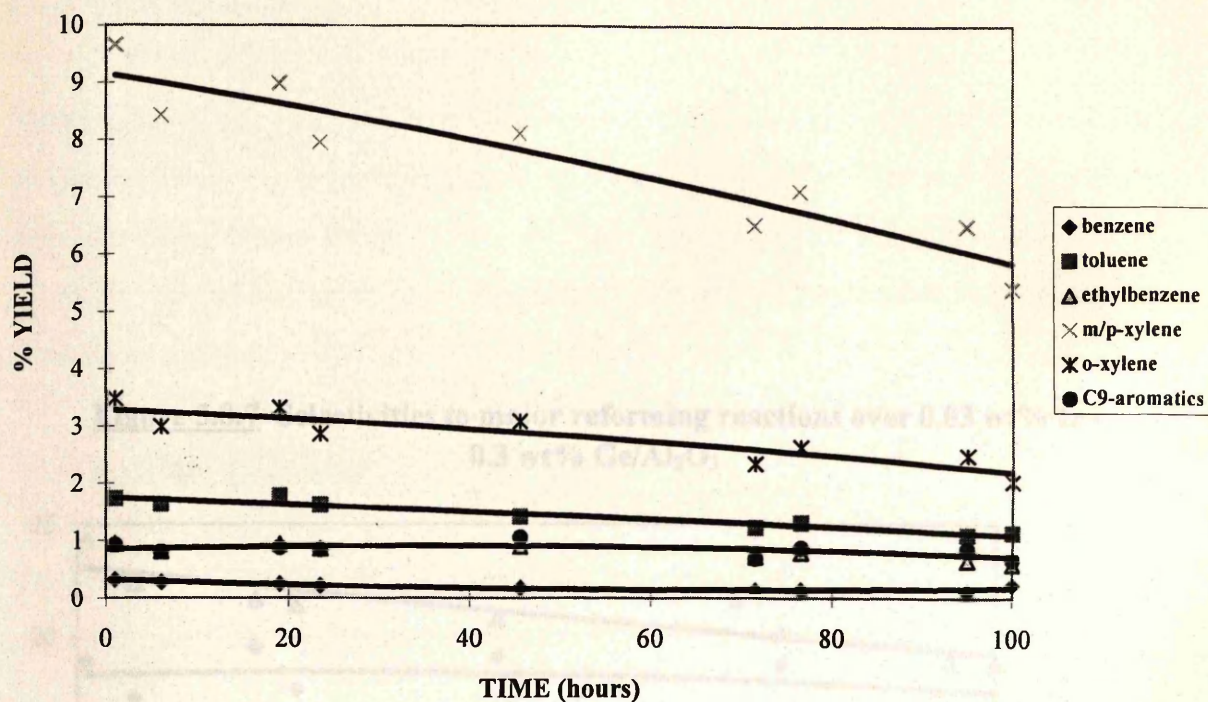
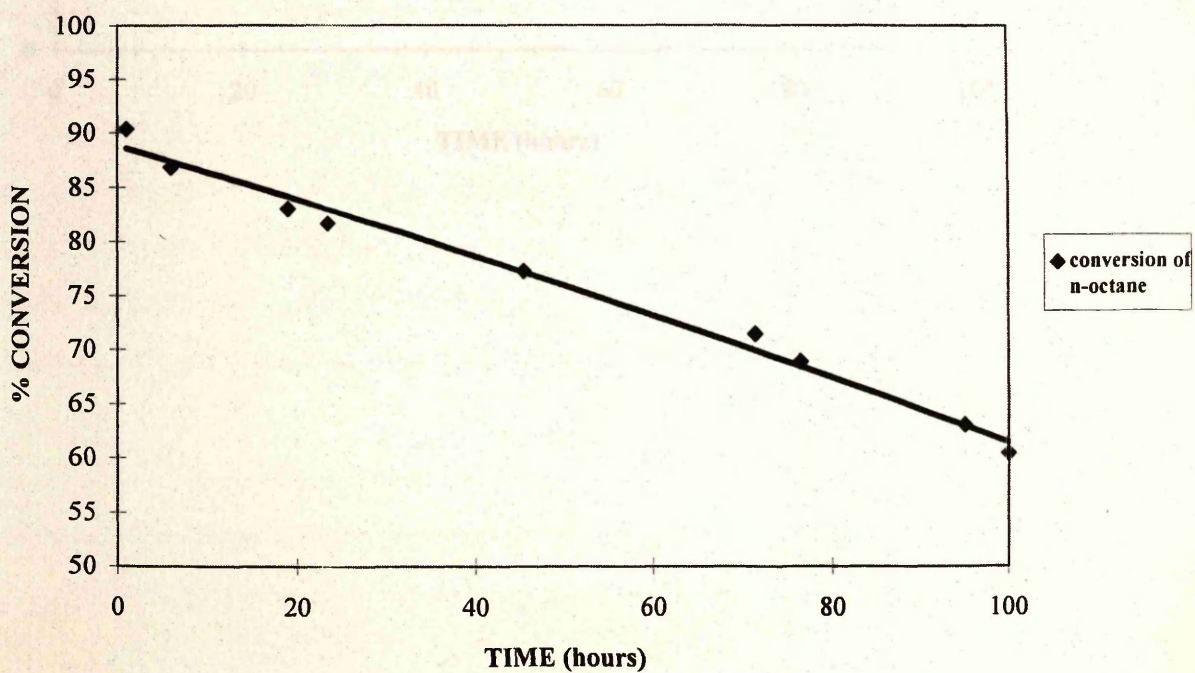


Figure 5.8.6 Conversion of n-octane over 0.03 wt% Ir - 0.3 wt% Ge/Al₂O₃



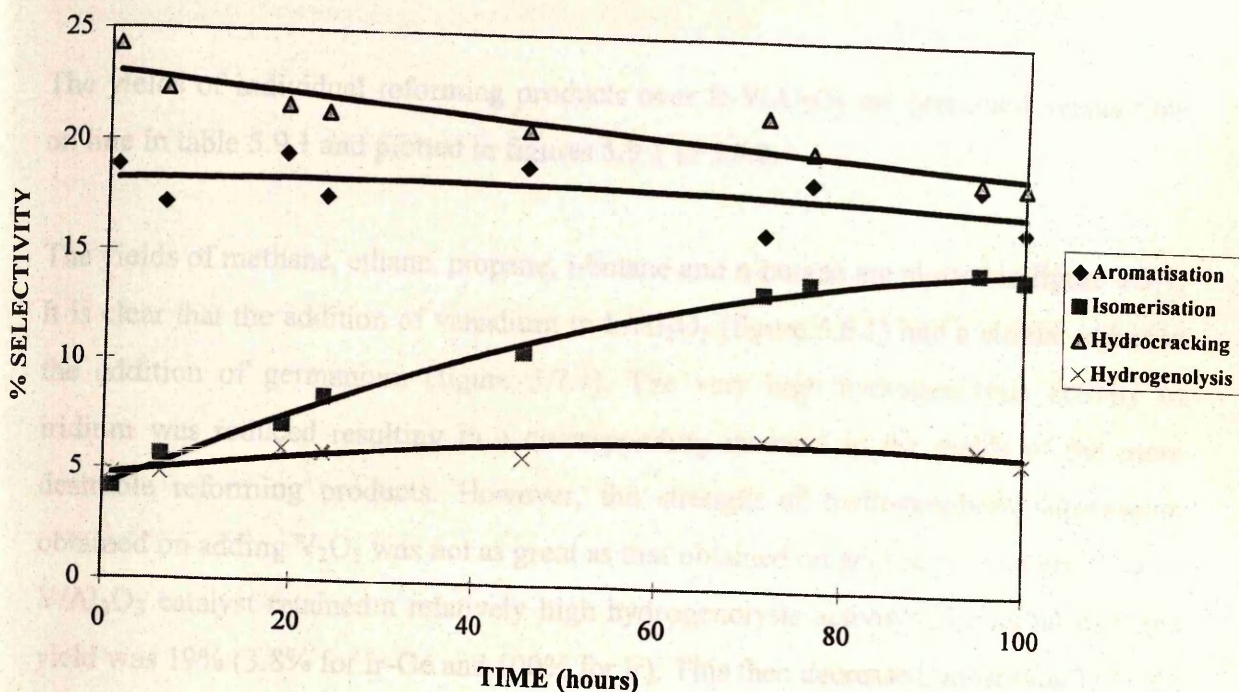
5.9. 0.3 wt% Ir - 0.3 wt% V/Al₂O₃

5.9.A TEM observations

TEM studies of this catalyst after both calcination/reduction and 144 hours on line at 510 °C could find no metal particles greater than 2 nm in diameter. This was in agreement with the observations made on the previous three catalysts (Ir, Ir-Ge and (0.03)Ir-Ge/Al₂O₃) that iridium tends to be very highly dispersed in these systems and was highly resistant to sintering in hydrogen rich atmospheres.

Figure 5.8.7 Selectivities to major reforming reactions over 0.03 wt% Ir - 0.3 wt% Ge/Al₂O₃

5.9.B n-Octane reforming



5.9. 0.3 wt% Ir - 0.3 wt% V/Al₂O₃

5.9.A TEM observations

TEM studies of this catalyst after both calcination/reduction and 144 hours on line at 510 °C could find no metal particles greater than 2 nm in diameter. This was in agreement with the observations made on the previous three catalysts (Ir, Ir-Ge and 0.03Ir-Ge/Al₂O₃) that iridium tends to be very highly dispersed in these systems and was highly resistant to sintering in hydrogen rich atmospheres.

5.9.B n-Octane reforming

The yields of individual reforming products over Ir-V/Al₂O₃ are presented versus time on line in table 5.9.1 and plotted in figures 5.9.1 to 5.9.7.

The yields of methane, ethane, propane, i-butane and n-butane are plotted in figure 5.9.1. It is clear that the addition of vanadium to Ir/Al₂O₃ (figure 5.6.1) had a similar effect to the addition of germanium (figure 5.7.1). The very high hydrogenolysis activity of iridium was reduced resulting in a corresponding increase in the yields of the more desirable reforming products. However, the strength of hydrogenolysis suppression obtained on adding V₂O₅ was not as great as that obtained on adding germanium. The Ir-V/Al₂O₃ catalyst retained a relatively high hydrogenolysis activity. The initial methane yield was 19% (3.8% for Ir-Ge and 100% for Ir). This then decreased, most rapidly in the initial stages and reached a final value of 10.0% after 144 hours on line. Similarly the ethane yield over Ir-V/Al₂O₃ was greater than the corresponding yield over Ir-Ge/Al₂O₃ (7.6% versus 4.0%). Interestingly the yields of propane, i-butane and n-butane were all significantly lower over Ir-V than Ir-Ge (compare with figure 5.7.1).

The yields of cycloalkanes over this catalyst are plotted in figure 5.9.2. The yields of these products were slightly greater than the corresponding yields over the Ir-Ge/Al₂O₃

catalyst. As with many of the catalysts studied the yields of C₇ and C₈ cycloalkanes were observed to increase with increasing time on line.

The yields of i-alkanes over this catalyst are plotted in figure 5.9.3. The yield of i-pentane, although initially significantly lower (5.4% versus 9.1%) than the corresponding value for Ir-Ge (figure 5.7.3) increased sharply in the initial stages and by 144 hours on line the yield of this product was similar over both catalysts (8.5%). The yields of i-hexane were also similar over these two catalysts, although in this case the yield over Ir-Ge was lower in the initial stages. The yields of i-heptane were slightly greater over Ir-V at all stages in the run than the corresponding values over Ir-Ge. Although the initial yield of i-octane was greater over Ir-V, after 144 hours on line both these catalysts gave the same yield of this product (9.0%).

The yields of n-alkanes over the Ir-V/Al₂O₃ catalyst are plotted in figure 5.9.4. The yield of n-pentane over this catalyst was observed to be considerably lower (~ 3%) than the corresponding value for Ir-Ge (~ 6% - figure 5.7.4) at all stages of the reforming run. The yields of n-hexane and n-heptane were roughly similar over these two catalysts although there did appear to be an initial dip in the yields of these products over Ir-V.

The yields of aromatic products over Ir-V/Al₂O₃ are plotted in figure 5.9.5. Comparing these values with those obtained over Ir-Ge (table 5.7.1 and figure 5.7.5) it is clear that there were major differences in the yields of aromatics over these catalysts. The yield of benzene (1.5% for Ir-Ge versus 2.7% for Ir-V) and toluene (3.8% versus 9.8%) were considerably greater over the Ir-V catalyst. However there was a corresponding decrease in the yields of ethylbenzene and xylenes. With increased time on line the yields of benzene and toluene over this catalyst gradually decreased. The yields of ethylbenzene and o-xylene remained relatively constant whilst the yield of m/p-xylene increased in the initial stages and then remained constant.

The conversion of n-octane versus time on line for this catalyst is plotted in figure 5.9.6. The change in conversion with use was found to be similar to that observed over Ir-Ge (figure 5.7.6) although the actual conversion values were slightly lower over Ir-V than Ir-Ge (e.g. initial values: 99.1 % and 100% respectively).

The selectivities to the four major reforming reactions over the Ir-V/Al₂O₃ catalyst are listed versus time on line in table 5.9.2 and plotted in figure 5.9.7. The selectivity to aromatics was relatively constant throughout the run. However this selectivity was lower than the corresponding value obtained for the Ir-Ge (table 5.7.2 and figure 5.7.7) catalyst (33.6% versus 27.6%). The selectivity to isomerisation was greater initially over Ir-V although by 144 hours on line this catalyst and Ir-Ge had similar values for isomerisation (10-11%). The selectivity to hydrocracking was found to be relatively constant throughout the run, apart for an initial increase, and was slightly lower than the corresponding values for Ir-Ge (21% versus 19%). In the case of hydrogenolysis Ir-V/Al₂O₃ was more selective at all stages of the run. The selectivity to this reaction did decrease with time on line however.

Table 5.9.1 Yields of individual products for catalyst 0.3 wt% Ir - 0.3 wt% V/Al₂O₃

Time (hours)	Methane	Ethane	Propane	i-Butane	n-Butane	c-Pentane	i-Pentane	n-Pentane
1.0	19.0	7.6	10.4	3.9	6.3	0.2	5.4	3.4
18.5	14.5	7.3	11.7	6.6	8.3	0.3	7.7	2.8
24.0	13.7	7.6	11.8	6.5	8.5	0.2	8.2	3.2
42.5	12.8	8.1	12.0	6.5	8.5	0.3	8.1	2.8
47.5	12.0	7.7	12.6	6.3	8.2	0.2	7.8	2.9
71.0	11.8	6.8	11.4	6.2	8.0	0.2	8.1	2.5
96.0	12.2	6.0	10.4	5.5	7.3	0.3	8.7	2.4
120.0	10.4	5.3	9.2	4.9	7.2	0.4	9.1	2.3
139.5	10.1	5.2	9.3	4.8	6.9	0.4	8.7	2.3
144.0	10.0	4.8	9.6	4.7	6.0	0.3	8.5	2.0

Table 5.9.1 (cont) Yields of individual products for catalyst 0.3 wt% Ir - 0.3 wt% V/Al₂O₃

Time (hours)	C6 c-Alkane	i-Hexane	n-Hexane	C7 c-Alkane	i-Heptane	n-Heptane	C8 c-Alkane	i-Octane
1.0	0.6	4.6	1.7	0.6	2.8	0.8	0.5	4.0
18.5	0.4	5.3	1.4	0.3	1.4	0.2	0.4	2.6
24.0	0.3	4.4	1.0	0.3	1.2	0.2	0.3	2.3
42.5	0.4	4.7	1.1	0.4	1.5	0.2	0.3	3.0
47.5	0.4	4.9	1.1	0.4	1.4	0.1	0.5	3.3
71.0	0.4	5.3	1.8	0.6	1.8	0.5	0.7	4.0
96.0	0.5	5.5	2.3	0.8	2.1	0.7	1.2	6.3
120.0	0.9	5.8	2.8	1.0	2.5	1.1	1.7	8.1
139.5	0.9	5.7	2.8	1.1	2.5	1.1	1.7	8.7
144.0	0.9	5.0	2.8	1.2	2.3	1.2	1.9	9.0

Table 5.9.1 (cont) Yields of individual products for catalyst 0.3 wt% Ir - 0.3 wt% V/Al₂O₃

Time (hours)	Benzene	Toluene	Ethyl- Benzene	m/p- Xylene	o-Xylene	C9 Aromatic	Total Conversion
1.0	2.7	9.8	1.6	8.2	4.7	0.3	99.1
18.5	2.6	9.4	1.0	9.4	4.6	0.7	98.9
24.0	2.5	9.5	1.0	10.6	4.4	0.9	98.9
42.5	2.1	9.1	1.0	10.4	4.4	0.8	98.6
47.5	2.1	9.0	1.1	11.2	4.6	0.9	98.5
71.0	2.0	8.3	1.1	11.2	4.6	1.0	98.5
96.0	1.5	6.9	1.1	10.8	4.5	0.9	97.9
120.0	1.2	6.2	1.1	10.4	4.4	0.8	97.0
139.5	1.4	5.9	1.3	10.9	4.3	0.9	96.7
144.0	1.3	6.3	1.3	11.3	4.6	0.9	95.9

Table 5.9.2 Selectivity to the major reforming reactions for 0.3 wt% Ir - 0.3 wt% V/Al₂O₃

Time (hours)	Selectivity to Aromatics	Selectivity to Isomerisation	Selectivity to Hydrocracking	Selectivity to Hydrogenolysis
1.0	27.6	6.9	14.0	19.1
18.5	28.1	4.1	19.8	14.7
24.0	29.3	3.6	19.4	13.8
42.5	28.2	4.6	19.6	13.0
47.5	29.4	4.8	19.2	12.2
71.0	28.6	5.9	19.9	12.0
96.0	26.2	8.6	20.1	12.4
120.0	25.0	10.9	20.4	10.8
139.5	25.4	11.6	19.8	10.5
144.0	26.9	11.8	19.0	10.5

Figure 5.9.1 Yields of individual products over 0.3 wt% Ir - 0.3 wt% V/Al₂O₃

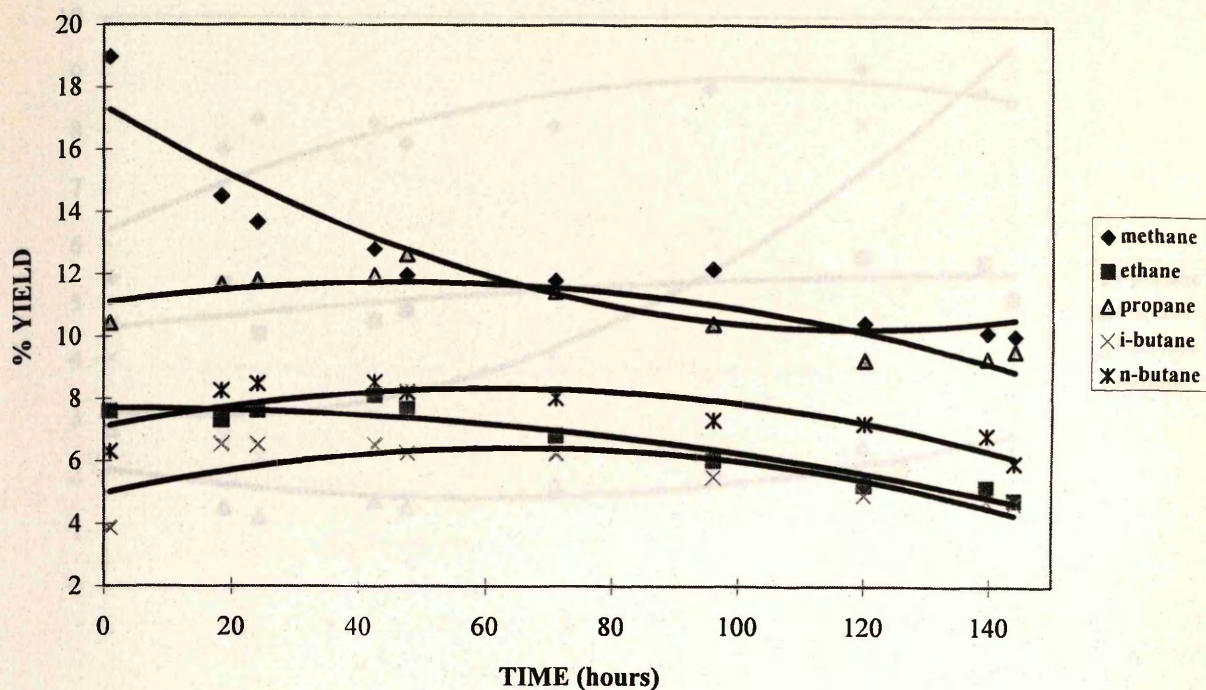


Figure 5.9.2 Yields of cycloalkanes over 0.3 wt% Ir - 0.3 wt% V/Al₂O₃

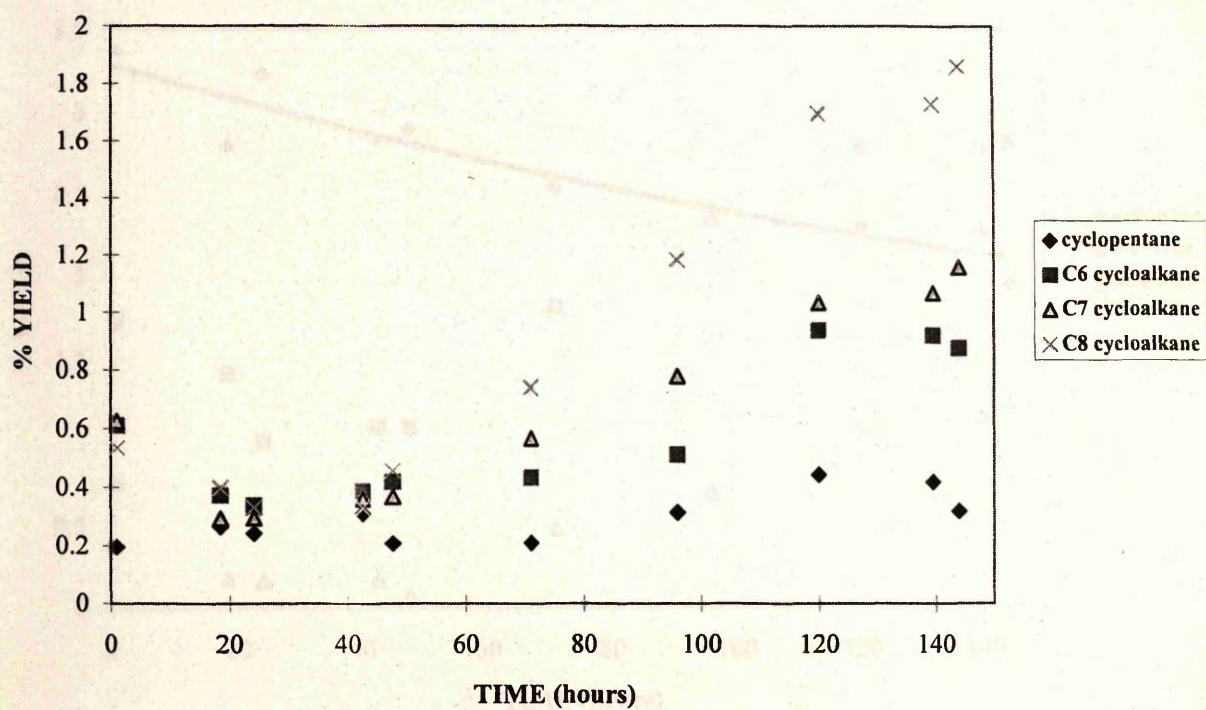


Figure 5.9.3 Yields of i-alkanes over 0.3 wt% Ir - 0.3 wt% V/Al₂O₃

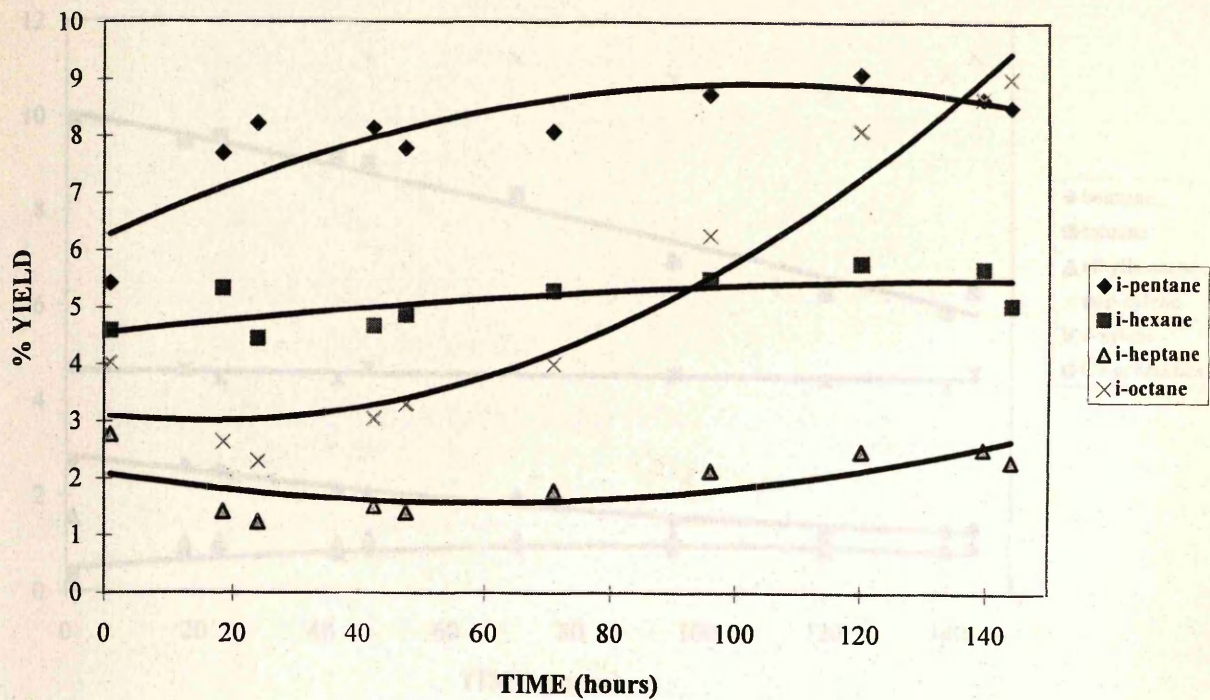


Figure 5.9.4 Yields of n-alkanes over 0.3 wt% Ir - 0.3 wt% V/Al₂O₃

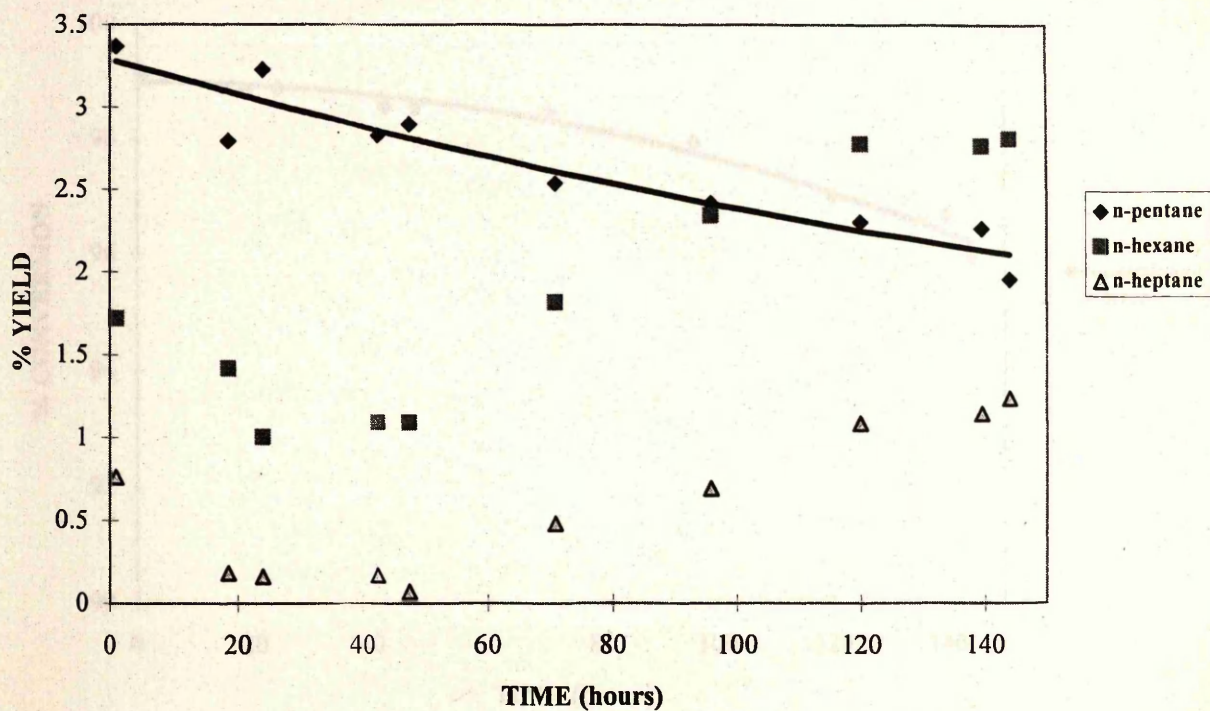


Figure 5.9.5 Yields of aromatics over 0.3 wt% Ir - 0.3 wt% V/Al₂O₃

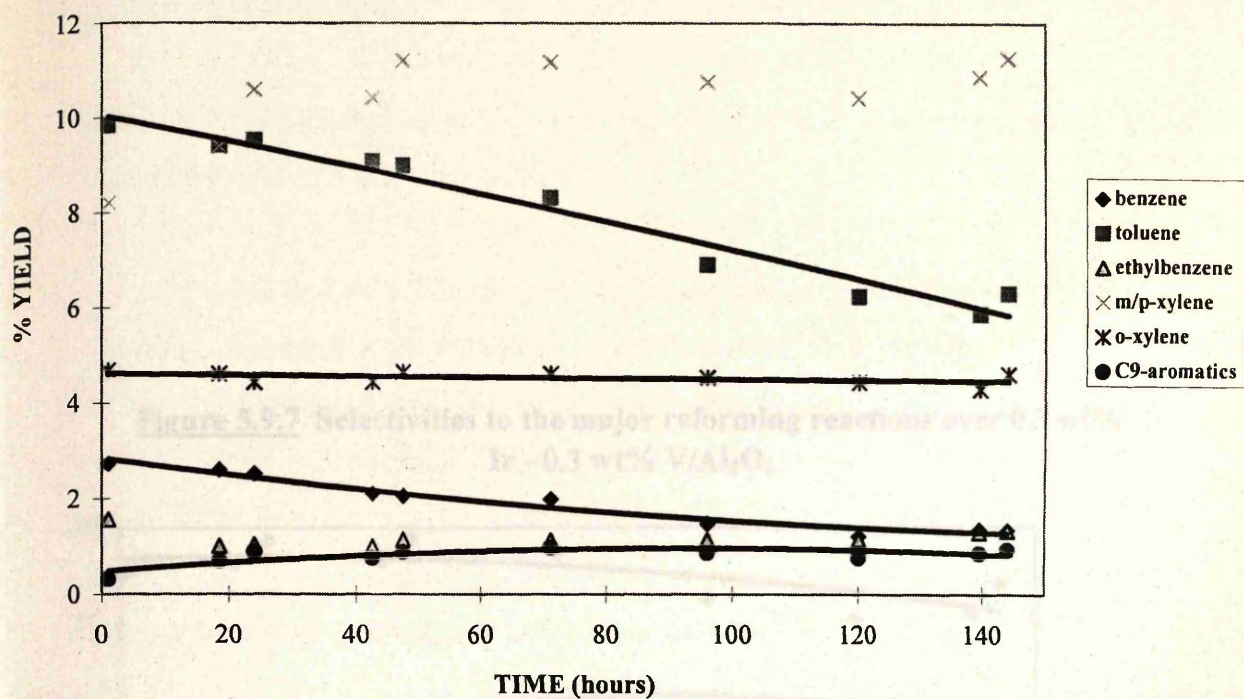
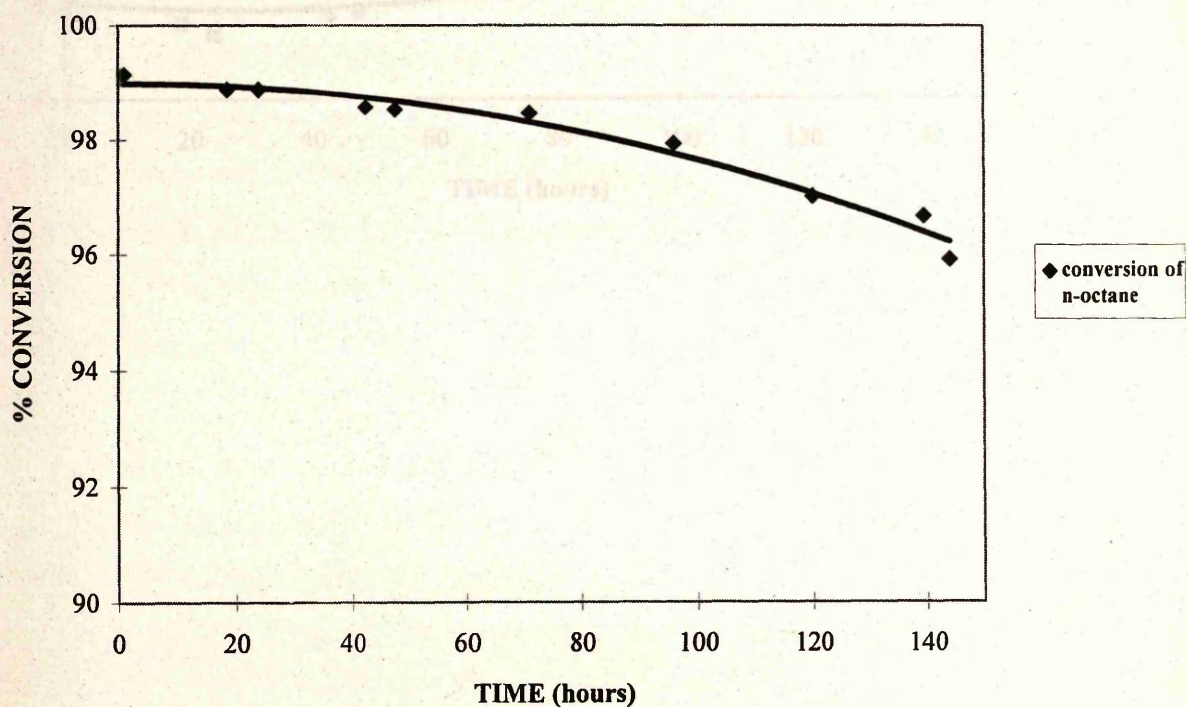


Figure 5.9.6 Conversion of n-octane over 0.3 wt% Ir - 0.3 wt% V/Al₂O₃



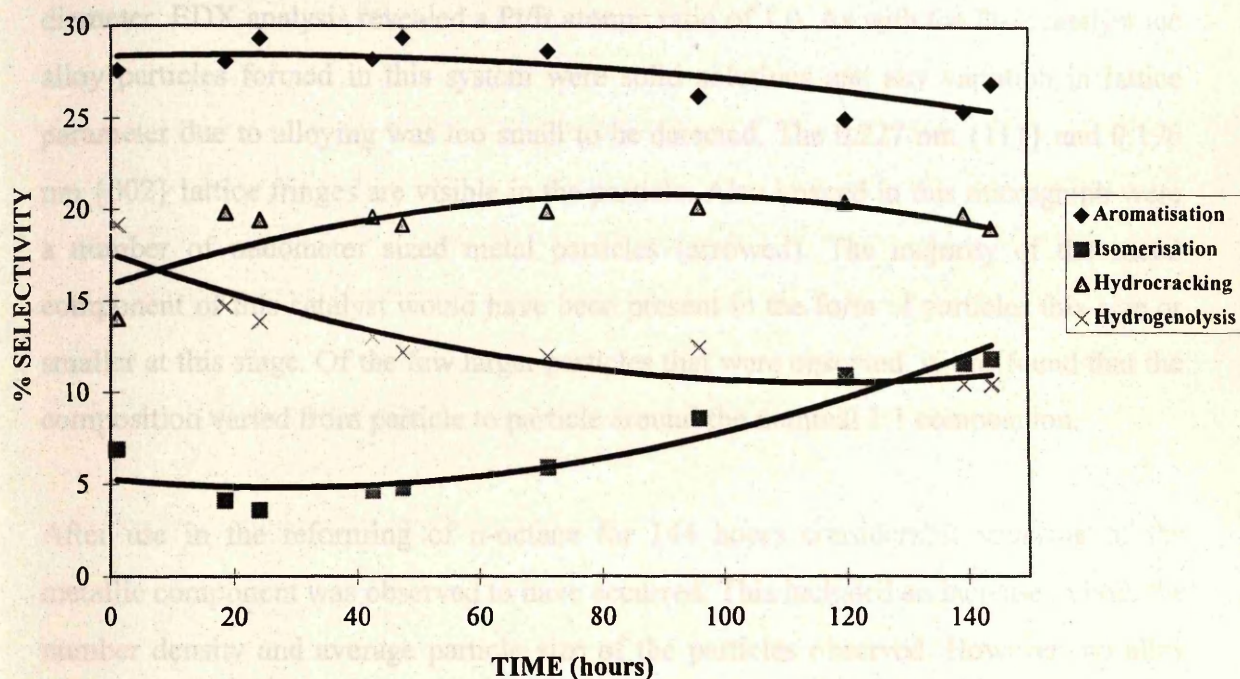
5.10. 0.3 wt% Pt - 0.3 wt% Ir - 0.03 wt% Ge/Al₂O₃

5.10.A TEM observations

The results of TEM studies of this catalysts were similar in every respect to those obtained on the Pt-Ir/Al₂O₃ catalyst.

After calcination and reduction the metallic component of this catalyst was present in a very highly dispersed form with only a small number of analysable particles being observed.

Figure 5.9.7 Selectivities to the major reforming reactions over 0.3 wt% Ir - 0.3 wt% V/Al₂O₃



5.10. 0.3 wt% Pt - 0.3 wt% Ir - 0.03 wt% Ge/Al₂O₃

5.10.A TEM observations

The results of TEM studies of this catalysts were similar in every respect to those obtained on the Pt-Ir/Al₂O₃ catalyst.

After calcination and reduction the metallic component of this catalyst was present in a very highly dispersed form with only a small number of analysable particles being observed. EDX analysis of these particles revealed that they were platinum-iridium alloys. An example is given in plate 32. This particle was approximately 6 nm in diameter. EDX analysis revealed a Pt/Ir atomic ratio of 1.0. As with the Pt-Ir catalyst the alloy particles formed in this system were solid solutions and any variation in lattice parameter due to alloying was too small to be detected. The 0.227 nm {111} and 0.196 nm {002} lattice fringes are visible in the particle. Also imaged in this micrograph were a number of nanometer sized metal particles (arrowed). The majority of the metal component of this catalyst would have been present in the form of particles this size or smaller at this stage. Of the few larger particles that were observed, it was found that the composition varied from particle to particle around the nominal 1:1 composition.

After use in the reforming of n-octane for 144 hours considerable sintering of the metallic component was observed to have occurred. This included an increase in both the number density and average particle size of the particles observed. However, no alloy particles containing germanium were detected in this catalyst. However, this does not exclude the possibility that a few weight percent of germanium may have been present in the particles analysed.

An example of a particle formed after 144 hours on line is given in plate 33. This particle was approximately 10 nm in diameter. The EDX spectrum obtained (inset) revealed that the particle was relatively rich in platinum, with a Pt/Ir atomic ratio = 2.3.

The particle was imaged in the (110) orientation with {111} and {002} lattice fringes visible. No germanium peaks were visible in the EDX spectrum.

The Pt/Ir ratio of the particles analysed was again found to vary about the nominal 1:1 ratio. Another example of a particle formed in this catalyst after 144 hours on line is shown in plate 34. This was a larger particle approximately 15 nm in diameter. The MBED pattern was indexed as the (110) pattern of platinum (or iridium) and the {111} and {002} lattice fringes are visible in the image. The EDX spectrum obtained in this case revealed a Pt/Ir atomic ratio of 1.4. Even in larger particles such as this, where the sensitivity of the EDX system is improved due to the increased quantity of material in the particle being analysed, still no evidence for the presence of germanium was obtained.

As with most of the catalysts studied, although considerable sintering of the metal component was observed to have occurred, relatively large particles such as those shown in plates 33 and 34 were still quite infrequently observed suggesting that a significant proportion of the metal remained in the form of nanometer sized particles.

5.10.B n-Octane reforming

The yields of individual reforming products obtained over this catalyst are presented versus time on line in table 5.10.1 and plotted in figures 5.10.1 to 5.10.6.

The yields of methane, ethane, propane, i-butane and n-butane are plotted in figure 5.10.1. It was observed that in the initial stages of the run this catalyst had a high hydrogenolysis activity. However when compared with the related Pt-Ir/Al₂O₃ catalyst (figure 5.5.1) it was observed that the initial methane yield was slightly lower over the Pt-Ir-0.03Ge catalyst (35.3% versus 42.8%) and that the ethane yield was substantially lower (11.5% versus 26.6%). This high hydrogenolysis activity resulted in lower initial yields of the remaining products. However, it was observed that the high hydrogenolysis

activity of this catalysts decreased very rapidly. After approximately 19 hours on line the yield of methane was below 10%. This rapid decrease in hydrogenolysis was accompanied by an increase in the yields of other products. This contrasts with the Pt-Ir/Al₂O₃ catalyst where the hydrogenolysis activity remained high throughout the run, resulting in the yields of the more desirable products remaining low.

The yield of propane over this catalyst was relatively high compared with most of the other catalysts studied (~ 9% as compared with 6-7% for Pt/Al₂O₃) and remained relatively constant throughout the run. The yields of i-butane and n-butane increased during the initial stages of the run and then remained relatively constant.

The yields of cycloalkanes over this catalyst are plotted in figure 5.10.2. The trends observed in this system for these products were similar to those shown by a number of the catalysts studied. The yields of cyclopentane and C₆ species remained relatively constant whilst the yields of C₇ and C₈ cycloalkanes increased throughout the run. When compared to the corresponding yields over platinum however (figure 5.1.2), although the yields of cyclopentane and C₆ species were similar, the yields of C₇ and C₈ cycloalkanes were much lower, initially and throughout the whole length of the run.

The yields of i-alkanes over Pt-Ir-0.03Ge/Al₂O₃ are plotted in figure 5.10.3. It was observed that the initial yields of these products were very low. However, the yields of i-pentane, i-hexane and i-heptane increased significantly during the first 20 hours on line and then remained relatively constant. The final yields of these products were similar to those obtained over Pt/Al₂O₃. The yield of i-octane increased at a more gradual pace throughout the run. However the increase in the i-octane yield over this catalyst was very small when compared with some of the other catalysts studied e.g. Pt, Pt-Sn and Pt-Ge (the final i-octane yield obtained over Pt/Al₂O₃ was 23% whilst over Pt-Ir-0.03Ge it was 1.9%).

The yields of n-alkanes over this catalyst are plotted in figure 5.10.4. As with the i-alkanes the initial yields of these species were very low but increased significantly during the initial stages of the run. The final yields obtained were similar to those observed over the Pt/Al₂O₃ catalyst.

The yields of aromatic products over Pt-Ir-0.03Ge/Al₂O₃ are plotted in figure 5.10.5. In the initial stages of the run this catalyst behaved in a similar manner to Pt-Ir (figure 5.5.4) producing large quantities of benzene and toluene and very little xylene or ethylbenzene. However, the yields of m/p-xylene, o-xylene and ethylbenzene all increased during the initial stages of the run whilst the yields of benzene and toluene decreased. After just ~ 20 hours on line the catalyst behaved more like Pt/Al₂O₃ or Pt-Ge/Al₂O₃, producing mostly xylenes. The yields of benzene and toluene did remain significantly higher than the corresponding values over platinum or Pt-Ge however (e.g. final toluene yields: Pt-Ge 1.4%, Pt-Ir-0.03Ge 9.6%).

The conversion of n-octane over this catalyst is plotted in figure 5.10.6. The initial conversion was 100% over this catalyst and only decreased slightly during the length of the run. Indeed this catalyst appeared to maintain its high conversion levels more effectively than the Pt-Ir/Al₂O₃ (although the difference between them is small, final values: 99.3% versus 98.6%).

The selectivities to the four major reforming reactions over this catalyst are presented versus time on line in table 5.10.1 and plotted in figure 5.10.7. As already stated, the high initial selectivity to hydrogenolysis over this catalyst decreased rapidly during the first 20 hours on line resulting in significant increases in selectivity to aromatisation and hydrocracking. The selectivities to these reactions then remained relatively constant throughout the remainder of the run. The selectivity to aromatics over this catalyst after 144 hours (45.5%) was significantly higher than the corresponding values over Pt (25.1%), Pt-Sn (25.8%) and Pt-Ge (26.2%) and similar to the value over Pt-Re (44.7%). The selectivity to isomerisation increased slowly throughout the entire length of the run

but remained relatively low even after 144 hours on line (final values: 3.1% versus 23.0% over $\text{Pt/Al}_2\text{O}_3$).



3 nm

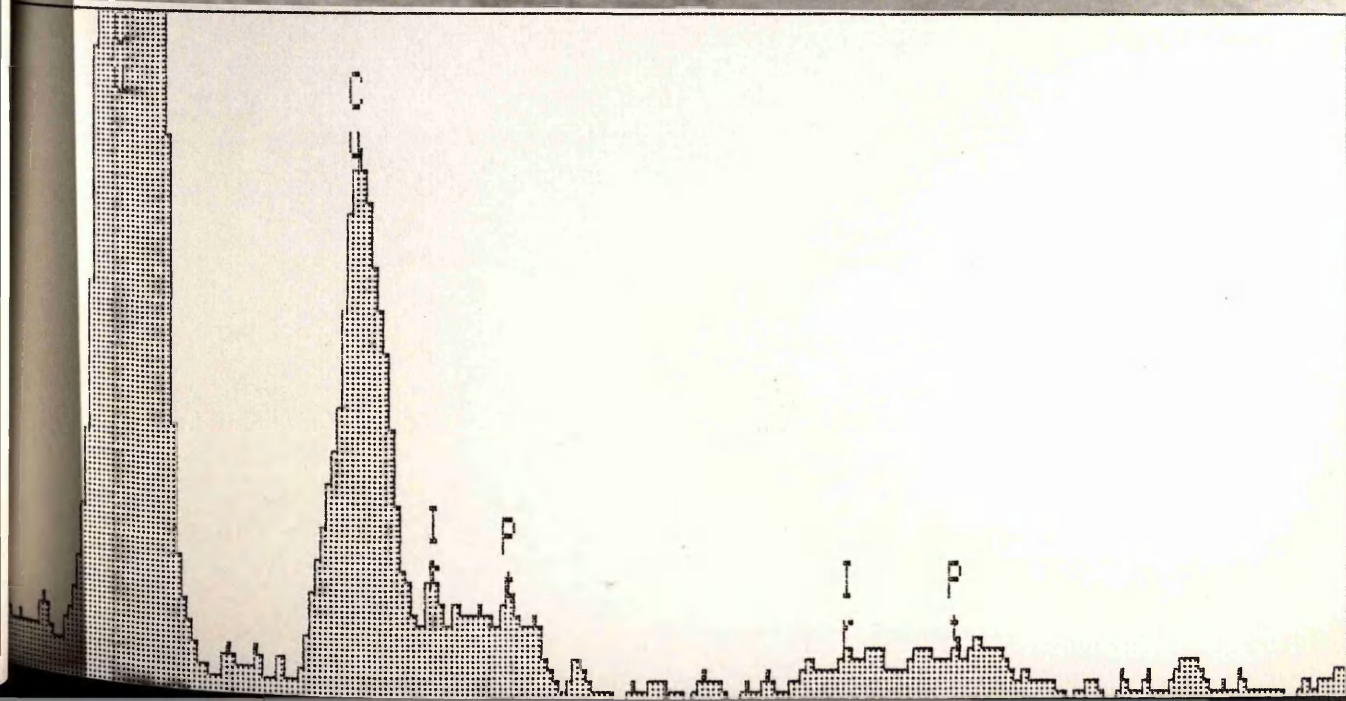
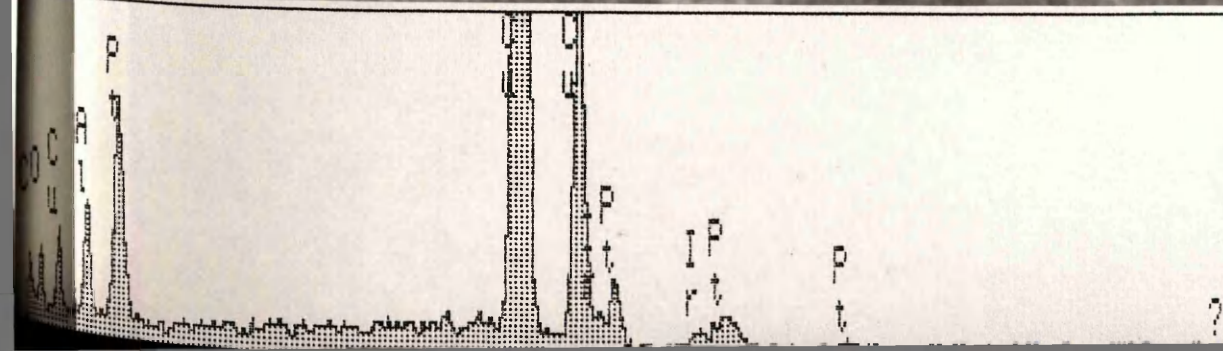
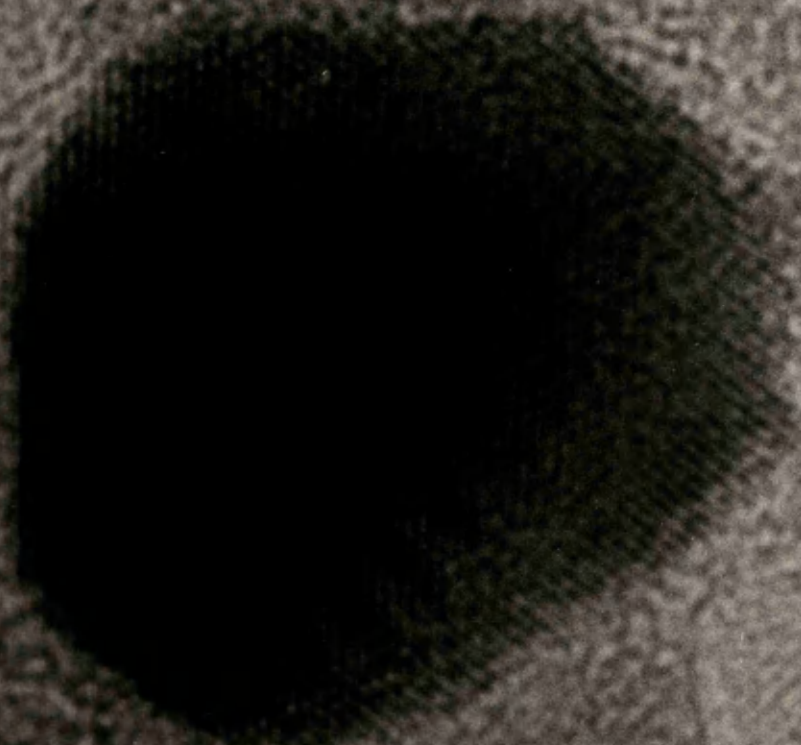


Plate 33

3 nm





3 nm

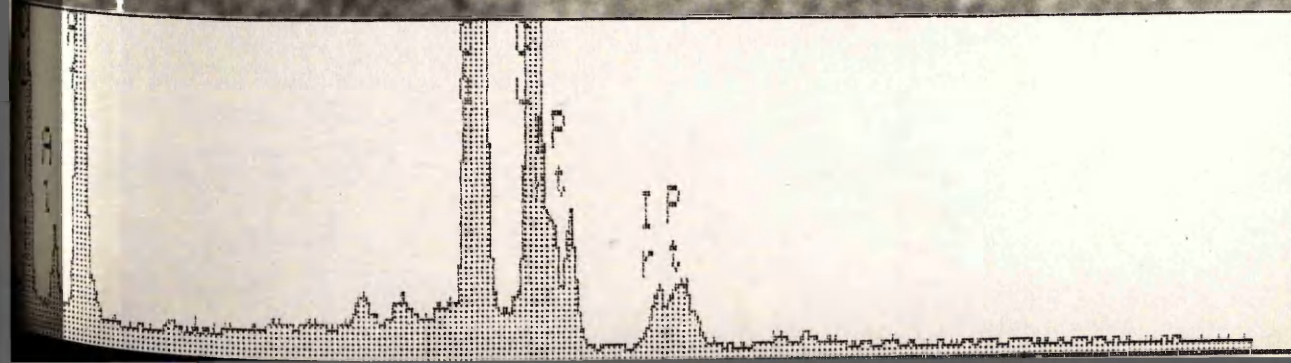
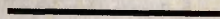


Table 5.10.1 Yields of individual products for 0.3 wt% Pt - 0.3 wt% Ir - 0.03 wt% Ge/Al₂O₃

Time (hours)	Methane	Ethane	Propane	i-Butane	n-Butane	c-Pentane	i-Pentane	n-Pentane
1.0	35.3	11.5	9.4	2.6	2.8	0.2	1.0	0.7
6.0	25.1	8.7	9.0	3.5	4.0	0.2	2.7	2.2
19.0	9.8	5.1	8.6	4.6	6.1	0.2	6.1	2.6
23.0	9.3	5.1	10.1	5.2	5.6	0.3	5.4	2.8
43.0	7.3	4.9	9.3	5.0	6.3	0.3	6.1	3.8
47.0	7.4	4.4	8.6	5.3	6.1	0.2	6.4	3.3
71.5	8.4	5.4	9.2	4.9	6.0	0.3	6.2	3.5
94.5	8.1	5.3	9.2	5.0	5.8	0.2	6.2	3.4
114.5	7.5	5.4	9.2	4.5	5.7	0.2	5.9	3.1
119.5	7.9	5.1	9.4	4.6	6.0	0.3	6.1	3.6
138.5	7.2	4.8	8.4	4.5	5.3	0.3	5.9	3.4
144.0	8.5	5.0	8.9	4.4	5.8	0.3	5.9	3.6

Table 5.10.1 (cont) Yields of individual products for 0.3 wt% Pt - 0.3 wt% Ir - 0.03 wt% Ge/Al₂O₃

Time (hours)	C6 c-Alkane	i-Hexane	n-Hexane	C7 c-Alkane	i-Heptane	n-Heptane	C8 c-Alkane	i-Octane
1.0	0.5	1.0	0.2	0.0	0.0	0.0	0.0	0.5
6.0	0.4	1.1	0.4	0.0	1.2	0.0	0.0	0.5
19.0	0.5	3.7	2.5	0.2	1.1	0.2	0.1	0.7
23.0	0.5	2.8	3.0	0.2	0.9	0.5	0.2	0.9
43.0	0.4	4.1	3.2	0.3	1.0	0.4	0.3	1.2
47.0	0.5	4.5	3.0	0.2	1.4	0.6	0.3	1.2
71.5	0.6	4.0	2.5	0.5	0.9	0.6	0.3	1.3
94.5	0.4	3.9	2.0	0.5	1.0	0.8	0.3	1.3
114.5	0.4	3.9	1.8	0.4	1.0	0.9	0.5	1.3
119.5	0.4	3.9	1.8	0.4	0.9	0.8	0.6	1.3
138.5	0.5	4.1	1.7	0.5	1.0	0.9	0.6	1.7
144.0	0.5	4.1	1.8	0.5	1.2	1.2	0.6	1.9

Table 5.10.1 (cont) Yields of individual products for 0.3 wt% Pt - 0.3 wt% Ir - 0.03 wt% Ge/Al₂O₃

Time (hours)	Benzene	Toluene	Ethyl- Benzene	m/p- Xylene	o-Xylene	C9 Aromatic	Total Conversion
1.0	8.1	17.1	0.1	6.1	2.8	0.1	100.0
6.0	5.6	16.4	0.4	12.7	5.7	0.4	100.0
19.0	2.8	10.1	3.7	21.3	9.0	0.9	99.8
23.0	3.1	10.4	3.3	20.3	8.7	1.1	99.7
43.0	2.5	8.4	4.1	20.0	9.0	1.5	99.6
47.0	2.3	7.9	4.5	21.1	9.0	1.5	99.7
71.5	2.5	9.7	4.0	19.4	8.5	1.1	99.6
94.5	2.6	10.0	3.8	19.7	8.7	1.1	99.4
114.5	2.8	10.3	4.0	20.3	9.1	1.0	99.4
119.5	3.0	10.6	3.7	19.4	8.6	1.2	99.5
138.5	2.7	9.8	4.2	20.9	9.7	1.4	99.5
144.0	2.7	9.6	3.9	19.3	8.5	1.1	99.3

Table 5.10.2 Selectivities for catalyst 0.3 wt% Pt - 0.3 wt% Ir - 0.03 wt% Ge/Al₂O₃

Time (hours)	Selectivity to Aromatics	Selectivity to Isomerisation	Selectivity to Hydrocracking	Selectivity to Hydrogenolysis
1.0	34.3	0.5	4.6	35.3
6.0	41.2	1.6	7.2	25.1
19.0	47.9	1.8	14.4	9.8
23.0	47.1	1.8	13.4	9.4
43.0	45.8	2.2	15.2	7.4
47.0	46.4	2.6	16.2	7.4
71.5	45.3	2.2	15.1	8.5
94.5	46.1	2.4	15.2	8.2
114.5	47.8	2.3	14.4	7.6
119.5	46.8	2.2	14.7	8.0
138.5	48.9	2.8	14.6	7.3
144.0	45.5	3.1	14.6	8.5

Figure 5.10.1 Yields of individual products over 0.3 wt% Pt - 0.3 wt% Ir - 0.03 wt% Ge/Al₂O₃

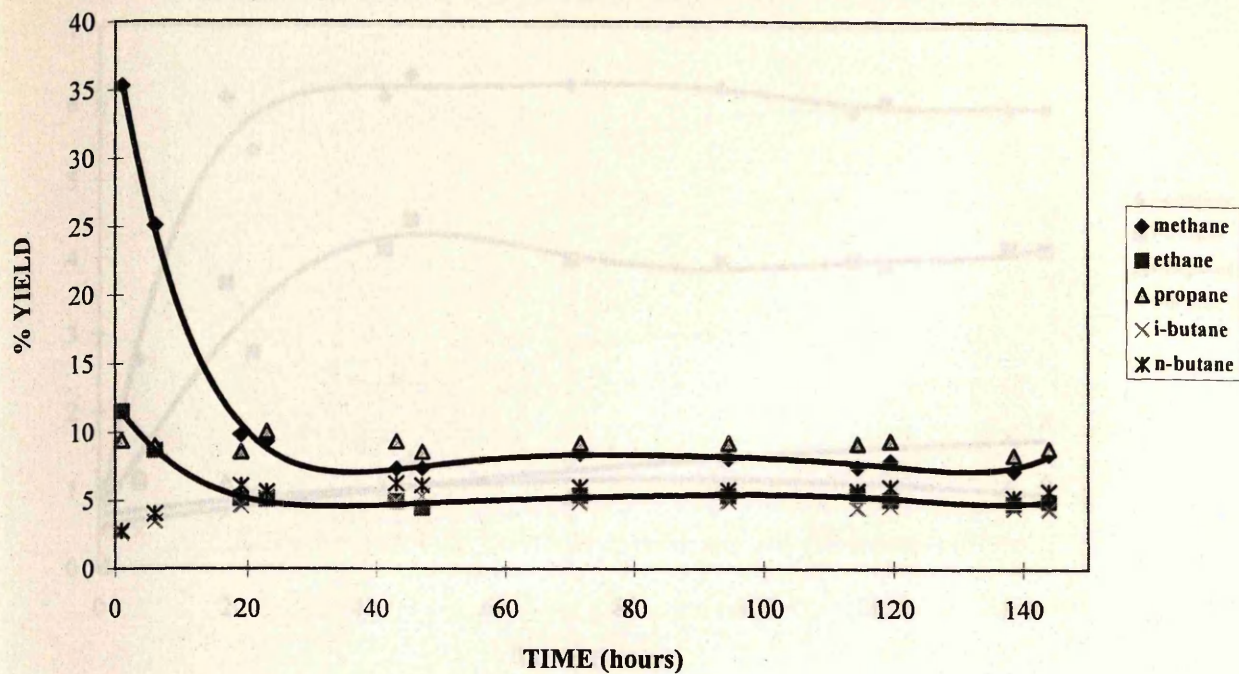


Figure 5.10.2 Yields of cycloalkanes over 0.3 wt% Pt - 0.3 wt% Ir - 0.03 wt% Ge/Al₂O₃

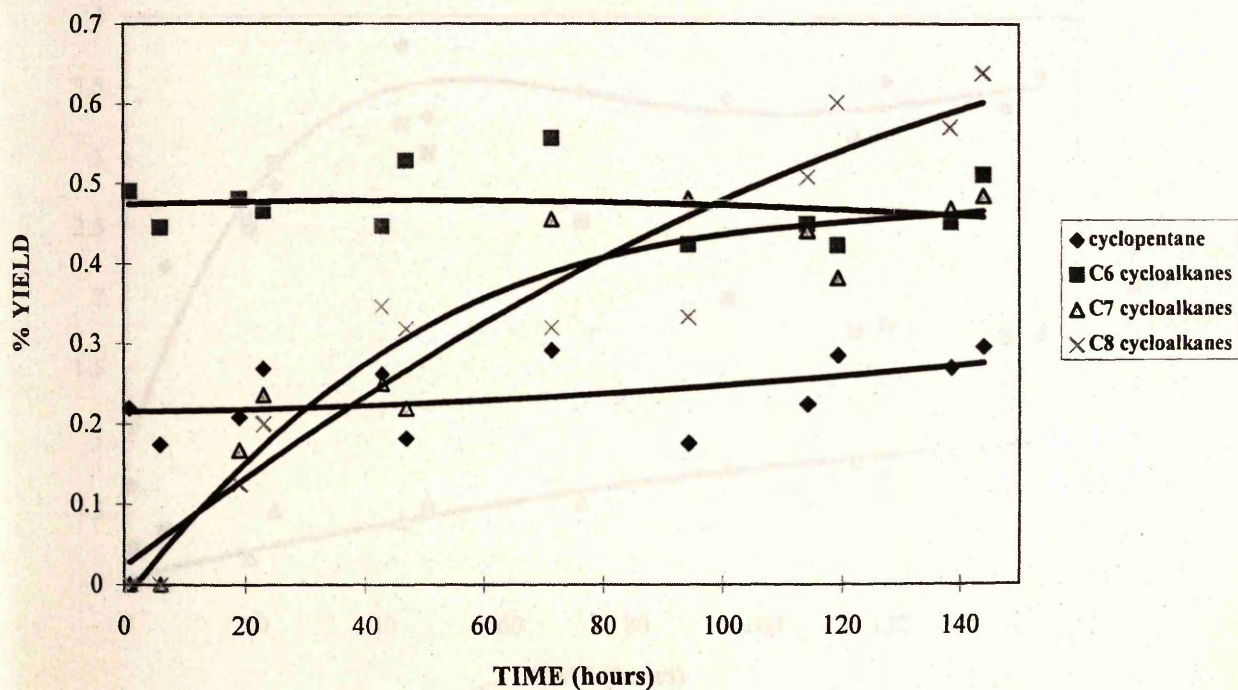


Figure 5.10.3 Yields of i-alkanes over 0.3 wt% Pt - 0.3 wt% Ir - 0.03 wt% Ge/Al₂O₃

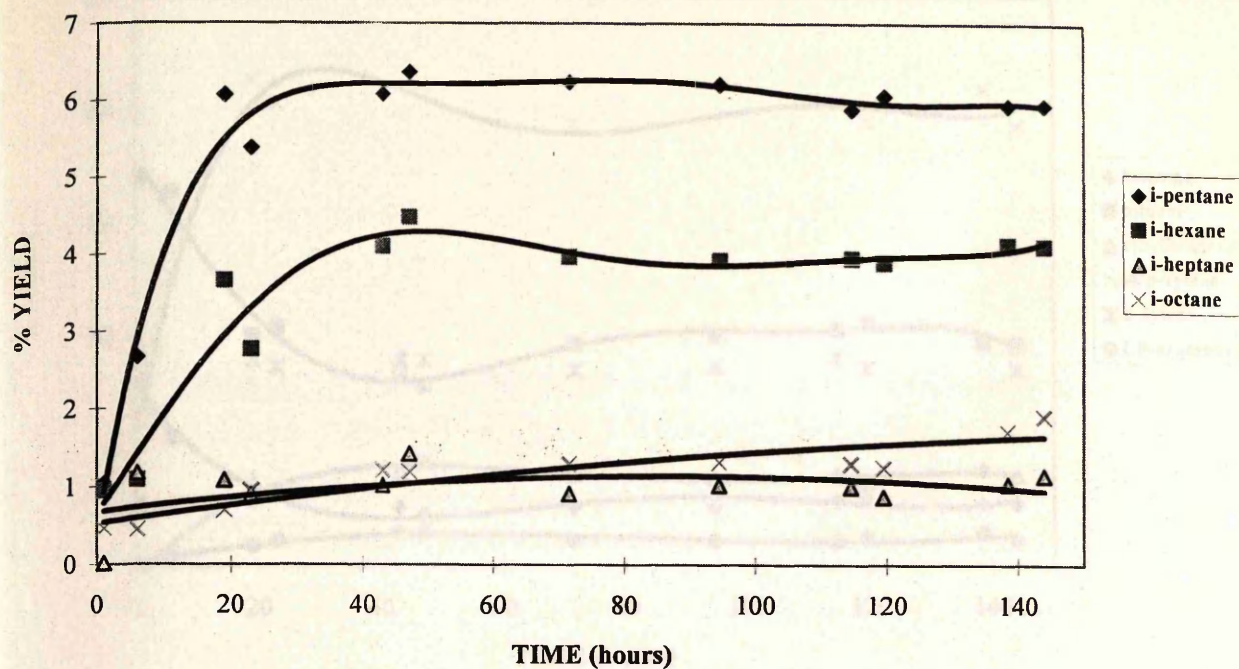


Figure 5.10.4 Yields of n-alkanes over 0.3 wt% Pt - 0.3 wt% Ir - 0.03 wt% Ge/Al₂O₃

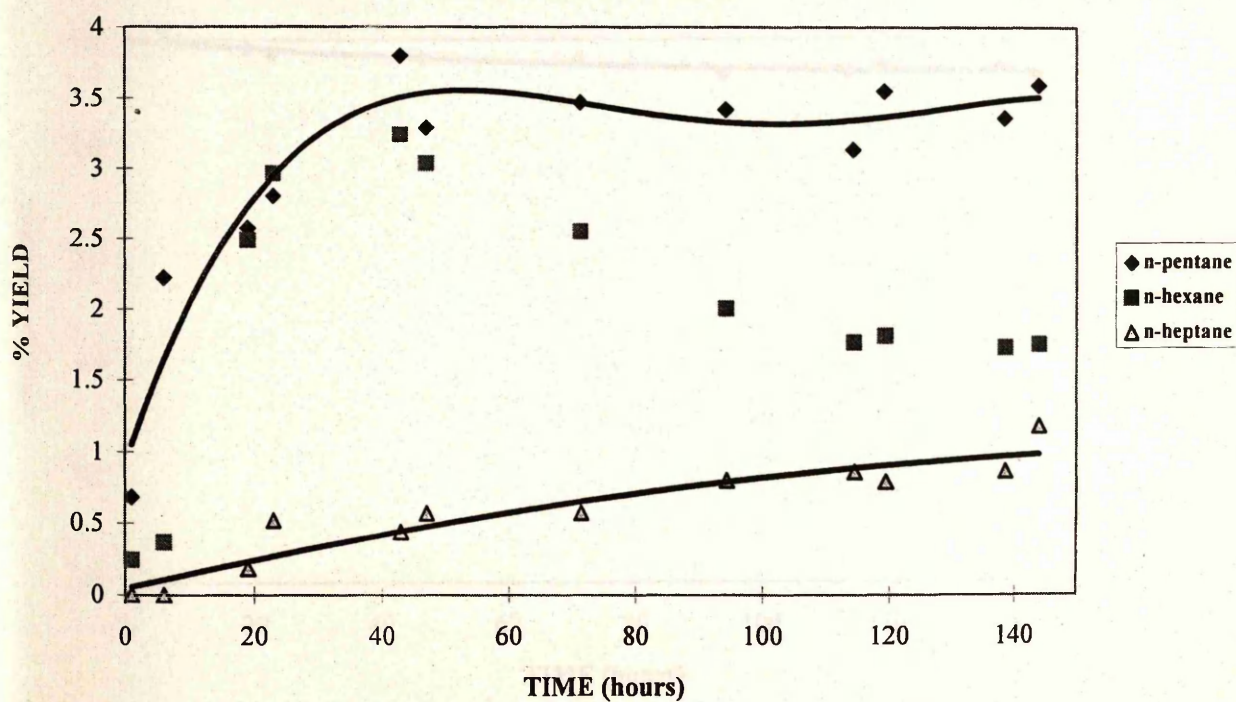


Figure 5.10.5 Yields of aromatics over 0.3 wt% Pt - 0.3 wt% Ir - 0.03 wt% Ge/Al₂O₃

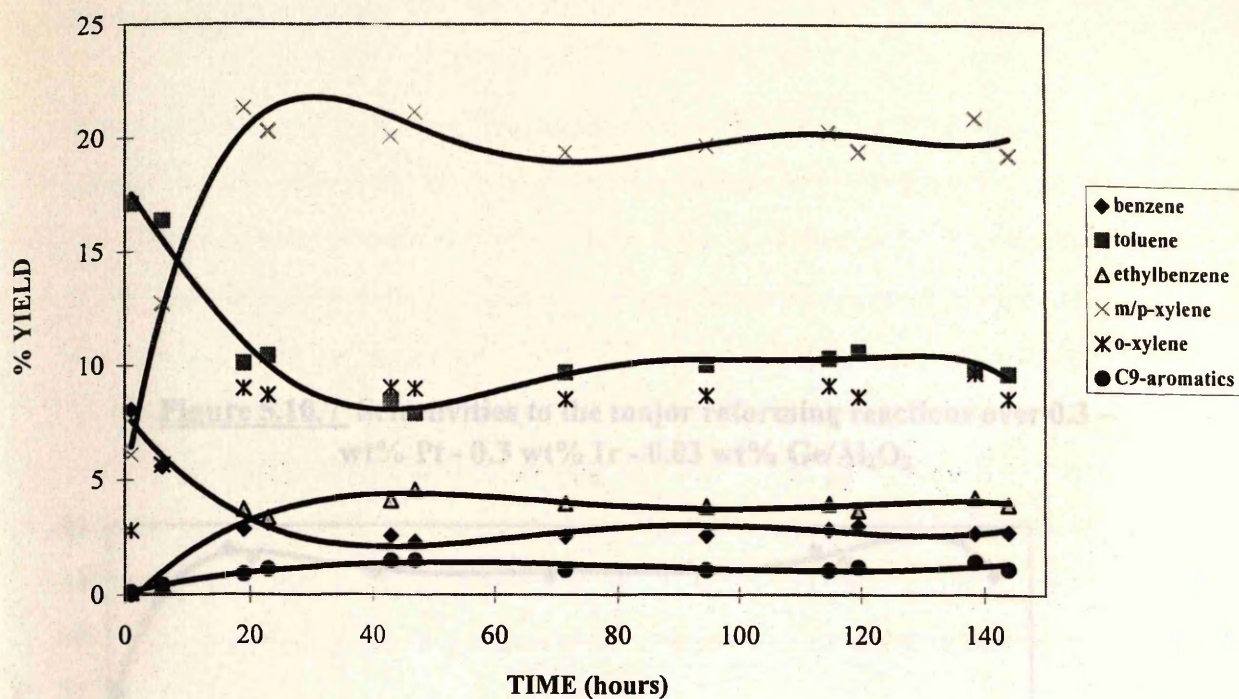
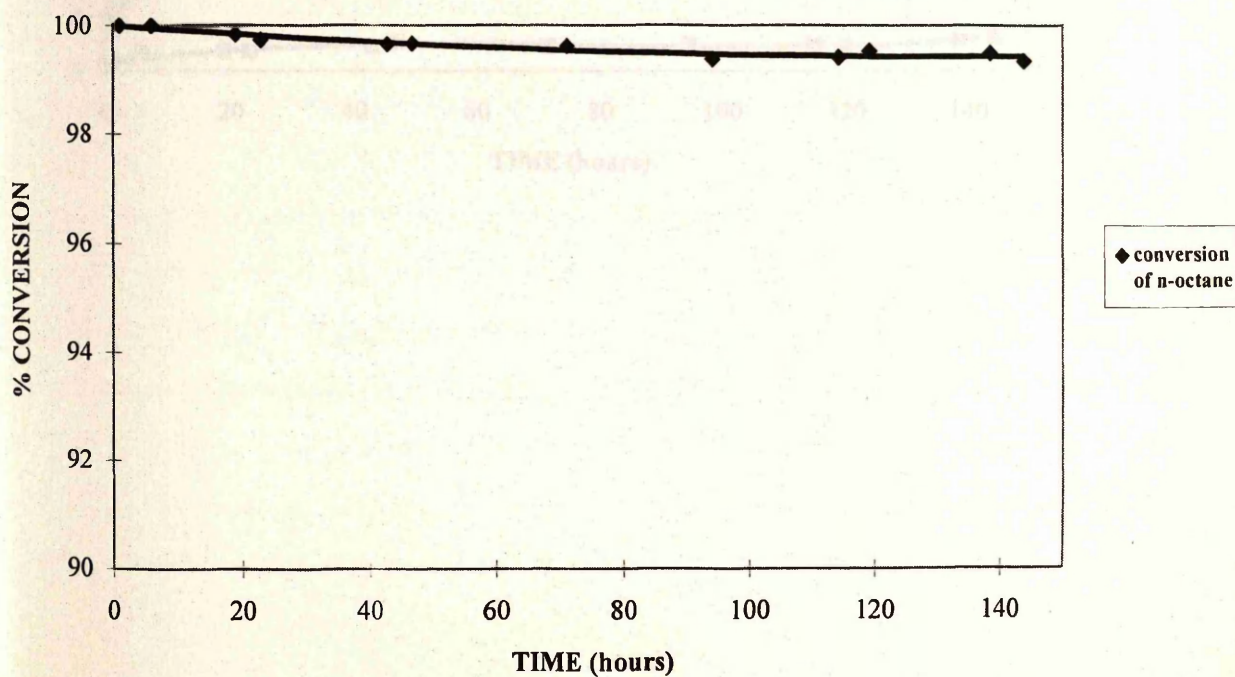


Figure 5.10.6 Conversion of n-octane over 0.3 wt% Pt - 0.3 wt% Ir - 0.03 wt% Ge/Al₂O₃

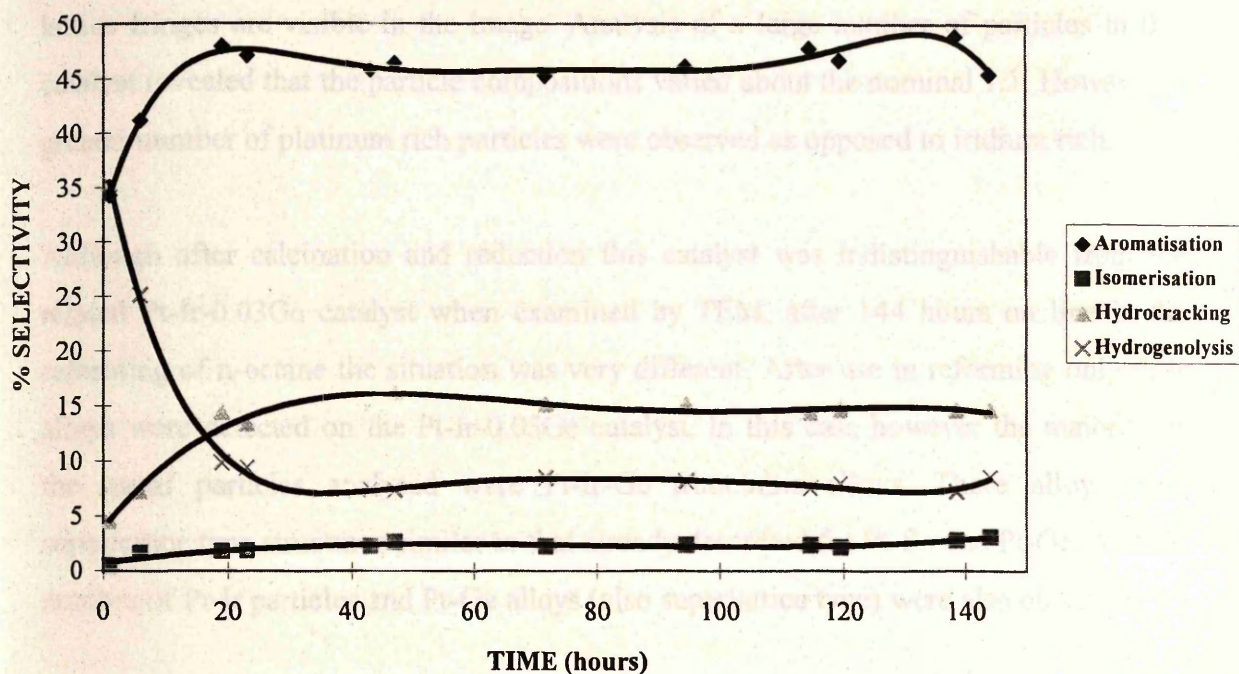


5.11. 0.3wt% Pt - 0.3 wt% Ir - 0.3 wt% Ge/Al₂O₃

5.11.A TEM observations

After calcination and reduction this catalyst was similar to the Pt-Ir and Pt-Ir-0.03% Ge catalysts already described. Again the metallic component was highly dispersed with only a small number of particles greater than 2 nm in diameter. EDX analysis of these particles revealed them to be Pt-Ir alloys. No germanium alloy particles were observed at this stage. An example is shown in plate 35. This particle was approximately 3 nm in diameter.

Figure 5.10.7 Selectivities to the major reforming reactions over 0.3 wt% Pt - 0.3 wt% Ir - 0.03 wt% Ge/Al₂O₃



5.11. 0.3wt% Pt - 0.3 wt% Ir - 0.3 wt% Ge/Al₂O₃

5.11.A TEM observations

After calcination and reduction this catalyst was similar to the Pt-Ir and Pt-Ir-0.03Ge catalysts already described. Again the metallic component was highly dispersed with only a small number of particles greater than 2 nm in diameter. EDX analysis of these particles revealed them to be Pt-Ir alloys. No germanium alloy particles were observed at this stage. An example is shown in plate 35. This particle was approximately 8 nm in diameter. The corresponding EDX spectrum obtained revealed a Pt/Ir atomic ratio of 1.5. The particle was in the (110) orientation. The 0.227 nm {111} and 0.196 nm {002} lattice fringes are visible in the image. Analysis of a large number of particles in this catalyst revealed that the particle compositions varied about the nominal 1:1. However, a greater number of platinum rich particles were observed as opposed to iridium rich.

Although after calcination and reduction this catalyst was indistinguishable from the related Pt-Ir-0.03Ge catalyst when examined by TEM, after 144 hours on line in the reforming of n-octane the situation was very different. After use in reforming only Pt-Ir alloys were detected on the Pt-Ir-0.03Ge catalyst. In this case however the majority of the metal particles analysed were Pt-Ir-Ge trimetallic alloys. These alloys were superlattice type structures similar to that already described for Pt-Sn and Pt-Ge. A small number of Pt-Ir particles and Pt-Ge alloys (also superlattice type) were also observed.

An example of a superlattice type particle formed on this catalyst after 144 hours on line is given in plate 36. This particle was approximately 15 nm in diameter. The EDX spectrum obtained (inset) revealed that the particle contained platinum, iridium and germanium. The relative atomic ratios were calculated as Pt/Ir = 1.2, Pt+Ir/Ge = 3.4. The MBED pattern obtained (inset) could be indexed as the (110) pattern of crystalline platinum or iridium (bright spots) with an extra set of (weaker) superlattice reflections between. The superlattice nature of this particle was also evident in the image. One set of

lattice planes corresponded to the 0.227 nm {111} lattice of the fcc metal. The other bolder set of planes running vertically up the page correspond to twice the {002} spacing, i.e. $2 \times 0.196 = 0.392$ nm.

The concentration of germanium in particles exhibiting superlattice particles was found to vary quite considerably. Another example is shown in plate 37. This particle was approximately 12 nm in diameter and again the EDX spectrum obtained revealed the presence of platinum, iridium and germanium. In this case however, the relative atomic ratios were calculated as $\text{Pt/Ir} = 1.0$, $\text{Pt+Ir/Ge} = 7.1$. The MBED pattern obtained from this particle again contained the characteristic superlattice reflections. The pattern was indexed as the (100) pattern of the fcc metal (bright spots) with extra superlattice spots between the main reflections. Also imaged in this micrograph were a number of nanometer sized particles (arrowed).

A further example of this type of particle is given in plate 38. This particle was approximately 30 nm in diameter. Again the EDX spectrum revealed the presence of platinum, iridium and germanium. In this case the relative atomic ratios were calculated to be $\text{Pt/Ir} = 1.0$, $\text{Pt+Ir/Ge} = 6.0$. The MBED pattern obtained (inset) was indexed as the (121) pattern of the fcc metal (bright spots) with again superlattice reflections between.

EDX analysis of a number of the larger sintered particles revealed that some of these did not have uniform elemental composition. An example is shown in plate 39. This very large particle was approximately 30-40 nm in diameter. EDX spectra from two regions of the particle (marked (A) and (B) in the image) were obtained with a 5 nm diameter probe. Region (A) (spectrum (A)) was found to be rich in iridium and germanium, $\text{Pt/Ir} = 0.8$, $\text{Pt+Ir/Ge} = 1.3$. Region (B) (spectrum (B)) was found to be mainly platinum with only a small fraction of iridium. The concentration of germanium was also much lower, with $\text{Pt+Ir/Ge} = 4.2$. A MBED pattern obtained (inset) taken from region (B) contained superlattice reflections. The bright spots correspond to the platinum (110) pattern whilst

the darker spots correspond to the superlattice reflections. The bold lattice fringes visible in region (B) had a spacing of 0.45 nm, twice the Pt {111} spacing.

Although Pt-Ir-Ge superlattice structures accounted for the majority of the larger particles observed in this system after 144 hours, other phases were also observed. Plate 40 gives an example of a particle containing a Pt-Ge superlattice phase. This particle was approximately 50 nm in diameter. The EDX spectrum obtained from the whole particle revealed a Pt/Ge atomic ratio of 13.6. The MBED pattern obtained, again using a probe which covered the entire particle, was indexed as the (110) pattern of platinum with characteristic superlattice reflections between. Evidence for superlattice structure was also obtained from the image, with some regions containing alternating bold and faint lattice fringes (as shown by the higher magnification insert of the area arrowed). Also imaged in this micrograph were a number of nanometer sized particles (some of which are also arrowed).

A small number of Pt-Ir alloys were also observed in this catalyst after 144 hours on line. An example is given in plate 41. This particle was 12 nm in diameter. The EDX spectrum obtained (inset) revealed the presence of platinum and iridium with an atomic ratio Pt/Ir of 2.1. The corresponding MBED pattern was indexed as the (110) pattern of the crystalline fcc metal. The lattice fringes visible in the image correspond to the {111} 0.227 nm and {002} 0.196 nm lattices.

It was evident that considerable sintering of the metal component had occurred on this catalyst during 144 hours on line. Both the particle number density and the average particle size were greater in this system than on any of the catalysts studied. However, it is possible that even at this stage a significant proportion of the metallic component of this catalyst remained in the form of nanometer sized metal particles similar to those imaged in plates 37 and 40.

5.11.B n-Octane reforming

The yields of individual products over the Pt-Ir-Ge/Al₂O₃ catalyst are listed versus time on line in table 5.11.1 and plotted in figures 5.11.1 to 5.11.6.

The yields of methane, ethane, propane, i-butane and n-butane over this catalyst are plotted in figure 5.11.1. It was found that the yield of methane over this catalyst was considerably lower than the corresponding yield over Pt-Ir/Al₂O₃ (5.5% versus 42.8%, figure 5.5.1). It was also much lower than the initial high methane yield observed over the Pt-Ir-0.03Ge/Al₂O₃ catalysts (35.3%). The actual yields observed were similar to those observed over the Pt/Al₂O₃ catalyst (figure 5.1.1) and remained relatively constant throughout the run. Similar observations can be made regarding the yield of ethane on this catalyst.

The yields of propane over this catalyst (9.6%) was initially similar to that observed over the Pt-Ir-0.03Ge catalyst (9.4%), but decreased slightly during the initial stages and then remained constant. The yield of this product was slightly higher than the corresponding yield over Pt/Al₂O₃ however (7.0%). The yields of i-butane and n-butane were relatively high over this catalyst (5.5% and 8.9% respectively), higher than the corresponding yields over Pt (3.9% and 5.9%) and Pt-Ir-0.03Ge (2.6% and 2.8%). The yields remained relatively constant throughout the run and actually obtained higher values after 12 hours.

The yields of cycloalkanes over this catalyst are plotted in figure 5.11.2. The yields of cyclopentane, C₆ and C₇ cycloalkanes remained relatively constant throughout the run whilst the yields of C₈ cycloalkanes over the catalyst increased. The final yield of C₈ cycloalkanes over this catalyst (0.9%) was lower than the corresponding value over Pt/Al₂O₃ (2.1%) but higher than the that obtained over Pt-Ir-0.03Ge/Al₂O₃ (0.6%).

The yield of i-alkanes over this catalyst are plotted in figure 5.11.3. The yield of i-pentane (8%) was relatively constant throughout the run and was observed to be slightly higher than the corresponding yield over Pt/Al₂O₃ (figure 5.1.3: 6%) and the stable yield (after the initial increase) over Pt-Ir-0.03Ge/Al₂O₃ (6%). The yield of i-hexane was also relatively stable throughout the run. In this case the yields obtained were again slightly higher at all stages of the run than the corresponding values over Pt-Ir-0.03Ge (6% versus 4%) but were roughly equivalent to the corresponding values over platinum. The yield of i-heptane also remained constant throughout the run but in the case of this product was similar to those obtained over both Pt/Al₂O₃ and Pt-Ir-0.03Ge/Al₂O₃.

The yield of i-octane over this catalyst was observed to increase very substantially throughout the run (from 4.3 to 17%). This behaviour is similar to that observed over Pt/Al₂O₃ and Pt-Ge/Al₂O₃ (figure 5.3.3). However the corresponding yield over Pt-Ir-0.03Ge (figure 5.11.3) only increased by a very small amount in comparison (from 0.55 to 1.9%).

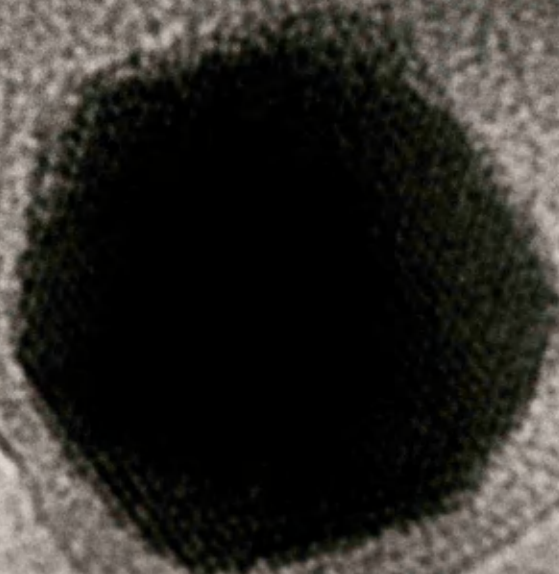
The yields of n-alkanes over this catalyst are plotted in figure 5.11.4. The yields of n-pentane decreased slightly throughout the run although it remained higher than the corresponding value over Pt-Ir-0.03Ge (figure 5.10.4). Similar observations can be made regarding the yield of n-hexane. The yield of n-heptane was also relatively constant over this catalyst. However, although the initial yield of n-heptane was higher over this catalyst than the corresponding value over the Pt-Ir-0.03Ge catalyst, the yield over Pt-Ir-0.03Ge increased throughout the run and actually obtained higher values after 144 hours on line.

The yields of aromatic products over the Pt-Ir-Ge/Al₂O₃ catalyst are presented in figure 5.11.5. The distribution of aromatic products was similar in many respects to that observed over the related Pt-Ge/Al₂O₃ catalyst (figure 5.3.5). However the initial yields of xylenes were observed to be significantly lower over this catalyst (e.g. m/p-xylene: 18.8% versus 23.6%). The corresponding yield of toluene was slightly greater. When

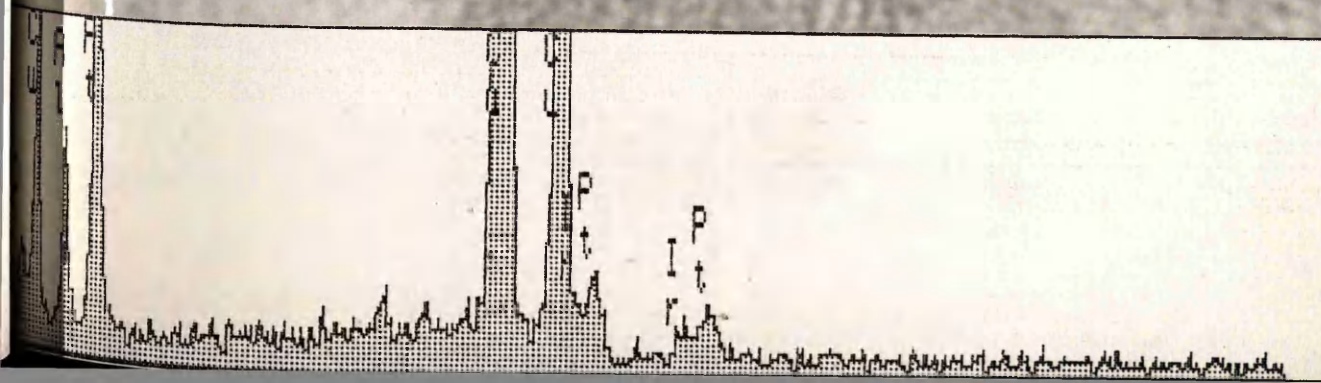
comparing these yields with the corresponding yields over the Pt-Ir-0.03Ge catalyst (figure 5.10.5) it was observed that after the initial increase over the Pt-Ir-0.03Ge catalyst, the yields of xylenes and ethylbenzene were similar over each, whilst the yield of benzene and toluene were higher over the Pt-Ir-0.03Ge catalyst (e.g. final toluene yields: Pt-Ir-Ge 1.9%; Pt-Ir-0.03Ge 9.6%). Also, the yields of aromatics, especially m/p-xylene decreased towards the end of the run over the Pt-Ir-Ge catalyst whilst they remained relatively constant over the Pt-Ir-0.03Ge catalyst (final m/p-xylene yields: Pt-Ir-Ge 14.6%; Pt-Ir-0.03Ge 19.3%).

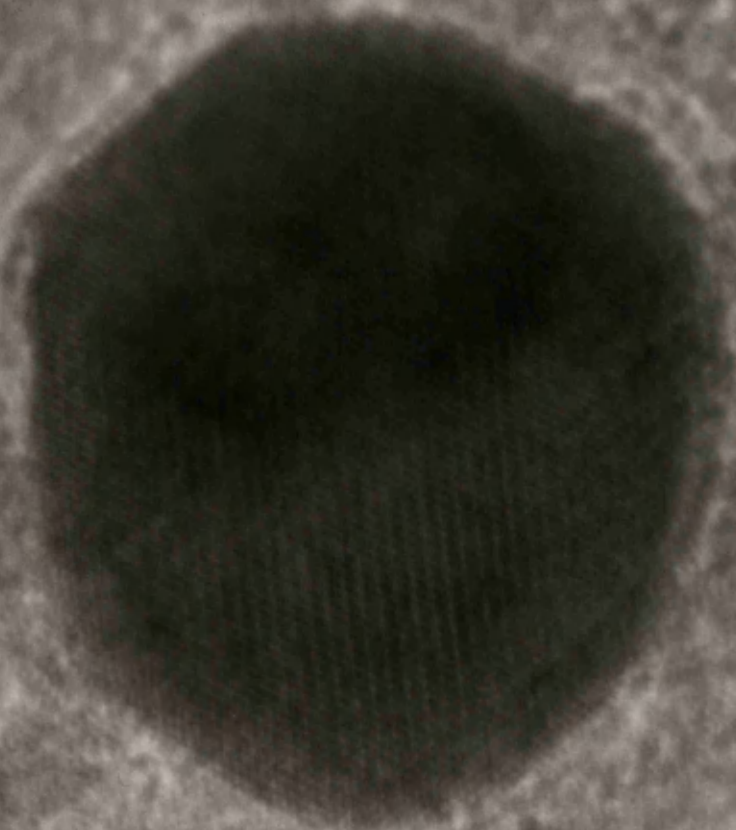
The total conversion of n-octane over Pt-Ir-0.03Ge/Al₂O₃ is plotted in figure 5.11.6. The conversion of n-octane over this catalyst followed a similar "accelerating" deactivation curve to that observed over Pt-Sn and Pt-Ge (figure 5.2.6 and 5.3.6 respectively). However the rate of loss of conversion in this trimetallic system was not as great as that observed over these bimetallic systems. However, it was considerably greater than that observed over the Pt-Ir-0.03Ge catalyst (final conversion: Pt-Ir-Ge 92.8%; Pt-Ir-0.03Ge 99.3%).

The selectivities to the four major reforming reactions over the Pt-Ir-Ge/Al₂O₃ catalyst are listed versus time on line in table 5.11.2 and plotted in figure 5.11.7. The selectivity to aromatics was observed to decrease significantly towards the end of the reforming run. The selectivity towards isomerisation was found to increase steadily throughout the run. However the extent of the increase in selectivity to isomerisation and decrease in selectivity towards aromatisation was not as great as observed in some of the related systems (e.g. Pt-Sn: figure 5.2.7, Pt-Ge: figure 5.3.7). The selectivity to hydrocracking over this catalyst remained relatively constant throughout the run, as did the selectivity to hydrogenolysis. However, the selectivity to hydrogenolysis was significantly lower than the corresponding values over Pt-Ir/Al₂O₃ and the initial values over Pt-Ir-0.03Ge/Al₂O₃.

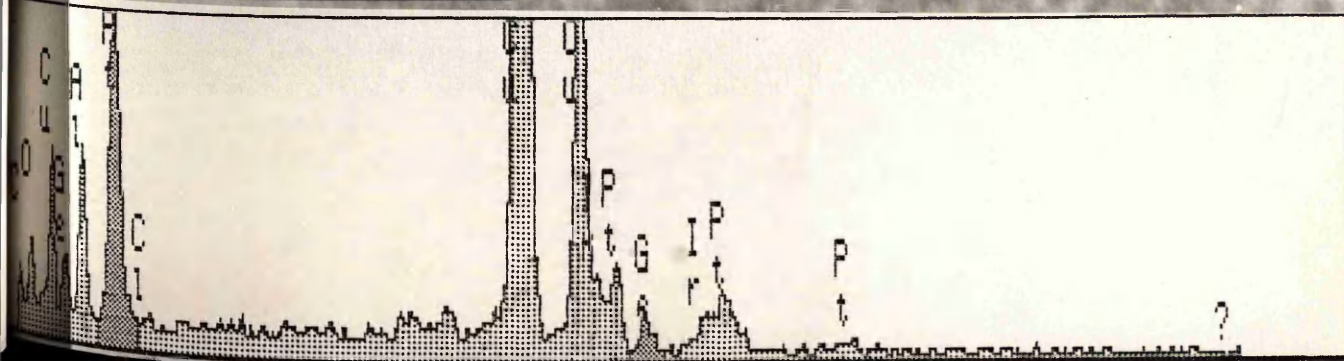


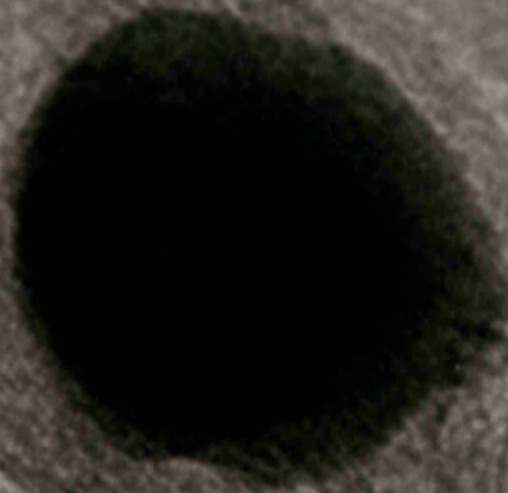
3 nm





3 nm





3 nm

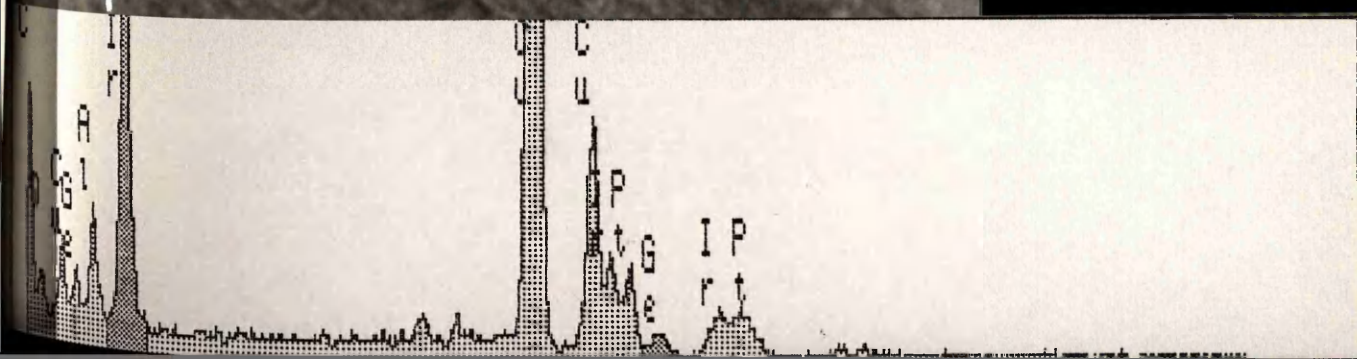
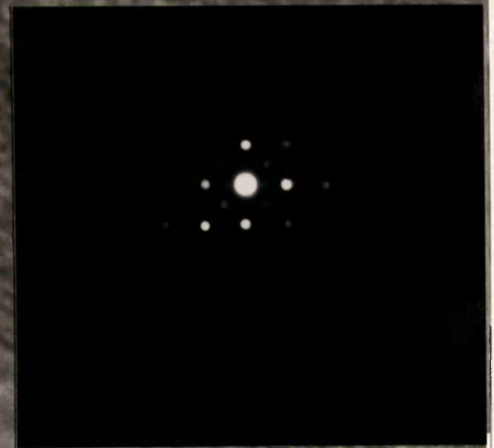
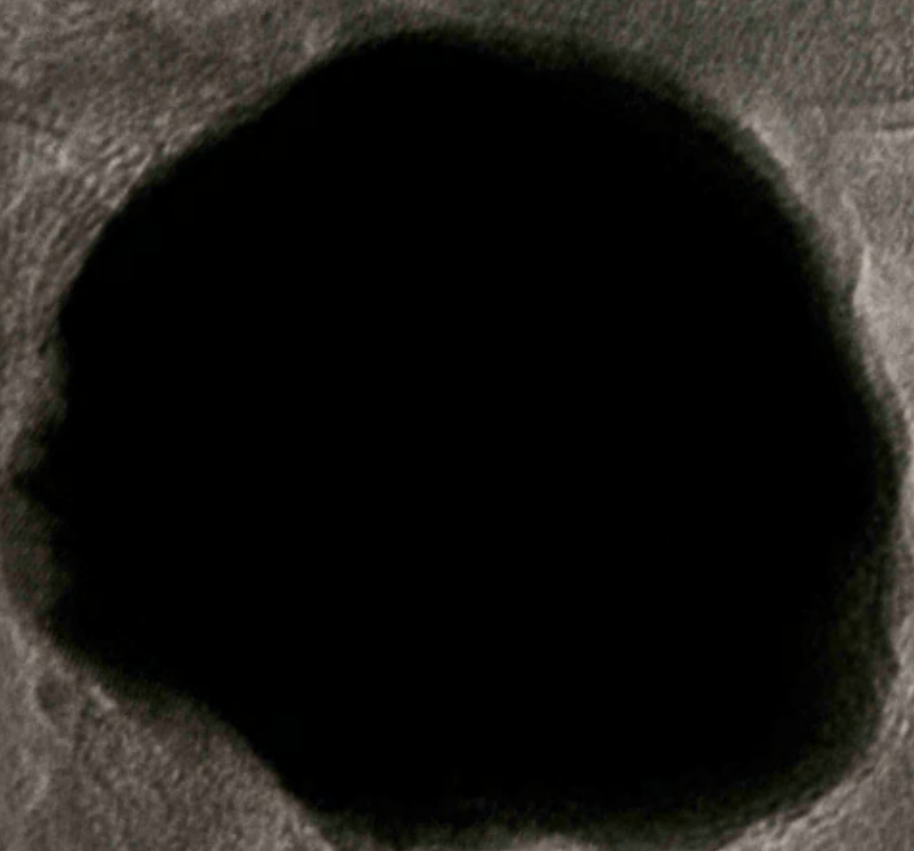
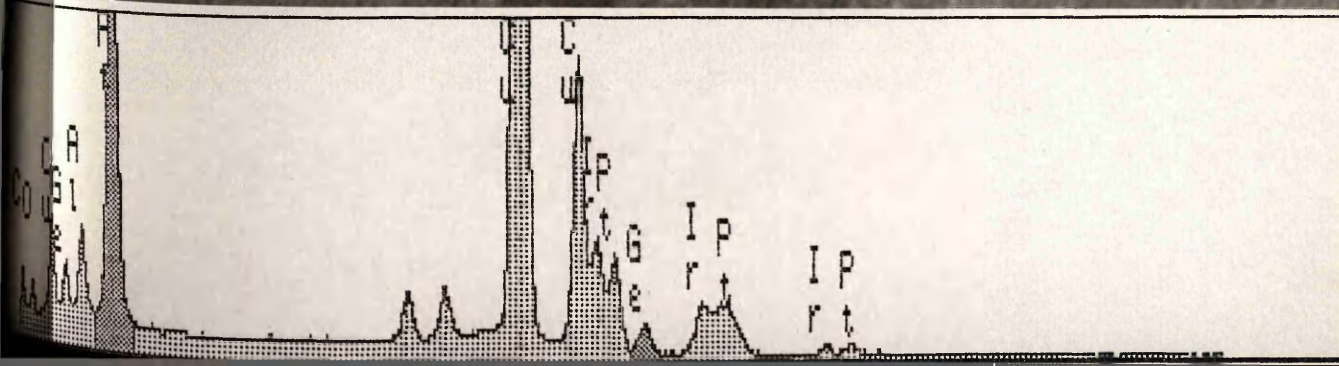


Plate 38



5 nm



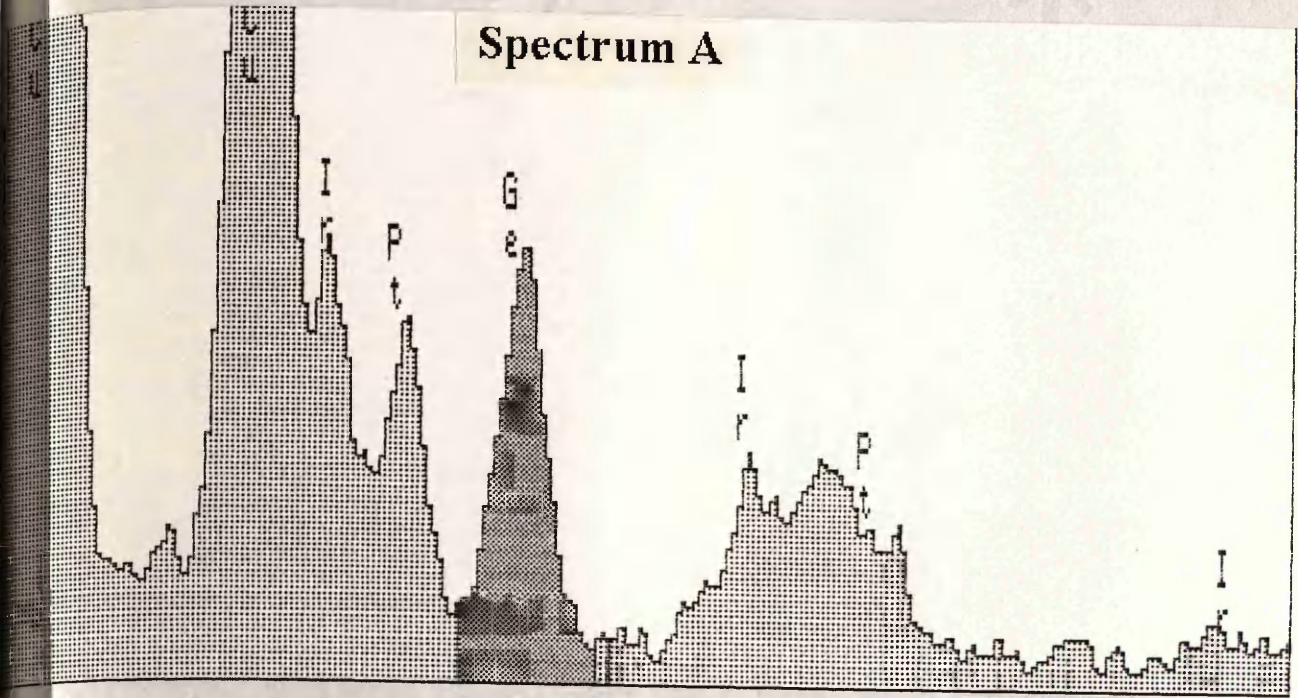
(A)

(B)

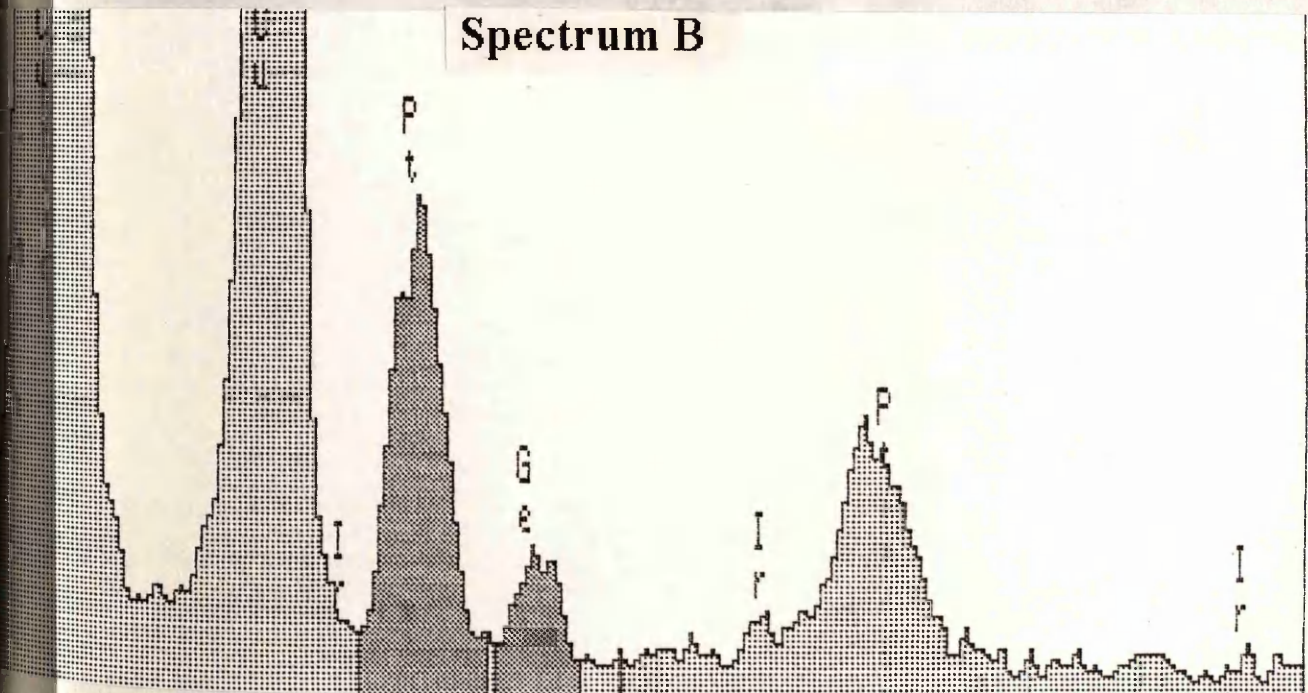
5 nm



Spectrum A



Spectrum B



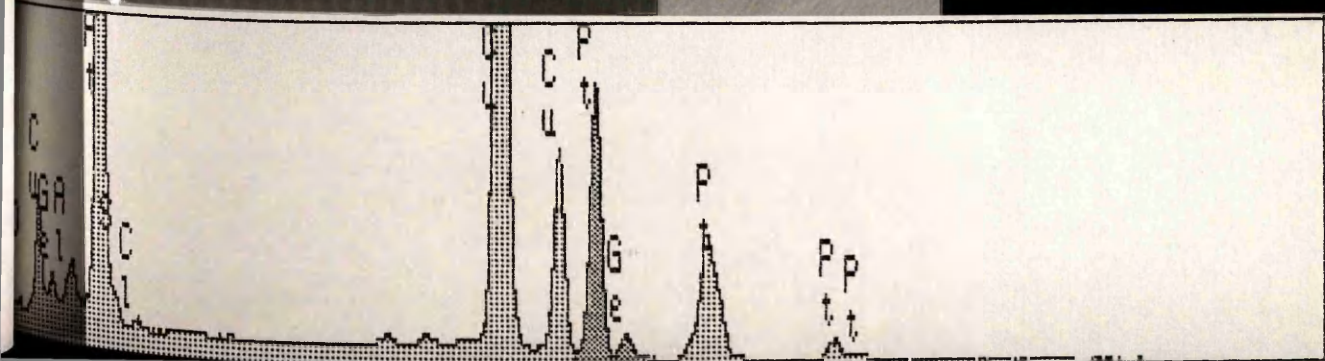
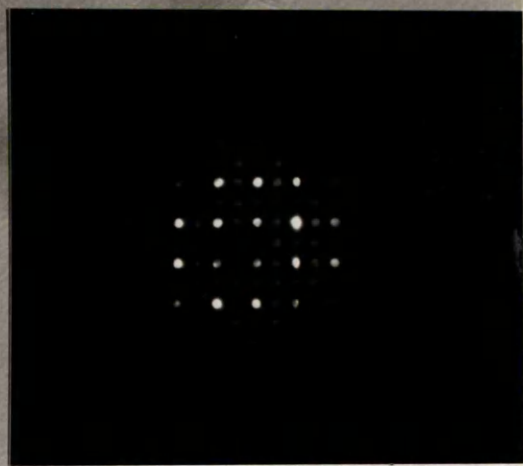
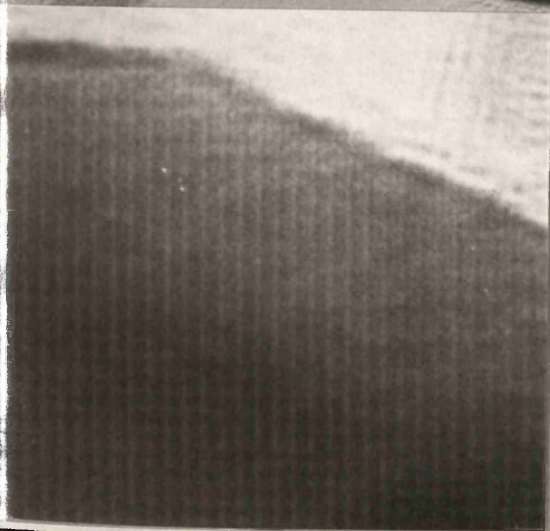
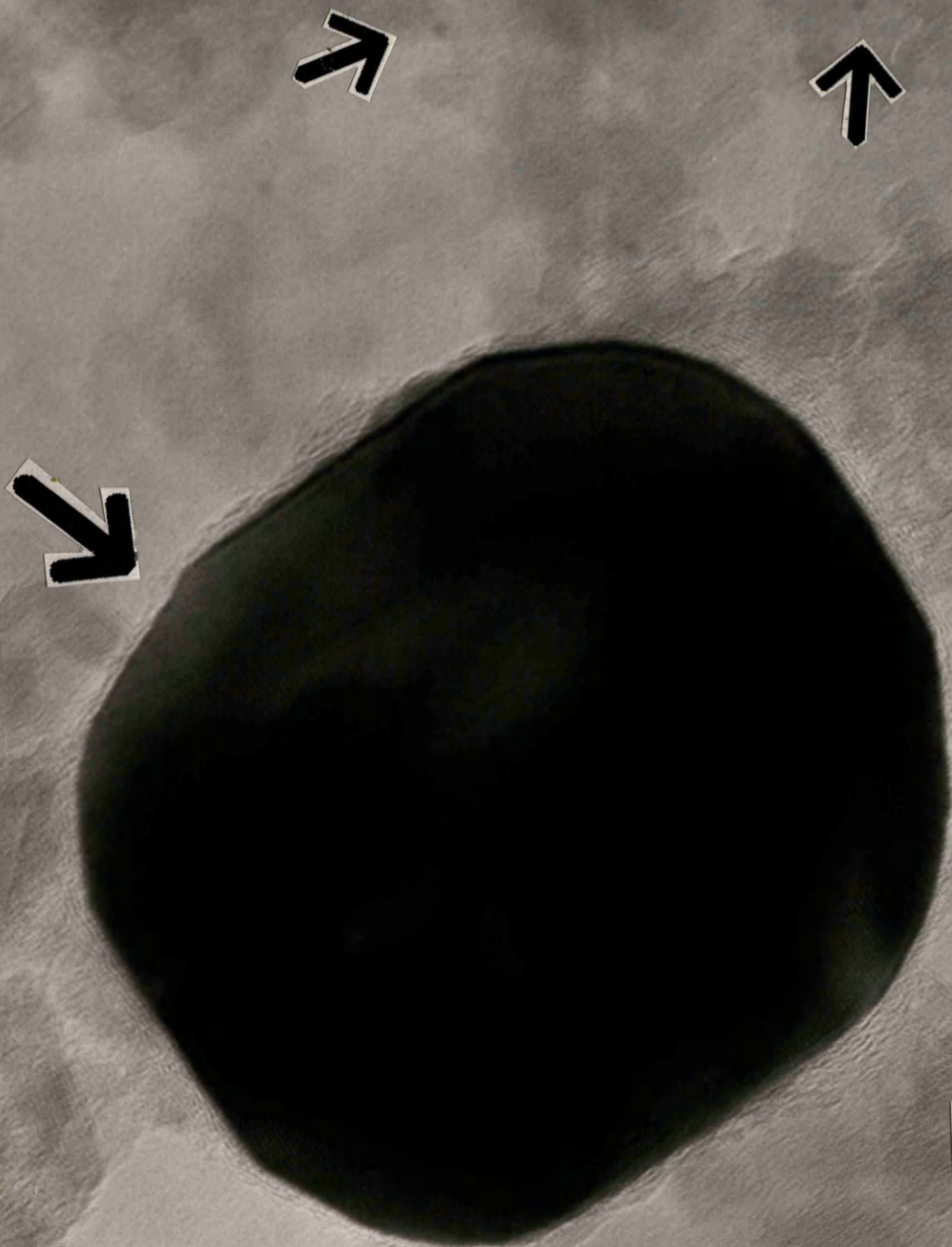
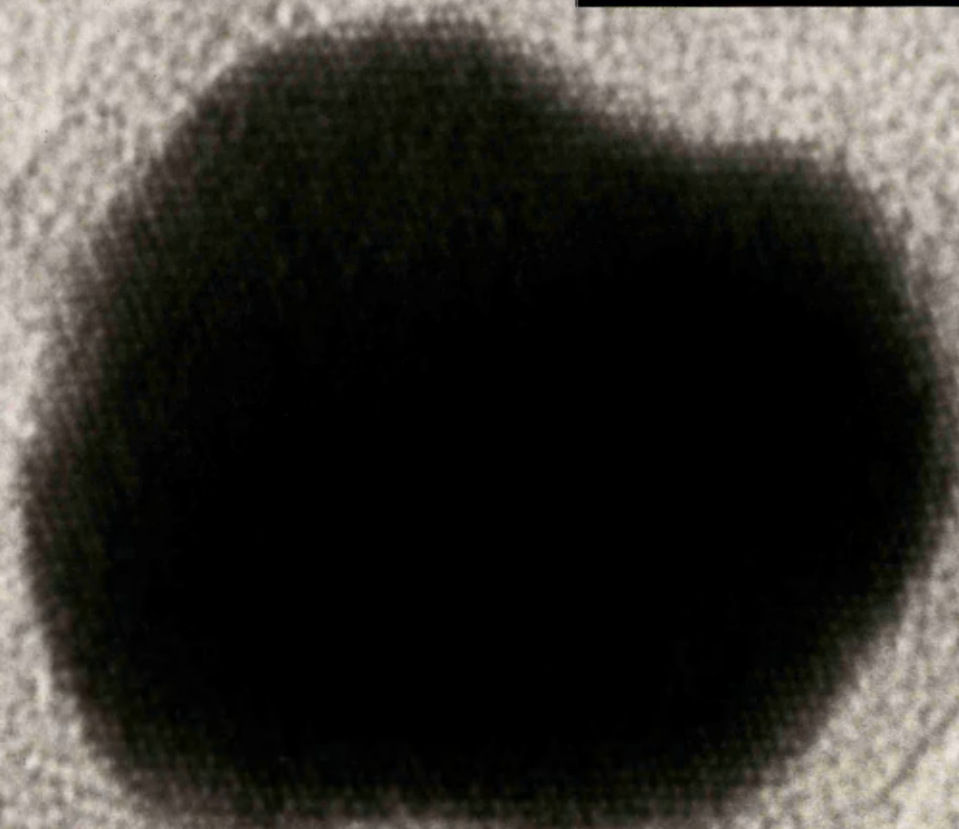


Plate 41



2 nm

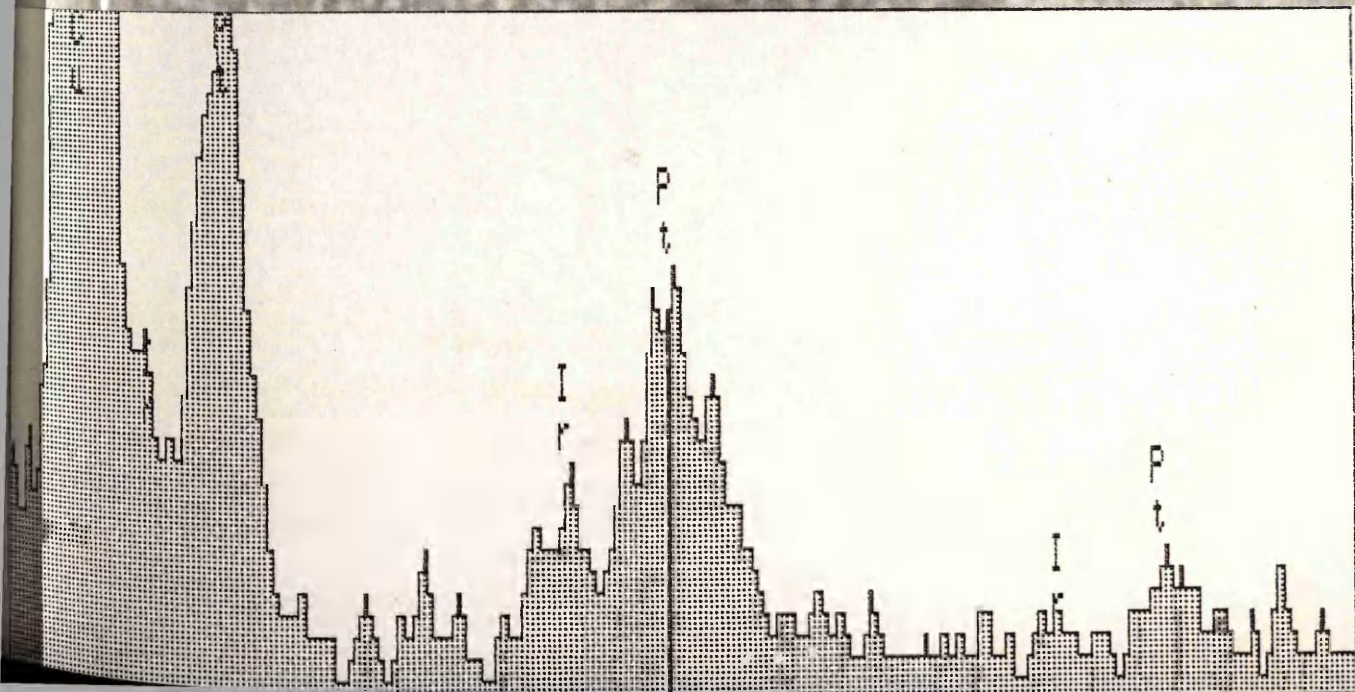


Table 5.11.1 Yields of individual products for catalyst 0.3 wt% Pt - 0.3 wt% Ir - 0.3 wt% Ge/Al₂O₃

Time (hours)	Methane	Ethane	Propane	i-Butane	n-Butane	c-Pentane	i-Pentane	n-Pentane
1.0	5.5	2.9	9.6	5.5	8.9	0.2	8.3	5.6
5.3	4.7	2.1	7.8	6.0	8.5	0.2	9.1	5.6
18.5	5.2	2.6	7.8	4.9	7.3	0.1	7.6	4.7
23.0	4.6	2.3	7.8	4.8	8.5	0.1	9.5	5.2
28.8	5.3	2.3	7.1	4.8	7.3	0.1	7.4	5.2
49.5	4.0	2.5	7.4	5.1	7.4	0.1	7.8	4.6
73.5	5.0	2.4	7.2	4.9	7.3	0.1	7.4	4.5
98.5	3.8	2.4	7.1	4.7	6.7	0.1	7.1	4.8
123.0	4.6	2.0	7.1	5.0	7.8	0.1	7.2	4.6
144.0	4.1	2.0	7.0	4.9	6.6	0.1	6.9	4.4

Table 5.11.1 (cont) Yields of individual products for 0.3 wt% Pt - 0.3 wt% Ir - 0.3 wt% Ge/Al₂O₃

Time (hours)	C6 c-Alkane	i-Hexane	n-Hexane	C7 c-Alkane	i-Heptane	n-Heptane	C8 c-Alkane	i-Octane
1.0	0.4	6.0	2.6	0.3	1.1	0.5	0.1	4.3
5.3	0.4	6.9	2.9	0.3	1.6	0.6	0.2	5.7
18.5	0.3	6.0	2.5	0.3	1.4	0.4	0.2	6.4
23.0	0.3	7.0	2.8	0.2	1.7	0.6	0.2	8.9
28.8	0.3	6.3	2.7	0.2	1.5	0.7	0.3	8.9
49.5	0.3	6.0	2.3	0.2	1.5	0.4	0.4	9.8
73.5	0.3	5.9	2.3	0.2	1.5	0.4	0.6	11.6
98.5	0.3	6.7	2.1	0.2	1.4	0.5	0.7	15.7
123.0	0.3	6.2	2.3	0.3	1.6	0.5	0.8	17.3
144.0	0.3	5.7	2.6	0.4	1.5	0.8	0.9	17.0

Table 5.11.1 (cont) Yields of individual products for 0.3 wt% Pt - 0.3 wt% Ir - 0.3 wt% Ge/Al₂O₃

Time (hours)	Benzene	Toluene	Ethyl- Benzene	m/p- Xylene	o-Xylene	C9 Aromatic	Total Conversion
1.0	0.8	3.6	3.9	18.8	9.5	0.7	99.3
5.3	0.6	2.7	3.5	19.0	8.8	0.5	97.9
18.5	0.6	2.7	4.4	20.6	11.2	0.7	98.0
23.0	0.5	2.2	3.7	17.9	8.2	0.6	97.6
28.8	0.5	2.4	4.0	20.2	9.5	1.0	98.0
49.5	0.5	2.3	4.2	20.1	9.2	1.1	97.3
73.5	0.4	2.1	4.6	18.2	8.4	1.3	96.5
98.5	0.4	2.0	3.5	16.7	7.3	0.9	95.1
123.0	0.4	1.9	3.1	14.4	6.2	1.0	94.6
144.0	0.4	1.9	3.2	14.6	6.2	1.2	92.8

Table 5.11.2 Selectivities for catalyst 0.3 wt% Pt - 0.3 wt% Ir - 0.3 wt% Ge/Al₂O₃

Time (hours)	Selectivity to Aromatics	Selectivity to Isomerisation	Selectivity to Hydrocracking	Selectivity to Hydrogenolysis
1.0	37.1	5.5	20.0	5.6
5.3	35.9	7.4	22.6	4.8
18.5	41.2	8.0	18.8	5.3
23.0	34.0	10.8	21.7	4.7
28.8	38.3	10.5	18.9	5.4
49.5	38.4	11.6	19.5	4.1
73.5	36.3	13.6	18.9	5.2
98.5	32.4	18.1	19.4	4.0
123.0	28.4	20.0	19.5	4.8
144.0	29.6	20.0	18.8	4.4

Figure 5.11.1 Yields of individual products over 0.3 wt% Pt - 0.3 wt% Ir - 0.3 wt% Ge/Al₂O₃

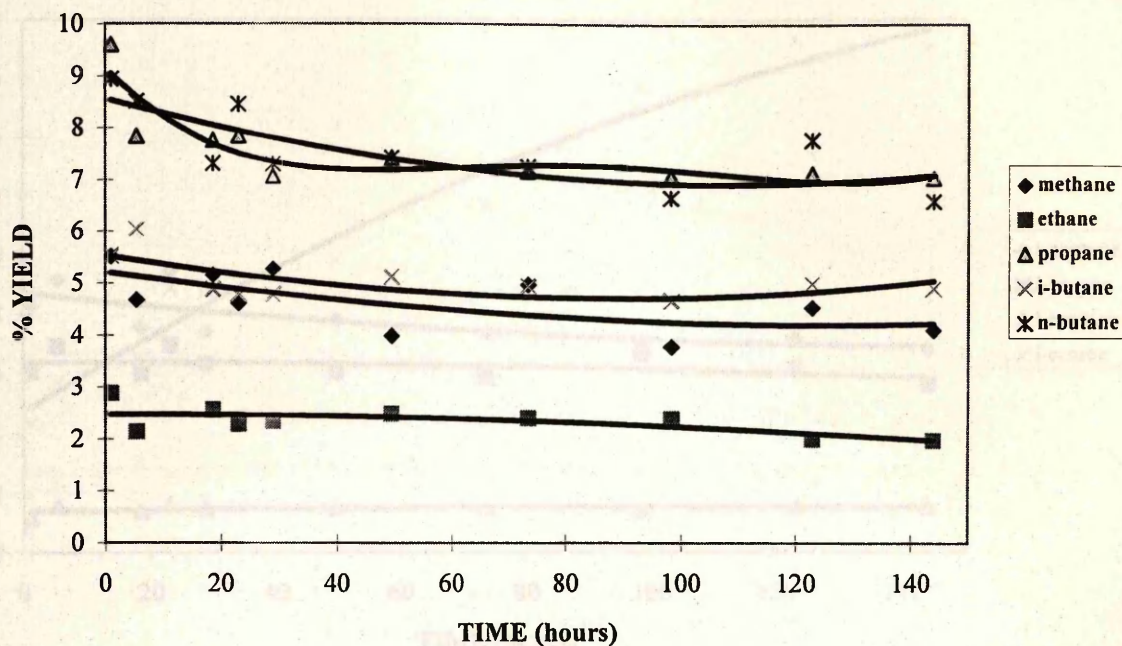


Figure 5.11.2 Yields of cycloalkanes over 0.3 wt% Pt - 0.3 wt% Ir - 0.3 wt% Ge/Al₂O₃

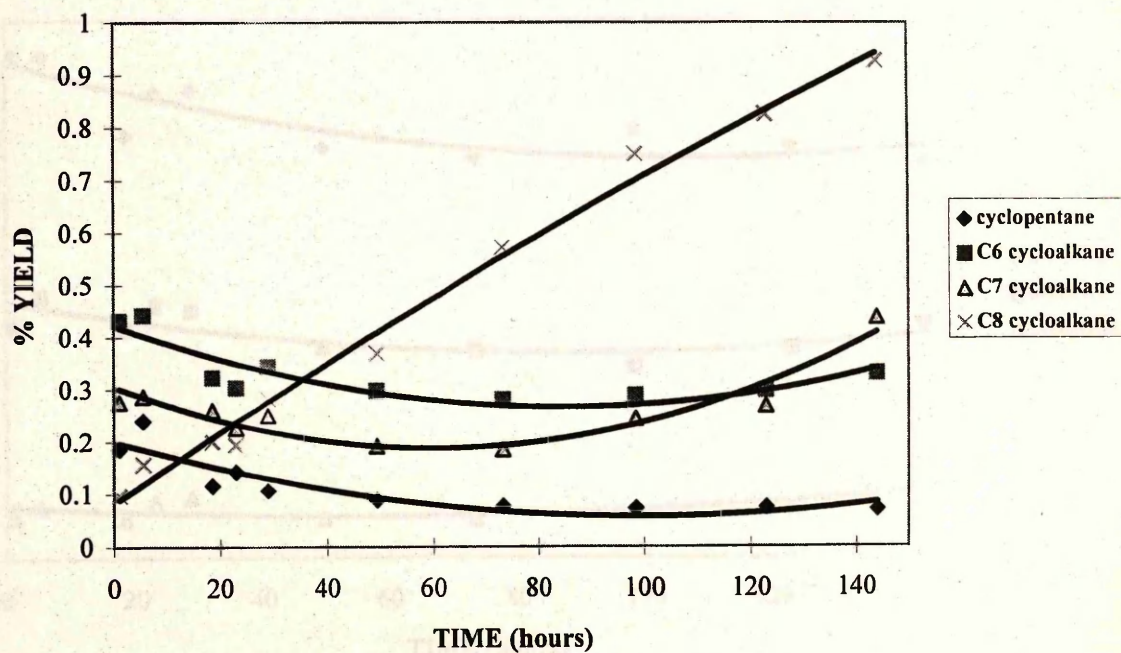


Figure 5.11.3 Yields of i-alkanes over 0.3 wt% Pt - 0.3 wt% Ir - 0.3 wt% Ge/Al₂O₃

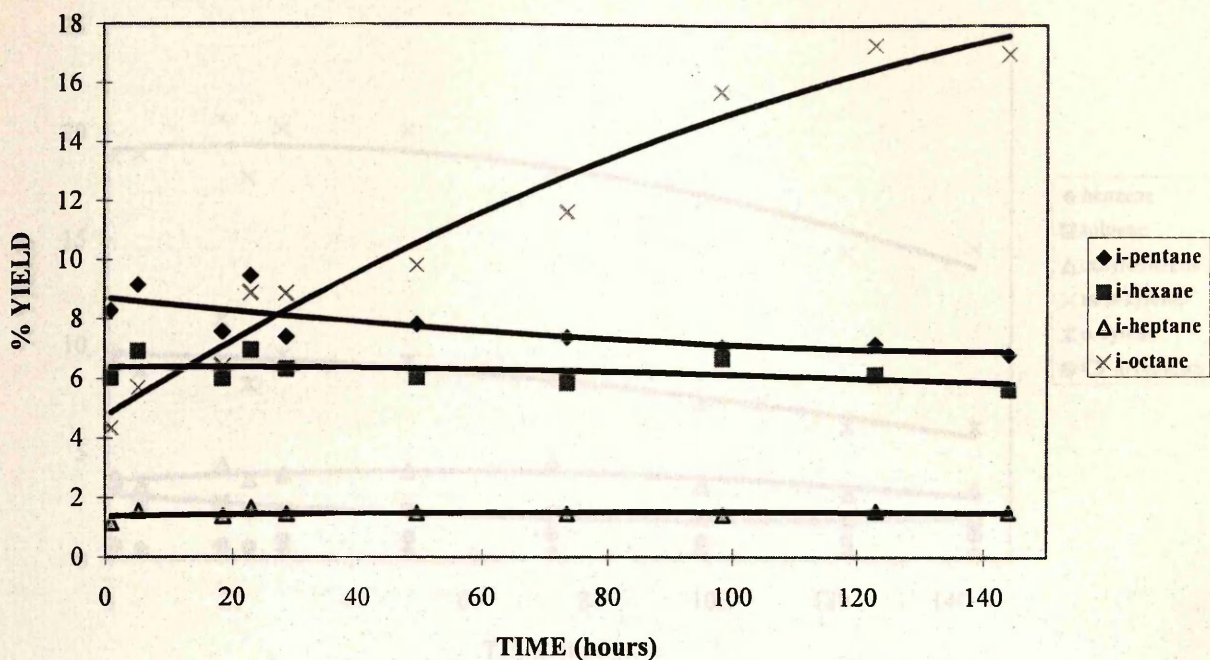


Figure 5.11.4 Yields of n-alkanes over 0.3 wt% Pt - 0.3 wt% Ir - 0.3 wt% Ge/Al₂O₃

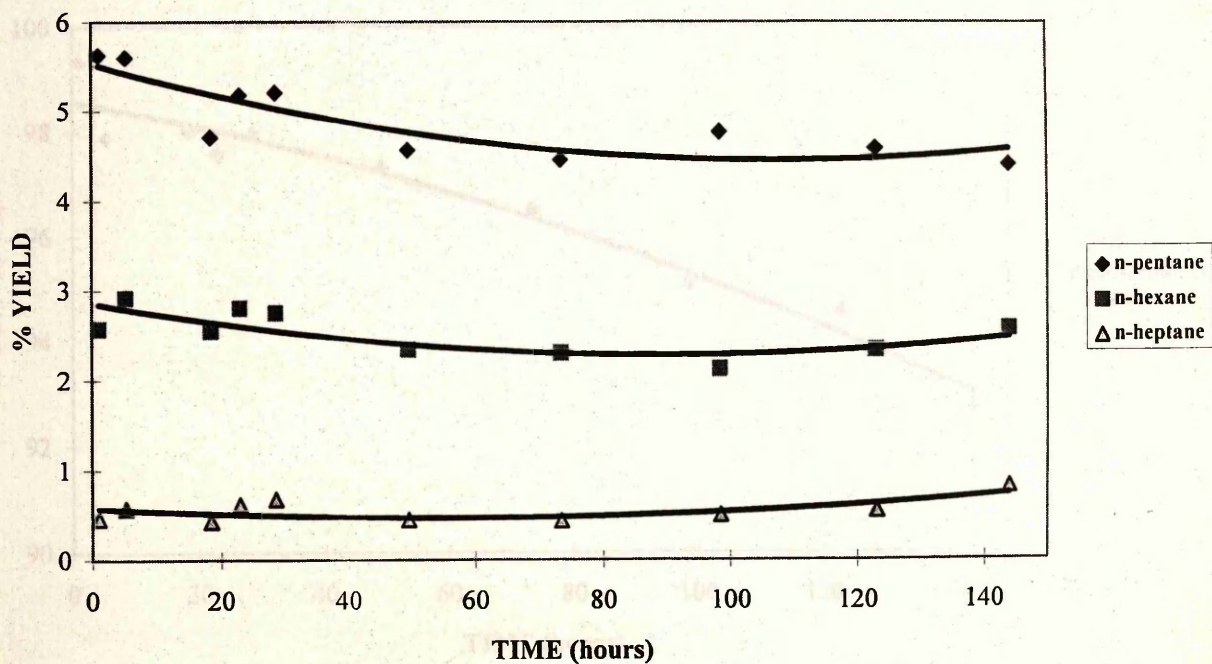


Figure 5.11.5 Yields of aromatics over 0.3 wt% Pt - 0.3 wt% Ir - 0.3 wt% Ge/Al₂O₃

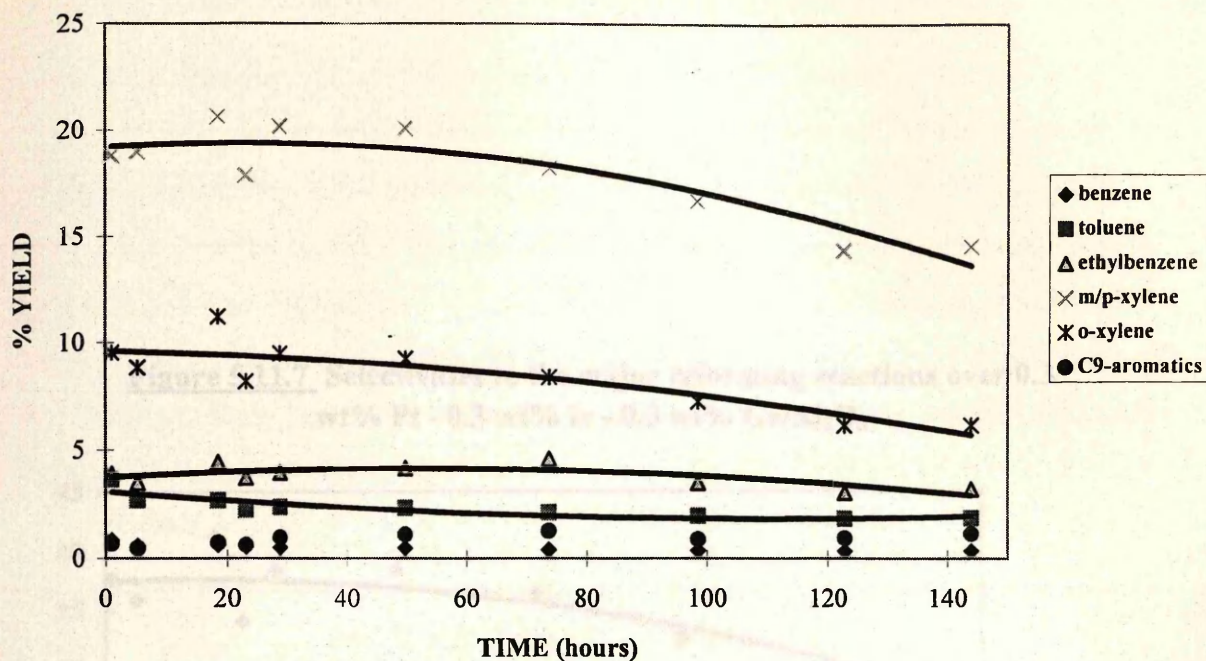
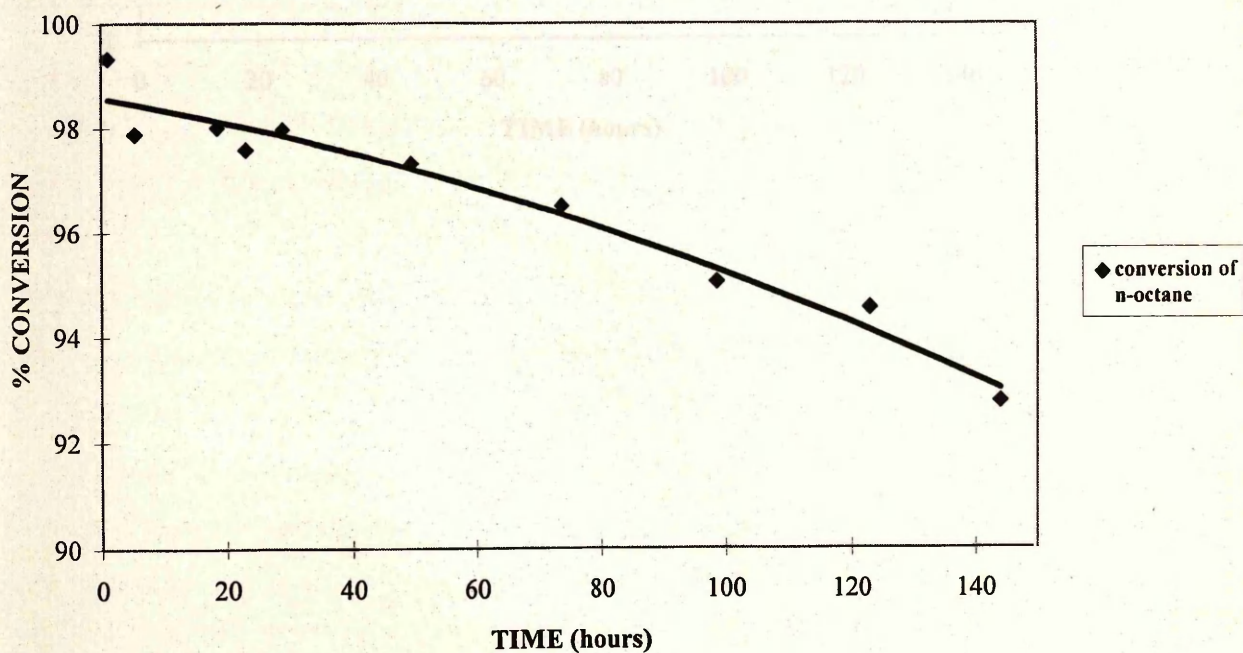


Figure 5.11.6 Conversion of n-octane over 0.3 wt% Pt - 0.3 wt% Ir - 0.3 wt% Ge/Al₂O₃

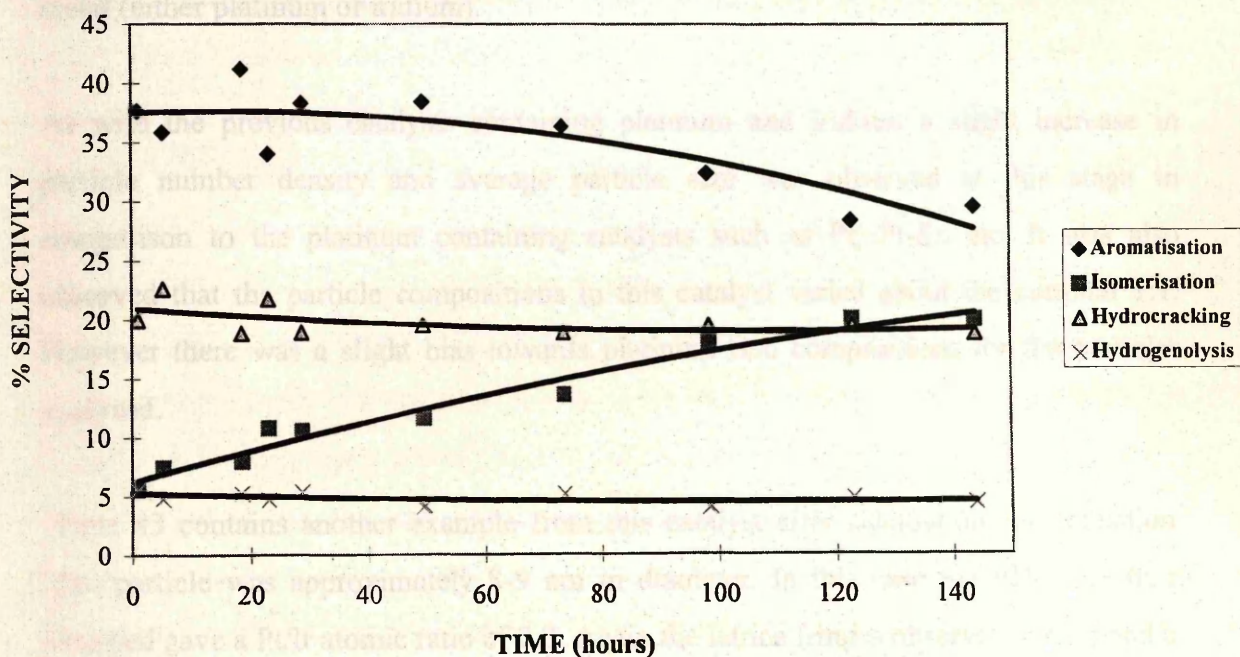


5.12. 0.3 wt% Pt - 0.3 wt% Ir - 0.3 wt% V/Al₂O₃

5.12.A. TEM observations

After calcination and reduction this catalyst showed similar features to the preceding Pt-Ir, Pt-Ir-0.03Ge and Pt-Ir-Ge catalysts. The metal component was found to be highly dispersed with only a small number of particulate particles being observed. EDX analysis of the larger 3-5 nm particles observed revealed that they were Pt-Ir alloys. An example of a particle formed at this stage is shown in plate 42. This particle was approximately 7 nm in diameter. The lattice fringes were observed at a spacing of 0.227 nm, which is consistent with the lattice spacing of the Pt-Ir alloy (rather than Pt or Ir alone).

Figure 5.11.7 Selectivities to the major reforming reactions over 0.3 wt% Pt - 0.3 wt% Ir - 0.3 wt% Ge/Al₂O₃



5.12. 0.3 wt% Pt - 0.3 wt% Ir - 0.3 wt% V/Al₂O₃

5.12.A. TEM observations

After calcination and reduction this catalyst showed similar features to the preceding Pt-Ir, Pt-Ir-0.03Ge and Pt-Ir-Ge catalysts. The metal component was found to be highly dispersed with only a small number of metallic particles being observed. EDX analysis of the larger 3-5 nm particles observed revealed that they were Pt-Ir alloys. An example of a particle formed at this stage is shown in plate 42. This particle was approximately 5 nm in diameter. The corresponding EDX spectrum (inset) revealed a Pt/Ir atomic ratio of 1.5. The lattice fringes visible in the image correspond to the {111} spacing of the fcc metal (either platinum or iridium).

As with the previous catalysts containing platinum and iridium a slight increase in particle number density and average particle size was observed at this stage in comparison to the platinum containing catalysts such as Pt, Pt-Sn etc. It was also observed that the particle compositions in this catalyst varied about the nominal 1:1. However there was a slight bias towards platinum rich compositions for the particles analysed.

Plate 43 contains another example from this catalyst after calcination and reduction. This particle was approximately 8-9 nm in diameter. In this case the EDX spectrum obtained gave a Pt/Ir atomic ratio of 2.3. Again the lattice fringes observed correspond to the {111} 0.227 nm fringes of the fcc metals.

At this stage it seems likely that the vanadium present in this catalyst was present as a highly dispersed oxide phase. (It is unlikely that V₂O₅ was reduced as far as the metal under the conditions used in this study²²⁷). Although EDX analysis could not find evidence for any vanadium species being in close contact with the metal particles (as has been discussed previously for Sn, Ge and Re species) this does not rule out the

possibility that a few weight percent of the vanadium present was in such a form. Indeed as will be shown, the reforming data suggests that it was highly likely that some of the vanadium was in close contact with the metal component.

After 144 hours on line some sintering of the Pt-Ir component was observed to have occurred. Again, EDX analysis of the particles formed after this time revealed that they were Pt-Ir alloys and that the particle compositions varied about the nominal 1:1. An example of a particle formed after 144 hours is shown in plate 44. This particle was approximately 12 nm in diameter and the EDX spectrum obtained (inset) revealed a Pt/Ir atomic ratio of 0.7. Another example is shown in plate 45. In this case a relatively large particle (20-30 nm) and a smaller particle (6-7 nm) were imaged in close proximity to one another. The EDX spectrum obtained from the larger particle (spectrum A) revealed that it was a Pt-Ir alloy with an approximate atomic ratio of Pt/Ir of 1.3. EDX analysis of the smaller particle (spectrum B) revealed the presence of platinum only. The lattice fringes visible in both particles corresponded to the {111} lattice of the metals. A number of dislocations were imaged in both particles.

Again it must be stated that although EDX analysis found no evidence for the presence of vanadium species in close proximity to the metal particles, this does not rule out the possibility that such species were present. Also, as with the previous catalysts, although substantial sintering was observed to have occurred after 144 hours on line, it is likely that a significant proportion of the metal component of this catalyst remained in the form of nanometer sized metal particles.

5.12.B. n-Octane reforming

The yields of individual products over the Pt-Ir-V/Al₂O₃ catalyst are listed versus time on line in table 5.12.1 and plotted in figures 5.12.1 to 5.12.6.

The yields of methane, ethane, propane, i-butane and n-butane over this catalyst are plotted in figure 5.12.1. The initial yield of methane over this catalyst was observed to be considerably lower than the corresponding yield over the Pt-Ir/Al₂O₃ catalyst (initial yield 42.8%). However, the initial methane yield of 16.4% was still relatively high when compared to most of the catalysts studied. This initial high yield decreased very rapidly in the initial stages of the run and then continued to decrease throughout the remainder of the run at a slower pace. Similar observations were made regarding the yield of ethane. The yield of propane was also high at the start of the run. This also decreased very quickly in the initial stages and then continued to decrease throughout the remainder of the run. This contrasts with the Pt-Ir catalyst where the yield of propane increased throughout the run, reaching the relatively high value of 12.4% after 144 hours. The yields of i-butane and n-butane were similar to those observed over a number of catalyst and decreased slowly as the run progressed.

The yields of cycloalkanes versus time on line over this catalyst are plotted in figure 5.12.2. The yields of all these products increased throughout the run with the largest increase being shown by the yield of C₈ cycloalkanes. This contrasts with the yield of these products over Pt-Ir/Al₂O₃ (table 5.5.1) where the yield of these products remained very low or zero throughout the run.

The yields of i-alkanes over Pt-Ir-V/Al₂O₃ are plotted in figure 5.12.3. The yields of i-pentane, i-hexane and i-heptane were similar to the yields obtained for most of the catalyst studied (the only exceptions being the starting yields of i-hexane and i-heptane which were low) and remained relatively constant throughout the run. The yield of i-octane, although very low initially (0.2%), increased sharply throughout the run and became the single major product after 144 hours on line (final yield 19.2%). This contrasts with the Pt-Ir/Al₂O₃ (figure 5.5.2) where the yield of all these products remained low.

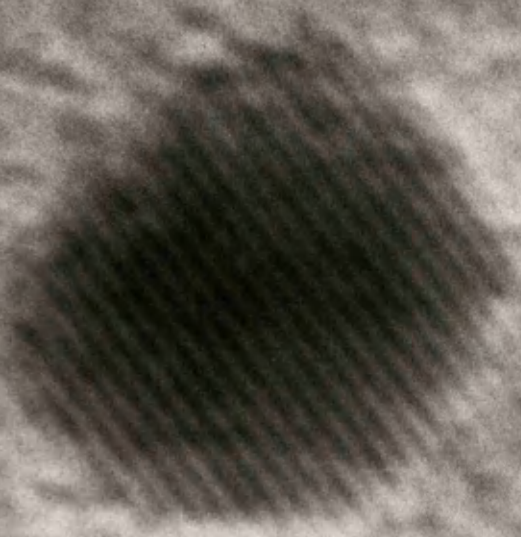
Plate 42

The yields of n-alkanes over this catalyst are plotted in figure 5.12.4. The yields of all these products were unusually low as compared with the corresponding yields over the majority of the catalysts studied.

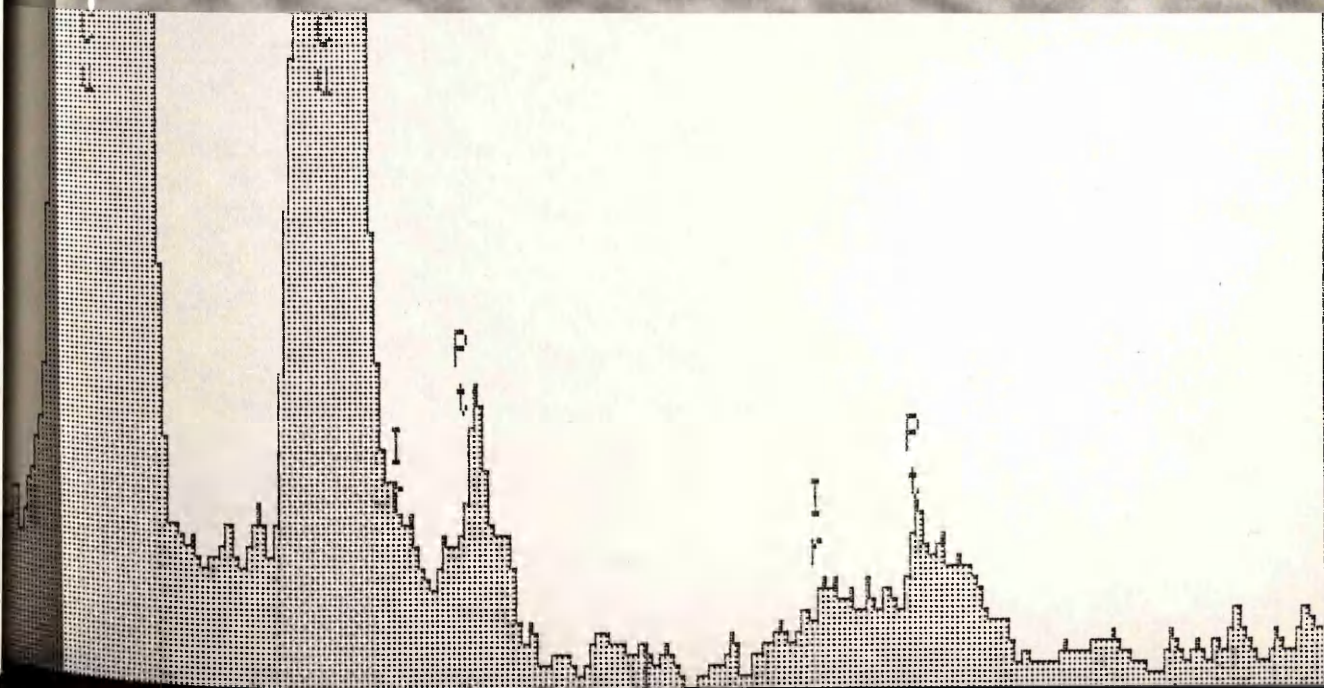
The yields of aromatics over this catalyst are plotted in figure 5.12.5. In a number of respects the yields of these products resembled the corresponding yields over the related Pt-Ir-0.03Ir/Al₂O₃ catalyst. In the initial stages the yields of benzene (5.8%) and toluene (16.1) were high whilst the yields of C₈ aromatics were relatively low (e.g. m/p-xylene 10.4%). The high initial yields of benzene and toluene decreased quite rapidly and this was accompanied by a corresponding increase in the yields of m/p-xylene (final value 16.5%), o-xylene and ethylbenzene (the trendlines in figure 5.12.5 for m/p xylene, o-xylene and ethylbenzene are not good representations of the actual data in the initial stages of the run).

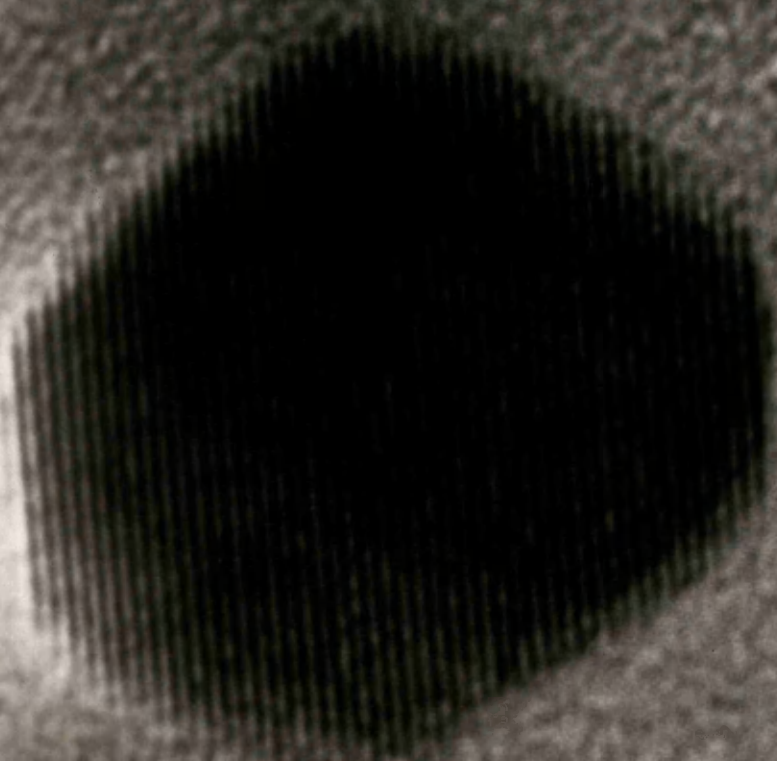
The conversion of n-octane versus time on line over this catalysts is plotted in figure 5.12.6. The initial conversion was essentially 100%. However this high conversion gradually decreased with time on line. The rate of loss of activity was relatively constant throughout the run. This contrasts with platinum, where the rate of deactivation was greatest in the initial stages, and also many of the bi(multi)-metallics (e.g. Pt-Sn, Pt-Ge, Pt-Ir-Ge) where the rate of deactivation was observed to increase as the run progressed.

The selectivities to the four major reforming reactions over Pt-Ir-V/Al₂O₃ are presented versus time on line in table 5.12.2 and plotted in figure 5.12.7. The selectivity to aromatics over this catalyst was observed to remain relatively high throughout the run (final value 38.5% versus 29.6% over Pt-Ir-Ge/Al₂O₃). The selectivity to isomerisation, as with many of the catalysts studied, was observed to increase during the run. The selectivity to hydrocracking appeared to increase, pass through a maximum, and then decrease. The selectivity to hydrogenolysis decreased rapidly in the initial stages and then continued to decrease at a slower rate during the remainder of the run.

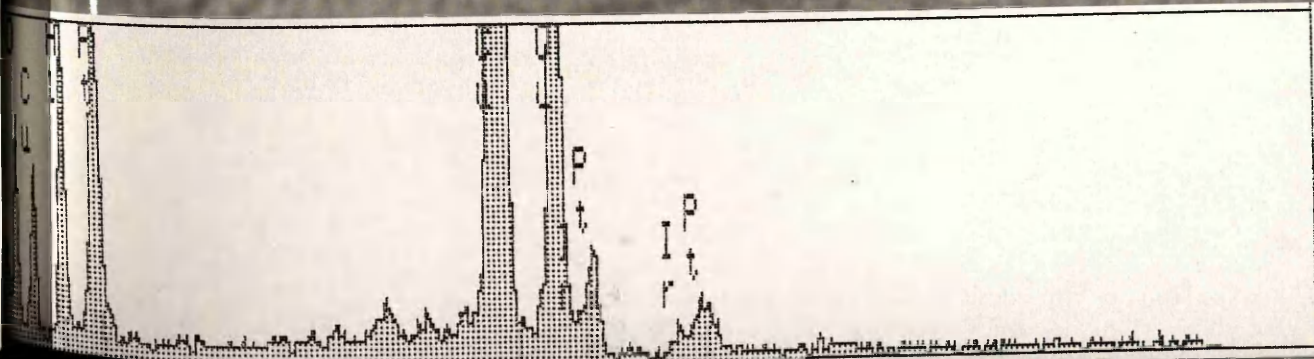


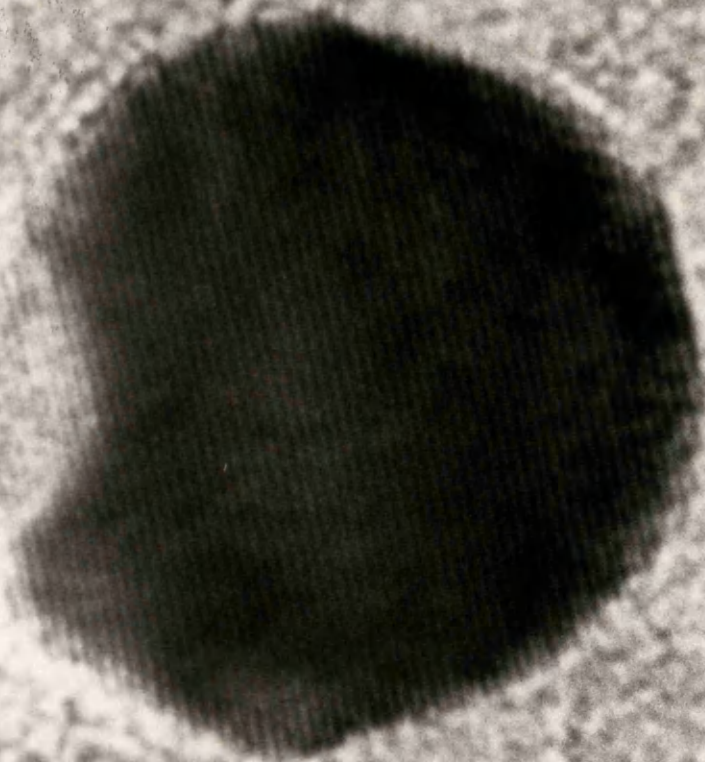
2 nm



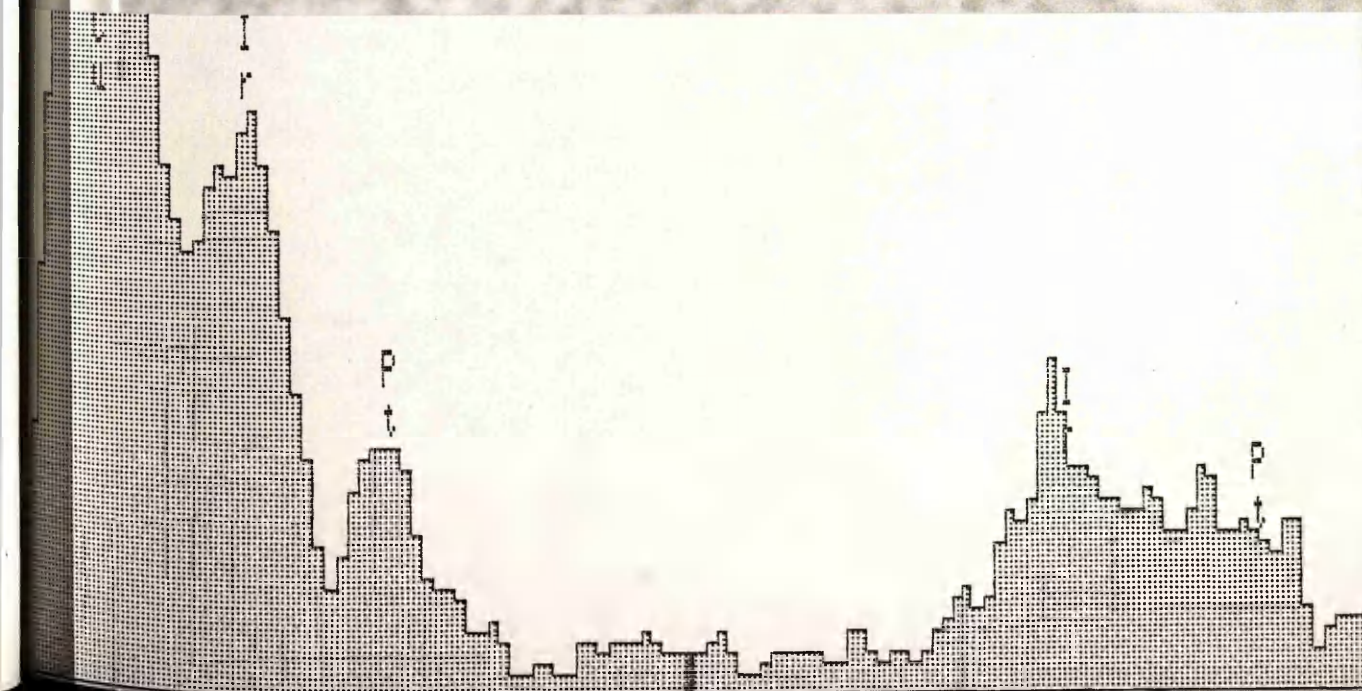


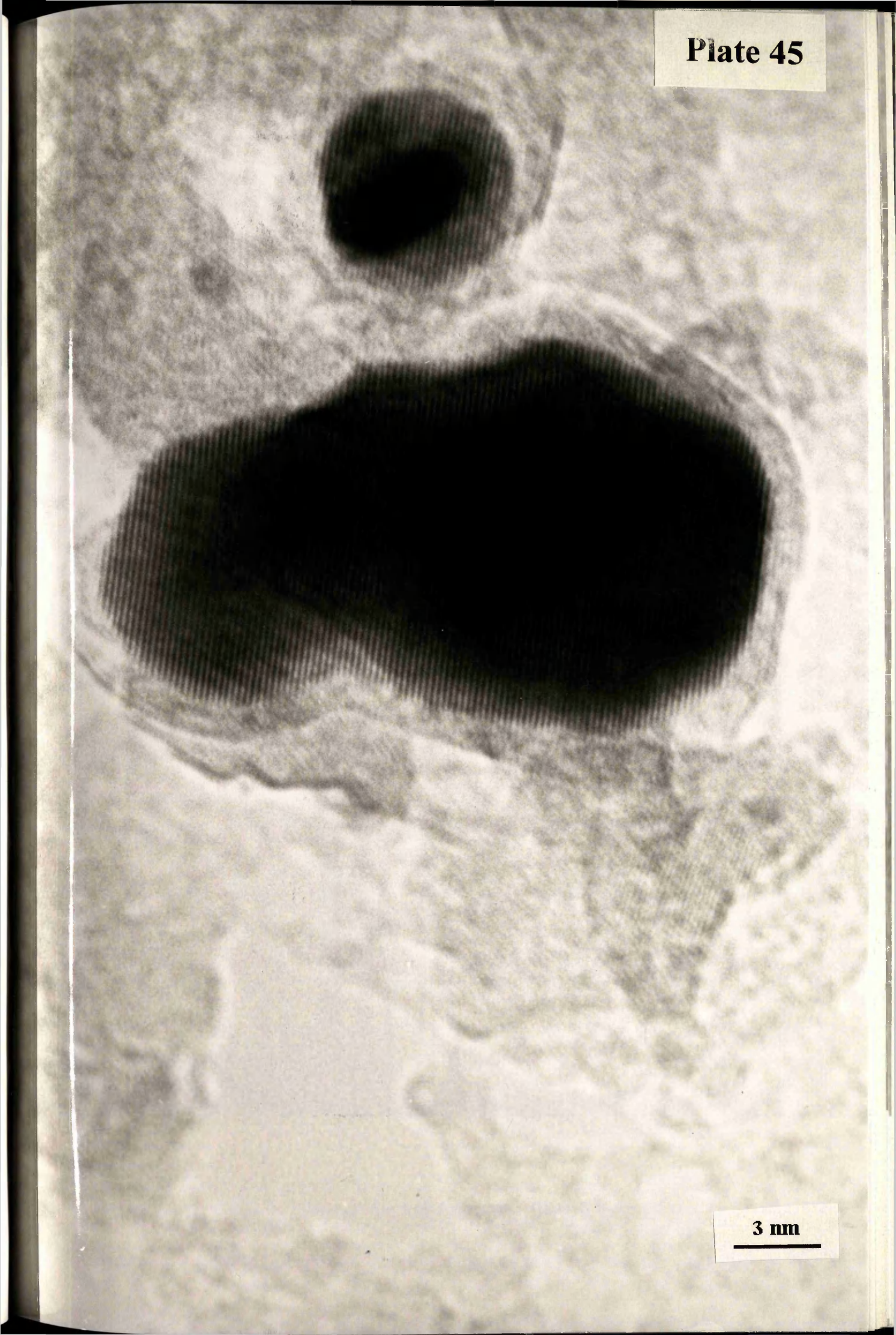
2 nm





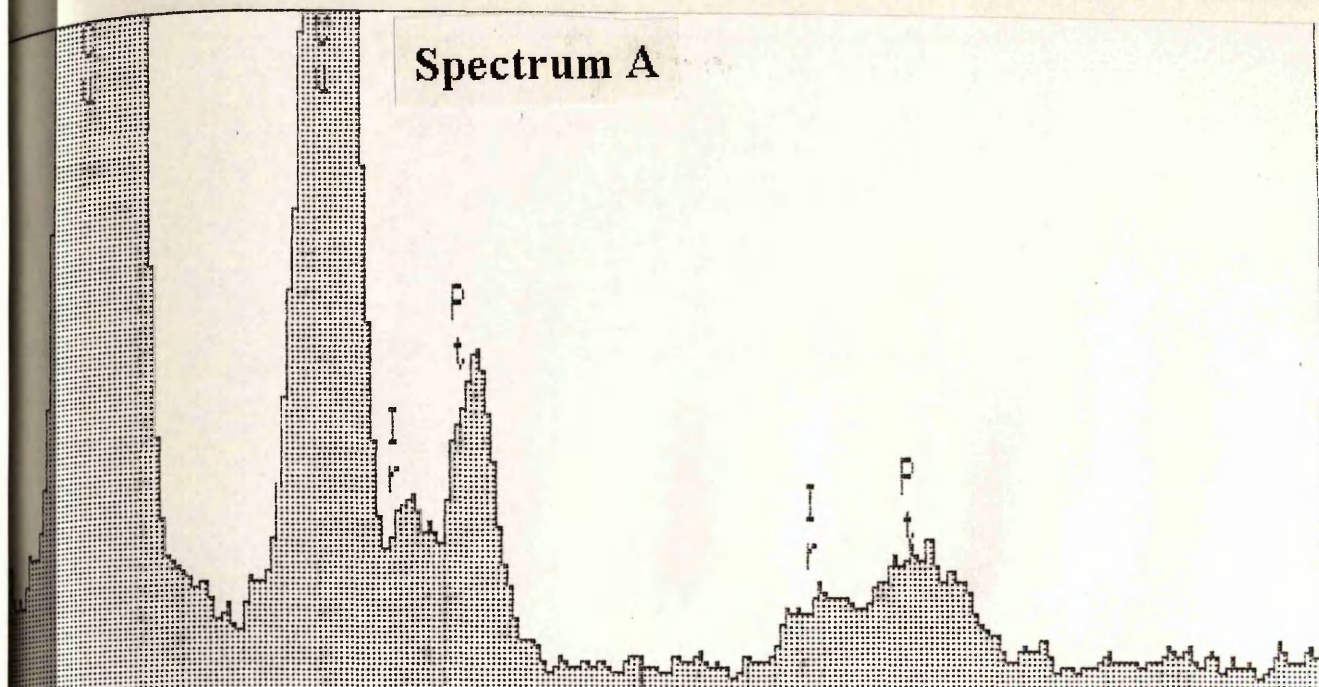
3 nm





3 nm

Spectrum A



Spectrum B

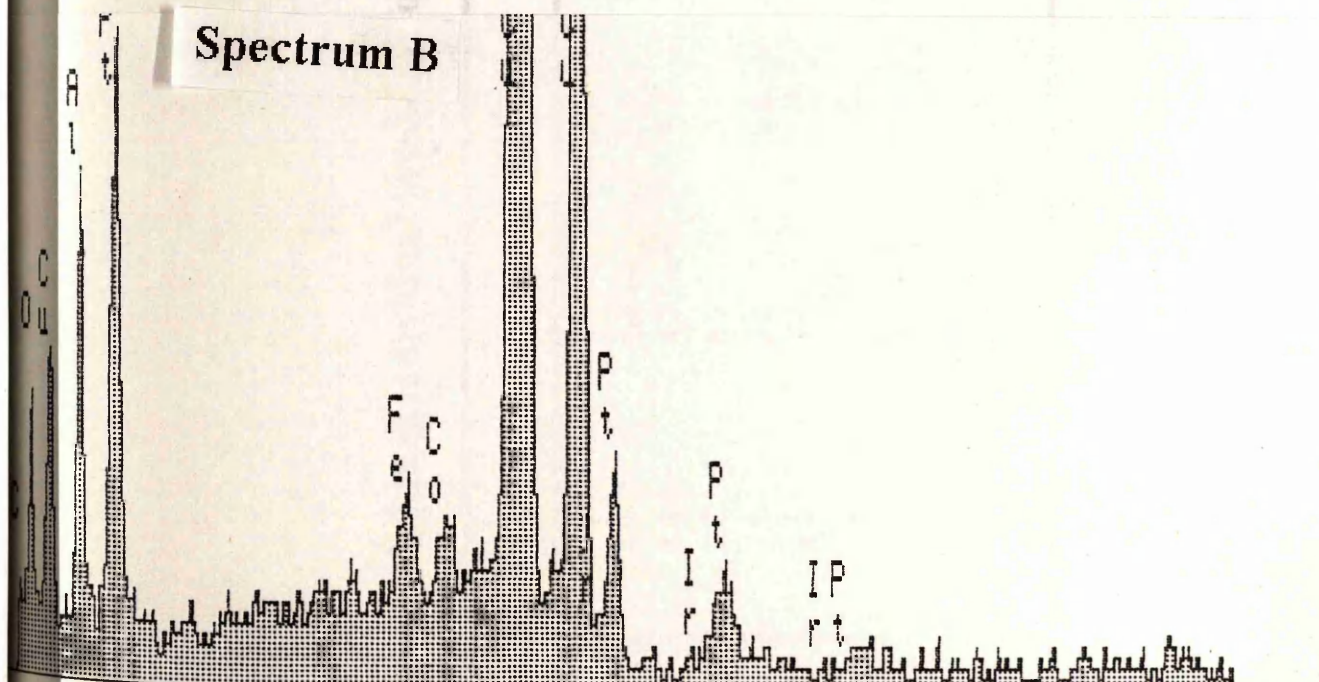


Table 5.12.1 Yields of individual products for catalyst 0.3 wt% Pt - 0.3 wt%Ir - 0.3 wt% V/Al₂O₃

Time (hours)	Methane	Ethane	Propane	i-Butane	n-Butane	c-Pentane	i-Pentane	n-Pentane
1.0	16.4	8.6	12.2	4.1	6.7	0.1	5.0	2.5
6.5	8.7	4.5	9.1	4.9	5.9	0.3	6.6	3.7
23.5	8.4	4.2	9.0	5.1	5.8	0.3	6.8	3.7
45.0	8.5	4.1	7.7	5.6	5.8	0.3	8.4	2.7
50.0	7.8	3.8	8.0	4.7	5.8	0.5	6.6	2.5
71.0	6.0	3.4	7.5	4.5	5.0	0.3	6.7	2.3
94.0	5.8	3.2	6.8	4.0	5.3	0.5	7.5	2.3
99.5	6.3	2.8	6.0	3.7	5.0	0.6	7.7	2.1
117.0	5.5	2.4	5.7	3.3	3.7	0.4	5.6	1.3
121.0	5.6	2.7	6.4	3.5	4.4	0.5	7.1	1.9
144.0	4.7	2.0	4.2	2.5	3.4	0.4	5.4	1.4

Table 5.12.1 (cont) Yields of individual products for 0.3 wt% Pt - 0.3 wt%Ir - 0.3 wt% V/Al₂O₃

Time (hours)	C6 c-Alkane	i-Hexane	n-Hexane	C7 c-Alkane	i-Heptane	n-Heptane	C8 c-Alkane	i-Octane
1.0	0.3	2.1	0.8	0.1	0.3	0.1	0.0	0.2
6.5	0.6	4.6	1.8	0.5	1.2	0.3	0.4	2.5
23.5	0.6	5.5	2.7	0.7	1.4	0.4	0.8	3.8
45.0	0.5	6.5	2.9	0.9	1.9	0.5	1.2	6.9
50.0	0.8	5.8	2.5	0.9	1.8	0.5	1.0	6.8
71.0	0.6	5.6	2.0	0.8	1.6	0.3	1.6	13.5
94.0	0.9	5.8	2.7	1.0	1.9	0.4	1.5	12.1
99.5	1.1	5.7	3.0	1.3	2.1	0.6	1.9	12.8
117.0	0.9	4.8	1.9	1.2	1.7	0.3	1.7	14.7
121.0	1.0	5.6	2.7	1.2	2.0	0.6	2.0	14.2
144.0	0.9	4.5	2.5	1.1	1.8	0.4	2.4	19.2

Table 5.12.1 (cont) Yields of individual products for 0.3 wt% Pt - 0.3 wt%Ir - 0.3 wt% V/Al₂O₃

Time (hours)	Benzene	Toluene	Ethyl- Benzene	m/p- Xylene	o-Xylene	C9 Aromatic	Total Conversion
1.0	5.8	16.1	2.0	10.4	5.6	0.3	99.9
6.5	2.6	8.8	4.5	18.8	8.3	0.9	99.4
23.5	2.0	6.8	4.1	18.3	7.3	0.9	98.9
45.0	1.5	5.0	3.5	16.1	6.4	0.9	97.8
50.0	1.5	5.7	4.1	17.8	7.1	1.0	97.1
71.0	0.9	4.3	3.3	17.6	7.1	1.2	96.2
94.0	1.1	4.3	3.5	16.6	6.8	1.2	95.2
99.5	1.0	3.8	3.2	16.0	6.7	1.0	94.2
117.0	0.9	4.2	4.0	19.9	8.2	1.5	93.9
121.0	0.9	3.9	3.4	17.1	6.9	1.5	95.0
144.0	0.9	4.2	4.6	16.5	7.5	1.9	92.5

Figure 5.12.1 Yields of individual products over 0.3 wt% Pt - 0.3 wt% Ir - 0.3 wt% V/Al₂O₃

Table 5.12.2 Selectivities for catalyst 0.3 wt% Pt - 0.3 wt% Ir - 0.3 wt% V/Al₂O₃

Time (hours)	Selectivity to Aromatics	Selectivity to Isomerisation	Selectivity to Hydrocracking	Selectivity to Hydrogenolysis
1.0	40.2	0.5	11.2	16.5
6.5	44.2	3.8	16.1	8.7
23.5	39.9	5.3	17.6	8.5
45.0	34.1	9.0	21.0	8.7
50.0	38.4	8.9	17.6	8.0
71.0	35.8	15.7	17.5	6.3
94.0	35.1	14.7	18.2	6.1
99.5	33.4	15.9	18.2	6.7
117.0	41.2	17.4	14.6	5.9
121.0	35.5	17.1	17.0	5.8
144.0	38.5	22.8	13.4	5.1

Figure 5.12.1 Yields of individual products over 0.3 wt% Pt - 0.3 wt% Ir - 0.3 wt% V/Al₂O₃

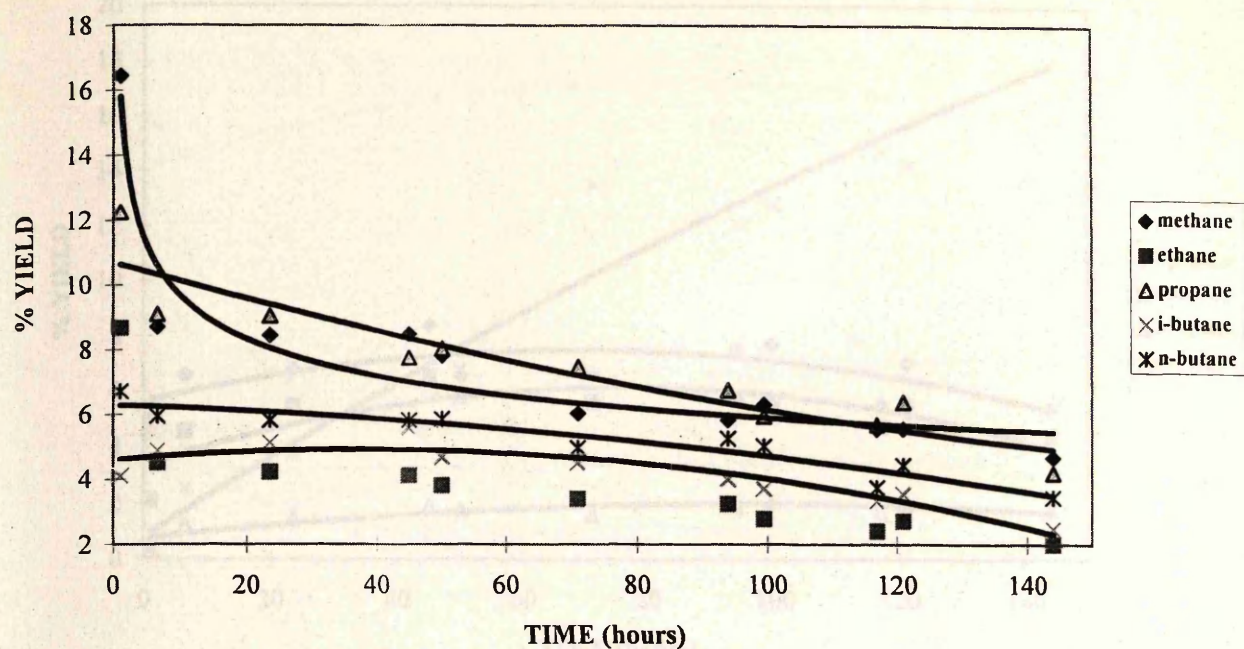


Figure 5.12.2 Yields of cycloalkanes over 0.3 wt% Pt - 0.3 wt% Ir - 0.3 wt% V/Al₂O₃

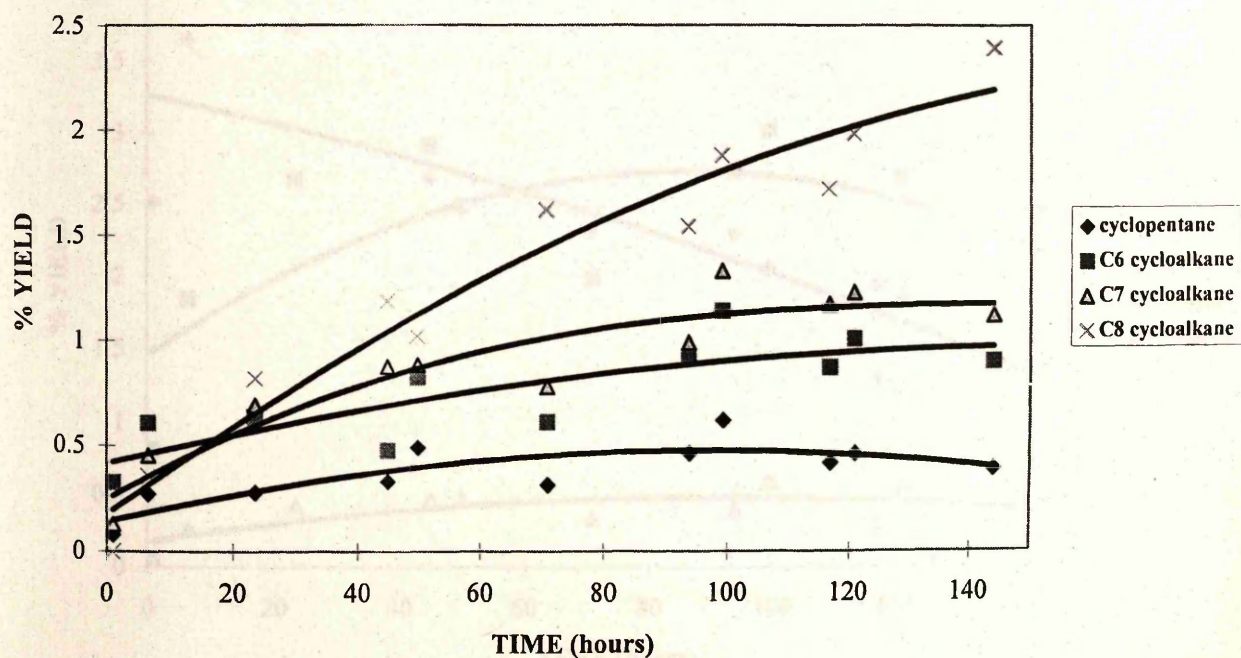


Figure 5.12.3 Yields of i-alkanes over 0.3 wt% Pt - 0.3 wt% Ir - 0.3 wt% V/Al₂O₃

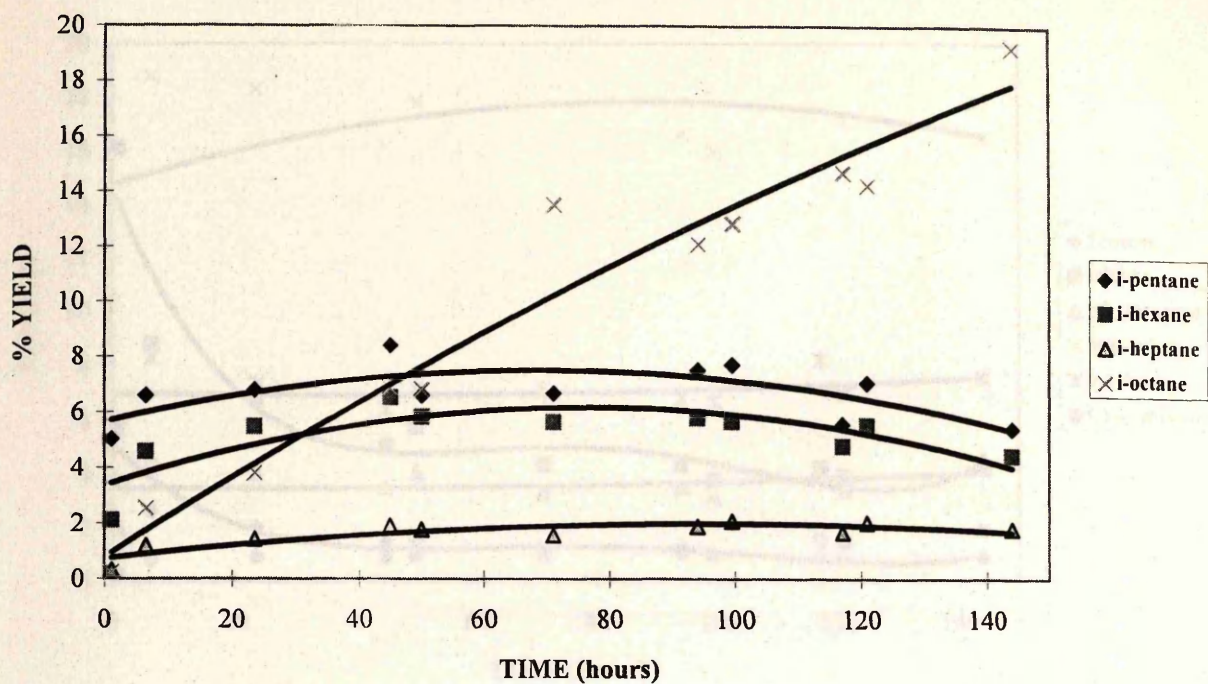


Figure 5.12.4 Yields of n-alkanes over 0.3 wt% Pt - 0.3 wt% Ir - 0.3 wt% V/Al₂O₃

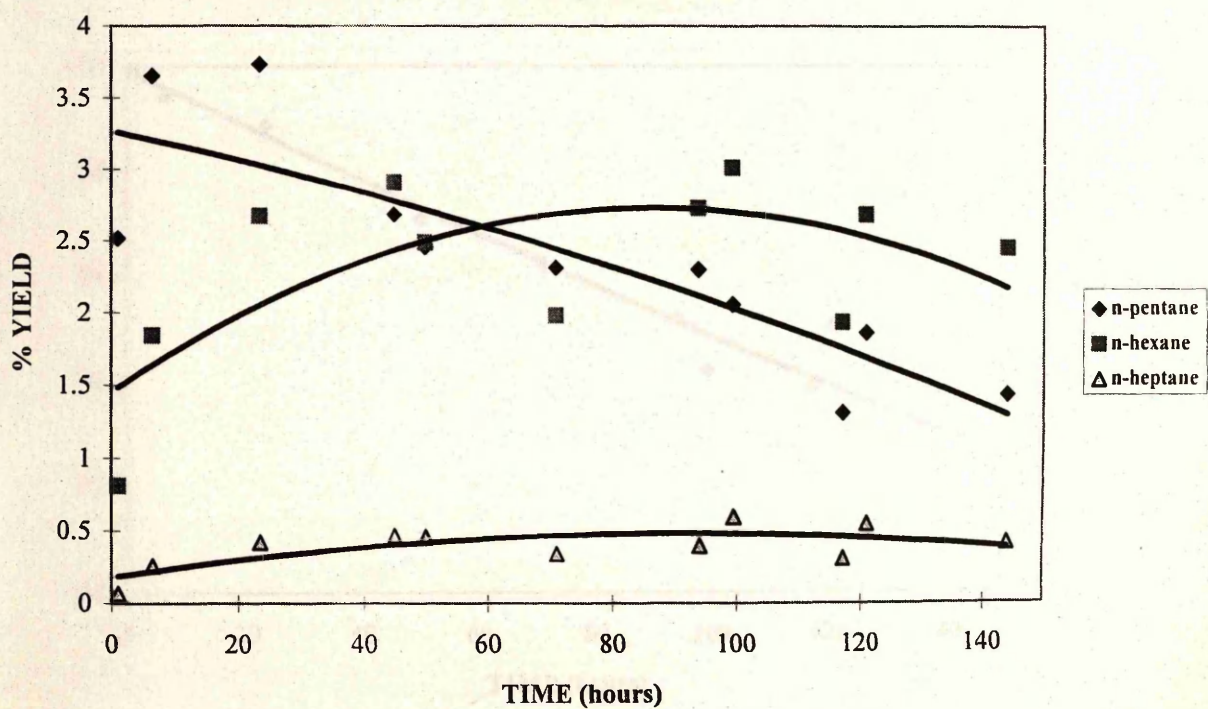


Figure 5.12.5 Yields of aromatics over 0.3 wt% Pt - 0.3 wt% Ir - 0.3 wt% V/Al₂O₃

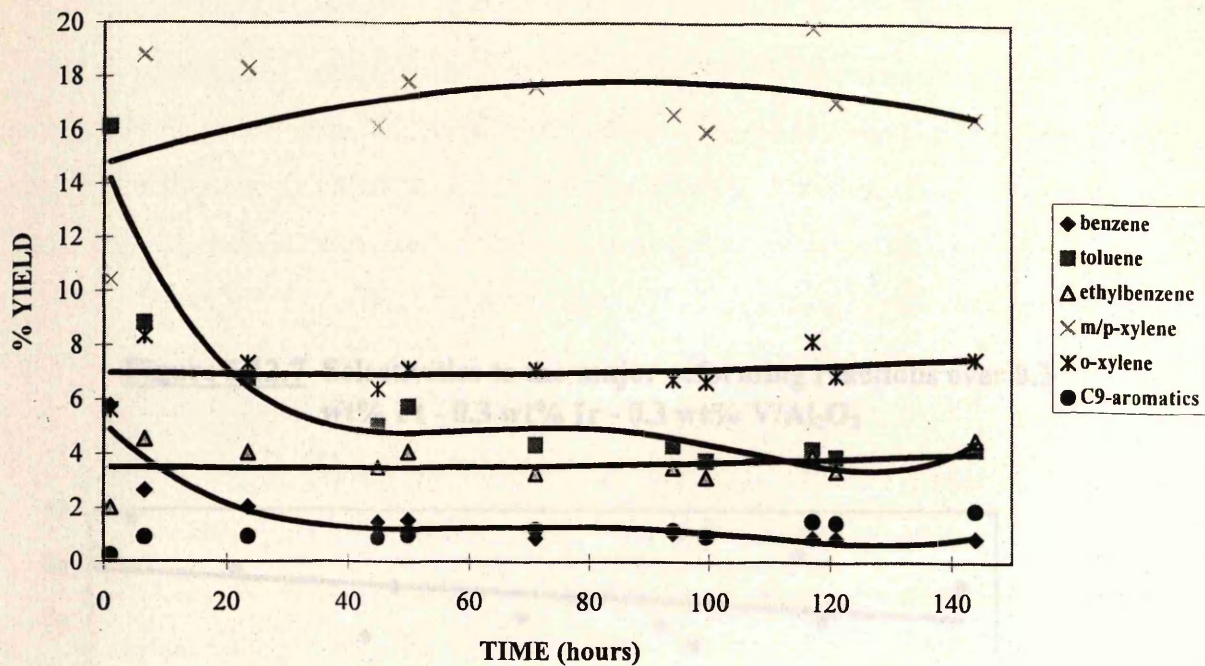
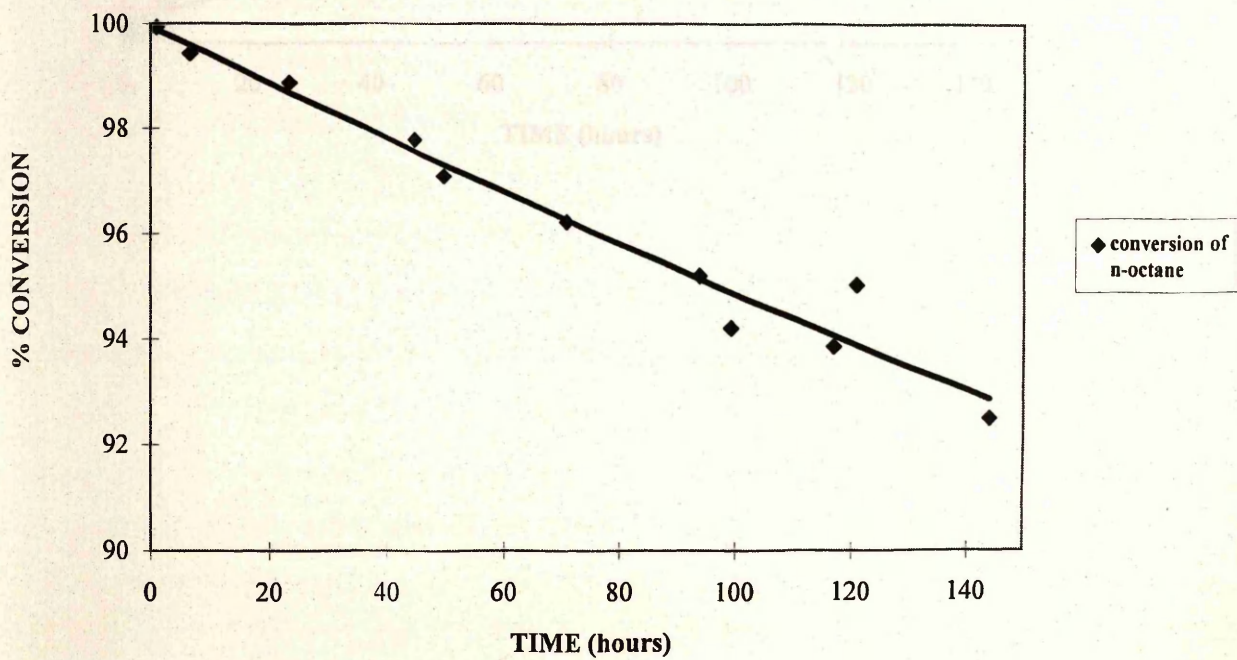


Figure 5.12.6 Conversion of n-octane over 0.3 wt% Pt - 0.3 wt% Ir - 0.3 wt% V/Al₂O₃

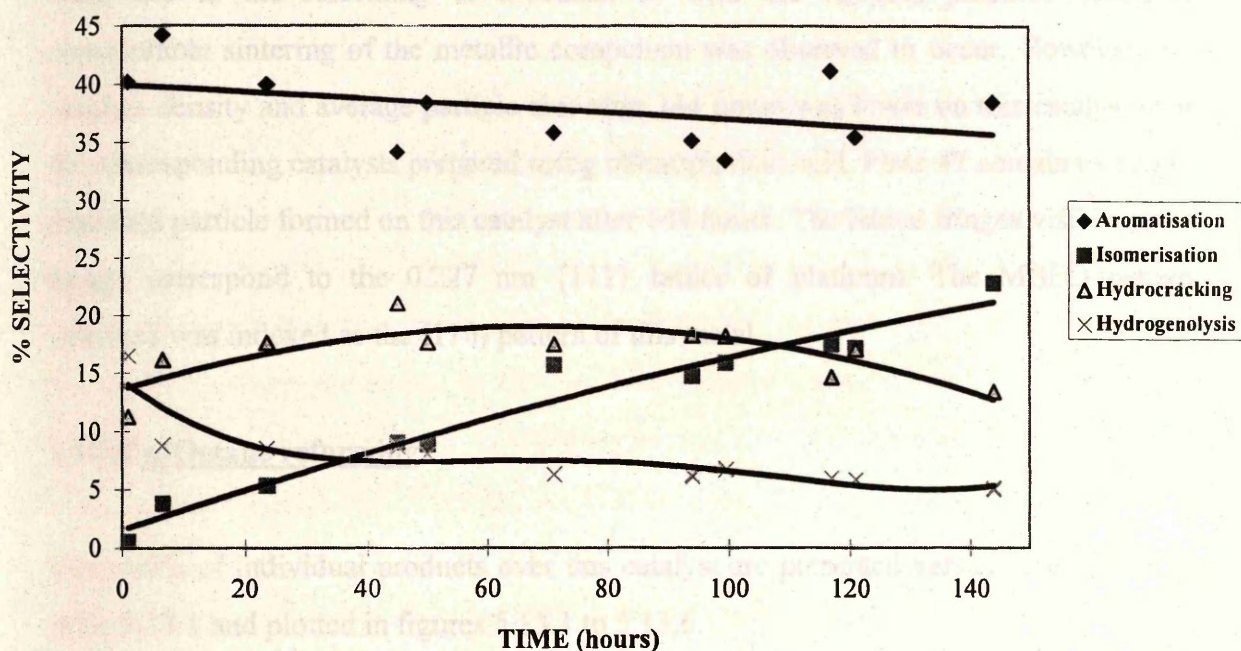


5.13. 0.3 wt% Pt/Al₂O₃ (Pt/acachi)

5.13.4 TEM observations

After calcination and reduction the metallic component of this catalyst was found to be in a highly dispersed state. The number of directly observable metal particles ($> 10^2$ nm) was lower than on the catalyst prepared using H₂PtCl₆. However, it is difficult to be more specific because the overall number of metal particles was very low in both cases. Figure 5.12.6 shows a 5 nm platinum particle formed on this catalyst after calcination and reduction.

Figure 5.12.7 Selectivities to the major reforming reactions over 0.3 wt% Pt - 0.3 wt% Ir - 0.3 wt% V/Al₂O₃



5.13. 0.3 wt% Pt/Al₂O₃ [Pt(acac)₂]

5.13.A TEM observations

After calcination and reduction the metallic component of this catalyst was found to be in a highly dispersed state. The number of directly observable metal particles ($> 1\text{-}2\text{ nm}$) was lower than on the catalyst prepared using H_2PtCl_6 . However, it is difficult to be more specific because the overall number of metal particles was very low in both cases. Plate 46 shows a 5 nm platinum particle formed on this catalyst after calcination and reduction.

With use in the reforming of n-octane, as with the H_2PtCl_6 prepared catalysts, considerable sintering of the metallic component was observed to occur. However, the number density and average particle size after 144 hours was lower on this catalyst than the corresponding catalysts prepared using chloroplatinic acid. Plate 47 contains a 12 nm platinum particle formed on this catalyst after 144 hours. The lattice fringes visible in the image correspond to the 0.227 nm {111} lattice of platinum. The MBED pattern obtained was indexed as the (110) pattern of this metal.

5.13.B n-Octane reforming

The yields of individual products over this catalyst are presented versus time on line in table 5.13.1 and plotted in figures 5.13.1 to 5.13.6.

The yields of methane, ethane, propane, i-butane and n-butane over this catalyst are plotted in figure 5.13.1. The initial yield of methane over this catalyst was slightly higher than the corresponding yield over the catalyst prepared using H_2PtCl_6 (figure 5.1.1: 7.8% versus 5.8%). This yield decreased slightly in the initial stages but remained higher than the value over the H_2PtCl_6 catalyst throughout the remainder of the run. The yield of ethane was slightly lower over this catalyst.

The yields of propane, i-butane and n-butane showed similar trends to those observed on the H_2PtCl_6 catalyst although the actual yields were significantly lower over the $\text{Pt}(\text{acac})_2$ prepared catalyst.

The yields of cycloalkanes over this catalyst are plotted in figure 5.13.2. The yields of cyclopentane and C_6 cycloalkanes over this catalyst were similar to those over the chloroplatinic acid prepared catalyst (figure 5.1.2). However the yields of C_7 and C_8 species were initially higher over this catalyst. The yields of C_8 cycloalkanes over the $\text{Pt}(\text{acac})_2$ prepared catalyst increased during the run and remained above the corresponding yield of the H_2PtCl_6 prepared catalyst (in which the yield of C_8 cycloalkanes increased in a similar manner).

The yields of i-alkanes are plotted in figure 5.13.3. This catalyst showed very similar trends in the yields of i-alkanes to those observed with the H_2PtCl_6 prepared catalyst (compare with figure 5.1.3). However the yields of i-pentane and i-hexane were lower over this catalyst whilst the yields of i-heptane were higher. The yields of these products remained relatively constant through the run. The yield of i-octane was found to increase sharply throughout the length of the run. The yield of i-octane over this catalyst was similar at all stages of the run to the corresponding values over the H_2PtCl_6 prepared catalyst (final values: 23.7% and 23.0% respectively).

The yields of n-alkanes over this catalyst are plotted in figure 5.13.4. The yields of n-hexane and n-heptane were similar to those obtained over the H_2PtCl_6 prepared catalyst (figure 5.1.4). The yield of n-hexane remained relatively constant while the yield of n-heptane increased slightly. The yield of n-pentane was slightly lower than the corresponding yields over the H_2PtCl_6 catalyst.

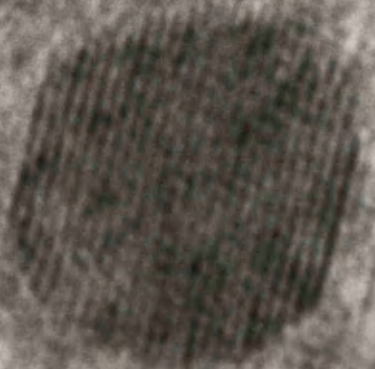
The yield of aromatics over this catalyst are plotted in figure 5.13.5. The yields of aromatics over this catalyst were essentially similar to those obtained over the H_2PtCl_6

catalyst (figure 5.1.5). The only major difference observed was that the initial yield of toluene was substantially higher (8.0%) over this catalyst as compared to the H_2PtCl_6 prepared catalyst (3.7%). This high toluene yield decreased rapidly and after 144 hours both these catalyst showed similar aromatic yields.

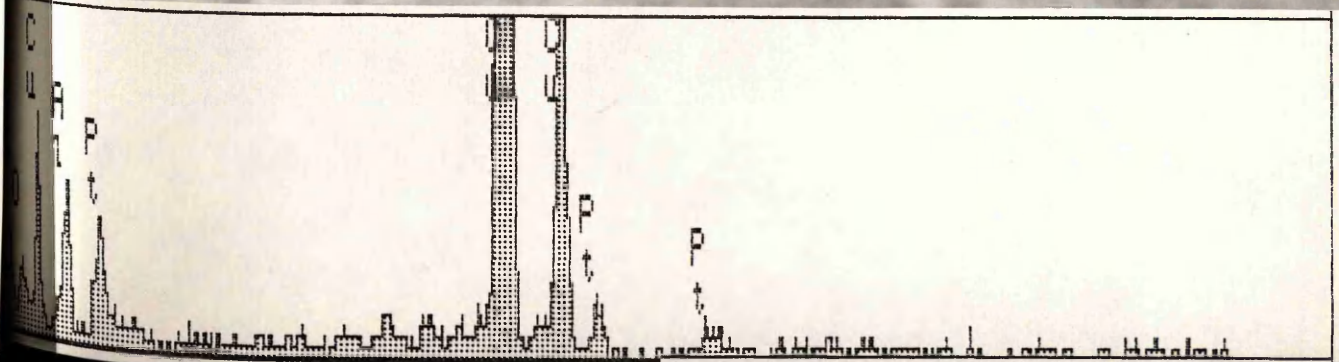
The conversion of n-octane over the $\text{Pt}(\text{acac})_2$ prepared catalyst is plotted versus time on line in figure 5.13.6. In comparison to the H_2PtCl_6 catalyst (figure 5.1.6) the initial conversion is significantly lower over this catalyst and decreases faster resulting in a much reduced final conversion (81.9% as opposed to 90.2% for the H_2PtCl_6 prepared catalyst).

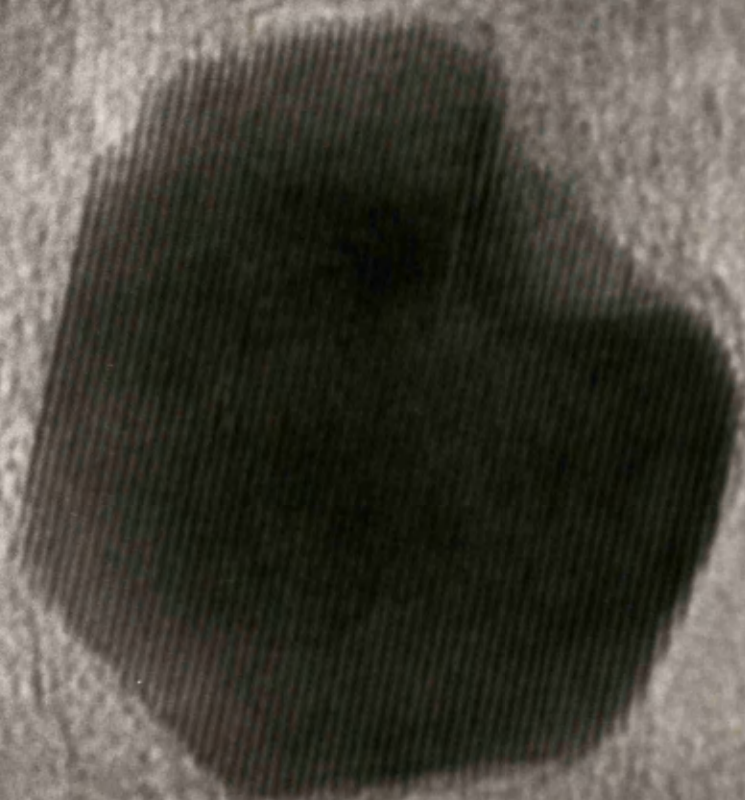
The selectivities to the four main reforming reactions for this catalyst are presented versus time on line in table 5.13.2 and plotted in figure 5.13.7. These selectivities follow similar trends to those observed over the H_2PtCl_6 catalyst. The selectivity to aromatisation decreases with time on line whilst the selectivity to isomerisation increases. The selectivity to hydrocracking and hydrogenolysis remained relatively unchanged. However on this catalyst the selectivities to isomerisation and hydrogenolysis were slightly higher at all stages of the run whilst the selectivity to hydrocracking was lower.

Plate 46



3 nm





3 nm

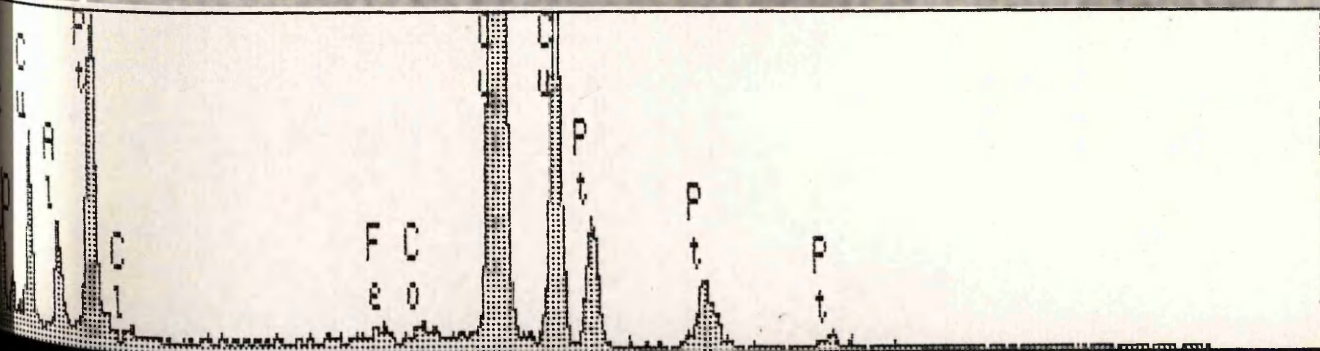


Table 5.13.1 Yields of individual products for catalyst 0.3 wt% Pt/Al₂O₃ [Pt(acac)₂]

Time (hours)	Methane	Ethane	Propane	i-Butane	n-Butane	c-Pentane	i-Pentane	n-Pentane
1.5	7.8	2.9	5.7	2.3	3.9	0.1	4.4	2.8
5.0	6.0	2.7	5.6	2.4	4.3	0.3	4.8	3.4
16.0	5.5	2.2	5.2	2.5	3.7	0.1	4.9	2.2
20.8	5.8	2.2	5.2	2.5	3.7	0.1	4.6	2.3
46.0	5.6	2.2	5.3	2.6	3.8	0.2	4.8	2.1
64.0	5.5	2.2	4.9	2.6	4.1	0.3	6.2	2.1
69.0	5.7	2.1	4.9	2.4	3.3	0.2	4.3	2.0
88.0	4.6	1.9	4.3	2.3	3.8	0.3	4.5	2.7
117.0	5.2	2.0	4.5	2.2	3.4	0.2	4.3	2.3
144.0	5.6	2.0	4.3	2.2	3.0	0.2	4.0	1.2

Table 5.13.1 (cont) Yields of individual products for catalyst 0.3 wt% Pt/Al₂O₃ [Pt(acac)₂]

Time (hours)	C6 c-Alkane	i-Hexane	n-Hexane	C7 c-Alkane	i-Heptane	n-Heptane	C8 c-Alkane	i-Octane
1.5	0.7	5.0	2.6	1.2	2.3	0.3	0.9	5.4
5.0	0.9	5.3	2.5	1.4	2.4	0.3	1.2	8.8
16.0	0.5	5.2	1.7	0.8	1.9	0.8	1.4	14.6
20.8	0.6	4.9	2.0	0.8	2.0	0.7	1.6	14.6
46.0	0.7	5.3	2.3	1.2	2.2	1.0	2.3	18.4
64.0	0.5	5.8	2.6	1.0	2.0	1.0	2.6	19.2
69.0	0.6	4.7	1.9	1.0	1.8	1.1	3.2	20.7
88.0	0.8	5.1	2.4	1.2	2.0	0.9	3.2	21.7
117.0	0.7	4.8	2.1	0.8	1.5	1.4	3.5	22.7
144.0	0.4	4.0	1.8	0.8	1.5	1.4	3.6	23.7

Table 5.13.1 (cont) Yields of individual products for catalyst 0.3 wt% Pt/Al₂O₃ [Pt(acac)₂]

Time (hours)	Benzene	Toluene	Ethyl- Benzene	m/p- Xylene	o-Xylene	C9 Aromatic	Total Conversion
1.5	1.8	8.0	8.9	18.4	10.3	0.8	96.6
5.0	1.3	5.4	8.2	17.1	9.0	1.0	94.3
16.0	0.9	3.8	7.4	18.6	9.3	1.3	94.7
20.8	0.9	3.7	7.2	17.1	8.7	1.6	92.7
46.0	0.7	2.6	5.4	14.1	7.0	0.9	90.8
64.0	0.6	2.1	4.3	12.7	5.6	0.9	88.9
69.0	0.6	2.0	4.2	12.4	5.5	0.9	85.7
88.0	0.4	1.7	3.7	11.1	4.9	0.9	84.2
117.0	0.4	1.7	3.5	10.9	4.6	0.8	83.4
144.0	0.4	1.7	3.4	11.0	5.0	0.8	81.9

Table 5.13.2 Selectivity to the major reforming reactions for 0.3 wt% Pt/Al₂O₃ [Pt(acac)₂]

Time (hours)	Selectivity to Aromatics	Selectivity to Isomerisation	Selectivity to Hydrocracking	Selectivity to Hydrogenolysis
1.5	49.9	8.0	12.2	8.1
5.0	44.5	11.9	13.3	6.4
16.0	43.7	17.5	13.3	5.9
20.8	42.3	17.9	12.8	6.2
46.0	33.8	22.8	14.0	6.2
64.0	29.5	23.8	16.4	6.2
69.0	30.0	26.2	13.4	6.7
88.0	26.8	28.2	14.1	5.5
117.0	26.1	29.1	13.5	6.2
144.0	27.1	30.7	12.4	6.8

Figure 5.13.1 Yields of individual products over 0.3 wt% Pt/Al₂O₃ [Pt(acac)₂]

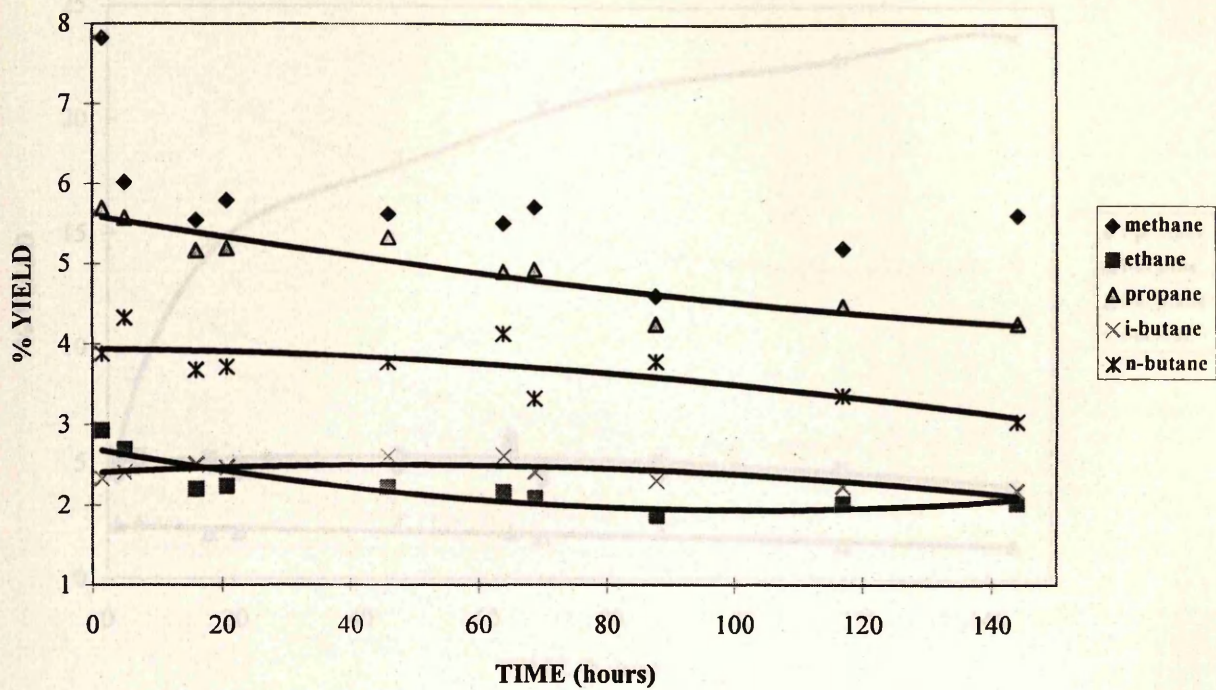


Figure 5.13.2 Yields of cycloalkanes over 0.3 wt% Pt/Al₂O₃ [Pt(acac)₂]

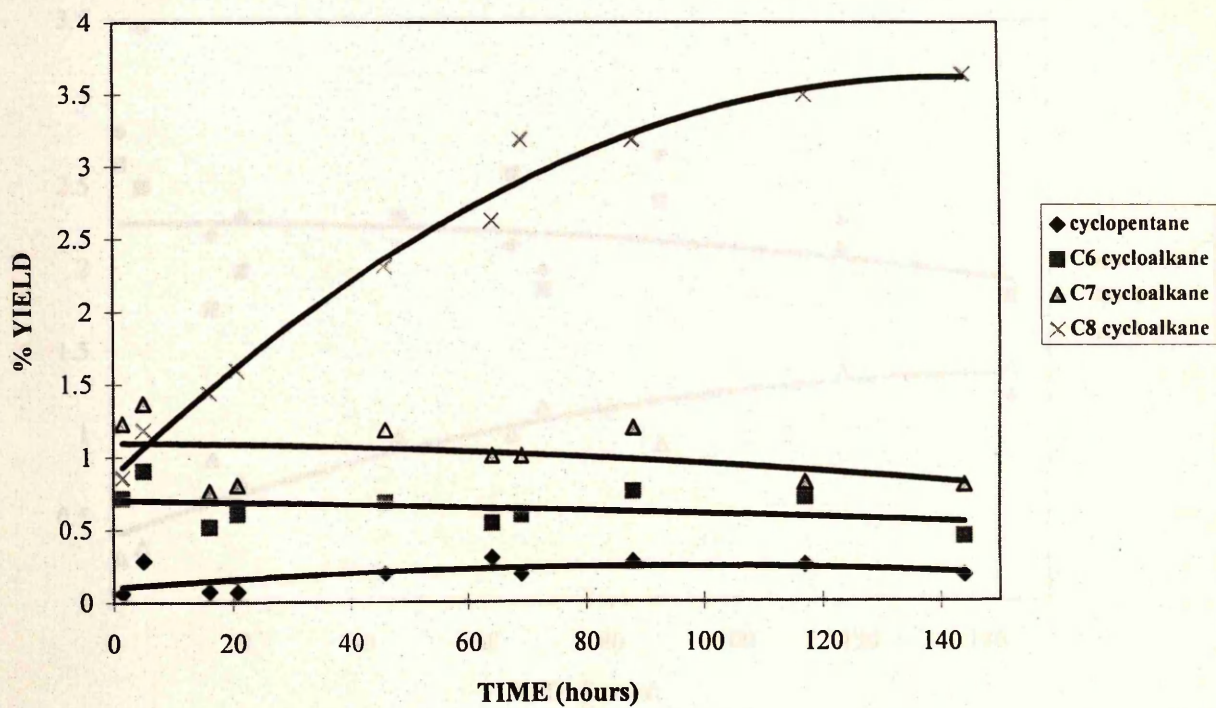


Figure 5.13.3 Yields of i-alkanes over 0.3 wt% Pt/Al₂O₃ [Pt(acac)₂]

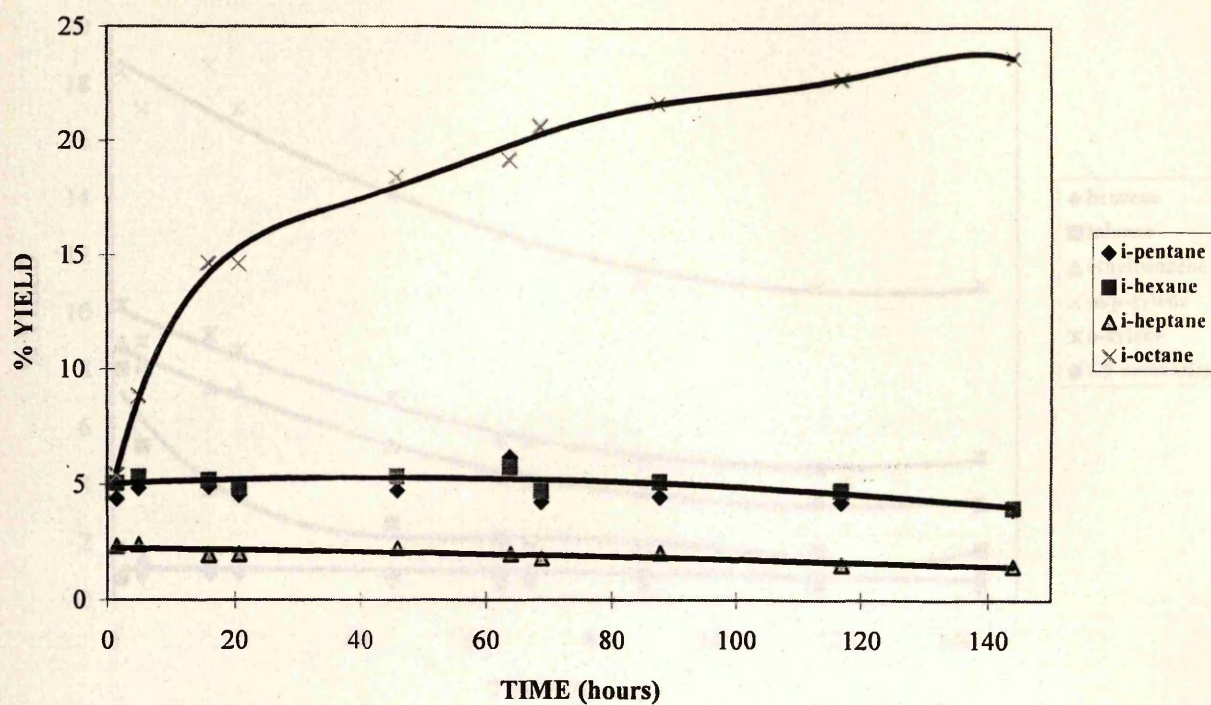


Figure 5.13.4 Yields of n-alkanes over 0.3 wt% Pt/Al₂O₃ [Pt(acac)₂]

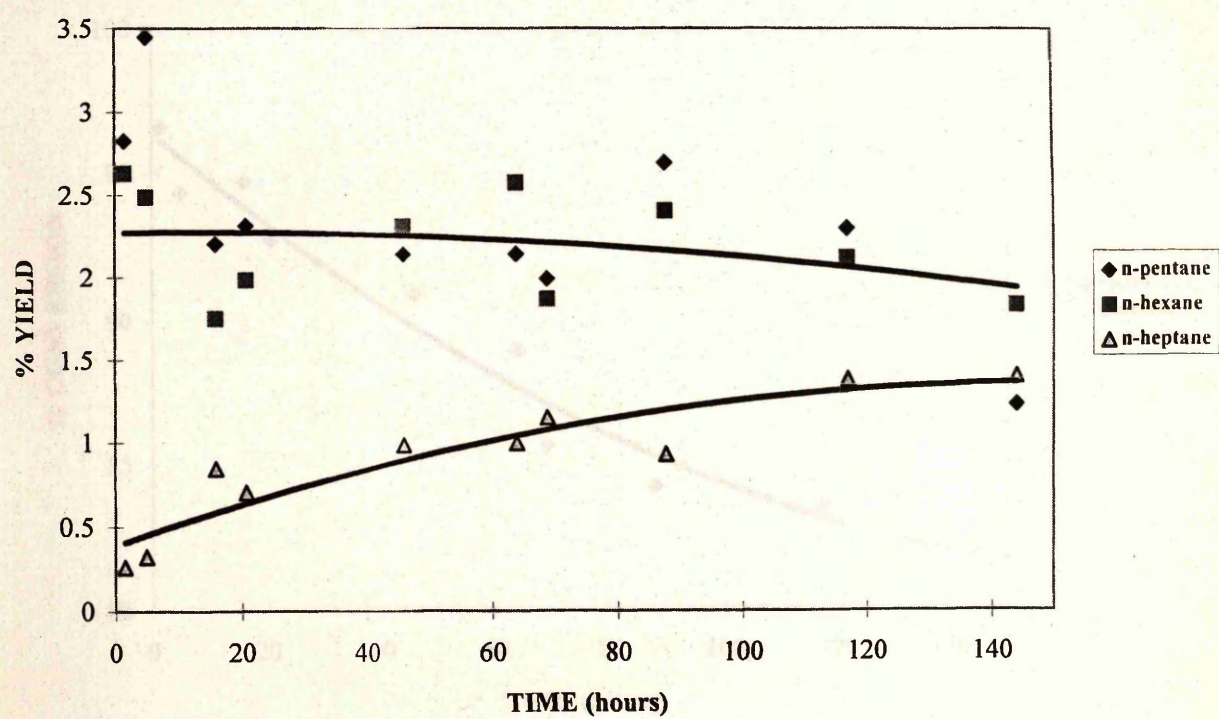


Figure 5.13.5 Yields of aromatics over 0.3 wt% Pt/Al₂O₃ [Pt(acac)₂]

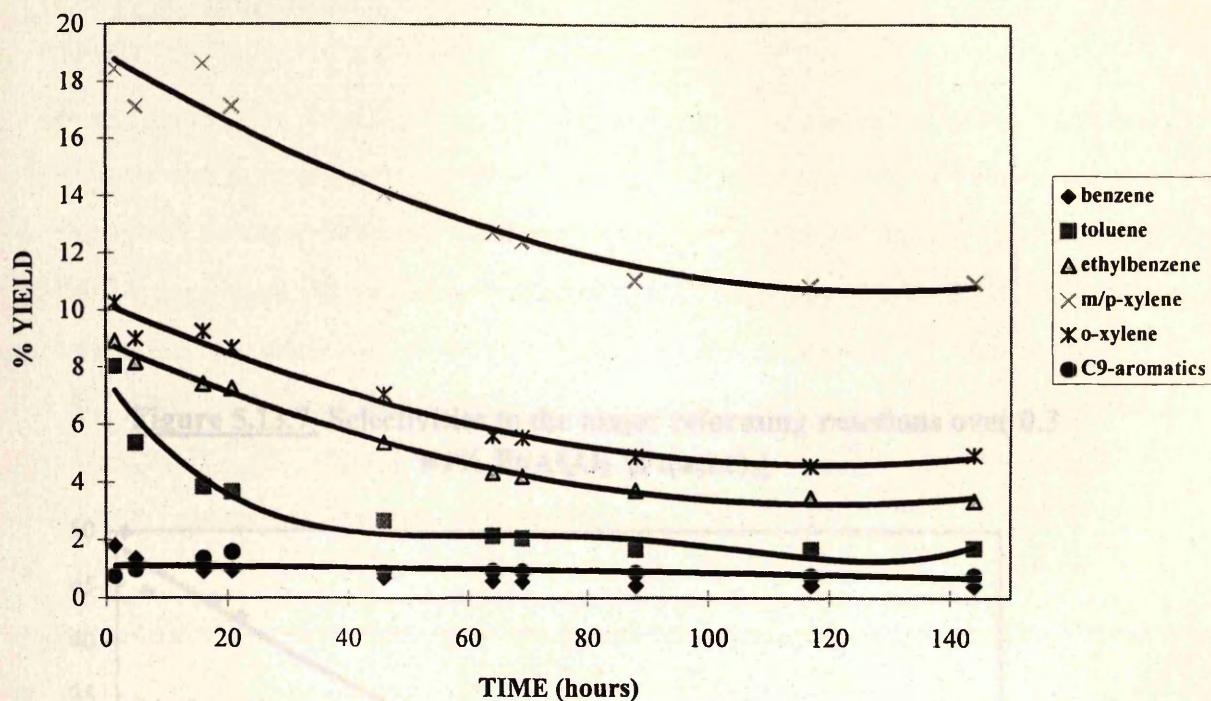
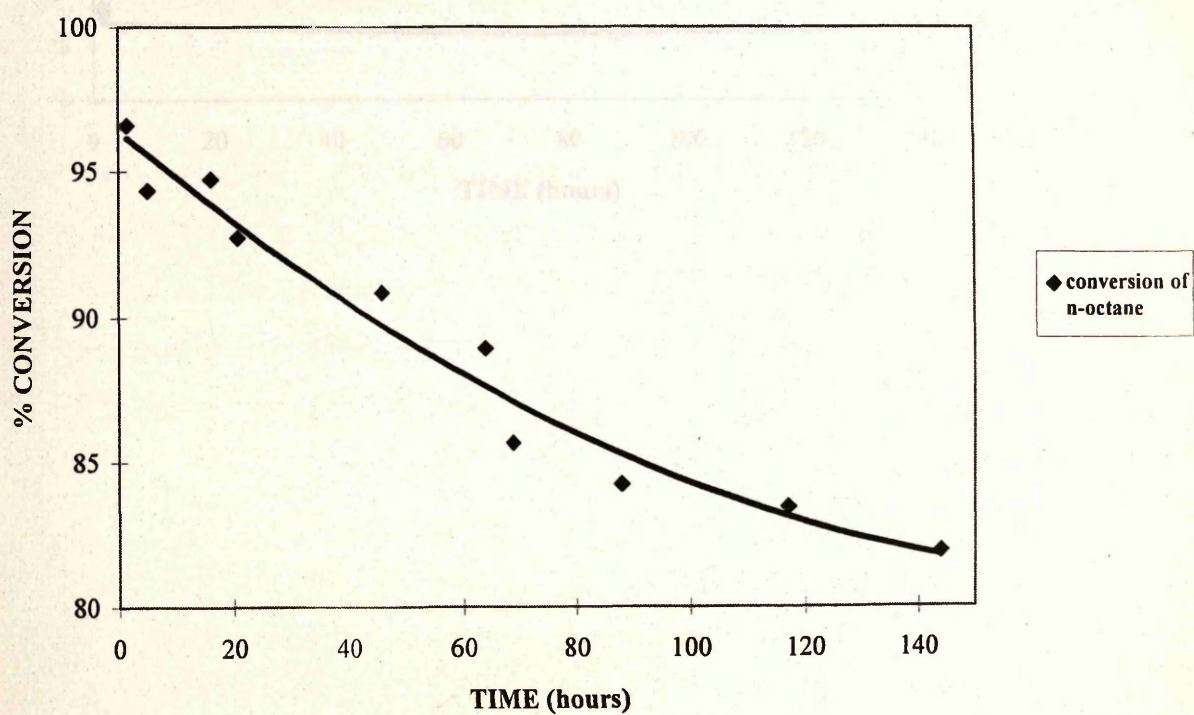


Figure 5.13.6 Conversion of n-octane over 0.3 wt% Pt/Al₂O₃ [Pt(acac)₂]

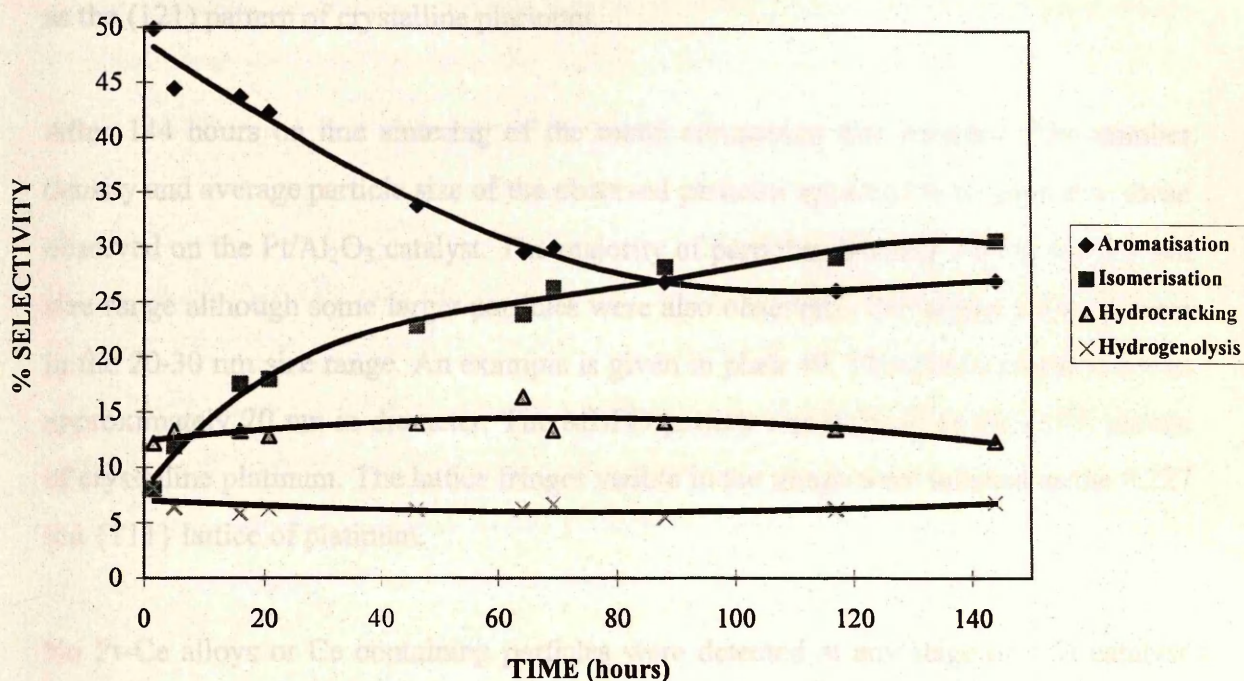


5.14. 0.3 wt% Pt - 0.3 wt% Ce/Al₂O₃

5.14.A TEM observations

After calcination and reduction this catalyst was found to be similar to Pt/Al₂O₃ (section 5.1). There was no noticeable alteration in either the number density or the average size of the particles observed due to the presence of cerium. Again the metal component was highly dispersed with the vast majority of the metallic component present in the form of monomer sized particles too small to be imaged by the microscope. A small number of 2-5 nm particles were observed.

Figure 5.13.7 Selectivities to the major reforming reactions over 0.3 wt% Pt/Al₂O₃ [Pt(acac)₂]



5.14. 0.3 wt% Pt - 0.3 wt% Ce/Al₂O₃

5.14.B n-Octane reforming

5.14.A TEM observations

After calcination and reduction this catalyst was found to be similar to Pt/Al₂O₃ (section 5.1). There was no noticeable alteration in either the number density or the average size of the particles observed due to the presence of cerium. Again the metal component was highly dispersed with the vast majority of the metallic component present in the form of nanometer sized particles too small to be imaged by the microscope. A small number of 2-5 nm particles were imaged however. An example is given in plate 48. This particle was 5 nm in diameter. The MBED pattern obtained from this particle (inset) was indexed as the (121) pattern of crystalline platinum.

After 144 hours on line sintering of the metal component had occurred. The number density and average particle size of the observed particles appeared to be similar to those observed on the Pt/Al₂O₃ catalyst. The majority of particles detected were in the 2-5 nm size range although some larger particles were also observed. The largest particles were in the 20-30 nm size range. An example is given in plate 49. This platinum particle was approximately 20 nm in diameter. The MBED pattern was indexed as the (110) pattern of crystalline platinum. The lattice fringes visible in the image were indexed as the 0.227 nm {111} lattice of platinum.

No Pt-Ce alloys or Ce containing particles were detected at any stage on this catalyst. The presence of Pt-Ce alloys was not expected as the temperatures used in this study were too low to cause reduction of ceria to the metal.²²⁸ It is likely that the cerium in this catalyst remained in the form of a highly dispersed oxide phase.

5.14.B n-Octane reforming.

The yield of individual products over this catalyst are presented versus time on line in table 5.14.1 and plotted in figures 5.14.1. to 5.14.6.

The yields of methane, ethane, propane, i-butane and n-butane are plotted in figure 5.14.1. The initial and final yields of methane over this catalyst were similar to those observed over the Pt/Al₂O₃ catalyst (figure 5.1.1). However this catalyst did not show the rapid initial decrease in methane yield observed over the platinum catalyst. In this case the gradual fall in yield was spread out over a longer period of time. The yield of ethane, propane, i-butane and n-butane showed similar trends over this catalyst to those observed over platinum. However in this case the yield of these products were lower than the corresponding values over Pt/Al₂O₃.

The yields of cycloalkanes over Pt-Ce/Al₂O₃ are plotted in figure 5.14.2. The yield of cyclopentane over this catalyst was similar to the corresponding yield over platinum (figure 5.1.2). However the yield of C₆ cycloalkane species was slightly higher. The yield of C₇ and C₈ species followed similar trends to those observed over platinum (slightly increase with time on line) although in this case the yields remained slightly lower after 144 hours on line (0.6% as opposed to 0.9% for C₇ cycloalkanes and 1.1% versus 2.1% for C₈ cycloalkanes).

The yields of i-alkanes over this catalyst are plotted in figure 5.14.3. The yield of i-alkanes over this catalyst were similar to those over the Pt/Al₂O₃ catalyst (although the yields of i-pentane and i-hexane were perhaps slightly lower) and showed similar trends. The yields of i-pentane, i-hexane and i-heptane remained relatively stable whilst the yield of i-octane increased significantly throughout the run.

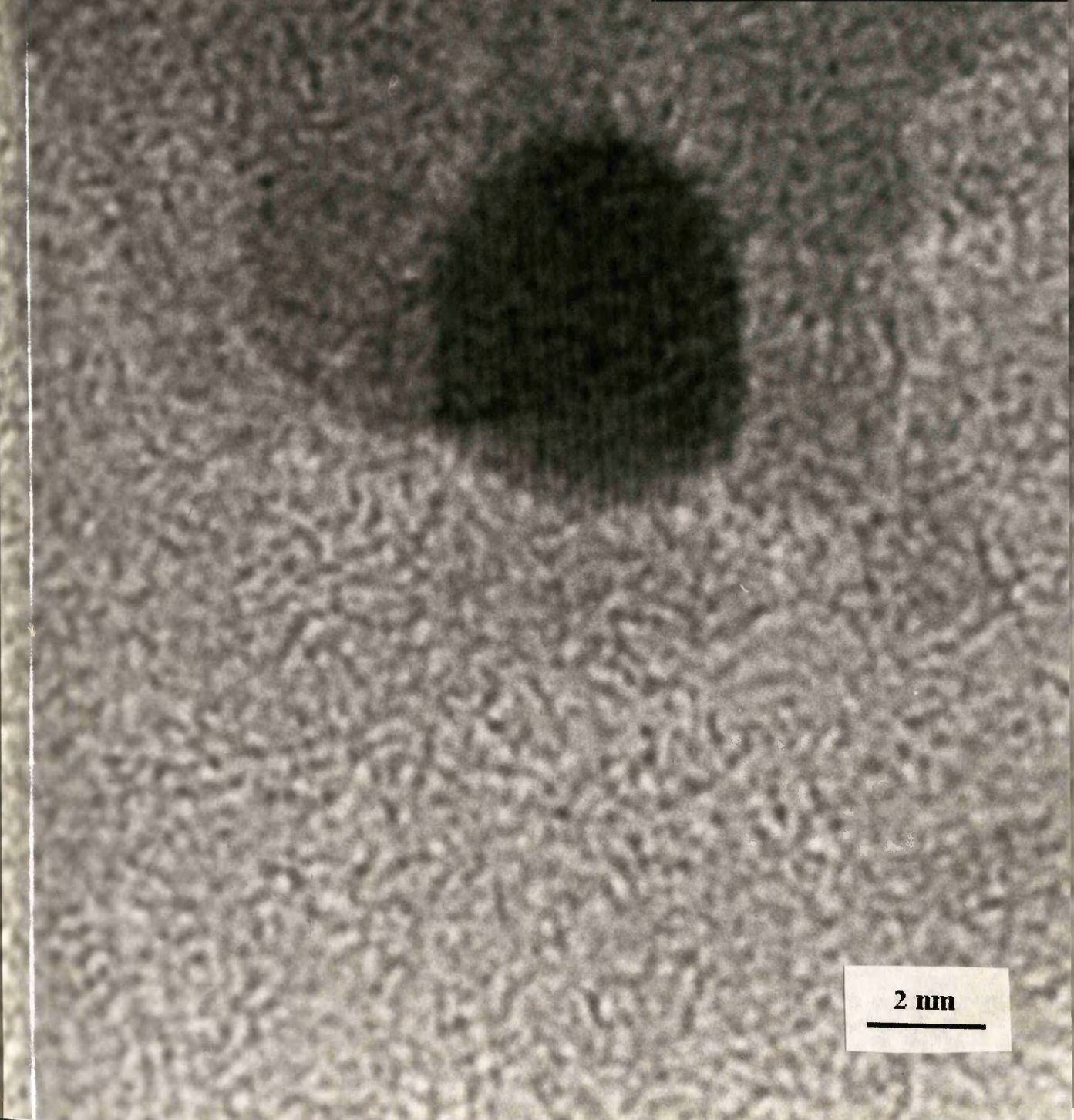
The yields of n-alkanes over this catalyst are plotted in figure 5.14.4. Again the yields of these products were similar to those obtained over the Pt/Al₂O₃ catalyst and did not vary significantly with time on line.

The yields of aromatic species over the Pt-Ce/Al₂O₃ catalyst are plotted in figure 5.14.5. The yields of these products were higher than those observed over platinum (figure 5.1.5). The yields of benzene, toluene, ethylbenzene and o-xylene were initially higher over Pt-Ce/Al₂O₃ whilst after 144 hours on line the yields of benzene, ethylbenzene, m/p-xylene and o-xylene were slightly higher over this catalyst.)

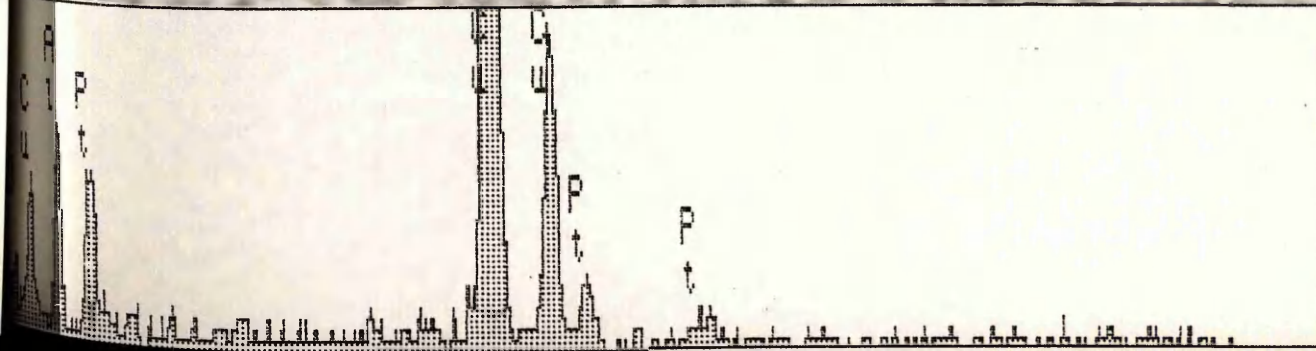
The conversion of n-octane versus time on line over Pt-Ce/Al₂O₃ is plotted in figure 5.14.6. The initial conversion of n-octane over Pt-Ce was very similar to that over Pt/Al₂O₃ (figure 5.1.6. :- 98.3% and 98.4% respectively) and followed a similar trend with time on line. However, the deactivation curve was slightly shallower over the Pt-Ce catalyst in the initial and the final conversion was therefore slightly higher over this catalyst (91.6% versus 90.2%).

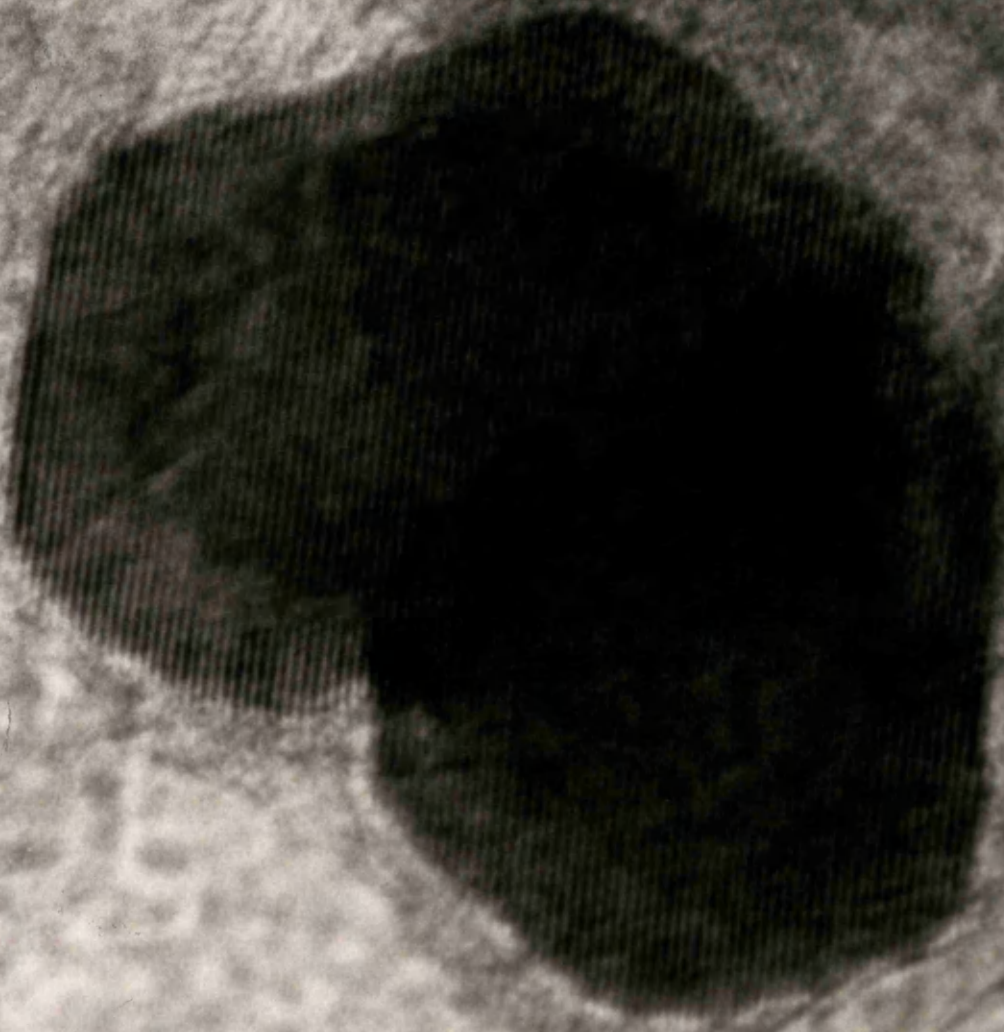
The selectivities to the four major reforming reactions for this catalyst are listed versus time on line in table 5.14.1 and plotted in figure 5.14.7. Comparison of these results with the selectivities over Pt/Al₂O₃ (figure 5.1.7) reveals that these two catalysts showed approximately similar trends in their selectivities. However, the initial (51.5% versus 45.2%) and final (28.2% versus 25.1%) selectivity to aromatics was higher over the Pt-Ce/Al₂O₃ catalyst as was the final selectivity to isomerisation (30.6% versus 26.9%). The selectivity to hydrocracking was lower over the Pt-Ce catalyst at all stages of the run whilst the selectivities to hydrogenolysis were similar throughout.

Plate 48



2 mm





3 nm

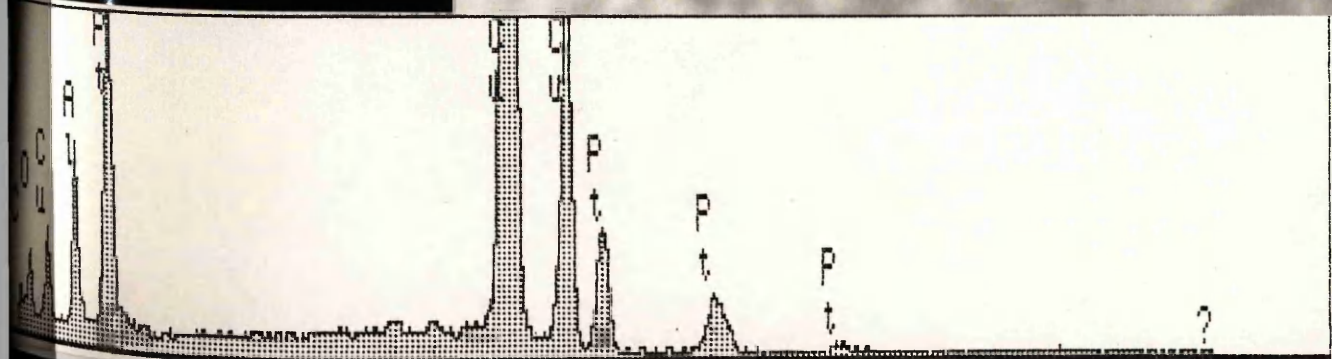


Table 5.14.1 Yields of individual products for catalyst 0.3 wt% Pt - 0.3 wt% Ce/Al₂O₃

Time (hours)	Methane	Ethane	Propane	i-Butane	n-Butane	c-Pentane	i-Pentane	n-Pentane
1.0	6.9	2.7	5.6	2.7	5.1	0.1	5.2	4.5
6.5	7.0	2.6	6.0	3.3	5.4	0.1	5.9	3.5
20.0	6.2	2.7	5.8	3.3	5.1	0.1	5.7	3.1
25.0	5.9	2.3	5.6	3.1	4.6	0.1	5.3	3.4
46.3	5.0	2.3	5.9	3.2	4.7	0.1	5.5	3.5
49.5	5.4	2.3	5.4	3.0	4.7	0.2	5.5	3.7
72.0	5.1	2.1	5.6	3.2	4.9	0.1	5.7	3.5
93.6	4.9	2.0	5.1	3.0	4.9	0.1	5.8	3.8
98.0	4.3	1.8	5.5	3.1	4.6	0.1	5.4	3.3
117.0	4.1	2.2	5.3	3.0	4.5	0.1	5.3	3.5
121.0	4.3	1.7	5.7	3.1	4.8	0.1	5.4	3.3
141.0	3.8	1.9	5.3	3.0	4.7	0.2	5.4	4.0
144.0	4.0	1.6	4.9	2.7	4.5	0.2	5.0	3.5

Table 5.14.1 (cont) Yields of individual products for catalyst 0.3 wt% Pt - 0.3 wt% Ce/Al₂O₃

Time (hours)	C6 c-Alkane	i-Hexane	n-Hexane	C7 c-Alkane	i-Heptane	n-Heptane	C8 c-Alkane	i-Octane
1.0	0.7	5.2	2.2	0.3	1.4	0.7	0.5	3.9
6.5	0.7	5.5	2.2	0.3	1.5	0.4	0.3	6.1
20.0	0.8	5.5	2.3	0.4	1.7	1.0	0.7	9.1
25.0	0.6	5.4	3.0	0.4	2.0	1.7	0.7	12.9
46.3	0.7	5.5	2.3	0.4	1.6	0.8	0.7	15.0
49.5	0.7	5.3	2.7	0.5	1.7	1.2	0.9	16.9
72.0	0.7	6.9	2.8	0.6	1.5	1.2	1.0	16.0
93.6	0.7	6.3	3.0	0.6	2.0	1.2	1.1	20.1
98.0	0.7	5.6	2.5	0.6	1.9	1.1	1.0	21.2
117.0	0.7	5.8	2.7	0.6	1.9	1.1	1.0	21.4
121.0	0.7	5.8	2.8	0.7	2.1	1.5	1.1	22.4
141.0	0.5	5.6	1.8	0.6	1.5	0.5	1.0	23.5
144.0	0.5	5.3	2.7	0.6	1.8	1.2	1.1	26.3

Table 5.14.1 (cont) Yields of individual products for catalyst 0.3 wt% Pt - 0.3 wt% Ce/Al₂O₃

Time (hours)	Benzene	Toluene	Ethyl- Benzene	m/p- Xylene	o-Xylene	C9 Aromatic	Total Conversion
1.0	2.0	5.8	11.7	19.2	11.4	0.6	98.3
6.5	1.6	4.8	9.7	20.6	10.6	0.6	98.5
20.0	1.2	3.7	8.3	19.9	10.0	0.7	97.3
25.0	1.0	3.4	7.1	18.3	8.9	0.6	96.4
46.3	0.9	3.0	6.8	18.2	8.5	0.9	95.6
49.5	0.8	2.7	5.8	17.0	7.9	0.7	95.1
72.0	1.0	2.7	5.6	16.7	7.0	0.8	94.7
93.6	0.8	2.3	4.7	14.5	6.6	0.7	94.2
98.0	0.7	2.3	5.1	15.7	6.9	0.9	94.2
117.0	0.6	2.2	5.0	14.6	6.7	0.6	92.9
121.0	0.5	1.9	4.3	13.4	5.7	0.7	92.0
141.0	0.5	2.1	4.4	14.2	6.2	0.7	91.7
144.0	0.7	1.9	4.1	13.0	5.6	0.7	91.6

Table 5.14.2 Selectivity to the major reforming reactions for 0.3 wt% Pt - 0.3 wt% Ce/Al₂O₃

Time (hours)	Selectivity to Aromatics	Selectivity to Isomerisation	Selectivity to Hydrocracking	Selectivity to Hydrogenolysis
1.0	51.5	5.3	13.3	7.0
6.5	48.5	7.8	14.9	7.1
20.0	44.9	11.1	14.9	6.4
25.0	40.9	15.4	14.3	6.2
46.3	39.9	17.4	14.9	5.2
49.5	36.7	19.6	14.5	5.7
72.0	35.7	18.5	16.7	5.4
93.6	31.5	23.4	16.1	5.2
98.0	33.5	24.5	14.9	4.6
117.0	32.0	25.0	15.0	4.5
121.0	28.9	26.6	15.6	4.6
141.0	30.8	27.3	15.2	4.2
144.0	28.2	30.6	14.1	4.4

Figure 5.14.1 Yields of individual products over 0.3 wt% Pt - 0.3 wt% Ce/Al₂O₃

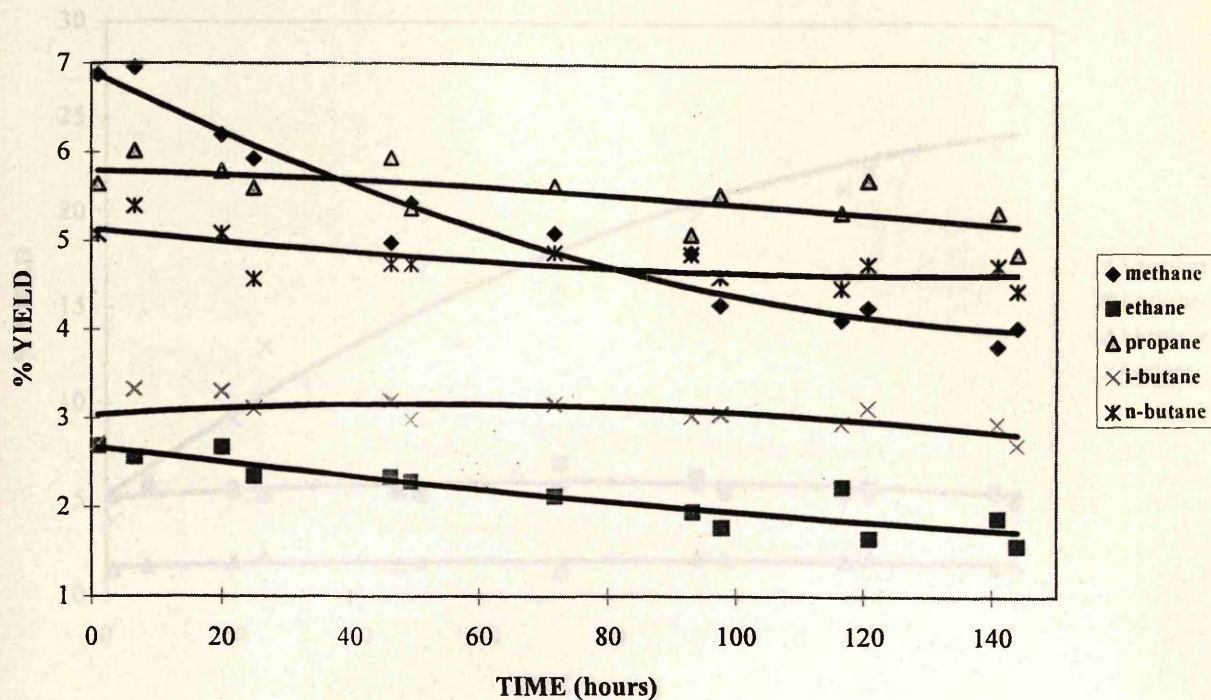


Figure 5.14.2 Yields of cycloalkanes over 0.3 wt% Pt - 0.3 wt% Ce/Al₂O₃

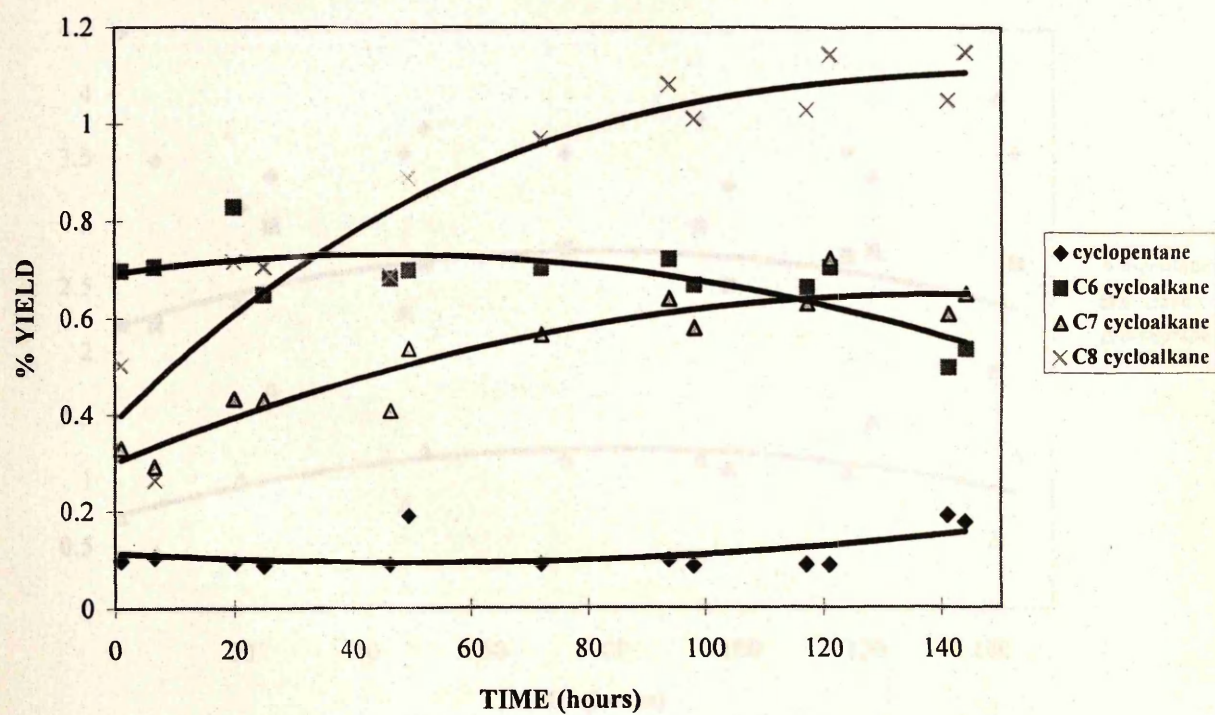


Figure 5.14.3 Yields of i-alkanes over 0.3 wt% Pt - 0.3 wt% Ce/Al₂O₃

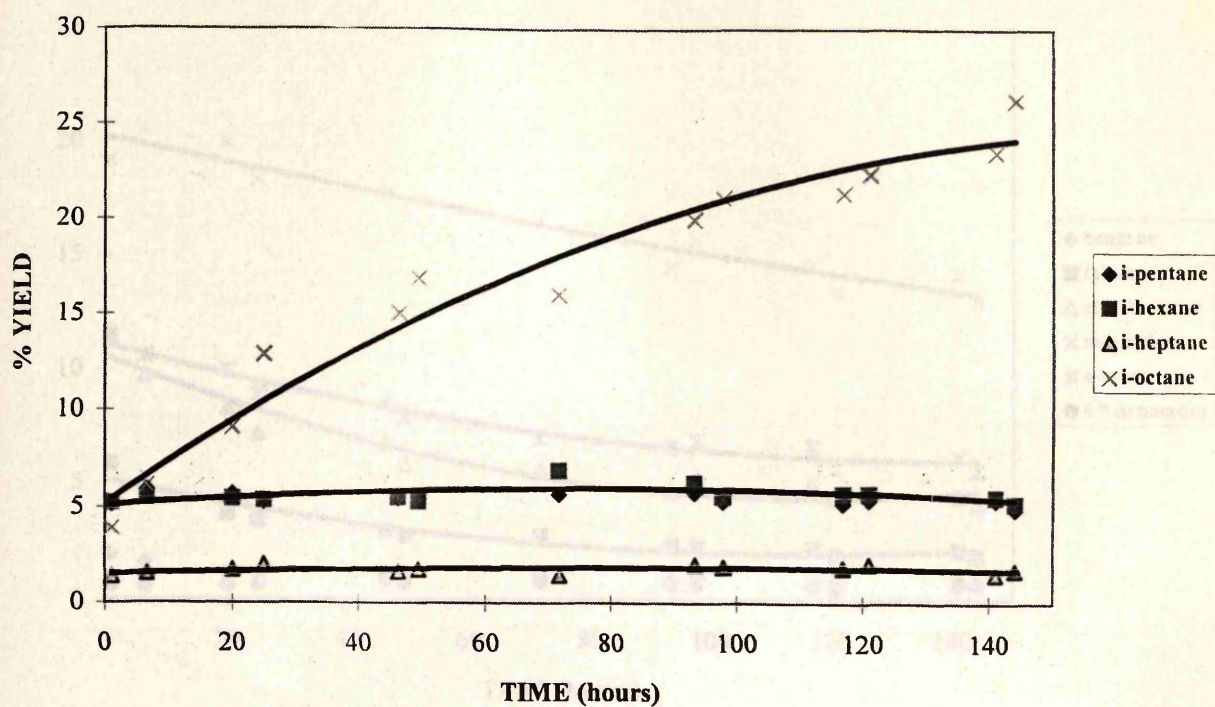


Figure 5.14.4 Yields of n-alkanes over 0.3 wt% Pt - 0.3 wt% Ce/Al₂O₃

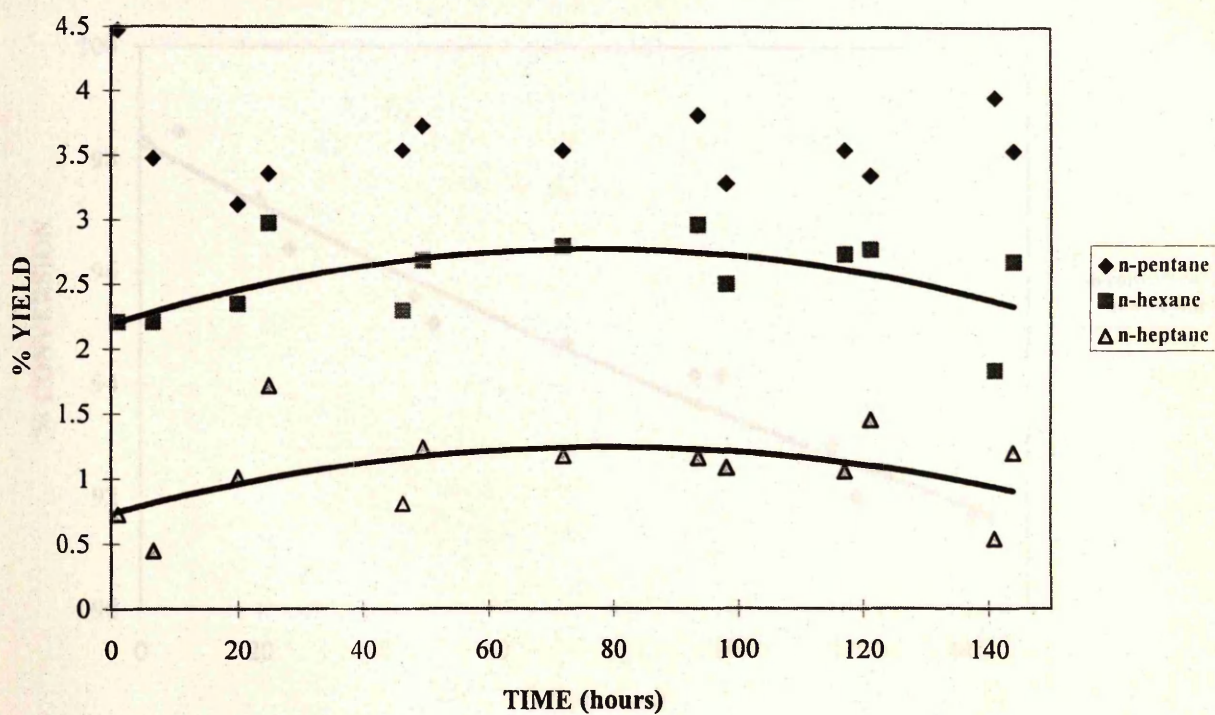


Figure 5.14.5 Yields of aromatics over 0.3 wt% Pt - 0.3 wt% Ce/Al₂O₃

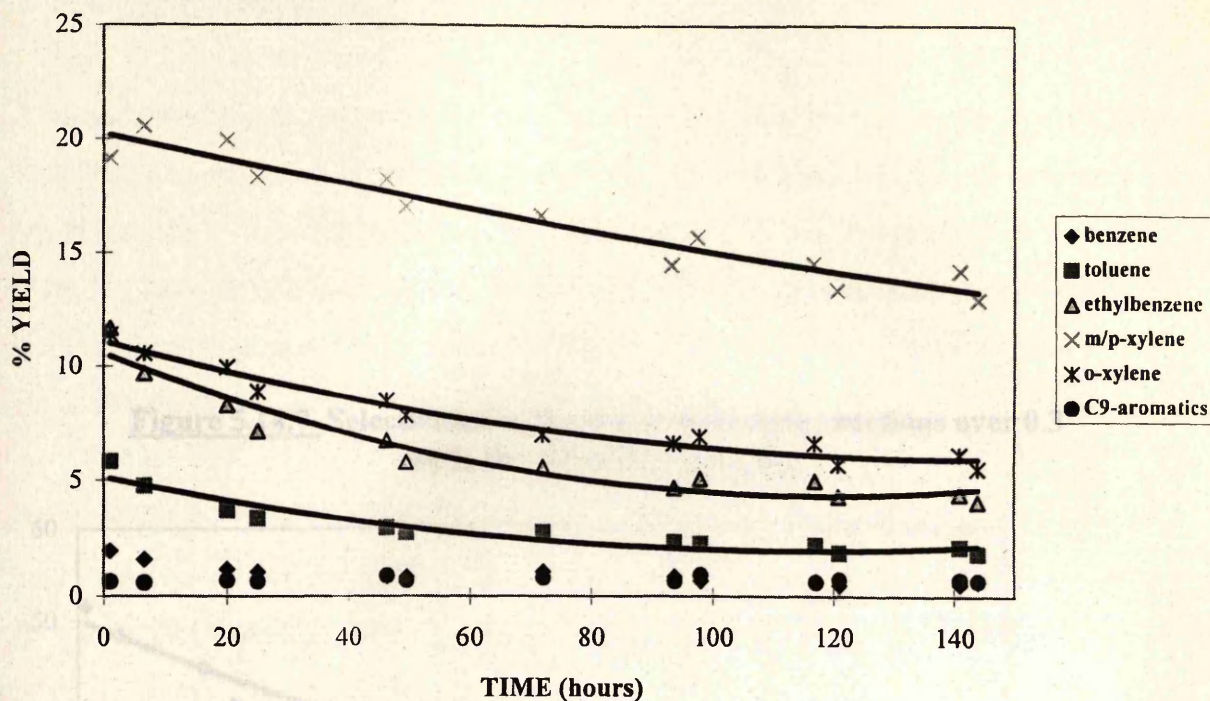
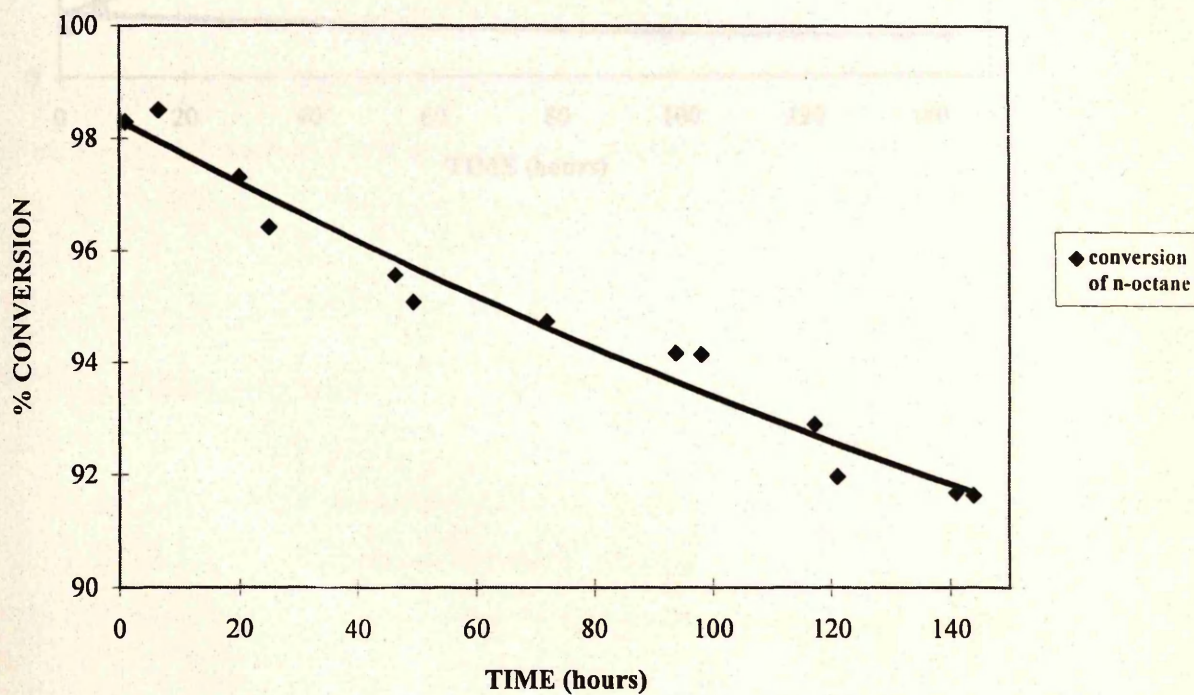


Figure 5.14.6 Conversion of n-octane over 0.3 wt% Pt - 0.3 wt% Ce/Al₂O₃

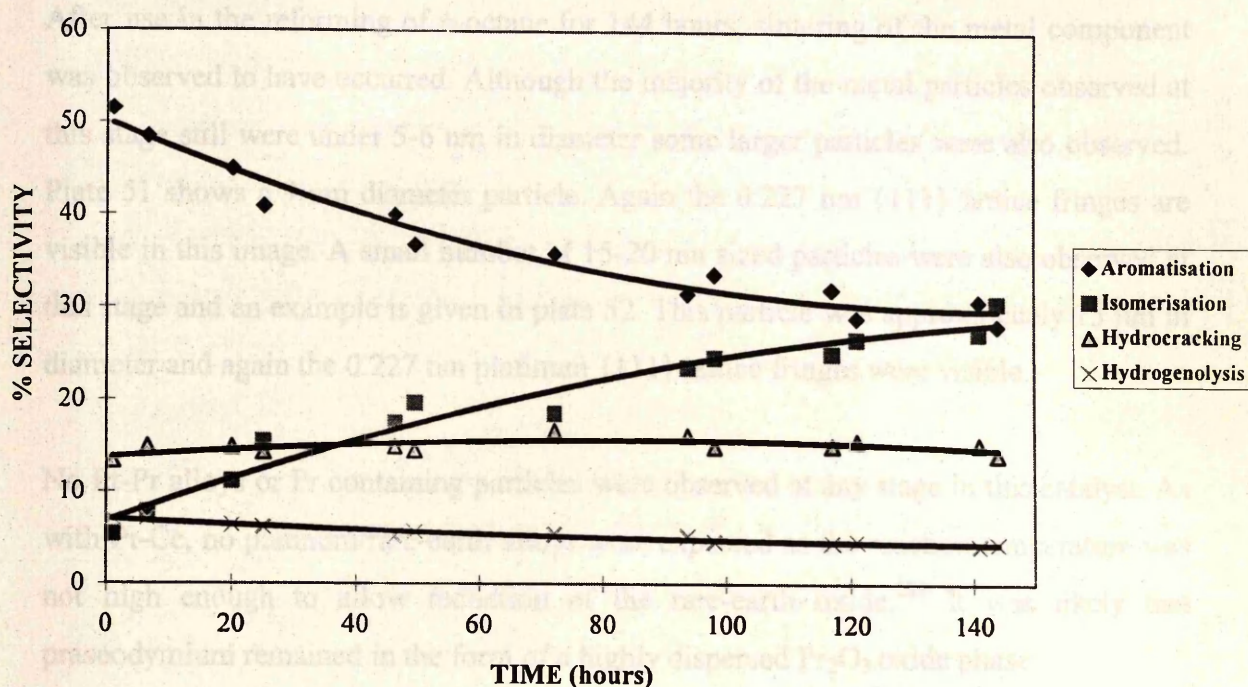


5.15. 0.3wt% Pt - 0.3 wt% Pr/Al₂O₃

5.15.A. TEM observations

After calcination and reduction the catalyst showed similar feature to the Pt-Ce/Al₂O₃ and Pt/Al₂O₃ catalysts. Again the metal component was highly dispersed with only a small fraction of particles in the 2-6 nm range being observed. An example is shown in plate 50. This particle was 6 nm in diameter. The lattice fringes imaged correspond to the 0.227 nm platinum (111) lattice. The HRTEM pattern obtained was indexed as the (123) pattern.

Figure 5.14.7 Selectivities to the major reforming reactions over 0.3 wt% Pt - 0.3 wt% Ce/Al₂O₃



5.15.B n-Octane reforming

The yields of individual products over the Pt-Pr/Al₂O₃ catalyst at 400 °C and 10 bar are shown in figure 5.15.1 and plotted in figures 5.15.4 to 5.15.6.

5.15. 0.3wt% Pt - 0.3 wt% Pr/Al₂O₃

5.15.A. TEM observations

After calcination and reduction this catalyst showed similar feature to the Pt-Ce/Al₂O₃ and Pt/Al₂O₃ catalysts. Again the metal component was highly dispersed with only a small fraction of particles in the 2-6 nm range being observed. An example is shown in plate 50. This particle was 6 nm in diameter. The lattice fringes imaged correspond to the 0.227 nm platinum {111} lattice. The MBED pattern obtained was indexed as the (123) pattern of platinum.

After use in the reforming of n-octane for 144 hours, sintering of the metal component was observed to have occurred. Although the majority of the metal particles observed at this stage still were under 5-6 nm in diameter some larger particles were also observed. Plate 51 shows a 9 nm diameter particle. Again the 0.227 nm {111} lattice fringes are visible in this image. A small number of 15-20 nm sized particles were also observed at this stage and an example is given in plate 52. This particle was approximately 15 nm in diameter and again the 0.227 nm platinum {111} lattice fringes were visible.

No Pt-Pr alloys or Pr containing particles were observed at any stage in this catalyst. As with Pt-Ce, no platinum/rare-earth alloys were expected as the reaction temperature was not high enough to allow reduction of the rare-earth oxide.²²⁸ It was likely that praseodymium remained in the form of a highly dispersed Pr₂O₃ oxide phase.

5.15.B n-Octane reforming

The yields of individual products over the Pt-Pr/Al₂O₃ catalyst are listed versus time on line in figure 5.15.1 and plotted in figures 5.15.1 to 5.15.6.

The yields of methane, ethane, propane, i-butane and n-butane over this catalyst are plotted in figure 5.15.1. The yield of methane over this catalyst, although similar initially, remained higher than the corresponding yield over Pt-Ce/Al₂O₃ (figure 5.14.1). The yield of ethane, propane and i-butane were similar to the yields over Pt-Ce and followed similar trends. These yields were lower than the corresponding yields over Pt/Al₂O₃ (figure 5.1.1). The yield of n-butane was found to be slightly lower over this catalyst than on Pt-Ce (which in turn had been found to produce less n-butane than Pt/Al₂O₃).

The yields of cycloalkanes over Pt-Pr are plotted in figure 5.15.2. The yields of cyclopentane, C₆ and C₇ cycloalkanes over this catalyst were observed to be similar to those found with Pt (figure 5.1.2) and Pt-Ce (figure 5.14.2) although the initial yields of C₆ cycloalkanes were slightly lower. The initial yield of C₈ cycloalkanes over this catalyst was similar to that over Pt/Al₂O₃ (0.2-0.3%) but lower than the corresponding value over Pt-Ce/Al₂O₃ (0.5%). However the yield of this product increased substantially through the run and by 144 hours on line was much higher than the corresponding yield over the Pt-Ce/Al₂O₃ catalyst (4.3% versus 1.1% respectively) and also the Pt/Al₂O₃ catalyst (2.1%).

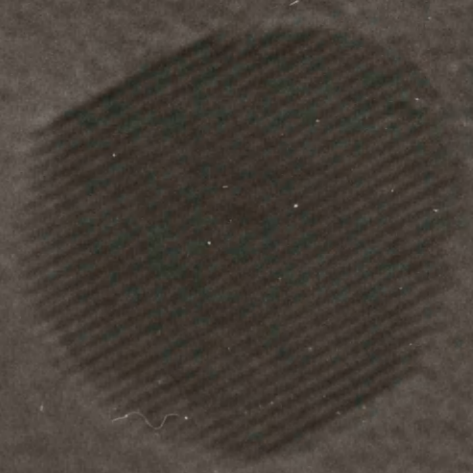
The yields of i-alkanes over the Pt-Pr/Al₂O₃ catalyst are plotted in figure 5.15.3. The yields of i-alkanes over this catalyst were similar to the corresponding yields over platinum (figure 5.1.3) and Pt-Ce (5.14.3) and also followed similar trends. The yield of i-pentane, i-hexane and i-heptane remained relatively stable whilst the yield of i-octane increased significantly through the run. The only minor difference observed between the yields of i-alkanes over this catalyst and Pt/Al₂O₃ was that the yields of i-pentane, i-hexane and i-octane were slightly lower over the Pt-Pr catalyst at all stages of the reforming run.

The yields of n-alkanes over this catalyst are plotted in figure 5.15.4. Again the yields of these products were similar to the corresponding yields over Pt/Al₂O₃ and Pt-Pr/Al₂O₃ (compare with figures 5.1.4 and 5.14.4 respectively). The only significant difference being that the yield of n-heptane was lower over this catalyst. Again the yields of these products remained relatively stable throughout the run.

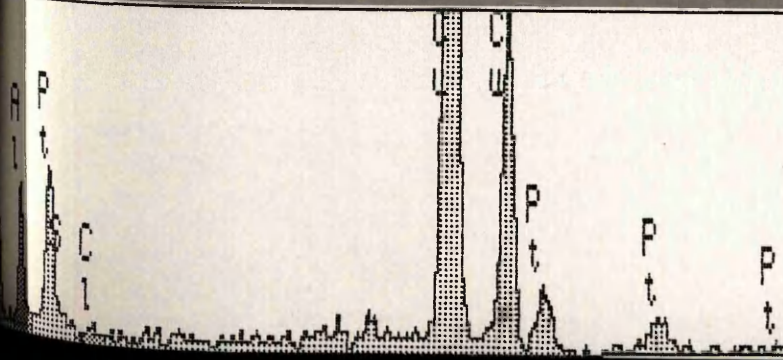
The yields of aromatic products over Pt-Pr/Al₂O₃ are plotted in figure 5.15.5. Although the trends in these yields are similar to those observed over Pt and Pt-Ce (compare with figures 5.1.5 and 5.14.5 respectively) the initial yield of toluene, ethylbenzene and xylenes over this catalyst were all significantly higher than the corresponding yields over Pt/Al₂O₃ and remained higher throughout the run. This effect was also observed with Pt-Ce/Al₂O₃ but was much more pronounced over this catalyst.

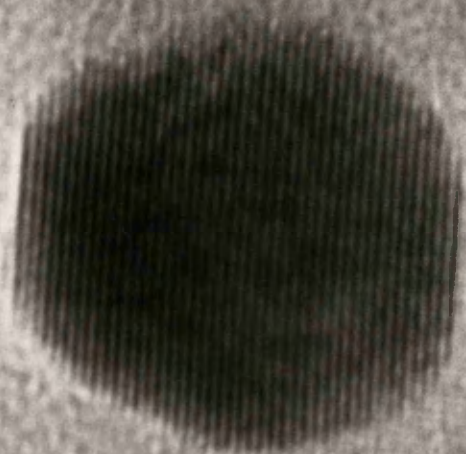
The conversion of n-octane over this catalyst is plotted versus time on line in figure 5.15.6. It was observed that the deactivation curve for this catalyst was similar to that obtained for Pt/Al₂O₃ (compare with figure 5.1.6). The initial and final conversions were similar and the rate of deactivation was greatest initially but gradually decreased during the run.

The selectivities to the four major reforming reactions over Pt-Pr/Al₂O₃ are listed versus time on line in table 5.15.2 and plotted in figure 5.15.7. The selectivity trends on this catalyst followed similar patterns to those observed over Pt/Al₂O₃ and Pt-Ce/Al₂O₃ (compare with figures 5.1.7 and 5.14.7 respectively). However, the selectivity to aromatics was substantially higher over this catalyst than either of the others and remained so throughout the run (initial values:- Pt 45.2%, Pt-Ce 51.5%, Pt-Pr 56.6%). Although the selectivity to isomerisation did increase it did not do so to the same extent as on the Pt and Pt-Ce catalyst (final values:- Pt 26.9%, Pt-Ce 30.6%, Pt-Pr 22.7%). The selectivity to hydrocracking on this catalyst remained relatively constant and was lower than the corresponding selectivity over Pt/Al₂O₃. The selectivity to hydrogenolysis was similar to that over Pt-Ce and Pt/Al₂O₃ (although slightly higher than the latter).

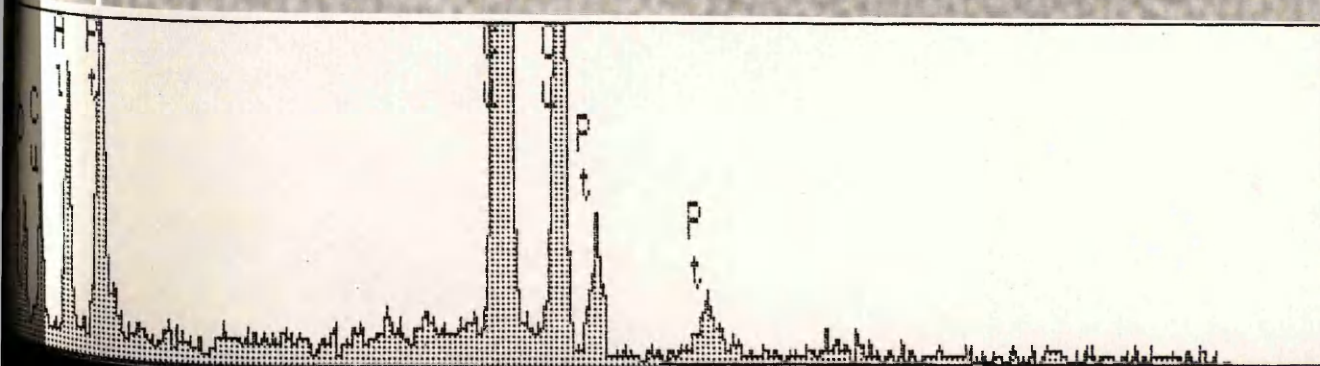


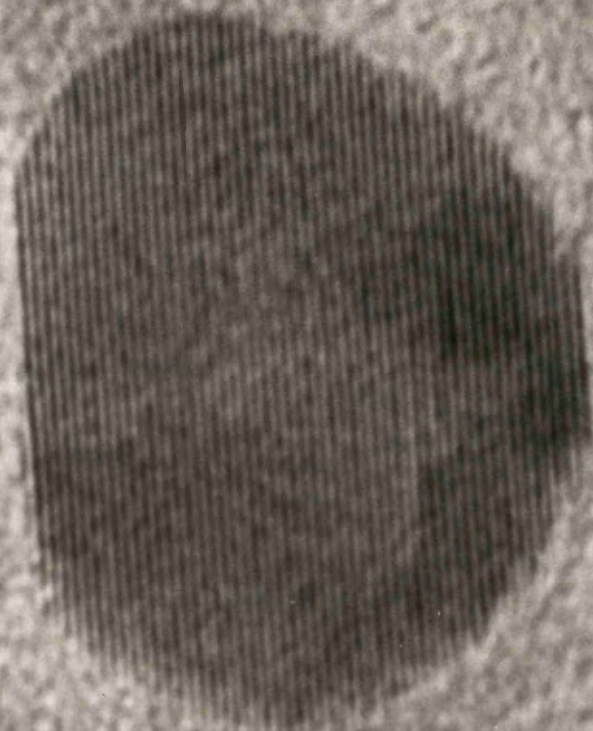
2 nm





3 nm





3 nm

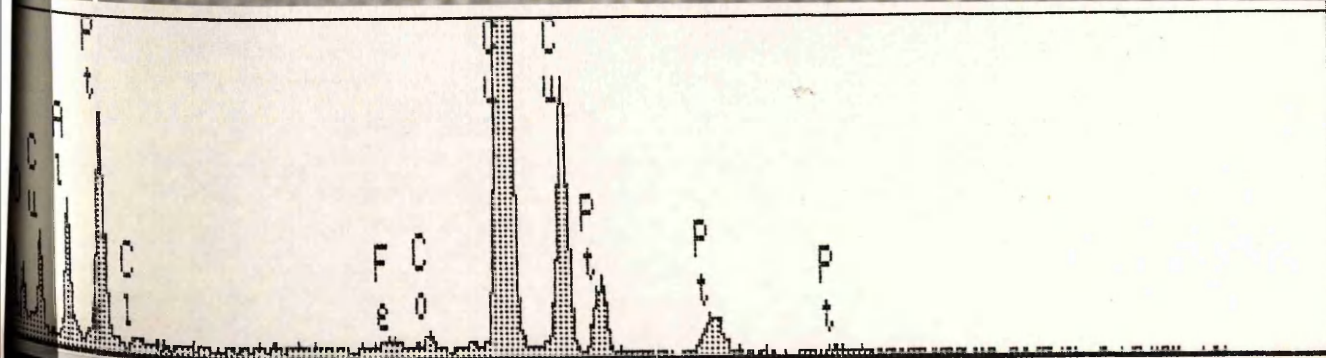


Table 5.15.1 Yields of individual products for catalyst 0.3 wt% Pt - 0.3 wt% Pr/Al₂O₃

Time (hours)	Methane	Ethane	Propane	i-Butane	n-Butane	c-Pentane	i-Pentane	n-Pentane
1.0	7.3	3.2	5.3	2.8	4.1	0.1	4.6	3.3
27.5	5.9	1.8	4.8	2.6	3.7	0.2	4.3	2.6
33.0	6.3	2.4	6.2	3.3	4.7	0.1	5.5	3.3
44.5	5.6	2.4	5.9	3.3	4.7	0.1	5.3	2.7
50.0	5.2	2.1	6.0	3.2	4.3	0.1	5.2	3.1
71.0	5.2	1.9	5.7	3.3	4.3	0.2	5.2	2.7
78.0	5.3	2.1	5.9	3.3	4.5	0.2	5.4	2.7
97.0	4.6	2.4	5.9	3.3	4.6	0.2	5.4	2.6
101.0	5.0	2.0	5.8	3.1	4.2	0.1	4.9	2.6
117.0	5.0	2.2	5.5	2.9	4.0	0.1	4.8	2.9
121.5	4.9	1.9	5.8	3.0	4.4	0.1	4.6	2.7
140.5	5.1	2.3	5.6	3.0	4.2	0.2	4.9	2.8
144.0	5.2	2.1	4.8	2.9	4.0	0.1	4.6	2.9

Table 5.15.1 (cont) Yields of individual products for catalyst 0.3 wt% Pt - 0.3 wt% Pr/Al₂O₃

Time (hours)	C6 c-Alkane	i-Hexane	n-Hexane	C7 c-Alkane	i-Heptane	n-Heptane	C8 c-Alkane	i-Octane
1.0	0.3	4.5	2.0	0.1	0.9	0.2	0.2	4.2
27.5	0.4	4.2	1.9	0.3	1.4	0.2	0.7	11.3
33.0	0.2	5.2	2.0	0.6	1.5	0.2	1.0	12.2
44.5	0.5	5.1	2.3	0.5	1.7	0.4	0.9	14.6
50.0	0.5	5.2	2.6	0.6	1.8	0.5	1.3	15.6
71.0	0.6	5.3	2.2	0.9	1.8	0.4	1.9	16.2
78.0	0.6	5.3	1.8	0.8	1.6	0.1	2.0	16.1
97.0	0.4	5.1	1.6	0.7	1.5	0.1	1.9	17.8
101.0	0.7	4.9	2.1	1.1	1.8	0.5	2.5	17.8
117.0	0.6	5.0	1.9	1.3	1.8	0.4	3.2	19.0
121.5	0.5	4.7	2.0	1.1	1.7	0.6	3.8	19.3
140.5	0.6	5.1	1.8	0.9	1.5	0.2	4.1	20.2
144.0	0.6	4.9	2.3	0.9	1.7	0.5	4.3	18.9

Table 5.15.1 (cont) Yields of individual products for catalyst 0.3 wt% Pt - 0.3 wt% Pr/Al₂O₃

Time (hours)	Benzene	Toluene	Ethyl- Benzene	m/p- Xylene	o-Xylene	C9 Aromatic	Total Conversion
1.0	1.7	5.1	11.6	23.6	13.0	0.9	98.8
27.5	1.5	5.0	11.8	19.4	11.4	1.7	97.0
33.0	0.8	3.0	6.8	21.2	9.4	1.1	97.0
44.5	0.7	2.7	6.5	19.1	8.7	1.1	94.7
50.0	0.7	2.7	6.0	18.9	8.3	1.1	94.9
71.0	0.6	2.6	5.7	18.2	8.0	1.2	94.2
78.0	0.7	2.6	5.6	18.2	7.9	1.0	93.9
97.0	0.5	2.5	5.4	17.4	7.6	1.1	92.7
101.0	0.6	2.5	5.0	16.9	7.1	1.0	92.1
117.0	0.6	2.3	4.8	15.4	6.7	1.0	91.4
121.5	0.5	2.3	4.6	15.3	6.5	0.9	91.3
140.5	0.6	2.2	4.4	14.5	6.3	1.1	91.5
144.0	0.5	2.3	4.4	15.3	6.6	1.1	91.0

Table 5.15.2 Selectivity to the major reforming reactions for 0.3 wt% Pt - 0.3 wt% Pr/Al₂O₃

Time (hours)	Selectivity to Aromatics	Selectivity to Isomerisation	Selectivity to Hydrocracking	Selectivity to Hydrogenolysis
1.0	56.6	5.1	12.0	7.4
27.5	52.3	13.0	11.5	6.1
33.0	43.5	14.2	14.4	6.4
44.5	40.9	17.2	14.5	5.9
50.0	39.7	18.3	14.3	5.4
71.0	38.6	19.1	14.7	5.5
78.0	38.4	18.8	14.9	5.7
97.0	37.3	20.8	14.9	5.0
101.0	35.9	21.3	14.1	5.4
117.0	33.6	22.8	13.9	5.5
121.5	32.9	23.0	13.5	5.4
140.5	31.7	23.8	14.3	5.5
144.0	33.2	22.7	13.7	5.7

Figure 5.15.1 Yields of individual products over 0.3 wt% Pt - 0.3 wt% Pr/Al₂O₃

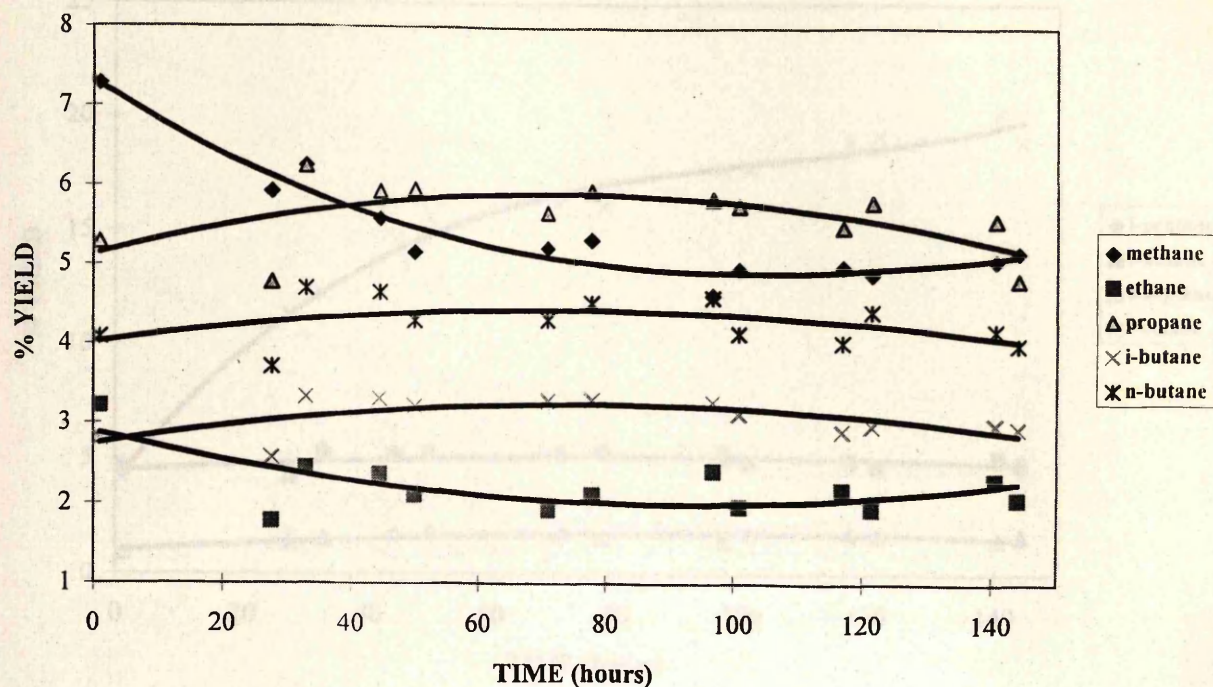


Figure 5.15.2 Yields of cycloalkanes over 0.3 wt% Pt - 0.3 wt% Pr/Al₂O₃

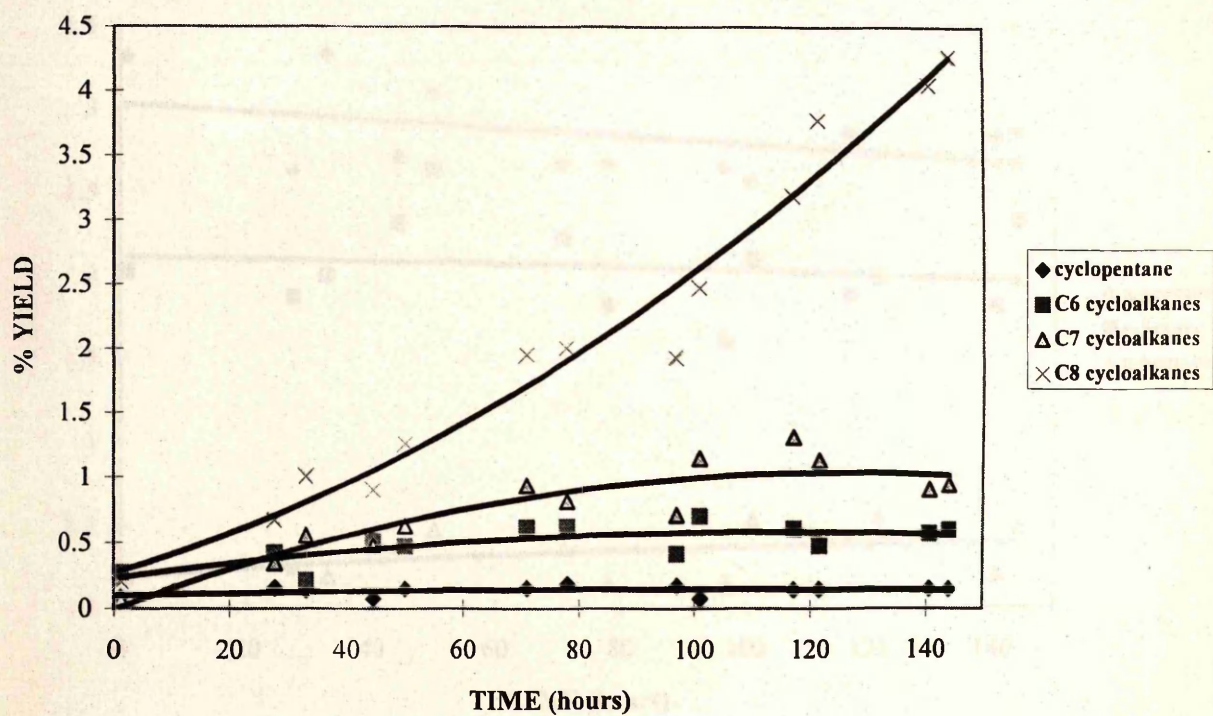


Figure 5.15.3 Yields of i-alkanes over 0.3 wt% Pt - 0.3 wt% Pr/Al₂O₃

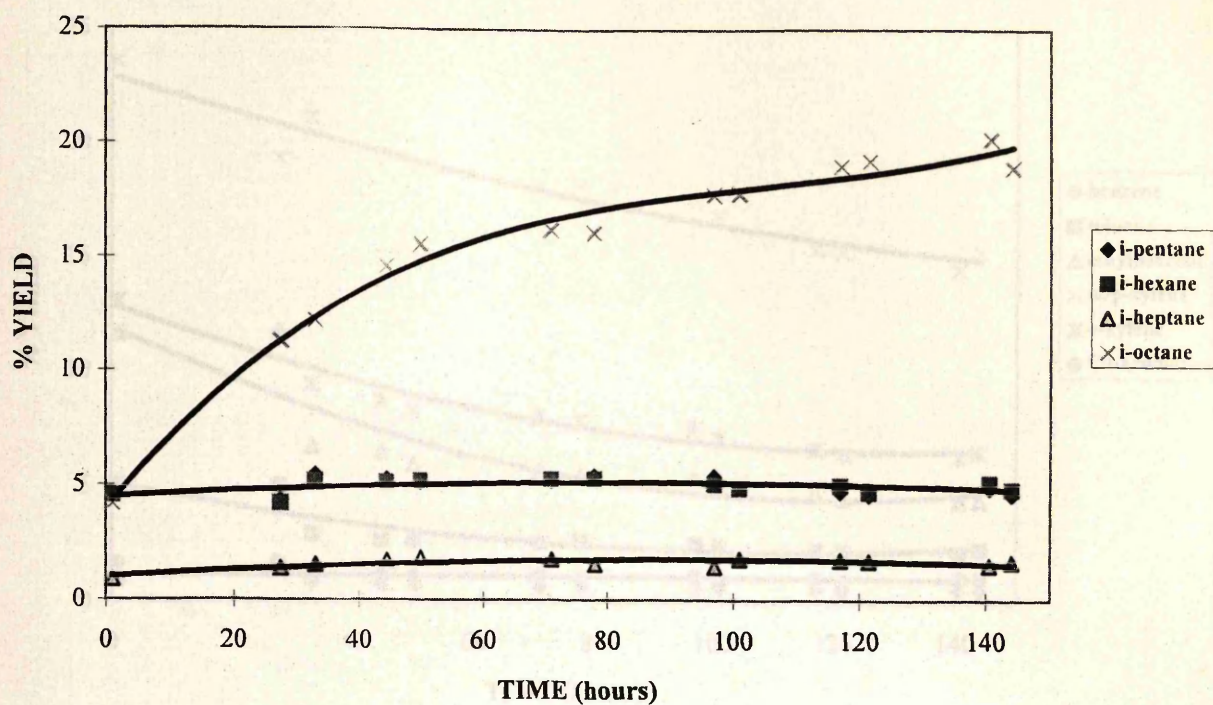


Figure 5.15.4 Yields of n-alkanes over 0.3 wt% Pt - 0.3 wt% Pr/Al₂O₃

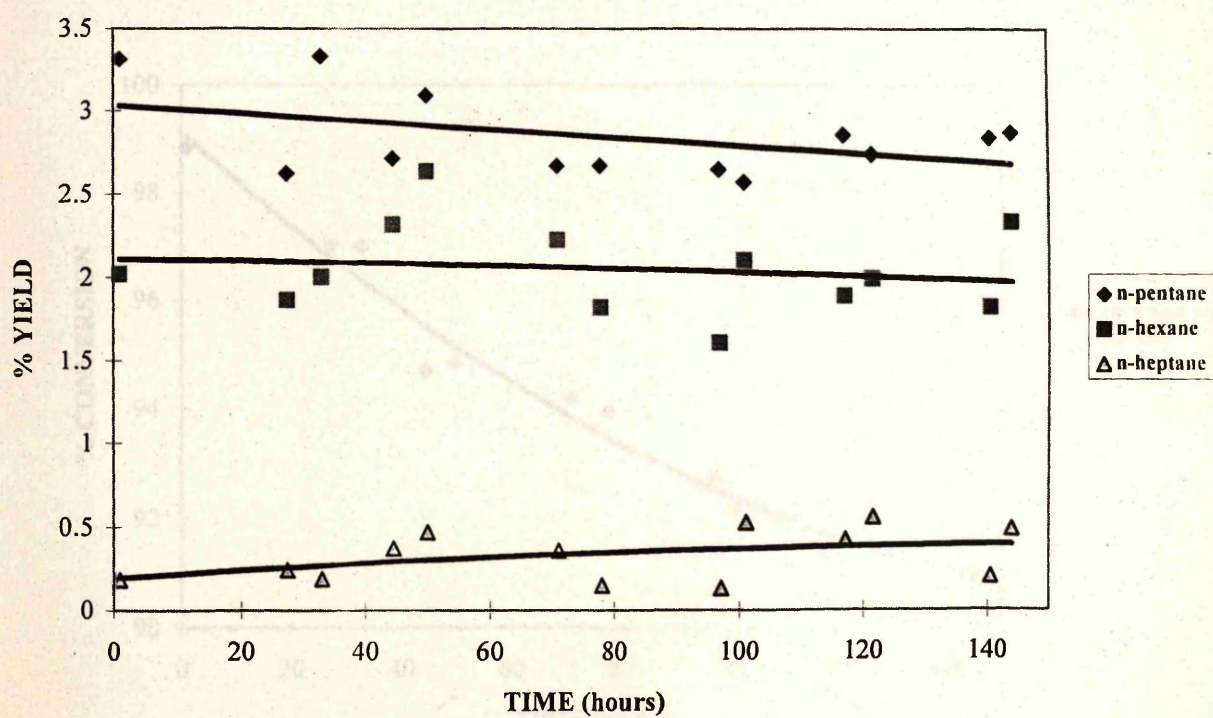


Figure 5.15.5 Yields of aromatics over 0.3 wt% Pt - 0.3 wt% Pr/Al₂O₃

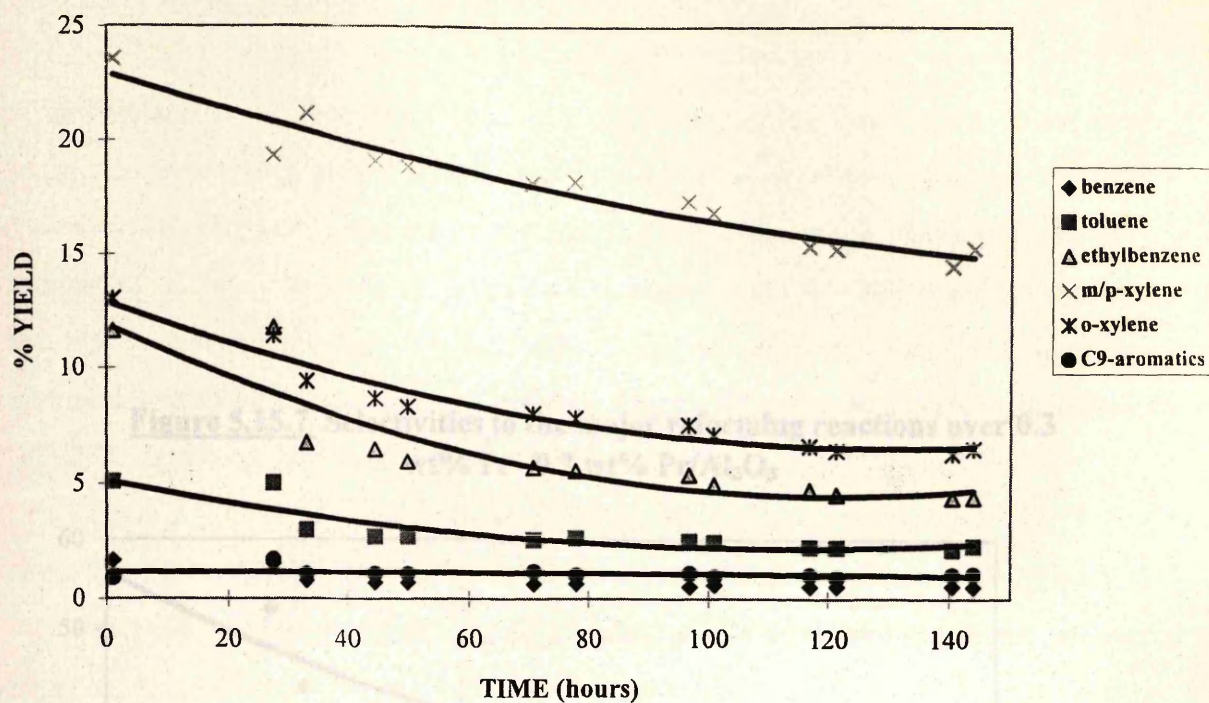
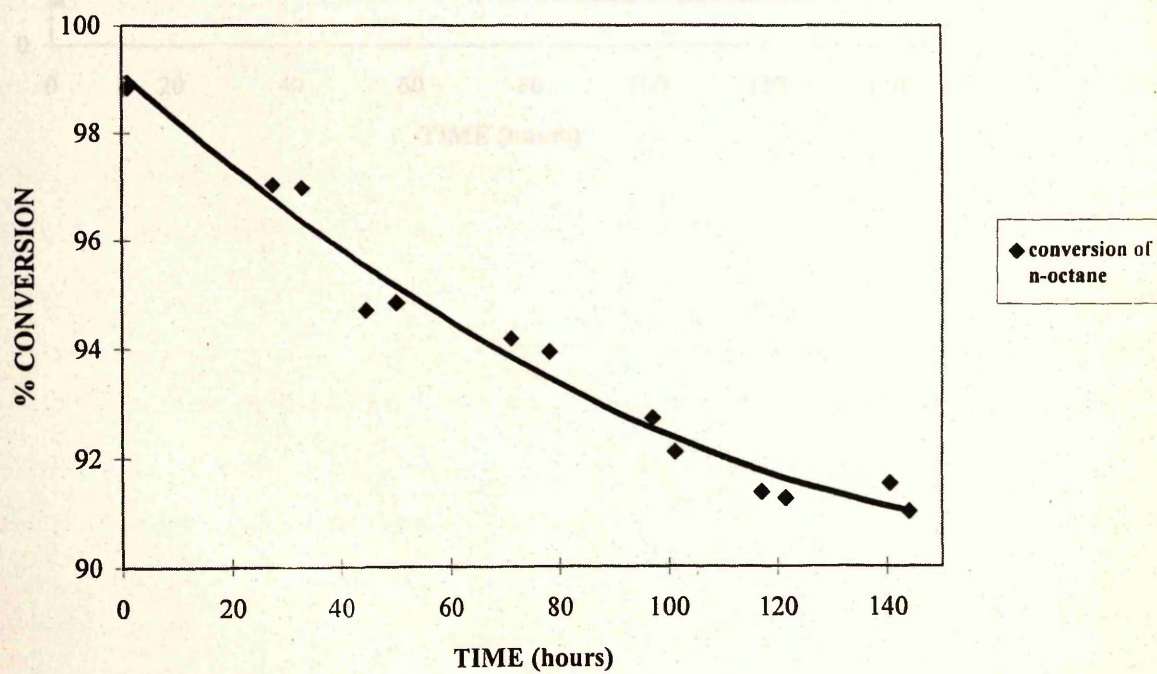


Figure 5.15.6 Conversion of n-octane over 0.3 wt% Pt - 0.3 wt% Pr/Al₂O₃

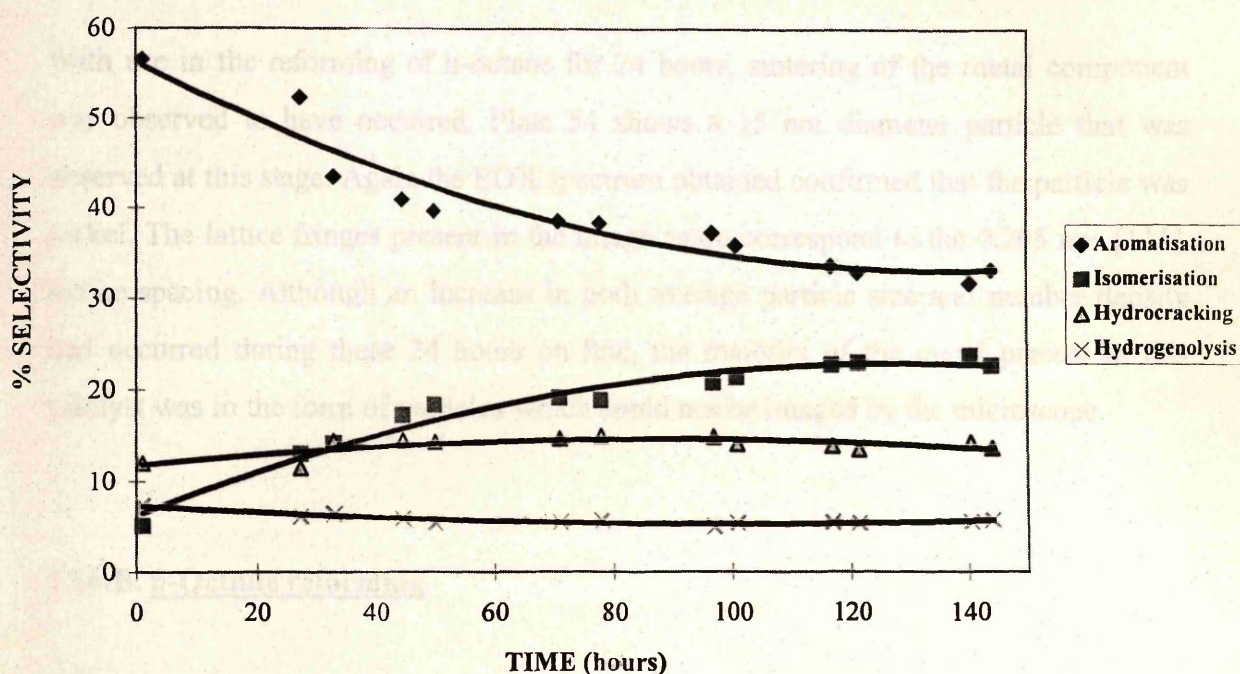


5.16. 0.3 wt% $\text{Ni}/\text{Al}_2\text{O}_3$

5.16.A. TEM observations

After calcination and reduction the metallic component of this catalyst was found to be highly dispersed with only a small number of particles large enough to be observed. However, the dispersion was not as high as on the corresponding platinum catalyst. A number of relatively large 10 nm particles were observed at this stage. Plate 53 shows an example. This particle was approximately 9 nm in diameter. The EDX spectrum obtained confirmed that it was nickel. The lattice fringes present in the image corresponded to the (111) 0.205 nm lattice spacing. Although an increase in both average particle size and number of particles occurred during these 24 hours on flow, the catalyst was still highly dispersed.

Figure 5.15.7 Selectivities to the major reforming reactions over 0.3 wt% Pt - 0.3 wt% Pr/ Al_2O_3



The yields of individual products over this catalyst are presented in Figure 5.16.1. The selectivities to the four major reforming reactions are shown in Figure 5.15.7. The selectivities to the four major reforming reactions are shown in Figure 5.15.7.

From these results that nickel was a much poorer catalyst than platinum. The yields of all the desired products were lower, particularly aromatics, over this catalyst.

5.16. 0.3 wt% Ni/Al₂O₃

5.16.A. TEM observations

After calcination and reduction the metallic component of this catalyst was found to be highly dispersed with only a small number of particles large enough to be observed. However, the dispersion was not as high as on the corresponding platinum catalyst. A number of relatively large 10 nm particles were observed at this stage. Plate 53 shows an example. This particle was approximately 9 nm in diameter. The EDX spectrum obtained confirmed it to be nickel. The lattice fringes visible in the image correspond to the {111} 0.205 nm lattice of nickel.

With use in the reforming of n-octane for 24 hours, sintering of the metal component was observed to have occurred. Plate 54 shows a 15 nm diameter particle that was observed at this stage. Again the EDX spectrum obtained confirmed that the particle was nickel. The lattice fringes present in the image again correspond to the 0.205 nm {111} lattice spacing. Although an increase in both average particle size and number density had occurred during these 24 hours on line, the majority of the metal present in this catalyst was in the form of particles which could not be imaged by the microscope.

5.16.B. n-Octane reforming

The yields of individual products over this catalyst are presented versus time on line in table 5.16.1. The selectivities to the four major reforming reactions are given in table 5.16.2.

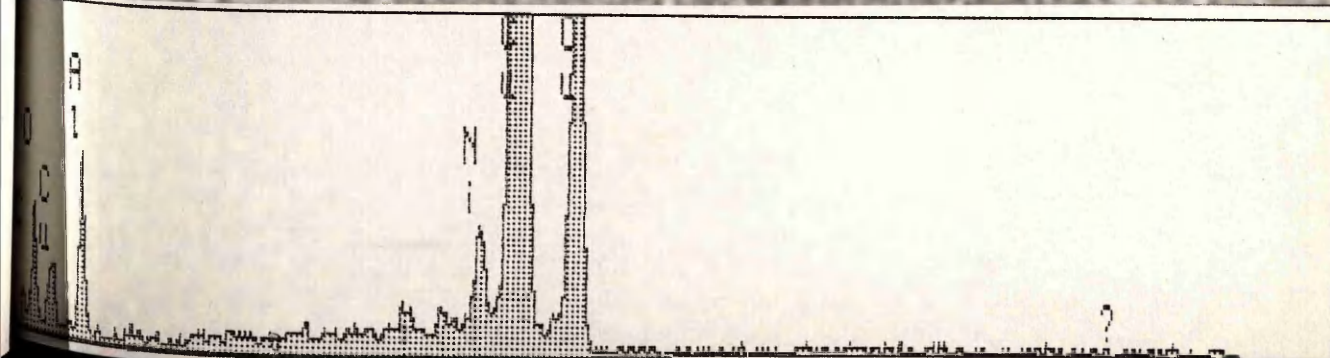
It is clear from these results that nickel was a much poorer catalyst for the reforming of n-octane than platinum. The yields of all the desired reforming products were considerable lower, particularly aromatics, over this catalyst than over Pt/Al₂O₃. The

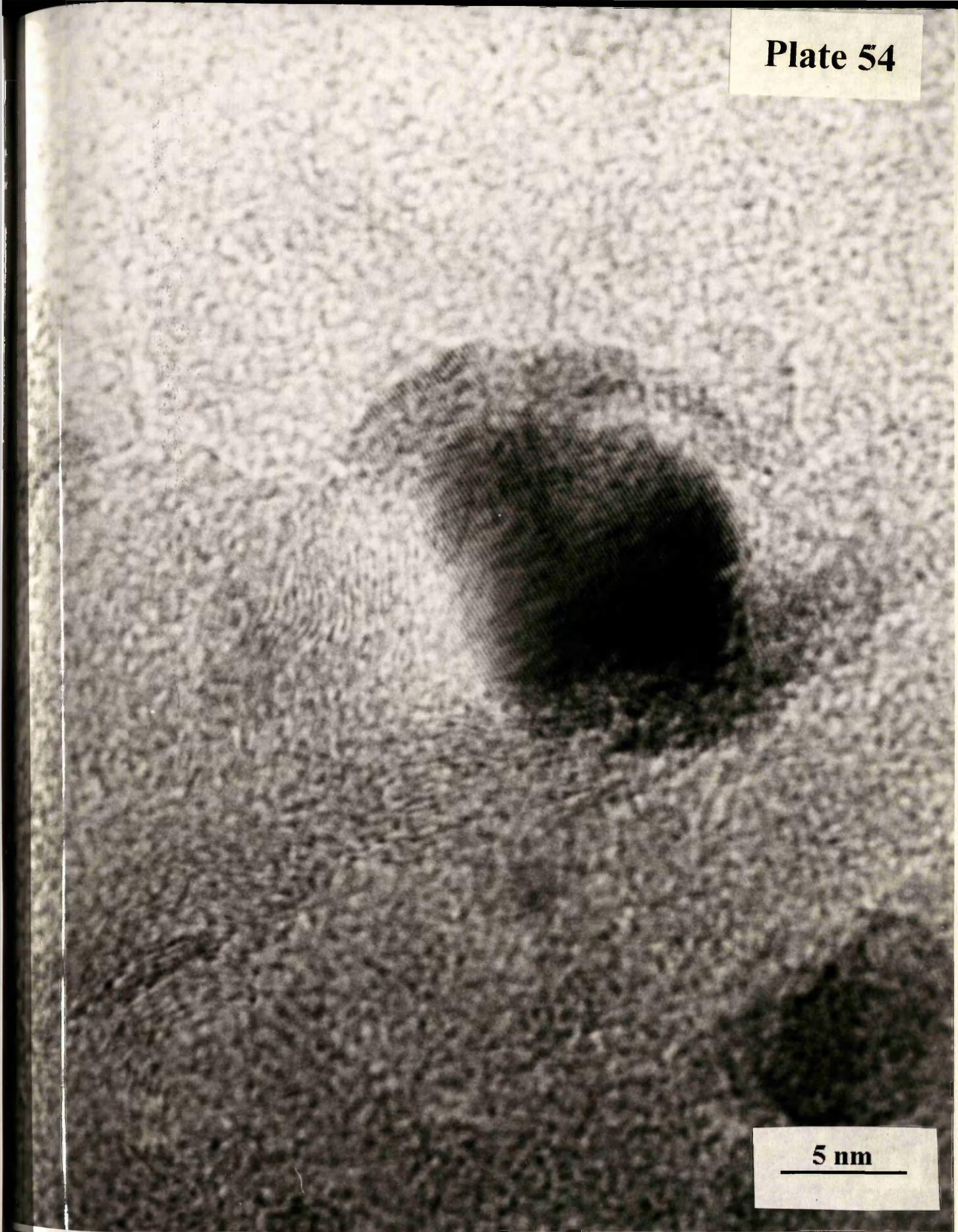
total conversion was also significantly lower. The only yield to show an increase relative to platinum was the yield of the undesirable methane product.

Due to the poor reforming properties of this catalyst the reaction was discontinued after 24 hours on line.



3 mm





5 nm

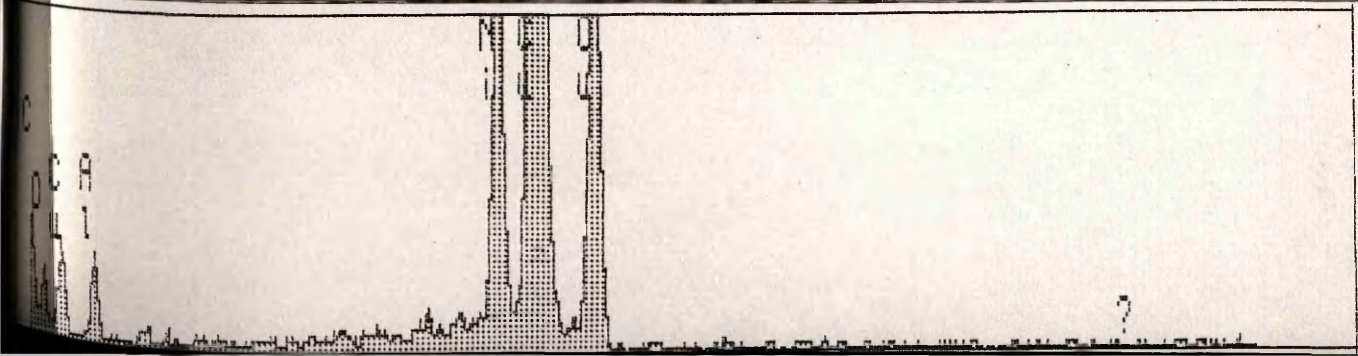


Table 5.16.1 Yields of individual products for catalyst 0.3 wt% Ni/Al₂O₃

Time (hours)	Methane	Ethane	Propane	i-Butane	n-Butane	c-Pentane	i-Pentane	n-Pentane
1.0	11.9	1.8	3.4	1.7	2.9	0.2	1.7	3.3
19.5	11.4	2.0	4.1	2.7	3.3	0.2	2.0	3.8
24.0	14.2	2.6	4.5	2.7	3.2	0.2	2.0	3.9

Table 5.16.1 (cont) Yields of individual products for catalyst 0.3 wt% Ni/Al₂O₃

Time (hours)	C6 c-Alkane	i-Hexane	n-Hexane	C7 c-Alkane	i-Heptane	n-Heptane	C8 c-Alkane	i-Octane
1.0	0.7	1.1	2.3	0.7	0.4	0.5	2.4	1.8
19.5	0.8	1.1	2.5	0.6	0.3	0.7	2.0	0.9
24.0	0.6	0.9	2.5	0.6	0.4	0.4	1.9	0.9

Table 5.16.1 (cont) Yields of individual products for catalyst 0.3 wt% Ni/Al₂O₃

Time (hours)	Benzene	Toluene	Ethyl-Benzene	m/p-Xylene	o-Xylene	C9 Aromatic	Total Conversion
1.0	0.3	1.1	0.1	1.4	0.6	0.1	40.5
	0.3	0.7	0.0	0.7	0.3	0.1	40.5
	0.2	0.7	0.0	0.7	0.3	0.1	43.2

Table 5.16.2 Selectivity to the major reforming reactions for 0.3 wt% Ni/Al₂O₃

Time (hours)	Selectivity to Aromatics	Selectivity to Isomerisation	Selectivity to Hydrocracking	Selectivity to Hydrogenolysis
1.0	9.0	5.4	11.1	29.5
19.5	5.0	3.1	14.3	28.2
24.0	4.6	2.9	12.8	32.7

5.17. 0.3 wt% Ni - 0.3 wt% Ge/Al₂O₃

5.17.A TEM observations

After calcination and reduction this catalyst was similar in every respect to the Ni/Al₂O₃ catalyst. The metal component was highly dispersed with only a small number of 2-10 nm particles being observed. At this stage no Ni-Ge or Ge particles were detected (as with Pt-Ge/Al₂O₃). It was therefore concluded that the germanium was present mainly as a highly dispersed oxide phase after these treatments.

After use in the reforming of n-octane for 23 hours however, Ni-Ge alloys were detected in this system. Some sintering of the metallic component was also observed to have occurred. Plate 55 gives an example of a Ni-Ge alloy formed in this system. This particle was approximately 8 nm in diameter. The EDX spectrum obtained revealed a Ni/Ge atomic ratio of 3.0. No MBED pattern was obtained from this particle. The lattice fringes visible in the image had a spacing of approximately 0.20 nm.

Another example of an alloy particle is given in plate 56. This particle contained two separate regions (marked (A) and (B) in the image). An EDX spectrum obtained from the whole particle (inset) revealed the presence of nickel and germanium in an approximate atomic ratio of 4.2. Unfortunately no MBED pattern was obtained. The crossed lattice imaged in region (A) corresponds to the {111} and {002} lattice planes of nickel with respective spacings of 0.205 nm and 0.176 nm. A number of apparently pure (within the limits of the EDX system) nickel particles were also observed at this stage.

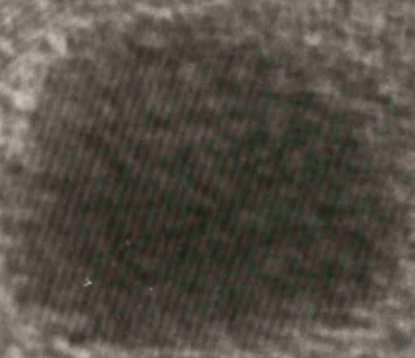
5.17.B n-Octane reforming

The yields of individual reforming products over Ni-Ge/Al₂O₃ are listed versus time on line in table 5.17.1. The selectivities to the four main reforming reactions are given in table 5.17.2.

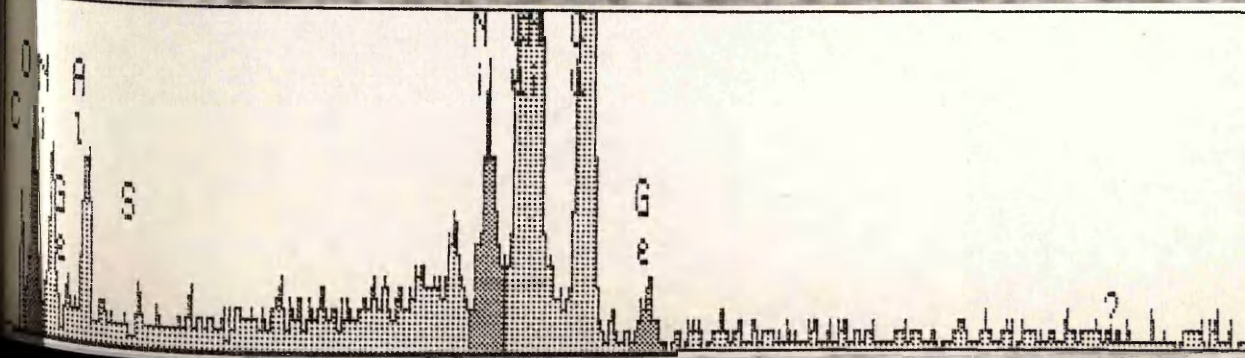
As with the related nickel catalyst the overall reforming properties of this catalyst were poor. The yield of aromatics and the overall conversion of n-octane were considerably lower than on the corresponding platinum or iridium containing catalyst.

However, the addition of germanium did induce some changes in the activity of Ni/Al₂O₃. The yield of methane was slightly decreased while the yield of hydrocracked products such as propane, i-butane, n-butane, i-pentane and n-pentane were enhanced. This increase in hydrocracking is also evident in the table of selectivities. However the selectivities to aromatisation did not seem to be altered significantly due to the addition of germanium.

Due to the poor nature of this catalyst the reaction was stopped after 23 hours.



3 nm



(A)

(B)

3 nm

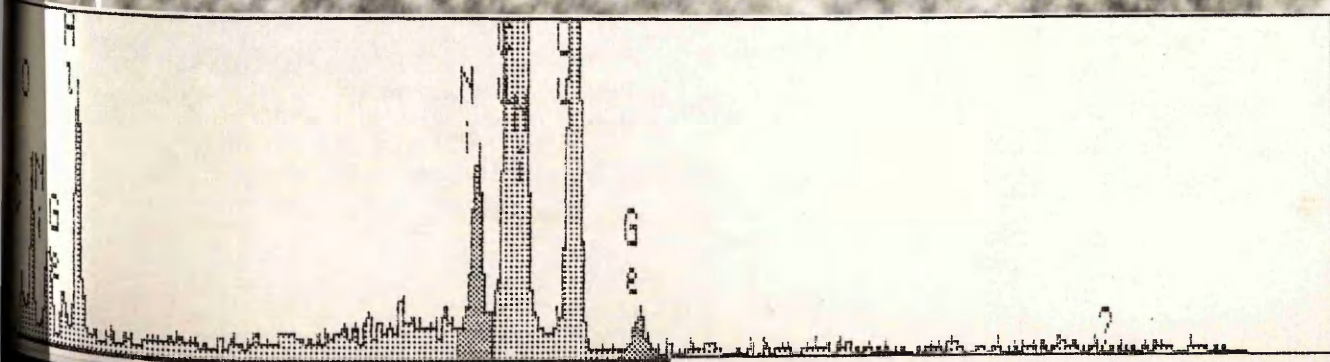


Table 5.17.1 Yields of individual products for catalyst 0.3 wt% Ni - 0.3 wt% Ge/Al₂O₃

Time (hours)	Methane	Ethane	Propane	i-Butane	n-Butane	c-Pentane	i-Pentane	n-Pentane
1.0	8.0	2.8	7.6	4.5	6.2	0.3	3.9	4.5
5.0	4.2	1.4	4.5	2.5	3.8	0.2	2.4	3.8
18.0	5.3	1.6	4.1	3.4	4.2	0.2	2.6	3.9
23.0	6.2	1.9	5.1	3.3	3.6	0.1	2.2	3.5

Table 5.17.1 (cont) Yields of individual products for catalyst 0.3 wt% Ni - 0.3 wt% Ge/Al₂O₃

Time (hours)	C6 c-Alkane	i-Hexane	n-Hexane	C7 c-Alkane	i-Heptane	n-Heptane	C8 c-Alkane	i-Octane
1.0	0.8	1.5	2.6	0.6	0.4	0.5	1.8	2.3
5.0	0.5	0.8	2.7	0.4	0.3	0.4	1.4	1.6
18.0	0.5	0.8	2.4	0.4	0.2	0.3	1.9	1.3
23.0	0.5	0.7	2.0	0.4	0.3	0.3	1.8	1.5

Table 5.17.1 (cont) Yields of individual products for catalyst 0.3 wt% Ni - 0.3 wt% Ge/Al₂O₃

Time (hours)	Benzene	Toluene	Ethyl-Benzene	m/p-Xylene	o-Xylene	C9 Aromatic	Total Conversion
1.0	0.1	1.0	0.1	2.2	0.8	0.3	52.8
5.0	0.1	0.4	0.0	0.9	0.3	0.2	32.8
18.0	0.0	0.4	0.0	0.6	0.2	0.1	34.4
23.0	0.0	0.4	0.0	0.7	0.3	0.1	35.0

Table 5.17.2 Selectivity to the major reforming reactions for 0.3 wt% Ni - 0.3 wt% Ge/Al₂O₃

Time (hours)	Selectivity to Aromatics	Selectivity to Isomerisation	Selectivity to Hydrocracking	Selectivity to Hydrogenolysis
1.0	8.7	5.2	18.7	15.1
5.0	5.6	5.8	17.3	13.0
18.0	3.8	4.5	19.7	15.3
23.0	4.5	4.9	17.8	17.6

5.18. 0.3 wt% Ru - 0.3 wt% Ge/Al₂O₃

5.18.A. TEM observations

After calcination and reduction the metallic component of this catalyst was again found to be in a highly dispersed form with only a small number of particles greater than 2 nm in diameter. The overall number density and average particle sizes on this catalyst suggested a dispersion similar to that of Pt/Al₂O₃. (It is not possible to be more precise due to the very low number of particles observed on both catalysts.) EDX analysis of those particles observed could not find any evidence for Ru-Ge alloy formation at this stage. An example of particles formed in this catalyst after calcination and reduction is shown in plate 57. This micrograph contained two particles in close proximity to one another. The larger particle was approximately 6 nm in diameter whilst the smaller particle was 3 nm. The EDX spectrum obtained from the larger particle using a 5 nm probe (inset) revealed that the particle was ruthenium. (Again the possibility that a few percent germanium was present in this particle cannot be ruled out.) The lattice fringes visible in both particles corresponded to the 0.214 nm {002} spacing of hcp ruthenium.

After 21 hours on line sintering of the metal component was observed to have occurred and the formation of Ru-Ge alloys had taken place. An example is given in plate 58. This particle was approximately 12 nm in diameter. The EDX spectrum obtained (inset) revealed an Ru/Ge atomic ratio of 1.4. The lattice fringes (vertical) imaged in this micrograph had spacing of approximately 0.34 nm and were therefore indexed as the 0.338 nm {110} lattice of the cubic RuGe structure. Also imaged in this micrograph was a strongly diffracting alumina crystallite. The highly faceted nature of this crystallite as compared to a metal particle is evident.

Another example of an alloy particle formed in this catalyst is given in plate 59. In this case the particle was 20 nm in diameter and was found to consist of a ruthenium core surrounded by a shell of RuGe alloy. An EDX spectrum obtained using a 4 nm electron

beam probe centered on the area marked (A) in the image (a portion of the probe was not incident on the particle) is given as spectrum (A) and revealed a Ru/Ge atomic ratio = 0.8. Another spectrum taken using the same probe diameter centered on the centre of the particle, marked (B) in the image, is given as spectrum (B). In this case the Ru/Ge atomic ratio was calculated to be 1.9. The smaller lattice spacing in the centre region of the particle had a spacing of 0.214 nm corresponding to the Ru {002} spacing whilst the larger lattice had a spacing of 0.338 nm corresponding to the {110} lattice of cubic RuGe. This type of particle containing a metallic core surrounded by an alloy region was not observed in any of the Pt-Sn, Pt-Ge or Pt-Ir-Ge catalysts.

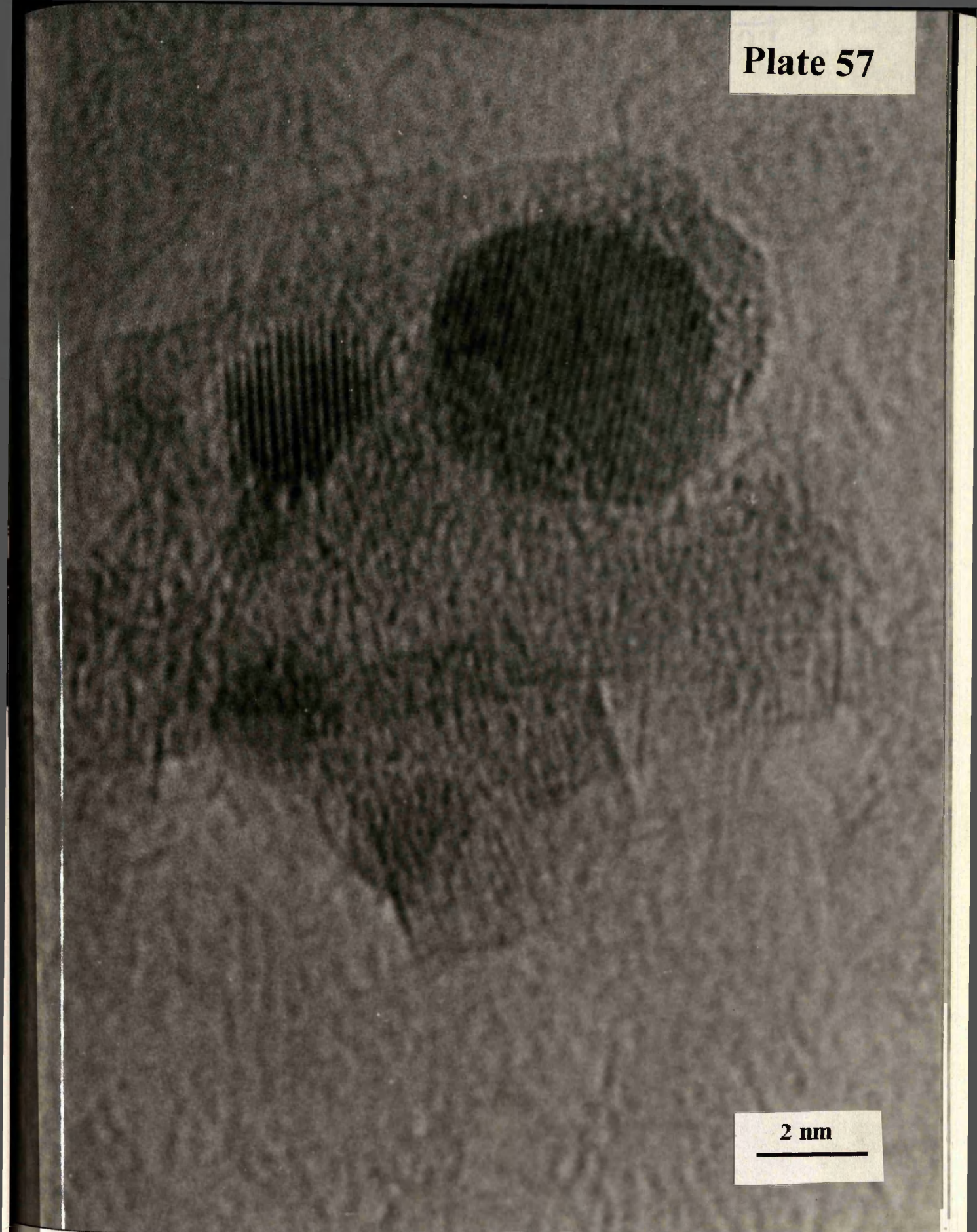
A number of apparently pure ruthenium particles were also observed in this catalyst after 21 hours on line. An example is given in plate 60. This particle was approximately 15-20 nm in diameter. The EDX spectrum obtained (inset) contained peaks due to ruthenium only. The MBED pattern (inset) obtained was indexed as the {100} pattern of hcp ruthenium. The lattice fringes in this micrograph were again indexed as the 0.214 nm {002} lattice of Ru.

5.18.B. n-Octane reforming

The yields of individual products over Ru-Ge/Al₂O₃ are listed versus time on line in table 5.18.1. The selectivities to the four major reforming reactions are given in table 5.18.2.

As with the nickel containing catalysts it was observed that the ruthenium catalyst showed very poor properties for the reforming of n-octane when compared to the related platinum or iridium catalysts. The yield of desirable aromatic products was very low as was the overall conversion. As with Ni-Ge, the yields of hydrocracked products such as propane, i-butane, n-butane and i-pentane were relatively high. This is also evident in the high selectivity shown by this catalyst for hydrocracking.

Due to the poor overall performance of this catalyst the reaction was discontinued after 21 hours on line.



2 nm

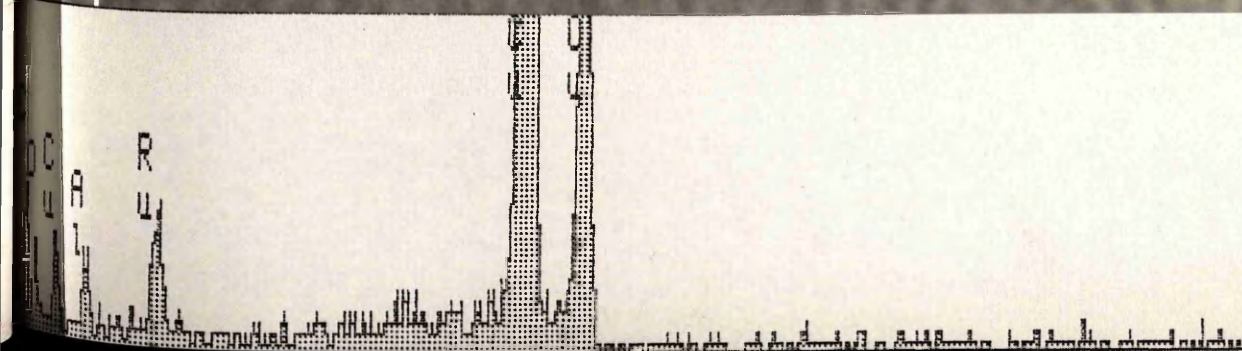
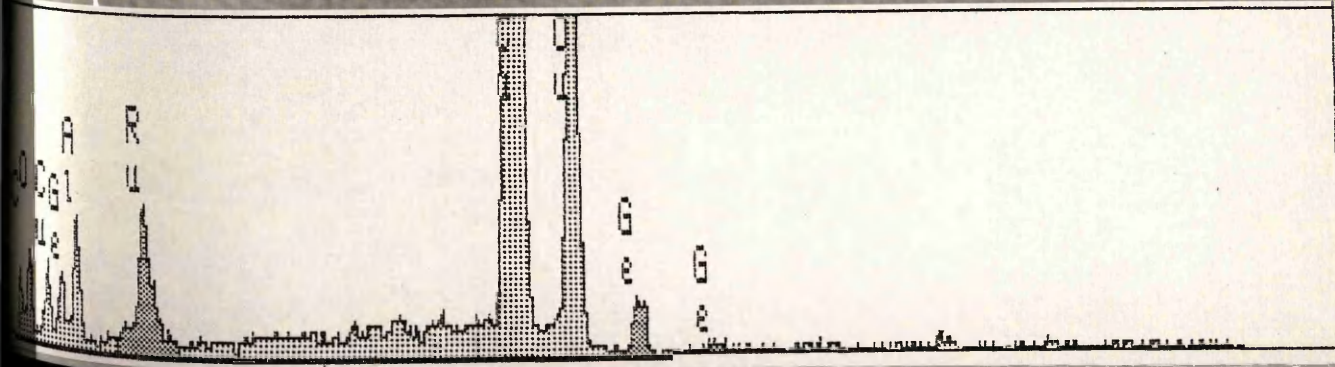
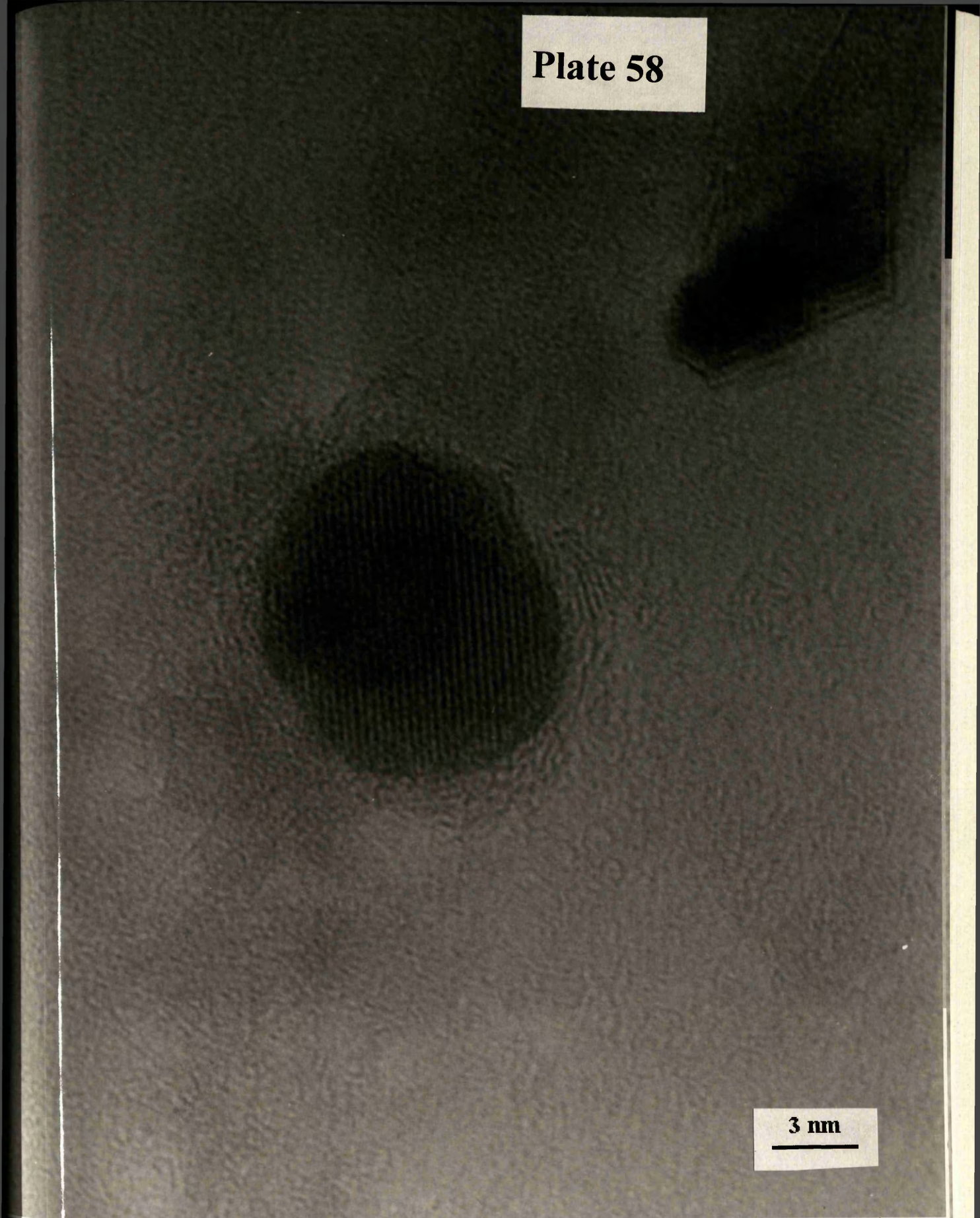
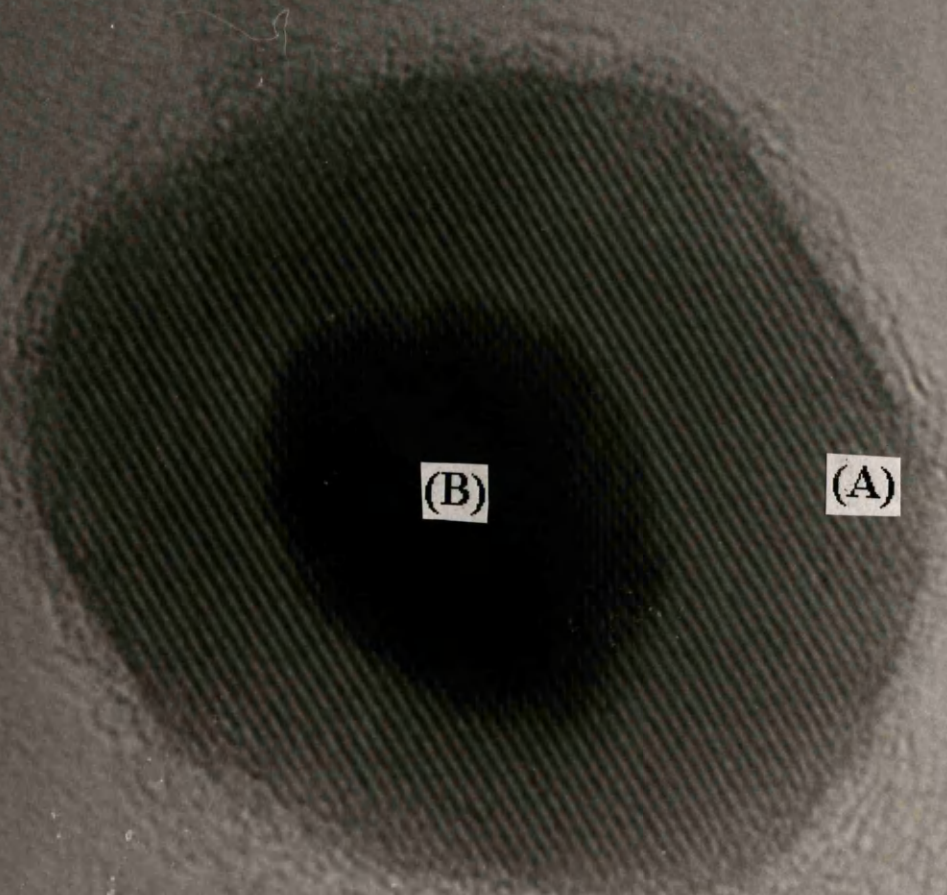


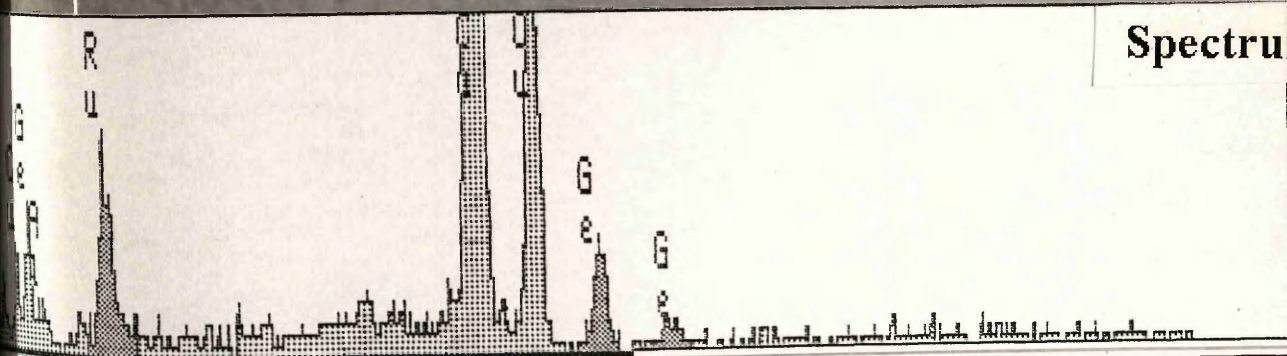
Plate 58



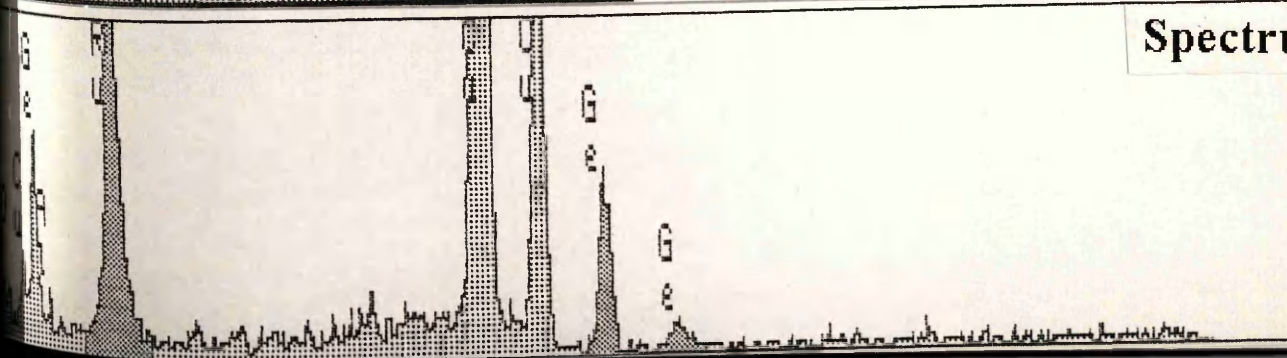


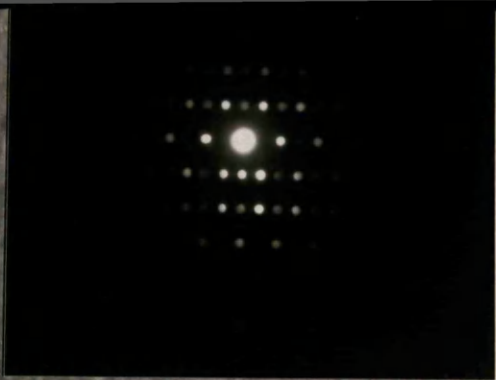
3 nm

Spectrum A



Spectrum B





3 nm

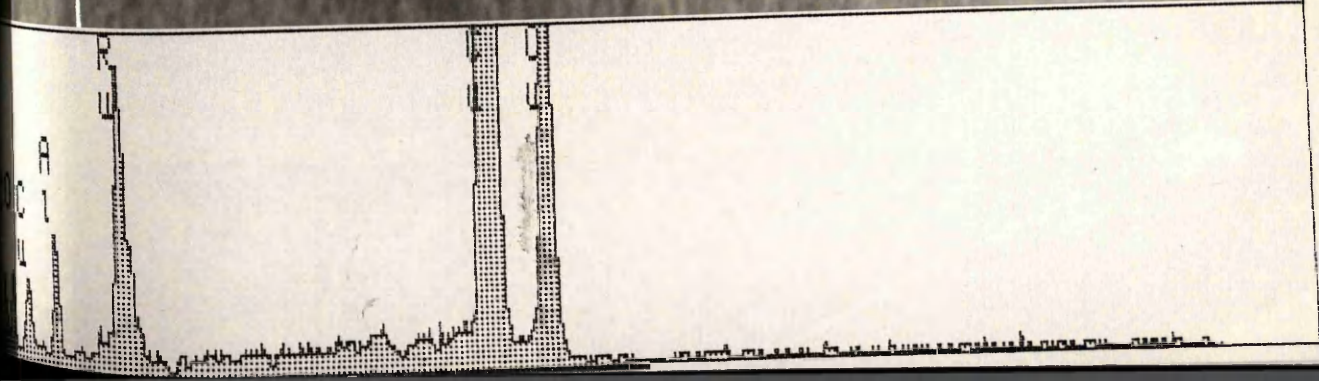


Table 5.18.1 Yields of individual products for catalyst 0.3 wt% Ru - 0.3 wt% Ge/Al₂O₃

Time (hours)	Methane	Ethane	Propane	i-Butane	n-Butane	c-Pentane	i-Pentane	n-Pentane
1.0	4.5	4.2	14.5	7.6	12.1	0.4	7.3	3.9
14.0	3.5	1.9	7.7	4.6	7.5	0.3	3.9	5.0
21.0	4.1	2.6	8.4	4.0	6.2	0.3	3.3	4.5

Table 5.18.1 (cont) Yields of individual products for catalyst 0.3 wt% Ru - 0.3 wt% Ge/Al₂O₃

Time (hours)	C6 c-Alkane	i-Hexane	n-Hexane	C7 c-Alkane	i-Heptane	n-Heptane	C8 c-Alkane	i-Octane
1.0	0.4	1.4	1.4	0.0	0.1	0.1	1.0	1.6
14.0	0.6	1.1	2.9	0.1	0.3	0.3	2.2	1.7
21.0	0.7	1.0	2.6	0.7	0.4	0.5	1.9	1.6

Table 5.18.1 (cont) Yields of individual products for catalyst 0.3 wt% Ru - 0.3 wt% Ge/Al₂O₃

Time (hours)	Benzene	Toluene	Ethyl-Benzene	m/p-Xylene	o-Xylene	C9 Aromatic	Total Conversion
1.0	0.2	1.5	0.2	2.4	0.9	0.4	66.1
14.0	0.0	0.6	0.1	1.0	0.4	0.2	45.8
21.0	0.1	0.7	0.1	1.2	0.5	0.2	45.5

Table 5.18.2 Selectivity to the major reforming reactions for 0.3 wt% Ru - 0.3 wt% Ge/Al₂O₃

Time (hours)	Selectivity to Aromatics	Selectivity to Isomerisation	Selectivity to Hydrocracking	Selectivity to Hydrogenolysis
1.0	8.3	2.6	24.6	6.8
14.0	5.1	4.3	21.1	7.5
21.0	6.0	4.4	18.2	9.0

5.19 Coke deposition

The weight percentage of carbon deposited on each catalyst after 144 hours (with one exception) is given in table 5.19.

Table 5.19 Coke deposition (wt%)

Catalyst	Coke (wt%)	Catalyst	Coke (wt%)
Pt	3.49	Ir-V	0.56
Pt-Sn	2.51	Pt-Ir-0.03Ge	2.35
Pt-Ge	3.74	Pt-Ir-Ge	3.95
Pt-Re	2.22	Pt-Ir-V	1.63
Pt-Ir	0.93	Pt [Pt(acac) ₂]	3.70
Ir	0.90	Pt-Ce	2.77
Ir-Ge	3.91	Pt-Pr	2.91
0.03Ir-Ge (100 hours)	1.82		

These results show that there is no simple relationship between the amount of carbon deposited and the rate of deactivation of these systems. It is known that the type of coke produced and where the coke is deposited are also important factors.

In general, additives such as Re, Sn, Ce and Pr tended to reduce the quantities of coke deposited. The presence of iridium however, reduced the quantity of carbon laid down much more significantly. In contrast germanium appeared to increase the quantity of coke formed, even when iridium was also present.

5.20 Chemisorption of CO and O₂ over Ir/Al₂O₃, Pt-Ir/Al₂O₃ and Pt-Ir-Ge/Al₂O₃

The chemisorption results are presented in table 5.20. Metallic platinum and iridium adsorb both CO and O₂ whilst Ge⁰ adsorbs only O₂.²²⁹

Table 5.20 Chemisorption results. (M = Ir + Pt)

Catalyst	Adsorbate	
	CO/M	O/M
Ir	1.18	1.78
Ir-Ge	0.61	1.47
Pt-Ir-Ge	0.43	0.93

The ability of highly dispersed iridium to show adsorption stoichiometries greater than unity has been reported previously for H₂^{137,140} and CO.¹⁴⁰ Although a lack of detailed knowledge regarding the stoichiometries of CO and O₂ adsorption on iridium prevented calculation of the metal dispersions, some useful qualitative conclusions could still be drawn.

The TEM studies revealed that both Ir and Ir-Ge were highly dispersed with particle sizes ≤ 1 nm. It is therefore unlikely that the differences in CO/M and O/M ratios obtained over these catalysts were due to particle size effect. It is more likely that dilution of the iridium surface by germanium resulted in the observed decrease in adsorption.

TEM observations of the Pt-Ir-Ge catalyst revealed a slight increase in particle size compared with the two preceding catalysts. It is therefore likely that at least part of the

further chemisorption suppression observed on addition of platinum was due to a decrease in dispersion. However, it is also likely that alloy formation between platinum and iridium played a significant role.

Chapter Six Discussion

Chapter Six: Discussion

6.1. Philosophy

6.1.1. Introduction

The overall objective of this study was to investigate the

relationship between the variables of interest, and to determine

the extent to which the findings are consistent with the

hypotheses derived from the theoretical framework.

The study was conducted in a

controlled environment, and the results are presented in

the following sections.

The first section discusses the

overall findings of the study, and the

second section discusses the

implications of the findings.

With regard to the first

observed that the results of the

study are consistent with the

hypotheses derived from the

theoretical framework, and the

results are consistent with the

hypotheses derived from the

theoretical framework, and the

results are consistent with the

hypotheses derived from the

theoretical framework, and the

In the following chapter the various activities and selectivities of the catalysts studied will be compared and contrasted. The reforming data will be correlated with the structural aspects of this study and the influence of processes such as coke formation, sintering and, in particular, alloy formation will be discussed. The advantages and disadvantages of the various promoters employed in this study will also be evaluated.

However, before a detailed discussion of the reforming properties of bi and multimetallic catalysts can be made, it is necessary to look in some detail at the monometallic Pt/Al₂O₃ catalyst on which these systems were based.

6.1 Pt/Al₂O₃

The overall conversion of n-octane over this catalyst was observed to fall significantly with time on line (figure 5.1.6) from 98.4% to 90.2%. The rate of activity decline was greatest in the initial stage of the run and gradually tailed off thereafter. This type of deactivation curve for Pt/Al₂O₃ has been observed in numerous studies of this catalyst.^{86,118,230,231} In these studies it is generally concluded that the initial rapid deactivation is caused by coke formation on the metal surface. Once the level of carbon on the metal obtains a steady state level, further deactivation of the catalyst proceeds via coke deposition on the support. Sintering of the metal particles also contributes to the overall activity decline by reducing the active surface area of the metal which is free to interact with gaseous hydrocarbons.

With regards to the yields of hydrogenolysis products (i.e. methane and ethane) it was observed that the yield of methane was higher at all stages of the run. This situation was repeated on all the catalysts studied. However, the yield of methane decreased rapidly in the initial stages of the run before stabilising, whilst the yield of ethane decreased in a slow, steady manner throughout the entire length of the run (figure 5.1.1). An initial

rapid decrease in hydrogenolysis activity over $\text{Pt}/\text{Al}_2\text{O}_3$ has been observed by many workers.^{72,86,118,230,231} This decrease is also believed to be linked to coking of the metal function. Hydrogenolysis reactions are considered to be structure sensitive^{25,26} (require specific numbers of adjacent metal atoms and/or geometries). Therefore dilution of the active metal surface results in selective loss of hydrogenolysis activity. This accounts for the rapid initial decrease in methane yield observed, although it is not clear why the yield of ethane was not affected in a similar manner.

For C_3 to C_7 products two general trends were observed in product distribution. First of all it was observed that within a particular alkane type (i.e. either normal, iso or cyclo) the yield decreased with increasing carbon number, e.g. for normal alkanes the yield decreased in the order: propane > n-butane > n-pentane > n-hexane > n-heptane. The only products which did not follow this rule were i-butane and c-pentane. The other general trend observed was that for a particular carbon number, the yield decreased in the order: i-alkane > n-alkane > c-alkane. Again the only exception to this rule was i-butane, whose yield was lower than that of n-butane. These trends were also seen on most of the bi/multimetallic catalysts studied.

Correlating the number of moles of products related by their carbon numbers such as C_3/C_5 , C_2/C_6 and C_1/C_7 reveals some interesting points. (N.B. the yields quoted are in terms of carbon number, see section 4.3.12, to obtain relative number of moles divide the total yield of C_3 , C_4 , C_5 etc. products by the number of carbon atoms). For this catalyst it was observed that the number of moles of C_3 and C_5 products produced were approximately equal, as were those of C_2 and C_6 species. This would suggest that the majority of these products were formed by a single scission of the n-octane molecule (rather than for example $\text{C}_8 \rightarrow \text{C}_5 + \text{C}_2 + \text{C}_1$). However, in the case of the C_1/C_7 relationship, it was observed that the number of moles of methane produced were considerably higher than the corresponding number of moles of heptanes + toluene. This strongly suggests that during hydrogenolysis of n-octane to produce methane (i.e. $\text{C}_8 \rightarrow \text{C}_{8-x} + x\text{C}_1$) multiple fragmentation of the molecule frequently occurred (i.e. $1 \leq x \leq 8$).

As described in section 1.2.5, i-alkanes predominate over n-alkanes due to rearrangement of the carbonium ions involved in hydrocracking to give more stable tertiary ions. Why this does not seem to be the case for butanes (the only exception) is not clear. The very low yield of cyclopentane may be related to the tendency of this molecule to form coke deposits.^{177,178}

With the exception of methane, all the aliphatic reforming products with six carbon atoms or less were observed to maintain relatively constant yields throughout the run (some yields decreased slightly). This contrasts with the yields of C₇ and C₈ compounds which were found to increase with time on line. The large increase in production of i-octane with time on line has also been observed in a number of related studies.^{118,232} This increase was mirrored by an equivalent decrease in the yields of C₈ aromatics (see figure 5.1.7). It was found that this change in selectivity occurred on a number of the catalysts studied and was always found to be accompanied by a corresponding decrease in overall conversion. It is thought that this change in selectivity with time on line occurred due to coke formation on the metal, which was responsible for decreasing the overall dehydrogenation activity of the catalyst.¹⁸⁶ This resulted in lower yields of aromatics, more isomerisation and lower conversion. This is consistent with the fact that most coke was formed on the metal in the initial stages and that the rate of change of all these reactions was greatest at that stage. It is unlikely that the particle size effects discussed in section 1.2.2¹⁶ were responsible for these observations as these effects refer to skeletal isomerisation on the metal surface alone, whilst in these acid catalysts the bifunctional mechanism has been shown to predominate (for example see Davis et. al.²³³).

It was also observed that the full range of possible aromatic compounds were formed over this catalyst. This is in agreement with the work of Davis et. al.^{117,233} For n-octane reforming at 100 psig over a monofunctional Pt catalyst (Pt/SiO₂ or Pt/Al₂O₃- non acidic alumina) these authors found that the only C₈ aromatics formed were those expected due

to direct six-carbon ring formation (i.e. ethylbenzene and o-xylene). However, over an acidic catalyst the mixture of C₈ aromatics produced was near the thermodynamic equilibrium mixture. (It was also found that the rate of aromatic formation was an order of magnitude higher over the bifunctional catalyst). This difference was attributed to the formation of five-membered-ring intermediates over the bifunctional catalyst and also to the ability of this catalyst to produce large quantities of i-octanes at low conversions (≈ 10%) which at higher conversions were converted into aromatics.

Significant yields of benzene and toluene were also observed over the Pt/Al₂O₃ catalyst. Regarding whether the loss of methyl or ethyl fragments necessary to form these products occurred before or after aromatisation, it is interesting to note that the concentration of toluene was higher than that of benzene. This is in contrast with the corresponding yields of alkanes, where the yield of hexane was considerably higher than the yield of heptanes. This suggests that these products were not formed by dehydrocyclisation of hexane or heptane molecules.

A small yield of C₉ aromatic products was also observed. It is thought that these species were formed via transalkylation between aromatic species. Such reactions were observed by Silva et. al.^{234,235} over bifunctional catalysts with mixtures of ethylbenzene and o-xylene. These authors also found that o-xylene was rapidly transformed into m/p isomers over bifunctional catalysts at 410 °C. Thus it is dangerous to draw conclusions about the mechanism of aromatisation of n-octane from the distribution of aromatics produced, especially in light of the very high conversions obtained in this study.

6.2 Pt-Sn and Pt-Ge

A number of the initial product yields over these two catalysts showed significant differences when compared to Pt/Al₂O₃. The correlations between related species which held for Pt/Al₂O₃, i.e. C₃/C₅ and C₂/C₆ ratios, were also found over these catalysts.

In the case of Pt-Sn/Al₂O₃, the most pronounced changes in the initial yields relative to platinum were an increase in aromatisation and a decrease in hydrocracking and isomerisation. This is shown in table 6.2.1.

Table 6.2.1 Initial and final conversions and selectivities over Pt, Pt-Sn and Pt-Ge.

<u>Reaction</u>	<u>Conversions and Selectivities</u>					
	<u>Pt</u>		<u>Pt-Sn</u>		<u>Pt-Ge</u>	
	I	F	I	F	I	F
Conversion	98.4	90.2	99.4	89.0	99.1	91.6
Aromatisation	45.2	25.1	51.0	25.8	43.9	26.2
Isomerisation	6.5	26.9	2.4	21.0	4.5	25.3
Hydrocracking	17.1	15.2	15.9	16.3	17.7	18.3
Hydrogenolysis	5.9	4.6	7.1	5.1	5.3	4.1

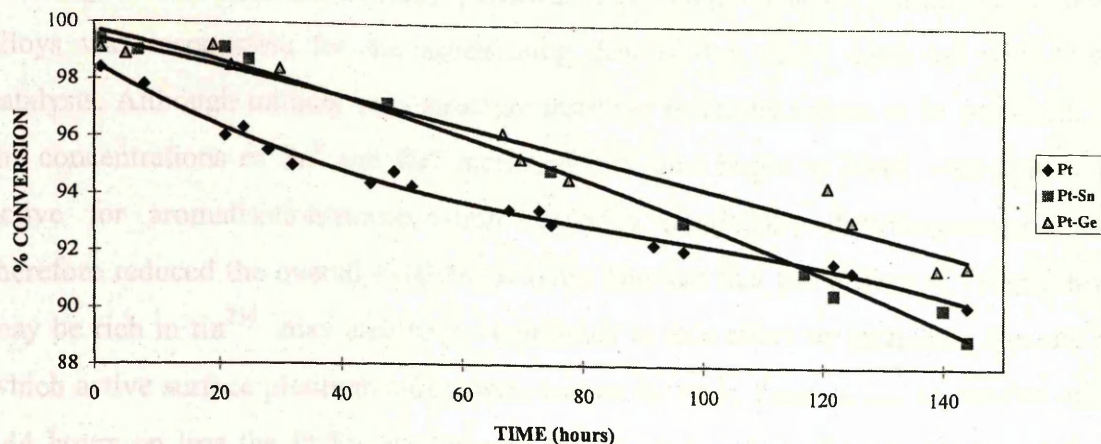
The ability of tin to promote aromatisation and decrease hydrocracking and isomerisation is well documented.^{93,99,112,117} The decrease in isomerisation/hydrocracking is generally thought to involve poisoning of the highly acidic sites on the alumina support by Sn^{II} ions.^{93,99} The increase in aromatisation is not well understood however. Some authors have concluded that the geometric effect of tin species on the metal surface actively promotes the aromatisation reaction.^{89,118,119} There is some support for this conclusion from the fact that sulphidation of Pt/Al₂O₃ catalysts

is also said to increase aromatisation. Other studies have found that the effect may be electronic in origin, i.e. the interaction between platinum and $\text{Sn}^{0(112,118)}$ or Sn^{II} ions^{89,118,119} results in modification of the electronic properties of platinum and hence its catalytic activity.

In the case of Pt-Ge/ Al_2O_3 , there was no enhancement of the initial yields of aromatics, the yield of isomerisation products was only slightly decreased whilst the yield of hydrocracked products was actually increased (N.B. the selectivity to aromatics quoted here does not include all the hydrocracked products). The increases in hydrocracking activity due to the presence of germanium was also observed in previous studies and was attributed to the acidity of GeO_2 species which were stabilised by the support.^{118,127} Although the overall yield of aromatics over Pt-Ge/ Al_2O_3 was similar to that observed over Pt/ Al_2O_3 , it was found that the distribution of products was different. The yield of ethylbenzene over Pt-Ge was very much lower (4.4% versus 8.8% over Pt/ Al_2O_3) whilst the yields of m/p-xylenes were increased (23.6% versus 19.4%). A similar effect was observed over Pt-Sn, although in this case the yield of ethylbenzene was only slightly suppressed (6.3%) whilst the yield of m/p-xylenes were strongly increased (27.4%). The reasons behind these changes in product distribution are not clear, although these differences do suggest that the influence of these promoters is not purely geometric in origin, (although as will be discussed, this is likely to be the major effect) and that electronic modification of platinum by these species may also play a significant role.

Although Pt-Ge and Pt-Sn did show differences in initial product distribution relative to the monometallic platinum catalyst, the more important influence of these promoters was to influence the way in which the product yields and overall conversions changed with time on line. The conversion of n-octane over these three catalyst versus time on line is plotted in figure 6.2.1. Similar graphs for the selectivities to aromatisation and isomerisation are presented in figures 6.2.2 and 6.2.3 respectively.

Figure 6.2.1 Conversion of n-octane versus time on line for Pt, Pt-Sn and Pt-Ge



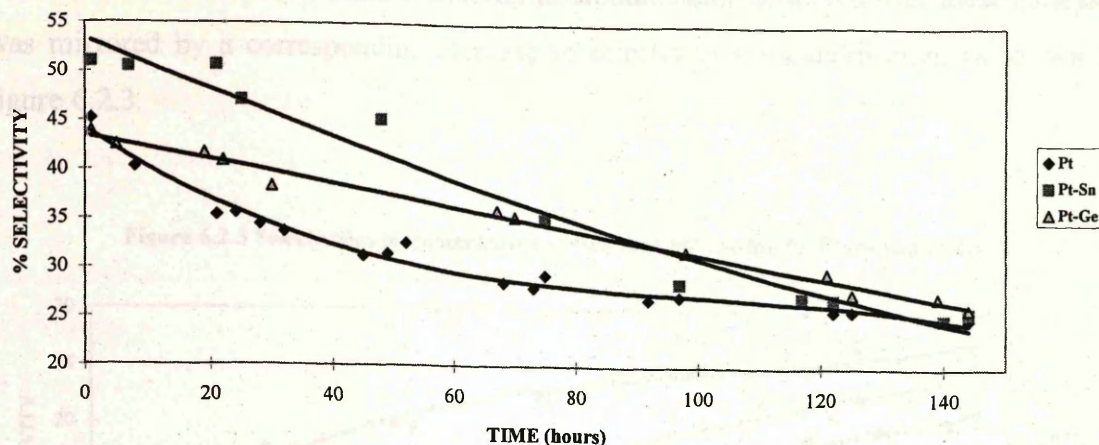
As discussed previously, the conversion over $\text{Pt}/\text{Al}_2\text{O}_3$ decreased most rapidly in the initial stages of the run due to coke formation on the metal surface. As the rate of formation of carbonaceous species decreased the rate of loss of catalytic activity also decreased. (An attempt to model these deactivation curves in terms of rate expressions was inconclusive) However, for Pt-Sn and Pt-Ge the deactivation curves were very different. In the case of these catalysts the rate of deactivation was lowest in the initial stages of the run and actually accelerated as the run progressed. The lower initial rate of deactivation of these systems was due to a geometric effect. Although previous studies in this department found that the total concentrations of Sn^0 and Ge^0 after calcination and reduction were low,^{120,128} nonetheless the reforming data presented in this work for the related Ir-Ge/ Al_2O_3 catalyst (section 5.7) showed that a very strong geometric/ensemble interaction had occurred between the dispersed metal and the promoter, i.e. dilution of the active metal surface into smaller ensembles. As coke formation on the metal surface is known to be structure sensitive, the dilution of these surfaces by Sn^0 or Ge^0 species results in a lower rate of coke deposition and hence deactivation. The possibility that SnO_x and GeO_x oxide species were involved in these geometric effects cannot be ruled out (c.f. V_2O_5 catalysts). This will be discussed in more detail in section 6.4.

However, with extended use the concentration of Sn^0 and Ge^0 species increases, resulting in the formation of alloy particles. It is thought that the formation of these alloys was responsible for the accelerating deactivation curve observed with these catalysts. Although initially only structure sensitive reactions appear to be poisoned, as the concentrations of Sn^0 and Ge^0 increased they also began to block sites that were active for aromatisation/isomerisation reactions (essentially dehydrogenation) and therefore reduced the overall catalytic activity. The fact that the surface of Pt-Sn alloys may be rich in tin²³⁶ may also have contributed to this effect by increasing the rate at which active surface platinum atoms were lost to the bulk. Figure 6.2.1 shows that after 144 hours on line the Pt-Sn catalyst was actually less active than Pt/ Al_2O_3 and that, given a sufficiently long period of time on line, the activity of Pt-Ge would also fall below that of Pt/ Al_2O_3 .

The effect of sintering on the catalytic properties of these systems was not clear from the data obtained. Although TEM studies revealed significant alloy formation in the Pt-Sn and Pt-Ge catalysts, the actual number density and average particle size of the particles observed were found to be similar to those observed over Pt/ Al_2O_3 . However, it is difficult to be very specific in this respect due to the low metal loadings that were employed in these systems.

The changes in selectivity to aromatics, which are shown in figure 6.2.2, over these three catalysts were found to follow similar trends to those of conversion of n-octane.

Figure 6.2.2 Selectivity to aromatics versus time on line over Pt, Pt-Sn and Pt-Ge

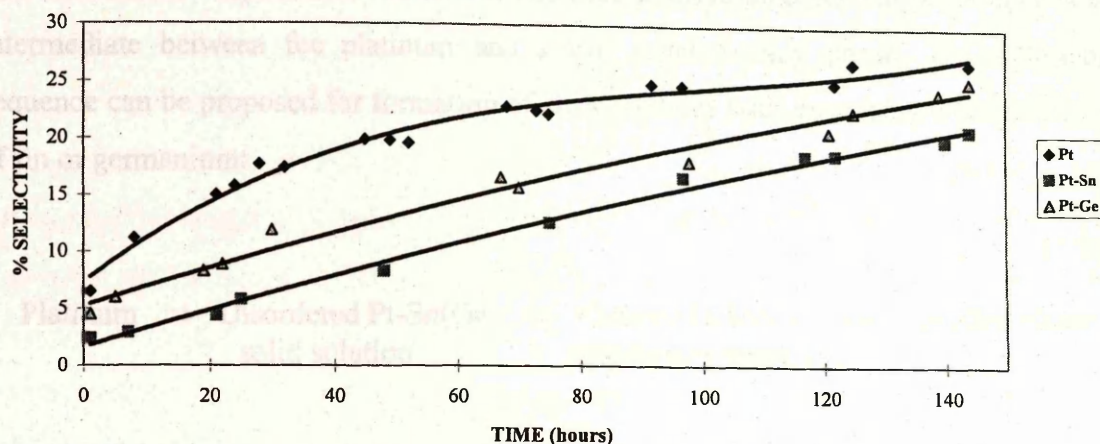


The selectivity to aromatisation was found to decrease most rapidly in the initial stages over Pt/Al₂O₃, again due to coke formation. On Pt-Sn and Pt-Ge the selectivities to these products did not undergo this initial decline but deactivated at a more constant level throughout the entire length of the run. Again it would appear that the selectivity to aromatisation over Pt-Sn and Pt-Ge would actually fall below that of Pt/Al₂O₃ given a sufficiently long period of time. As with the overall conversion, the initial improved properties of Pt-Sn and Pt-Ge were due to a geometric effect decreasing the rate of carbon deposition in the initial stages. However over extended periods blocking of the active sites by Sn⁰ and Ge⁰ species contributed to the overall rate of deactivation.

Comparison of the initial hydrogenolysis activities of these catalysts would perhaps suggest significant geometric effects did not occur in these systems due to the fact that the hydrogenolysis activities of Pt-Sn and Pt-Ge were not lower than the corresponding activity of platinum. However, it must be remembered that the initial yields quoted in this work were obtained after one hour on line. It is likely that the initial hydrogenolysis activity of the Pt/Al₂O₃ catalyst had decreased substantially before the first sampling point was reached. Indeed, a number of studies, where the detection and quantification of reforming products could be performed in a matter of minutes as opposed to the 3 hours required in this study, have found that very rapid initial hydrogenolysis decline does occur over platinum.^{72,118,231}

The decrease in conversion and selectivity to aromatisation observed over these catalysts was mirrored by a corresponding increase in selectivity to isomerisation, as shown in figure 6.2.3.

Figure 6.2.3 Selectivities to isomerisation versus time on line for Pt, Pt-Sn and Pt-Ge

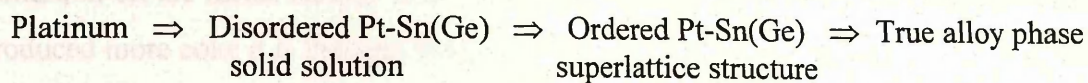


Again it was observed that the rate of change in the selectivity was greatest in the initial stages over Pt/ Al_2O_3 , whilst over Pt-Ge and Pt-Sn the increase in isomerisation occurred at a more constant rate throughout the run. It is interesting to note that the isomerisation activity of the Pt-Ge catalyst remained above that of the Pt-Sn catalyst throughout the run. This may have been due to the increased acidity of this catalyst due to the presence of GeO_2 species.

It is also interesting to note that the rate of activity decline, both in terms of conversion and selectivity to aromatisation, was greater over the Pt-Sn catalyst than the Pt-Ge catalyst. It is thought that this may have been due to the relative ease of reduction of tin and germanium oxide species. Consideration of the relative TPR studies described in sections 1.3.3B and 1.3.3C reveals that the position of the reduction peaks assigned to germanium in the TPR profiles of Pt-Ge/ Al_2O_3 catalysts were found at consistently higher temperatures than the corresponding tin peaks in the profiles of Pt-Sn/ Al_2O_3 catalysts. This suggests that tin oxide species are more easily reduced than germanium

and that the concentration of Sn^0 present in these catalysts would therefore increase more rapidly than the corresponding concentration of Ge^0 . This may also explain why most of the Pt-Sn alloys observed were hcp PtSn whilst for germanium a greater distribution of alloy compositions were observed, most with Pt/Ge atomic ratios less than unity (also, the atomic percent of germanium was actually higher than that of tin in these systems).

The modified or “superlattice” structures observed in these catalysts can be thought of as intermediate between fcc platinum and a true ordered alloy phase. The following sequence can be proposed for formation of alloy particles with increasing concentrations of tin or germanium:



In the initial stages the solute atoms occupied completely random sites in the platinum lattice. However, as the concentration of these atoms increased it became necessary for them to occupy specific sites in the lattice in order to reduce lattice strain. Eventually when the concentration of solute atoms obtained a certain value it was possible for true ordered alloy phases to form.

The ordered nature of the lattice sites occupied by Ge and Sn accounts for the presence of extra “superlattice” reflections in the diffraction patterns obtained from these phases. When a disordered solid solution formed the structure factors for the solute atoms would sum to zero and the diffraction pattern obtained would be essentially that of pure platinum. However, if these atoms occupied specific ordered sites in the lattice, then the structure factors become non-zero and extra superlattice reflections would appear in addition to the underlying fcc diffraction pattern. It is also interesting to note that different types of superlattice reflections were observed. If the diffraction patterns for plates 11 and 17 are compared it is apparent that the latter contains more reflections. The pattern in plate 11 was indexed as the Pt (110) pattern (bright spots) with extra {100}

and $\{110\}$ spots (which are forbidden for pure fcc metals). However in plate 17 it is apparent that a further set of reflections were present midway between each of the $\{111\}$ spots, with a d-spacing equivalent to $2 \times \{111\} = 0.453$ nm, i.e. larger than the platinum unit cell. These extra spots occurred due to double diffraction.

It must be remembered that even after 144 hours on line it is possible that a significant proportion of the metallic component in Pt-Sn and Pt-Ge catalysts was present in the form of particle 1 nm in diameter or less.

Although tin was found to decrease the total quantity of coke formed on this catalyst it is likely that its major influence was on where this coke was deposited,¹¹⁸ i.e. coke formation on the metal surface was reduced. Although the Pt-Ge/ Al_2O_3 catalyst actually produced more coke it is thought likely that the metal component of the catalyst was kept free of carbonaceous deposits in a similar manner. Promotion of the overall quantity of coke deposited on catalysts containing germanium was also observed by Beltamini and Trim¹²⁷ and was attributed by these authors to the increased acidity of this catalyst.

It would appear that Pt-Sn and Pt-Ge offer improved performance to Pt/ Al_2O_3 catalysts in the initial stages of the reforming run via geometric effects which reduce coke deposition on the metal and, particularly in the case of tin, improve the selectivity to aromatics. It is likely that this improvement would become even more noticeable under more severe operating conditions (lower pressure, higher hydrocarbon/ H_2 ratio, higher temperature) where the formation of both aromatics and coke are favoured. With increased time on line the formation of alloy particles contributed to the overall rate of deactivation of these systems. Indeed, given a sufficiently long period of time on line the activity of these catalysts would have fallen below that of platinum. This may explain the preferred use of Pt-Sn/ Al_2O_3 catalysts in refineries which allow continuous regeneration of the catalyst. In such systems the Pt-Sn catalyst is preferred due to its improved selectivity to aromatics and the ease of its regeneration (does not require the lengthy sulphur treatment procedures needed for Pt-Re and Pt-Ir). As will be discussed in the

following section Pt-Re and Pt-Ir catalysts are used in refineries where the catalyst must remain active over very long periods of time.

It is worth drawing attention to the similarity in the effects of addition of Sn, Ge and sulphur to Pt/Al₂O₃ catalysts. All three influence the quantity of coke deposited on the metal function via a geometric effect and improve the selectivity of the catalyst.⁶¹ However, it is well known that addition of larger quantities of sulphur poison the activity of reforming catalysts (therefore sulphur levels in naphtha feedstocks must be controlled) and it would appear from this work that relatively large quantities of Sn⁰ and Ge⁰ can produce similar effects. The poisoning effects of Sn⁰ and Ge⁰ have been noted in a number of previous studies.^{112,117}

6.3 Pt-Re/Al₂O₃ and Pt-Ir/Al₂O₃

The initial product yields over these catalysts were significantly altered from those of monometallic Pt/Al₂O₃. For Pt-Re it was observed that the initial yield of methane was significantly higher than the corresponding yield over platinum. It was also found that the correlation between the number of moles related species, i.e. C₂/C₆ and C₃/C₅, no longer held. In both cases the number of moles of the lower molecular weight product was considerably greater. This suggests that multiple fragmentation/hydrogenolysis reactions were considerably enhanced over this catalyst relative to Pt/Al₂O₃. This increase in fragmentation is also evident in the distribution of aromatic products formed over this catalyst, with yields of benzene and toluene being considerably enhanced at the expense of C₈ species.

For the Pt-Ir catalysts this trend towards hydrogenolysis and multiple fragmentation reactions was even more pronounced. The yields of methane, ethane and, in the latter stages, even propane were considerably greater whilst those of C₄, C₅, C₆, C₇ and C₈ compounds were much lower (in some cases zero). The enhanced propane yield

observed over this catalyst during the later stages of the run was not caused by increased hydrocracking. Rather these species were the remnants of C₈ molecules that had undergone multiple splitting reactions yielding methane and ethane. As the overall hydrogenolysis activity of the catalyst decreased slightly with use, the number of C₃ units remaining intact at the end of the catalyst bed increased, as did the yields of butanes and some other products. On this catalyst the major aromatic products formed were benzene and toluene while only small amounts of C₈ aromatics were produced.

The increased hydrogenolysis activity of the Pt-Ir catalyst was caused by the presence of metallic iridium which is well known to have a high hydrogenolysis activity.^{23,24} The TEM studies revealed that this iridium was found in the form of Pt-Ir alloys whose compositions varied about the nominal 1:1. Comparison of the activity of this alloy catalyst with that of pure iridium (section 5.5) reveals that the presence of platinum significantly decreased the hydrogenolysis activity of iridium.

As has been discussed in section 5.5, the Pt-Ir and Pt-Re catalysts showed similarities in their product distributions. These are summarised in table 6.3.1.

Table 6.3.1 Similarities in product yields over Pt-Re and Pt-Ir

<u>Product</u>	<u>Yield</u>		
	Pt	Pt-Re	Pt-Ir
Methane	5.8	10.0	42.8
C ₆ + C ₇ Aromatics	5.0	14.0	21.0
C ₈ Aromatics	38.4	31.4	0.7

Both catalysts showed increased hydrogenolysis relative to platinum and a shift in the production of aromatics towards benzene and toluene at the expense of C₈ species. These

similarities strongly suggest that a significant proportion of the rhenium in Pt-Re catalysts must have been present in the metallic state. The TEM/EDX studies performed in this work, and previous studies performed in this department involving TEM/EDX and chemisorption methods,⁸⁵ could find no evidence to suggest the presence of Pt-Re alloys or Re^0 metal.

Why these methods did not detect any Re^0 is not clear although a number of possible explanations may be discussed. Sinfelt et. al.¹⁶⁴, studying a series of Pd-Re catalysts utilising EXAFS, found evidence for oxidation of rhenium on switching from hydrogen to nitrogen atmospheres. It was concluded by these authors that after changing to nitrogen some Re^0 reacted with lattice oxygen from the Al_2O_3 support. This suggests the possibility that metallic rhenium may have oxidised on removing the catalyst from the reactor. However, if relatively large Pt-Re alloys were present in this catalysts, as was found in the case of Pt-Ir, then oxidation of rhenium would be expected to produce platinum particles surrounded by a shell of rhenium oxide (similar to the tin oxide layer visible in plate 11). However this was not observed. It must also be remembered that rhenium is an hcp metal whilst platinum and iridium are fcc. Rhenium is not miscible with platinum in the bulk whilst platinum and iridium are completely miscible. This would suggest that even if significant quantities of Re^0 were formed, they would not form alloy particles in a similar manner to Pt-Ir. It may be the case that alloy particles or bimetallic clusters could only form for very small particle sizes, i.e. 1 nm in diameter or less and that as the particle size increased the atomic fraction of rhenium that could be incorporated into the lattice decreased (and always remained below the sensitivity limits of the EDX system). A further possibility was that rhenium atoms were only found at surface positions in these particles.

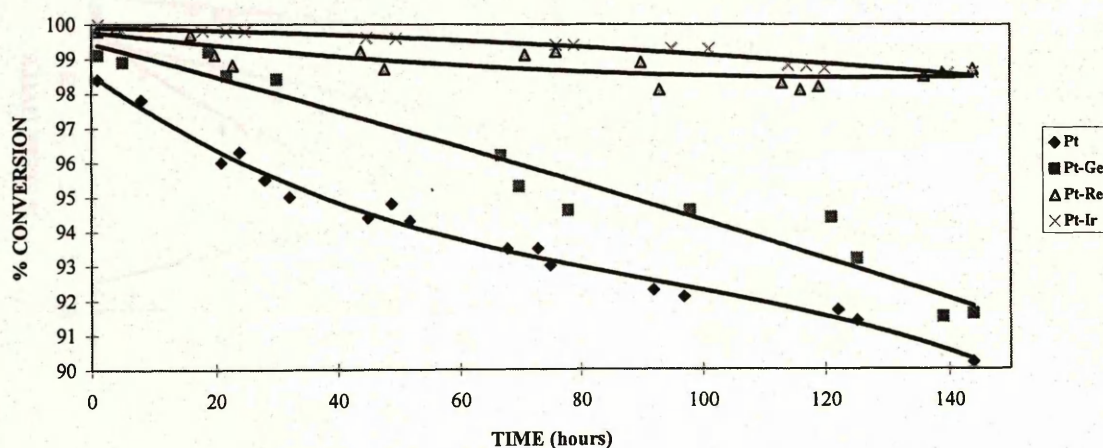
A further possibility that must be considered was that rhenium was not significantly associated with platinum but formed separate nanometer sized particles. If these particles did form it is likely that they would not sinter significantly throughout the 144 hours on line, as was found with iridium particles in $\text{Ir}/\text{Al}_2\text{O}_3$ (relative melting points: Pt - 1769

°C, Ir - 2443 °C and Re - 3170 °C). It is likely therefore that these particles, if formed, would remain invisible to TEM observation. However, it is not thought likely that these separate Re particles were formed. If a large proportion of rhenium was present as separate rhenium particles then the catalyst properties would be dominated by these particles and a very high hydrogenolysis activity would result. However, if rhenium was alloyed with platinum, or in the form of small bimetallic clusters, then this high hydrogenolysis activity would be modified to some degree, as was found on addition of platinum to iridium.

It must also be stated that although the activity of metallic rhenium for alkane hydrogenolysis reactions is higher than that of platinum, it is not considered to be as high as iridium.²³ Therefore the observation that the hydrogenolysis activity of the Pt-Re catalyst was lower than that of Pt-Ir does not necessarily imply that only a small proportion of the rhenium was in the metallic state.

As well as modifying the initial activity of these catalysts, rhenium and iridium also significantly altered the way in which the yields changed with time on line. The conversion of n-octane versus time on line for these catalysts is plotted in figure 6.3.1 along with the corresponding values for Pt/Al₂O₃ and Pt-Ge/Al₂O₃, to aid comparison.

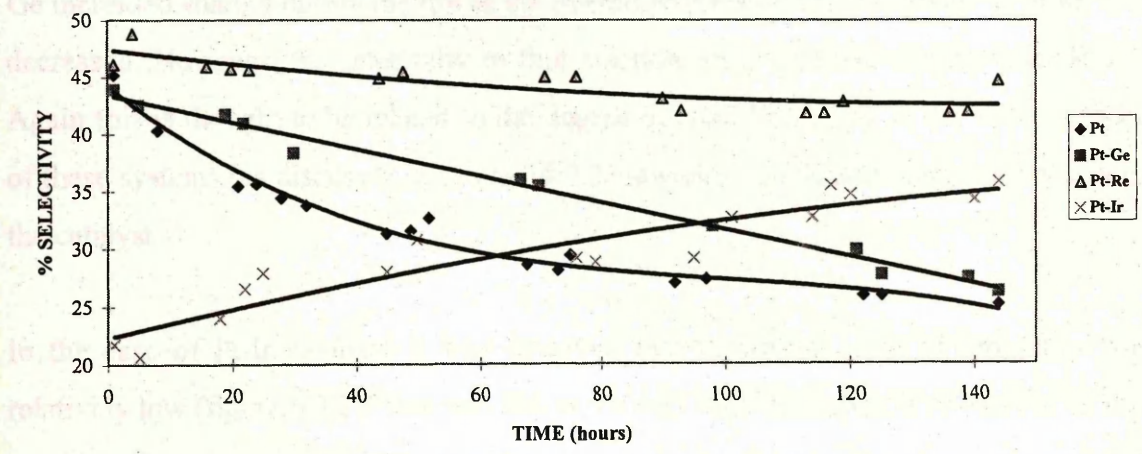
Figure 6.3.1 Conversion versus time on line over Pt, Pt-Ge, Pt-Re and Pt-Ir



It is clear from this graph that the presence of rhenium and iridium significantly improved the available lifetime of these catalyst by maintaining high conversion levels. Indeed, the conversion over these systems was found to decrease by only 1-2% during 144 hours on line. This is a well known property of Pt-Re and Pt-Ir catalysts and has been discussed at some length in the literature.^{61,72,135,139-141} It is generally concluded that, in the non sulphided form (the effect of sulphur addition will be discussed at the end of this section), rhenium and iridium prevent coke formation on the metal surface. However, this is not a geometric effect as with tin and germanium. In this case the high hydrogenolysis activities of these metals provide sites for the hydrogenolysis /hydrogenation of coke deposits that form on the metal surface (or of the precursors which are known to produce large quantities of coke e.g. methylcyclopentane). In this way the metal surface is kept relatively clean and the overall activity is maintained.

Some interesting points are also observed when we look at the selectivities of these catalysts. The selectivities to aromatisation versus time on line for these catalysts are plotted in figure 6.3.2., again with the corresponding data for Pt/Al₂O₃ and Pt-Ge/Al₂O₃ for comparison.

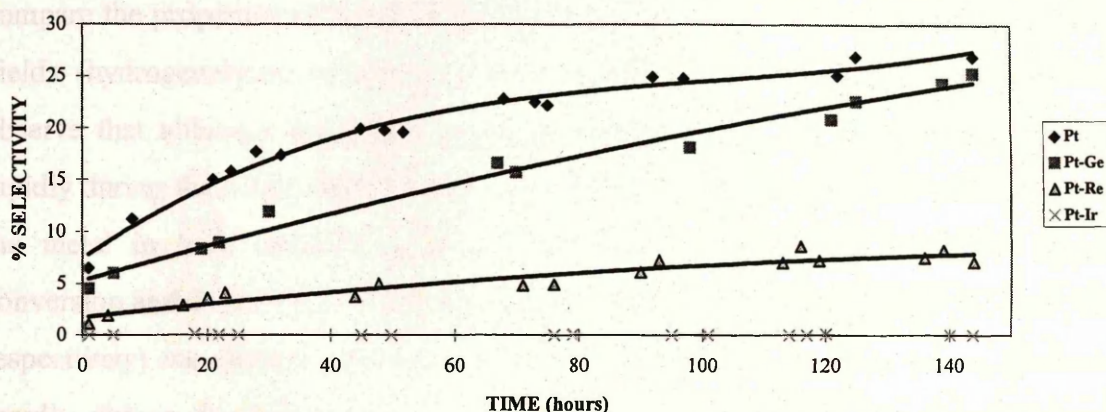
Figure 6.3.2 Selectivity to aromatics versus time on line for Pt, Pt-Ge, Pt-Re and Pt-Ir



First of all it is noted that the Pt-Re catalyst maintained an excellent yield of aromatics even after 144 hours on line. This is in contrast to the Pt and Pt-Ge (and Pt-Sn) catalysts which deactivated significantly during the run as discussed previously. Again this was due to the ability of rhenium to prevent the formation of large scale coke deposits which would reduce the selectivity to aromatics.

This point is also important when looking at the selectivities to isomerisation, which are plotted for the same four catalysts in figure 6.6.3.

Figure 6.3.3 Selectivities to isomerisation versus time on line for Pt, Pt-Ge, Pt-Re and Pt-Ir



As was discussed in the previous section the selectivity to isomerisation over Pt and Pt-Ge increased sharply during the run as the overall conversion and selectivity to aromatics decreased. However, the selectivity to this reaction only increases slightly over Pt-Re. Again this is thought to be related to the degree of coke formation on the metal surface of these systems (as discussed in section 6.2.2) lowering the dehydrogenation activity of the catalyst.

In the case of Pt-Ir catalysts it was observed that the initial yield of aromatics was relatively low (figure 6.3.2). This was due to the very high hydrogenolysis activity of this catalyst. However, as the run progressed the yields of aromatics were observed to increase steadily. This corresponded to a decrease in the activity for hydrogenolysis.

Again this phenomenon is thought to be related to coke formation on the metal surface (there is an apparent contradiction here which will be discussed in more detail shortly). Hydrogenolysis, as has been discussed previously, is a structure sensitive reaction which is known to require specific reaction sites/ensembles of metal atoms and therefore its activity is most severely affected by any residues or surface species that adhere to the metal surface. The activities of the remaining reactions are not affected greatly by these species and therefore the selectivity of the catalyst moves away from hydrogenolysis towards aromatisation etc.

To address the apparent contradiction regarding the formation of carbonaceous residues either improving the catalytic properties or resulting in deactivation, it is useful to compare the properties of Pt and Pt-Re catalysts. First of all if we compare the methane yields (hydrogenolysis) of these catalysts (figures 5.1.1 and 5.4.1 respectively) we observe that although the initial values were higher over Pt-Re, they both decreased rapidly during the initial stages of the run. This has been attributed to coke deposition on the metal in both cases as discussed. However, if we now compare the overall conversion and selectivities to aromatics over these two catalysts (figures 6.2.1 and 6.2.2 respectively) we observe that over the Pt/Al₂O₃ catalyst both these values decreased rapidly during the initial stages whilst over the Pt-Re catalyst the conversion and selectivity to aromatics remained constant throughout the run. This suggests that rhenium modified the quantity of coke that formed, allowing sufficient carbon to be deposited to decrease structure sensitive hydrogenolysis reactions but not enough to affect the remaining reactions. On pure platinum the level of coke deposited on the metal was higher and therefore aromatisation and total conversion levels were also affected.

It is also possible that the type of coke deposited, or the position where this coke was deposited on the metal surface, also played significant roles. Blakely and Somorjai²⁹ and a subsequent paper by Coughlin et.al.⁷⁵ proposed that the hydrogenolysis sites on metal surfaces were high index, low coordination sites such as corners, edges etc. It was also proposed that initial carbon deposition occurs on these sites thereby poisoning

hydrogenolysis. As further carbon deposition occurs the higher coordination or terrace type sites begin to be blocked resulting in deactivation of dehydrocyclisation reactions. It was further proposed by Coughlin et. al. that the function of rhenium was to retard the deposition of carbon and/or prevent its rearrangement into graphitic structures on the high coordination or terrace sites and thereby slow the deactivation of the dehydrocyclisation reaction. Both Pt-Re and Pt-Ir, particularly Pt-Ir, were found to produce significantly less coke than platinum. Again however there is no simple relationship between the quantity of coke produced and the rate of deactivation, e.g. Pt-Re did not deactivate any faster than Pt-Ir even though more carbon was produced.

For Pt-Re the rate of sintering was found to be similar to that of Pt/Al₂O₃. It is therefore thought unlikely that a major influence of rhenium, in the form of Re^{IV} ions, was to stabilise small metal particles as suggested by some studies.²³⁷ Also, the role played by any electronic modification of platinum induced by either alloy formation⁷¹ or interaction with Re^{IV} species⁸⁵ was not clear from the data obtained. The Pt-Ir catalyst was found to sinter more noticeably than Pt and Pt-Re. Whether this produced a significant change in the reforming properties of this catalyst is not clear. The reduction in methane yield, and by implication the deposition of coke on the metal surface, occurred at a much lower rate on Pt-Ir than Pt-Re but continued throughout the entire length of the run.

Finally, as Pt-Re and Pt-Ir catalysts are always treated with sulphur before use, it is necessary to discuss what effect this process would have on the corresponding catalytic properties. It is likely that the effect of adding small quantities of sulphur to the Pt-Re catalyst would be essentially the same as the effects produced by coke formation in the initial stages of the run. That is, to selectively decrease hydrogenolysis whilst retaining the activity for the desirable reforming products. In the case of the Pt-Ir catalyst a similar process would occur. In this case however the suppression in hydrogenolysis activity by sulphur would be much greater than that observed due to gradual coking. The fact that the selectivity to aromatics was still increasing after 144 hours on line suggests that over

the sulphided catalysts (where the hydrogenolysis activity is similar to that of Pt/Al₂O₃) the selectivity for this reaction would be higher still. Indeed, Sinfelt et. al.¹⁴⁰ found that a sulphided Pt-Ir catalysts was approximately twice as active as a similar Pt-Re catalyst for the dehydrocyclisation of alkanes. It is not clear however whether such a large difference in activity would exist under the conditions employed in this study.

6.4 Ir/Al₂O₃, Ir-Ge/Al₂O₃, 0.03Ir-Ge/Al₂O₃ and Ir-V/Al₂O₃

It was shown in chapter 5 that addition of germanium and vanadium species to Ir/Al₂O₃ catalysts produced dramatic alterations in the catalytic properties of these systems.

The Ir/Al₂O₃ catalyst (section 5.6), as expected, was found to have a very high hydrogenolysis activity. In the initial stages this catalysts converted the entire octane feed into methane. With extended use the selectivity to methane decreased very slightly, due to a small amount of coke deposition. It was again observed that this change occurred most noticeably in the initial stages of the run (see figure 5.6.1). The quantity of coke formed on this catalyst was significantly lower than on the Pt/Al₂O₃ (Pt - 3.49 wt% versus Ir - 0.9 wt%: these are total carbon contents, it is not known what fraction of each was associated with the metal function) and therefore this catalyst retained very substantial hydrogenolysis activity even after 144 hours on line. It is interesting to note that although the hydrogenolysis selectivity decreased slightly through the run, the overall conversion remained at 100%. This again highlights the sensitivity of the hydrogenolysis reaction relative to the other reforming processes.

As the selectivities to hydrogenolysis decreased, the yields of some of the other products increased. Those that increased most significantly were ethane, propane, benzene and i-octane. This reveals some interesting points. First of all, the observation that the i-octane yield increased much more significantly than those of hexanes or heptanes suggests that multiple fragmentation reactions occurred during a single adsorption step. If multiple

adsorption-fragmentation-desorption steps were involved one would expect to have seen an equivalent increase in the yields hexanes and heptanes, which was not observed. The observation that the yields of ethane and propane (and to lesser extent butanes) increased throughout the run was due to increasing quantities of C₂, C₃ and C₄ units desorbing from the metal surface before further hydrogenolysis/fragmentation could occur.

It is also interesting to note that the aromatic yields which increased most significantly were benzene and toluene. Again it is not thought that these products were formed by dehydrocyclisation of C₆ and C₇ species. It is more likely that C₈ aromatics, once formed, were susceptible to dealkylation reactions. The observation that iridium was significantly more resistant to sintering than platinum in hydrogen rich atmospheres was also made by Fiedorow et. al.²³⁸ These authors also explained this observation in terms of the relative melting points of the metals, as discussed in section 6.3 (melting points: Pt - 1769 °C, Ir - 2443 °C).

The properties of this base Ir/Al₂O₃ catalyst were altered significantly by the addition of germanium and vanadium species to the catalyst. Table 6.4.1 contains the initial (1 hour) and final (144 hour) selectivities and conversions for the four catalysts discussed in this section.

Table 6.4.1 Initial and final conversions and selectivities over Ir, Ir-Ge, 0.03Ir-Ge and Ir-V

<u>Reaction</u>	<u>Conversions and Selectivities</u>							
	<u>Ir</u>		<u>Ir-Ge</u>		<u>0.03Ir-Ge</u>		<u>Ir-V</u>	
	I	F	I	F	I	F	I	F
Conversion	100.0	100.0	100.0	97.1	90.4	60.4	99.1	95.9
Aromatisation	0.0	6.0	33.6	32.2	18.9	16.7	27.6	26.9
Isomerisation	0.0	2.2	0.0	10.8	4.1	14.5	6.9	11.8
Hydrocracking	0.0	2.2	21.0	21.5	24.3	18.7	14.0	19.0
Hydrogenolysis	100.0	80.7	3.8	2.9	4.8	6.0	19.1	10.5

It is clear from this table that the major influence of these promoters was to dramatically decrease hydrogenolysis, which in turn resulted in a very large increase in the selectivities to the remaining more desirable reactions. This indicates that a very strong geometric effect occurred, particularly in the case of the germanium catalyst. Indeed the product distribution obtained over this catalyst had more in common with the $\text{Pt}/\text{Al}_2\text{O}_3$ catalyst than with $\text{Ir}/\text{Al}_2\text{O}_3$.

First of all in the case of the Ir-Ge catalyst, it was observed that the methane yield over this system was actually lower than the corresponding yield over $\text{Pt}/\text{Al}_2\text{O}_3$. It is not clear why this should be the case, although factors such as the degree of reduction of germanium, the strength of the interaction between germanium and iridium relative to germanium and platinum, and particle size effects must all be considered.

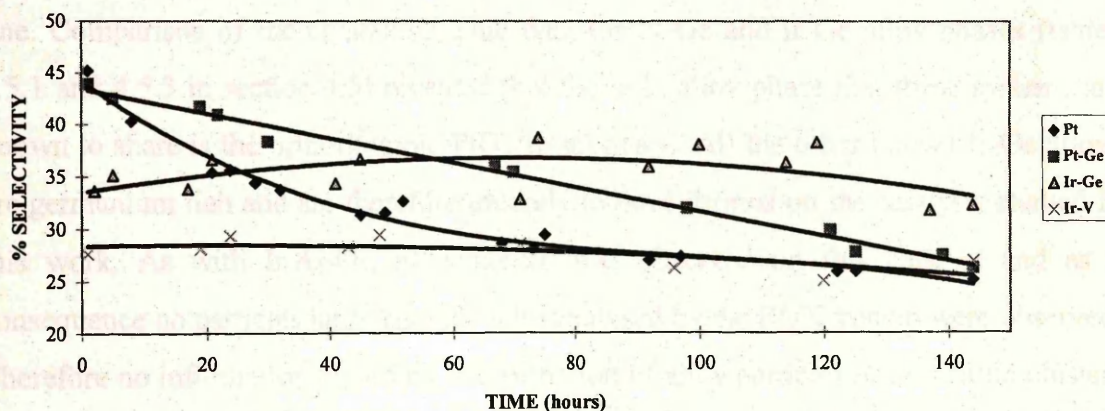
If we consider the yields of C_3 to C_8 aliphatic species over Ir-Ge (table 5.7.1), Pt (table 5.1.1) and Pt-Ge (table 5.1.3) some interesting differences were again observed. The initial yields of C_3 , C_4 and C_5 species were found to be considerable higher over the Ir-Ge catalyst whilst the corresponding yields of C_6 , C_7 and C_8 species were lower. If we look at the correlation between the number of moles of C_2/C_6 and C_3/C_5 produced on these catalysts it is observed that whilst these correlations hold reasonably well over Pt and Pt-Ge, over Ir-Ge not enough C_5 species were produced to account for all the propane and not enough C_6 species were produced to account for all the ethane.

One explanation to account for these observations was that the presence of acidic germanium oxide sites in the Ir-Ge catalyst increased the hydrocracking activity resulting in more C_3 , C_4 and C_5 species being produced. The fact that the number of moles of C_3/C_5 and C_2/C_6 did not correlate may have been caused by a significant fraction of the C_6 and C_5 molecules produced undergoing a further cracking reaction.

Although a similar effect was observed over the Pt-Ge catalyst (increased production of C₃, C₄ and C₅ relative to C₆, C₇ and C₈) the effect was not as pronounced. Whether this observation can be explained in terms of the degree of reduction of germanium in these two related catalysts is not clear.

In terms of the production of aromatics it was observed that the initial yields and selectivities for these products were significantly lower over Ir-Ge (tables 5.7.1 and 5.7.2) than Pt (tables 5.1.1 and 5.2.1). This was due almost exclusively to a decrease in the production of o-xylene and particularly ethylbenzene, the two products which could be formed by direct six-ring closure of the n-octane molecule. Again it is not clear why this was the case. However, when examining the way in which the selectivity to aromatics changed with time on line over these catalysts, figure 6.4.1, it was observed that whilst over Pt and Pt-Ge the selectivity to aromatisation decreased progressively with time on line, over the Ir-Ge catalyst the selectivity remained relatively constant throughout the run. Indeed, the Ir-Ge catalyst had a higher selectivity to aromatics after 144 hours on line than either Pt or Pt-Ge.

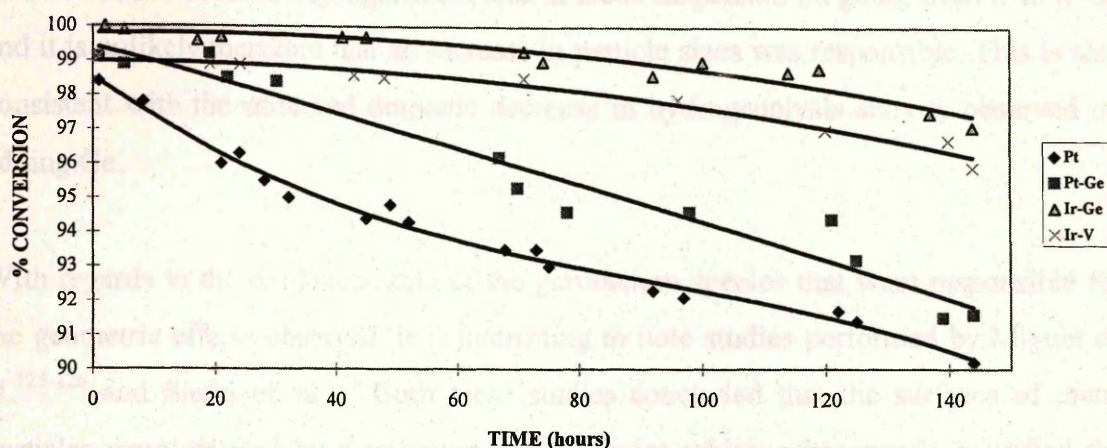
Figure 6.4.1 Selectivities to aromatisation versus time on line over Pt, Pt-Ge, Ir-Ge and Ir-V



Similar differences to those found with the selectivities to aromatics were also found with the n-octane conversion over these three systems, as shown in figure 6.4.2. Whilst

over Pt/Al₂O₃ and Pt-Ge/Al₂O₃ the overall conversion had decreased significantly during 144 hours on line, over Ir-Ge the decrease was much less pronounced. As has been discussed, the conversion over platinum decreased rapidly in the initial stages due to coke formation on the metal. Over Pt-Ge the rate of deactivation was slower initially but increased during the run. This was attributed to alloy formation between platinum and germanium.

Figure 6.4.2 Conversion of n-octane versus time on line over Pt, Pt-Ge, Ir-Ge and Ir-V



The Ir-Ge catalyst followed the same type of deactivation curve, although much shallower, as that seen with Pt-Ge, i.e. the rate of deactivation increased with time on line. Comparison of the crystallographic data for Pt-Ge and Ir-Ge alloy phases (tables 4.5.1 and 4.5.3 in section 4.5) revealed that the only alloy phase that these systems are known to share is the orthorhombic PtGe(IrGe) phase. All the other known Ir-Ge alloys are germanium rich and are therefore unlikely to have formed on the catalysts studied in this work. As with Ir/Al₂O₃, no sintering was observed on this catalyst and as a consequence no particles large enough to be analysed by the EDX system were observed. Therefore no information regarding the formation of alloy particles or bimetallic clusters was obtained for this catalyst. Nevertheless, the reforming data and chemisorption studies both showed that the germanium species present did have a very strong influence on the metal.

The total amount of coke formed over Ir-Ge was much greater than over Ir (3.91 wt% versus 0.90 wt%). This may have been due to the high acidity of GeO_2 . However, this coke did not appear to significantly alter the catalytic properties of this catalyst. It is therefore concluded that the majority of this carbon was deposited on the support surface rather than on metal crystallites.

The suppression in chemisorption capacity observed on adding Ge to an Ir/ Al_2O_3 catalyst was due to the presence of germanium species on the surface of metal crystallites. TEM studies did not observe any significant loss in metal dispersion on going from Ir to Ir-Ge and it is unlikely therefore that an increase in particle sizes was responsible. This is also consistent with the observed dramatic decrease in hydrogenolysis activity observed on adding Ge.

With regards to the oxidation state of the germanium species that were responsible for the geometric effects observed, it is interesting to note studies performed by Miguel et. al.¹²⁵⁻¹²⁶ and Sierra et. al.²³⁹ Both these studies concluded that the surfaces of metal particles were covered by germanium oxide species which subsequently modified the catalytic properties. However, a large number of studies have concluded that the species responsible for the geometric effects observed was $\text{Ge}^{0(112,122,127)}$. In this study it is not clear whether Ge^0 or GeO_2 species were responsible for the geometric effects observed, although comparison with the related Pt-Ge system suggests that significant amounts of both species would have been present. A further point worth noting is that the Ir-V/ Al_2O_3 catalyst (section 5.9) demonstrated that oxide species could indeed produce significant geometric effects.

With regards to alloying and the poisoning effects of large quantities of Ge^0 , it is worth discussing a study by Frety et. al.^{240,241} on related Ir-Sn catalysts. Addition of tin to Ir/ Al_2O_3 catalysts²⁴⁰ was found by these authors to produce a similar suppression in hydrogenolysis to that observed with germanium in this study. A later study compared the properties of high loadings (10 wt%) of iridium and tin (1:1 ratio) supported either

on alumina or silica supports.²⁴¹ Mössbauer spectroscopy and TEM/EDX investigations found that for the alumina supported catalyst, whilst some Sn^0 was formed, the majority of the particles observed (1-10 nm particle sizes) were found to be pure iridium or at least contain very little tin. For the silica supported catalyst the situation was very different. Essentially all the tin present was found as Sn^0 and alloyed with iridium. The particles observed had the nominal 1:1 composition. When the catalytic activity for benzene hydrogenation was compared over these two catalysts, it was found that the Ir-Sn/ Al_2O_3 catalyst was two orders of magnitude more active than Ir-Sn/ SiO_2 when the catalysts were reduced at 330 °C. For reduction at higher temperatures the Ir-Sn/ SiO_2 catalysts became completely inactive. Again this strongly suggests that alloy formation between Ir (or Pt) and inactive Sn or Ge can significantly contribute to the overall rate of deactivation of these systems.

For the Ir-Ge/ Al_2O_3 catalysts studied in this work therefore, it is concluded that coverage of the iridium surface by small concentrations of Ge^0/GeO_2 species produced a strong geometric effect which reduced the hydrogenolysis activity of the catalysts and increased its selectivity for aromatisation etc. The small degree of deactivation observed on this catalyst (although the rate was increasing with time on line) may have been due to the increasing quantities of Ge^0 species present.

On decreasing the iridium metal loading to 0.03 wt%, it was observed that the initial conversion was almost 10 % lower (90.4 %). Not surprisingly reactions which relied mainly on the acidic support were initially higher relative to Ir-Ge, i.e. the initial selectivities to isomerisation and hydrocracking were higher over this catalyst. However, the aromatisation reaction, which required the high dehydrogenation activity of the metal, was significantly reduced due to the lower metal content (18.95 versus 33.6% over Ir-Ge).

Perhaps the most significant difference however between Ir-Ge and 0.03 Ir-Ge was in the rate of catalyst deactivation. After 100 hours on line the total conversion over this

catalyst had fallen from 90.4 to 60.4%. This 30% decrease in the level of conversion was by far the highest observed on any of the platinum or iridium containing catalysts studied. It is also interesting to note that the rate of deactivation was relatively constant throughout the run. (figure 5.8.6). Although this increased deactivation was perhaps to be expected, it is not clear whether the major deactivating process was increased coke deposition on the metal or encapsulation of iridium by Ge^0 or GeO_2 . Certainly (as expected) the TEM investigation confirmed that sintering was not a major factor. The overall quantity of coke deposited (1.82 wt% over 100 hours) was lower than over Ir-Ge (3.91 wt% over 144 hours). As has been discussed it is very difficult to relate the actual amount of coke deposited with the rate of deactivation.

Before discussing the reforming properties of the Ir-V catalyst it is necessary to discuss the likely oxidation state(s) of vanadium species present in this catalyst. Bond and Flamerz²²⁷ used TPR to study a series of $\text{Ru}/\text{V}_2\text{O}_5/\text{Al}_2\text{O}_3$ catalyst with V_2O_5 loadings ranging from 0.9 to 6.6 wt%. It was concluded by these authors that after reduction at 475 °C the majority of vanadium was present as V^{3+} . This species was found to strongly suppress the n-butane hydrogenolysis activity of the $\text{Ru}/\text{Al}_2\text{O}_3$ catalyst.

Similar observations have been made in a number of studies regarding the suppression of metal hydrogenolysis activity by V_2O_5 and TiO_2 oxides incorporated either as the support or as supported oxide component (as in the case of the present study). The fall in hydrogenolysis activity which occurs in these systems is attributed to a strong metal support interaction^{242,243} (SMSI) which is thought to involve encapsulation of metal particles by oxide species.

The large drop in hydrogenolysis activity observed on addition of V_2O_5 to $\text{Ir}/\text{Al}_2\text{O}_3$ observed in this study was therefore due to an SMSI type interaction between some vanadium oxide species (perhaps V_2O_3) and the metal crystallites. However, the degree of hydrogenolysis suppression produced by this interaction was not as great as on the addition of germanium. The initial yields of methane and ethane over this catalyst were

significantly higher than over Ir-Ge or platinum. It is interesting to note that the yield of propane was slightly higher than over Pt/Al₂O₃. This was due to multiple fragmentation of n-octane molecules to produce a greater number of C₃ fragments. As a result of this higher hydrogenolysis activity, the correlation's between C₂/C₆ and C₃/C₅ no longer held in this system.

The conversion of n-octane over Ir-V/Al₂O₃ (figure 6.4.2) was found to decrease more significantly with time on line than over Ir-Ge. It is not clear whether this was due to increased coking of the metal function over Ir-V (even though the overall coke content was lower on this catalyst) or due to increased site blocking by vanadium species.

When comparing the selectivities of Ir-Ge and Ir-V, it is clear that the selectivity to aromatics was lower over Ir-V (figure 6.4.1). As discussed previously this may have been linked to the dehydrogenation activity of these catalysts. This would also explain the initial higher selectivity to isomerisation observed over the vanadium catalyst. The increase in selectivity to isomerisation with time on line over this catalyst was due to a corresponding decrease in hydrogenolysis.

6.5 Pt-Ir-0.03Ge/Al₂O₃, Pt-Ir-Ge/Al₂O₃ and Pt-Ir-V/Al₂O₃

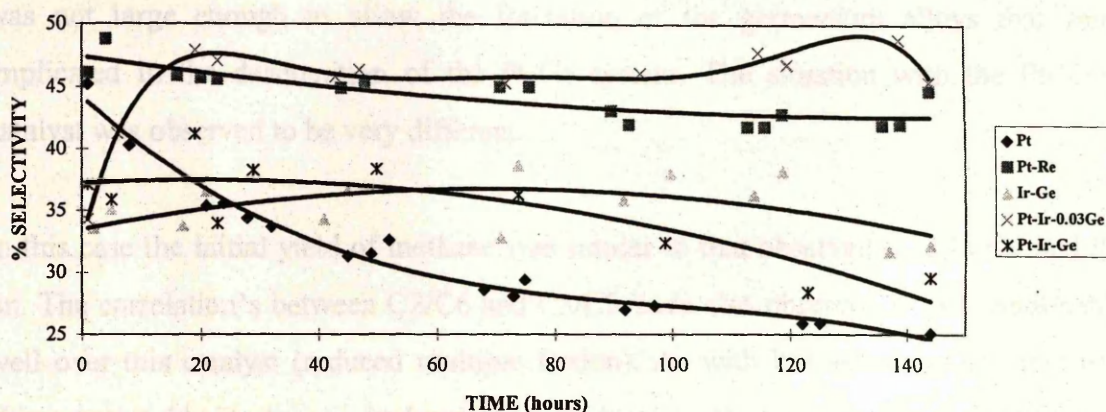
These three catalysts all showed significant differences in product yields compared to the Pt-Ir/Al₂O₃ catalyst on which they were based.

In the case of the Pt-Ir-0.03Ge catalyst it was observed that although the initial hydrogenolysis activity was only slightly lower than over Pt-Ir, this activity fell very rapidly and after approximately 19 hours on line had fallen below 10%. Due to this high initial hydrogenolysis activity the correlations between C₂/C₆ and C₃/C₅ did not hold over this catalyst. The explanation for the rapid decrease in hydrogenolysis was as follows: initially the small germanium loading was highly dispersed over the surface of

the support, most likely as an oxide, whilst only a small fraction of germanium was associated with the metal. However, with use in reforming germanium gradually migrated to the metal crystallites producing the geometric/ensemble effect observed. This migration of germanium species may have involved oxide species or Ge^0 which was produced by reaction with hydrogen spilt over from metal crystallites.

This suppression of hydrogenolysis produced a very rapid increase in the selectivity to aromatisation in the early stages of the run, as shown in figure 6.5.1.

Figure 6.5.1 Selectivity to aromatics versus time on line over Pt, Pt-Re, Ir-Ge, Pt-Ir-0.03Ge and Pt-Ir-Ge



Once this initial increase in aromatisation occurred, the selectivity towards this reaction remained high and relatively constant throughout the remainder of the run, in a similar manner to Pt-Re. The selectivity to isomerisation remained low throughout the run, again in a similar to Pt-Re. Also, the overall conversion of n-octane over this catalyst remained very high, as shown in figure 6.5.2, having decreased by less than 1 % during 144 hours (this catalyst appeared to be more resistant to deactivation than Pt-Ir).

As the rate of sintering on this catalyst was actually slightly greater than that observed over Pt, Pt-Sn, Pt-Re etc, it is thought that the main reason for the stability of this catalyst was control of coke deposition on metal crystallites. This may have occurred due to a combination of two processes:

1). Hydrogenolysis of coke deposits/precursors by iridium. Although the hydrogenolysis activity of this catalyst after 144 hours on line was much lower than over Pt-Ir, it was higher than over Pt and therefore the contribution of this activity to the control of coking may have been significant.

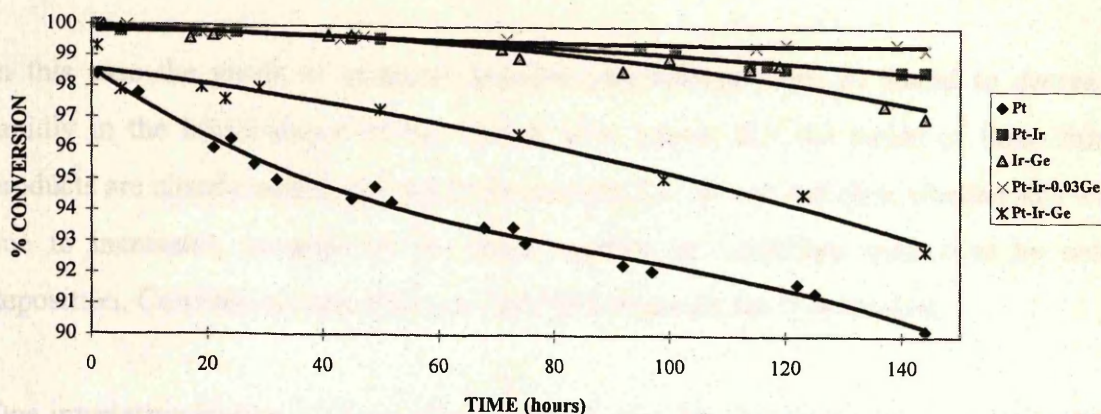
2). Reduction of coke deposition on the metal by a geometric effect induced by the small concentrations of germanium present. This is similar to effects seen in the initial stages over Pt-Sn and Pt-Ge.

An important point about this catalyst was that the concentration of germanium present was not large enough to allow the formation of the germanium alloys that were implicated in the deactivation of the Pt-Ge system. The situation with the Pt-Ir-Ge catalyst was observed to be very different.

In this case the initial yield of methane was similar to that observed over Pt-Ge and Pt-Sn. The correlation's between C2/C6 and C3/C5 were also observed to hold reasonably well over this catalyst (reduced multiple fission). As with Pt-Ge and Ir-Ge, there was also a noticeable increase in hydrocracked products on this catalyst due to the presence of GeO₂ species.

As the hydrogenolysis selectivity of this catalyst was low, the corresponding initial aromatisation selectivity was high. However, the initial yields of aromatics were slightly lower than the corresponding yields over Pt and Pt-Ge. Why this should be is not clear although it is possible that there may have been more Ge⁰ present in the initial stages in this catalyst. What is clear however is that with extended use this catalyst deactivated in a similar manner to that observed over Pt-Ge and Pt-Sn, as shown in figure 6.5.2, i.e. the level of conversion was observed to decrease with time on line and the rate of loss was found to be greater towards the end of the run.

Figure 6.5.2 Conversion of n-octane versus time on line over Pt, Pt-Ir, Ir-Ge, Pt-Ir-0.03Ge and Pt-Ir-Ge



The aromatisation selectivity also decreased during the run and was matched by an increase in selectivity to isomerisation. Again the relative rates of decrease in aromatisation was greatest at the end of the run (figure 6.5.1). Similar observations were made with Pt-Ge and Pt-Sn, where these changes were attributed to the formation of Pt-Ge and Pt-Sn alloys. It was therefore concluded that in this catalyst the formation of Pt-Ir-Ge alloys resulted in similar deactivation. However, in this case the relative proportion of active metal (Pt + Ir) to inactive support (Ge) was higher and therefore the level of deactivation observed after 144 hours was not as great. TEM studies revealed that this catalyst sintered more noticeably than any of the other catalysts studied, probably due to the higher overall loading. The quantity of coke deposited (3.95 wt%) was also relatively high.

In the case of the Pt-Ir-V catalyst, as with the Ir-V system, the suppression of hydrogenolysis activity, although large, was not found to be as great as on the corresponding germanium catalyst. The differences in product distribution observed over this catalyst as compared to Pt-Ir was attributed to the presence of vanadium (perhaps $V_2O_3^{227}$) species on the surface of metal crystallites. This produced the decrease in structure sensitive hydrogenolysis and corresponding increase in the other reactions. In the initial stages the correlation between C_2/C_6 and C_3/C_5 products did not hold due to

multiple fission reactions. However, by 144 hours on line the correlations were in reasonable agreement, reflecting the lower hydrogenolytic splitting occurring.

In this case the yields of methane, benzene and toluene were all found to decrease rapidly in the initial stages (it has already been shown that the yields of these three products are closely related e.g. see Pt-Re, section 5.4). It was not clear whether this was due to increasing coverage of the metal crystals by vanadium species or by coke deposition. Certainly no such changes were observed over the Ir-V catalyst.

One interesting feature of this catalyst was that although the selectivity to isomerisation increased throughout the run, this was not accompanied by a decrease in aromatisation, as was found in most cases. On this catalyst the increased selectivity to isomerisation was at the expense of C₁-C₄ products, the yields of which decreased continuously throughout the run.

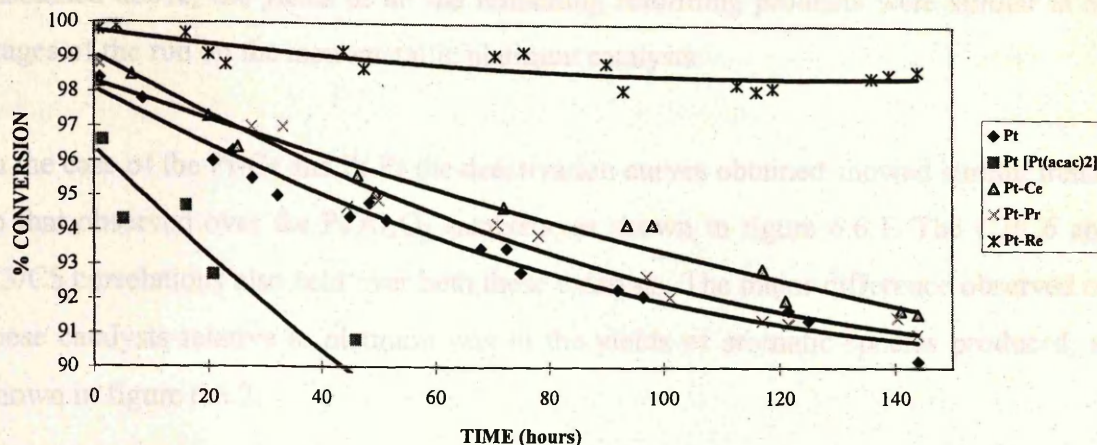
The conversion of n-octane over this catalyst was observed to decrease continuously and quite steadily throughout the run. Again the relative contributions of coke formation and gradual poisoning of active sites by vanadium species in producing this effect was not clear. It is interesting to note that the relative deactivation caused by addition of 0.3 wt% germanium and vanadium to Pt-Ir/Al₂O₃ catalysts was much greater than the corresponding deactivation caused in iridium only catalysts (i.e. Ir-Ge and Ir-V). This is one indication that sintering may also have played some role in the deactivation of these catalysts.

6.6 Pt/Al₂O₃ [Pt(acac)₂] and rare-earth containing catalysts

All three of these catalysts showed features which were significantly different from the Pt/Al₂O₃ catalyst.

First of all in the case of $\text{Pt}/\text{Al}_2\text{O}_3$ [$\text{Pt}(\text{acac})_2$] it was observed that a major difference was in the rate of deactivation. The conversion of n-octane versus time on line for these catalysts is plotted in figure 6.6.1 along with the corresponding data for Pt and Pt-Re to aid comparison.

Figure 6.6.1 Conversion of n-octane over Pt, Pt [$\text{Pt}(\text{acac})_2$], Pt-Ce, Pt-Pr and Pt-Re



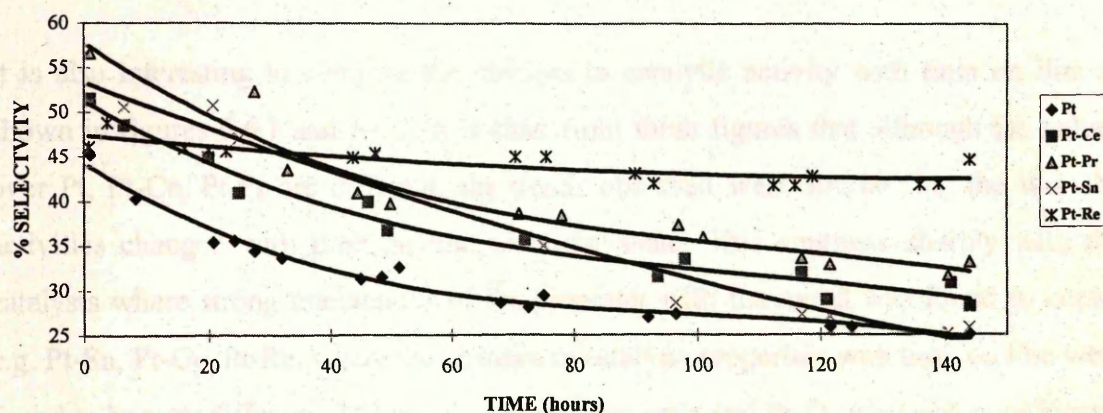
It is clear from this figure that the $\text{Pt}(\text{acac})_2$ prepared catalysts deactivated much more significantly during the run than did the H_2PtCl_6 catalysts. This may have been due to the relative amount of chlorine on these two catalysts. The $\text{Pt}/\text{Al}_2\text{O}_3$ catalysts were prepared with a dilute HCl solution of H_2PtCl_6 (to give a Cl^- loading of ~ 1 wt%) whilst the $\text{Pt}(\text{acac})_2$ catalysts were prepared using a toluene solution of $\text{Pt}(\text{acac})_2$. When the relative yields over these two catalysts are compared it is seen that the increased deactivation over the $\text{Pt}(\text{acac})_2$ catalyst was due to the fact that the yields of C_3 to C_6 products (i.e. hydrocracked products) were consistently and significantly lower over this catalyst than on $\text{Pt}/\text{Al}_2\text{O}_3$. The possibility that some carbonaceous species were retained by the catalyst from the impregnation procedure must also be considered. It is interesting to note that the yields of isomerisation and aromatisation products did not seem to be affected.

One other significant difference between the two monometallic catalysts was in the yield of toluene. The yield of this product was initially much higher over the $\text{Pt}(\text{acac})_2$

catalysts and this was solely responsible for the higher initial selectivity to aromatics observed on this system. This initial high toluene yield decreased rapidly and at the end of the run the yield of this product was similar over both catalysts. One possible explanation for this observation was that the alumina support retained some toluene from the impregnation solution (which was $\text{Pt}(\text{acac})_2$ dissolved in toluene, section 4.1) during the drying, calcination and reduction procedures. With the exception of the products discussed above, the yields of all the remaining reforming products were similar at all stages of the run on the monometallic platinum catalysts.

In the case of the Pt-Ce and Pt-Pr the deactivation curves obtained showed similar trends to that observed over the $\text{Pt}/\text{Al}_2\text{O}_3$ catalysts, as shown in figure 6.6.1. The C2/C6 and C3/C5 correlations also held over both these catalysts. The major difference observed on these catalysts relative to platinum was in the yields of aromatic species produced, as shown in figure 6.6.2.

Figure 6.6.2 Selectivity to aromatics versus time on line over Pt, Pt-Ce, Pt-Pr, Pt-Sn and Pt-Re



For both Pt-Ce and Pt-Pr it was observed that the selectivity to aromatics was considerably enhanced relative to $\text{Pt}/\text{Al}_2\text{O}_3$. This improvement in aromatisation was at the expense of $\text{C}_3\text{-C}_6$ hydrocracked products. Similar findings were made by Fengi et. al.¹⁴⁴⁻¹⁴⁷, who also found that that addition of rare-earth oxides decreased the selectivity of the catalyst for hydrocracking and increased the selectivity for aromatisation.

However, these authors attributed their findings to electronic modification of platinum by the rare-earth. The results of this study would suggest that this is not the case, as will be discussed below.

As already stated, the increased yields of aromatics over rare-earth containing catalysts was due to a corresponding decrease in the yields of C_3 - C_6 hydrocracked products. This would suggest that the effect of these promoters was to modify the acidic properties of the support. This may also explain the reduced coking over these catalysts. It is interesting to compare these systems with the Pt-Sn catalysts (the selectivity to aromatics over Pt-Sn are included in figure 6.6.2 to aid comparison). In this case an increase in selectivity to aromatics was also observed relative to Pt/ Al_2O_3 . This improvement was mainly at the expense of isomerisation (mainly i-octane) products. A number of studies^{93,99} concluded that one of the effects of tin was that Sn^{II} poisoned the highly acidic sites on alumina resulting in less hydrocracking and/or isomerisation. It is possible that a similar effect occurred with Ce^{4+} (or Ce^{3+}) and Pr^{3+} ions. The rare-earth ions may have poisoned acid sites with different strengths from those poisoned by tin. This would account for the fact that C_3 - C_6 yields were decreased more significantly than i-octane.

It is also interesting to compare the changes in catalytic activity with time on line as shown in figures 6.6.1 and 6.6.2. It is clear from these figures that although the values over Pt, Pt-Ce, Pt-Pr are different, the trends observed were similar, i.e. the way the activities changed with time on line were the same. This contrasts sharply with the catalysts where strong interactions of the promoter with the metal was found to occur, e.g. Pt-Sn, Pt-Ge, Pt-Re, where the changes in catalytic properties with time on line were found to be very different. This would suggest that ceria and Pr_2O_3 were not significantly associated with the metal function.

A number of studies on ceria supported catalysts²⁴⁴⁻²⁴⁸ have found evidence for strong metal support interactions similar to those observed with TiO_2 and V_2O_5 . Perhaps the concentration of rare-earths used in this study was too low to allow significant SMSI

interactions to occur. Another possibility is that the rare-earth oxide interacted strongly with the alumina support, thereby preventing the formation of SMSI states under high temperature reduction. An excellent method to check for SMSI interactions in these catalysts would have been to prepare an Ir-Ce (or Pr)/Al₂O₃ catalyst and tests its hydrogenolysis activity. Any significant drop in hydrogenolysis produced by the rare-earth would strongly suggest that such an interaction had occurred.

One other often quoted effect produced by ceria is the stabilisation of small metal particles against sintering. The TEM studies performed found no evidence for this effect (the average particle sizes and number densities over Pt, Pt-Ce and Pt-Pr were similar after 144 hours on line). However, it must be stated that the weight percent of ceria generally employed is considerably higher than the 0.3 wt% used in the present study.

6.7 Ni/Al₂O₃, Ni-Ge/Al₂O₃ and Ru-Ge/Al₂O₃

Nickel and ruthenium containing catalysts were observed to have very poor reforming properties under the conditions used in this study. This was due to the poorer dehydrogenation activity of these metals relative to platinum. The major reaction occurring on these catalysts was hydrocracking. The yields of aromatic products were particularly low in comparison to the platinum or iridium containing systems. Addition of germanium to nickel reduced the hydrogenolysis activity of this catalyst in a similar manner to Ir-Ge. Ni-Ge and Ru-Ge alloys were formed in these catalysts during reaction at 510 °C in a hydrogen rich atmosphere.

Although the reforming properties of these catalysts were poor, there is growing interest in the use of germanium and tin modified Ni, Pd, Ru and Rh catalysts. For example, the addition of promoters to nickel has been found to improve its catalytic properties for some dehydrogenation reactions^{249,250} and tin and germanium modified ruthenium

catalysts have been tested for the hydrogenation of citral and cinnamaldehyde²⁵¹ and the hydrogenation of halonitroaromatics to haloanilines.²⁵²

6.8 General Conclusions

It has been shown that the addition of various promoters to Pt/Al₂O₃ catalysts can significantly effect the catalytic properties.

In the case of Pt-Sn and Pt-Ge catalysts, the initial improvement in catalytic properties was produced by a geometric effect which reduced the quantity of coke deposited on metal crystallites. However, with extended use the formation of Pt-Sn and Pt-Ge alloys contributed to the overall rate of deactivation of these systems. A number of alloy phases were identified in both catalysts.

For Pt-Re and Pt-Ir catalysts, which showed the highest stability, it was concluded that hydrogenolysis/hydrogenation of coke precursors by Re⁰ and Ir⁰ resulted in the observed improvements in catalytic properties. TEM observations revealed that the metallic component of the Pt-Ir/Al₂O₃ catalyst consisted of PtIr alloy particles. TEM studies of the Pt-Re catalyst found no evidence for Re⁰ or Pt-Re alloys. However, the similarities between the reforming properties of these catalysts strongly suggests that Re⁰ was present.

The very high hydrogenolysis activity of iridium requires that Pt-Ir catalysts are pretreated with sulphur before use in industrial reforming units. It has been shown that the addition of germanium to iridium containing catalysts (Ir-Ge/Al₂O₃, Pt-Ir-Ge/Al₂O₃ and Pt-Ir-0.03Ge/Al₂O₃) had similar effects to the addition of sulphur, i.e. reduced the high hydrogenolysis activity of these catalysts and improved their selectivity to the desired reforming products. However, in the case of the Pt-Ir-Ge catalysts, formation of

germanium alloy particles contributed to the overall rate of deactivation of this system. The major alloy phase observed was a trimetallic Pt-Ir-Ge superlattice structure. No such alloys were observed on the Pt-Ir-0.03Ge catalyst and it was observed that this catalysts, along with Pt-Re, showed the highest selectivity to aromatics after 144 hours on line.

Addition of V_2O_5 , (which is known to exhibit "SMSI" properties) to iridium containing catalysts was found to produce similar alterations in the reforming properties to the addition of germanium. However, the suppression of hydrogenolysis was not as great in this case.

Iridium was found to be much less susceptible to sintering in the hydrogen rich atmospheres employed in this study than was platinum. This was due to the higher melting point of this metal.

Addition of the rare-earth oxides CeO_2 and Pr_2O_3 was found to significantly affect the acidic nature of the support and thus improve the properties of Pt/ Al_2O_3 catalysts. No evidence for a significant interaction between the rare-earth oxide and the metal component was obtained although the presence of such an interaction cannot be ruled out.

Nickel and ruthenium containing catalysts were found to have very poor reforming properties relative to platinum under the conditions employed in this study.

References

1. Farnsworth, J. D. "The History of the American Film Industry." *Harvard Film Review*, 1965, 37(1), 1-10.

2. Farnsworth, J. D. "The History of the American Film Industry." *Harvard Film Review*, 1965, 37(1), 1-10.

3. Jones, J. R. "The History of the American Film Industry." *Harvard Film Review*, 1965, 37(1), 1-10.

4. Jones, J. R. "The History of the American Film Industry." *Harvard Film Review*, 1965, 37(1), 1-10.

5. Jones, J. R. "The History of the American Film Industry." *Harvard Film Review*, 1965, 37(1), 1-10.

6. Jones, J. R. "The History of the American Film Industry." *Harvard Film Review*, 1965, 37(1), 1-10.

7. Jones, J. R. "The History of the American Film Industry." *Harvard Film Review*, 1965, 37(1), 1-10.

8. Jones, J. R. "The History of the American Film Industry." *Harvard Film Review*, 1965, 37(1), 1-10.

9. Jones, J. R. "The History of the American Film Industry." *Harvard Film Review*, 1965, 37(1), 1-10.

10. Jones, J. R. "The History of the American Film Industry." *Harvard Film Review*, 1965, 37(1), 1-10.

11. Jones, J. R. "The History of the American Film Industry." *Harvard Film Review*, 1965, 37(1), 1-10.

12. Jones, J. R. "The History of the American Film Industry." *Harvard Film Review*, 1965, 37(1), 1-10.

13. Jones, J. R. "The History of the American Film Industry." *Harvard Film Review*, 1965, 37(1), 1-10.

14. Jones, J. R. "The History of the American Film Industry." *Harvard Film Review*, 1965, 37(1), 1-10.

15. Jones, J. R. "The History of the American Film Industry." *Harvard Film Review*, 1965, 37(1), 1-10.

1. Satterfield, C. N., "Heterogeneous Catalysis in Industrial Practice," 2nd Edition, McGraw-Hill, New York, (1991)
2. Edmonds, T., "Catalysis and Chemical Processes," (Pearce, R., and Patterson, W. R., Eds) Leonard-Hill, London, (1981)
3. Gates, B. C., Katzer, J. R., and Schuit, G. C., "Chemistry of Catalytic Processes," McGraw-Hill, New York, (1979)
4. Le Page, J.F., "Applied Heterogeneous Catalysis: Design, Manufacture and Use of Solid Catalysts", Editions Technip, Paris , (1987)
5. Pines, H., "The Chemistry of Catalytic Hydrocarbon Conversion", Academic Press, New York, (1981)
6. Sinfelt, J.H., Catal. Sci. and Technology Vol 1., (Anderson, J.R., and Boudart, M., Eds) New York, Springer-Verlag, (1981)
7. Sinfelt, J.H., Advan. Chem. Eng. **5**, 37, (1964)
8. Rossini, F.D., Pitzer, K.S., Arnett, R.L., Braum, R.M., and Pimentel, G.C., "Selected values of physical and thermodynamic properties of hydrocarbons and related compounds." API Res. Project 44, Carnegie Press Inc, Pittsburgh, (1953)
9. Ciapetta, F.G., Dobres, R.M., and Baker, R.W., "Catalytic reforming of pure hydrocarbons and petroleum naphthas." Catalysis Vol 6, p 495, Reinhold, New York, (1958)
10. Mills, G.A., Heinemann, H., Milliken, T.H., and Oblad, A.G., Ind. Eng. Chem. **45** 134 (1953)
11. Roessner, F., and Roland, U., J. Mol. Catal. A. **112** 401 (1996)
12. Weisz, P.B., and Swegler, E.W., Science **126** 31 (1957)
13. Sinfelt, J.H., Hurwitz, H., and Rohrer, J.C., J. Phys. Chem. **64** 892 (1960)
14. Anderson, J.R., and Avery, N.R., J. Catal. **7** 315 (1967)
15. Gault, F.G., Adv. Catal. **30** 1 (1981)
16. Corolleur, C., Corolleurs, S., and Gault, F.G., J. Catal. **24** 385 (1972)

-
17. Sinfelt, J.H., and Roher, J.C., *J. Chem. Eng. Data* **8** (1) 109 (1963)
 18. Sinfelt, J.H., Hurwitz, H., and Roher, J.C., *J. Phys. Chem.* **65** 1458 (1961)
 19. Sinfelt, J.H., Hurwitz, H., and Roher, J.C., *J. Catal.* **1** 481 (1962)
 20. Dautzenberg, F.M., and Platteeuw, J.C., *J. Catal.* **19** 41 (1970)
 21. Davis, B.H., *Proc. 8th Intern. Congr. Catal.* **Vol 2** 469 (1984)
 22. Pollitzer, E.L., Hayes, J.C., and Haensel, V., *Am. Chem. Soc. Refining Petrol. Chem. Symp.*, New York, Sept. 7-12, (1969)
 23. Sinfelt, J.H., *Adv. Catal.* **23** 91 (1973)
 24. Broekhoven, E.H., Ponec, V., *J. Molec. Catal.* **25** 109 (1984)
 25. Boudart, M., Aldag, A., Benson, J.E., Dougharty, N.A., and Harkins, C.G., *J. Catal.* **6** 92 (1966)
 26. Augustine, S.M., and Sachtler, W.M.H., *J. Catal.* **106** 417 (1987)
 27. Mckerverey, M.A., Rooney, J.J., and Samman, N.G., *J. Catal.* **30** 330 (1973)
 28. Schaik, J.R.H. van, Dessing, R.P., and Ponec, V., *J. Catal.* **38** 273 (1975)
 29. Blakely, D.W., and Somorjai, G.A., *J. Catal.* **42** 181 (1976)
 30. Myers, C.G., and Munn, G.W., *Ind. Eng. Chem.* **50** 1727 (1958)
 31. Ciapetta, F.G., Dobres, R.H., and Baker, R.W., "Catalytic Reforming of Pure Hydrocarbons and Petroleum Naphthas" *Catalysis Vol 6*, p 495, Reinhold, New York (1958)
 32. de Boer, J.H., and Lippens, B.C., *J. Catal.* **3** 38 (1964)
 33. Lippens, B.C., and de Boer, J.H., *J. Catal.* **3** 44 (1964)
 34. Lippens, B.C., and Steggeron, J.J., "Physical and Chemical Aspects of Adsorbents and Catalysts", Academic Press, New York, 171 (1970)
 35. Kotanigawa, T., Yamamoto, M., Utiyama, M., Hattori, H., and Tanabe, K., *Appl. Catal.* **1** 185 (1981)
 36. Leonard, A.J., van Cauwelaert, F., and Fripiat, J.J., *J. Phys. Chem.* **71** 695 (1967)

-
37. Peri, J.B., and Hannan, R.B., J. Phys. Chem. **64** 1526 (1960)
38. Peri, J.B., J. Phys. Chem. **69** 220 (1965)
39. Parry, E.P., J. Catal. **2** 371 (1963)
40. Pines, H., and Haag, W.D., J. Am. Chem Soc. **82** 2471 (1960)
41. Krzywicki, A., Marczewski, M., Modzelewski, R., Pelszik, K., and Marinowski, S., React. Kinet. and Catal. Lett. **13** 1 (1980)
42. Krzywicki, A., and Marinowski, M., J. Chem. Soc. Faraday Trans. **76** 1311 (1980)
43. Basset, J., Naccache, C., Mathieu, M., and Pettre, M., J. Chem. Phys. **66** 1522 (1969)
44. Hall, W.K., Lutinski, F.E., and Gerberich, H.R., J. Catal. **3** 514 (1964)
45. Hightower, J.W., Gerberich, H.R., and Hall, W.K., J. Catal. **7** 57 (1967)
46. Tanaka, M., and Ogasawara, S., J. Catal. **16** 179 (1970)
47. Cai, T., Qü, J., Wong, S., Song, Z., and He, M., Appl. Catal. **97** 113 (1993)
48. Kluksdahl, H.E., U.S. Patent 3,415,737 (1968)
49. Johnson, M.F.L., and LeRoy, V.M., J. Catal. **35** 434 (1974)
50. Johnson, M.F.L., J. Catal. **39** 487 (1975)
51. Webb, A.N., J. Catal. **39** 485 (1975)
52. Yao, H.C., and Shelef, M., J. Catal. **44** 392 (1976)
53. Bolivar, C., Charcosset, R., Frety, R., Primet, M., Tournayan, L., Betizeau, C., Leclercq, G., and Maurel, R., J. Catal. **39** 249 (1975)
54. McNicol, B.D., J. Catal. **46** 438 (1977)
55. Isaacs, B.H., and Petersen, E.E., J. Catal. **77** 43 (1982)
56. Wagstaff, N., and Prins, R., J. Catal. **59** 434 (1979)
57. Sermon, P.A., and Bond, G.C., Catal. Rev. **8** 211 (1973)

-
58. Kramer, R., and Andre, M., *J. Catal.* **58** 287 (1979)
59. Mieville, R.L., *J. Catal.* **87** 473 (1984)
60. Bolivar, C., Charcosset, R., Frety, R., Primet, M., Tournayan, L., Betizeau, C., Leclercq, G., and Maurel, R., *J. Catal.* **45** 163 (1975)
61. Biloen, P., Helle, J.N., Verbeek, H., Dautzenberg, F.M., and Sachtler, W.M.H., *J. Catal.* **63** 112 (1980)
62. Shpiro, E.S., Avaev, V.I., Antoshin, G., Ryashentseva, M.A., Minachev, K.M., *J. Catal.* **55** 402 (1978)
63. Short, D.R., Khalid, S.M., Katzer, J.R., and Kelley, M.J., *J. Catal.* **72** 288 (1981)
64. Meitzner, G., Via, G.H., Lytle, F.W., and Sinfelt, J.H., *J. Chem. Phys.* **87** 6354 (1987) March 20-25 (1983)
65. Kelley, M.J., Freed, R.L., Swartzfager, D.G., *J. Catal.* **78** 445 (1982)
66. Peri, J.B., *J. Catal.* **52** 144 (1978)
67. Isaacs, B.H., and Petersen, E.E., *J. Catal.* **85** 1 (1984)
68. Isaacs, B.H., and Petersen, E.E., *J. Catal.* **85** 8 (1984)
69. Charcosset, H., Frèty, R., Leclercq, G., Mendès, E., Primet, M., and Tournayan, L., *J. Catal.* **56** 468 (1979)
70. Jossens, L.W., and Petersen, E.E., *J. Catal.* **76** 265 (1982)
71. Betizeau, C., Leclercq, G., Maurel, R., Bolivar, C., Charcosset, H., and Tournayan, L., *J. Catal.* **45** 179 (1976)
72. Parera, J.M., and Beltramini, J.N., *J. Catal.* **112** 357 (1988)
73. Bond, G.C., and Cunningham, R.H., *J. Catal.* **163** 328 (1996)
74. Bertolacini, R.J., and Pellet, R.J. "Catalyst Deactivation" (Delmon, B., and Froment, G.F., Eds.) p73. Elsevier, Amsterdam, (1980)
75. (a) Coughline, R.W., Hasan, A., and Kawakami, K., *J. Catal.* **88** 150 (1984)
(b) Coughline, R.W., Hasan, A., and Kawakami, K., *J. Catal.* **88** 163 (1984)
76. Menon, D.G., and Prasad, J., *Proc. 6th Intern. Congr. Catal.* (Bond, G.C., Well, P.B., and Tompkins, F.C., Eds.) p1601, The Chemical Society, London, (1977)

-
77. Sachtler, W.M.H., and van Santen, R.A., *Adv. Catal.* **26** 69 (1977)
78. Boudart, M., Aldag, A., Benson, J.E., Dougharty, N.A., and Harkins, C.G., *J. Catal* **6** 92 (1966)
79. Lankhorst, P.P., de Jongste, H.C., and Ponec, V., "Catalyst Deactivation" (Delmon, B., Froment, F.F. Eds.) p43, Elsevier, Amsterdam, (1980)
80. Apesteguia, C.R., Brena, C.E., Garetto, T.F., Borgna, A., and Parera, J.M., *J. Catal* **89** 52 (1984)
81. Parera, J.M., Beltramini, J.N., Querini, C.A., Martinelli, E.E., Churin, E.J., Alue, P.E., and Figoli, N.S., *J. Catal.* **99** 39 (1986)
82. Sachtler, W.M.H., and Biloen, P., Div. Pet. Chem., Am.Chem. Soc., Seattle Meeting, March 20-25 (1983)
83. Barbier, J., Corro, G., Zhang, Y., Bournville, J.P., and Frank, J.P., *Appl. Catal.* **16** 169 (1985)
84. Antos, G.J., Hayes, J.C., and Mitsche, R.T., U.S. Patent 4,178,268 (1979)
85. Huang, Z., Fryer, J.R., Park, C., Stirling, D., Webb, G., *J. Catal.* **148** 478 (1976)
86. Davis, B.H., Westfall, G.A., Watkins, J., and Pezzanite, J., *J. Catal.* **42** 247 (1976)
87. Ponec, V., Bond, G.C., "Studies in Surface Science and Catalysis, 95, Catalysis by metals and alloys", p660, Elsevier, Amsterdam (1995)
88. Burch, R., *J. Catal.* **71** 348 (1981)
89. Duatzenberg, F.M., Helle, J.N., Biloen, P., and Sachtler, W.M.H., *J. Catal.* **63** 119 (1980)
90. Völter, J., Lietz, G., Uhlemann, M., and Hermann, M., *J. Catal.* **68** 42 (1981)
91. Völter, J., and Kürschner, U., *Appl. Catal.* **8** 167 (1983)
92. Palazov, A., Ponec, C., Shopov, D., Lietz, J., Sárkanay, A., and Völter, J., *J. Catal.* **103** 249 (1987)
93. Burch, R., and Garla, L.C., *J. Catal.* **71** 360 (1981)
94. Muller, A.C., Engelhard, P.A., and Weisang, J.E., *J. Catal.* **56** 65 (1979)

-
115. Schwank, J., Balakrishnan, K., and Sachder, A., *Proc. 10th Intern. Cong. Catal.*, 1440, Akademiai Kiado, Budapest (1993)
95. Balakrishnan, K., and Schwank, J., *J. Catal.* **138** 491 (1992)
96. Lieske, H., and Völter, J., *J. Catal.* **90** 96 (1984)
116. Srinivasan, R., and Davis, B.H., *J. Molec. Catal.* **88** 343 (1984)
97. Baronetti, G.T., de Miguel, S.R., Scelza, O.A., and Castro, A.A., *Appl. Catal.* **24** 109 (1986)
117. Jenkins, J.W., Srinivasan, R., and Davis, B.H., *J. Molec. Catal.* **88** 359 (1984)
98. Sexton, B.A., Hughes, A.E., and Fogar, K., *J. Catal.* **88** 466 (1984)
99. Bariás, O.A., Holmen, A., and Blekkan, E.A., *J. Catal.* **158** 1 (1996)
100. Balakrishnan, K., Schwank, J., *J. Catal.* **127** 287 (1991)
101. Adkins, S.R., and Davis, B.H., *J. Catal.* **89** 371 (1984)
118. Jenkins, J.W., *Paper presented at the Surface Reaction Conference, Nottingham, U.K. (1976)*
102. Davis, B.H., and Srinivasan, R., *Plat. Metals. Rev.* **36(3)** 150 (1992)
122. Jenkins, J.W., *Paper presented at the Surface Reaction Conference, Nottingham, U.K. (1976)*
103. Li, Y.X., Stencel, J.M., and Davis, B.H., *Appl. Catal.* **64** 71 (1990)
104. Merlen, P., Beccat, P., Bertolini, J.C., Delichère, P., Zanier, N., Didillion, B., *J. Catal.* **159** 178 (1996)
105. Srinivasan, R., de Angelis, R.J., and Davis, B.H., *J. Catal.* **106** 449 (1987)
106. Srinivasan, R., Rice, L.A., and Davis, B.H., *J. Catal.* **129** 257 (1991)
107. Bacaud, R., and Bussière, P., *J. Catal.* **69** 399 (1981)
119. Li, Y., Klabunde, J.K., and Davis, B.H., *Appl. Catal.* **60** 47 (1990)
108. Li, Y., Klabunde, J.K., and Davis, B.H., *J. Catal.* **128** 1 (1991)
127. Behrman, J.N., and Trimm, D.L., *Proc. 9th Intern. Cong. Catal.*, 1140, Akademiai Kiado, Budapest (1989)
109. Hobson, M.C., Gores, S.L., and Khav, G.P., *J. Catal.* **142** 641 (1993)
110. Meitzner, G., Via, G.H., Lytle, F.W., Fung, S.C., and Sinfelt, J.H., *J. Phys. Chem.* **92** 2925 (1988)
111. Caballero, A., Dexpert, H.D., Didillion, B., LePeltier, F., Cluase, O., and Lynch, J., *J. Phys. Chem.* **97** 11283 (1993)
130. Sinfelt, J.H., *U.S. Patent 3,953,345 (1979)*
112. Coq, B., and Figueras, F., *J. Catal.* **85** 197 (1984)
131. Wagstaff, N., and Pines, R., *J. Catal.* **79** 432 (1982)
113. Sachder, A., and Schwank, J., *J. Catal.* **120** 353 (1989)
132. Fogar, K., and Jach, H., *J. Catal.* **87** 222 (1981)
114. Balakrishnan, K., and Schwank, J., *J. Catal.* **132** 451 (1991)
133. Wagstaff, N., and Pines, R., *J. Catal.* **81** 353 (1981)

-
115. Schwank, J., Balakrishnan, K., and Sachder, A., "Proc. 10th Intern. Cong. Catal., Budapest, 1992", (Guczi, L., Solymosi, F., and Tetenyi, P., Eds.) p140, Akadémiai Kiadó, Budapest (1993)
116. Srinivasan, R., and Davis, B.H., J. Molec. Catal. **88** 343 (1994)
117. Sparks, D.E., Srinivasan, R., and Davis, B.H., J. Molec. Catal. **88** 359 (1994)
118. Beltramini, J., and Trimm, D.L., Appl. Catal. **32** 71 (1987)
119. Coq, B., Chaqroune, A., and Nciri, B., Appl. Catal. **82** 231 (1991)
120. Huang, Z., Fryer, J.R., Park, C., Stirling, D., Webb, G., J. Catal **159** 340 (1996)
121. McNicol, B.D., Paper presented at Surface Reactivity and Catalysis Group Meeting, Nottingham, U.K. (1976)
122. Jenkins, J.W., Paper presented at the Surface Reactivity and Catalysis Group meeting, Brunel, U.K., (1979)
123. Goldwasser, J., Bernardo, A., Bolivar, C., Castro, G., Rodriguez, A., Fleitas, A., and Giron, J., J. Catal. **100** 75 (1986)
124. Bouwman, R., and Biloen, P., J. Catal. **48** 209 (1977)
125. Miguel, S.R., Scelza, O.A., and Castro, A.C., Appl. Catal. **44** 23 (1988)
126. Miguel, S.R., Correa, J.A.M., Baronetti, G.T., Castro, A.A., and Scelza, O.A., Appl. Catal. **60** 47 (1990)
127. Beltramini, J.N., and Trimm, D.L., (Proc. 9th Intern. Cong. Catal.) **vol 3**, p 1268 (1988)
128. Huang, Z., Fryer, J.R., Park, C., Stirling, D., and Webb, G., Submitted to J. Catal. for publication.
129. Huang, Z., Fryer, J.R., Stirling, D., and Webb, G., Phil. Mag. A **72** 1495 (1995)
130. Sinfelt, J.H., U.S. Patent 3,953,368 (1979)
131. Wagstaff, N., and Prins, R., J. Catal. **59** 446 (1979)
132. Foger, K., and Jaeger, H., J. Catal. **67** 252 (1981)
133. Wagstaff, N., and Prins, R., J. Catal **67** 255 (1981)

-
134. Huang, Y.-J., Xue, J., and Schwatz, J.A., *J. Catal.* **111** 59 (1988)
135. Huang, Y.-J., Fung, S.C., Gates, W.E., and McVicker, G.B., *J. Catal.* **118** 192 (1989)
136. Sinfelt, J. H., and Via, G.H., *J. Catal* **56** 1 (1979)
137. Garten, R.L., and Sinfelt, J.H., *J. Catal.* **62** 127 (1980)
138. Sinfelt, J.H., Via, G.H., Lytle, F.W., *J. Chem. Phys.* **76** 2779 (1982)
139. Rasser, J.C., Beindorff, W.H., Scholten, J.J.F., *J. Catal* **59** 211 (1979)
140. Carter, J.L., McVicker, G.B., Weissman, W., Kmak, W.S., and Sinfelt, J.H., *Appl. Catal.* **3** 327 (1982)
141. Rice, W.R., and Lu, K., *J. Catal.* **77** 104 (1982)
142. Ponec, V., Dees, M.J., *J. Catal.* **115** 347 (1989)
143. Bonivardi, A.L., Ribeiro, F.H., and Somorjai, G.A., *J. Catal.* **160** 269 (1996)
144. Guangzhong, Z., Jianhui, L., Qiujie, S., and Fengyi, L., *J. Less Comm. Metals* **148** 399 (1989)
145. Shibiao, C., Fengyi, L., Laitao, L., and Zaoping, C., *React. Kinet. Catal. Lett.* **48**(2) 437 (1992)
146. Shibiao, C., Fengyi, L., and Laitai, L., *React. Kinet. Catal. Lett.* **57**(1) 119 (1996)
147. Wang, T., and Fengyi, L., *J. Alloys and Comps.* **207** 393 (1994)
148. Fan, Y., Lin, L., and Xu, Z., (Proc. 10th Intern. Cong. Catal., 1992, Budapest, Hungary) p2507, Elsevier, Amsterdam (1993)
149. Daniels, L.J., Sperling, P., and Rouquier, A.G., *J. Oil Gas, May* **8** 78 (1980)
150. Prins, R., "Chemistry and Chemical Engineering of Catalytic Processes" p388 (Prins, R., and Schult, Eds.) Elsevier, Netherlands (1980)
151. Haldemann, R.G., and Bolty, M.C., *J. Phys. Chem.* **63** 489 (1959)
152. Parera, J.M., Figoli, N.S., and Traffano, E.M., *J. Catal* **79** 481 (1983)

-
153. Sato, Y., Kamo, M., and Setaka, N., Carbon **10** 279 (1978)
154. Lespade, P., Al-Jishi, R., and Dresselhaus, M.S., Carbon **20** 427 (1982)
155. Stencel J.M., "Raman spectroscopy for catalysis," Van Nostrand Rheibhold, New York (1990)
156. Nikiel, D., Jagodzinski, P.W., Carbon **31** 1313 (1993)
157. Espinat, D., Dexpert, H., Freund, E., Martino, G., Couzi, M., Lespade, P., and Cruege, F., Appl. Catal. **16** 343 (1985)
158. Lespade, P., Marehand, A., Couzi, M., and Cruege, F., Carbon **22** 375 (1984)
159. Sinha, K., and Menendez, J., Phys. Rev. B **41** 10845 (1990)
160. Espinat, D., Freund, E., Dexpert, H., and Martino, G., J. Catal. **126** 496 (1990)
161. Wolf, E.E., and Petersen, E.E., Catal. Rev. Sci. Eng. **24** 329 (1982)
162. Parmaliana, A., Fruster, F., Nestro, G.A., Paukshtis, E.A., and Giordano, N., "Catalyst Deactivation," (Belmon, B., and Fromet, G.F., Eds.) p197, Elsevier, Amsterdam (1987)
163. Datka, J., Sarbak, Z., and Eischens, R.P., J. Catal. **145** 544 (1994)
164. Posazheynikova, R.P., Buyano, R.A., Koloniichuk, V.N., and Shadrin, L.P., J. Catal. **15** 671 (1974)
165. Cabrol, R.A., and Oberlin, A., J.Catal **89** 256 (1983)
166. Marchese, L., Borello, E., Coluccia, S., Martra, G., Zecchina, A., (Proc. 10th Intern. Cong. Catal., 1992, Budapest) Elsevier, Amsterdam (1993)
167. Chang, T.S., Rodriguez, N.M., and Baker, R.T.K., J. Catal. **123** 486 (1990)
168. Querini, C.A., Fígoli, N.S., and Parera, J.M., Appl. Catal. **52** 249 (1989)
169. Trimm, D.L., Appl. Catal. **5** 263 (1983)
170. Parera, J.M., Beltramini, J.N., Figoli, N.S., Churin, E.G., and Cabriol, R.A., (Proc. 8th Intern. Cong. Catal, 1984, Berlin) p593, Verlag Chemie, Berlin (1984)
171. Trimm, D.L., Appl. Catal. **5** 263 (1983)

-
172. Biswas, J., Bickle, G.M., Gray, P.G., Do, D.D., and Barbier, J., *Cat. Rev. Sci. Eng.* **30(2)** 161 (1988)
173. Krebs, H.J., and Bonzel, H.P., *Surf. Sci.* **99** 570 (1980)
174. Wolf, E.E., and Petersen, E.E., *J. Catal.* **46** 190 (1977)
175. Salmeron, M., and Somorjai, G.A., *J. Phys. Chem.* **86** 341 (1982)
176. Trimm, D.L., "Deactivation and Poisoning of Catalysts," (Oudar, J., and Wise, H., Eds.) p151, Dekker, New York (1985)
177. Zhoroz, Y.M., Panchekov, G.M., and Kartashev, Y.N., *Kinet. Catal.* **21(3)** 776 (1980)
178. Copper, B.J., Trimm, D.L., "Catalyst Deactivation" (Delmon, B., and Froment, G.F., Eds.) p63, Elsevier, Amsterdam (1980)
179. Beltramini, J.N., Martinelli, E.E., Churin, E.J., Figoli, N.S., and Parea, J.M., *Appl. Catal.* **7** 43 (1983)
180. Figoli, N.S., Beltramini, J.N., Querini, C.A., and Parera, J.M., *Appl. Catal.* **15** 41 (1985)
181. Barbier, J., Marecot, P., and Churin, E., *J. Catal.* **126** 228 (1990)
182. Shum, V.K., Butt, J.B., and Sachtler, W.H.M., *J.Catal.* **99** 126 (1990)
183. Cristoffel, E.G., and Paál, Z.J., *J. Cata.* **73** 121 91982)
184. Barbier, J., Marecot, P., and Churin, E., *J. Catal.* **126** 288 (1990)
185. Beltramini, J., and Trimm, D.L., *Appl. Catal.* **31** 113 (1987)
186. Figoli, N.S., Beltramini, J.M., Martinelli, E.E., Sad, M.R., and Parera, J.M., *Appl. Catal.* **5** 19 (1983)
187. Bond, G.C., *Surf. Sci.* **156** 966 (1985)
188. White, D., Ph.D. Thesis, University of Glasgow (1982)
189. Smith, D., White, D., Baird, T., and Fryer, J.R., *J. Catal.* **81** 107 (1983)
190. White, D., Baird, T., Fryer, J.R., Freeman, L.A., Smith, D.J., and Day, M., *J. Catal.* **81** 119 (1983)

-
211. Fryer, J.R., "The Chemical Applications of Transmission Electron Microscopy",
191. Chu, Y.F., and Ruckenstein, E., Surf. Sci. **67** 517 (1977)
192. Chu, Y.F., and Ruckenstein, E., J. Catal. **55** 281 (1978)
193. Sushumna, I., and Ruckenstein, E., J. Catal. **109** 433 (1988)
194. Yao, H.C., Sieg, M., and Plummer, H.K., J. Catal. **59** 365 (1979)
214. Spence, J.C.H. and Zuo, J.M., "Electron Microdiffraction", Plenum Press, New York (1979)
195. Ruckenstein, E., and Pulvermacher, B., J. Catal. **29** 244 (1973)
196. Flynn, P.C., and Wanke, S.E., J. Catal. **34** 390 (1974)
197. Flynn, P.C., and Wanke, S.E., J. Catal. **34** 400 (1974)
216. Andrews, K.W., Dyson, D.J., and Keown, S.R., "Electron Diffraction: Theory and Practice", Plenum Press, New York (1990)
198. Wyblatt, P., and Gjostein, N.A., "Progress in Solid State Chemistry Vol 9" (McCaldin, J.O., and Somorjia, G.A., Eds.) p 21, Pergamon Press, New York (1975)
217. Beeston, B.F.P., Horne, R.W., and Markham, R., "Practical Methods in Electron Microscopy", Plenum Press, New York (1974)
199. McVicker, G.B., Garten, R.L., and Baker, R.T.K., J. Catal. **54** 129 (1978)
200. Wynblatt, P., and Ahn, T.M., Mat. Sci. Res. **10** 83 (1975)
"Electron Microscopy of Thin Crystals", 2nd Edition, Krieger Verlag, Zurich (1975)
201. Harris, P.F.J., Boyes, E.D., and Cairns, J.A., J. Catal. **82** 127 (1983)
202. Harris, P.F.J., J. Catal. **97** 527 (1986)
203. de Broglie, L., Ann. de Physiques, **3** 22 (1925)
"Electron Microscopy", Plenum Press, New York (1974)
204. Davisson, G., and Germer, L.H., Phys. Rev. **30** 705 (1927)
221. Russ, J.C., "Fundamentals of Energy Dispersive X-ray Spectroscopy", Plenum Press, New York (1979)
205. Knoll, M., and Ruska, E., Z. Physik **78** 318 (1932)
206. Spence, J.C.H., "Experimental High-Resolution Electron Microscopy", Oxford University Press, Oxford (1981)
207. Busek, P., Cowley, J., and Eyring, L., "High Resolution Transmission Electron Microscopy", Oxford University Press, New York (1988)
208. Cowley, J.M., and Moodie, A.F., Acta Cryst. **10** 609 (1957)
209. Cowley, J.M., "Diffraction Physics", North Holland, Amsterdam (1975)
210. Scherzer, O., J. Appl. Phys. **20** 20 (1949)
227. Bond, G.C., and Flannery, S., J. Chem. Soc., Faraday Trans. 2, **76** 1111 (1980)

-
211. Fryer, J.R., "The Chemical Applications of Transmission Electron Microscopy", Academic Press, London, (1979)
212. Jones, W., Surf. Defect. Prop. Solids. **5** 65 (1975)
213. Siegel, B.M., and Beaman, D.R., "Physical Aspects of Electron Microscopy and Microbeam Analysis", Wiley, London (1975)
214. Spence, J.C.H., and Zuo, J.M., "Electron Microdiffraction", Plenum Press, New York (1992)
215. JCPDS-ICDD Powder Diffraction File (formerly ASTM index) Swarthmore, Pennsylvania (1990)
216. Andrews, K.W., Dyson, D.J., and Keown, S.R., "Electron Diffraction Patterns" Hilger, London (1967)
217. Beeston, B.E.P., Horne, R.W., and Markham, R., "Practical Methods in Electron Microscopy", (Glauert, A.M., Ed) North Holland, Amsterdam (1972)
218. Hirsch, P.B., Howie, A., Nicholson, R.B., Pashley, D.W., and Whelan, M.J., "Electron Microscopy of Thin Crystals", 2nm Edition, Krieger Butterworths, London, (1965)
219. Dorset, D.L., "Structural Electron Crystallography" Plenum Press, New York (1995)
220. Hren, J., Goldstein, J.I., and Joy, D.C., "Introduction to Analytical Electron Microscopy", Plenum Press, New York, (1979)
221. Russ, J.C., "Fundamentals of Energy Dispersive X-ray Analysis", Butterworths, Boston (1984)
222. Williams, D.B., and Carter, C.B., "Transmission Electron Microscopy", Plenum Press, New York (1996)
223. Jackson, S.D., Glanville, B.M., Willis, J., McLellan, G., Webb, G., Moyes, R.B., Simpson, S., Wells, P.B., and Whyman, R.J., J. Catal. **139** 207 (1993)
224. Park, C., Ph.D. Thesis, University of Glasgow (1994)
225. Zhu, J., and Cowley, J.W., Acta. Crystallogr. **A38** 718 (1982)
226. Zhu, J., and Cowley, J.W., J. Appl. Crystallogr. **16** 171 (1983)
227. Bond, G.C., and Flamerz, S., J. Chem. Soc. Faraday Trans. **87(5)** 767 (1991)

-
228. Bernal, S., Calvino, J.J., Gatica, J.M., Larese, C., Lopez-Cartes, C., and Perez-Omil, J.A., *J. Catal.* **169** 510 (1997)
229. Bond, G.C., "Catalysis by Metals" Academic Press, London (1962)
230. Fan, Y., Xu, Z., Zang, J., and Lin, L., in "Catalyst deactivation 1991" (Bartholemew, C.H., and Butt, J.B., Eds) p683, Elsevier, Amsterdam (1991)
231. Burch, R., and Mitchell, J., *Appl. Catal* **6** 121 (1983)
232. Querini, C.A., and Fung, S.C., *J. Catal.* **141** 389 (1993)
233. Sparks, D.E., Srinivasan, R., and Davis, B.H., *J. Molec. Catal.* **88** 325 (1994)
234. Silva, J.M., Ribeiro, M.F., Ramôa Ribeiro, F., Benazzi, E., and Guisnet, M., *Appl. Catal.* **125** 1 (1995)
235. Silva, J.M., Ribeiro, M.F., Ramôa Ribeiro, F., Benazzi, E., and Guisnet, M., *Appl. Catal.* **125** 15 (1995)
236. Strohl, J.K., and King, T.S., *J. Catal.* **116** 540 (1989)
237. Yermakov, Y.I., (Proc. 7th Int. Congr. Catal., Tokyo) Vol A p57, Kodansha/Elsevier (1981)
238. Fiedorow, R.M.J., Chahar, B.S., and Wanke, S.E., *J. Catal.* **51** 193 (1978)
239. Sierra, M.C.S., Ruiz, J.G., Proietti, M.G., and Blasco, J., *J. Molec. Catal.* **108** 95 (1996)
240. Fréty, R., Benaichouba, B., Bussière, P., Santos Cunha, D., and Lam, Y.L., *J. Molec. Catal.* **25** 83 (1994)
241. Lázár, K., Bussière, P., Guénies, M., and Fréty, R., *Appl. Catal.* **38** 19 (1988)
242. Tauster, S.J., Fung, S.C., and Garten, R.L., *J. Am. Chem. Soc.* **100** 170 (1978)
243. Tauster, S.J., and Fung, S.C., *J. Catal.* **55** 29 (1978)
244. Cunningham, J., O'Brien, S., Sanz, J., Rojo, J.M., Soria, J.A., and Fierro, J.L.G., *J. Molec. Catal.* **57** 379 (1990)
245. Binet, C., Jodi, A., Lavelly, J.C., and Boutonnetkizling, M., *J. Chem. Soc. Faraday Trans.* **88** 2079 (1992)

-
246. Bernal, S., Calvino, J.J., Cauqui, M.A., Cifredo, G.A., Jobacho, A., and Rodriguez-Izquierdo, J.M., *Appl. Catal.* **99** 1 (1993)
247. Fan, L., and Fujimoto, K., *J. Catal.* **150** 217 (1994)
248. Cochrane, H.D., Hutchison, J.C., White, D., Parkinson, G.M., Dupas, C., and Scott, A.J., *Ultramicroscopy* **34** 10 (1990)
249. Lanh, H.D., Khoai, N., Thoang, H.S., and Völter, J., *J. Catal.* **129** 58 (1991)
250. Masai, M., Honda, K., Kubota, A., Ohnaka, S., Nishikawa, Y., Nakahara, K., Kishi, K., and Ikeda, S., *J. Catal.* **50** 419 (1977)
251. Neri, G., Mercadante, L., Milone, C., Pietropaolo, R., and Galvangno, S., *J. Molec. Catal.* **108** 41 (1996)
252. Tijani, A., Coq, B., and Figueras, F., *Appl. Catal.* **76** 255 (1991)